QC
851
.G73
V.12

Air Ministry
Meteorological Research Committee
MRP 1055-1098 (non-inclusive)

MRP No.	Title	Author
1055 AD 205149	Observations From Aircraft of Temperatures and Humidities Near Stratocumulus Cloud.	D.G. James
1056 AD 223148	Forecast Verification: a Critical Survey of the Literature.	D.H. Johnson
1058	Horizontal Diffusion in the Atmosphere in the Light of Air Trajectories.	C.S. Durst A.F. Crossley N.E. Davis
1062	Spectral Estimates From Subdivided Meteorological Series.	H. Charnock G.D. Robinson
1063	Two-parameter Techniques of Numerical Forecasting Applied to a Small Intense Depression.	J.S. Sawyer
1064 AD 208931	Temperature, Humidity and Cloud Near Fronts in the Middle and Upper Troposphere.	J.S. Sawyer
1065	The Southern Circumpolar Westerlies: Broad Characteristics and Apparent Associations.	H.H. Lamb
1066 AD 158566	Average Height of the Standard Isobaric Surfaces Over the Temperate and Tropical Regions in July.	H. Heastie
1068 AD 216170	The Origin of Radar 'Angels'.	W.G. Harper
1069	Some Airborne Observations of Condensation Nucleus Concentration. I. Variations in the Vertical.	G.J. Day
1070	The Measurement of Wind at Altitude by Airborne Instruments.	R.J. Murgatroyd N.C. Helliwell
1071	A Diagram for Obtaining True Air Temperatures From Indicated Air Temperatures for Aircraft Resistance Thermometers.	W.G. Durbin
1073	Convection-diffusion Processes Below a Stable Layer - Part II. (Porton Technical Paper No. 619).	F.B. Smith
1074	Some Observations on the Composition of Fogs.	K.H. Stewart
1075	Average Water-vapour Content of the Air.	J.K. Bannon L.P. Steele

MRP No.	Title	Author
1077	The Development of Precision Aneroids - Interim Report.	R. Frith
1078	Conservation of Vorticity at 100 mb.	J.R. Probert-Jones
1079	Some Measurements of Temperature and Humidity Near the Sea Surface.	H.C. Shellard
1080 AD 216168	The Relation Between Anomalies of Surface Air Temperature and of 1000-500 mb Thickness Over the Atlantic Sector of the Northern Hemisphere.	C.A.S. Lowndes
1084	The Phosphorus Pentoxide Electrolytic Hygrometer.	A.W. Brewer
1098	Index of M.R.P.'s Approved for General Distribution.	

M.R.P. 1055
S.C.111/ 237
S.C.11/236
17th May, 1957
AD 205149

Observations from aircraft of temperatures and humidities near stratocumulus cloud

by

D. G. James

(Meteorological Office)

AIR MINISTRY

METEOROLOGICAL RESEARCH COMMITTEE

58-94

At the time of issue this report has not been published. Any author desiring to quote this paper should refer to it as "A paper of the Meteorological Research Committee (London), M.R.P. No. 1055 by Dr. D.G. James
A copy is available in the Library of the Meteorological Office."

M.R.P.1055
S.C.III/237
S.C.II/236
17th May, 1957

AIR MINISTRY

METEOROLOGICAL RESEARCH COMMITTEE

Observations from aircraft of temperatures and humidities near stratocumulus cloud

by

D. G. James (Meteorological Office)

1. Introduction

Previous work on the dissipation of stratocumulus cloud (James, 1955) suggested that certain features of the environment of the cloud sheet are significant in determining the subsequent behaviour of the cloud. In particular, a significant difference was thought to exist in the hydrolapses above and below cloud, the temperature lapse rate above cloud, and the cloud thickness between cases when the cloud sheet persisted and cases when it dissipated within a given time. As lack of better agreement may have been due to inaccuracies in surface observations of cloud base, and in radio sonde measurements of temperatures and dewpoints, it was recommended that a series of flights should be made by aircraft of the Meteorological Research Flight in order to make accurate measurements of some of the features associated with an extensive sheet of non-frontal stratocumulus cloud.

Flights subsequently carried out by the Meteorological Research Flight were such that, following an ascent from ground to about 10,000 ft, the aircraft made level runs of 3-5 min at 250 ft intervals from 1,000 ft below cloud base to cloud top, then at 100 ft intervals up to 500 ft above cloud top, thereafter at 250 ft intervals to 2,000 ft above cloud top, and finally two level runs of 8 min at 200 ft above cloud top and 200 ft below cloud base. Height, airspeed, temperature and frost point were observed every 250 ft on the ascent, and every 30 sec on the level runs along which the observations were supplemented by accelerometer records. In cloud, an attempt was made to obtain measurements of the liquid water content.

Selection of the occasions for the flights was made in the Forecasting Research Division, Dunstable, and the analysis of the flight data was also carried out there. Some modifications of the flight plan were made from time to time, but these did not affect the basic scheme.

To conform with operational requirements all flights were performed in the Farnborough area so that the aircraft could be followed by radar whilst flying in cloud.

2. Flights by M.R.F. aircraft

Eight flights were made during November, 1955 by aircraft of the M.R.F. in connection with the stratocumulus investigation. On four of these flights only an ascent and descent through the cloud was made, but on the remaining four flights a full set of data was obtained. Figs. 1 (a - h) show the vertical distribution of temperature and dewpoint as obtained from the aircraft observations, together with details of the cloud base and top.

/Although

Although temperatures and frost points cannot be measured accurately in cloud, there were occasions when the stratocumulus was quite thin and tenuous, and then readings were taken of temperatures and sometimes frost points also. These values have been included in Figs. 1 (a - h) where they occur.

The second half of November, 1955 was particularly favourable for the presence of extensive sheets of stratocumulus cloud. An anticyclone at first centred over Scotland moved slowly westwards, and then slowly returned, finally turning southeast and moving into France. In general during this period, southeast England was in an anticyclonic weak northeasterly flow which was accompanied by extensive stratocumulus cloud; sometimes the cloud dissipated. Table 1 gives the dates of the flights together with cloud bases and tops and probable times of dissipation.

On level runs near the cloud, an accelerometer was used. Some of the traces from one of the flights are given in Fig. 5. These are traces obtained on the flight of 14th November, 1955, but they are quite characteristic of all such records made near stratocumulus cloud.

3. Analysis of observations

3.1 Temperature

Temperature measurements were made by a flat plate thermometer, the lag of which is about 8 sec. A level run of 3-5 min allows ample time for the thermometer to settle down and the readings obtained will give a good indication of actual fluctuations of temperature along the aircraft track at a given height. In Figs. 1 (a - h) one of the vertical profiles is obtained by plotting the means of corrected temperatures recorded on level runs. It can be seen that the inversions of temperature immediately above cloud top as shown by these means are considerably greater than might be expected from an appropriate radio-sonde ascent, Figs. 2 (a - d). Furthermore, the measured temperature gradients in the inversion increase as the height interval between observations is decreased.

If there is turbulent mixing at cloud top then large temperature fluctuations should be apparent at cloud top. Figs. 3 (a - d) present the standard deviations of temperature measured on level runs at given heights. It is clear that in all four cases there is a large increase in the standard deviation of temperature at cloud top. A return to normal values of standard deviation is indicated at 200 ft above cloud top and at greater heights. It must be pointed out, however, that the standard deviations recorded are not true deviations of horizontal temperature. The variations in height of the aircraft on a horizontal run probably account for some of the observed fluctuations, though the altimeter records are not sufficiently accurate to obtain a good correlation between temperature and height variations. Little significance can be attached to absolute values of temperature measured in cloud due to the liquid water deposited on the thermometer, but it is thought that the temperature fluctuations are of the right order of magnitude, and they have been included in Figs. 3 (a - d).

Table 2 shows the lapse rates of temperature upwards from cloud top over various distances.

Figs. 1 (a - h) show that:-

(1) when level runs are made at 100 ft intervals above cloud top the estimated temperature gradients in the inversion directly above cloud are significantly greater than when measurements are taken every 250 ft on an ascent. Thus to obtain accurate measurements of $\Delta T/\Delta Z$ above cloud, temperatures must be obtained at intervals of 100 ft or less.

/(2)

(2) The gradient of temperature with height within 300 ft of cloud top is of the order of 3°C per 100 ft.

(3) In some cases, the inversion extends as far as 1,000 ft above cloud top, though in general there is a reversal of sign of $\Delta T/\Delta z$ within 5-600 ft.

(4) On the occasions when the cloud had already dispersed or was well broken, the inversions were not as intense as on the other occasions.

(5) Below cloud the measured temperatures indicate the presence of a dry adiabatic lapse rate.

3.2. Frost point

Frost points were measured by a Dobson-Brewer manual hygrometer. In the range in which observations of frost points and dewpoints were taken, i.e., -20°C to +10°C, this instrument is accurate to within 0.5°C. The instrument suffers from the disadvantage that frost points are obtained manually, and hence, in general, the readings obtained are not synchronous with the temperature observations. Further, in a region where the humidity is variable, the frost point measurements are frequently missed by over-shooting from one reading to the next.

Figs. 1 (a - h) show the profiles of dewpoints with pressure for the eight flights made. In all cases it is clear that there is a sharp decrease of humidity just above cloud top. On some occasions the cloud was so thin and tenuous that frost points were measured in the cloud layer, and the corresponding dewpoints have been shown in the figures. Nevertheless, complete saturation was not measured.

Figs. 4 (a - d) present the standard deviation of frost points measured on level runs near cloud. The standard deviations shown may be expected to be less than those which would have been obtained had a fully automatic hygrometer been used: with a fluctuating frost point there will be a tendency to record fewer observations with the manual hygrometer; also there will be considerable bias towards recording successive values of the frost point which are approximately of the same value. Thus the tendency for an increase in the standard deviation at or just above cloud top is probably real.

It is interesting to note that both the standard deviations of temperature and frost point recorded on 14th November, 1955, Figs. 3 (a) and 4 (a), are considerably greater over an 8 min run above cloud than for a 3 min run at the same height. For the 16th November, 1955 and 22nd November, 1955, Figs. 3 (b) and 4 (b) and Figs. 3 (c) and 4 (c), there is no significant difference between standard deviations over 8 min and those over 3 or 5 min. Examination of the individual values of temperature and frost point recorded on the 8 min run at 5,800 ft on 14th November, 1955 shows that the temperature increased throughout the run, whilst the frost points decreased, the wet bulb potential temperature remaining constant, and equal to that above cloud. However, during this 8 min run, the aircraft increased height by about 80 ft, which, using the slope of the inversion directly above cloud, would lead to an increase in temperature of about $1\frac{1}{2}$ to $2\frac{1}{2}$°C. This would account for nearly all of the discrepancy between the standard deviations recorded on the 3 min and 8 min runs at the same height. It should be emphasised that the so-called level 3-5 min runs frequently admitted of variations in height of up to ± 20 or 30 ft.

In general the values of $\Delta x/\Delta z$ obtained from Figs. 1 (a - h) are less than ± 0.3 gm/Kg per 100 ft, but above cloud there is a sudden increase when values of up to -1.5 gm/Kg per 100 ft are measured.

/The

The case of the 15th November, 1955, when there was no cloud, and that of the 21st November, 1955, when the cloud was well broken, are worthy of note. Both show that a significant change in the lapse rate of humidity mixing ratio is still present; on the other hand Figs. 1 (b) and 1 (f) do not indicate the presence of such a sharp temperature inversion on those dates as on the occasions of continuous cloud sheets.

3.3. Accelerometer records

A photographically recording accelerometer was used on most of the flights on which level runs were made. Figs. 5 (a - g) show sections of the traces obtained near cloud during the flight of 14th November, 1955. The traces are typical of the bumpiness experienced by the aircraft on all other flights near cloud base and top.

On all occasions when accelerometer records were obtained the traces well above cloud top were very different from those just above and below cloud top. The former, as can be seen from Fig. 5, exhibit considerably fewer bumps than do the latter, though the occasional bumps, when they do occur, are of comparable magnitudes with those experienced below cloud top. However, the most striking difference between the two sets of traces is the almost complete absence of high frequency (1 - 3 c/s) disturbances i.e., disturbance with spatial dimensions of 80 - 250 ft in the region well above cloud top. The natural frequency of the loaded spring constituting the accelerometer is 3 c/s, but the change in the character of the trace must correspond to a decrease in the small scale turbulence in the atmosphere. High frequency components are clearly evident in Figs. 5 (a - d) but almost entirely absent in Figs. 5 (e - g). The line of demarcation between the two types of traces is well marked. On all occasions the sharp division occurred between 200 and 300 ft above cloud top; the traces above this height are very smooth, increasingly so with height, whilst below this level the traces are extremely disturbed. Accurate assessment of vertical velocities from the accelerometer traces (see Jones, 1953) was found to be impossible since a recording altimeter was not used, and therefore the zero error could not be applied accurately to the integrated traces. There was also considerable doubt in some cases as to the speed of the film in the accelerometer.

4. Discussion

4.1. General considerations

Although eight flights were carried out by the M.R.F. aircraft, full sets of data were obtained on only four of them. Consequently the following discussion relates only to these four cases though there is no evidence that the profiles obtained from the remaining four flights were materially different.

For the flights considered the stratocumulus sheet had been in existence for some 10 hours or more, and persisted for some hours afterwards. It is unlikely, therefore, that at the times of observation the observed temperature and humidity structures were changing rapidly.

The effect on the cloud of the following processes will be considered:-

(a) Radiation

(b) Turbulent diffusion of heat and water vapour at cloud base and top

(c) Subsidence.

It is not proposed to consider advection because the stratocumulus sheets extended well upstream and downstream from the area of flight and successive radio-sonde soundings showed no change in air mass.

/The

The remaining processes are considered below with particular reference to the data of 14th November, 1955, but corresponding results for the other three cases of complete data will be given later in the discussion.

4.2. Evidence from flight measurements

All flights in the region of a stratocumulus cloud sheet indicate the presence of a marked inversion extending for 10 mb or so above cloud top surmounted by at least a further 20 mb of very dry air with a stable lapse rate. The accelerometer records indicate significant turbulence in the lower part of the inversion layer directly above cloud.

The observed turbulence will transfer heat downwards into cloud top and water vapour upwards into the inversion layer and tend to change the observed character of the temperature inversion and hydrolapse. However, since these latter are fairly constant from flight to flight it is necessary to explain how the observed character of the inversion layer is maintained. Moreover, although the flights were of limited duration, there was little indication of systematic changes in the level of cloud top during them. We are therefore led to the conclusion that the air immediately above cloud top is continually being replaced by subsidence which operates against the turbulence to give an approximately steady state at and immediately above cloud top.

Before we evaluate the rate of subsidence necessary to maintain a steady state, we will first consider the heat and water vapour budgets of the cloud and air below and also those of the inversion layer. In the calculations we will make an initial choice of 3×10^3 cm^2/sec for the value of the coefficient of eddy diffusion, K, appropriate to the inversion layer, both in respect of heat and water vapour. This is the value given by Taylor (1915) for stable conditions at lower levels over the sea with winds of about 10 kt. The effect of a different value of K will be evident at any stage and indeed we shall see later that it is necessary to consider other values.

4.3. The heat budget of the cloud and air below

4.3.1. Radiation

Radiation measurements above a stratocumulus or stratus cloud sheet (Neiburger, 1949, Fritz, 1950, Murgatroyd, 1956) suggest that the albedo of such a sheet varies considerably with cloud thickness. Values between 0.3 and 0.8 are given for thicknesses from 'very thin' to 4,500 ft. For a cloud about 500 ft thick an albedo of 0.5 is probably close enough for our purposes.

Measurements at Kew show that, during a clear day in November, about 180 cal/cm^2 are available at the surface from solar radiation, an average of 20 cal/cm^2/hr between sunrise and sunset. Other measurements (Berry, Bollay and Beers, 1945, Houghton, 1954) also suggest an average during November of about 20 cal/cm^2/hr at the surface at about latitude 50°N. In the calculations below it is more convenient for us to assume durations of 8 and 16 hours for day and night respectively in November; also some allowance has to be made for the fact that events at a height of about 5,000 ft are under consideration. It will therefore be assumed that during daylight hours in November an average of about 25 cal/cm^2/hr is available at 5,000 ft from solar radiation. Thus with an albedo of 0.5 about 13 cal/cm^2/hr pass into cloud top.

The loss of heat by long-wave radiation at cloud top may be obtained by use of the Elsasser radiation chart. For 14th November, 1955 this loss was about 10 cal/cm^2/hr.

/Thus

Thus during the day there is a flux of heat of about 3 cal/cm^2/hr downwards through cloud top, whilst at night there is an outward flux of 10 cal/cm^2/hr.

The long-wave radiative loss occurs in the top 50 ft or so of the cloud and consequently this thin layer will at all times be tending to cool rapidly. Convective turbulence must therefore occur, causing rapid mixing of the air within the cloud; also mixing with the dry air below in which the observed lapse rate is dry adiabatic over a considerable depth. Thus cooling initiated at cloud top is quickly spread over a considerable depth below.

4.3.2. Conduction and evaporation

Measurements made at Kew suggest that, during November, about 1 cal/cm^2/hr is conducted into the earth during the day, the heat being restored to the surface at the same rate during the night.

The evaporation of water at the surface accounts for some heat also. Data available in the British Climatology Branch of the Meteorological Office show that evaporation from tanks of water at Kew was at the rate of about 7×10^{-2} gm/cm^2/24 hr on the dates of the flights. It is known that the average rate of evaporation during the day is some 3 or 4 times that at night. We will therefore assume that the average rates of evaporation during the day and night on the dates of the flights were 6.0×10^{-3} gm/cm^2/hr and 1.5×10^{-3} gm/cm^2/hr respectively. The quantities of heat required for these rates of evaporation are approximately 4 cal/cm^2/hr and 1 cal/cm^2/hr.

4.3.3. Turbulence

In the case of 14th November, 1955, assuming a saturated adiabatic lapse rate in the cloud and also a linear variation of temperature with pressure from cloud top at 851 mb to the top of the inversion at 838 mb, then the average $\Delta\theta/\Delta p$ (θ is potential temperature) through the stable layer is 0.44°C/mb. The flow of heat downwards is thus

$$F = \rho C_p K \frac{T}{\theta} \frac{\partial \theta}{\partial z} \simeq 1 \text{ cal/cm}^2\text{/hr}$$

taking $K = 3 \times 10^3$ cm^2/sec.

4.3.4. Summary of heat budget of cloud and air below

The above figures show that during the day the net loss of heat by the cloud and air below would be 1 cal/cm^2/hr. Assuming that this loss is uniformly distributed from cloud top to ground - all flights show a dry adiabatic lapse rate in a layer of some depth below cloud base - the cloud and air below cools by about 0.2°C during daylight hours.

At night there would be a net loss of 9 cal/cm^2/hr giving a cooling of the cloud and air below of 3.3°C during the night. This is about twice as great as is actually observed from radiosonde ascents at 12 hr intervals through the same air mass, and must therefore be considered further.

The main factor responsible for the rate of cooling thus calculated is the radiative loss from cloud top evaluated as 10 cal/cm^2/hr using the Elsasser diagram. However, measurements from aircraft of the flux of long-wave radiation near

/stratocumulus

stratocumulus cloud by Houghton and Brewer (1955) (about 9 cal/cm^2/hr at night) confirm the value we have taken. We must therefore turn to some other factor to operate against this excessive rate of cooling. Possibly the value of K we have assumed (3×10^3cm^2/sec) is too low, especially at night. A value of K of 10^4cm^2/sec would, through more rapid transfer of heat downwards in the inversion layer (4 cal/cm^2/hr), restrict the cooling of the cloud and air below to 2.2°C during the night, and this is much nearer what is observed. There is thus some indication that we may need to consider the effect of values of K greater than 3×10^3cm^2/sec in the inversion layer.

4.4. The water vapour budget of the cloud and air below

4.4.1. Evaporation

From 4.3.2. the water vapour available through evaporation at the surface is about 6.0×10^{-3}gm/cm^2/hr by day and 1.5×10^{-3}gm/cm^2/hr by night. Since all flights show that the humidity mixing ratio is constant in a considerable depth below cloud base, it is likely that the turbulence, as shown by the accelerometer traces, is sufficient to distribute the evaporated water through the cloud and air below.

4.4.2. Turbulence

The cloud loses water vapour by turbulent diffusion upwards at cloud top. The measurements of water content in the cloud are not reliable but it is reasonable to assume that the humidity mixing ratio in the cloud (including liquid water) is determined by observed temperature immediately below cloud base (dry adiabatic lapse) and the observed level of cloud base, extended upward by a saturated adiabatic lapse rate in cloud. Then for the data of 14th November, 1955, the average hydrolapse $\Delta x/\Delta p$ through the inversion layer immediately above cloud is 0.20×10^{-3}gm/gm/mb so that the flux of water vapour upwards is

$$F = \rho K \frac{\partial x}{\partial z} \simeq 2.2 \times 10^{-3}\text{gm/cm}^2\text{/hr},$$

using $K = 3 \times 10^3$ cm^2/sec.

4.4.3. Summary of the water vapour budget of the cloud and air below

During the day there would be a net gain of water vapour of 3.8×10^{-3}gm/cm^2/hr by the cloud and air below; by night a loss of 0.7×10^{-3}gm/cm^2/hr. Thus the changes in humidity mixing ratio of the air below cloud top would be about +0.2 gm/Kg during daylight hours and -0.06 gm/Kg by night, K being 3×10^3cm^2/sec. For $K = 10^4$ the changes would be -0.05 gm/Kg by day and -0.5 gm/Kg by night.

4.5. The balance of the inversion layer

The accelerometer records indicate considerable turbulence in and below the layer from cloud top to about 10 mb above but none whatever higher up in the dry air. It must therefore be assumed that the heat gained by the cloud and air below through turbulent diffusion, is taken entirely from this layer; also that the water vapour lost by the cloud and air below is accumulated in this layer. As we have seen in 4.2. above this would lead to observable changes in temperature and humidity in this layer and changes in the character of the temperature and dewpoint profiles in and immediately around the inversion. As no systematic variation in the level of cloud top was observed on any flight we proceed to calculate

/the

the rate at which the air in the inversion layer needs to be replaced by subsidence in order to counteract the effects of turbulent transfer and to maintain cloud top at the same level.

If air is subsiding then the amount of heat added to a layer is proportional to the rate of subsidence and to the difference in potential temperature at the limits of the layer. In the case of 14th November, 1955, the assumptions in 4.3.3. give a difference of 6°C in the potential temperature at cloud top at 851 mb and the top of the inversion at 838 mb. Thus a subsidence rate of rather less than 1 mb per hour would be sufficient to balance the heat loss to the cloud by turbulence (1 cal/cm^2/hr with $K = 3 \times 10^3$).

Similarly if the transport of water vapour downwards by subsidence is to equal that upwards by turbulent diffusion; then, with the assumptions given in 4.4.2., taking an average value of 2.6 gm/Kg for the humidity mixing ratio in the inversion layer, a rate of subsidence of rather less than 1 mb/hr is also sufficient to balance the upward transfer of water vapour by turbulence in the inversion layer.

The rate of subsidence required for this balance is directly proportional to the value of K assumed to be operative in the inversion layer. With $K = 10^4$ subsidence of rather less than 3 mb/hr would be required.

It will be appreciated that when subsidence operates there is divergence out of any column of air extending from cloud top to the ground. However, the heat and water vapour budgets of the cloud and air below remain as above (we assume constant potential temperature and humidity mixing ratio below cloud).

4.6. Extension to the four cases of complete data

Table 3 presents the results of calculations on all four occasions of complete data, carried out in the same manner as in 4.3. to 4.5. above. The table also includes estimates of the behaviour of the cloud if the assumed conditions were operating, and also the observed behaviour of the cloud. We will summarise here the assumptions made in obtaining the figures.

4.6.1. Complete saturation was not observed in cloud on any flight. The observations of humidity in the cloud were therefore regarded as unreliable and it was assumed that the (corrected) dry bulb temperatures below cloud (approximately on a dry adiabat for 50 mb at least) were correct. The humidity mixing ratio below cloud was assumed to be that given by these dry bulb temperatures and the observed cloud base. Similarly the temperature and frost point immediately above cloud top were assumed to be those determined by a wet adiabatic lapse rate in cloud.

4.6.2. The change in temperature and humidity mixing ratio of the cloud and air below were calculated on the assumption of complete mixing down to M.S.L. by both day and night. Whilst this is not necessarily true it gives a basis for comparison. As the relevant figures are inversely proportional to the layer mixed, adjustment for this assumption may readily be made.

4.6.3. Estimates of the observed behaviour of the cloud refer to the area of cloud near which the aircraft observations were made; so that, in determining from the synoptic chart whether or not it dispersed, an estimate of the movement of this parcel of cloud had to be made.

/4.7.

4.7. Deductions

4.7.1. The value of K in the inversion layer

On at least three of the occasions considered in detail the flights occurred in mid-afternoon and it may be assumed that the observed conditions applied at sunset. We are therefore interested at first in the figures against night in Table 3. If the expected and observed behaviour of the cloud are compared, it can be seen that the operative value of K in the inversion layer must be at least 10^4 cm^2/sec, if not rather greater, by night, if the expected behaviour is to approach the observed behaviour. With a K of $3 \times 10^3 cm^2$/sec unreasonable rates of subsidence would be required to disperse the cloud in the first two cases by 6 hours after sunset. On the other hand, if the observed profiles existed at sunrise there would be some reason to believe that the operative value of K by day is less than $10^4 cm^2$/sec because in all cases the cloud persisted by day.

General considerations support the possibility that the value of K in our problem is higher than might otherwise be expected in inversions of the magnitude we are considering; and that the value by night could well be higher than that by day. Excluding orographic effects, the turbulence in the cloud is maintained by the cooling of the top 50 ft or so of the cloud by reason of the outgoing long-wave radiation; as no fixed boundaries are involved the convective turbulence thus caused must have an effect in the (shallow) inversion layer above cloud; moreover the turbulence in the cloud may be expected to be greater by night than by day due to absorption of solar radiation by day.

4.7.2. Subsidence

The rate of subsidence, neglecting the small amount which may result from night cooling, is a function of the general synoptic regime only and not, ceteris paribus, of the time of day. Thus if the rate of subsidence is greater/less than the figures given in Table 3 cloud top will fall/rise. Rates of subsidence substantially greater than those given to maintain cloud top at the same level, K being $10^4 cm^2$/sec, are unlikely in general. As we have seen that K may well exceed $10^4 cm^2$/sec in the inversion above a stratocumulus sheet by night, it is probable that, in most cases, cloud top rises by night; although the cloud may still disperse through decrease of the humidity mixing ratio below the inversion.

5. Conclusions

5.1. The temperature inversion and lapse rate of water vapour content above a sheet of stratocumulus cloud are considerably greater than those shown by a radio-sonde ascent through the same air mass. Temperature increases of up to 3°C/100 ft and lapse rates of humidity mixing ratio of up to 1.5 gm/Kg/100 ft have been measured. For all cases of continuous cloud sheets the change from the saturated cloudy air to the warmer drier air above occurred almost entirely within the first 300 ft above cloud top.

5.2. The standard deviations of the temperature fluctuations on level runs near the cloud may be of an order of magnitude greater in the first 300 ft above cloud top than at any other level. The standard deviations of frost points measured on these runs exhibit similar features, but the increase directly above cloud is less well marked. In general, the standard deviation of temperature is of the same order as that of frost point.

5.3. The accelerometer records for level runs near cloud show a marked change at 200-300 ft above cloud top. Few bumps were experienced above

/this

this height, and there was a complete lack of high frequency disturbances (1-3 cycles/sec) i.e., disturbances of spatial dimensions of 80-250 ft. It is suggested that eddies of these dimensions play a major part in the transport of heat and water vapour by turbulence.

5.4. Consideration of the observed temperature and humidity profiles together with the effects of radiation, turbulent diffusion of heat and water vapour, and subsidence lead to the conclusion that the approximately steady state in a persistent layer of stratocumulus is maintained by turbulence operating against subsidence.

5.5. It is probable that the operative value of K, the coefficient of eddy diffusion, in the inversion layer immediately above cloud is close to $10^4 cm^2/sec$; and that K is greater by night than by day.

5.6. With K = $10^4 cm^2/sec$, subsidence of 3 mb/hr would keep cloud top at the same level in the cases considered. Subsidence rates greater/less than 3 mb/hr would result in cloud top falling/rising.

REFERENCES

Berry, Bollay and Beers	1945	Handbook of Meteorology.
Fritz, S.	1950	Bull. Am. Met. Soc., 31, p.251.
Houghton, H.G.	1954	J. Met., 11, No. 1.
James, D.G.	1955	Meteorological Research Papers, Air Ministry, London, No.913.
Jones, R.F.	1953	Meteorological Research Papers, Air Ministry, London, No.820.
Murgatroyd, R.J.	1956	Meteorological Research Papers, Air Ministry, London, No.995.
Neiburger, M.	1949	J. Met., 6, p.28.
Roach, W.T.	1955	Meteorological Research Papers, Air Ministry, London, No.936.
Robinson, G.D.	1955	Meteorological Research Papers, Air Ministry, London, No.929.
Taylor, G.I.	1915	Phil. Trans. Roy. Soc.
Brewer, A.W. and Houghton, J.T.	1955	Meteorological Research Papers, Air Ministry, London, No.914.

TABLE I

Date	Duration of flight	Cloud Base(ft.)	Cloud Top(ft.)	Probable time of dissipation
14:11:55	1400 – 1630	5,250	5,500	2300/14
15:11:55	1500 – 1620	No cloud		——
16:11:55	1430 – 1700	3,150	4,000	2200/16
17:11:55	1520 – 1620	5,000	6,100	2200/17
18:11:55	1410 – 1525	4,200	5,000	Not before 0600/19
21:11:55	1430 – 1530	3,000	3,500(well broken)	Possibly 1800/21
22:11:55	1340 – 1630	6,750	7,750	Not before 0600/23
28:11:55	1100 – 1330	4,250	4,750	Not before 0600/29

TABLE 2

Mean lapse rate from cloud top to specified heights above cloud top

$\frac{\Delta T}{\Delta Z}$ in °C / 100 ft.

		Height above cloud top (ft.)								
Date	Cloud cover	100	200	300	400	500	750	1000	1250	1500
14:11:55	8/8 sheet	3·06	1·81	1·37	0·95	0·85	0·49	0·32	0·25	0·18
15:11:55	Nil									
16:11:55	8/8 sheet	2·62	1·58	0·98	0·77	0·57	0·32	0·19	0·11	0·05
17:11:55	8/8 sheet	–	–	–	0·87	–	–	0·32	–	0·15
18:11:55	8/8 sheet	–	–	–	–	0·56	–	0·32	–	0·22
21:11:55	Well broken	–	–	-0·02	–	0·11	0·17	0·24	–	–
22:11:55	8/8 sheet	–	1·93	2·00	1·64	1·27	–	–	–	–
28:11:55	8/8 sheet	1·60	0·94	1·09	1·14	1·17	–	–	–	–

DATE AND TIME OF FLIGHT	M.S.L. PRESSURE (MB.)	CLOUD TOP (MB.)	CLOUD THICKNESS (MB.)	ASSUMED K (CM^2/SEC)	DAY 8 NIGHT 16 (HRS.)	CHANGE TEMP. CLOUD AND AIR BELOW °C PER DAY AND NIGHT	CHANGE HUM. MIXING RATIO CLOUD AND AIR BELOW (G M./KG. DAY/NIGHT)	SUBSIDENCE TO KEEP CLOUD TOP AT SAME LEVEL (MB./HR.)	EXPECTED BEHAVIOUR OF CLOUD +THICKNESS (MB. DAY/NIGHT)	OBSERVED BEHAVIOR OF CLOUD
14:11:55 1400-1630	1025	850	10	3×10^3	DAY	−0·2	+0·2	1	+15	CLOUD PATCHY WITH BREAKS BY DAY. OBSERVED ARE OF CLOUD PROI ABLY DISPERSE 2200Z
					NIGHT	−3·3	−0·1		+40	
				10^4	DAY	+0·4	−0·1	3	−10	
					NIGHT	−2·2	−0·5		−5	
16:11:55 1430-1700	1040	900	25	3×10^3	DAY	0·0	+0·2	1	+10	DISPERSED 2200Z
					NIGHT	−3·7	−0·1		+40	
				10^4	DAY	+1·0	−0·1	3	−20	
					NIGHT	−1·7	−0·7		−20	
22:11:55 1340-1630	1035	780	22	3×10^3	DAY	0·0	+0·1	1	+5	PERSISTED AT LEAST OVERNIG
					NIGHT	−2·0	0·0		+25	
				10^4	DAY	+0·7	0·0	3	−5	
					NIGHT	−0·6	−0·2		0	
28:11:55 1100-1330	1020	860	12	3×10^3	DAY	−0·1	+0·2	1	+10	PERSISTED AT LEAST OVERNIG
					NIGHT	−3·4	−0·1		40	
				10^4	DAY	+0·6	−0·1	2 HEAT	−10	
					NIGHT	−2·0	−0·5	3W. VAPOUR	0	

Table 3 Estimates and observations on occasions of complete data

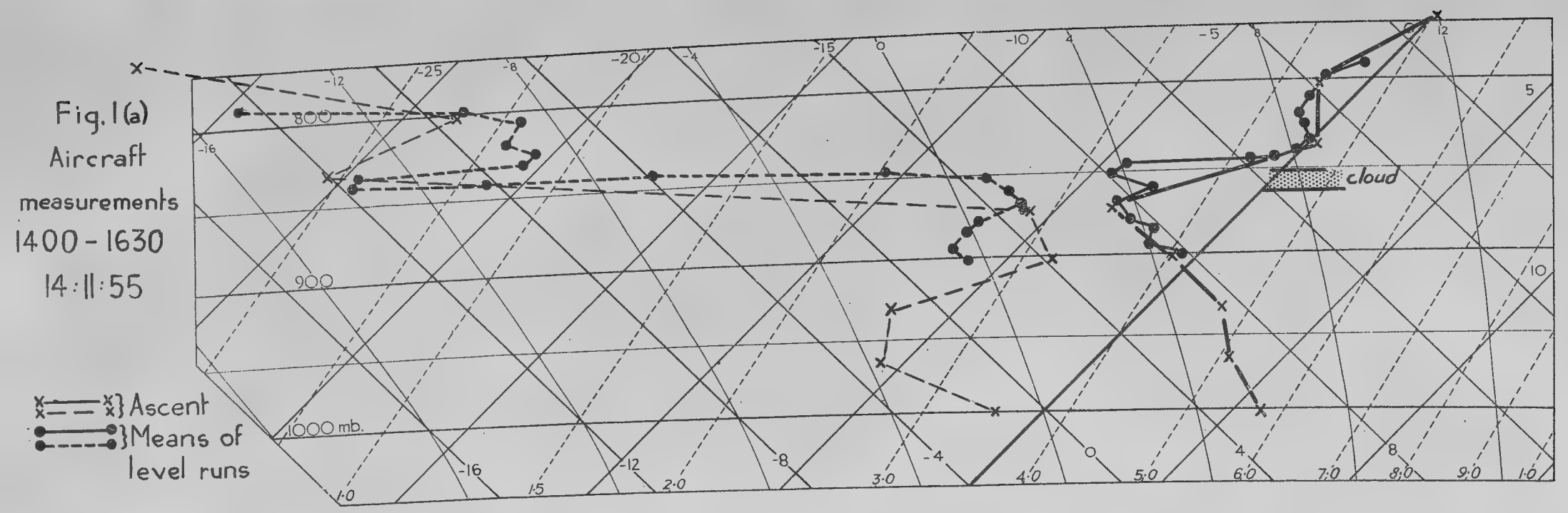

Fig. 1(a)
Aircraft measurements
1400 - 1630
14:11:55

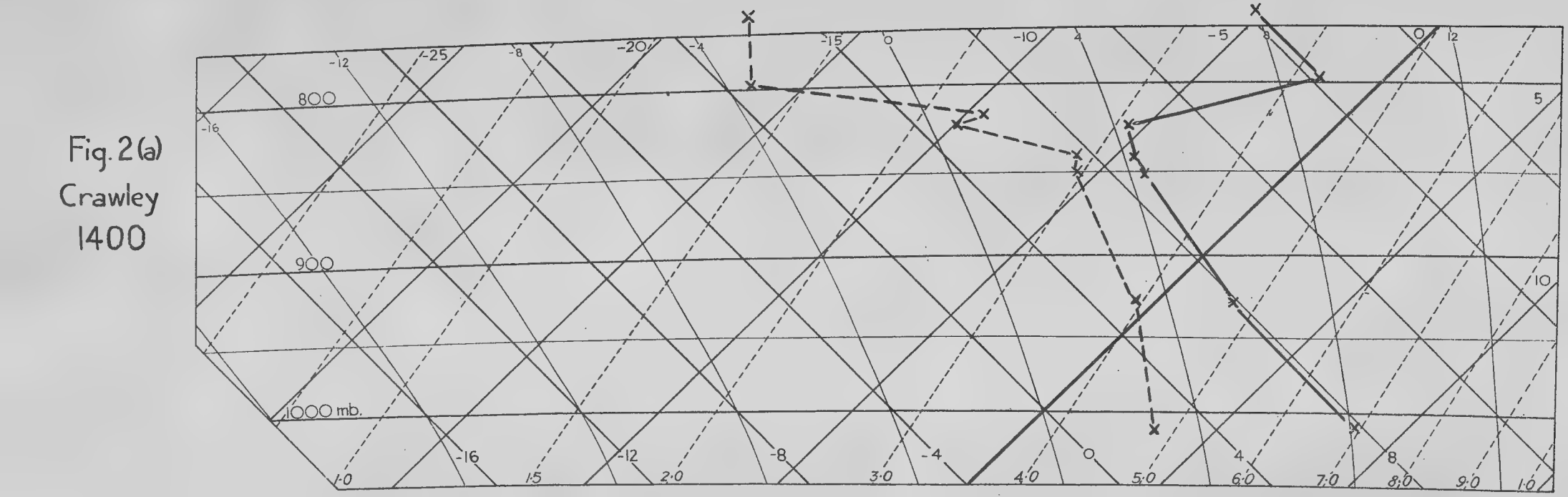

Fig. 2(a)
Crawley
1400

Fig 1 (b)
Aircraft
ascent
1500-1620
15:11:55

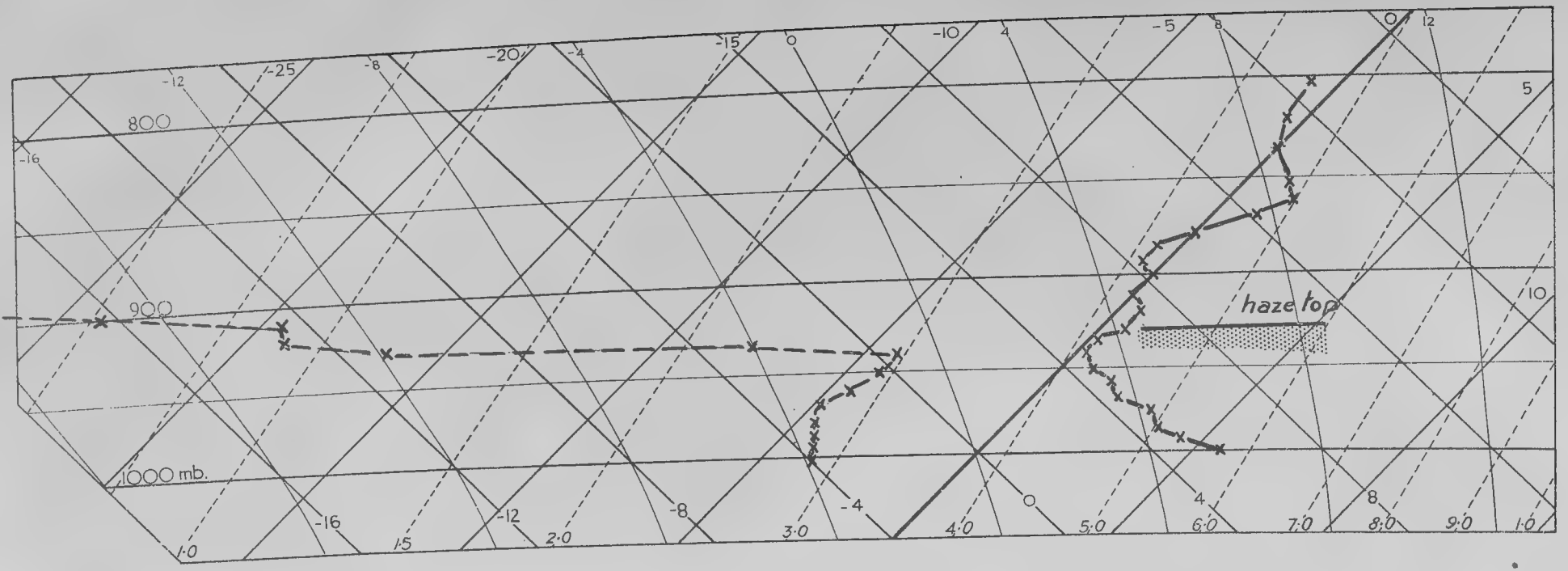

Fig. 1 (d)
Aircraft
ascent
1520-1620
17:11:55

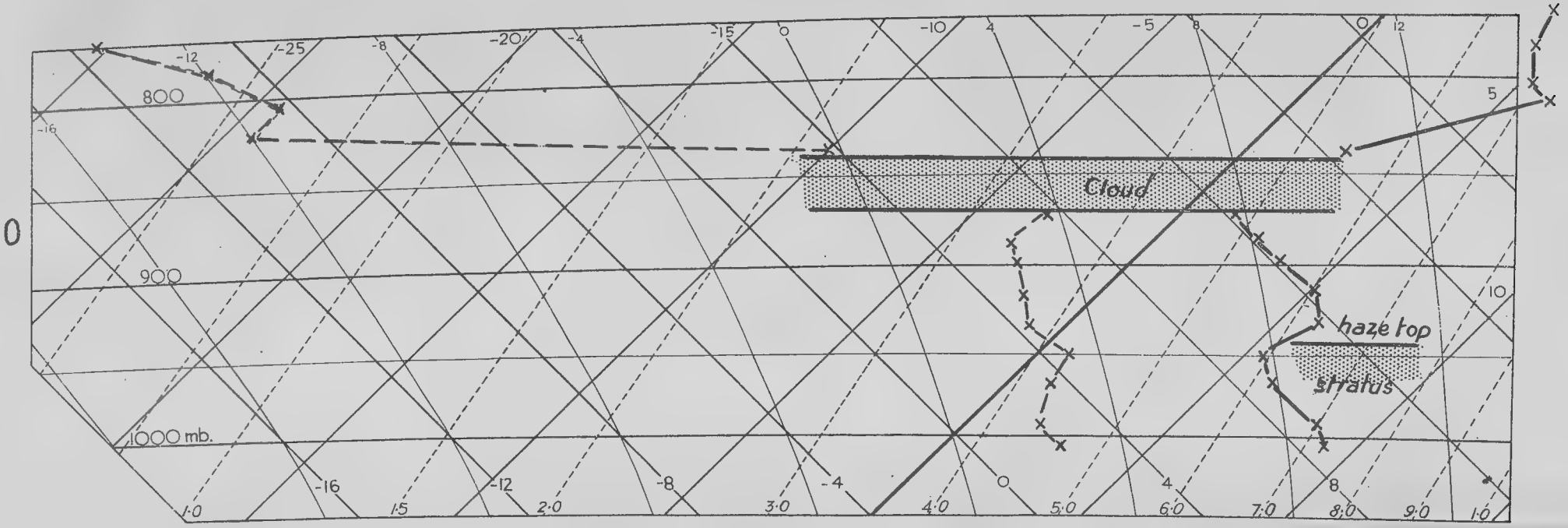

M.R.P. 1055

Fig 1(c)
Aircraft
measurements
1430-1700
16:11:55

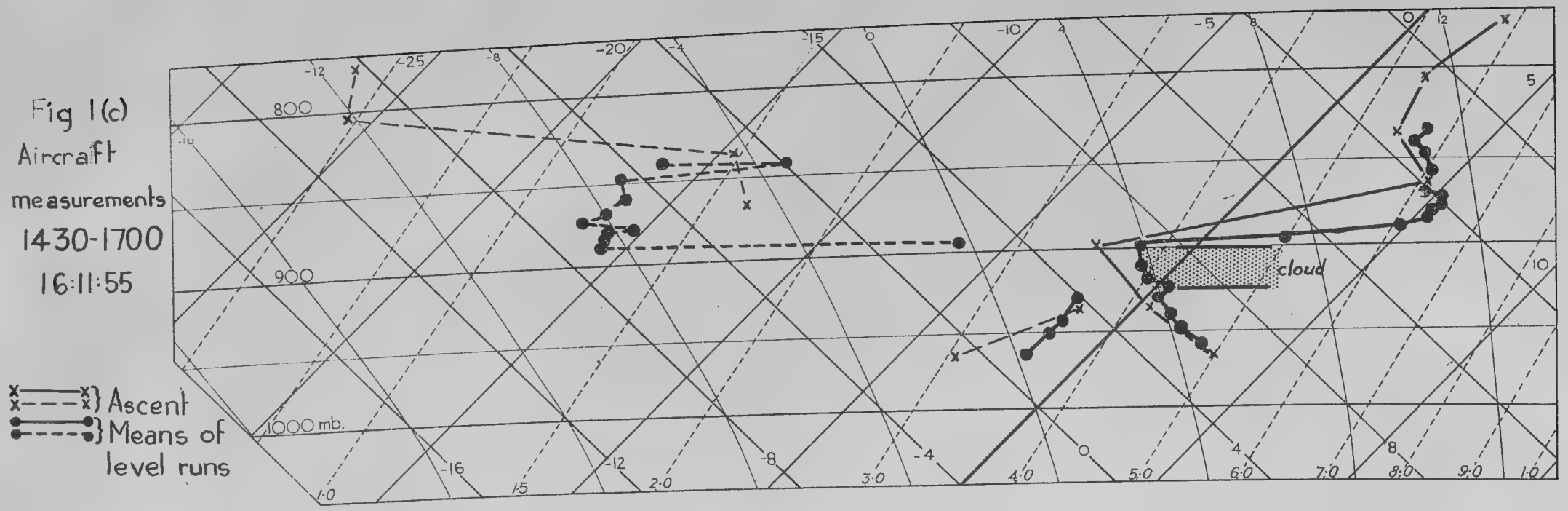

Fig. 2 (b)
Crawley
1400

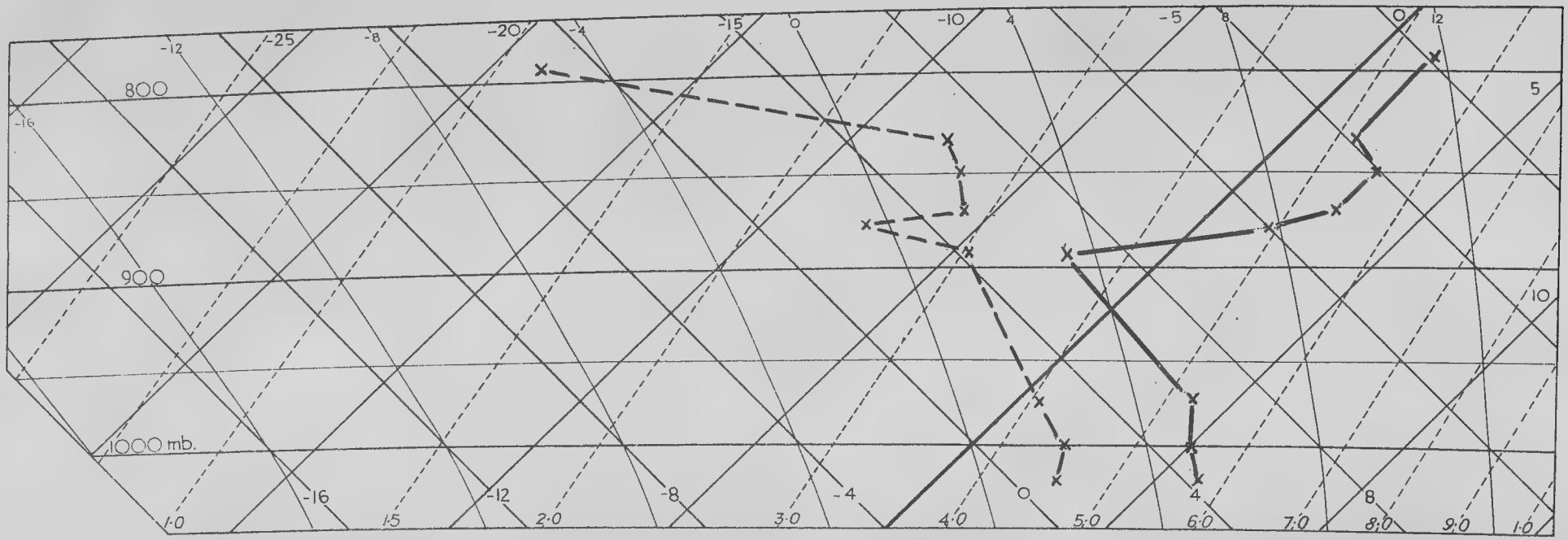

M.R.P. 1055

Fig 1(e)
Aircraft
ascent
1410-1525
18:11:55

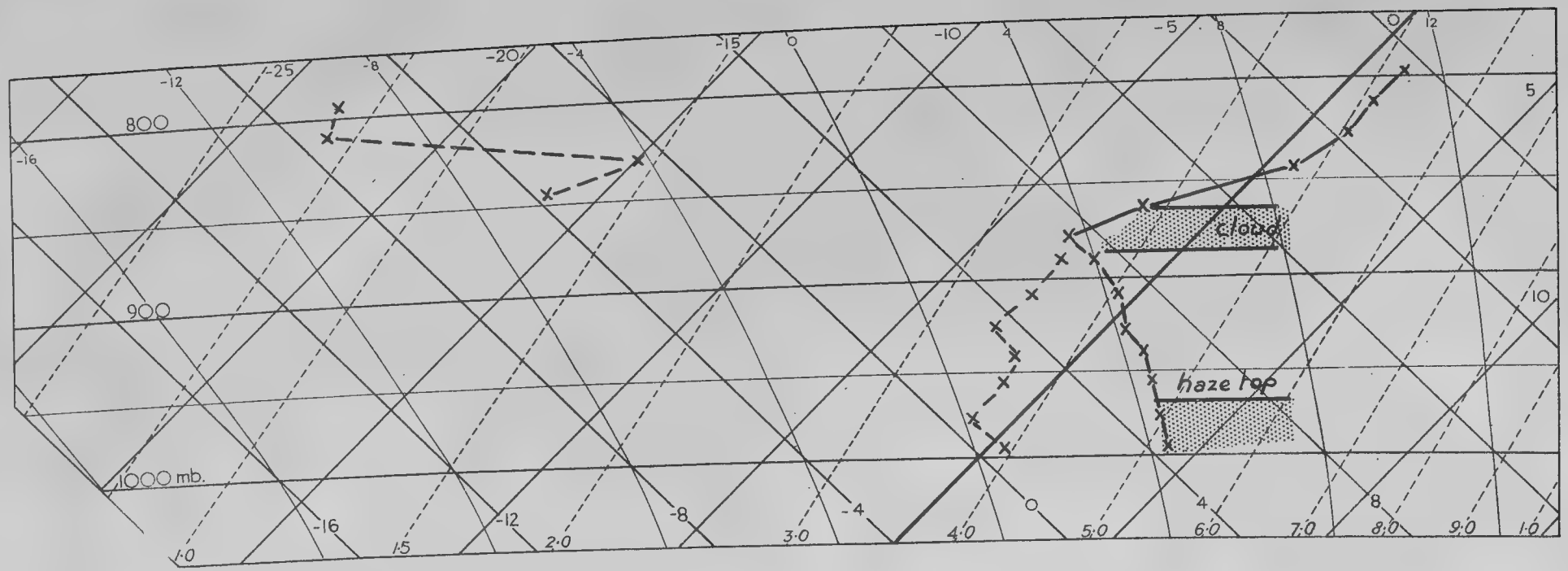

Fig. 1(f)
Aircraft
ascent
1430-1530
21:11:55

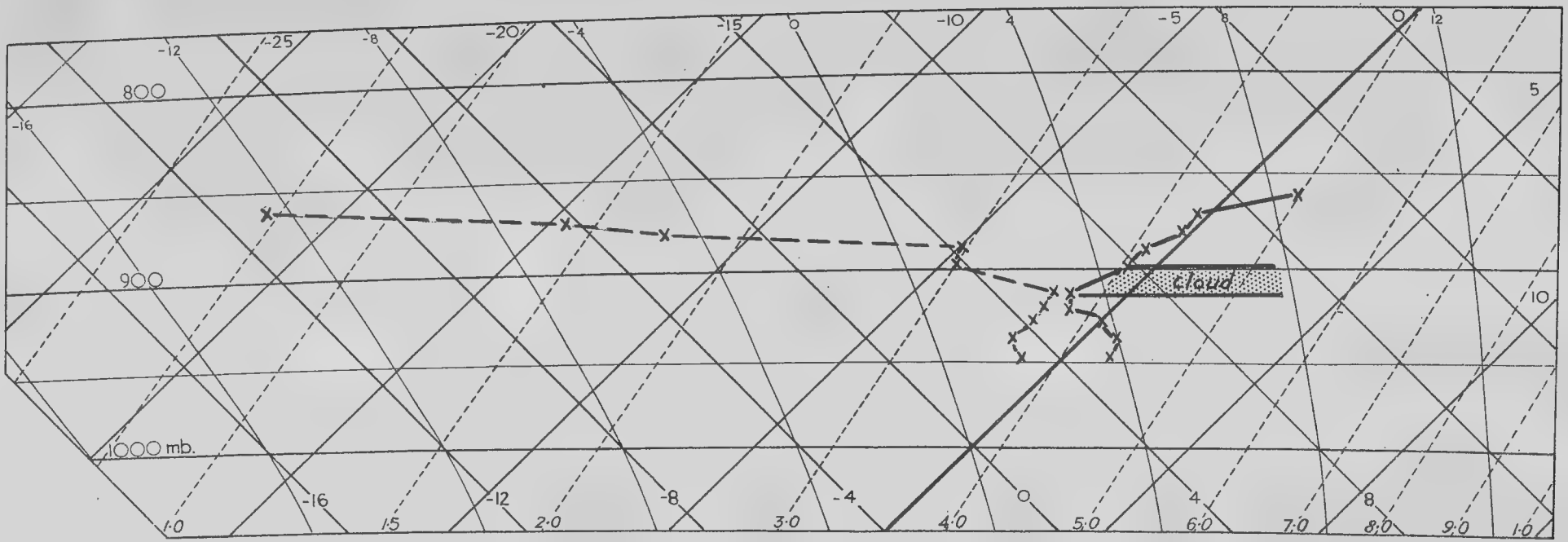

M.R.P. 1055

Fig. 1(g)
Aircraft
measurements
1340-1630
22:11:55

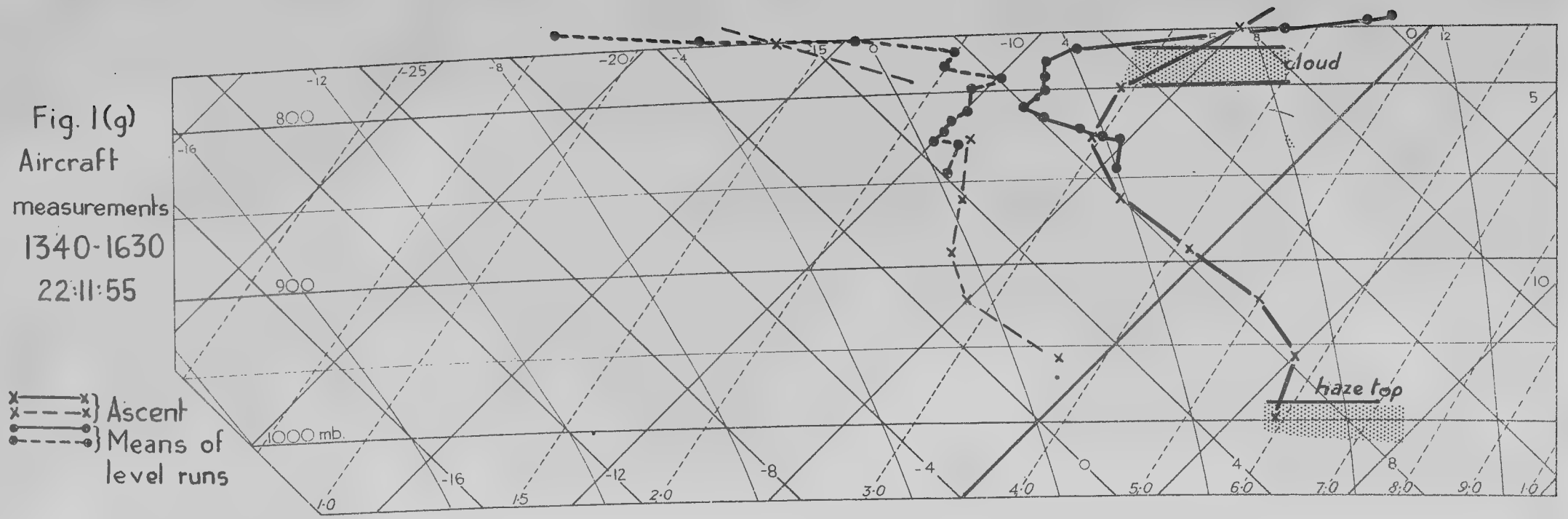

Ascent
Means of level runs

Fig. 2(c)
Crawley
1400

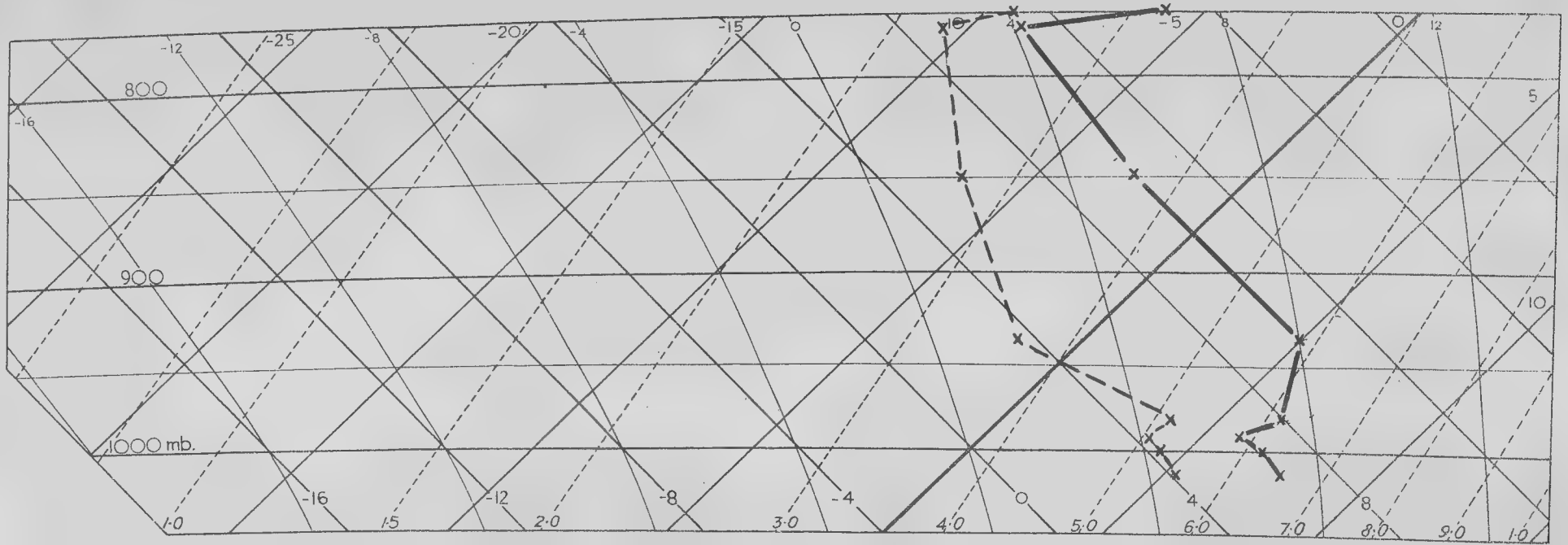

Fig. 1(h)
Aircraft
measurements
1100-1330
28:11:55

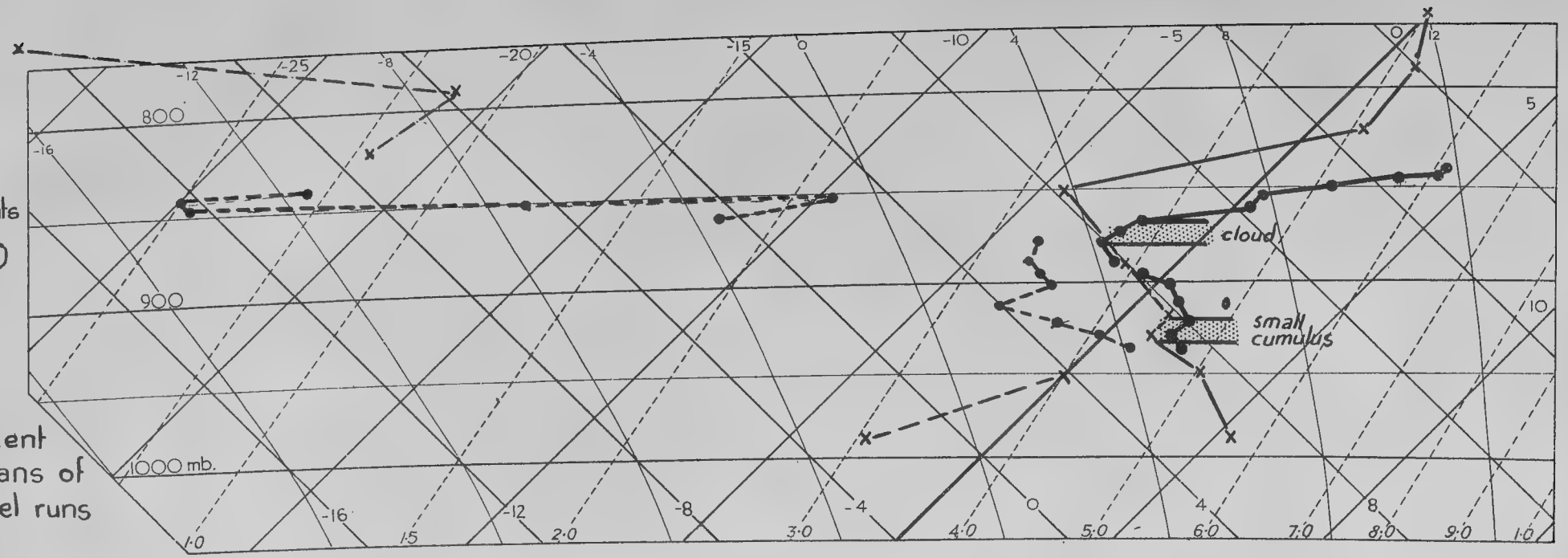

Fig. 2(d)
Crawley
1400

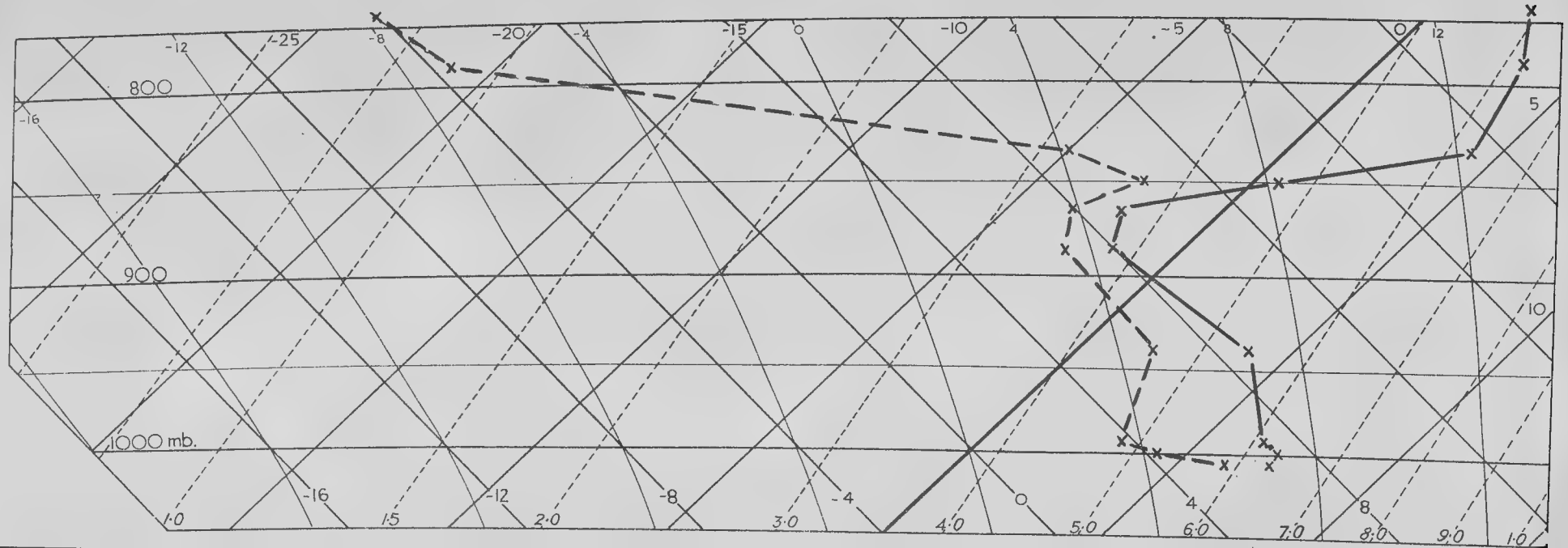

Standard deviations of temperature on level runs

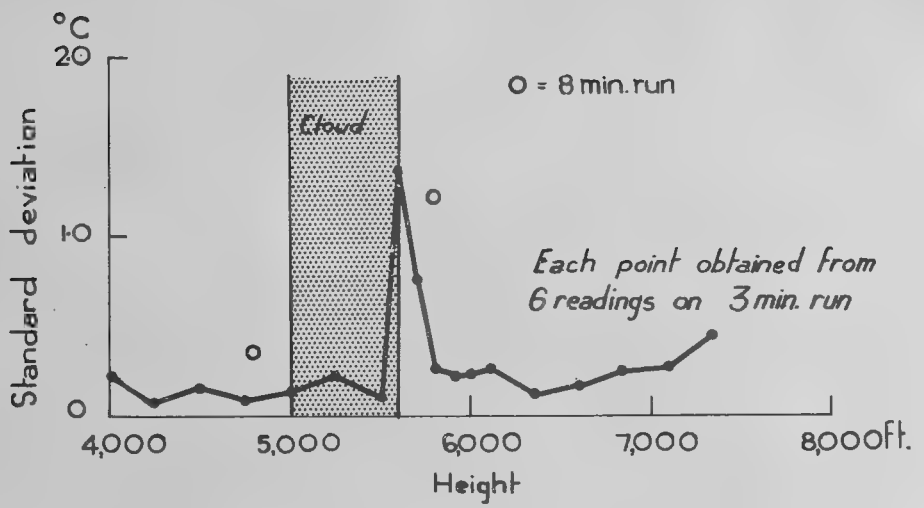

(a) 14:11:55

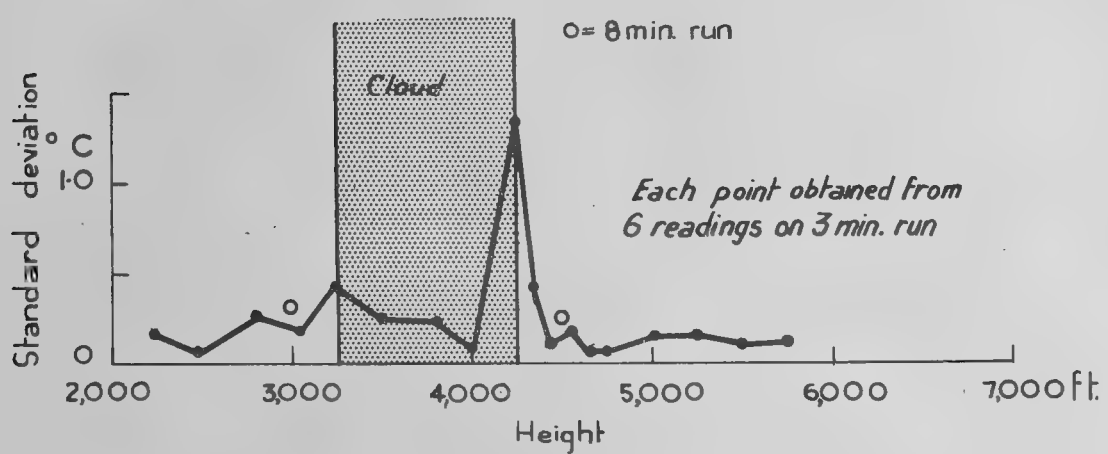

(b) 16:11:55

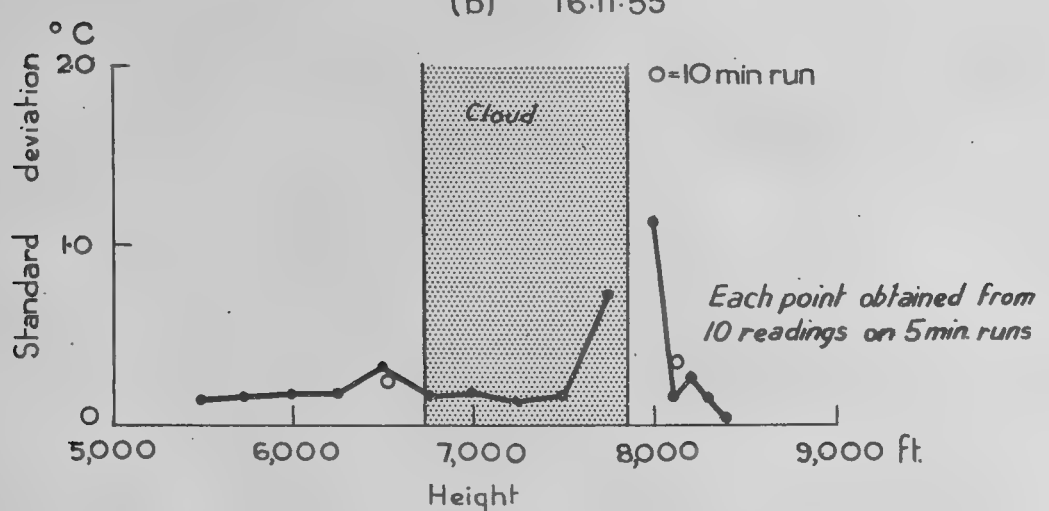

(c) 22:11:55

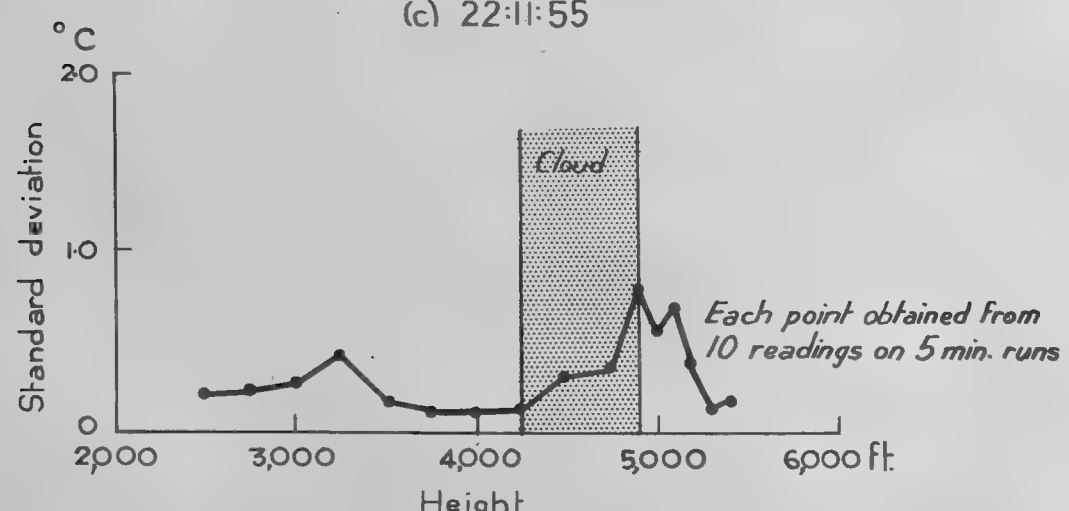

(d) 28:11:55

Fig. 4

Standard deviations of frost point on level runs

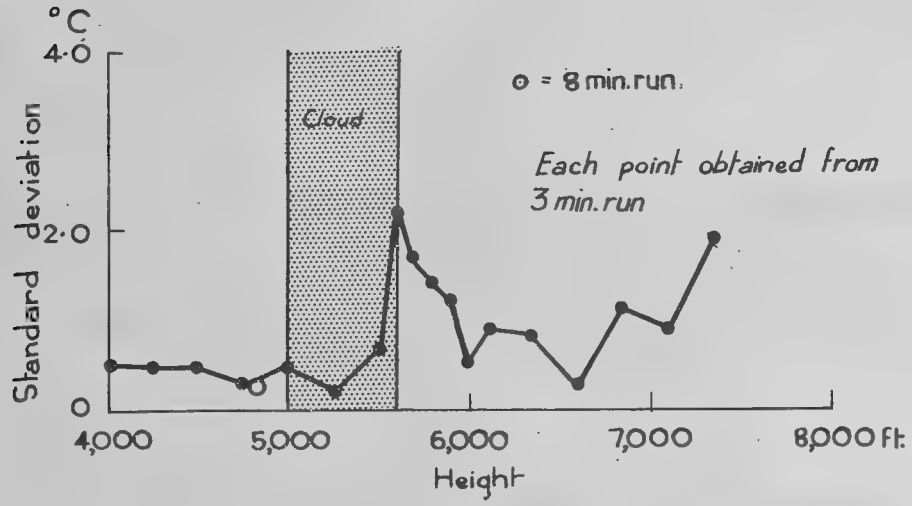

(a) 14:11:55

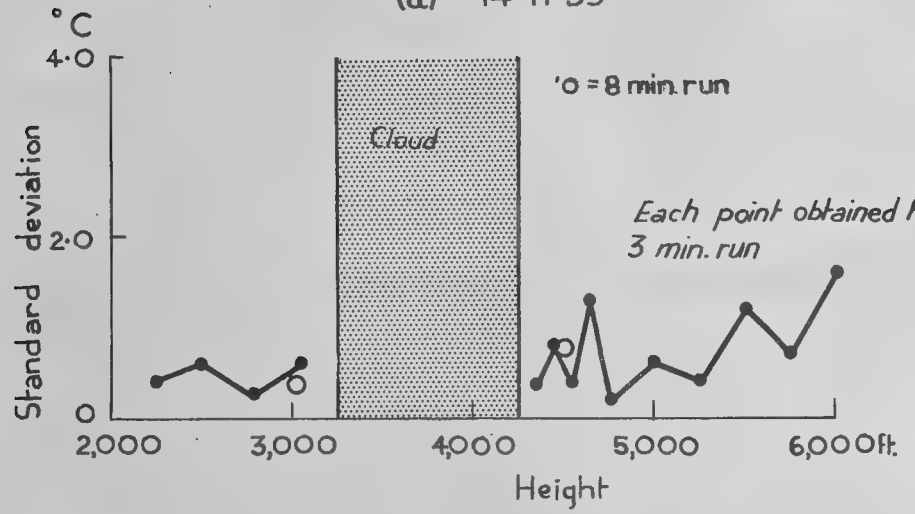

(b) 16:11:55

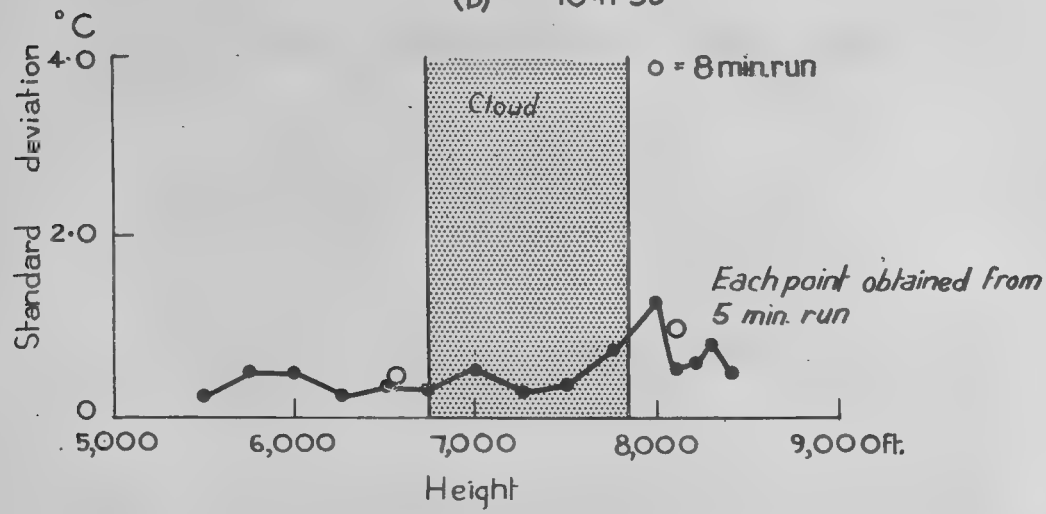

(c) 22:11:55

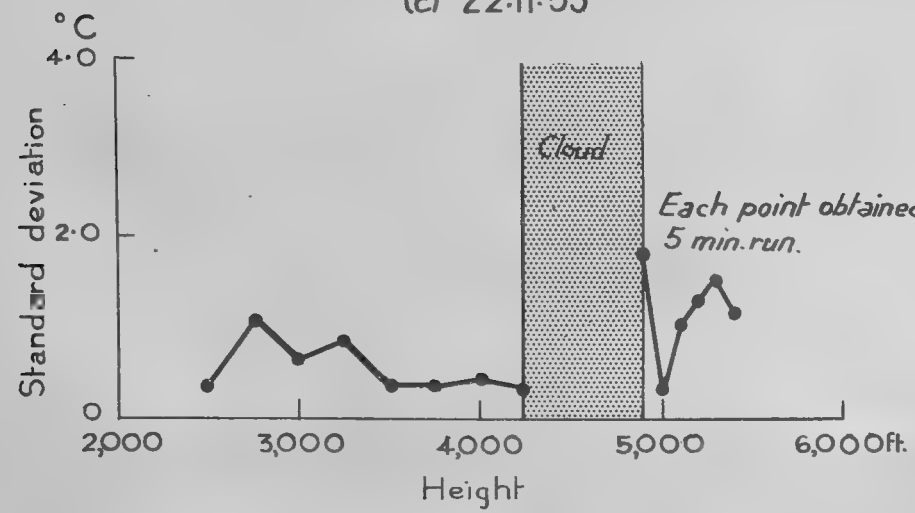

(d) 28:11:55

Fig.5 Accelerometer records for 14:11:55

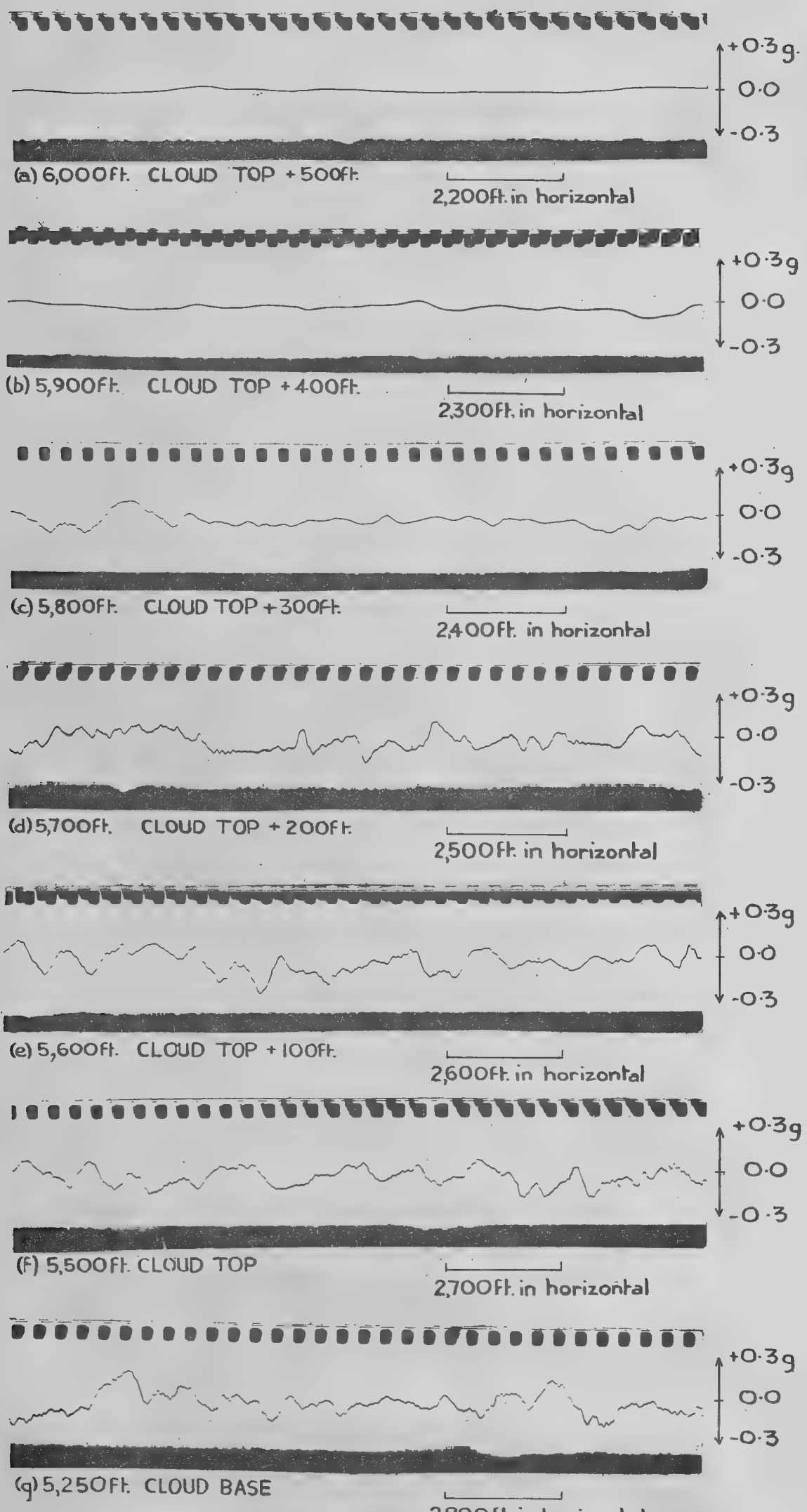

M.R.P. 1056
S.C.11/237
11th June, 1957

Forecast verification: a critical survey of the literature

by

D. H. Johnson

(Meteorological Office)

AIR MINISTRY

METEOROLOGICAL RESEARCH COMMITTEE

58-94

At the time of issue this report has not been published. Any author desiring to quote this paper should refer to it as "A paper of the Meteorological Research Committee (London), M.R.P. No. 1056 by Mr. D.H. Johnson. A copy is available in the Library of the Meteorological Office."

M.R.P. 1056
S. C. II/237
11th June, 1957

AIR MINISTRY
METEOROLOGICAL RESEARCH COMMITTEE

Forecast verification: a critical survey of the literature

by
D. H. Johnson (Meteorological Office)

1. Introduction

1.1. Brier and Allen (1951) have defined forecast verification as the entire process of comparing the predicted weather with the actual weather, utilizing the data so obtained to produce one or more indexes or scores and then interpreting these scores by comparing them with some standard, depending on the purpose to be served by the verification.

1.2. Verification schemes have been devised with one or more of the following ends in view:

(i) To measure the economic value of forecasts;

(ii) To investigate the nature and cause of forecast errors and so indicate the direction in which improvement is most required;

(iii) To assess the relative merits of alternative techniques;

(iv) To provide methods of quality control by which long or short-term variations in the accuracy of forecasts can be detected;

(v) To measure the skill of individuals;

(vi) To demonstrate the value of weather services to the general public or other non-scientific bodies.

Regarding item (vi), Köppen (1893) writes: "If one will study critically the prediction service ..... A report to the public should, in this case, be as free as possible from numerical data, because figures on this subject are generally misunderstood and really carry practical convictions only in certain directions and only to specialists. For such a report, a statement as direct and as free from excuses as possible, with concrete examples and the opinion of specialists is the most convincing and suitable." Later writers endorse this view. The layman cannot be expected to understand and interpret correctly the statistical concepts appurtenant to verification; he realises that even the simplest statistical devices are open to abuse and distrusts them accordingly.

The assessment of forecasting skill (item (v)) in terms of a single numerical score with a view to classifying individuals according to their forecasting ability, has inspired a number of papers, particularly in the United States. Some writers express doubts as to the wisdom of this practice, convenient though it may be for administrative purposes. Wagemann (1935) maintained that forecasters could not be judged solely by statistics, the proper purpose of verification being not the objective assessment of skill

/but

but the detection of flaws in forecasting techniques. Petterssen (Columbia Branch, 1952) states: "Chiefs of offices are required to judge individuals but collectively we should check on our methods, not on each other ....." Schmidt (Columbia Branch, 1952) says: "..... verifications are obtained on day-by-day forecasts, not according to individuals. From these verifications come ideas for research and forecast improvement. Individual testing schemes must involve controlled experiments where everyone has the same data, for the period is never long enough to smooth out the influences of extraneous factors," and Mook (Columbia Branch, 1952): "Particularly within a given weather office, the verification system should encourage teamwork rather than pit individuals against one another."

In the present work, it has been assumed that verification procedures are required to assess the scientific and economic values of forecasts. Problems raised by items (v) and (vi) have not been primarily considered. The economic aspects are discussed in Section 2. Section 3 is concerned mainly with items (ii) to (iv).

Questions of statistical significance are not discussed in the main paper, but are dealt with in Appendix II.

2. Measuring the economic value

2.1. Perfect forecasting is unknown and the forecaster generally takes a calculated risk in issuing a particular forecast. When action is taken on the assumption that the forecast will be correct, choice of forecast for a given operation depends not only upon the meteorological probabilities but also upon the economics of the operation. The first to make this point was Peirce (1884). More recently the relevance of the economics has been discussed by Bilham (1922), Bijvoet and Bleeker (1951), Gringorten (1951), and Thompson and Brier (1955).

2.2. Gringorten (1951) gives the following approach. Suppose a forecaster must predict one of n mutually exclusive events. Let α_{ki} be the profit accruing from operations put in hand when the kth event is forecast and the ith event occurs. Let $p_1, p_2, \ldots\ldots p_n$ be the probabilities that the 1st, 2nd,.....nth events will occur, given a certain set of initial conditions. Then the profit netted, under the working assumption that event k will occur, when averaged over all forecasts based on these initial conditions, is proportional to A_k where

$$A_k = p_1\alpha_{k1} + p_2\alpha_{k2} + \ldots\ldots + p_k\alpha_{kk} + \ldots\ldots p_n\alpha_{kn}$$

There are n such relations, one for each of the n possible working assumptions. The best working assumption is the one which maximizes A_k.

For verification in purely economic terms the important factor is simply the average profit $\frac{1}{N}\sum\alpha_{ki}$. Gringorten proposes a verification score $\sum\alpha_{ki}/\sum\alpha_{ii}$, $\sum\alpha_{ii}$ being the total profit attainable through perfect forecasting.

2.3. Bijvoet and Bleeker (1951) consider in detail the case where there are only two alternatives: either to take precautions against unfavourable weather or not. Suppose during a period of N days, unfavourable weather was experienced on n days. Let the loss due to unfavourable weather on a day when no precautions were taken be L. Let the daily cost of preventative measures be P. Two cases arise depending on whether the cost of taking precautions on every day exceeds the total loss when no precautions are taken, i.e., whether $nL < \text{or} > NP$.

/Suppose

Suppose there are:

a days when unfavourable weather was forecast and did occur, cost of preventative measures = aP;

b days when the meteorologist failed to give warning of unfavourable conditions, loss = bL;

c days when unfavourable conditions were predicted and did not occur, cost of needless preventative measures = cP;

N - (a + b + c) days when no warning was given and weather was favourable, no loss, no precautions.

For $nL < NP$ the "economic benefit", B, of the forecasts is given by $nL - (aP + bL + cP)$, or, since $a + b = n$, $B/L = n - (n - b + c)\,P/L - b$.

The ratio B/L is termed the "economic benefit factor" and P/L, the "specific industry factor". Figure 1 is a graph, prepared by Bijvoet and Bleeker, showing the relation between B/L and P/L for the case n = 10, N = 100 for various values of b and c. An important consideration emerges from a comparison between curves b = 2, c = 4 and b = 4, c = 2. The total number of meteorological failures, b + c, is the same for both curves, but the economic values of the two sets of forecasts are equal only when $2P = L$. When $2P < L$ it is desirable that b should be minimized, but for $2P > L$ it is better if c is small.

A similar analysis can be made for the case $nL > NP$, when it is invariably preferable to have b minimized rather than c, subject to the total number of failures being constant.

2.4. The foregoing treatments illustrate the type of approach taken in verifying forecasts for individual commercial undertakings when the economic circumstances are known. Often it is impossible to determine the economic value of the forecasts. For example, one could not assess the monetary value of the gale warning service. Further, it is impracticable to verify on an economic basis when the same forecasts must serve large numbers of recipients whose interests diverge and conflict. Moreover, such scores as the average profit will not reflect the scientific worth of the forecasts. A general scheme of verification requires a system which measures simply "the approach to the truth" (Brier and Allen, 1951). Such systems are discussed in the following section.

3. Scientific value of forecasts

3.1. Verification techniques are required to meet the following circumstances:

(i) a choice is made between one of two alternatives (dichotomous classification);

(ii) a selection is made between several mutually exclusive alternatives (manifold classification);

(iii) the forecast and observed values form continuous distributions;

(iv) a composite forecast which refers to several elements is made; this is often written but sometimes contains numerical values;

(v) the future pressure pattern, together with positions of fronts, is specified on a field basis.

No single formula or procedure can cater for the diversity of circumstances listed above. The first four possibilities will be considered in turn. The fifth class is rather special and is omitted from the present survey.

/3.2.

3.2. Dichotomous classification

3.2.1. A surprisingly large range of forecasts can be adapted for verification in dichotomous (black or white) terms. Some phenomena, such as thunder, can only be treated on an occurrence or non-occurrence basis. Other elements, rain, wind and temperature for example, form continuous distributions but can nevertheless be verified by dichotomous classification: rain/no rain; gale/no gale; frost/no frost; temperature, above/below normal. Crossley (1954) used "black or white" indexes to verify four-day forecasts (change or no-change of weather type), forecasts of development of secondary depressions, warnings of ice on conductor rails, and visibility forecasts.

3.2.2. The information required in verifying black or white forecasts can be expressed in a 2 x 2 contingency table as follows:

		Forecast		
		Black	White	Total
Observed	Black	c	o - c	o
	White	p - c	s - o -p + c	s - o
	Total	p	s - p	s

This notation was given by Gilbert (1884). Other writers have used alternative layouts but Gilbert's notation will be used throughout the following discussion. The problem of deriving a satisfactory verification index is essentially that of measuring association between attributes, which is discussed from a statistical standpoint by Kendall (1948).

The forecast and observed events can be considered independent if there is the same proportion of black (or white) occurrences amongst the forecasts of black, as amongst the forecasts of white, i.e., if $c/p = (o - c)/(s - p)$ or $cs - op = o$. Taking an alternative view: o/s is the expectation that black will occur on any day of the trial period, so op/s represents the expected number of correct forecasts when p forecasts of black are issued at random. If $c > op/s$, then the observed and forecast events are positively associated; if $c < op/s$, there is negative association. The quantity $cs - op$ occurs in the numerator of several proposed indexes of forecasting success.

Verification can proceed from two complementary aspects. One can examine (i) the probability that a prediction will be fulfilled, and (ii) the chance that an occurrence will be predicted. A measure of (i) is c/p; (ii) is measured by c/o. (Doolittle, 1885; Grossmann, 1895; etc.). The Weather Division, U.S.A.A.F. (1944) has termed aspect (i), the "postagreement" and (ii), the "prefigurance". These terms are inelegant, but no others have been suggested. Which is the more important aspect depends on the use to be made of the forecasts. A film director, awaiting fine weather for a costly day on location, might not mind missing a few good days if he could be certain that when a fine day is confidently forecast, a fine day will occur. For him postagreement is essential. On the other hand, in a typhoon warning service, it is essential that all storms which occur should be forecast, even though some warnings are not fulfilled. Here prefigurance is more important than postagreement. In a general purpose index, postagreement and prefigurance should receive equal weight. The following paragraphs discuss the merit of proposed verification coefficients.

/3.2.3.

3.2.3. Percentage correct. The percentage of the forecasts which are correct is given by $100\ (2c + s - o - p)/s$. This simple score has some virtue if blacks and whites have equal probabilities of occurrence, but it can be misleading when one of the probabilities is small. An oft-quoted example concerns Finley's verification of tornado prediction (Finley, 1884). Tornadoes were forecast on 100 out of 2803 occasions. 51 storms occurred and 28 warnings were fulfilled. Finley remarks on the high percentage correct (96.6), but several writers have pointed out that the percentage correct would have been 98.2 if "no tornadoes" had been forecast perpetually. Yet the predictions clearly had some merit since $28/100 > 51/2803$ $(c/p > o/s)$.

3.2.4. Gilbert's scores. Gilbert (1884) proposed two indexes. The first was the ratio of the successful forecasts of black to the sum total of the forecasts of black plus the unforecast occurrences of black: $c/(p + o - c)$. This is a bad index from several points of view: (i) a different answer is obtained if white forecasts are considered instead of black (the formula is incapable of inversion); (ii) the index varies between zero and one but the expected value for the random issue of p black forecasts is $op/(sp + so - op)$, which varies with o/s; (iii) a perpetual forecast of black gives a value o/s, which is high when $o \gg (s - o)$.

Gilbert's second index is based upon the first, the number of successful black forecasts, c, being replaced by $c - op/s$, which represents the difference between the total number of correct forecasts of black and the number expected to be correct by chance. The formula is:

$$\frac{c - op/s}{(c - op/s) + (p - c) + (o - c)} \quad \text{or} \quad \frac{cs - op}{s\,(o + p - c) - op}$$

This index overcomes the drawbacks of Gilbert's first index, but its lower limit, $-o\,(s - o) / (s^2 - os + o^2)$, is not fixed.

3.2.5. Doolittle's scores. Recognising the significance of c/p and c/o, Doolittle (1885) formed an index c^2/op, but this suffers from the defects of Gilbert's first score. Doolittle then argued that out of p predictions, op/s successes could be ascribed to chance, so that the quantities $p - op/s$ and $o - op/s$ represent "the fields which chance leaves for science to conquer".

The first index was therefore amended to become:

$$\frac{(c - op/s)}{(o - op/s)} \cdot \frac{(c - op/s)}{(p - op/s)} = \frac{(cs - op)^2}{op\ (s - o)\ (s - p)}$$

The latter form has much to recommend it. It takes values between zero and one, zero being the score attained through a random issue of forecasts. A drawback is that a value of one is obtained not only for a completely correct set of forecasts, but also for complete failure. Doolittle justifies this by remarking that complete failure is as difficult to attain as complete success. While this is true, it is still undesirable to use an index which does not conform with the ordinary idea of success.

3.2.6. Peirce's index. Peirce (1884) suggested use of the expression:

$$\frac{c}{o} - \frac{(p - c)}{(s - o)} = \frac{cs - op}{o\ (s - o)}$$

c/o is the probability of a black event being correctly forecast; $(p - c)/(s - o)$ is the probability that a white event will be forecast as black. Peirce's formula avoids most of the pitfalls and varies between -1 and +1, -1 corresponding to complete failure and +1 to complete success. It can be criticised for giving too much weight to prefigurance.

/3.2.7.

3.2.7. Lacour's index. Lacour (1906) in verifying Danish storm warnings, used the ratio of the probability of a black event following a black prediction to the probability of a black event following a white prediction. Symbolically, the ratio is:

$$\frac{c}{p} \cdot \frac{(o - c) + s - (o + p - c)}{o - c} = \frac{c\,(s - p)}{p\,(o - c)}$$

This score is open to abuse by the cautious forecaster, who can obtain a high value by forecasting white only when it is almost certain to occur. If black and white events are inverted a different value is obtained.

3.2.8. Clayton's index. Clayton (1934) proposed the use of the difference between the probability of a black event following a black prediction and the probability of a black event following a white prediction, i.e.:

$$\frac{c}{p} - \frac{o - c}{(o - c) + s - (o + p - c)} = \frac{cs - op}{p\,(s - p)}$$

This score is complementary to Peirce's index in forming part of Doolittle's formula. It weights postagreement rather than prefigurance.

3.2.9. Crossley's indexes. Crossley (1952) termed c/p the "useful effort" and c/o the "forecast accuracy". He suggested that when economy of effort is the main consideration and time of lesser importance the forecasts should maximise the "useful effort". Realising that the "useful effort" was not a satisfactory verification index, Crossley (1954) proposed the quantity,

$$\frac{1}{2}\left(\frac{c}{o} + \frac{s - (o + p - c)}{s - o}\right) = \frac{1}{2}\left(\frac{cs - op}{o(s - o)} + 1\right)$$

which he termed the "usefulness".

c/o is the "forecast accuracy" of the black forecasts and $(s - o - p + c)/(s - o)$ is the "forecast accuracy" of the white forecast. The formula is basically that proposed by Peirce, apart from the constants. Crossley's index ranges from 0 to 1 with a value of 1/2 as the lower limit for worthwhile forecasting.

3.2.10. The skill score. The skill score has been much used in the U.S.A. in recent years. It is usually given in the form:

$$S = \frac{\text{number of correct forecasts} - \text{number correct by chance (persistence)}}{\text{total number of forecasts} - \text{number correct by chance (persistence)}}$$

and is attributed to Heidke (1926). Symbolically,

$$S = \frac{c + s - o - p + c - \left[op/s + (s - p)(s - o)/s\right]}{s - \left[op/s + (s - p)(s - o)/s\right]} = \frac{2\,(cs - op)}{o\,(s - p) + p(s - o)}$$

S is zero if forecasts are no better than chance or if either black or white is perpetually forecast. S is one for perfect forecasting except in the special case when no blacks occur and none is forecast, when the score is undefined. The possible range of negative values is not fixed: the score for complete failure is $-2o\,(s - o)/\,(o^2 + (s - o)^2)$, which depends upon the observed proportion of blacks and attains its minimum value of -1 only when $o = s/2$.

A diagram which permits rapid calculation of skill scores has been prepared by Jorgensen (1956).

/3.2.11.

3.2.11. Improved percentage correct. Bleeker (1946) remarked that the percentage correct could be rendered less susceptible to abuse if the successful black and white predictions were weighted in proportion to the frequencies of black and white occurrences. The index thus obtained is:

$$\frac{c\,(s - o)/s + (s - o - p + c)\,o/s}{c\,(s - o)/s + (p - c) + (o - c) + (s - o - p + c)\,o/s}$$

Bleeker himself rejects the index on the grounds that the expected value for random forecasting, namely $o(s - o)/(sp + 2os - 2op + o^2)$, is not fixed.

3.2.12. Yule's indexes. The indexes hitherto discussed were devised with the meteorological problem in mind. In the early years of the present century, the task of devising measures of association between attributes drew the attention of several eminent statisticians. Yule (1912) in a comprehensive review, quotes the following measures of association:

(a) The coefficient of association $Q = \dfrac{c(s - o - p + c) - (o - c)(p - c)}{c(s - o - p + c) + (o - c)(p - c)}$

$$= \frac{cs - op}{c(s - o - p + c) + (o - c)(p - c)};$$

(b) The coefficient of colligation $Y = \dfrac{\sqrt{c}\,(s - o - p + c) - \sqrt{(o - c)(p - c)}}{\sqrt{c}\,(s - o - p + c) + \sqrt{(o - c)(p - c)}};$

(c) $$V = \frac{c\,(s - o - p + c) - (o - c)(p - c)}{\sqrt{op\,(s - o)\,(s - p)}}$$

$$= \frac{cs - op}{\sqrt{op\,(s - o)(s - p)}}\ .$$

These three coefficients vanish when the attributes are independent ($cs = op$), take values ranging between +1 and -1, and decrease as the cell frequencies proceed from association to disassociation. Q and Y become +1 when $p = c$ or $c = o$, and -1 when either c is zero or $(s - o - p + c)$ is zero. V becomes +1 only when $p = c$ and $c = o$, and -1 only when c is zero and $(s - o - p + c)$ is zero.

Kendall (1948) defines the condition in which all As are B, though not all Bs are A as "complete association". The state when all As are B and all Bs are A is termed "absolute association". Thus Q and Y are +1 for both complete and absolute association. V becomes +1 only for absolute association. On account of this difference Kendall prefers Q and Y to V. The preference is understandable in the common circumstances when the observer or experimenter has no control over the relation between the attributes. In meteorology however, one attribute is determined by the forecaster and it may not be difficult for him to "play the system" so as to obtain complete association even though the majority of his forecasts are valueless. For general verification it is desirable that an index should achieve its highest value for absolute association alone, and V is therefore preferred to Q or Y.

To derive V, Yule used the concept of correlation. The attributes can be regarded as variates, which take only the values zero and one. V then represents the coefficient of correlation between the two variates. V can be interpreted in terms other than those of correlation since it is also given by the square root of Doolittle's index or by the square roots of Peirce's and Clayton's indexes in combination. It gives equal weights to postagreement and prefigurance and is closely related to the important chi-squared statistic: for a 2 x 2 table, $\chi^2 = sV^2$. Chi-squared itself is a measure of the strength of the relation between attributes but since chi-squared is a function of the total number of observations as well as of the relative proportions of the cell frequencies, it is strictly a measure of statistical significance* and is not suitable for use as a coefficient of association.

*See Appendix II

/In

In common with the skill score and other indexes, V is undefined if black (or white) perpetually occurs and is perpetually forecast. In such circumstances a measure of association is hardly called for. V is always numerically greater than or equal to the skill score.

3.2.13. Of the indexes discussed V is perhaps the most suitable for use as a general verification index, both in view of its intrinsic properties and because it is closely linked with well-understood statistical quantities. The use of V in forecast verification was advocated by Wallén (1921) and later by Bleeker (1946). Bleeker attributes the formula to Wallén, although Wallén himself acknowledges the debt to Yule. Heidke (1928) criticised Wallén's formula (Yule's V) on the grounds that it was not based on probability calculations: it did not explicitly measure the improvement over chance as did the skill score. The criticism is hardly justified. While it is not obvious from the correlation derivation of V, it is clear from the alternative derivations following Doolittle or Peirce and Clayton, that chance successes are allowed for implicitly.

Values of Peirce's index, Clayton's index, Yule's V and the skill score for some sample contingency tables are given below. The effects of the relative weightings given to prefigurance and postagreement are apparent.

1)

		Forecast B	Forecast W	Total
Observed	B	10	0	10
	W	10	80	90
	Total	20	80	100

2)

		Forecast B	Forecast W	Total
Observed	B	10	0	10
	W	60	30	90
	Total	70	30	100

3)

		Forecast B	Forecast W	Total
Observed	B	10	0	10
	W	80	10	90
	Total	90	10	100

4)

		Forecast B	Forecast W	Total
Observed	B	1	9	10
	W	0	90	90
	Total	1	99	100

5)

		Forecast B	Forecast W	Total
Observed	B	1	0	1
	W	1	98	99
	Total	2	98	100

Contingency Table No.	Peirce's Index (prefigurance)	Clayton's index (postagreement)	Yule's V	Skill Score
(1)	.89	.50	.67	.62
(2)	.33	.14	.22	.09
(3)	.11	.11	.11	.02
(4)	.10	.91	.30	.08
(5)	.99	.50	.70	.66

/3.2.14.

3.2.14. Comparative indexes. Some authors (e.g., Clayton, 1889; Weather Division, H.Q., U.S.A.A.F., 1944) have objected to the calculation of the chance successes from the observed frequencies for the trial period. They maintain that the climatic normals should be used as the standard of comparison, since the use of observed frequencies implies a degree of foreknowledge of the observed weather. It is difficult to see the logic of this argument. It is true that before the event, an estimate of the expected success of forecasts issued at random is given by the climatic normals. Nevertheless, in assessing, post facto, the number of forecasts which could have been correct by chance during the trial period, the determination of the expected value must be based on the observed frequencies. The chance forecasts are assumed by definition to have been made without foreknowledge.

It is often desirable to compare the success of a forecasting system with the success of less subtle (and usually less costly) techniques such as predicting persistence or the climatic normals. Some writers have devised indexes which measure the success relative to the simpler technique. Heidke (1926) proposed the use of an index $G = (E - B)/(1 - B)$, where E is the number of correct forecasts expressed as a fraction of the total number of forecasts, and B is the number of correct persistence forecasts also expressed as a fraction of the total number of forecasts. B could be replaced by any convenient standard. If the fraction correct by chance is substituted for B the skill score is obtained. Heidke (e.g., 1935) repeatedly stressed his preference for a persistence base because persistence normally gives a higher score than pure chance or climatology.

Crossley (1954) suggests that improvement over persistence, or any other forecasting system, be measured by the index $J = (I - I_o)/(1 - I_o)$ where I is the value, appropriate to the system under test, of some verification index taking a maximum value of one, and I_o is the value scored by the standard.

A distinction should be recognised between indexes discussed in previous sections which measure the association between observed and forecast events, and indexes such as Heidke's G or Crossley's J which measure the relative success of forecast systems. Whether indexes of the latter type have much value is a moot point. Statements of the verification statistics for the forecast technique and for persistence, separately, contain more information and are better interpreted than hybrid indexes which measure relative success.

The accuracy of conventional forecast techniques is higher during periods when the weather displays a greater degree of persistence. Indexes which measure gain over persistence have therefore been used in attempts to make comparisons between verification data obtained for different periods more fair. There are two objections to this practice. Firstly, it may be found that the greater the variability of the weather, the more the forecaster gains relative to persistence (cf. remarks made in section 3.4.8. regarding Priestley's index). Secondly, it cannot be admitted that the inherent forecasting difficulty posed by a synoptic sequence is to be measured simply in terms of persistence. A suggestion due to Brier and Allen (1951), that indexes can be adjusted for difficulty using a regression equation $I' = I + a\,(Ip - \overline{Ip})$, where Ip is the persistence score corresponding to a forecasters score I, is open to similar objections. It is preferable to avoid these difficulties by verifying alternative techniques on the same series of weather situations. If the problem must be met, for example, if the variation of forecast accuracy with time is to be measured, periods compared must be long enough to contain well-varied selections of weather types and allowance must be made for diurnal and seasonal effects.

For historical interest mention is made of two other types of standard with which routine forecasts have been compared. Mascart (1922) had forecasts made for each day of a year, in advance, a knowledge of local climate being assumed. Dinies (1936) used daily forecasts made in 1929 and 1933 as forecasts for 1934.

/3.3.

3.3. Manifold classification

3.3.1. Categorical forecasts

3.3.1.1. The data essential to the verification of forecasts which represent a choice made from several mutually exclusive alternatives can be expressed in a p x p contingency table:

		Forecast Class				
		A_1	A_2	A_i	A_p	Total
Observed class	B_1	X_{11}	X_{21}	X_{i1}	X_{p1}	(B_1)
	B_2	X_{12}				(B_2)
	B_j	X_{1j}		X_{ij}	X_{pj}	(B_j)
	B_p	X_{1p}		X_{ip}	X_{pp}	(B_p)
Total		(A_1)	(A_2)	(A_i)	(A_p)	N

X_{ij} is the number of occasions when class j occurred, class i having been forecast. (A_i), (B_j) are the forecast and observed frequencies of classes i and j respectively. N is the total number of occasions.

Classes A_i and B_j are defined as independent when

$$\frac{X_{ij}}{(A_i)} = \frac{(B_j)}{N}$$

For complete success entries should occur only in the leading diagonal of the table. The percentage correct is given by the ratio of the sum of the leading diagonal entries to the total number of occasions. Reasons were given in para. 3.2.3. for interpreting this statistic with caution. When the classes are formed by division of a range of values of some variate, the number falling into each class depends on the number of classes formed. The percentage correct can be varied by adjusting the number of classes, although the basic data remain unchanged.

The contingency table was one of the earliest tools employed in verification. The Deutsche Seewarte introduced tabular summaries as a routine (Köppen, 1884). Clayton (1889) used them to show where the greatest need for improvement lay. With a similar end in view, Ekholm (1907), in verifying storm warnings, computed values of $X_{ii}/(A_i)$ and $X_{ii}/(B_i)$ for a series of values of the observed Beaufort force. $X_{ii}/(A_i)$ and $X_{ii}/(B_i)$ measure postagreement and prefigurance respectively.

Bleeker (1946) points out that "black or white" verification indexes can be computed for each class, black forecasts corresponding to forecasts of the class in question and white forecasts, to forecasts of all other classes. By this method, which could even be applied when the forecast classes overlap, the variation of success between the classes can be examined. Crossley (1954) used a similar device to verify forecasts of visibility at Northolt Airport. The visibility forecasts were classified dichotomously, taking a succession of visibility limits as the dividing lines. Crossley's index (para. 3.2.9.) was computed for each limit.

/3.3.1.2.

3.3.1.2. The skill score. Most of the measures of association discussed in section 3.2. apply only to black or white forecasts and cannot be generalised simply, to cover the manifold case. One exception is the skill score. The formula,

$$S = \frac{(\text{No. of correct forecasts}) - (\text{No. correct by chance})}{(\text{Total no. of forecasts}) - (\text{No. correct by chance})}$$

becomes for manifold classification,

$$S = \frac{\sum X_{ii} - \sum (A_i)(B_i)/N}{N - \sum (A_i)(B_i)/N}$$

S varies from +1 for complete success to a negative score ($\geqslant -1$), which depends upon the observed frequencies, for complete failure.

3.3.1.3. The skill index. The Weather Division, H.Q. U.S.A.A.F. (1944) refer to a "skill index" given by,

$$I = \left[\sum_i X_{ii}\{N-(B_i)\} + \sum_i X_{ii} - N\right] \Big/ N(p-1)$$

I is +1 for complete success, zero if the diagonal frequencies take their "chance" values, and $-1/(p-1)$ when the diagonal frequencies are zero.

When applied to the "black or white" case, $p = 2$ and the formula reduces to $(cs - op)/o\,(s - o)$ in the notation of section 3.2. This is Peirce's index (para. 3.2.6.).

3.3.1.4. The skill score and the skill index depend only upon the frequencies in the leading diagonal and the border frequencies of the contingency table. They are applicable to the special case (statistically speaking) of the bivariate frequency table: it is assumed that the classes are arranged in order, being formed by division of the range of some variate. No allowance is made for "near misses"; the indexes depend upon the hits alone and do not explicitly measure the extent to which the shots are grouped around the target. The values of the indexes depend upon the number of classes into which the data are divided.

3.3.1.5. Vernon's deviation and quadratic skill scores. Vernon (1953) devised two scores which weight the incorrect forecasts according to the degree of error. The deviation skill score is defined as,

$$S_d = \frac{\sum (A_i)(B_j) d_{ij}/N - \sum_{ij} X_{ij} d_{ij}}{\sum_{ij} (A_i)(B_j) d_{ij}/N}$$

where d_{ij} is equal to the number of class intervals by which the cell in the ith row and jth column is removed from the "perfect hit" cell in the same column. $d_{ij} = |j - i|$. The $(A_i)(B_j)/N$ are the expected frequencies.

/The

The quadratic skill score is

$$S_q = \frac{\sum_{ij}(A_i)(B_j)d_{ij}^2/N - \sum_{ij} X_{ij} d_{ij}^2}{\sum_{ij}(A_i)(B_j)d_{ij}^2/N}$$

The two scores are analogous to the conventional skill score, to which they reduce in the "black or white" case. They differ from each other only in degree of weighting, which is, of course, quite arbitrary. The scores become +1 for complete success and are zero when success is no better than chance. Table 1 contains a hypothetical example, taken from Vernon's paper, of the application of the scores to two contingency tables.

A common fault of systems which award marks for near misses, is that they encourage the forecaster to play safe. Professor J.G. Bryan, who collaborated in U.S. Air Force experiments in verification, has said that when attempts were made to allot partial credit to a nearly correct forecast, the scheme was compromised to a point where it was possible to "play the system", usually by forecasting the most frequent event or by forecasting persistence (Gringorten, 1951). However, Vernon's scores do not appear to suffer from this drawback in practice and Vernon shows that, for the data considered in Table 1, the forecasters would have lost by always forecasting the middle of the range (see Table 2).

3.3.1.6. Pearson's coefficient of contingency. The value of the chi-squared statistic for a p x p contingency table is

$$\sum_{ij}\left[\left\{X_{ij} - (A_i)(B_j)/N\right\}^2 \Big/ \left\{(A_i)(B_j)/N\right\}\right]$$

Chi-squared may be used to test the significance of the association displayed in the contingency table, but for reasons given in para. 3.2.12. it cannot be used as a coefficient of association. Pearson proposed a measure based on chi-squared namely,

$$C = \sqrt{\frac{\chi^2}{N+\chi^2}}$$ (Kendall 1948)

C vanishes when there is no association but takes a value $((p - 1)/p)^{\frac{1}{2}}$ which depends upon the number of classes, for absolute association. This is a disadvantage from a verification point of view. It is possible to "correct" C, so that it shall have an upper limit of +1, using a scaling factor appropriate to the number of classes (Brooks and Carruthers, 1953).

3.3.1.7. Tchuprow's coefficient. Tchuprow devised a coefficient of association which like Pearson's C is a function of chi-squared, but which has the advantage of a fixed upper limit. For a p x p contingency table, Tchuprow's coefficient is,

$$T = \sqrt{\frac{\chi^2}{N(p-1)}}$$ (Kendall 1948)

T is +1 for absolute association and is zero if there is no relation. For the "black or white" case T reduces to Yule's V (para. 3.2.12.).

/3.3.1.8.,

3.3.1.8. The coefficients of Pearson and Tchuprow take all the cells of the contingency table into account, but they do not depend upon any ordering of the classes, i.e., any two rows or columns may be interchanged without affecting the value of the index. They measure association, but they do not require that a given row should be associated with any particular column. Where the classes represent divisions of a visibility or temperature scale, for example, the forecasts may have an appreciable bias and yet achieve a high coefficient of association. The indexes need not necessarily be rejected on this account; one does not reject the correlation coefficient because it is insensitive to errors of bias and scale; but the limitations must be borne in mind. A further difficulty arises because, like Doolittle's index (para. 3.2.5.), the coefficients take their minimum values for chance success and their maximum values for both complete success and complete failure. Chi-squared is undefined if a row or column total is zero.

3.3.1.9. Correlation coefficient. When the contingency table is a bivariate frequency table and the number of classes is sufficiently large, a coefficient of correlation may be calculated, due allowance being made for grouping (vide para. 3.4.4.). The correlation coefficient is sensitive to the ordering of the classes and takes negative values for negative association.

3.3.1.10. Gringorten's verification scheme. Gringorten (1951) has devised a system which forces the forecaster to select, not the most probable event, but the event whose probability is most increased in proportion to the climatic frequency. If α_{ki} is the mark awarded for predicting the kth event when the ith event occurs, then $\alpha_{ki} = 0$ for $k \neq i$ and $\alpha_{ii} = 1/Q_k$ where Q_k is the climatological probability that the kth event will occur.

The score for completely erroneous forecasting is zero. The expected value of the score for perpetual forecasting of the kth event is $\sum_{r=1}^{N} Q_r \alpha_{kr} = 1$. Similarly the score for forecasts issued at random is one. Gringorten suggests that to eliminate any gain due to forecasting persistence the "climatic frequencies" should be calculated for each basic class of antecedent weather, so that the expected score for "blind" forecasting will be unity, regardless of whether the blind forecast is a perpetual forecast, a persistence forecast or a forecast of pure chance.

The expected score for forecasting the kth event on any occasion is $\sum_r q_r \alpha_{kr} = q_k/Q_k$ where q_r is the true probability that event r will occur on that occasion. The forecaster is therefore encouraged to predict the event whose probability is most increased in relation to the climatological probability.

An index which is zero for "blind" forecasting and unity for perfect forecasting is given by

$$K = \frac{\sum^{N} \alpha_{ki} - N}{\sum^{N} \alpha_{ii} - N},$$

where $\sum^{N} \alpha_{ki}$ is the forecaster's accumulated score and $\sum^{N} \alpha_{ii}$ is the accumulated score for perfect forecasting.

/When

When the forecaster is permitted to predict that the event will fall into one of two or more alternative classes (i.e., he is not required necessarily to choose a single class) then a similar verification scheme can be applied. The score for correctly predicting that the event would fall into one of the classes u, v,.....z becomes

$$1 \Big/ \sum_{r=u}^{z} Q_r$$

This method of verification is unsuitable for checking routine forecasts, since the forecast selected with a view to maximising the score might often differ from that normally issued. The scheme was devised with the object of assessing the forecaster's skill and requires that a special set of forecasts be made. It might be used to test the insight into the meteorological probabilities provided by alternative forecast techniques, particularly if those techniques yielded objective estimates of the probabilities.

The opinion that certain scores leave too much room for hedging have led some (e.g., McKillip, Columbia Branch, 1952) to suggest that the forecaster should be unaware of the nature and existence of the checking scheme. By contrast, Gringorten's approach to verification, exemplified by the system presently discussed and by that given in para. 2.2., requires the forecaster deliberately to play the system. "If the scoring system influences the forecaster adversely, then it is the fault of that particular scoring system. A good system when 'played' by the forecaster will force him to use his meteorological know-how" (Columbia Branch, 1952).

Gringorten, Lund and Miller (1955) discuss the practical application of Gringorten's system to verification made over a period of two years at four U.S. Air Force stations.

Verification methods which apply solely to probability forecasts are discussed in the following section.

3.3.2. Probability forecasts

3.3.2.1. Checking systems for probability forecasts have not been so widely studied as those applicable to categorical predictions, presumably because numerical estimates of likelihood do not usually accompany routine forecasts, although subjective verbal qualifications are common. Cooke (1906) is generally credited with the first attempt to verify probability statements. The proportions of erroneous forecasts were simply compared with the degree of confidence indicated.

Brier (1944) offers a convenient form of tabulation, used in verifying 6-hr. precipitation forecasts for Washington as follows:

/Verification

Verification of statements of probability of precipitation

F/c probability of precipitation	No. of cases (n)	Average probability (p)	No. of precipitation cases expected (np)	observed	Observed proportion of precipitation cases
.00 - .09	56	.036	2.0	1	.018
.10 - .19	38	.162	6.2	13	.342
.20 - .29	6	.222	1.3	1	.167
.30 - .39	10	.326	3.3	3	.300
.40 - .49	25	.439	11.0	13	.520
.50 - .59	9	.558	5.0	2	.222
.60 - .69	9	.654	5.9	5	.556
.70 - .79	13	.755	9.8	10	.769
.80 - .89	10	.835	8.4	8	.800

A table of this type will indicate:

(i) the correlation between forecast and observed probabilities;

(ii) errors of scale; the forecaster may be either optimistic or pessimistic in the assessment of risks;

(iii) what proportion of the forecasts fall into high or low probability classes; these are generally the most useful forecasts.

3.3.2.2. Brier's index. Brier (1950) has devised an index P for use when an event can occur in one of r possible classes,

$$P = \frac{1}{n} \sum_{j=1}^{r} \sum_{i=1}^{n} \left(f_{ij} - E_{ij} \right)^2$$

where f_{ij} is the forecast probability that the event will fall in the jth class on the ith occasion. E_{ij} is an indicator which takes the value one, if the event does occur in the jth class on the ith occasion, but is zero if the event falls in some other class. Summations are taken over r classes and n events. $\sum_{j=1}^{r} f_{ij} = 1, \quad i = 1, 2, \ldots n$.

P ranges from zero for complete success to two for complete failure. Complete success requires a forecast probability of one to be correctly given on every occasion. P depends on the frequency distribution of the forecast probability statements and on the correlation between forecast and observed probabilities. If p_j is the relative frequency with which jth class occurred during the forecast trial, then the minimum score which can be got by predicting the same set of probabilities for every occasion is

$$P = 1 - \sum_{j=1}^{r} p_j^2 ,$$

which occurs when $f_{ij} = p_j$ for all i. If the jth event is categorically forecast on every occasion $P = 2 (1 - p_j)$ and if categorical forecasts are made at random, the expected value of P is $2 (r - 1)/r$. The score must be

/interpreted

interpreted with caution, since repeated issue of the climatic probabilities will give a relatively small value in some circumstances. A perpetual forecast of an event which has a probability of occurrence of .9 yields a score as low as .2.

To achieve a score S* which increases with increasing success Leight (1953) has transformed S by the relation $S^* = 1 - S/2$.

3.3.2.3. Information theory. A novel way of verifying probability forecasts, based on information theory, is given by Holloway and Woodbury (1955). In a situation with several outcomes, the "information" is defined as $I = \sum_i p_i \log_e p_i$ where p_i is the probability of the ith possible outcome. Maximum information is available when $p_r = 1$ and $p_i = 0$ for $i \neq r$; then, $I = 0$. Smaller amounts of information correspond to negative values of I. If there are n outcomes, it can be shown that I takes its minimum value when $p_1 = p_2 = \ldots\ldots\ldots = p_n = 1/n$.

Holloway and Woodbury define the Information Ratio for probability forecasts by the relation

$$(I.R.)_p = \frac{\sum_{i=1}^{n} \log_e p_i'/p_i}{\sum_{i=1}^{n} \log_e 1/p_i}$$

where p_i' is the probability forecast for the event which occurred and p_i is the corresponding climatic probability. Summations are taken over n forecasts. $(I.R.)_p$ is described as the ratio of the increase in information given by the forecast beyond that provided by climatology, to the amount of information beyond climatology required for a perfect forecast. This description does not exactly agree with the definition of "information" previously given. $(I.R.)_p$ is one for perfect forecasting and zero if the climatic probabilities are predicted but, as defined above, it becomes minus infinity if zero probability is forecast for the event which occurs.

Information theory can also be applied to the verification of categorical forecasts. The Information Ratio is then defined by the relations

$$(I.R.)_c = \frac{\sum_i \sum_j \frac{X_{ij}}{N} \log_e \frac{X_{ij}}{(A_i)} - \sum_j \frac{(B_j)}{N} \log_e \frac{(B_j)}{N}}{-\sum_j \frac{(B_j)}{N} \log_e \frac{(B_j)}{N}}$$

$$= \frac{\sum_i \sum_j X_{ij} \log_e X_{ij} - \sum_i (A_i) \log_e (A_i) - \sum_j (B_j) \log_e (B_j) + N \log_e N}{N \log_e N - \sum_j (B_j) \log_e (B_j)}$$

using the notation of Section 3.3.1.

/Some

Some of the properties of $(I.R.)_C$ differ from those of $(I.R.)_P$. $(I.R.)_C$ is one for perfect forecasting but zero is the value expected for forecasts issued at random. Using the categorical forecast definition it is possible to attain the maximum score for forecasts which are completely wrong since $(I.R.)_C$ is a measure of association which is not concerned with the ordering of the classes (cf. Pearson's C and Tchuprow's coefficient, Section 3.3.1.).

Holloway and Woodbury compare the Information Ratio with the skill score by computing the indexes for sample tetrachoric tables. Skill scores of zero and one correspond to Information Ratios of zero and one, but an Information Ratio of 0.5 corresponds to skill scores ranging from .71 to .78. The authors state: this implies one can make a very good forecast having only half the information required for a perfect forecast. This questionable remark illustrates the danger of attaching a plain language label which has a broad everyday connotation to a verification score; the Information Ratio is a mathematical function only loosely connected with the subjective notion of information; it could be variously defined so as to give several different answers for the fraction of information available. Heidke's "value" (para. 3.4.6.) and Crossley's "usefulness" (para. 3.2.9.) are other examples of names which may mislead.

3.4. Continuous distribution

3.4.1. If the forecast is expressed as a single value chosen from a continuous distribution or a variate scale, the simplest verification statistic is the forecast error. The distribution of forecast errors is examined using some sort of frequency curve, either a histogram or a cumulative frequency curve or both. Alternatively, the information can be given in tabular form. Important features of the error distribution are measured by the mean forecast error or "bias" and the root-mean-square (r.m.s.) error. These statistics provide convenient methods of discriminating between error distributions of alternative techniques; their standard errors can readily be estimated, even when the errors themselves are serially correlated.

3.4.2. R.m.s. error. The r.m.s. error of a series of forecast errors $x_1, x_2 \ldots\ldots\ldots\ldots x_n$ is $\left[\frac{1}{N}\sum_{r=1}^{N} x_r^2\right]^{\frac{1}{2}}$. This can be expanded as $\left[\frac{1}{N}\sum_{r=1}^{N}(x_r-\bar{x})^2 + \bar{x}^2\right]^{\frac{1}{2}}$ i.e., the r.m.s. error contains contributions from the bias and the standard deviation of the forecast errors. The bias is usually small, so the r.m.s. error is largely a measure of dispersion. An alternative measure of dispersion is the mean modulus of the errors, but the r.m.s. error gives more weight to the larger errors and is more convenient for statistical manipulation.

It is sometimes objected that the r.m.s. error encourages the forecaster to play the middle of the range. An oft-quoted example concerns the forecaster faced with the problem of predicting the night minimum temperature. He may be reasonably sure that the minimum will be 30 degrees if cloud disperses and 40 degrees if cloud remains. To play safe he forecasts 35 degrees even though such a minimum is unlikely. In some circumstances, for example in forecasting route winds for aviation, where safety considerations are involved, it may be desirable that the forecaster should avoid the risk of making large errors by cutting down on the bad failures at the expense of the spectacular successes.

3.4.3. Correlation coefficient. The correlation coefficient is the measure of association most commonly used in measuring association between variates. It is insensitive to errors of bias and scale and its function is complementary to those of the bias and r.m.s. error.

/If

If $F_1, F_2 \ldots F_N$ and $O_1, O_2, \ldots O_N$ are series of forecast and observed values, the coefficient of correlation between them is

$$\frac{\sum_{r=1}^{N}(F_r-\bar{F})(O_r-\bar{O})}{\sqrt{\sum_{r=1}^{N}(F_r-\bar{F})^2 \sum_{r=1}^{N}(O_r-\bar{O})^2}}$$

When F and O are vectors this formula gives the stretch vector correlation coefficient (Durst, 1954), provided that the product terms are scalar products. Both the correlation coefficient and the stretch vector correlation coefficient take values between -1 and +1, being zero when there is complete linear independence; but for the stretch vector correlation to be maximised, corresponding pairs of vectors must have the same direction as well as satisfy a linear relation.

Correlations between forecast and observed values contain components due to climatic and synoptic trends which are common to both sets of data. A more sensitive coefficient is got when the forecast and observed changes are compared. Complications due to trends are then less intrusive, unless there is a marked diurnal variation which has not been eliminated by choice of forecast period.

3.4.4. The bias, r.m.s. error and correlation coefficients are numerical digests from which characteristic properties of the error distribution can be inferred. For some purposes it will be important to know the percentage of errors which fall within or beyond specific limits, in which case reference should be made to the basic frequency distribution of errors. It may also be pertinent to examine the two aspects, postagreement and prefigurance discussed in previous sections. The Weather Division, U.S.A.A.F. (1944) observe that the distribution of postagreement and prefigurance are cross-sections of the bi-variate surface of forecast and observed values. The two distributions are not generally the same, nor will either distribution remain invariant over the whole range of events.

In some cases the importance of an error of given size varies with the range of the element in question. Murray and Smith (1956) remark that an error of a few degrees may be vital when temperatures are around freezing, but is relatively unimportant on a hot summer's day. Likewise Best and Panofsky (1956) on forecasting precipitation amounts: an error of half an inch of precipitation is much more important if the precipitation is observed to be zero than if it is observed to be five inches; for such types of forecast, it is better to define a number of categories for the forecast variable, which cover larger ranges for larger precipitation amounts, and find the actual number of categories by which the prediction missed the actual amount. Similar considerations lead Brier and Allen (1951) to mention the possibility of expressing errors in such elements as cloud height and visibility as percentages of the actual value.

3.4.5. Comparative indexes. Comments on the use of special indexes in assessing the relative success of forecast techniques were made in para. 3.2.14. Similar indexes which apply particularly to the type of forecast discussed in the present section have been devised by Heidke (1929) and Priestley (1945).

/3.4.6.

3.4.6. Heidke's index. Heidke's index, W, which he terms the "value" is defined as

$$W = \frac{\sum|x'| - \sum|x|}{\sum|x|} ,$$

where x' is the forecast error and x is the error given by persistence.

3.4.7. Priestley's index. Priestley defined a "percentage success", P, by the relation

$$P = 100\left[1 - \frac{\epsilon^2}{\sigma_t^2}\right]^{\frac{1}{2}} ,$$

where ϵ is the r.m.s. error of the forecasts and σ_t is the r.m.s. error of corresponding persistence forecasts.

Sawyer (1953) remarks that this index is particularly flattering to the forecaster because a small reduction from one in the ratio ϵ/σ_t produces an apparently large success; for example if $\epsilon = .8\,\sigma_t$, P = 60%.

It should not be forgotten that the percentage success measured by Priestley's P is purely relative. For example, the "percentage successes" of routine 18-hr. wind forecasts at 30,000 ft. and 50,000 ft. are 73 and zero respectively; yet the forecast errors are actually less at 50,000 ft. than at any lower level. It was mentioned in para. 3.2.14. that the errors of most techniques vary from period to period, being greater at times when persistence errors are large. For this reason, indexes such as Priestley's are sometimes used to make tests of forecasts issued during different periods or seasons more comparable. However, Murray (1954) has indicated that the "percentage success", when computed for upper wind forecasts, is not independent of the winds' variability, high values of P being got when persistence errors are large. Murray concludes that large changes can usually be forecast better than small changes, although the absolute errors are greater for the large changes.

3.4.8. For some purposes it may be convenient to classify data which form a continuous distribution and treat them by the methods of Section 3.3. A system developed by the Weather Information Branch, H.Q., U.S.A.A.F. (1943) is an example of this type of approach. The main purpose of the system was to classify personnel but it contains features of more general interest. The first stage was to divide the distribution of an element into thirty intervals of equal probability (trentiles) on the basis of past records. No complications arise for an element such as atmospheric pressure which, when measured to the nearest tenth of a millibar, takes very many values over a wide range. In less normal distributions a single value may occupy a number of trentiles. For example, the authors give a rainfall case where the "no rain" category occupies twenty trentiles; "trace" requires three trentiles, whilst all other possible rainfall amounts are contained in the remaining seven trentiles. The mark awarded for each forecast is simply the number of trentiles which separate the forecast and observed values. When a value which occupies one trentile or less is correctly forecast, the mark is zero. When a value which occupies more than one trentile is correctly forecast, the mark awarded is $(n^2 - 1)/3n$, where n is

/the

the number of trentiles occupied. $(n^2 - 1)/3n$, the "deviational penalty score", is the mark which would be got by random forecasts within a group of n trentiles. If the forecast value differs from the observed value, and either the forecast value or the observed value or both occupy more than one trentile, then the mark awarded is $\frac{1}{2}(n_1 + n_2) + K$, where n_1 and n_2 are the number of trentiles occupied by forecast and observations and K is the number of trentiles separating those containing the two values. This system of penalties compensates for the relatively greater ease with which some categories can be predicted. Taking the rainfall data mentioned above, a correct forecast of "no rain" receives a high penalty mark (6.7) because two out of three "no rain" predictions will be correct by chance. A correct forecast of "trace" has a low penalty mark (0.9) because only one in ten will succeed by chance.

When the above scheme had been in operation for some time, it was found that the average scores achieved varied with the difficulty of the weather situation (Weather Inf. Branch, H.Q. U.S.A.A.F., 1944). Each individual score was therefore standardised by subtracting from it the mean of all the scores for that day and dividing the difference by the standard deviation. Standardisation facilitates combination of scores and adjusts for difficulty, but standardised scores are useless for measuring improvements due to changes of technique, etc.

3.4.9. To afford a comparison between some of the verification indexes discussed in sections 3.2., 3.3. and 3.4., values have been computed for a series of 24-hr. temperature forecasts. These are examined in Appendix I.

3.5. Written and composite forecasts

3.5.1. Most weather forecasts specify the future state of several elements. A number of verification systems have been designed to give a single index of the success of the whole forecast. In many cases the predictions are not numerical but are expressed in words. Inevitably these systems are more arbitrary than those so far discussed.

3.5.2. The verification rules for an early scheme used by the U.S. Signals Office are listed by Harrington (1889). A verifying officer estimated the areas of a forecast region affected by rain, warmer or colder conditions, etc. consulting synoptic charts for two hours of the 24-hr. forecast period. On this basis, the percentage success was estimated subjectively for each of the factors: weather and temperature; display of cautionary and storm signals; warnings of cold waves. Weights of five, two and one respectively were given to these factors in computing "the general monthly percentage of verifications of all indications". The use of subjective estimates was evidently unsatisfactory, for Harrington comments: ..... the low average of verification of late years as compared with early years of the service is due to increased care and precision in estimating the verifications.

Another subjective check which has been used from time to time in various meteorological services is known as the jury method. Verification is made by a small committee who award the forecast some mark on an arbitrary scale, perhaps ranging from zero for failure to five or ten for close agreement. Resort to the jury method is made when the meteorologists have difficulty in laying down acceptable objective criteria, but subjectivity does not solve the problems, although it may obscure them. Fresh difficulties are raised; a subjective mark does not carry with it the climate of thought which led to its fixing and there is no knowing afterwards, or perhaps even at the time, just how much weight was given to the different factors. Variations with time of subjectively fixed indexes may be due to changes in forecast success or to changes in the critical standards of the assessors. An objective system may have its flaws but they will bear investigation and its judgment will not lack in consistency. Freybe (1911) defended subjective verification on the grounds that it was better than no verification at all.

/3.5.3.

3.5.3. The desire to eliminate subjectivity led to two developments. Firstly, some weather services prescribed all the terms and phrases which were to be used in forecasting, each being given a specific meaning. Secondly, verification systems increased in complexity. Milham (1912) quotes the current U.S. Weather Bureau verification regulations. For precipitation these were:

"Rain or snow forecast and all modifications thereof containing the terms 'possibly', 'probably', etc. will be verified by the occurrence of .01" or more of precipitation. Precipitation to the amount of .01" or more which is not forecast or which is forecast and does not occur will be charged as a failure. A forecast of precipitation will be considered as neither a success nor a failure when a trace of precipitation is recorded within the period specified."

In determining the percentage of verification, the number of forecasts verified will constitute the dividend, the divisor will be the sum of the forecasts verified, the number of forecasts not verified and the number of occurrences of .01" or more of precipitation which were not forecast. Corresponding rules were given for temperature, storm warnings, etc. and the individual percentages were then averaged to give an overall figure. On the basis of this system, the Weather Bureau claimed that the forecasts were 80% to 85% correct.

3.5.4. Ferraz (1924) submitted to an international conference a complex scheme used in Brazil. All permitted weather terms and expressions were listed. The verification rules "are based on agriculture's necessities and not on those of urban life, where people are much more severe, and unnecessarily so, in exacting absolute correctness". 24-hr. forecasts were made in three categories: weather; wind (light, moderate, etc.); temperature (stationary, small rise, moderate rise, etc.). In each category a fully verified forecast received a maximum of twelve points. Forecasts were verified at each station. Forecasts for a whole region, state, or province were considered as verified when the sum of the points obtained for n stations (well distributed) was equal to or greater than $(1 + n/2)10$. As an example, a forecast of "fair" received: 10 points when rain did not exceed one mm. within 30 continuous minutes, with a minimum of four hours sun; 8 points with local thunder not forecast; 8 points if unsettled without rain; 8 points with rain over one mm. within 15 minutes or with intermittent inappreciable rain within one hour; 8 points with no sunshine but clouds of good character (no dark shades); 5 points if threatening. More complicated forecasts such as "fair, changing to unsettled with rain" received points as follows: 8 points, when the first part of the forecast was verified during at least the first three hours or within the maximum period of 21 hours, and the second part, during at least the last three hours or within the maximum period of the last 21 hours, verification being strictly in accordance with the rules established (when minimum periods of three hours were considered, the limits put down by the rules could be halved); 5 points when the forecast was verified only in the maximum period; 5 points when the forecast was verified only in the second part during the last three hours, except in the case when there was no change of weather during the total period of the forecast. Forecasts made separately for day and night were verified separately, the points being halved and one added as a premium, so the maximum number of points obtainable for the 24 hours was 12. In such cases the limits established by the rules were halved.

3.5.5. While checking the accuracy of forecasts based on "perfect" prebaratics Murray and Smith (1956) devised a points system for verifying simple forecasts expressed in Beaufort letters. Table 3 contains the marking system. The results of verifying a set of 528 spot forecasts for mid-day are given in Table 4 (Table IV of Murray and Smith's paper). Precipitation forecasts were verified against the weather observed during the hour preceding mid-day. The average score for the 528 forecasts, expressed as a

/percentage

percentage, was 65. Table 4 shows that the fair weather occasions (b, bc and c) are heavily weighted by virtue of their numerical preponderance. The success in forecasting the important, but less common, phenomena, fog, hail, snow and thunder, contributes little to the final overall score. To increase deliberately the effect of the rarer categories by some artificial weighting system might not be a particularly good solution, because it is the day in and day out "rain or no rain", "sunshine or cloud" considerations which most continually affect the everyday lives of the general public, even though rarer events assume considerable importance when they do occur. These difficulties would not arise, were the forecast elements verified individually rather than in combination.

Routine use of Murray and Smith's system might encourage "hedging", since the score for a perpetual forecast of bc equals the percentage attained in practice. This consideration does not apply to the verifications of Table 4 since the checking system had not been devised when the forecasts were made.

3.5.6. Restriction of the expressions used in weather predictions to defined terms has not generally met with approval. Milham (1912) remarked that it hampered individuality and free expression of opinion even though he considered it necessary to prevent ambiguity and hedging and make possible systematic verification. In recent years many papers have dealt with the verification of numerical or simply classified forecasts but no schemes have been advanced for checking written forecasts, issued to the general public. Bleeker (1946) and Brier and Allen (1951) each refer to the undesirability of limiting the forecasters' terms. Nevertheless, there is no wish to return to subjective methods. Brier and Allen (1951) summarise the common view: "One essential for satisfactory verification is objectivity, which requires that the forecasts be explicitly stated, either numerically or categorically, thus permitting no element of judgment to enter into the comparison of the forecast with subsequent observation." And yet the forecaster who writes for the general public cannot eliminate subjective considerations; he has to interpret for the public and maintain its interest. Bleeker (1946) discusses the difficulties:

> Statements about the future value of four of five meteorological elements do not necessarily say what the weather will be like. Weather is a very complicated matter, it is namely the integral of the influences of various meteorological factors upon our senses. "With the eye", says Schmaus (1942) "we observe the colours of the sky, the clouds, the electric discharges, the precipitation. The ear tells us something of the sounds of wind and thunder, our feeling sense something about the temperature and our skin about the moisture." Every meteorologist will agree with Schmaus that it is very difficult to form a picture of the weather on a past day by combining the elements published in a year book. This can only be done in certain cases, e.g., for fine days. The reader of forecasts inevitably has the same difficulty when he tries to form an idea about the future weather from the objectively given elements of a forecast which he will experience subjectively. This subjectivity is a great handicap for the forecaster, especially if he is serving different groups of the public. Seamen, farmers, townspeople, etc. are all interested in different elements of the forecast, they apply different standards and criticize from different points of view.

How can the dilemma be resolved? The alternatives seem to be to straight-jacket the forecasts or to abandon the possibility of strict checking. Brier and Allen (1951) wash their hands of the public forecasts: "If every forecast is accompanied by a definition of the terms used, the forecaster sometimes objects that it hinders his freedom to express himself adequately. Only those forecasts which are expressed in objective terms can be verified satisfactorily as forecasts. The extent to which public forecasts satisfy the public is a different question which can be answered, it appears, only by public opinion polls; and the answer will generally contain little information about the agreement of forecast and actual weather." Bleeker, however, mentions a kind of compromise. In some meteorological services, two forecasts are compiled,

/one

one for issue to the public and one for checking: the two forecasts must not contradict each other, but the forecaster has complete liberty in the choice of his terms for the public forecasts. The system of double forecasts was introduced in Holland in 1939 for rainfall forecasts "to the great satisfaction of the acting meteorologists". Apart from allowing public forecasts to be made more colourful, such a system considerably simplifies the verification problem: more use can be made of numerical values and strict classifications, elements can be checked separately, probability statements can be made objective and difficulties of verifying area forecasts are ameliorated. The forecaster can object, sometimes with good justification, that the synopic reporting stations in a given region do not give a good objective picture of the weather over the area, although he may be able to infer from them subjectively the sort of conditions which generally obtain. It may be unfair to verify the area forecasts against the limited number of reports. If the forecaster is aware that forecasts will be checked against reports from certain stations, he may be tempted to phrase his predictions to cater particularly for those stations. This is legitimate if the forecasts are for checking purposes alone: it is not desirable when the forecasts are to be issued to the public.

3.5.7. Apart from the problems raised in the last paragraphs, certain other difficulties attend the verification of the elements of a forecast in combination. The Weather Division, H.Q., U.S.A.A.F. (1944) discuss predictions of weather type. It is remarked that if the probability of correctly forecasting one element within specified limits is 0.70, then the probability of successfully forecasting a composite of four such elements is 0.24, assuming the elements to be independent. A study of 24-hr. forecasts of air route terminal conditions is quoted. This showed that while forecasters had considerable skill in forecasting pressure, temperature and precipitation separately, they were badly beaten by persistence forecasts of the composite weather conditions. The authors conclude that if forecasts of weather type are demanded by a user, such forecasts should be furnished only in addition to, and not in place of, predictions of the respective components.

3.5.8. Most composite or semi-objective checking systems produce as their final score a "percentage correct". It was mentioned in para. 3.2.1.1. that the percentage correct depends upon the limits arbitrarily set for "correct" forecasts. Thomas (1933) for example, quotes Berlin Meteorological Office regulations which rule that an error up to two degrees in temperature is 100% correct, errors between two and four degrees are 50% correct and errors greater than four degrees are zero per cent correct. Van Everdingen (1908) gives a method used by the Royal Nederland Meteorological Institute which employs a nine-point scale for each element. According to Koppen (1893) most German institutes verified on a three-point scale, although a five-point scale was in use in Bavaria (0%, 25%, 50%, etc). And so on. Moreover, there is no agreement regarding the weights to be given to the separate elements in computing the overall percentage. Thus "percentage correct" has no meaning for those unacquainted with the details of the verification. The meteorologist himself cannot interpret the meaning of "X% correct" precisely; it cannot be inferred that the forecasts were X% correct on every occasion, neither can it be assumed that the forecasts were completely correct for X% of the occasions.

3.5.9. The foregoing paragraphs have indicated the considerable advantages to be gained in checking the meteorological content of public forecasts by having parallel forecasts made in a form suited to the verification problem. If the meteorologist is faced with written or partly written forecasts which have already been made over a long period and he is required to judge the changes in accuracy which have been effected through the years, then the parallel forecast solution is inapplicable, since there is obviously no hope of applying it in retrospect. In this case subjectivity in the comparisons is unavoidable, and the verification scheme can only attempt to minimise the inherent uncertainties. Individual elements can still be checked separately. The verifier, reading the forecasts, would place each expected state of the element into one of a number of classes. Similar treatment of

/the

the observed weather would yield a set of data which could be handled objectively from that stage, by the methods described in sections 3.2. and 3.3. The difficulties and doubts entering into the initial classification may easily be appreciated by all who are familiar with the forms in which written forecasts are given, but acceptance of a measure of subjective judgement would be implicit in a decision to check past written issues.

4. Concluding remarks

The preceding sections have shown that there is no lack of verification techniques and scores covering many of the contingencies which may arise. In most cases, the problem facing the verifier is to select the statistic or system which best suits his purpose. When fresh systems must be devised, there exists a body of experience which should enable many potential pitfalls to be avoided. When forecasting trials are held, the experiments should be designed with the verification technique and the problems of statistical significance well in mind.

5. References

The following list of references does not constitute an exhaustive bibliography, since it was not found necessary in the foregoing discussion to refer to every paper which was consulted and some papers which touch on verification indirectly may have been overlooked. An annotated bibliography has been published by Muller (1944) and a very comprehensive list of references is furnished by Bleeker (1946).

Best, W.H. and Panofsky, H.A.	1956	'Some application of statistics to Meteorology', College of Mineral Industries, Pennsylvania State University.
Bijvoet, H.C. and Bleeker, W.	1951	'The value of weather forecasts', Weather, 6, p. 36.
Bilham, E.G.	1922	'A problem in economics', Nature, 109, p. 341.
Bleeker, W.	1946	'The verification of weather forecasts,' Mededeelingen en Verhandelingen, Serie B.1, No. 2.
Brier, G.W.	1944	'Verification of a forecaster's confidence and the use of reliability statements in weather forecasting', Washington Weath. Bur. Res. Pap. No. 16.
	1950	'Verification of forecasts expressed in terms of probability', Mon. Weath. Rev., 78, p. 1.
Brier, G.W. and Allen, R.A.	1951	'Verification of weather forecasts', Compendium of Meteorology, Amer.Met. Soc., p. 841.
Brooks, C.E.P. and Carruthers, N.	1953	Handbook of statistical methods in meteorology, London (H.M.S.O.).
Clayton, H.H.	1889	'Verification of weather forecasts', Am. Met. J., 6, p. 211.
	1934	'Rating weather forecasts', Bull. Amer. Met. Soc., 15, p. 279.
Columbia Branch, American Met.Soc.	1952	'Panel discussion on forecast verification', Bull.Amer. Met. Soc., 33, p. 274.

/Cooke,

Cooke, W.E.	1906	'Forecasts and verifications in Western Australia,' Mon. Weath.Rev., 34, p. 23.
Crossley, A.F.	1952	'Usefulness of forecasts', Met. Mag., 81, p. 193.
	1954	'Measures of success in forecasting', Met. Mag., 83, p. 66.
Dinies, E.	1936	'Vorhersageprufungen', Erf. Ber. deutchen Flugwetterdienstes, Sonderband 5, Teil 2.
Doolittle, H.M.	1885	'The verification of predictions', Am. Met. J., 2, p. 327.
Durst, C.S.	1954	'Variation of wind with time and distance,' Geophys. Mem., 12, No. 93.
Ekholm, N.	1907	'Uber die unperiodischen Luftdruckschrankungen und einige damit Zusammerhengende Erscheinungen, Met. Zeit., 24, p. 145.
Ferraż, de Sampaio	1924	'Verification of daily weather forecasts,' International Conf. of Directors (1923), Koninklijk Nederlandsch Met. Inst. No. 112, Appendix N.
Finley, J.P.	1884	'Tornado predictions,' Am. Met. J., 1, p. 85.
Freybe, O.	1911	'Die Traffsicherheit der Prognosen', Wetter, 28, p. 117.
Gilbert, G.K.	1884	'Finley's tornado predictions,' Am. Met. J., 1, p. 166.
Gringorten, I.I.	1951	'The verification and scoring of weather forecasts,' J. Amer. Statist. Ass., 46, p. 279.
	1955	'Tests of significance in a verification problem,' J. Met., 12, p. 179.
Gringorten, I.I., Lund, I.A. and Miller, M.A.	1955	'A program to test skill in terminal forecasting,' Air Force Surveys in Geophysics, No. 80, Geophysics Research Directorate, Cambridge, Mass.
Grossmann, L.	1898	'Die Sturme und die Sturmwarnungen an die deutche Kuste,' Aus dem Archiv der deutschen Seewarte, 21, No. 4.
Harrington, M.W.	1889	'Verifications at the Signals Office,' Am. Met. J., 6, p. 19.
Heidke, P.	1926	'Berechnung der Erfolges und der Gute der Windstarkevorhersagen im Sturmwarnungdienst, Geografika Annaler, 8, p. 310.
	1928	'Erfolg und Gute Ortlicher Vorhersagen im taglichen Wetterdienst,' Aus dem Archiv der deutschen Seewarte, 45, No. 1.

/1929

	1929	'Zur objektiven Prufung ortlicher Vorhersagen im taglichen Wetterdienst,' Beitrage Zur Physik der freien Atmosphare, 15, p. 202.
	1935	'Erfolg und Gute von Hamburger und Konigsberger Frostvorhersagen fur die nächste Nacht,' Ann. der Hydr., 63, p. 40.
Holloway, J.L. and Woodbury, M.A.	1955	'Application of information theory and discriminant function analysis to weather forecasting and forecast verification', Tech. Rep. of Met. Statistics Project of Inst. Co-op. Res., Univ. of Pennsylvania.
Johnson, D.H.	1955	'The success achieved in forecasting upper winds by orthodox and statistical techniques,' Meteorological Research Papers, Air Ministry, London, No. 953.
Jorgensen, D.L.	1956	'A graphical solution of the conventional skill score involving two categories,' Mon. Weath. Rev., 83, p. 139.
Kendall, M.G.	1948	Advanced theory of statistics, 1, (Charles Griffin and Co., London).
Köppen, W.	1893	'The best method of testing weather predictions,' Rep. of International Met. Congress, Chicago, Part 1.
Lacour, D.M.	1906	'Kritik af Stormvarselst Jenesten i Denmark i Aaret 1905, Meddelt af Meteorologisk Institut,' Arkiv for Soevaesen, p. 47.
Leight, W.G.	1953	'The use of probability statements in extended forecasting,' Mon. Weath. Rev., 81, p. 349.
Lewis, R.P.W. and McIntosh, D.H.	1952	'Some effects of coherence in meteorological time series,' Met. Mag., 81, p. 242.
Mascart, J.	1922	'La proportion des réussites dans la provision du temps,' Academie des Sciences, Comptes Rendus, 175, p. 627.
Milham, W.I.	1912	'The accuracy and verification of predictions' Meteorology, p. 404. (Macmillan, New York).
Muller, R.H.	1944	'Verification of short-range weather forecasts,' Bull. Amer. Met. Soc., 25, p. 18.
Murray, R.	1954	'On the accuracy of contour charts in forecasting upper winds,' Met. Office, London, Prof. Notes. No. 110.
Murray, R. and Smith, C.V.	1956	'The attainable accuracy of weather forecasts derived from 24-hr. prebaratic charts.' Unpublished.

/Peirce,

Peirce, C.S.	1884	'The numerical measure of the success of predictions,' Science, 4, p. 453.
Priestley, C.H.B.	1945	'Accuracy of upper air forecasts,' Meteorological Research Papers, Air Ministry, London, No. 222.
Sawyer, J.S.	1953	'The correlation coefficient, as a measure of success in forecasting,' M.O.21, Tech. Notes, No. 76, Met. Office, Dunstable.
Schmauss, A.	1942	'Das Problem der Wettervorhersage,' Leipzig.
Thomas, H.	1933	'Zur Prufung der synoptischen Vorhersagen,' Met. Zeit, 50, p. 29.
Thompson, J.C. and Brier, G.W.	1955	'The economic utility of weather forecasts,' Mon. Weath. Rev, 83, p. 249.
Vernon, E.M.	1953	'A new concept of skill score for rating quantitative forecasts,' Mon. Weath. Rev., 81, p. 326.
Wagemann, H.	1935	Prognosenprufung, Annalen der Hydrographie, 63, p. 270.
Wallén, A.	1921	'Sur le Contrôle des Annonces de tempêtes,' Geograf. Ann., 3, p. 267.
Weather Division, H.Q., U.S.A.A.F.	1944	'Critique of verification of weather forecasts,' Weather Division, H.Q. U.S.A.A.F., Rep. No. 669.
Weather Information Branch, H.Q., U.S.A.A.F.	1943	'Short range forecast verification programme,' Weather Information Branch, H.Q., U.S.A.A.F., Rep. No. 602.
	1944	Ibid., Supplement to Rep. No. 602.
Yule, G.U. and Kendall, M.G.	1937	Introduction to the theory of statistics, (Charles Griffin and Co., London).

Table 1. Contingency tables of precipitation forecasts by A and B (after Vernon 1953)

Forecasts by A

Observed	0	0.01-0.20	0.21-0.50	0.51-1.00	⩾ 1.01	Total
0	65	5	2	1	1	74
0.01 - 0.20	9	6	3	3	1	22
0.21 - 0.50	4	5	4	2	1	16
0.51 - 1.00	1	2	3	3	1	10
⩾1.01	1	1	2	2	2	8
Total	80	19	14	11	6	130

Conventional skill score = 0.362
Deviation " " = 0.498
Quadratic " " = 0.602

Forecasts by B

Observed	0	0.01-0.20	0.21-0.50	0.51-1.00	⩾ 1.01	Total
0	65	9				74
0.01 - 0.20	10	6	6			22
0.21 - 0.50	5	4	4	2	1	16
0.51 - 1.00			4	3	3	10
⩾1.01				6	2	8
Total	80	19	14	11	6	130

Conventional skill score = 0.362
Deviation " " = 0.639
Quadratic " " = 0.824

G. 23021/IKW/7/57/50

Table 2. Contingency tables of biased precipitation forecasts by A and B (after Vernon 1953)

Forecasts by A

Observed	0	0.01-0.20	0.21-0.50	0.51-1.00	⩾ 1.01	Total
0	65		9			74
0.01 - 0.20	9		13			22
0.21 - 0.50	4		12			16
0.51 - 1.00	1		9			10
⩾ 1.01	1		7			8
Total	80		50			130

Conventional skill score = 0.323
Deviation " " = 0.469
Quadratic " " = 0.582

Forecasts by B

Observed	0	0.01-0.20	0.21-0.50	0.51-1.00	⩾ 1.01	Total
0	65		9			74
0.01 - 0.20	10		12			22
0.21 - 0.50	5		11			16
0.51 - 1.00			10			10
⩾ 1.01			8			8
Total	80		50			130

Conventional skill score = 0.310
Deviation " " = 0.482
Quadratic " " = 0.631

G. 23021/IKW/7/57/50

Table 3. Scoring system for weather forecasts (Murray and Smith 1956)

Observed Weather

Forecast Weather	b	bc	c	f	pr	prs	ps	ph	tl	r	rs	s
b	5	4	3	3	1	1	1	1	0	0	0	0
bc	4	5	4	3	2	2	2	2	0	0	0	0
c	3	4	5	3	2	2	2	2	0	0	0	0
f	3	3	3	5	0	0	0	0	0	0	0	0
pr	1	2	2	0	5	4	3	4	3	3	2	1
prs	1	2	2	0	4	5	4	4	3	2	3	2
ps	1	2	2	0	3	4	5	4	3	1	2	3
ph	1	2	2	0	4	4	4	5	3	2	2	2
tl	0	0	0	0	3	3	3	3	5	3	3	3
r	0	0	0	0	3	2	1	2	3	5	4	3
rs	0	0	0	0	2	3	2	2	3	4	5	4
s	0	0	0	0	1	2	3	2	3	3	4	5

Table 4. Results of Press forecasts (Murray and Smith 1956)

Observed Weather

Forecast Weather	b	bc	c	f	pr	prs	ps	ph	tl	r	rs	s	Total
b	18	7	11	3	1					1			41
bc	30	70	60	7	22		1			22			212
c	5	32	44	1	4		1	1		27		1	116
f			5							2			7
pr	3	13	14		18			2		14	1		65
prs		1						1					2
ps						1	2	1					4
ph							1						1
tl													0
r	3	16	23	1	8		2			25	1		79
rs			1										1
s													0
Total	59	139	158	12	53	1	7	5	0	91	2	1	528

Forecast verification: Appendix I

Some representative values of the verification indexes

1. A series of 212 routine 24-hr. temperature forecasts for October and November 1956 have been checked to compare values of some of the verification indexes.

2. Tables A and B are contingency tables for routine forecasts versus the observed values and for persistence forecasts versus the observed values. Measures of postagreement ($X_{ii}/(A_i)$) and prefigurance ($X_{ii}/(B_i)$) (para. 3.3.1.1. of the survey) suggest that the forecasts had greater success over the middle of the range than at the extremes. The routine forecasts were more successful than the persistence forecasts in most categories, but there is a close relation in the values achieved by the two techniques.

3. The tetrachoric tables C and D classify the forecasts dichotomously according as the temperatures forecast were below the seasonal normal or not. The routine forecasts improved upon persistence for both prefigurance (c/o) and postagreement (c/p) (para. 3.2.2. of the survey), but the gain was greatest for postagreement.

4. Table E contains values of some of the more useful of the indexes discussed in the survey. The numerical values of these indexes vary widely but it is noteworthy that they all place the two sets of forecasts in the same order of merit.

5. Table F gives values of a few of the indexes, based on the same data, for which the forecast changes rather than the forecasts themselves are considered. These indexes are generally smaller than their counterparts in Table E, since the success they represent owes nothing to persistence.

Table A. Contingency table for routine 24-hr. forecast temperatures versus observed values

		Forecast temperature range in degrees Fahrenheit									Totals	Prefigurance
		36-38	39-41	42-44	45-47	48-50	51-53	54-56	57-59	60-62		$(X_{ii}/(B_i))$
Observed temperature range in degrees Fahrenheit	36-38	1	2								3	.33
	39-41	2	1	3	3						9	.11
	42-44	1	1	1	4	3					10	.10
	45-47			1	13	10	3				27	.48
	48-50			2	12	28	7	3			52	.54
	51-53		1		2	20	13	8	3		47	.28
	54-56					4	8	14	4		30	.47
	57-59						2	8	10	7	27	.37
	60-62						1		6		7	.00
	Totals	4	5	7	34	65	34	33	23	7	212	
Postagreement $(X_{ii}/(A_i))$		.25	.20	.14	.38	.43	.38	.42	.43	.00		

G. 23021/IKW/7/57/50

Table B. Contingency table for persistence 24-hr. forecast temperatures versus observed values

		Forecast temperature range in degrees Fahrenheit									Totals	Prefigurance
		36-38	39-41	42-44	45-47	48-50	51-53	54-56	57-59	60-62		$(X_{ii}/(B_i))$
Observed temperature range in degrees Fahrenheit	36-38	1	2								3	.33
	39-41	1	1	2	2	3					9	.11
	42-44		2		5	2		1			10	.00
	45-47		2	3	5	8	7	1	1		27	.19
	48-50	1		4	9	23	13	1	1		52	.44
	51-53			2	4	14	12	13	2		47	.26
	54-56				1	2	8	11	6	2	30	.37
	57-59						4	7	11	5	27	.41
	60-62							1	5	1	7	.14
	Totals	3	7	11	26	52	44	35	26	8		
Postagreement $(X_{ii}/(A_i))$		.33	.14	.00	.19	.44	.27	.31	.42	.13		

Table C. Tetrachoric table classifying routine forecast and observed temperatures as below or not below normal

		Routine Forecast		
		not below	below	total
Observed Temperature	not below	57	26	83
	below	21	108	129
	total	78	134	212

Prefigurance

$\frac{c}{o}$ = .69

Postagreement

$\frac{c}{p}$ = .73

Table D. Tetrachoric table classifying persistence forecasts and observed temperatures as below or not below normal

		Persistence Forecast		
		not below	below	total
Observed Temperature	not below	53	30	83
	below	32	97	129
	total	85	127	212

Prefigurance

$\frac{c}{o}$ = .64

Postagreement

$\frac{c}{p}$ = .62

Table E. Verification indexes for 24-hr. temperature forecasts (forecast versus observed values)

Classification	Index	Routine Forecast	Persistence
dichotomous (below normal or not)	Peirce	.52	.39
	Clayton	.54	.39
	Yule's V	.53	.39
	skill score	.53	.39
manifold	skill score	.25	.17
	Vernon's S_d	.60	.50
	Vernon's S_q	.81	.72
	Pearson's C	.79	.73
	Pearson's C (adjusted)	.84	.78
	Tchuprow's T	.46	.38
	correlation (grouped)	.81	.72
continuous distribution (forecast v. observed value)	mean error	+.17°F	-.26°F
	root mean square error	3.06	3.63
	correlation coefficient	.82	.74

Table F. Verification indexes for 24-hr. temperature forecasts (forecast versus observed changes)

Classification	Index	Routine Forecast
dichotomous (colder or not colder)	Peirce	.31
	Clayton	.31
	Yule's V	.31
	skill score	.31
Continuous distribution (forecast change v. observed change)	mean error	+.17°F
	root mean square error	3.06
	correlation coefficient	.61

Forecast verification: Appendix II

Tests of statistical significance in forecast verification

1. Representativeness of data

1.1. When forecasts are verified it is necessary to estimate whether the results of the verifications are likely to be of general validity. This question is particularly relevant when the purpose of the checking is to decide the relative merits of two sets of forecasts. The use of tests of statistical significance in this connexion has increased in recent years, although it is still far from general. Owing to the underlying assumptions, standard treatments given in statistical text-books are often inadequate to deal with the meteorological case, the most frequently invalid supposition being that successive data are independent.

1.2. The representativeness of the weather types occurring during the period of the verifications must also be considered. Suppose, for example, that a forecast trial showed one forecast technique to achieve a (statistically) significantly greater success than another. If the weather during the trial happened to be predominantly anticyclonic, then the significance of the difference in the forecast successes would have been established for anticyclonic conditions, but the significance tests would have nothing to say about the success achieved in a generality of weather types. In brief, verification samples are rarely random.

2. Tests on independent data

2.1. If the data can be selected so that successive forecasts and successive occurrences are independent, then statistical significance can be estimated by standard methods.

2.2. For dichotomous and manifold classifications questions of significance are best resolved by applying a chi-squared test to the basic contingency table, although this test should be used only when the expected frequency is not less than five in any cell (Brooks and Carruthers, 1953).

In some cases formulae for the standard errors of verification indexes are available. For Yule's V, in the notation of section 3.2. of the survey, the standard error is given by the square root of the expression,

$$\frac{1}{S}\left[1 - V^2 + \frac{(V + \frac{1}{2}V^3)(2o-s)(2p-s)}{(op(s-o)(s-o))^{\frac{1}{2}}} - \frac{3V^2s^2\,(p(s-p) - o(s-o))}{4op\,(s-p)(s-o)}\right]$$

Yule (1912) derived this expression assuming that the observed cell frequencies may be used in place of the population cell frequencies and that successive trials are independent.

2.3. The standard errors of many of the statistics discussed in section 3.4. of the survey (continuous distribution) are well-known.

For the mean error, or bias, the standard error is given by $\sigma/\sqrt{N}$ where σ is the standard deviation of the N forecast errors.

The standard error of the difference between two biases is $\sqrt{(\sigma_x^2+\sigma_y^2)}/\sqrt{N}$ where σ_x and σ_y are the standard deviations of the two error distributions. For small (uncorrelated) samples Student's 't' test is available.

/The

The standard error of the difference between two standard deviations is given by

$$\left[\text{standard error of } (\sigma_1 - \sigma_2)\right]^2 = \frac{\mu_4 - \mu_2^2}{4\mu_2 N} + \frac{\nu_4 - \nu_2^2}{4\nu_2 N},$$

where μ_4, μ_2 and ν_4, ν_2 are the fourth and second moments of the forecast error distribution and N is the number of cases (Yule and Kendall, 1937). When the errors are normally distributed, this formula reduces to $(\sigma_1^2 + \sigma_2^2)/2N$

Correlation coefficients are usually tested for significance by means of Fisher's Z-test. Kendall (1948) advises against the use of the standard error in this case since the usual assumptions of normality of the sampling distribution, etc. do not hold unless N is very large; how large N should be it is not easy to say but values as high as 500 are unsatisfactory.

Vector errors require special consideration. Components may be treated individually but it is often convenient to sum departures from the vector mean error over all directions to get a scalar variate which can be handled along the lines discussed above.

3. Serially correlated data

3.1. An attempt can be made to avoid serial correlation by spacing the forecasts so that the persistence effects are minimised, but, as Gringorten (1955) rightly remarks, it is difficult to avoid the problem completely because there is persistence of weather patterns on all scales, even from month to month. Gringorten continues: it is better to live with this difficulty and assume that it will be negligible. This view is hardly tenable; the effects of serial correlation are often far from negligible; for example, even when the serial correlation in a set of observations is as low as 0.35, for the purpose of estimating the accuracy of the mean, the equivalent number of independent values is only one half of the total number of observations.

3.2. Although the difficulties arising in extending the theory of significance tests to cover cases where successive values are not independent have not been generally solved, a rigorous approach is possible when the verification statistic can be expressed as a mean value.

For a series of N terms, having standard deviation σ and serial correlations p_1 between consecutive terms, p_2 between alternate terms, etc., the standard error of the mean value is

$$\sigma\left[1 + \frac{2}{N}\left\{(N-1)p_1 + (N-2)p_2 + \ldots\ldots\ldots + p_{N-1}\right\}\right]^{\frac{1}{2}} \Big/ N^{\frac{1}{2}}$$

When the mean values of two such series, $x_1, x_2 \ldots\ldots x_N, y_1, y_2 \ldots\ldots y_N$, are to be compared, the square of the standard error of the difference between the means is given by

$$\frac{\sigma_x^2 + \sigma_y^2}{N}\left[1 + \frac{2\left\{P\sigma_x^2 + Q\sigma_y^2 - \sigma_x\sigma_y(r + 2T)\right\}}{\sigma_x^2 + \sigma_y^2}\right]$$

/where

where, $P = \frac{1}{N}\left((N-1)p_1 + (N-2)p_2 + \_\_\_\_\_ + p_{N-1} \right)$;

$Q = \frac{1}{N}\left((N-1)q_1 + (N-2)q_2 + \_\_\_\_\_ + q_{N-1} \right)$;

$T = \frac{1}{N}\left((N-1)t_{1,2} + (N-2)t_{1,3} + \_\_\_\_\_ + t_{1,N} \right)$;

r is the correlation between the x and y; p_1, p_2, etc. are correlations in the x; q_1, q_2, etc. are correlations in the y; $t_{i,j}$ are cross-correlations between the x_i and y_j (Johnson, 1955). These formulae can be applied when N is sufficiently large for the following assumptions to hold:

(i) the sample standard deviations and correlations may be used as estimates of the population values;

(ii) the sampling distribution of the bias is approximately normal.

These conditions become better fulfilled as N increases. When the serial correlations are about .3, a good approximation is probably obtained for $N > 60$ but when higher serial correlations exist a larger number is required. In estimating this number it may be helpful to calculate the "equivalent number of independent observations" (Lewis and McIntosh, 1952).

3.3. The above method of estimating the standard error can be applied to the bias (continuous distribution, para. 3.4.1.), when the x and y are simply the forecast errors. The serial correlations in forecast errors are usually substantially smaller than the serial correlations in the forecast or observed values, but it must not be assumed that they are negligible. In a set of 18-hr. upper wind forecasts, for example, significant serial correlations in the forecast errors of about 0.2 were found. The errors made in upper wind forecasts issued from two independent stations were correlated with a coefficient as high as 0.6 (Johnson, 1955).

Other indexes which essentially award a mark for each forecast made can be adapted for similar treatment. Examples are: percentage correct (para. 3.2.3.); Vernon's scores (para. 3.3.1.4.); Gringorten's score (para. 3.3.1.9.); Brier's Index (para. 3.3.2.2.); variance of the forecast errors (para. 3.4.2.).

3.4. The problem of allowing for serial correlation in dealing with other types of verification score, such as the correlation coefficient, has not yet been satisfactorily solved, to the writer's knowledge. A possible approach is to estimate an "equivalent number of independent terms" (Lewis and McIntosh, 1952) or an "equivalent number of independent comparisons" (Johnson, 1955), but this method involves the working assumption that the equivalent number of independent terms is about the same for the correlation coefficient as for a mean value.

Fig. 1

The relation between the specific industry factor, (P/L) and the economic benefit factor, (B/L) for 10 unfavourable days out of 100, total loss being smaller than the total cost of preventive measures (After Bijvoet and Bleeker)

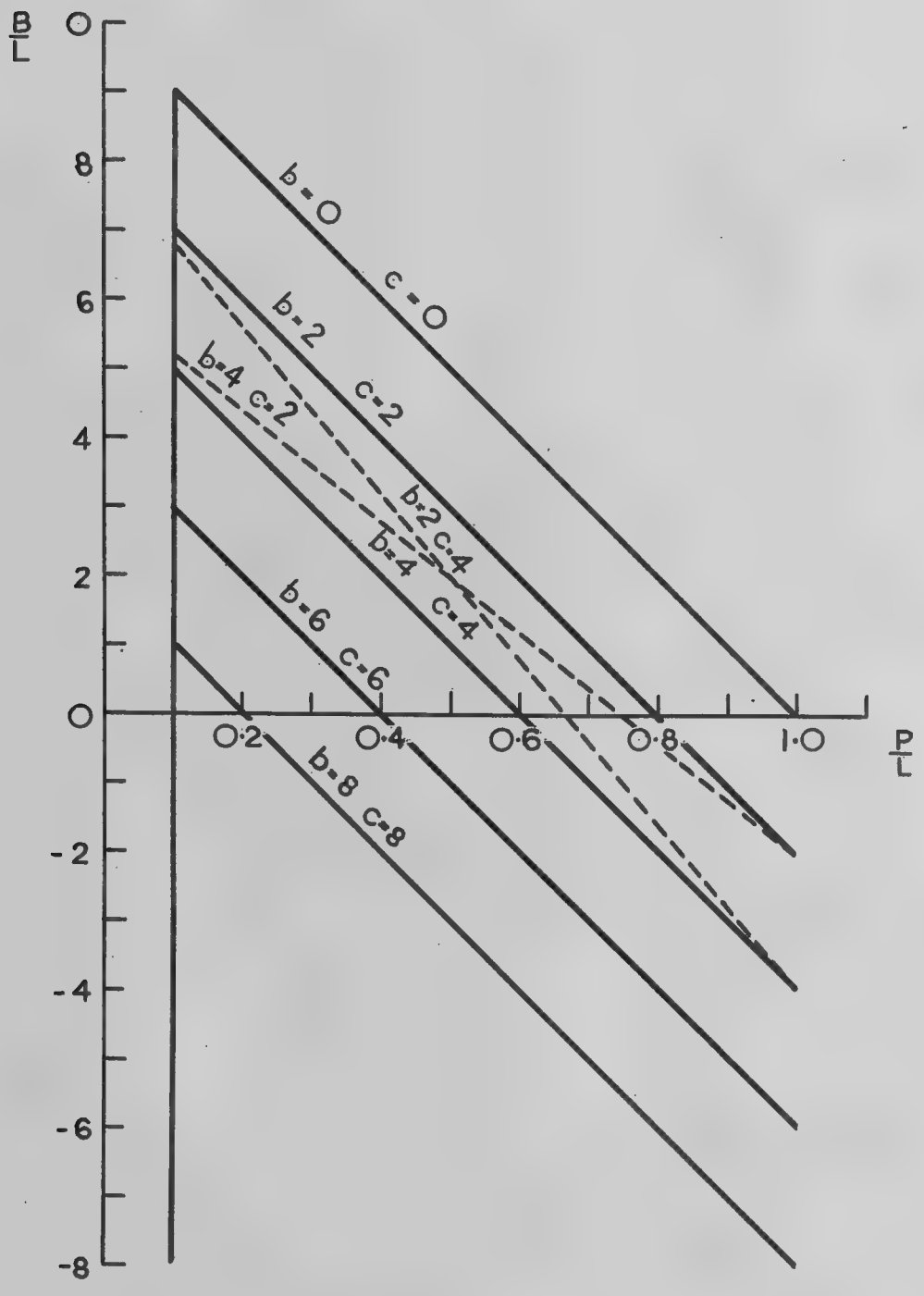

M.R.P. 1058
S.C.111/238
31st May, 1957

AD

Horizontal diffusion in the atmosphere in the light of air trajectories.

by

C. S. Durst, A. F. Crossley and N. E. Davis

(Meteorological Office)

AIR MINISTRY

METEOROLOGICAL RESEARCH COMMITTEE

MASTER FILE COPY
NOT TO BE REMOVED
FROM AWS TECH FILES

At the time of issue this report has not been published. Any author desiring to quote this paper should refer to it as "A paper of the Meteorological Research Committee (London), M.R.P. No. 1058 by Messrs. C.S. Durst, A.F. Crossley & N.E. Davis
A copy is available in the Library of the Meteorological Office."

M.R.P. 1058
S.C.III/238
31st May, 1957

AIR MINISTRY

METEOROLOGICAL RESEARCH COMMITTEE

Horizontal diffusion in the atmosphere in the light of air trajectories

by
C.S. Durst, A.F. Crossley and N.E. Davis (Meteorological Office)

Summary

The dispersion of the end points of geostrophic trajectories is examined for a considerable number of cases. The standard vector deviations of the end points of these trajectories are computed after various times, and also correlation coefficients are calculated between the initial wind velocities and the velocities at later times following the trajectories. An attempt is made to determine an empirical law connecting the standard vector deviation of the end points with the time during which the trajectories had been pursued. There is good agreement with a law based on an exponential value for the Lagrangian correlation coefficient of wind with time.

Introduction

If a trajectory of the free air is drawn from a point it will follow a meandering path; if at subsequent times a second, third and successive trajectories are initiated from the same point at equal time intervals, their paths will form a plume flowing out in the direction of the general wind stream, as is shown in Figures 1a and 1b. These plumes are not of exactly the same type as for example the plume of smoke from a chimney emitting a continuous source of pollution but are more closely parallelled by the pattern on the ground of the pollution deposited from such a chimney. The analogy is not exact in the case of geostrophic trajectories because in a smoke plume the individual particles are free to move vertically as well as horizontally. A geostrophic trajectory is the quasi-horizontal path of a point element, but the cross-section of a smoke plume is affected by the eddies within itself and in its surroundings. Sutton (1) emphasised this feature of smoke and in his hypothesis he has suggested that the dimensions of the eddies which operate on the smoke are essentially related to the distance which the smoke has travelled from its source. Thus it may be that there is a difference between the plume of smoke and the bundle of trajectories but such studies as are given in this paper may it is hoped enable the fundamental characteristics of large scale turbulence to be more clearly understood. For that reason we have included the summarised data concerning the trajectories in an appendix so that they may be available to other workers.

To discuss these plumes of trajectories we should follow the true paths of selected elements of air, but since it is not in general possible to do so on the scale of synoptic charts, there have been substituted instead "geostrophic trajectories". These are formed, according to common practice, by measuring the geostrophic wind near the point of origin on a synoptic or pressure contour chart, plotting the position which the air at that point will have reached after half the time interval to the next chart, measuring the geostrophic wind on the next chart, at the position at which the air will probably have arrived at the time of that (second) chart, drawing the probable track of the air up to the mid time between the second and third charts and so on. There are errors inherent in this process which do not necessarily cancel out but nevertheless when a large number of trajectories are drawn it is believed that the technique serves to produce some important data concerning the atmosphere.

The purpose of this paper is to discuss the distribution of the end points of air trajectories, initiated at regular intervals (i) at a point above the earth's surface and pursued for a given length of time (t). It is clear that the distribution is related not only to the time during which the trajectories are pursued but also to the length of the period (T) over which they are regularly initiated. Thus there are three time scales, but if N is the number of trajectories followed $(N-1)\,i = T$ and provided N is reasonably large the plume can be considered fairly representative of the wind régime and so the magnitude of i does not appear to be significant to the same extent as that of t and T. It is clear that the value of T is of importance in relation to the general pattern of the wind régime prevailing during the period when the trajectories are being drawn. This is at once apparent in the comparison of Figures 1a and 1b which are drawn at 700 mb over N. America where data for a large area are most complete. In the former case the general circulation was strong and uniform, in the latter there was much greater meandering of the trajectories and greater variability of the individual winds. The effect is not necessarily seasonal but it can readily be seen to be dependent on the frequency and type of eddies (depressions and anticyclones) which were passing during the period. For instance, if numerous centres of disturbances were passing over the neighbourhood of the initiation point the plume would have greater spread than if the centres of depressions were following a track to the north. Another pair of plumes is shown in Figures 2 and 3 also initiated at 700 mb. In these cases the date of the individual trajectories is indicated by a figure at the end.

General theory

Let us suppose that a large number (N) of trajectories be drawn at regular intervals of time T/N from a particular point in the earth's atmosphere. After an interval of t hours a typical trajectory has extended to the point x_t, x_t being the vector from the point of origin to the end point of the trajectory as shown in Figure 4. Let V be the vector wind at any point on the trajectory. Then by the simple summation of vectors

$$x_t = \int_o^t V\,dt \qquad (1)$$

Further, if we sum over the N trajectories we get

$$\frac{\sum x_t}{N} = \frac{1}{N}\int_o^t \sum V\,dt \qquad (2)$$

which may be written $$[x_t]_T = \int_o^t [V]_T\,dt \qquad (3)$$

the brackets indicating that a mean over the period T is taken and accordingly

$$x_t - [x_t]_T = \int_o^t \{V - [V]_T\}\,dt = \int_o^t v_T\,dt \qquad (4)$$

where v_T is the vector departure from the mean taken over the period T. That is, the vector departure from mean of the trajectory ends can be obtained from the integral with time of the vector departure from means of the wind. Moreover if S is the standard vector deviation of the end point of the trajectories at time t after initiation

$$S^2 \equiv \overline{\{x_t - [x_t]_T\}^2} = \int_o^t \{v(a)\}\,da \int_o^t \{v(b)\}\,db \qquad (5)$$

If we define σ_T to be the standard vector deviation of wind in the period T, i.e.,

$$\sigma_T^2 = \overline{\{v(a)\}^2} = \overline{\{v(b)\}^2} \tag{6}$$

equation (5) gives

$$S^2 = \sigma_T^2 \int_0^t da \int_0^t r_T(a-b)\, db \tag{7}$$

where $0 \leq a \leq t$, $0 \leq b \leq t$ and $r_T(a-b)$ is the stretch vector correlation coefficient* between $v(b)$ and $v(a)$. But $r_T(a-b)$ is an even function so if we consider only $a \geq b$ and put $a-b=\xi$, $0 \leq \xi \leq a$, then the contribution to the double integral from $a \geq b$ is

$$\sigma_T^2 \int_0^t da \int_0^a r_T(\xi)\, d\xi \tag{8}$$

and there is an equal contribution from $a < b$ whence

$$S^2 = 2\,\sigma_T^2 \int_0^t \int_0^a r(\xi)\, d\xi\, da \tag{9}$$

Differentiating twice we see that

$$r_T(t) = \frac{1}{2\sigma_T^2} \frac{d^2 S^2}{dt^2} \tag{10}$$

Expression (9) is of the same type as that given by Taylor (2).
Now

$$\overline{\{V(a)-V(t)\}_T^2} = \overline{\{v(a)-v(b)\}_T^2} = \overline{v(a)_T^2} + \overline{v(b)_T^2} - 2\,\overline{v(a)_T \cdot v(b)_T} \tag{11}$$

$$= 2\,\sigma_T^2 - 2\,\sigma_T^2\, r_T \tag{12}$$

and from equations (9) and (12) we can say

$$S^2 \equiv \overline{\{x_t - [x_t]\}^2} = \sigma_T^2 t^2 - \int_0^t \int_0^b \overline{\{V(a)-V(b)\}^2}\, da\, db \tag{13}$$

The form of $r(t)$

It was pointed out by Sutton (1) (p.284) that for motion near a smooth boundary dimensional considerations require

$$r(t) = f\left(\frac{\omega' t}{V}\right) \tag{14}$$

/where

* For the definition of the "stretch vector correlation coefficient" vide Geophysical Memoir 93 or Prof. Notes 121.

where ν is the kinematic viscosity and $\overline{\omega^2}$ the mean square eddy velocity. For large scale horizontal diffusion a similar argument would lead to

$$\tau(t) = f\left(\frac{\sigma^2 t}{K}\right) \tag{15}$$

where σ is the standard vector deviation of wind and K the eddy viscosity for lateral mixing.

Sutton proposed the expression

$$\tau(t) = \left(\frac{\nu}{\nu + \overline{\omega^2} t}\right)^n \tag{16}$$

where n is a numerical constant between 0 and 1. When the boundary is dynamically rough, the kinematic viscosity may be replaced by the macro-viscosity $N = u_* z_0$ where u_* is the friction-viscosity and z_0 the roughness-length (Sutton p.82).

Thus N has no direct counterpart in the free atmosphere. Sutton pointed out that provided ν in equation (16) could be ignored in relation to $\overline{\omega^2} t$, S in equation (9) had the form of a power law. The success of this treatment was attributed to the power law taking account of the effects of larger and larger eddies, the further and further the observational position receded from the source of smoke in Sutton's experiments.

Now for values of t greater than, say, t^* large scale diffusion in the free air is controlled by the largest eddies, which in middle latitudes consist of travelling cyclones and anticyclones, and the general long wave pattern, and which are not restricted in size in the way that eddies are restricted by the proximity of a physical boundary. The eddies in the free atmosphere that are concerned in any long period of diffusion may indeed be of various sizes, but their average size does not change with time in any systematic way. Hence $\tau(t)$ might well approximate to a simple exponential function

$$\tau(t) = \exp.(-\alpha t) \quad , \; t \text{ greater than } t^* \tag{17}$$

Taylor and others have suggested the exponential law in the past but we infer from the previous argument that the coefficient α has dimensions of σ^2/K. In the sequel this form is taken as

$$\tau(t) = \exp.\left(-\frac{\sigma^2 t}{K}\right) \tag{18}$$

which is shown to be physically reasonable, although there may be a suppressed non-dimensional factor of order unity in the index.

It is to be noted that if in expression (16) we put K the eddy viscosity for lateral mixing in place of ν and σ the standard vector deviation of wind in place of $\left(\overline{\omega^2}\right)^{\frac{1}{2}}$, K cannot be ignored in relation to $\sigma^2 t$ unless t is of the order of days. Hence it cannot be argued by a precisely similar argument to that put forward by Sutton that $\tau(t)$ should obey a power law for diffusion on the scale discussed in this paper. Nevertheless a large amount of work has been done on fitting a power law to the data obtained from trajectories and a considerable success has been obtained to which reference is made at the end of the present paper.

It is important to realise that for testing the form of $\tau(t)$ measurements must be made within ranges which are rather strictly confined. It has been pointed out by Taylor that when t is small and $\tau(t)$ is nearly unity then S is initially nearly $\sigma_1 t$; also that if $\tau(t)$ is zero for all $t \geq t_1$, $\int_0^t \tau(\xi)\, d\xi$ tends to a finite limit as t increases and consequently S varies as $\sqrt{t}$ when t is much greater than t_1 no matter what the form of $\tau(t)$

is for values of t less than t_1. More particularly we have for t greater than t_1, $S^2(t) = k(t - t_1) + S^2(t_1)$ where k is a constant. This gives a simple formula for diffusion for times exceeding t_1 and incidentally shows clearly that if we wish to examine the form of $\gamma(t)$, it will not help if we extend the time during which the samples are followed much beyond this critical time t_1.

In the case of geostrophic trajectories in the free air the critical time would appear to be about 40 hours but for the surface trajectories about 18 hours. Consequently in the discussions of the form of $\gamma(t)$ we have not made use of data for trajectories beyond 36 and 18 hours respectively.

However, if we assume that $\gamma(t)$ is exponential in form we can calculate the dispersion of the end points of the trajectories after they have been followed for a given time t by use of (9) which on integration gives

$$\frac{S}{\sigma_T} = \frac{\sqrt{2}}{\alpha}\sqrt{\alpha t - 1 + e^{-\alpha t}} \qquad (19)$$

and the values of S can then be compared with data such as those given in Appendix I.

It is to be noted that for times somewhat greater than t_1, which make $e^{-\alpha t}$ small but for which αt is not great in comparison with unity, there is a range in which S^2 is approximately equal to $2\sigma_T^2\left(\frac{t}{\alpha} - \frac{1}{\alpha^2}\right)$ and so given values of S_1 and S_2 at times t_1 and t_2, both of which are greater than the critical value mentioned above, we can obtain the value of α from the formula

$$\alpha = 2\sigma_T^2 \frac{t_2 - t_1}{S_2^2 - S_1^2} \qquad (20)$$

or since $\alpha = \frac{\sigma_T^2}{K}$ we can obtain K in the form

$$K = \frac{\sigma_T^2}{\alpha} = \frac{S_2^2 - S_1^2}{2(t_2 - t_1)} \qquad (21)$$

Here K is the eddy viscosity for lateral mixing and is seen to be obtainable directly from the spread of the end points of the trajectories, no matter what the standard deviation of the wind, provided always that the assumption of an exponential form for γ is correct.

Magnitude of errors involved in using geostrophic trajectories

Before proceeding to the discussion of the results a word must be said as to the errors likely to arise in taking the geostrophic trajectories as representative of the true motion of the atmosphere. The principal causes of error are (a) inaccuracy in measurement of geostrophic winds and (b) the inherent unrepresentativeness of the geostrophic wind as a picture of the true air flow. The magnitude of these errors over the British Isles is given by Murray (11) and a note on their effects on trajectories by Durst and Davis (12).

Let the true wind be $V + v$ and the error be ϵ then the erroneous correlation coefficient between $v(a)$ and $v(b)$ becomes $\gamma_T' = \frac{\{v(a) + \epsilon_1\}\{v(b) + \epsilon_2\}}{\sigma_T^2 + \epsilon^2}$

/instead

instead of the true value $\frac{\overline{v(a).v(b)}}{\sigma_T^2}$. Moreover, if we can assume there is little or no correlation between ϵ_1 and ϵ_2 or between ϵ_1 and $v(a)$ ....., except possibly very near time $t = 0$,

$$r_T' = \frac{\overline{v(a).v(b)}}{\sigma_T^2 + \overline{\epsilon^2}} \qquad (22)$$

If $\overline{\epsilon^2}$ is small in comparison with σ_T^2 we get

$$r_T - r_T' \doteq \frac{\overline{\epsilon^2}}{\sigma_T^2} r_T \qquad (23)$$

If we go back to equation (9) and use the value of σ_T^2 deduced from the actual measurements of velocities (i.e., if we really use $\sigma_T^2 + \overline{\epsilon^2}$) we see that $\sigma_T^2 + \overline{\epsilon^2}$ occurs in fact in both numerator and denominator and in consequence there is no consistent error in S due to errors in the measurements of velocities.

It is true that a large value of ϵ_1 will lead to the apparent trajectory running away from the true trajectory with in consequence a large value of ϵ_2. This effect is discussed by Durst and Davis (12). After 36 hours the results of this effect might produce an error of 250 to 350 km for individual trajectories at 700 mb and when one looks at the magnitude of the standard deviation of end points given in Appendix I it is clear that an error of such an amount may on some occasions produce an effect which is an appreciable proportion of the true S. However, on the whole the error involved in using geostrophic trajectories in determining the values of S is probably not more than 10 per cent at any rate for trajectories extending to 36 or 48 hours.

Empirical values of the correlation coefficient $r(t)$

The values of $r(t)$ have been evaluated from two types of data, (a) from a series of constant level balloons which were flown at 300 mb for periods of 2, 3 or 4 days, the results of which have been published (3) in America, (b) from a considerable series of geostrophic trajectories at levels of 300, 500, 700 mb and some from surface charts. The values from the constant level balloons are set out in Table I, those of the geostrophic trajectories in Table II.

Table I. Values of $r(t)$ derived from constant level balloons flown at 300 mb over America and the North Atlantic in latitudes north of 40° N.

Time interval (hours) (t)		2	4	6	8	10	12	14
Number of pairs of observations		59	51	43	35	31	27	24
Standard differences	N-S	19	22	28	30	33	38	39
	E-W	17	19	22	25	28	30	32
	Vector	26	29	35	39	43	49	50
r (t)		0.72	0.66	0.50	0.38	0.24	0.02	-0.02
α x 10^5 sec^{-1}		4.5	2.9	3.2	3.4	3.9	?	?

In Table I the value of $r(t)$ has been calculated from the mean square differences between observed velocities at a different time interval by means of equation (12), the standard vector deviation being 35 kt. By proceeding in this way it was possible to obtain a considerable number of comparisons from a limited number of trajectories. The correlation coefficients nearly follow an exponential law and values of α have been calculated on the assumption that $r(t)$ is of the form $e^{-\alpha t}$. The mean value of α is 3.6×10^{-5} sec^{-1} (or 0.13 hr^{-1}). If α is $\frac{\sigma^2}{K}$ we find the value of K to be 9.3×10^{10} in c.g.s. units.

/There

There is however a difficulty in that there are errors in the positioning of the balloons which are stated to range from 20 miles in the case of good fixes to 40 miles in the case of moderately good fixes and up to 60 miles in the case of poor fixes. From internal evidence, however, it is clear that these figures are excessively high, and although any correction for position error will tend to increase all the correlation coefficients, the resulting increase in the value of K would be hardly significant.

Secondly we can use data derived from geostrophic trajectories. In Appendix I there are set out the standard vector deviations of the end points after the trajectories had been followed for various times and also the vector mean distance that the end points had reached during those times.

Further, for a number of groups of trajectories the winds have been tabulated after each time interval and the actual correlation coefficients between the velocity at one time and that at a subsequent time on the same trajectory have been calculated. In Table II there are given the correlation coefficients between measured geostrophic winds at one time and measured geostrophic wind at the appropriate point on the same trajectory at a subsequent time. The number of trajectories on which they are based is given but on each trajectory a number of pairs of points can be taken with the same time interval so that the correlation coefficients are based on several times as many pairs as the number of trajectories, the number of pairs being entered in brackets in the table. Correlation coefficients are given separately for the south-north direction (S) and the east-west direction (W) and a vector correlation coefficient is also calculated and entered below the others. In October and November, 1949 each month was split up into six periods of five days and departures from 5-day means were formed so that the average correlation coefficients were calculated for 5-day periods of initiation. Some specimens of the relationship between $\log_{10} r(t)$ and t are shown in Fig. 5.

The mean value of the logarithms of the correlation coefficients for 12 hours in Table II is -0.238, for 24 hours is -0.464, and for 36 hours is -0.703; the mean value of the standard vector deviation is 18 kt. These values of $\log_{10} r(t)$ have been plotted in Fig. 6 and fit a relationship such that

$$r(t) = e^{-\alpha t}$$

where $\alpha = 1.25 \times 10^{-5}$ sec^{-1} or 0.045 hr^{-1}

If then $\alpha = \frac{\sigma^2}{K}$ and $\sigma = 18$ kt,

$$K = 6.8 \times 10^{10} \text{ cm}^2/\text{sec}.$$

During 1943 to 1946 a very close network of stations was maintained over the British Isles and observations were plotted at 3-hour intervals. Surface geostrophic trajectories were drawn from two points over the British Isles on eight days chosen at random. These trajectories were pursued for 24 hours and new ones initiated every three hours (nine times) so that the period of initiation of each family of trajectories was 27 hours. The winds were measured every three hours and correlation coefficients were calculated for 6, 12, 18 and 24-hour intervals from the 18 comparisons for each family. The results are set out in Table III.

/Table III

Table III. Vector correlation coefficients from surface geostrophic trajectories over the British Isles

Date	Number of trajectories	Standard vector deviation (kt)	Time interval (hours) 6	12	18	24
21/22 Sept., 1943	18	11.3	0.27	0.04	0.02	-0.06
25/26 Sept., 1943	18	7.7	0.43	0.59	0.10	0.21
3/4 March, 1944	18	8.7	0.18	-0.08	0.01	0.13
6/7 March, 1944	18	6.9	0.16	0.02	0.18	0.01
16/17 June, 1944	18	12.9	0.56	0.14	0.07	-0.33
22/23 June, 1944	18	6.9	0.36	-0.29	-0.59	-0.55
12/13 Dec., 1946	18	4.9	0.19	-0.04	0.17	-0.16
16/17 Dec., 1946	18	8.7	0.09	0.07	0.35	0.33
Mean		8.5	0.28	0.06	0.04	-0.05
α $\{$ or $-\frac{1}{t}\log_e r(t)\}$ $\times 10^5$ sec^{-1}			6.1	6.4	5.0	

from which $K = 3.3 \times 10^9$ cm^2/sec.

There seems then to be fairly strong evidence that the correlation coefficients between the winds at the end points of the trajectories follow closely an exponential law in view of the small difference in α calculated for various times in Tables I and III and the impressive linearity in the points on Figure 6. The calculated values of K differ somewhat in the three cases but they are of the same order of magnitude as the values deduced by Haurwitz (4) who quotes 4×10^7 gm/cm/sec for the exchange coefficient derived from the transport of heat across parallels of latitude. To obtain the corresponding figure for the eddy viscosity we have to divide this value by the density, i.e., by 9×10^{-4} gm/cm^3 at 700 mb and 7×10^{-4} gm/cm^3 at 500 mb, so obtaining $4 \times 10^{+10}$ cm^2/sec for 700 mb and $6 \times 10^{+10}$ cm^2/sec for 500 mb. Other values of the exchange coefficient have been derived by Lettau (5) which vary with latitude from 4.4×10^7 gm/cm/sec in latitude 35° to a maximum of 8.2×10^7 gm/cm/sec in latitude 50° to 55° (these correspond to $K = 5 \times 10^{10}$ and 9×10^{10} cm^2/sec respectively).

This then gives some grounds for believing that the identification of K derived from trajectories with the coefficient of eddy viscosity for lateral mixing is correct.

In Table IV, values of α and K are set out which have been derived in three independent ways. First in the columns marked A, they have been derived by the direct calculation of correlation coefficients from the velocities at various intervals of time. These coefficients given in Tables II and III have been fitted to an exponential from which α has been derived and hence K.

Secondly in the columns marked B, the values of S/σ_T have been calculated from the data in Appendix I for various values of t up to 36 hours for the trajectories in each group at 300, 500 and 700 mb (18 hours for the surface

/trajectories).

trajectories). These have been plotted on diagrams such as Figure 7 and the value of α was chosen for which the S/σ_T gave the best fit, and again K was appropriately calculated. Figure 8 shows some specimens of the fits. Thirdly in the columns marked C, the value of K has been calculated from the data in Appendix I by the use of equation (21). In these calculations t_1 was chosen to be 36 hours in the upper air groups (and 18 hours in the surface trajectories), t_2 was chosen appropriate to the biggest value of t available, (72 hours in many cases).

Thus there were two, or in some cases three, estimates of K available, and a mean value of these was taken, and compared with the corresponding standard vector deviation (σ). The correlation coefficient of K and σ was found to be 0.85, but the correlation between σ and α was small.

The regression equation of K on σ is

$$K = 7.8 \times 10^7 \sigma - 10^{10} \qquad (24)$$

where K is measured in cm^2/sec and σ in cm/sec. Figure 9 shows by dot diagram the distribution of the results of groups of trajectories. In the diagram, the large filled-in circles are used to represent initiation periods of two or three months, and three crosses indicate the mean values of K deduced from Tables I, II and III. It may be noted that if the two groups measured at 300 mb July, 1947 and February, 1948 were excluded, the correlation coefficient would be even higher at 0.883 leading to a regression equation

$$K = 9.7 \times 10^7 \sigma - 2.75 \times 10^{10} \qquad (25)$$

The expression of S as a power of the distance travelled

Contemporaneously with the preceding analysis work was done on fitting the data contained in the appendix to a power law of the form

$$S = \frac{C}{\sqrt{2}} (x)^{1-\frac{n}{2}} = \frac{C}{\sqrt{2}} (x)^{a} \qquad (26)$$

where S, as before, is the standard vector deviation of the end points of the trajectories, x the mean vector distance from the point of initiation and C and n are arbitrary constants.* Regression equations were formed of log S on log x for various time intervals up to 24 or 36 hours. This was done in the 27 cases set out in Appendix I. The correlation coefficients were very high, being 0.94 or over in all cases and 0.99 or over in 25 out of the 27, but not too much weight can be attached to such values when the logarithms of numbers are being compared. The value of a varied from 0.53 to 1.21 with an average value of 0.870. The values of C varied, of course, with the unit used, but also with the period of initiation three months, one month, a fortnight or 27 hours as the case might be; more will be said of this below.

On quite a different scale there are some rather similar data available made from series of smoke puffs fired from aircraft above a camera obscura, in a manner described by Durst (6). These puffs were plotted in the camera obscura with trajectories lasting a minute or a minute and a half; the period of initiation was generally $\frac{3}{4}$ hour to an hour. From these trajectories a plume could be made up in just the same way as is shown in Figure 1 and standard vector deviations of the end points of these trajectories were found after various time intervals. Ten such families of trajectories were worked up; the mean value of a was 0.926, the mean value of C was 0.15 in kilometre units and 0.21 in metre units.

/A

* Expression (26) is of the same form as that which Sutton derives from (16). His derivation cannot however be appealed to here as it would require $K/\sigma^2 t$ to be negligible and that is not the case over the range of t concerned in this paper. Hence (26) must be regarded as a purely empirical formula.

A further collection of wind observations made by smoke puffs at various heights has been discussed by Jones (7). In that case the trajectories were initiated over half-hourly periods and the value of C found when units are in centimetres was 0.275 $cm^{\frac{2}{3}}$. The value of the index, a, is not available, however, if we assume arbitrarily that the index is 0.875, the value of C in metre units is 0.16 and in kilometre units is 0.06.

The American constant level balloons referred to earlier were not suitable to provide data for working up in this manner but Moore, Smith and Gaalswick (8) have discussed some cases in which two or three balloons have been launched at the same time from neighbouring sites. From photographs in the Journal of Meteorology it would seem that the initial distance apart of the balloons was of the order of 100 feet. This would correspond to a time interval of release of no more than 30 seconds even in a very light wind. In three cases two balloons were released together and in one case three balloons, which gave in all six pairs of balloons. The distance apart of the pairs after they had travelled for a long time were as follows:

Table V. Distance apart of constant level balloons

Number of balloons	Distance of flight		Distance balloons apart		Distance apart "corrected" to 1200 miles (1930 km)
	statute miles	km	statute miles	km	
2	850	1360	20	32	43 km
2	775	1250	13	21	31 km
3	1200	1930	1, 5, 5	$1\frac{1}{2}$, 8, 8	$1\frac{1}{2}$, 8, 8 km
2	1640	2630	18	29	22 km

Since the distances of the flights (l) were not the same a "correction" was made to the separation of the balloons by the formula -

$$\text{corrected separation} = \text{observed separation} \times \left(\frac{1930}{l}\right)^{0.875}$$

The root mean square of these "corrected" distances is 24 km after travel of 1930 km and the value of the vector standard deviation of a cluster of balloons which were separated by these distances would be $24/\sqrt{2}$ km or 17 km. If we assume that this standard deviation is $C/\sqrt{2}$ times the distance travelled raised to the power of 0.875, we can get a value of C from the equation

$$\log \frac{C}{\sqrt{2}} = -0.875 \log (1930) + \log 17 \qquad (27)$$

When the units are kilometres, C is 0.032 (or 0.018 for 100 kilometre units).

In addition Sutton (9) made an estimate of the value of C from the dispersion of balloons described by Richardson (10). They were released over about three hours and the value of C was 0.92 $cm^{\frac{2}{3}}$. Sutton also made an estimate of C of 0.30 $cm^{\frac{2}{3}}$ from his own observations of smoke over a grass lawn, the observations lasting about 3 minutes. If the value of a is 0.875 these amounts are equivalent to 0.52 in metre units and 0.22 in kilometre units in the case of Richardson's balloons and 0.17 in metre units and 0.07 in kilometre units in the case of Sutton's observations.

Summary of comparisons of C and a and T

The values of C derived from all the observations mentioned above have been collected together in Table VI and classified according to the period of initiation T.

/Table IV

Table VI. Mean values of a and C arranged according to the duration of the "period of initiation" (T)

Type of observation	Period of initiation (T)	Duration of trajectories	Number of cases	Mean value of a	Value of C' 100 km	km	m
Geostrophic trajectories	3 months	36 hours	2	0.865	3.08	7.67	-
" "	2 months	36 hours	1	0.815	2.35	5.40	-
" "	1 month	36 hours	8	0.844	(3.07)	(8.36)	-
" "	15-28 days	36 hours	8	0.909	(1.82)	(2.23)	-
" "	27 hours	24 hours	8	0.848	(0.63)	(1.43)	-
Richardson's balloons	5 hours	-	-	-	-	0.22	0.52
Smoke puffs	$\frac{3}{4}$ hour	1 minute	10	0.926	-	(0.12)	(0.21)
Smoke puffs	$\frac{1}{2}$ hour	-	-	-	-	0.06	0.16
Sutton's smoke	3 minutes	-	-	0.875		0.07	0.17
Constant level balloons	$\frac{1}{2}$ minute	-	6	-	0.02	0.03	-

The modal values of C are put in brackets when they can be derived. The modal value of a for all the geostrophic trajectories combined is 0.878 and for the 10 smoke puffs is 0.95.

These have been compared by plotting the logarithm of "the period of initiation" (T) against the logarithm of the mean value of C in kilometre units. The result is shown in Figure 10. The correlation coefficient between $\log T$ and $\log C$ is 0.973 and the regression equation is

$$\log T = 1.99 \log C + 5.07$$

which gives $$C = 0.003\ T^{\frac{1}{2}} \qquad (28)$$

where C is expressed as $km^{\frac{1}{8}}$ and T in seconds

or $$C = 0.18\ T^{\frac{1}{2}} \qquad (29)$$

where T is expressed in hours with the qualification that it is greater than 0. It has been pointed out to us by Sir Graham Sutton that this result has been obtained theoretically by E. Inoue (15) who has shown that the diffusion angle of a smoke plume near its source increases in proportion to the square root of the time of averaging, or in our notation S at a constant distance from the source is nearly proportional to $T^{\frac{1}{2}}$.

The diffusion laws in relation to time scale

From this work it would seem that there is a remarkable agreement between the values of K (the coefficient of large scale horizontal diffusion) which we have found and that derived by other workers by quite different methods. The inference is that the Lagrangian correlation coefficients follow an exponential law. However, the empirical relation between C and T set out above would seem to support the hypothesis that the power law applies to this type of diffusion.

We believe that both are indeed correct and that the scheme below sets out the modes of diffusion.

/Eddies

$t=0$ t^* t_2 $\rightarrow \infty$

	Eddies small in scale, effective size increasing with t		Diffusion controlled by large eddies, size distribution constant	
$r(t)$	near unity	given by power law	given by exponential law	effectively zero
Diffusion	$\sigma_T t$	$\frac{C}{\sqrt{2}}(\bar{u}t)^a$	$\frac{\sqrt{2}\,\sigma_T}{\alpha}\sqrt{\alpha t - 1 + e^{-\alpha t}}$	$P\sigma_T\sqrt{t}$

In this t is time along the trajectory, σ_T is the standard deviation of wind in the appropriate period of initiation, T, $\bar{u}$ is the mean velocity (so that $\bar{u}t$ is x) and P is a constant. It may be noted that C is a function of T and σ_T is also a function of T as can be seen in Appendix II, therefore C must itself be a function of σ_T.

It is perhaps to be expected that the value of t^* should not be precise, and that the power law and exponential forms should overlap over a considerable range of t, and this is indeed supported by what we have found from the geostrophic trajectories. We should expect the magnitude of t^* would vary from one experiment to another and to be intimately connected with the period of initiation.

Application of results to large scale diffusion in two dimensions

Instantaneous emission. In this case a 'cloud' is produced instantaneously at the source. The centre of gravity of the cloud travels along a wind trajectory, meanwhile the cloud itself spreads out (relative to its c.g.) by small scale diffusion. The examination of (geostrophic) trajectories through the source shows the area within which the centre of gravity of the cloud will have arrived after time t from the moment of generation. The most probable position will be that point arrived at by the mean trajectory (the trajectory followed by the mean wind) through the source (e.g., the appropriate monthly mean wind). If the distribution of the trajectory end-points and their standard deviation is known, the probability of the centre of gravity of the cloud arriving at any particular point at time t can be set down by assuming that the trajectories are distributed according to the exponential law. We have not been able to assemble any data on the growth of smoke clouds which would show the values of the constants in the exponential formula which are applicable to such short "periods of initiation" as are necessary for following a single cloud, if indeed the exponential law holds down to that range. Instead we have to fall back on empirical power law data which we have given in the second part of this paper. The growth of the cloud while it moves along the trajectory will take place according to local (small scale) diffusion; an approximation to the size of the cloud can be obtained by the assumption of a spreading by a power law. For this we need to know the "time of initiation" (T).

If we suppose the cloud from an explosion to be represented by a circle diameter A.B. (Figure 11) after the explosive effects are completed, which is embedded in a general wind of velocity V, the point A will be near B at a time AB/V, and we can expect the growth of the cloud after time t, represented by the difference between $A'B'$ and AB to be dependent on AB/V in the same way as the divergence of trajectories is dependent on the time of initiation.

From equation (29) we can expect then that the value of C appropriate to the diffusion of material from an explosion cloud will be given by $0.18\left(\frac{AB}{V}\right)^{1/2}$ if AB is measured in nautical miles and V is measured in knots.

If we use this value of C and a value of a of 0.875 it is possible to calculate the cross-wind dimensions of the cloud at various distances down wind. Suppose for instance that the wind in which the cloud is travelling is 15 kt and the initial diameter after the explosive effects have subsided is $\frac{1}{4}$ miles then

/ C expressed

C expressed in kilometre units is $0.052\ km^{\frac{1}{8}}$. After 12 hours the cloud would have travelled 180 miles (or 330 km) and from equation (26) S is 5.83 km or $3\frac{1}{4}$ n. miles. We can then suppose that this diffusion has taken place at each end of the diameter $C'D'$ in Figure 11 and in consequence the lateral diameter of the cloud will be of the order of 9 or 10 n. miles after 12 hours.

It will be noticed that in this example it has been assumed that there is no shear in the wind across the direction of travel of the cloud. Any such shear would tend to increase the spread of the cloud but that subject need not be pursued here.

Continuous emission. In this case only a point source need be considered. The cloud of particles is emitted as a continuous plume which broadens by small scale diffusion as it gets further and further (in time) from the source. First, however, we simply ignore the broadening of the plumes and concentrate on the distribution which results from the continuous variation of the trajectories with time. The distribution of the superposed end-points of trajectories emitted over a period may as a first approximation be assumed to follow the normal (circular) law. From this it follows that the probability of an end-point falling within an elemental area $dx\,dy$ is

$$\frac{1}{\pi S^2}\exp\left\{-\frac{x^2+y^2}{S^2}\right\}dx\,dy \qquad (30)$$

where S is the standard deviation of the distance of the end-points from the centre of mass and x, y are rectangular co-ordinates with origin at the centre of mass. The x-axis is taken in the positive direction of the mean trajectory. When referred to the source as origin, x must be replaced by $(s-\bar{u}t)$ where s is distance along the mean trajectory and $\bar{u}$ the constant (or average) velocity along it.

In the case of continuous emission the successive trajectories through the source may be considered as lying within a gradually broadening "plume" and we have to consider the concentration of material across the plume (i.e., normal to the mean trajectory) at a distance s from the source. This concentration is obtained by integrating (30) over all values of t. Making the substitution for x, we obtain an expression for the concentration of diffusing substance,

$$\chi = \int_{-\infty}^{\infty}\frac{Q}{\pi S^2}\exp\left\{-\frac{(s-\bar{u}t)^2+y^2}{S^2}\right\}dt \qquad (31)$$

where Q is the rate of emission (units of mass per unit time) and S, the scatter, is dependent on the standard deviation of the wind appropriate to the "time of initiation" and also the coefficient of horizontal diffusion. This expression gives the concentration per unit length across the mean trajectory at a distance s along it, i.e., it gives the concentration along the y-axis. The integration cannot, of course, be carried out explicitly but we notice that most of the matter comprising the concentration (31) will have left the source at about the time t previously, and for matter leaving much before or after that time the contribution to χ diminishes rapidly because of the exponential factor. Hence an approximation to (31) is obtained by regarding S as appreciably constant over a small range of t centred at $s/\bar{u}$. Thus approximately;

$$\chi = \frac{Q}{\pi S^2}\exp\left(-\frac{y^2}{S^2}\right)\int_{-\infty}^{\infty}\exp\left\{-\frac{(s-\bar{u}t)^2}{S^2}\right\}dt \qquad (32)$$

$$= \frac{Q}{\pi^{\frac{1}{2}} S\bar{u}}\exp\left(-\frac{y^2}{S^2}\right) \qquad (33)$$

in which S may now be regarded as a function of time or of distance, in either case measured along the mean trajectory through the source to the region considered.

If the broadening of the plume by small scale diffusion is taken into account, it may be shown that (32) remains a first approximation since the "coefficient of diffusion" appropriate to the trajectories is several magnitudes greater than the coefficient of small-scale diffusion.

Moreover S is dependent on the period of initiation in precisely the same way as has been discussed for the geostrophic trajectories and hence we can see how the plume gradually broadens with time owing to S increasing.

References

1. Sutton, O.G. Micrometeorology. McGraw-Hill, 1953.
2. Taylor, G.I. Diffusion by continuous movements. Proc. London Math. Soc., Ser.2, Vol.20, Part 3, 1920.
3. Mastenbrook, H.J. and A.D. Anderson. NRL Memo., Rep.240.
4. Haurwitz, B. Dynamic Meteorology. McGraw-Hill, 1941, p.266.
5. Lettau, H. Beit. Phys. Atm., 23, 45, 1936.
6. Durst, C.S. The fine structure of wind in the free air. Q.J.R. Met.S., 74, July-October, 1948, p.349.
7. Jones, R.F. Unpublished.
8. Moore, Smith and Gaalswyck. Journal of Meteorology. Vol. 11, p.167.
9. Sutton, O.G. Proc. Roy. Soc., A, Vol.135, p.158.
10. Richardson, L.F. and Procter. Mem.R. Met.S., Vol.1, No. 1.
11. Murray, R. On the accuracy of contour charts in forecasting upper winds. A.M. Prof. Note, 110, 1954.
12. Durst, C.S. and N.E. Davis. On the accuracy of geostrophic trajectories.
13. Durst, C.S. Variation of wind with time and distance. G.M.93, 1954.
14. Inoue, E. On the Lagrangian correlation coefficient for turbulent diffusion. Air Force Cambridge Research Center, Geophys. Res. Papers No. 19, Dec., 1952, p.397.

Table II. Values of $\Upsilon(t)$ derived from geostrophic trajectories

Date	Height	Number of trajectories	Standard deviation (kt)	Time interval 6h	12h	18h	24h	30h	36h	42h	48h
			S W	S W	S W	S W	S W	S W	S W	S W	S W
1-20 Feb., 1948	700 mb	20	19.5 21.5 29.0	0.696 0.797 0.745(240)	0.539 0.513 0.517(200)	0.402 0.487 0.437(160)	0.366 0.522 0.428(120)	0.326 0.435 0.364(80)	0.262 0.346 0.299(40)	- -	- -
17 Ap. - 4 May, 1950	700 mb	16	11.1 12.3 16.5	0.723 0.779 0.777(224)	0.577 0.628 0.609(192)	0.369 0.440 0.409(160)	0.262 0.350 0.314(128)	0.100 0.282 0.210(96)	0.076 0.295 0.210(64)	0.020 0.386 0.246(32)	
5-20 May, 1950	700 mb	16	6.3 6.9 9.4	0.731 0.700 0.715(224)	0.709 0.520 0.560(192)	0.500 0.457 0.477(160)	0.428 0.420 0.423(128)	0.271 0.438 0.362(96)	0.302 0.381 0.345(64)	0.140 0.183 0.162(32)	
1-15 June, 1950	700 mb	15	6.3 9.4 11.3	0.666 0.828 0.785(210)	0.463 0.750 0.663(180)	0.326 0.607 0.512(150)	0.304 0.505 0.443(120)	0.232 0.500 0.416(90)	0.262 0.337 0.310(60)	0.276 0.139 0.377(30)	
Oct., 1949	500 mb	30	21.2 18.1 27.9	- -	0.600 0.408 0.490(120)	- -	0.356 0.230 0.275(90)	- -	-0.013 0.148 0.057(60)	- -	-0.422 0.109 -0.150(30)
Nov., 1949	500 mb	30	13.3 18.0 22.4	- -	0.468 0.784 0.671(120)	- -	0.257 0.641 0.499(90)	- -	0.154 0.392 0.293(60)	- -	-0.057 0.156 0.055(30)
April, 1948	700 mb	15	11.2 13.7 17.7	- -	0.560 0.651 0.613(60)	- -	0.219 0.472 0.369(45)	- -	-0.115 0.284 0.095(30)	- -	-0.582 0.249 -0.075(15)
May, 1948	700 mb	16	11.4 11.8 16.4	- -	0.615 0.607 0.610(72)	- -	0.221 0.238 0.229(48)	- -	0.079 0.173 0.126(32)	- -	-0.009 0.080 0.037(16)
June, 1948	700 mb	15	11.6 10.0 13.2	- -	0.723 0.737 0.725(60)	- -	0.540 0.524 0.528(45)	- -	0.336 0.206 0.262(30)	- -	0.535 0.195 0.328(15)
1-15 Nov., 1947	700 mb	30	18.4 14.4 23.5	- -	0.617 0.653 0.635(150)	0.401 0.662 0.549(120)	0.371 0.548 0.468(90)	0.427 0.452 0.430(60)	0.456 0.395 0.401(30)	- -	- -
1-15 Aug, 1947	700 mb	30	7.5 6.0 9.6	- -	0.638 0.179 0.364(150)	0.385 0.070 0.204(120)	0.303 0.092 0.173(90)	0.295 -0.023 0.114(60)	0.330 0.013 0.130(30)	- -	- -
5-day periods											
Oct., 1949	500 mb	30	13.1 12.2 17.9	- -	0.336 0.168 0.251(120)	- -	0.135 0.060 0.118(90)	- -	-0.117 -0.021 -0.072(60)	- -	-0.380 0.132 -0.162(30)
Nov., 1949	500 mb	30	10.5 12.2 16.1	- -	0.378 0.680 0.554(120)	- -	0.149 0.441 0.312(90)	- -	0.193 0.392 0.324(60)	- -	-0.006 0.315 0.207(30)

Table IV. Values of α and K deduced from the geostrophic trajectories by various methods

Date	Height	Period of initiation	Average velocity over 36 hours		Standard vector deviation of wind (σ) (a) at point of initiation		(b) from all points up to 36 hours		Coefficient of eddy diffusivity for lateral mixing (A) derived from correlation coefficients		(B) derived from end-points of trajectories (0 to 36 hours)		(C) derived from end-points of trajectories by $K = \frac{S_2^2 - S_1^2}{2(t_2 - t_1)}$	
	mb	days	kt	m/s	kt	m/s	kt	m/s	hr^{-1}	cm^2/sec	hr^{-1}	cm^2/sec	hr^{-1}	cm^2/sec
Ap. to June, 1948	700	91	7	3.6	18	8.9					0.05	6.3×10^{10}	0.04	8.0×10^{10}
Oct. to Dec., 1949	500	92	21	10.3	28	14.4					0.05	14.8×10^{10}	0.07	10.5×10^{10}
17 Ap. to 15 June, 1950	700	47	9	4.6	14	7.2					0.05	9.3×10^{10}	0.04	5.0×10^{10}
April, 1948	700	30	14	7.0	21	10.4	18	9.1	0.049	6.1×10^{10}	0.07	4.6×10^{10}	0.05	7.0×10^{10}
May, 1948	700	31	6	3.1	15	7.7	16	8.3	0.053	4.8×10^{10}	0.03	6.1×10^{10}	0.05	4.5×10^{10}
June, 1948	700	30	3	1.3	11	5.7	13	6.8	0.030	5.5×10^{10}	0.02	5.8×10^{10}	0.02	5.5×10^{10}
October, 1949	500	30	25	12.6	33	16.9	28	14.4	0.064	11.6×10^{10}	0.03	3.4×10^{10}	0.10	10.5×10^{10}
November, 1949	500	30	14	6.9	28	14.0	22	11.5	0.032	14.8×10^{10}	0.07	8.3×10^{10}	0.06	11.5×10^{10}
December, 1949	500	31	21	10.3	21	10.5					0.06	6.6×10^{10}	0.03	12.0×10^{10}
July, 1949	700	20	8	4.2	15	7.4					0.01	2.0×10^{10}		
August, 1949	700	20	14	6.8	21	10.6					0.04	10.2×10^{10}		
February, 1948	700	20	24	12.0	24	12.1	29	14.5	0.042	17.5×10^{10}	0.06	8.7×10^{10}		
17 Ap. - 4 May, 1950	700	16	9	4.6	17	8.4	16	8.1	0.046	5.1×10^{10}	0.04	6.3×10^{10}	0.04	6.5×10^{10}
5 - 20 May, 1950	700	16	10	5.2	13	6.4	9	4.7	0.041	1.9×10^{10}	0.06	2.4×10^{10}	0.05	3.0×10^{10}
1 - 15 June, 1950	700	15	8	4.1	13	6.3	11	5.8	0.034	3.5×10^{10}	0.05	2.8×10^{10}	0.03	5.5×10^{10}
1 - 15 Aug., 1947	700	15	14	6.8	8	3.8	10	4.8	0.075	1.1×10^{10}	0.01	5.2×10^{10}	0.06	3.9×10^{10}
1 - 15 Nov., 1947	700	15	17	8.5	16	7.9	23	11.7	0.031	15.7×10^{10}	0.02	11.4×10^{10}	0.04	6.0×10^{10}
July, 1947	300	30	22	11.0	29	19.6					0.10	13.9×10^{10}	0.14	9.8×10^{10}
February, 1948	300	28	26	13.0	45	22.9					0.15	12.1×10^{10}	0.15	12.5×10^{10}
October, 1949	500	5					18	9.1	0.070	4.4×10^{10}				
November, 1949	500	5					16	8.3	0.043	5.8×10^{10}				
		hours	over 24 hours								(0 to 18 hours)			
21 - 22 Sept., 1943	Surface	27	16	7.8	10	5.0	11	5.8			0.15	8×10^9	0.09	10×10^9
25 - 26 Sept., 1943	"	27	14	7.1	8	4.1	8	3.9			0.10	5×10^9	0.61	1×10^9
3 - 4 March, 1944	"	27	18	9.2	6	2.9	9	4.4			0.20	3×10^9	0.04	7×10^9
6 - 7 March, 1944	"	27	11	5.7	4	1.9	7	3.5			0.35	1×10^9	0.07	2×10^9
16 - 17 June, 1944	"	27	13	6.4	14	7.0	13	6.6			0.10	15×10^9	0.13	14×10^9
22 - 23 June, 1944	"	27	8	4.0	5	2.6	7	3.5			0.50	1×10^9	0.24	1×10^9
12 - 13 Dec., 1946	"	27	17	6.8	3	1.6	5	2.5			0.75	0.3×10^9	0.09	1×10^9
16 - 17 Dec., 1946	"	27	14	6.8	5	2.4	9	4.4			0.30	2×10^9	0.03	7×10^9

G.23063(b)/MFW/7/57/50

Appendix I

Standard vector deviations of end-points of trajectories after various times

A. Cases at 300 mb

Time Hours	July, 1947 (300 mb) (30 trajectories) σ km	S km	February, 1948 (300 mb) (28 trajectories) σ km	S km
6	483	423	258	494
12	805	780	610	800
18	970	1060	940	990
24	1160	1210	1190	1180
30	1340	1420	1490	1410
36	1420	1570	1680	1580
42	1570	1760	1900	1750
48	1730	1820	2100	1890

B. Cases at 700 mb

Time Hours	August 1-15, 1947 (30 trajectories) σ km	S km	November 1-15, 1947 (30 trajectories) σ km	S km
6	124	83	211	171
12	237	209	417	362
18	409	266	597	510
24	513	344	765	687
30	666	390	905	805
36	887	430	1100	950
42	1026	460	1288	1098
48	1253	521	1500	1198
54			1742	1293
60			1975	1391

C. Cases at 700 mb

Time Hours	April, 1948 (15 trajectories) σ km	S km	May, 1948 (16 trajectories) σ km	S km	June, 1948 (15 trajectories) σ km	S km	April - June, 1948 (46 trajectories) σ km	S km
6	198	225	81	166	25	123	98	192
12	392	462	161	317	51	245	193	363
18	500	603	197	464	103	352	252	482
24	575	727	260	617	129	458	297	650
36	915	922	405	838	167	644	462	888
48	1255	1162	489	985	240	933	621	1142
60	1685	1435	563	1208	312	1168	801	1436
72	2045	1630	710	1357	423	1343	1014	1686

D. Cases at 500 mb

Time Hours	October, 1949 (31 trajectories) σ km	S km	November, 1949 (30 trajectories) σ km	S km	December, 1949 (31 trajectories) σ km	S km	Oct.-Dec., 1949 (92 trajectories) σ km	S km
6	197	364	87	302	183	226	150	310
12	442	688	218	509	372	424	330	566
18	690	1042	380	658	541	583	523	800
24	980	1337	510	890	770	744	755	1050
30	1291	1600	682	1100	1066	882	1030	1270
36	1630	1675	897	1378	1375	1028	1330	1430
42	1924	1870	1033	1562	1710	1160	1620	1630

Time Hours	October, 1949 (31 trajectories) x km	S km	November, 1949 (30 trajectories) x km	S km	December, 1949 (31 trajectories) x km	S km	Oct.-Dec., 1949 (92 trajectories) x km	S km
48	2255	1973	1253	1760	2100	1285	1950	1770
54	2485	2087	1500	1915	2358	1427	2225	1910
60	2655	2155	1710	2042	2750	1598	2530	2060
66	2820	2155	1937	2157	2840	1827	2700	2110
72	-		2250	2205	3530	2035	2800	2170

E. Cases at 700 mb

Time Hours	17th Ap.-4th May, 1950 (32 trajectories) x km	S km	5-20th May, 1950 (32 trajectories) x km	S km	1-15th June, 1950 (30 trajectories) x km	S km	17th Ap.-15th June, 1950 (94 trajectories) x km	S km
6	99	181	96	138	81	135	89	155
12	203	339	197	240	176	226	186	274
18	317	470	328	349	262	340	302	393
24	408	604	441	440	358	432	397	501
30	523	754	565	523	447	534	510	618
36	600	947	670	576	533	628	600	743
42	717	1067	805	682	621	747	716	853
48	837	1174	885	756	722	856	815	950
54	972	1325	975	832	810	968	912	1064
60	1127	1415	1110	914	867	1049	1046	1157
66	1244	1520	1225	995	1130	1220	1195	1270
72	1389	1613	1387	965	1410	1358	1388	1348

F. Cases at 700 mb

Time Hours	1-20th February, 1948 (40 trajectories) x km	S km	July, 1949 (20 trajectories) x km	S km	August, 1949 (20 trajectories) x km	S km
6	375	261	134	160	171	230
12	675	490	223	317	287	450
18	918	629	329	469	453	651
24	1113	807	405	615	594	827
30	1327	987	480	759	749	973
36	1549	1160	547	887	887	1137

G. Surface cases with time of initiation 27 hours

Time Hours	21/22nd Sept., 1943 (18 trajectories) x km	S km	25/26th Sept., 1943 (18 trajectories) x km	S km	3/4th Mar., 1944 (18 trajectories) x km	S km	6/7th Mar., 1944 (18 trajectories) x km	S km
3	87	54	49	44	105	31	77	21
6	183	103	90	79	202	63	145	43
9	275	144	174	103	295	94	201	59
12	375	186	261	144	407	113	254	71
15	472	223	351	158	502	148	311	88
18	554	257	453	180	613	167	345	113
21	618	293	528	191	709	210	419	134
24	671	331	611	197	792	247	496	150

Time Hours	16/17th June, 1944 (18 trajectories) x km	S km	22/23rd June, 1944 (18 trajectories) x km	S km	12/13th Dec., 1944 (18 trajectories) x km	S km	16/17th Dec., 1944 (18 trajectories) x km	S km
3	81	75	45	28	77	17	82	26
6	168	138	88	59	151	37	165	59
9	253	194	130	79	225	48	236	81
12	321	242	167	91	300	55	300	104
15	381	283	201	89	378	61	378	143
18	447	321	244	79	452	68	453	169
21	504	365	290	81	520	80	527	195
24	553	365	343	95	587	93	585	225

G.23063(c)/MFW/7/57/50

Appendix II

The values of σ_T over Southern England

The standard deviation of wind (σ_T) taken over intervals of duration T bears a ratio to the standard deviation over a long period (σ) depending on the value of T.

The ratios have been set out in Tables A and B. Table A was derived from the comparison of winds at 500 mb observed during 15 years at Larkhill (or Crawley) in the months of January and July. Table B was derived from data given in Geophysical Memoir 93 (14) which enabled the ratios σ_T to σ to be calculated.

Table A Value of σ_T (in kt) for various values of T

	T	1 day	2 days	4 days	8 days	1 mth.	3 mth.	5 mth.	15 mth.
January	σ_T	17.7	24.4	29.4	32.6	38.8	40.6	41.6	41.8
	σ_T/σ_{15}	0.40	0.58	0.70	0.78	0.93	0.97	0.99	1.00
July	σ_T	11.6	16.2	19.4	22.6	28.4	29.3	29.5	29.6
	σ_T/σ_{15}	0.39	0.55	0.65	0.76	0.96	0.99	1.00	1.00

Table B Values of σ_T/σ for various values of T

T	5 min.	15 min.	30 min.	1 hr.	6 hr.	12 hr.	24 hr.
σ_T/σ	0.037	0.062	0.088	0.111	0.22	0.30	0.41

σ being the long period value of the standard vector deviation of wind which is a constant for the appropriate region, season and level.

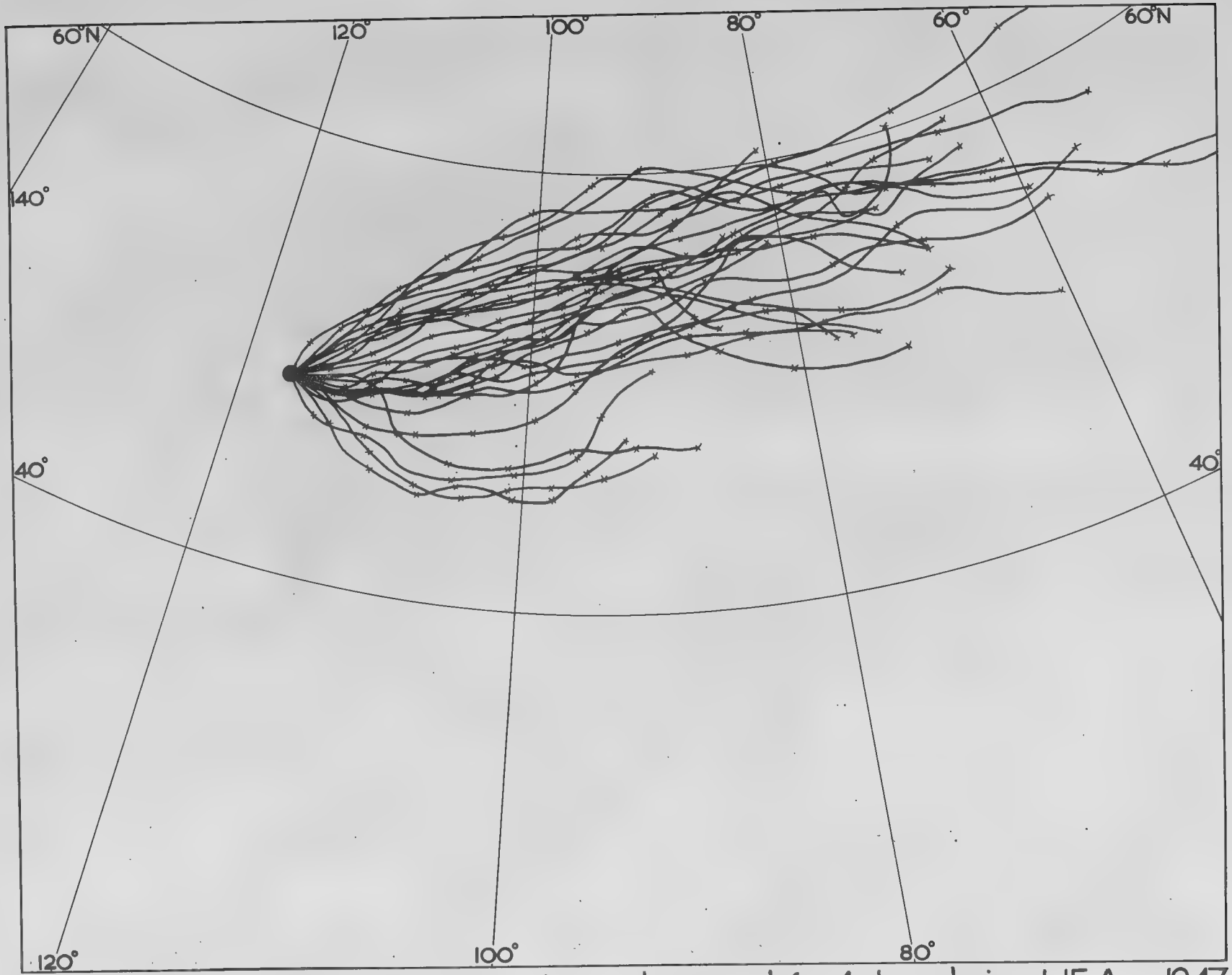

Fig. 1a Trajectories initiated twice a day and pursued for 4 days during 1-15 Aug. 1947.

Fig. 1b Trajectories initiated twice a day and pursued for 4 days during 1-15 Nov. 1947.

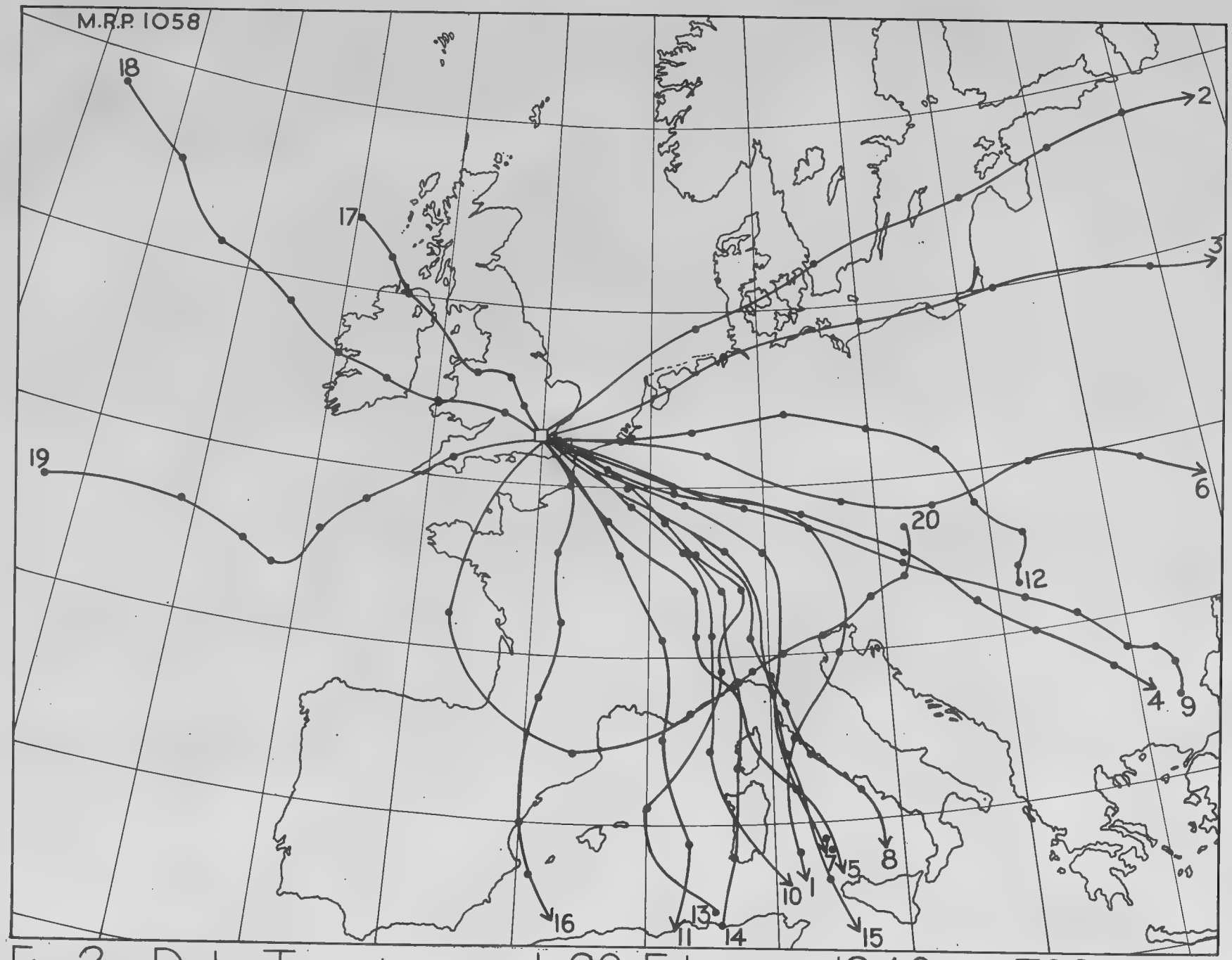

Fig. 2 Daily Trajectories. 1-20 February 1948 at 700 mb.

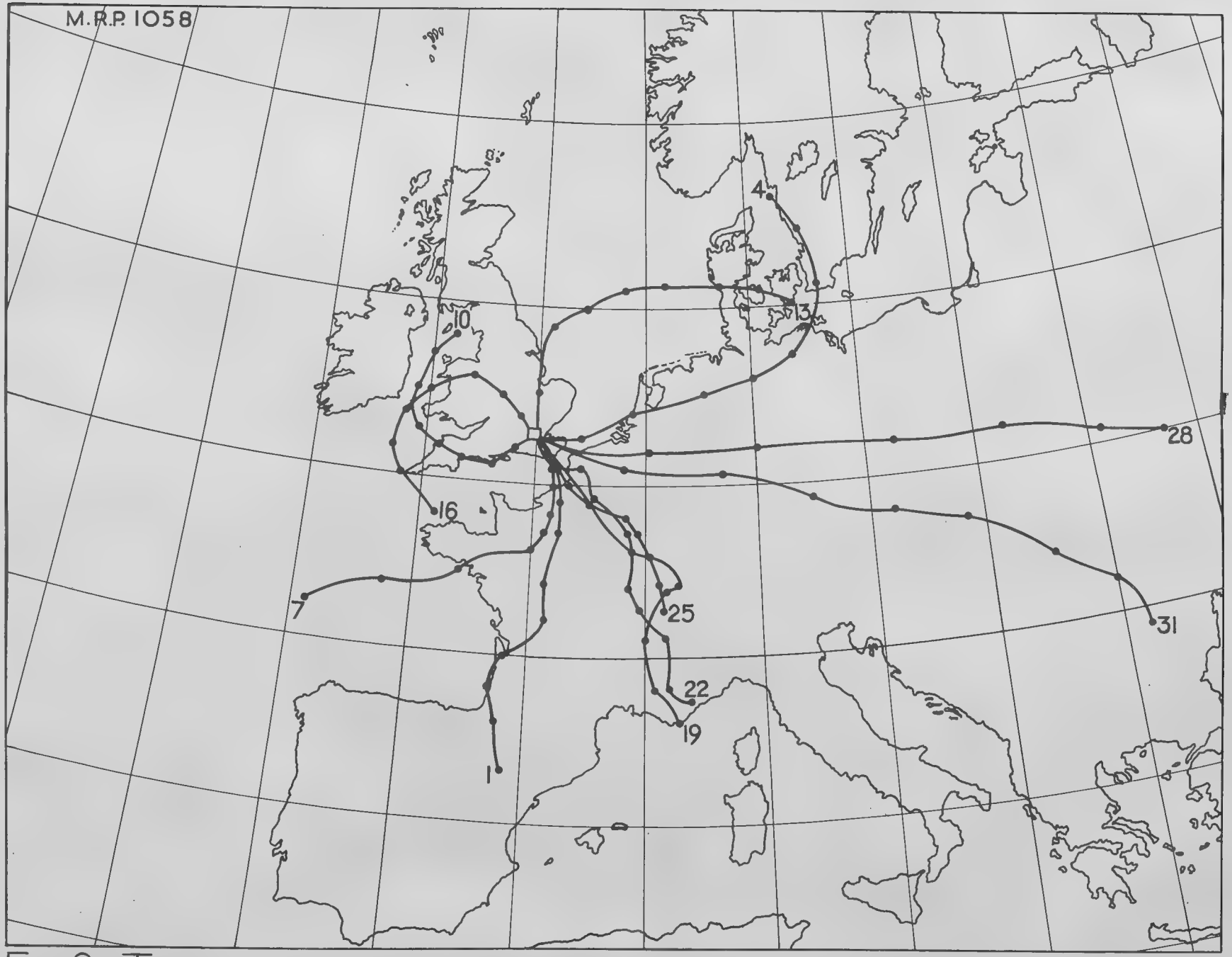

Fig. 3 Trajectories starting every third day. July 1949 at 700 mb.

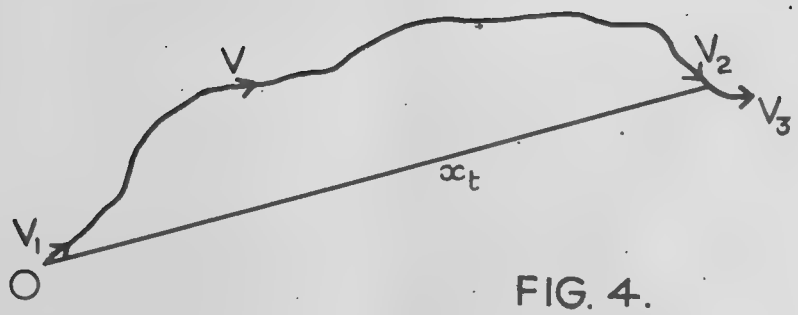

FIG. 4.

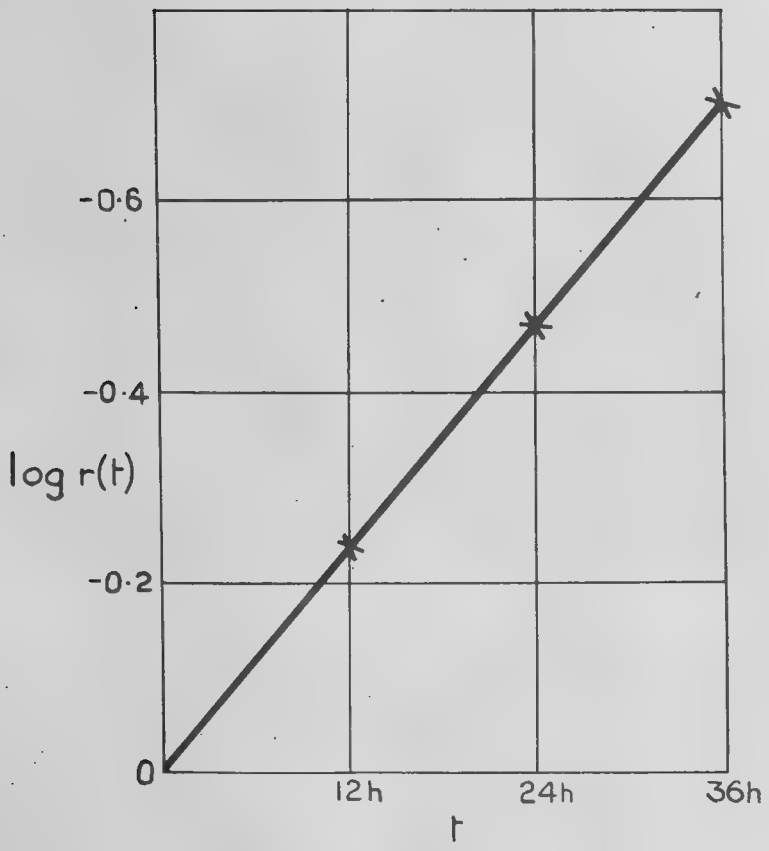

FIG 6. Relation of r(t) and t.

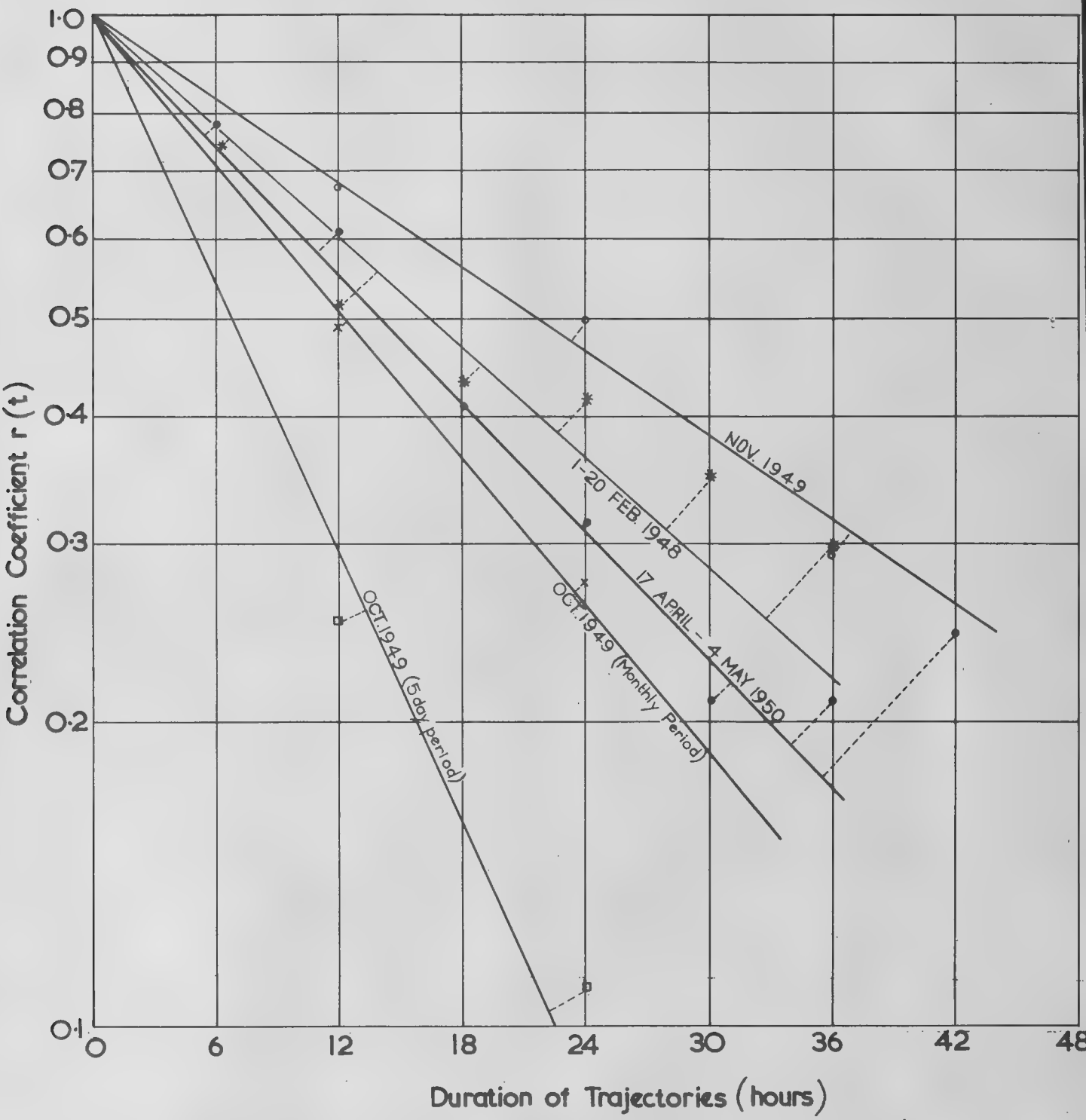

Fig. 5. Relation between correlation coefficient and the duration of trajectories.

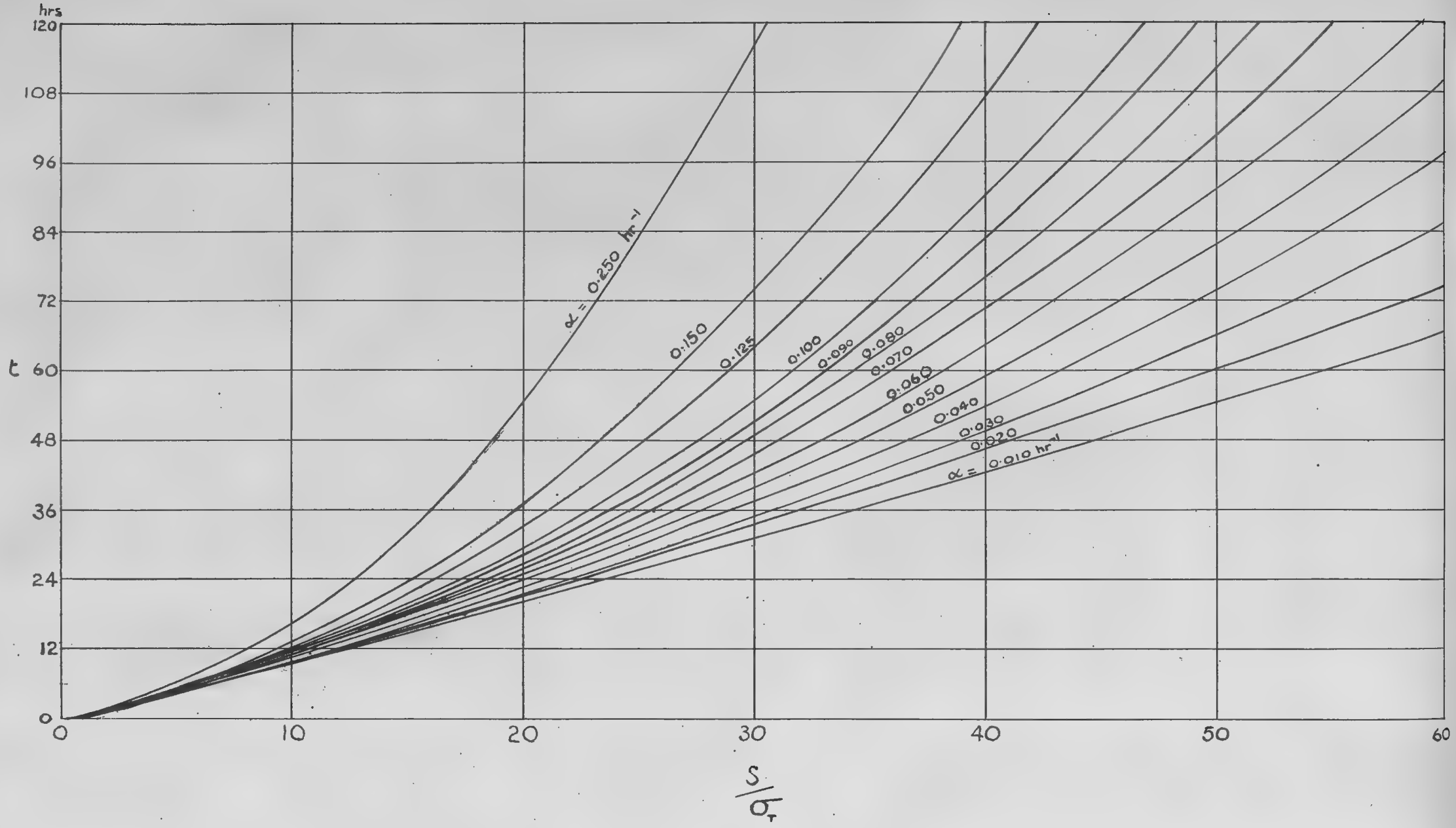

Fig 7 Values of ratio $\frac{S}{\sigma_T}$ for various values α and t

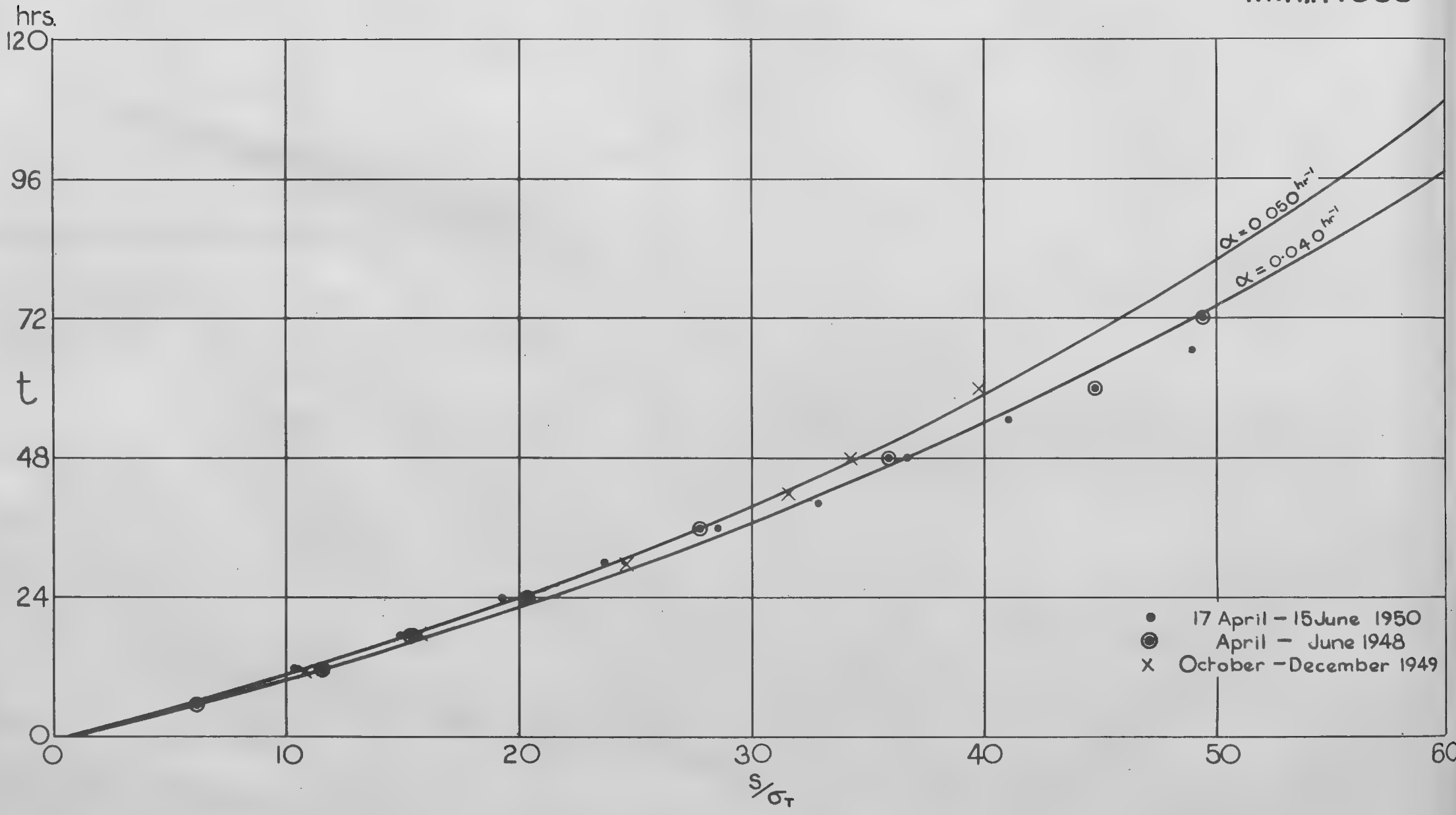

Fig 8 α obtained from Trajectories

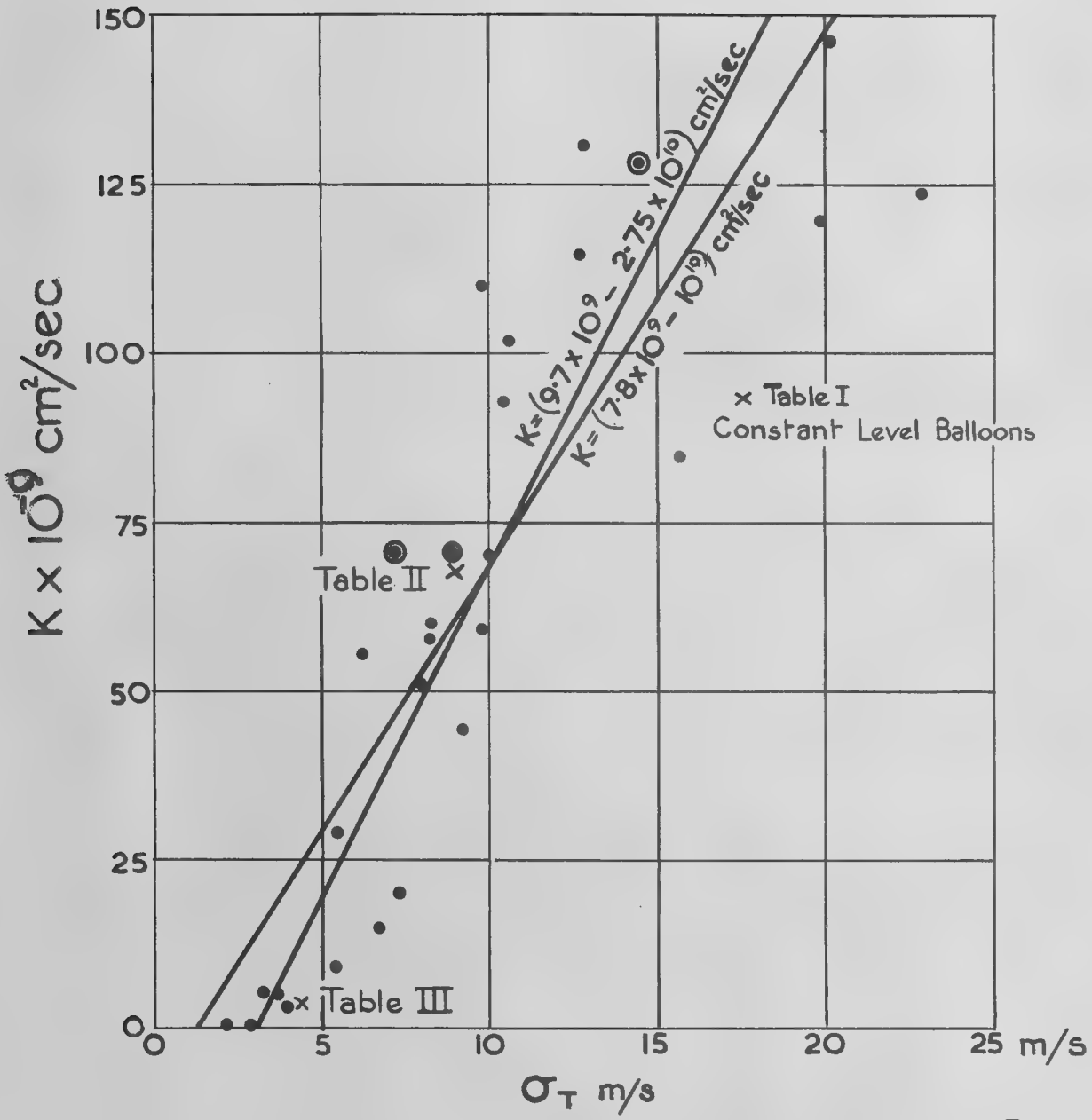

FIG. 9 Relationship between Standard Vector Deviation of wind (σ_T) and Coefficient of Eddy Viscosity for Lateral Mixing (K).

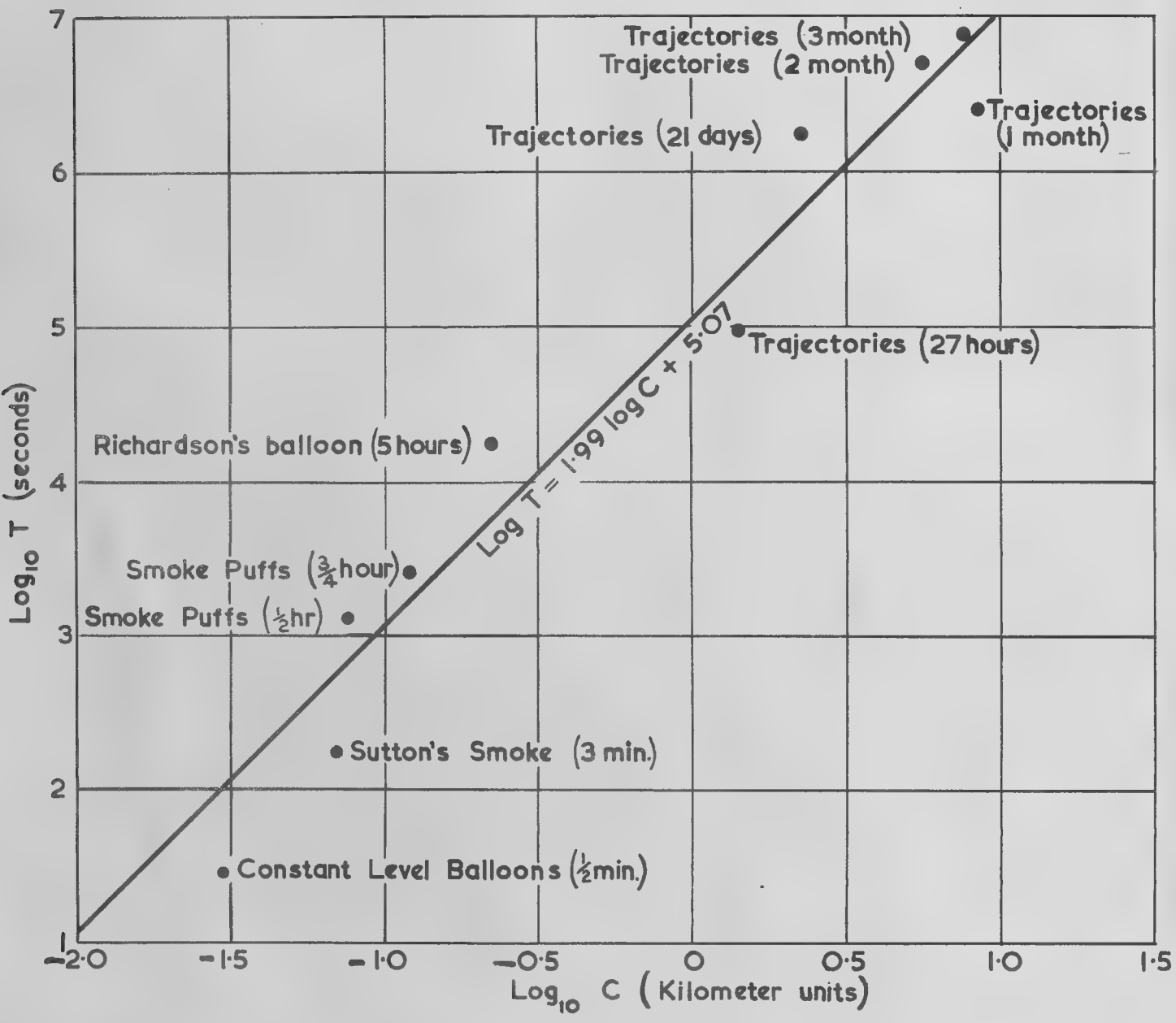
Trajectories (3 month)
Trajectories (2 month)
Trajectories (21 days)
Trajectories (1 month)
Trajectories (27 hours)
Log T = 1·99 log C + 5·07
Richardson's balloon (5 hours)
Smoke Puffs (¾ hour)
Smoke Puffs (½ hr)
Sutton's Smoke (3 min.)
Constant Level Balloons (½ min.)
Log10 T (seconds)
Log10 C (Kilometer units)
7
6
5
4
3
2
1
−2·0
−1·5
−1·0
−0·5
0
0·5
1·0
1·5

FIG. 10

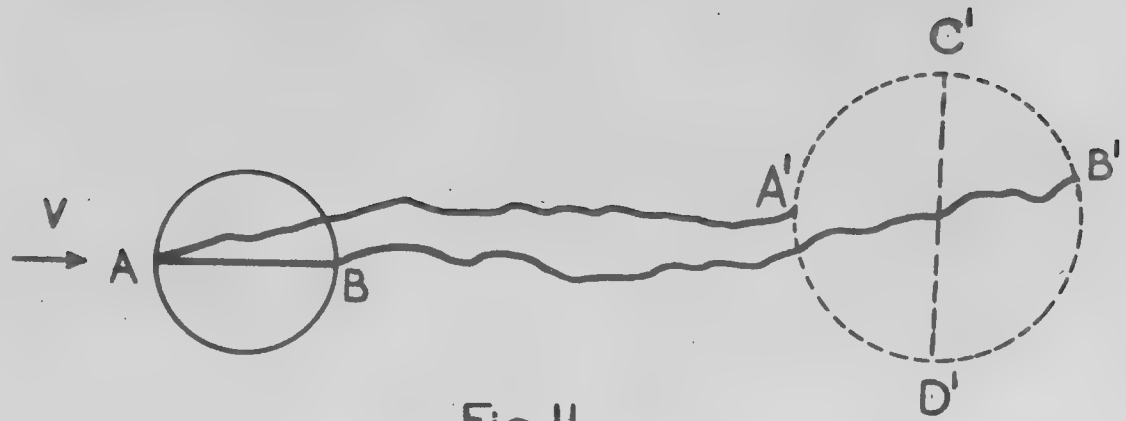

Fig 11

M.R.P. 1062
S.C.111/240
27th August, 1957

Spectral estimates from subdivided meteorological series

by

H. Charnock
(National Institute of Oceanography)
and
G. D. Robinson
(Kew Observatory, Meteorological Office)

AIR MINISTRY

METEOROLOGICAL RESEARCH COMMITTEE

MASTER FILE COPY
NOT TO BE REMOVED
FROM AWS TECH FILES

At the time of issue this report has not been published. Any author desiring to quote this paper should refer to it as "A paper of the Meteorological Research Committee (London), M.R.P. No. 1062 by Mr. H. Charnock and Dr. G.D. Robinson. A copy is available in the Library of the Meteorological Office."

M.R.P. 1062
S.C.III/240
27th August, 1957

AIR MINISTRY

METEOROLOGICAL RESEARCH COMMITTEE

Spectral estimates from subdivided meteorological series

by

H. Charnock (National Institute of Oceanography)

and

G.D. Robinson (Kew Observatory, Meteorological Office)

Abstract

The relation $\frac{1}{2}\frac{\partial^2}{\partial s^2}\left(s^2\bar{\Phi}(s)\right) = 1 - R_+(s)$

between $\bar{\Phi}(s)$, the average fraction of the covariance contained in subseries of s terms, and $R_+(s)$, the even part of the cross-correlogram, is simply derived. Its use and practical limitations are illustrated by the analysis of an artificial series.

The form $\bar{\Phi}(s) = s/(a + s)$ appears to be a suitable approximation for certain series involving vertical wind near the ground. The corresponding spectrum is discussed.

1. Introduction

Meteorologists in several countries are making estimates of turbulent fluxes and intensities by what has been called the 'direct' method. The usual technique is to compute mean products of the type

$$F(N) = (1/N)\sum_{t=1}^{N}(U_t - \bar{U})(W_t - \bar{W})$$

$$= (1/N)\sum_{t=1}^{N} u_t w_t \qquad (1)$$

Here U_t, W_t are values of appropriate meteorological variables measured at equal intervals of time over a total duration T.

$$\bar{U} = (1/N)\sum_{1}^{N} U_t \quad \text{and} \quad \bar{W} = (1/N)\sum_{1}^{N} W_t$$

F(N) is then taken to be proportional to the flux or intensity required. For instance, if U were a horizontal and W the vertical component of wind, then F(N) may be supposed to be a measure of the horizontal shearing stress in the direction of U.

Among the various theoretical and experimental difficulties which arise there is the problem of specifying the duration T over which the observations should be made. A method devised by Swinbank (see Swinbank, 1955, and Deacon, 1955) has been used to check that a chosen duration is appropriate. The record, over duration T, containing N observations, is divided into m sub-records each containing s. Mean products similar to those of Equation (1) are computed for each sub-record, and the average value of the m mean products is taken as the value of F(s):

$$F(s) = \frac{1}{N}\sum_{a=0}^{m-1}\left[\sum_{t=as+1}^{s(a+1)} u_t w_t - \frac{1}{s}\sum_{t=as+1}^{s(a+1)} u_t \sum_{t=as+1}^{s(a+1)} w_t\right] \qquad (2)$$

The process is repeated for different values of s, and $\Phi(s) \equiv F(s)/F(N)$ plotted against s/N. If $\Phi(s)$ approaches unity for $s < N$, then the duration s is deemed adequate.

In this note we are concerned to interpret this test in terms of other statistics of the variables, in particular their lag-covariance, and a suitable relation is derived by elementary methods. It is possible to derive the even part of the lag-covariance (or the co-spectrum) from the statistics of sub-records of a stationary process: an example shows that the method, though difficult in practice, can be useful.

Some of the additional difficulties associated with non-stationary meteorological series are mentioned. Further examples show that series involving the vertical velocity near the surface have special properties from which plausible and interesting results can be derived.

2. The relation between F(s) and the lag-covariogram, C(s)

We seek a relation between F(s) and C(s) where

$$C(s) = \frac{1}{N-s}\sum_{t=1}^{N-s} u_t w_{t+s} \qquad s \geq 0$$

$$= \frac{1}{N+s}\sum_{t=1}^{N+s} u_{t-s} w_t \qquad s \leq 0$$

Our derivation is by elementary argument and has no pretence to rigour.*

/We

* Whilst this paper was in preparation Kahn (1957) published a more general derivation.

/We

We write Equation (2) as

$$F(s) = F(N) - \overset{*}{F}(m) \quad , \text{ where}$$

$$Ns\,\overset{*}{F}(m) = \sum_{a=0}^{m-1} \left[\sum_{t=as+1}^{s(a+1)} u_t \sum_{t=as+1}^{s(a+1)} w_t \right] \qquad (3)$$

If we now evaluate $Ns\overset{*}{F}(m)$ by straightforward cross-multiplication we get rm terms of type $u_t\, w_{t-(s-r)}$ and $u_t\, w_{t+(s-r)}$, where $1 \ll r \ll s$.

Our best estimate for the sum of the mr samples of type $u_t\, w_{t+(s-r)}$ is rm $C(s-r)$, so that

$$\overset{*}{F}(m) \simeq \frac{1}{s}\left[\frac{1}{s}C(1-s) + \frac{2}{s}C(2-s) + \cdots + C(0) + \cdots + \frac{1}{s}C(s-1)\right] \qquad (4)$$

i.e., $F(N) - F(s)$ can be estimated from $C(s)$ by using a weighted mean.

If we consider $C(s)$ and s as continuous functions, all the summations being re-defined as corresponding integrals,

$$F(N) - F(s) \simeq \frac{1}{s}\int_{-s}^{s} C(k)\left(1 - \frac{|k|}{s}\right)dk \qquad (5)$$

We can define $C_+(s)$ as the even part of $C(s)$ by

$$2C_+(s) = C(s) + C(-s)$$

when (5) becomes

$$F(N) - F(s) \simeq \frac{2}{s}\int_{0}^{s} C_+(k)\left(1 - \frac{k}{s}\right)dk \qquad (6)$$

Formulae similar to (6) turn out to be fairly common. They are to be found in textbooks of statistics, for example that of Brooks and Carruthers (1953), for estimating the variance of mean values in a single auto-correlated series. Ogura (1950) (1952) has used a similar formula to interpret single series of atmospheric turbulent fluctuations in terms of the similarity theory of isotropic turbulence. Equation (6) can be transformed by using a spectral function $S(n) = \int_0^\infty C(s)/C(0).\cos 2\pi ns\,ds$ to

$$\Phi(s) = \int_0^\infty S(n)\,(1 - \chi^2)\,dn \qquad (7)$$

where $\chi\,(sn) = (\sin \pi sn)/\pi sn$.

This is the form given by Webb (1955) and attributed by him to van der Hoven and Panofsky (1954).

/Equation

Equation (6) can be written in a more useful form by multiplying by s^2 and differentiating twice with respect to s to get

$$\frac{1}{2}\frac{\partial^2}{\partial s^2}\left(s^2 F(s)\right) = C(0) + C_+(s) \qquad (8)$$

and correspondingly

$$\frac{1}{2}\frac{\partial^2}{\partial s^2}\left(s^2 \Phi(s)\right) = 1 - C_+(s)/C(0)$$

$$= 1 - R_+(s) \qquad (9)$$

where $R_+(s)$ is the even part of the cross-correlogram as usually defined.

3. Stationary processes: an artificial example

For the hypothetical stationary process, where statistics such as $\bar{U}$, $C(s)$, $S(n)$, etc. are well defined, Equation (8) shows how $C_+(s)$ can be determined from $F(s)$.

Given a finite record which is approximately stationary, $F(s)$ is easier to compute than $C(s)$, but it seems likely that the double differentiation with respect to s will make the method difficult to apply in practice. We have investigated the method using an artificial series published by Kendall (1946). This series (Kendall's experimental series 1) consists of 480 terms constructed according to the formula

$$u_{t+2} = 1.1\, u_{t+1} - 0.5\, u_t + \epsilon_{t+2}$$

The element ϵ was obtained by taking two-figure random numbers between -49 and +49*.

Values of $1 - \Phi(s)$ were computed for all integral factors of 480 and are plotted against $\log_{10} s$ in Fig. 1a. The scatter is such as to preclude the direct estimation of $R(s)$ by double differentiation of $s^2 \Phi(s)$. First differences were therefore read from a smooth curve drawn by eye, and approximate values of $(1/2)\,\partial/\partial(\log s)\left(1-\Phi(s)\right)$ plotted. Another smooth curve provided estimates of $\frac{1}{2}\frac{\partial^2}{\partial(\log s)^2}\left(1-\Phi(s)\right)$, which in turn were smoothed. Corresponding ordinates of the three smooth curves were added to give the estimated variation of $R(s)$ shown in Fig. 1b. The values computed directly, tabulated by Kendall, are also plotted and the form of $R(s)$ which would be expected from an indefinitely long record is also indicated. The graphical method appears to give useful smoothed results, in spite of its subjective nature. We should perhaps mention that the smooth curves of Fig. 1 were drawn by a disinterested person (the wife of one of the authors).

4. Statistics of series involving vertical wind near the surface

Meteorological series are characteristically non-stationary and statistics such as $\bar{U}$, $C(s)$, $S(n)$ vary with T, the total duration of the series available for analysis, as well as in space and time. Such difficulties have

/been

* The mean of the series was found to be 0.821; Kendall's value of 8.821 appears to be a misprint.

been reviewed by Charnock (1957) and we shall not discuss them further here. We have analysed several sets of observations made to test the 'direct' method for estimating the flux of heat and momentum, and we have found that series which involve the vertical wind component close to (i.e., about 1 m above) the surface have, approximately, some of the attributes of stationary series. For example, $R_+(s)$ approaches zero at relatively small and practicable values of s. It may not be entirely misleading to apply methods appropriate to stationary series to the study of these particular examples.

Observations of this type are made by instruments which integrate the wind components over a certain period of time. The individual members of the series, w_t etc., are not 'instantaneous' winds, but means over a time depending on the time-constants of the equipment used. We have found that for a given N, within fairly wide limits, and for the time-constants of the apparatus we have used (over a hundred-fold range), $F(s)$ and $R_+(s)$ are approximately independent of the time-constant of the apparatus.

We can use this observed (approximate) property to establish a functional form for $F(s)$ and hence for $R_+(s)$. We have (Equation 3)

$$F(N) \equiv F(s) + \overset{*}{F}(m), \qquad N = sm$$

If we take it, from observation, that

$$\overset{*}{F}(m) \simeq F(m),$$

then $$F(N) \simeq F(m) + F(s),$$

i.e., $$1 \simeq \underset{\sim}{\Phi}(m) + \underset{\sim}{\Phi}(s) \qquad (10)$$

Equation (10) is satisfied generally by the solution $\underset{\sim}{\Phi}(s) = \log_N s$, and for a given N, in the physically significant range $2 \ll s \ll \frac{1}{2}N$, by the family $\underset{\sim}{\Phi}(s) = 1 - 1/((s^2/N)P + 1)$, which in the particular case of $p=\frac{1}{2}$ reduces to

$$\underset{\sim}{\Phi}(s) = \frac{s}{s+N^{\frac{1}{2}}} \equiv \frac{s}{s+a} \qquad (11)$$

This simple expression has proved an adequate fit to many of our observations.

Fig. 2 shows an example. The series used are of 2000 observations of vertical wind, W, and temperature, Θ at $\frac{1}{4}$-sec intervals, the individual observations being instrumental integrations over about 1/10 sec. The points plotted are of $\underset{\sim}{\Phi}(s)$ for $w\theta$ with N = 1600, the curve being $\underset{\sim}{\Phi}(s) = s/(s + 40)$. For comparison the more general solution of Equation (10), $\underset{\sim}{\Phi}(s) = \log_{1600} s$, is also plotted.

This is not an isolated example; we have speculated that Equation (11) may be of general application to similar series.

5. The frequency spectrum of series involving vertical velocity near the ground

Applying Equation (9) to Equation (11), we have

$$R_+(s) = 1 - \frac{1}{2}\frac{\partial^2}{\partial s^2}\left(s^2 \underset{\sim}{\Phi}(s)\right) = \frac{a^3}{(s+a)^3} = \frac{1}{(1+s')^3} \qquad (12)$$

where $s \equiv as'$ and, if Δ is the number of seconds between observations, $\Delta as' = t$. Then, writing $b = 2\pi a \Delta n$ and taking the Fourier cosine transform of Equation (12) we have

$$\frac{1}{a\Delta} S(b) = \int_0^\infty \frac{\cos bs'}{(1+s')^3} ds' = \frac{1}{2} + \frac{b^2 \cos b}{2} Ci(b) + \frac{b^2 \sin b}{2}\left(Si(b) - \frac{\pi}{2}\right) \qquad (13)$$

Equation (13) is not readily computed in the interesting range of b from the easily available tables of the sine and cosine integrals Si(b) and Ci(b), and we are indebted to the Mathematics Division of the National Physical Laboratory for the tabulation which is illustrated in Figs. 3 and 6. The expression is asymptotic to $3/b^2$. Equation (13) relates the frequency spectrum of a series (or of course the co-spectrum of two series) for which Equation (12) holds to the value of a, where a^2 is the number of terms in the series or the number of terms at which the steady value of flux or intensity is attained, if this occurs.

6. Some examples

Fig. 4a shows $\Phi(s)$ for a series of 300 observations at 1/30-sec intervals of the vertical wind integrated over 1/60 sec. The series was taken at about 1.25 m above short grass, in a mean wind about 2.5 $m.sec^{-1}$, with a heat flux of about 10 mw cm^{-2} upwards. The series fits reasonably well to Equation (11) with a = 10 or a = 15. In Fig. 4b the curves show Equation (13) with these values for a, the points being the computed Fourier cosine transform of a curve drawn smoothly through values of the lag correlation R(s) which had been computed directly from the series.

Similar agreement can be found with a computed auto-correlogram given by Jones (1957). The three series analysed, each of 240 terms, were observations of $2\frac{1}{2}$-sec averages of wind inclination to the horizontal and were made at 2000 ft above Cardington. Fig. 5a shows values of $\bar{\Phi}(s)$ computed from the original data which were kindly provided by Mr. Jones. The curve drawn is of $s/(s + a)$ with $a = (240)^{\frac{1}{2}}$. Fig.5b shows the corresponding auto-correlogram, the directly computed values of R(s) for one of the series (No. 2), and the mean of R(s) for the three series.

Other observations which involve the vertical velocity at considerable height have been obtained by Crane and Chilton (1956) from an aircraft at 1700 ft above Chesapeake Bay. They display their results in the form of the composite spectrum shown in Fig. 6. The smooth curve is of Equation (13); it provides a reasonable interpretation of the observations.

7. Tentative extrapolation to higher frequencies

There is considerable interest in the form of the spectrum of the turbulence of the wind near the ground and several attempts have been made (Taylor, 1955, Macready, 1953, Webb, 1955) to demonstrate the existence of the form $S(k) \propto k^{-5/3}$ for the wave-number spectrum. This form follows by dimensional argument from the hypotheses of Kolmogoroff. Our observations and arguments have been in terms of frequency spectra, but we assume, with others, that they can be made applicable to wave-number spectra by multiplication by a constant velocity*.

The spectrum we suggest does approximate to $k^{-5/3}$ over an appreciable range, but appears to be asymptotic to k^{-2}. It must however be emphasised that we have computed the spectra of observed series, not necessarily the true turbulence spectrum, and that the observed properties of these series, which we have summarised in Equation (10), are such that the same form of spectrum, displaced appropriately along the frequency axis, is found whatever the time scale of observation, within the fairly wide (100-fold) limits we have used. This is another aspect of the facts summarised in Webb's (1955) remark "A value = (-) 5/3 ..... is clearly indicated for eddy scales ..... where it is certainly believed isotropy does not extend." It shows the danger of regarding the statistics of observed series as statistics of turbulence, unless there is independent evidence that the turbulence statistics are well defined.

/A

---

* Priestley and Sheppard (1952) and Robinson (1953) argued on dimensional grounds that frequency and wave-number spectra in the 'inertial sub-range' should differ. This appears to be in error. Knowledge of frequency only gives no knowledge of a typical length of the field, so viscous dissipation cannot be expressed in terms of frequency only and the dimensional argument as applied to frequency spectra is invalid.

A spectrum of type k^{-2} is of considerable physical interest, as it implies an equipartition of the viscous dissipation over the range of eddy sizes for which it holds. Our own observations suggest such a spectrum over a limited range: they certainly do not establish it.

The observations of Crane and Chilton (1956), however, extend to somewhat higher frequency and were made at greater heights. It seems reasonable to interpret their observations as showing a k^{-2} type of spectrum over a hundred-fold range of k and down to the short wavelength limit of their observations.

Acknowledgements

We are grateful to several of our colleagues who have helped in the collection and analysis of observations and in other ways. Mr. J. Crease has been particularly helpful.

References

Brooks, C.E.P. and Carruthers, N. 1953 Handbook of Statistical Methods in Meteorology, London.

Charnock, H. 1957 J.R. Statist. Soc. (in press).

Crane, H.L. and Chilton, R.G. 1956 N.A.C.A. Tech. Note 3702 (27).

Deacon, E.L. 1955 Divn. Met. Phys. C.S.I.R.O., Melbourne, Tech. Pap. No. 4.

Jones, R.A. 1957 Meteorological Research Papers, Air Ministry, London, No.1044.

van der Hoven, I. and Panofsky, H.A. 1954 Div. Met. Penn. St. Univ., Final Report Con.AF.19 (604)-166.

Kahn, A.B. 1957 J. Met., 14, p.9.

Kendall, M.G. 1946 Contributions to the study of oscillatory time series, Cambridge.

Macready, P.B. 1953 J. Met., 10, p.434.

Ogura, Y. 1950 Geophys. Notes, Tokyo, 3, (26).

Ogura, Y. 1952 J. Met. Soc. Japan, 30, p. 103.

Priestley, C.H.B. and Sheppard, P.A. 1952 Quart. J.R. Met. Soc., 78, p. 488.

Robinson, G.D. 1953 Meteorological Research Papers, Air Ministry, London, No. 808.

Swinbank, W.C. 1955 Divn. Met. Phys. C.S.I.R.O., Melbourne, Tech. Pap. No. 2.

Taylor, R.J. 1955 Aust. J. Phys. 8 (4), p. 535.

Webb, E.K. 1955 Divn. Met. Phys. C.S.I.R.O., Melbourne, Tech. Pap. No. 5.

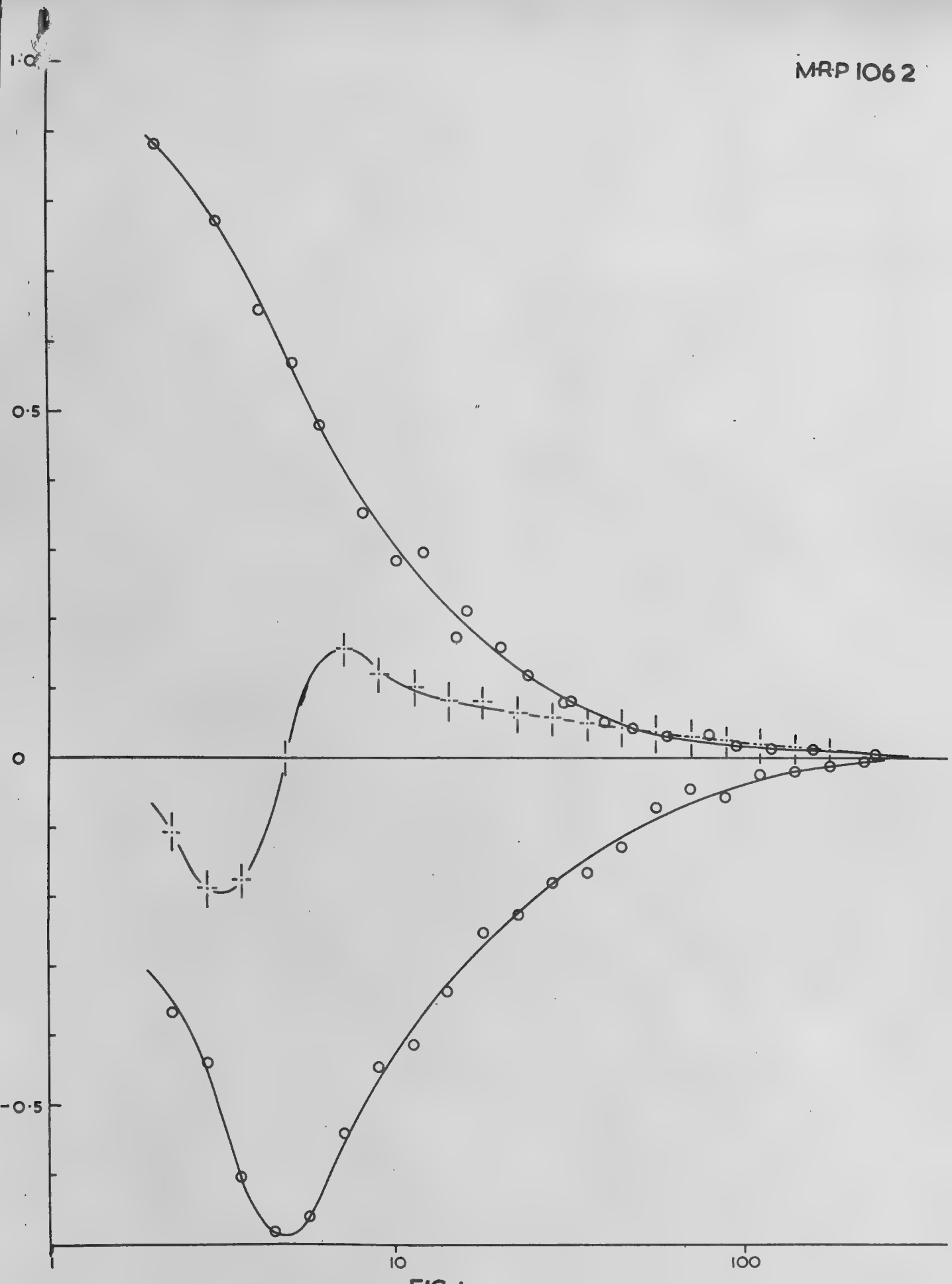

FIG. 1a.

ANALYSIS OF AN ARTIFICIAL SERIES (KENDALL No 1)

$\left\{1-\Phi(s)\right\}$, $\frac{3}{2}\frac{\partial}{\partial(\log s)}\left\{1-\Phi(s)\right\}$, $\frac{1}{2}\frac{\partial^2}{\partial(\log s)^2}\left\{1-\Phi(s)\right\}$ AGAINST Log s

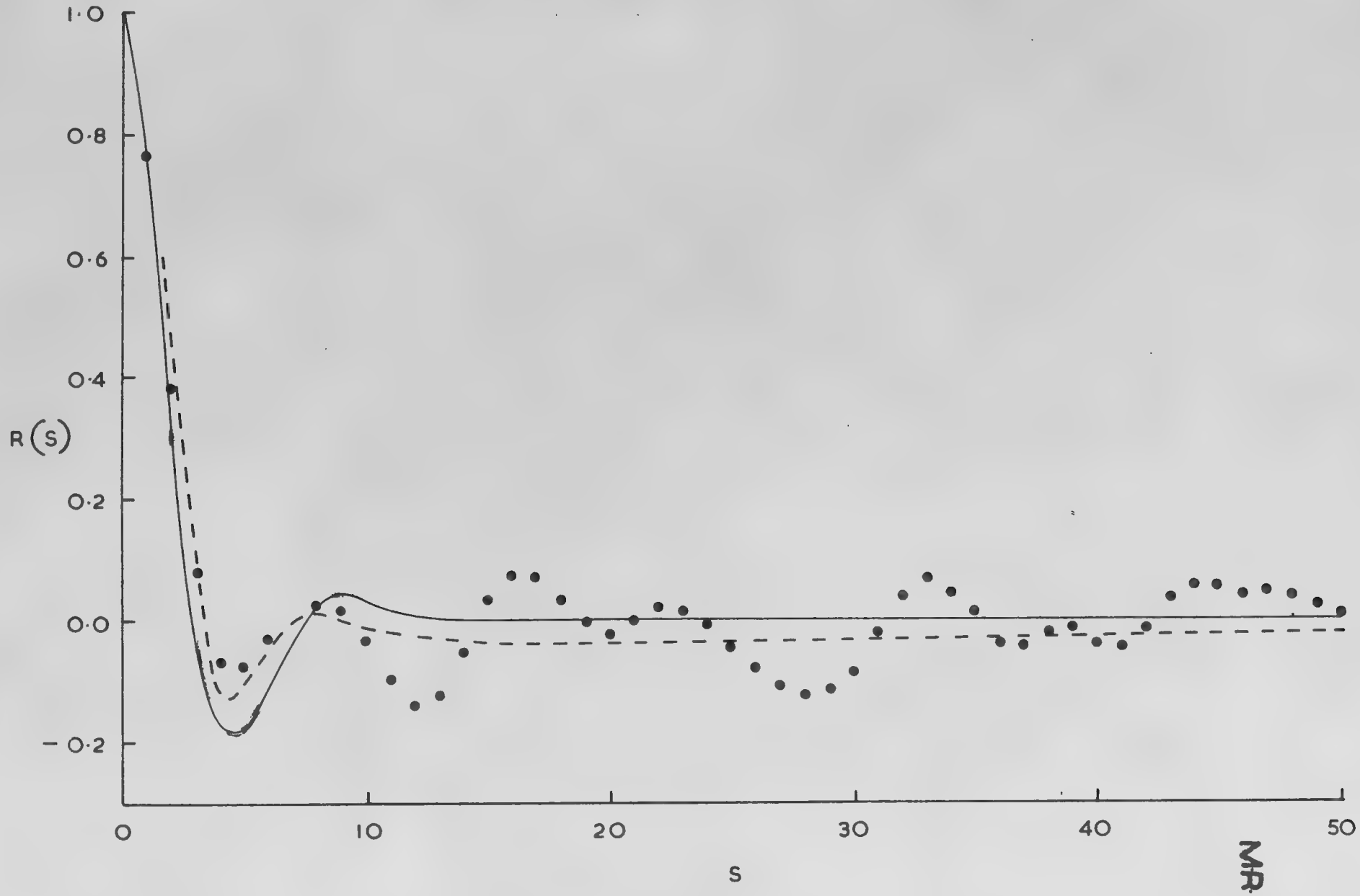

FIG. 1 b.

ANALYSIS OF AN ARTIFICIAL SERIES (KENDALL No 1)

R(s) FOR INFINITE SERIES ——— BY PRESENT ANALYSIS - - - - - -
BY DIRECT COMPUTATION (KENDALL) ●●●●●

M.R.P. 1062

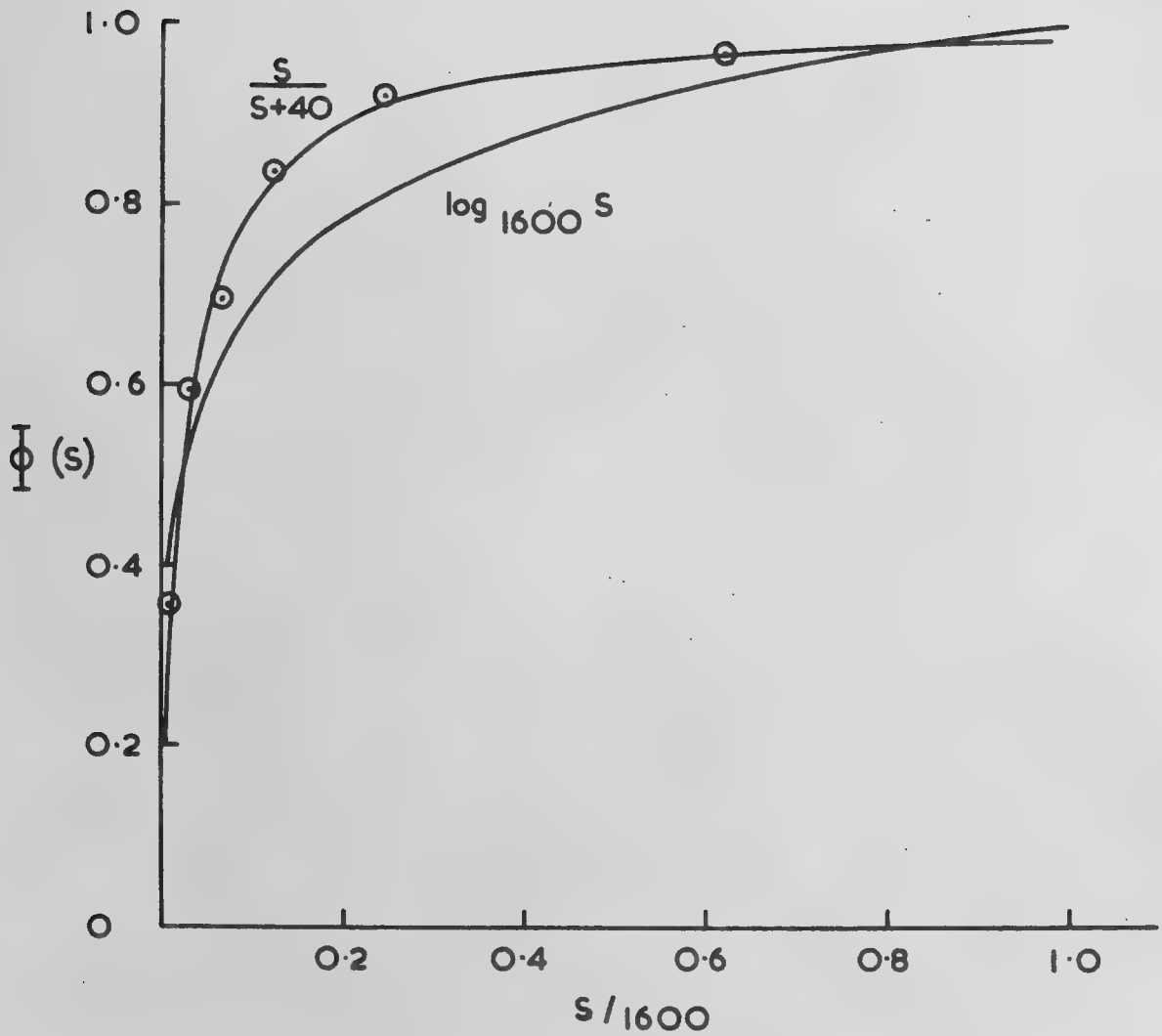

FIG. 2.

Φ(s) AGAINST s/a^2 a = 40. 2000 OBSERVATIONS AT Im ΘF PRODUCT wθ. INTERVAL ¼ Sec. CARDINGTON 31 AUGUST 1954.

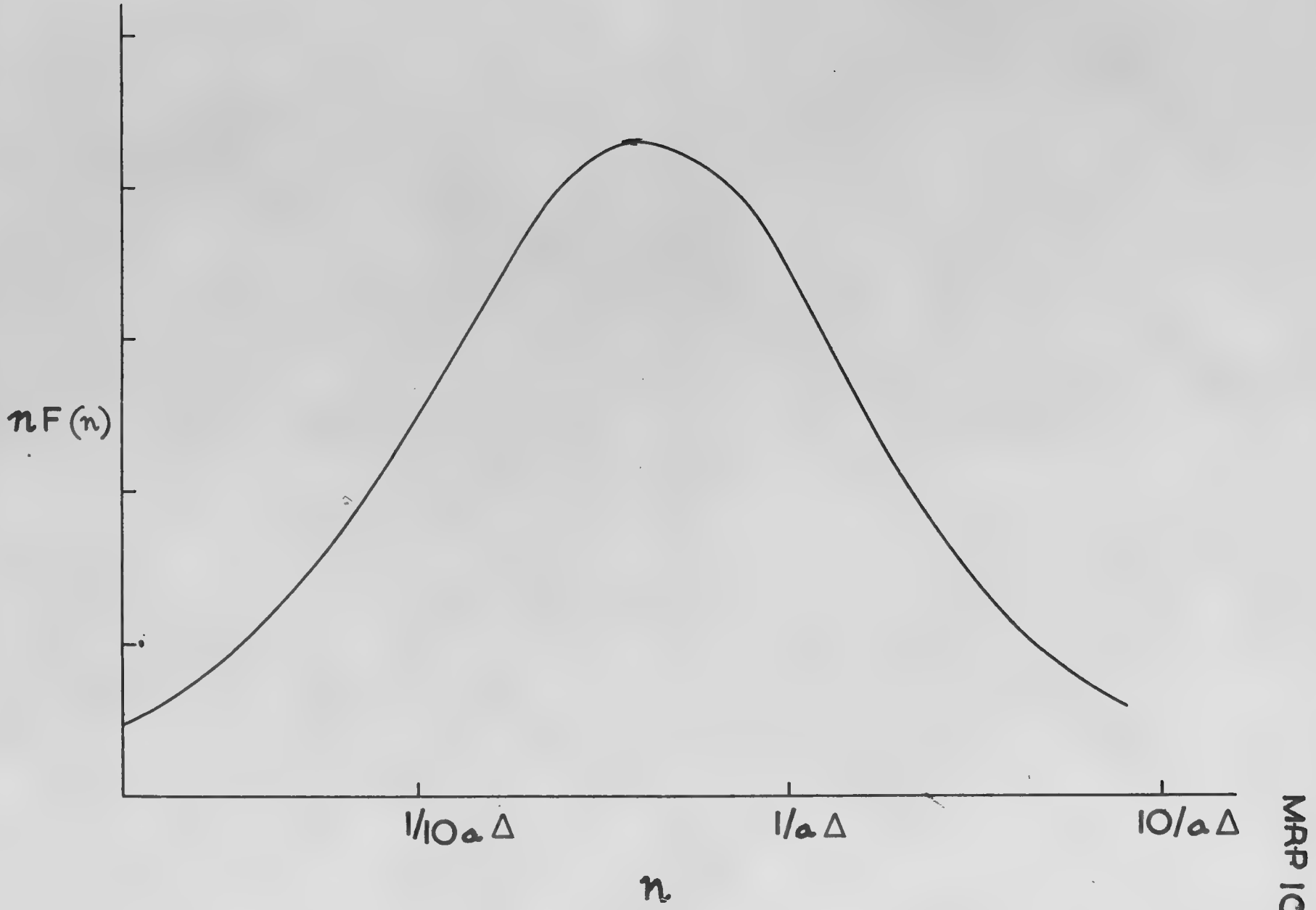

MRP 1062

FIG. 3.

PROPOSED FREQUENCY SPECTRUM OF W ETC. (Eq. 13)

M.R.P. 1062

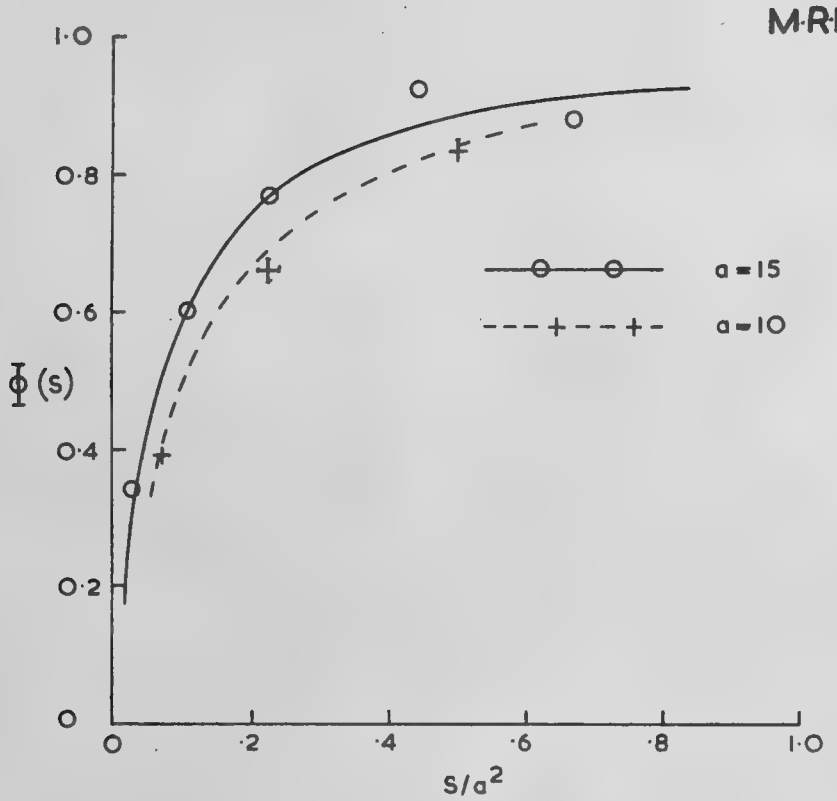

FIG. 4a.

FREQUENCY SPECTRUM OF W. 300 OBSERVATIONS AT 1m. INTERVAL 1/30 SEC. KEW 9 JUNE 1953
Φ(s) AGAINST s/a²

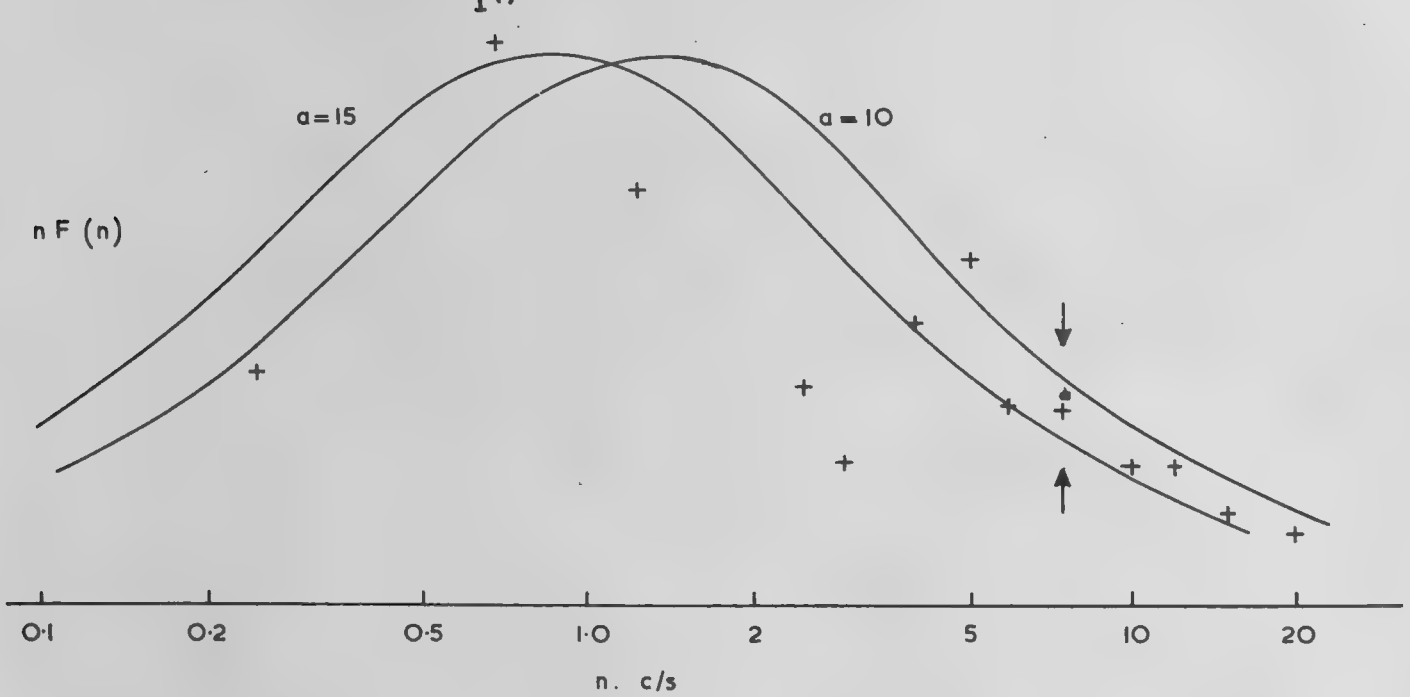

FIG. 4 b.

FREQUENCY SPECTRUM OF W. 300 OBSERVATIONS AT 1m. INTERVAL 1/30 SEC. KEW 9 JUNE 1953
FREQUENCY SPECTRUM. DIRECTLY COMPUTED POINTS FITTED IN POSITION INDICATED BY ARROW.

FIG 5. LAG CORRELOGRAM OF INCLINATION OF WIND TO HORIZONTAL.
3 SERIES OF 240 OBSERVATIONS AT 2000 ft. CARDINGTON (JONES 1957)

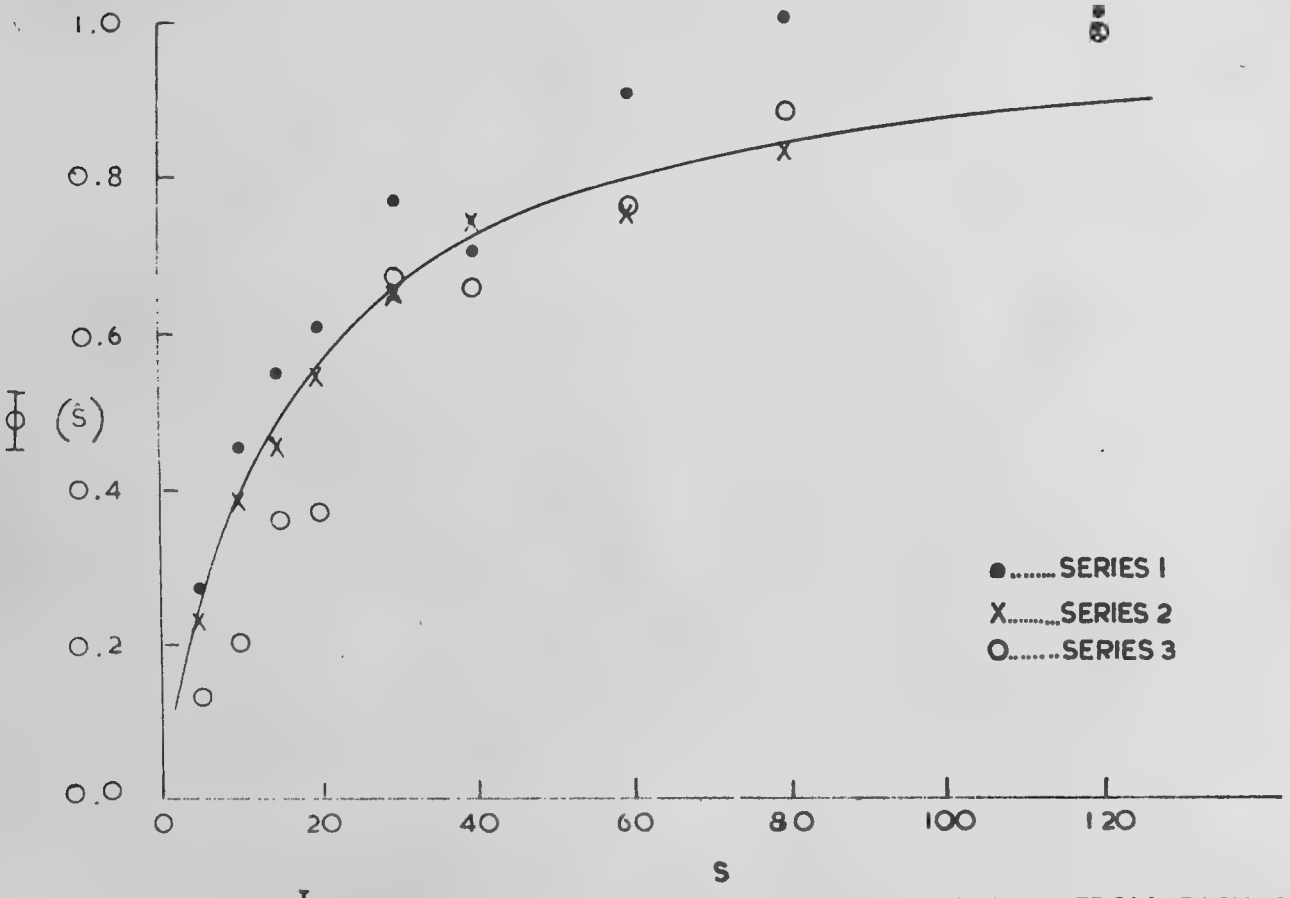

FIG 5a $\Phi(s)$ AGAINST s POINTS ARE COMPUTED DIRECTLY FROM EACH SERIES

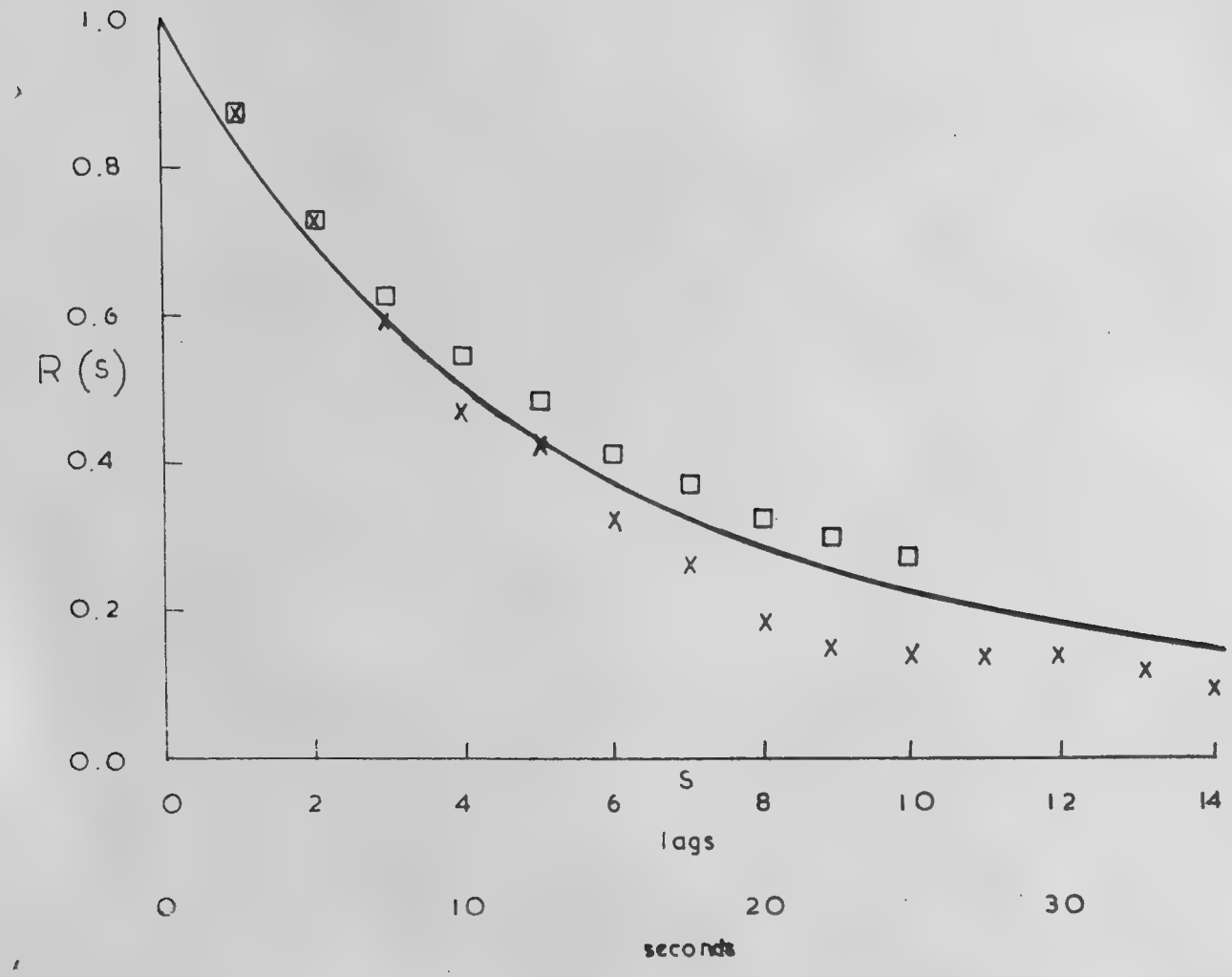

FIG 5b LAG CORRELOGRAM. CURVE BY Eq. 12 WITH $a=(240)^{\frac{1}{2}}$
POINTS ARE COMPUTED DIRECTLY FROM THE OBSERVATIONS
X..... SERIES 2. □.....MEAN OF THE THREE SERIES

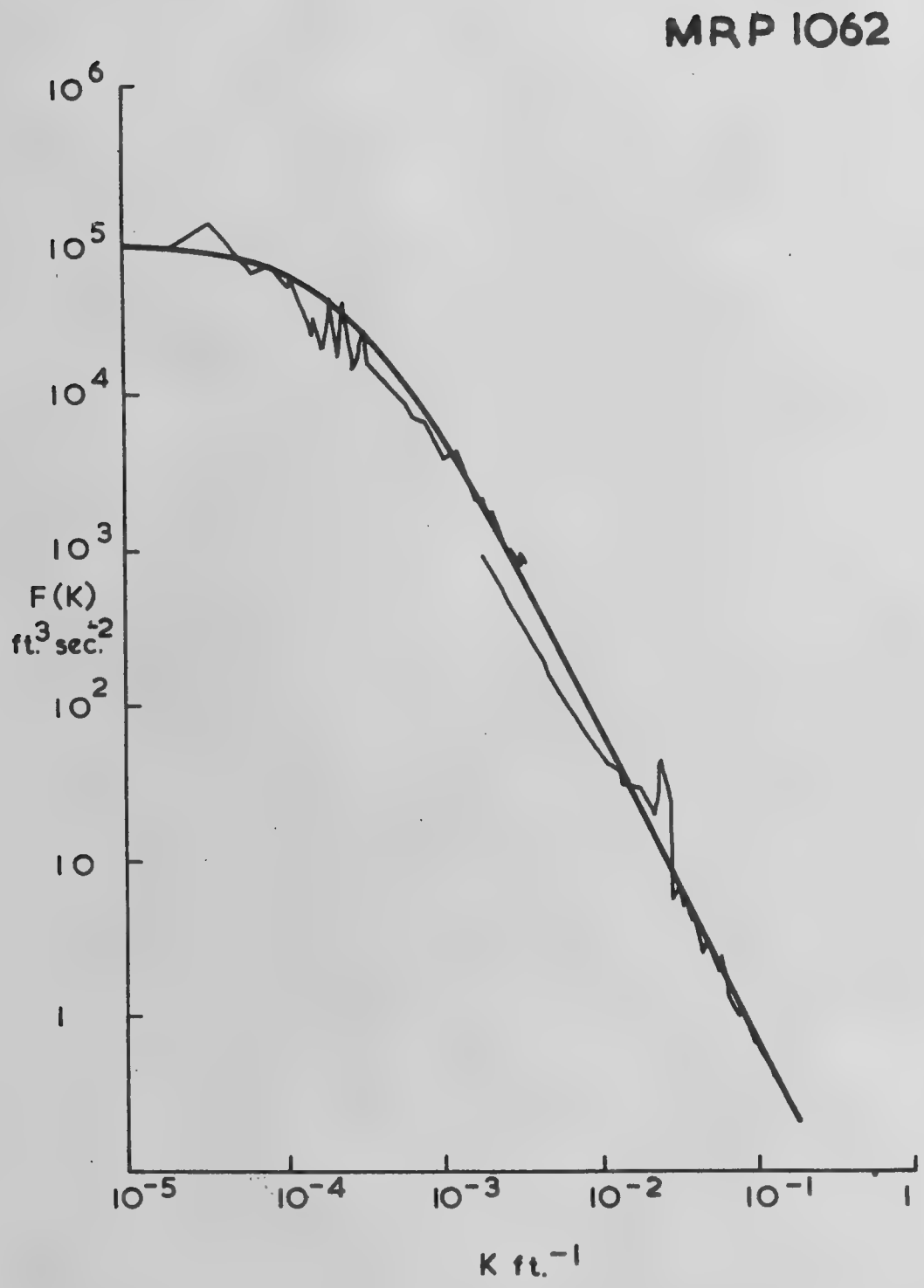

FIG 6 FREQUENCY SPECTRUM OF W AT 1700ft (CRANE AND CHILTON 1956) SMOOTH CURVE IS Eq. 13

MA 7 S

M.R.P. 1063
S.C.11/240
26th August, 1957

Two-parameter techniques of numerical forecasting applied to a small intense depression

by

J. S. Sawyer

(Meteorological Office)

58-231

AIR MINISTRY

METEOROLOGICAL RESEARCH COMMITTEE

At the time of issue this report has not been published. Any author desiring to quote this paper should refer to it as "A paper of the Meteorological Research Committee (London), M.R.P. No. 1063 by Mr. J.S. Sawyer A copy is available in the Library of the Meteorological Office."

M.R.P.1063
S.C.II/240
26th August, 1957

AIR MINISTRY

METEOROLOGICAL RESEARCH COMMITTEE

Two-parameter techniques of numerical forecasting applied to a small intense depression

by

J. S. Sawyer (Meteorological Office)

1. Introduction

From time to time small depressions deepen very rapidly over the Atlantic and when such a development takes place near to the coasts of the British Isles the forecaster is usually unable to foresee the coming changes until large barometric tendencies appear. Important errors in the forecasting of the gales and associated bad weather occur. It is relevant to enquire whether the newly developed techniques of numerical forecasting can be expected materially to assist the forecaster on these occasions.

2. The depression of 28-29 July 1956

A suitable case for study occurred on 28-29 July 1956. The synoptic situation at 1500 GMT 28 July 1957 is illustrated in Fig. 1. At that time a rather shallow depression was centred about 250 miles west-south-west of Cornwall with a trough of low pressure extending northeastward over most of the British Isles. Over the previous twelve hours the depression had moved northeastward at about 25 kt and had deepened slowly, the central pressure falling from 1000 mb to about 994 mb. Although at 1200 GMT there were a number of ships around the centre none reported winds in excess of 20 kt and it was very difficult to forecast the coming gales with confidence. The depression lay just to the east of a trough in the 1000-500 mb thickness lines, and the axis of the 500 mb trough was about 200 miles west of the centre. Deepening of the depression was therefore to be expected, but it was the rapidity of this deepening which poses the problem.

In the 12 hours which followed the situation illustrated in Fig. 1, the central pressure of the depression fell by 15 mb to a little below 980 mb. By 0300 GMT 29 July when the centre was just off the north coast of Cornwall, surface winds of 40 kt were being reported from all sides of the centre except the northeast. The gale reached 58 kt at the Lizard and a gust of 87 kt was recorded. Considerable damage was caused. Additional details are given by D. M. Houghton (1956).

Calculations of the expected changes in 1000 mb and 500 mb heights were carried out by numerical forecasting methods over 24-hour intervals starting from the synoptic situation at 0300 GMT 28 July and from that at 1500 GMT 28 July. The two-parameter model described by Sawyer and Bushby (1953) was used, and the technique followed that described by Bushby and Hinds (1955) in which allowance is made for warming of the air by heat from the sea. Although both of these calculations successfully indicated the larger scale synoptic

changes, the north-east movement of the depression and the eastward displacement of the 500 mb and thickness troughs, neither of them gave any indication of the phase of very rapid deepening during the evening and night of 28 July. Both of the computations indicated a deepening of about 6 mb over 24 hours and the correlation coefficients between the calculated and observed 24-hour changes of surface pressure were 0.90 and 0.81 in respect of the two computed charts.

3. The problem of prediction in small depressions

Inspection of the relevant synoptic charts shows that the rapid deepening of the depression was a phenomenon confined to an area of 200 to 300 miles radius around the centre. Outside this region the pressure changes were not unexpectedly large and the errors of the numerical predictions were not important.

Techniques of numerical weather prediction based upon geostrophic winds and a simple two-parameter model of an adiabatic atmosphere were not designed for such relatively small scale phenomena. One might expect that to describe properly developments on this scale it would be necessary to formulate a new model, abandoning the geostrophic condition, considering the release of latent heat and elaborating the simple vertical distribution of wind assumed in the two-parameter model. However, before attempting to reformulate the problem in such a general way, there are advantages to be gained by examining whether the simple two-parameter predictions can be brought into closer accord with the observed developments by relatively minor modifications of computing technique. Besides possibly providing a "short-cut" to a practical technique, such a procedure can throw light upon the physical and mathematical factors which are important.

It is the results of computations with such a modified two-parameter model which are reported in the present paper. The calculations were all carried out over the 12-hour period of maximum deepening (namely 1500 GMT 28 July to 0300 GMT 29 July).

The principal effect which has been examined is that of the release of latent heat during condensation and precipitation, particularly in regard to its effect on the static stability of the air. The air over England on the 28th was notably warm and moist and during the period of active deepening of the depression an extensive area of heavy rain covered eastern Ireland and St. George's Channel. Rainfall amounts exceeded 40 mm in western Wales and 15 mm at Roches Point in southern Ireland. Thunderstorms were also reported in the rain area. It thus seems that a warm and moist air mass was ascending in this area under conditions in which the lapse rate differed little from the saturated adiabatic. The significance of these conditions will be discussed further in the following section together with the theoretical basis of the method adopted to examine their effects.

A second important reason why the numerical calculations might fail in respect of a depression with a small and intense core, such as that occurring on 28 July, lies in the occurrence of non-geostrophic motion. The ageostrophic wind component can be expected to become larger when the scale of disturbance is made smaller. A comprehensive treatment is however beyond the scope of the present paper but some allowance for non-geostrophic effects will be made by use of the "balance equation".

A third reason why the first calculations might have proved inadequate lies in the mathematical technique for solution of the equations. This was based on finite differences on a grid of about 150 miles mesh-length. The whole phenomenon of intense deepening thus falls within the length of four grid intervals, and may be inadequately described by so coarse a grid. For this reason some experiments were carried out using a finer mesh over the critical area.

/4.

4. The effects of ascent of moist air on numerical forecasts

It is characteristic of active fronts and other intense synoptic features of relatively small scale that the vertical motion, as evidenced by the rainfall, is much greater than that computed by the quasi-geostrophic methods of numerical forecasting; the generation of cyclonic vorticity is also greater. Sawyer (1956) considered the vertical circulation at fronts on the basis of non-geostrophic motion perpendicular to the front, but making various simplifying assumptions about motion parallel to the front. This discussion showed that the large vertical velocities could be explained if, within the cloud mass, the limiting condition for inertial instability was approached, namely $(\partial u/\partial y)_{\theta'} = -f$ where f is the Coriolis parameter and $(\partial u/\partial y)_{\theta'}$ is the (anticyclonic) wind shear measured along a surface of constant wet-bulb potential temperature (θ' = constant). The significance of this condition is that a parcel of air displaced along a surface of constant wet-bulb potential temperature is in equilibrium at its new location both as regards hydrostatic equilibrium (it has the same density as the environment) and also in respect of dynamical equilibrium, because it has the same velocity as the environmental air at its new location. There is no restoring force tending to return the displaced parcel to its original or any other location.

An essential feature of the two-parameter models for numerical forecasting is contained in the thermodynamic equation which takes into account the effect of ascending motion in cooling the atmosphere and of descending motion in heating it. If, however, upward motion takes place under the conditions postulated in the preceding paragraph no such cooling takes place. Moreover the slope of the surfaces of constant wet-bulb potential temperature is fairly steep (say 1 in 30) and, as a first approximation, we can maintain the pattern of divergence assumed in the two-parameter models in which the convergence in the lower atmosphere is balanced by divergence in the upper troposphere directly above it, ignoring the tilt of the line joining areas of convergence and divergence which should accompany the motion up the sloping wet-bulb potential temperature surfaces.

Thus in order to study the effect of ascent of saturated air in areas of neutral inertial stability (and probably in areas of inertial or hydrostatic instability) upon the large-scale dynamics of the horizontal motion, it appears possible to treat the problem as if vertical motion had no effect upon the temperature field at points lying within the region of neutral inertial stability. Mathematically expressed, this implies that at such points the equation given by Sawyer and Bushby (1951) to determine the rate of change of their thickness parameter h', namely (in their notation):-

$$\nabla^2 \frac{\partial h'}{\partial t} + J\left(h_m, \frac{\beta}{f}\nabla^2 h'\right) + J\left(h', \frac{\beta^2 g}{f}\nabla^2 h_m + f\right)$$

$$= \frac{4g}{RA\Gamma_p}\left(\frac{\beta^2}{f}J(h'h_m) - \frac{\partial h'}{\partial t}\right)\left(\nabla^2 h_m + \frac{f^2}{\beta^2 g}\right) \qquad (1)$$

should be replaced by an equation expressing simply the horizontal advection of thickness. The appropriate equation is

$$\frac{\partial h'}{\partial t} = \frac{\beta^2 g}{f} J(h', h_m) \qquad (2)$$

The vertical velocity then has to be obtained (if required) by the evaluation of $\partial p/\partial t \equiv \Pi_m$ from the equation

$$\frac{4\Pi_m \left(\nabla^2 h_m + f^2/\beta^2 g\right)}{p_0 - p_1} = \nabla^2 \frac{\partial h'}{\partial t} + J\left(h_m, \frac{\beta^2 g}{f} \nabla^2 h'\right) + J\left(h', \frac{\beta^2 g}{f} \nabla^2 h_m + f\right) \qquad (3)$$

It is, of course, necessary in any practical computation to determine the points of the grid at which equation (2) is to be used in preference to equation (1). In the study of the depression of 28 July, equation (2) was used for three fixed points of the computational grid which fell within the area of extensive rain throughout the period of 12 hours through which the calculation was continued. There seemed good reason to think that the postulated conditions occurred in that area. Equation (2) was applied to calculate $\partial h'/\partial t$ at these points and subsequently equation (1) was solved by the modified Liebmann process of iteration regarding the points for which $\partial h'/\partial t$ had already been calculated as additional (internal) boundary points.

If such a method were used in day-to-day numerical forecasting a scheme would have to be devised by which the points for the application of equation (2) would be determined either by extrapolation of known areas of near neutral inertial stability or from the vertical motion pattern itself.

5. Results

The results of calculations of the 500 mb and 1000 mb height distributions at 0300 29 July 1956 on the basis of the corresponding distribution 12 hours earlier are illustrated in Fig. 2 and 3. (For convenience the distribution of 1000 mb height has been converted to a sea-level pressure map).

Comparison of Fig. 2(a) with 2(b) and of 3(a) with 3(b) shows the shortcomings of the calculations based on the simple two-parameter model. The eastward motion of the 500 mb trough has been slightly underestimated, and in particular values of 500 mb height are about 60 m too high over southwest England where the deep surface depression had formed. The error in the surface pressure map is more striking. The calculated chart shows a flat depression extending from south-west England to the Scottish border and contains no indication of the intense centre over Cornwall. Pressure calculated over Cornwall is 995 mb and is no lower than the initial pressure in the depression off southern Ireland. On the other hand, the position of the 1000 mb isobar is essentially correct and errors outside this are of a minor character.

In order to study the possible effect of the release of latent heat in the region of near neutral stability over Ireland, the calculations were repeated following the method outlined in the previous section. Equation (2) was applied at three adjacent grid points forming a triangle covering most of the south-eastern half of Ireland. The calculated 500 mb heights were practically unaffected by the changed procedure, but an improvement was effected in the calculated distribution of sea-level pressure. The calculated pressure between southern Ireland and Cornwall was about 991 mb - about 4 mb lower than in the first calculations, but the low pressure centre was still flat and elongated towards the Irish Sea.

/In

In order to ascertain whether more realistic results would be obtained using a smaller computation grid, the calculations were repeated on a grid with a mesh length of about 75 nautical miles, half of that used in the previous calculations. The area covered by the calculations, roughly that illustrated in Fig. 2 and 3, was only one quarter of the area for which the previous calculations had been performed, and the changes calculated in the first calculations were used as boundary values in the computations on the smaller grid. The points at which equation (2) was substituted for equation (1) are shown in Fig. 2(c) - these form a smaller triangle than the points used in the calculations on the larger grid.

The change to the finer grid resulted in a slight further improvement in the computed results. The computed central pressure for the depression was lowered to 989 mb and a closed centre placed off south-east Ireland. At 500 mb the trough line was advanced slightly eastward but the computed 500 mb heights were nowhere changed by more than 20 m.

Full discussion of the importance of departures from geostrophic balance would be impossible without a complete reformulation of the "model" of the atmosphere which has been used as a basis for comparison. However, some allowance for non-geostrophic motion can be made by first using the "balance equation", proposed by Charney (1955), to obtain a stream function which would correspond to non-divergent flow in the initial pressure field, by secondly using this stream function in place of the geopotential in the time-integrations and finally by recomputing the final geopotential field again from the "balance equation". This technique has been used by Bushby (1956) who applied the "balance equation" at the 600 mb level only, and also by others. In the present calculations the "balance equation" was used to determine a stream function at both the 600 mb and 1000 mb levels. In a region of strongly curved and slowly changing isobars the effect of using the balance equation is somewhat similar to the use of the gradient wind in place of the geostrophic wind, and its importance in the present case is that it takes into account the sub-geostrophic wind velocities in the strongly curved contours in the region of the developing depression.

The results of the computations based upon stream functions determined from the balance equations are illustrated in Fig. 2(c) and 3(c). The smaller grid referred to in previous paragraphs was used and allowance for the release of latent heat in the rain area over southern Ireland was made in the manner previously described. The result of all of these changes in technique has been to produce computed charts which are substantially better than those produced by the simple two-parameter model (Fig. 2(b) and 3(b)). The calculated depth of the depression is 987 mb compared with 980 mb observed - a calculated deepening of 8 mb compared with the observed deepening of 15 mb in 12 hours. The depression is also computed to be almost 100 mi too far west.

At 500 mb the trough line is computed to be about 80 miles further east than with the simple two-parameter model and coincides closely with the observed position. Maximum errors are now reduced to about 40 m and occur over central England. The improvement at 500 mb arises almost entirely from the use at 600 mb of the stream function determined from the "balance equation."

As might be expected on occasions of rapid deepening, the results of such numerical computations are rather sensitive to the assumed initial distribution of pressure. Thus, although computations based on two slightly different analyses of the initial 1500 GMT both indicated no deepening of the depression when the simple two-parameter model was used, a third similar integration gave a different result when it was based on an analysis adjusted to take into account the greater depth of the centre observed at 1800 GMT - starting with a depth of 992 mb at 1800 GMT instead of 995 mb at 1500 GMT in the previous calculations. This latter integration gave a deepening of the centre of 6 mb in 9 hours.

/6.

6. Conclusions

The experiments reported here represent only a few of those which must be made if the greatest practical help to forecasters is to be obtained from methods of numerical forecasting. One cannot adopt such modifications of the computation procedure as have been discussed here, without ensuring that they do not introduce as great errors on some occasions as they cure on others. Nevertheless, the results are interesting as suggesting that the present rather simple numerical forecasting models can perhaps be adapted to meet the needs of the forecaster whose concern is with the developments of medium-scale systems within 24 hours. They also indicate that modification of the vertical stability of the air by the release of latent heat in regions of ascent may be an important factor in accelerating the deepening of small pressure centres.

Acknowledgements

I wish to acknowledge the assistance of Miss M. K. Hinds in preparing the programmes for the computations used in the present study and of Mr. F. H. Bushby and Miss Hinds in carrying them out on the Manchester University electronic computer.

References

Bushby, F. H. and V. M. Huckle	1956	The use of a stream function in a two-parameter model of the atmosphere. Quart. J.R. Met. Soc., Vol. 82, p. 409.
Bushby, F. H. and M. K. Hinds	1955	Further computations of 24-hr pressure changes based on a two-parameter model. Quart. J.R. Met. Soc., Vol. 81, p. 396.
Charney, J. G.	1955	The use of the primitive equations of motion in numerical prediction. Tellus, Vol. 7, p. 22.
Houghton, D. M.	1956	The gale of July 29, 1956. Met. Mag., Vol. 85, p. 289.
Sawyer, J. S.	1956	The vertical circulation at fronts and its relation to frontogenesis. Proc. Roy. Soc., A, Vol. 234, p. 346.
Sawyer, J. S. and F. H. Bushby	1953	A baroclinic model atmosphere suitable for numerical integration. J. Met., Vol. 10, p. 54.

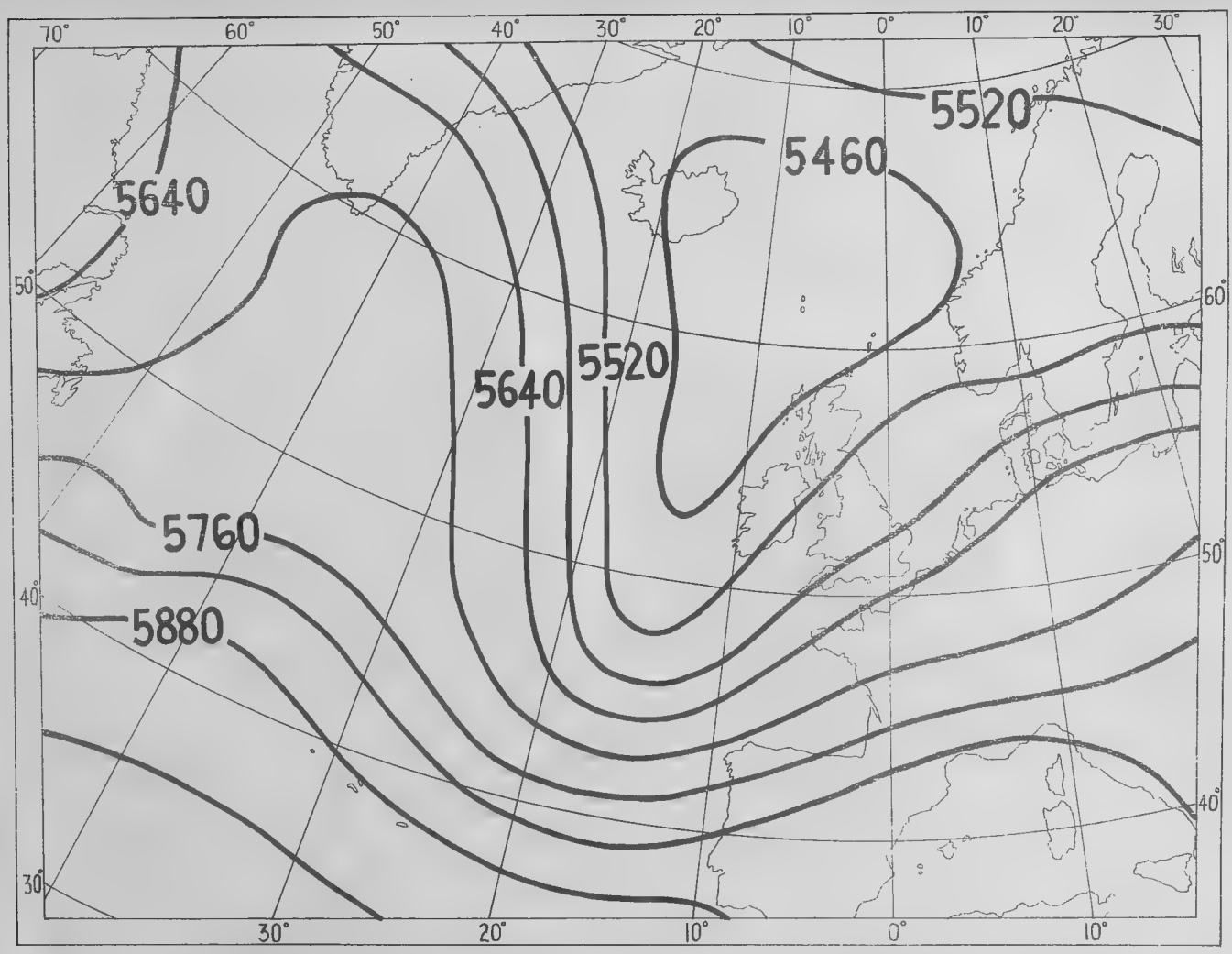

Fig.1 (a) 500 mb. contours (metres) 1500 G.M.T. 28:7:56

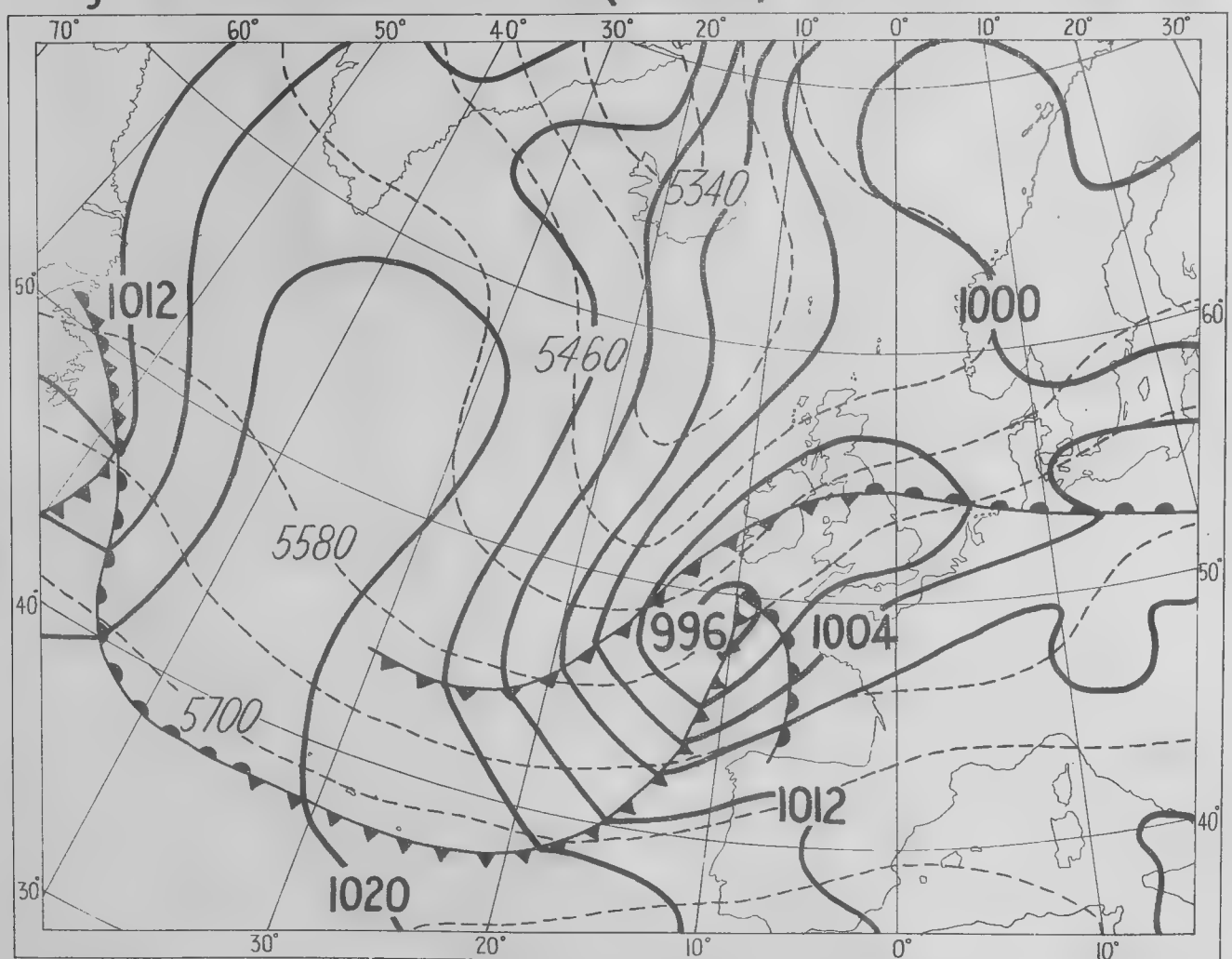

Fig.1 (b) Surface isobars and 1000-500 thickness lines (metres)
1500 G.M.T. 28:7:56

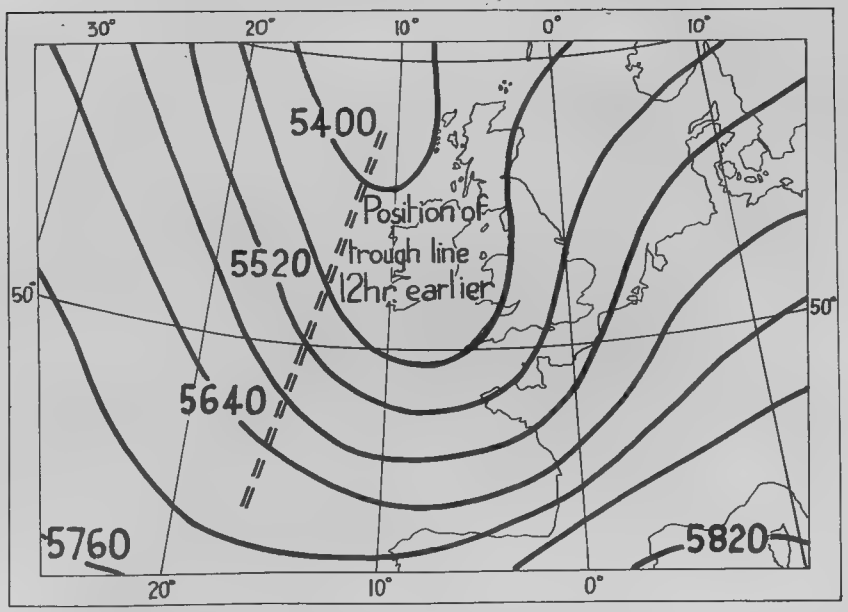

Fig 2(a) 500mb contours (metres) 0300 G.M.T. 29:7:56

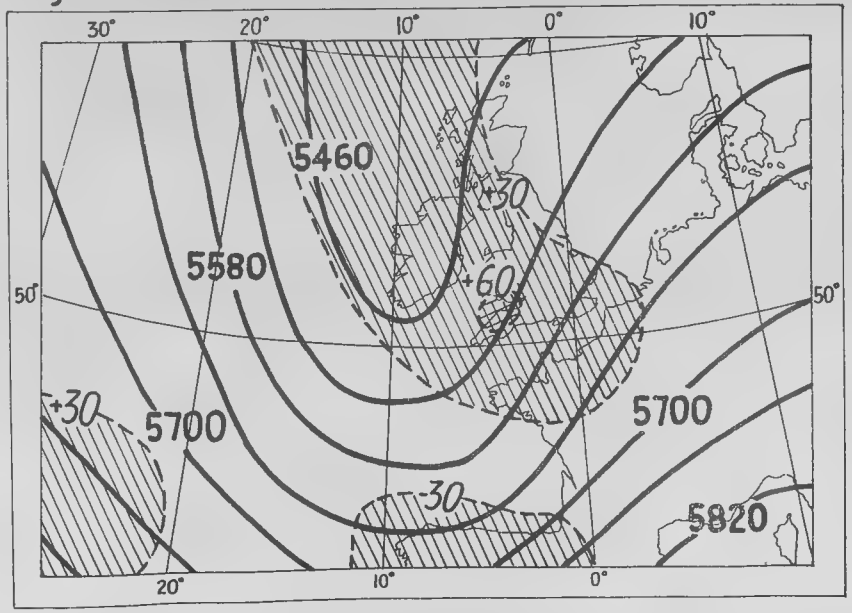

Fig 2(b) Calculated 500mb. contours (metres) 0300 G.M.T. 29:7:56 (12hr. prediction with simple two level model)

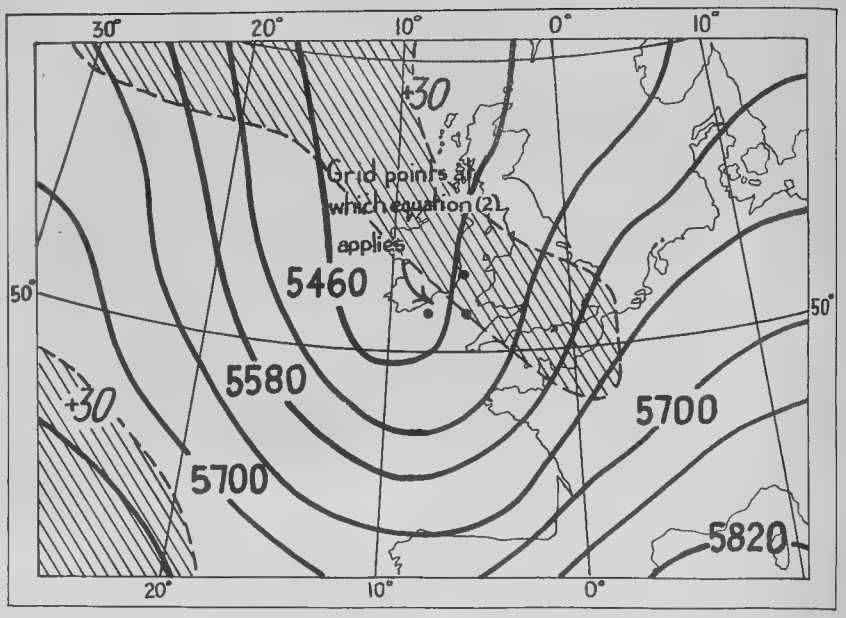

Fig 2(c) Calculated 500mb. contours (metres) 0300 G.M.T. 29:7:56 (12hr. prediction - modified stability stream function used at two levels)

Error field

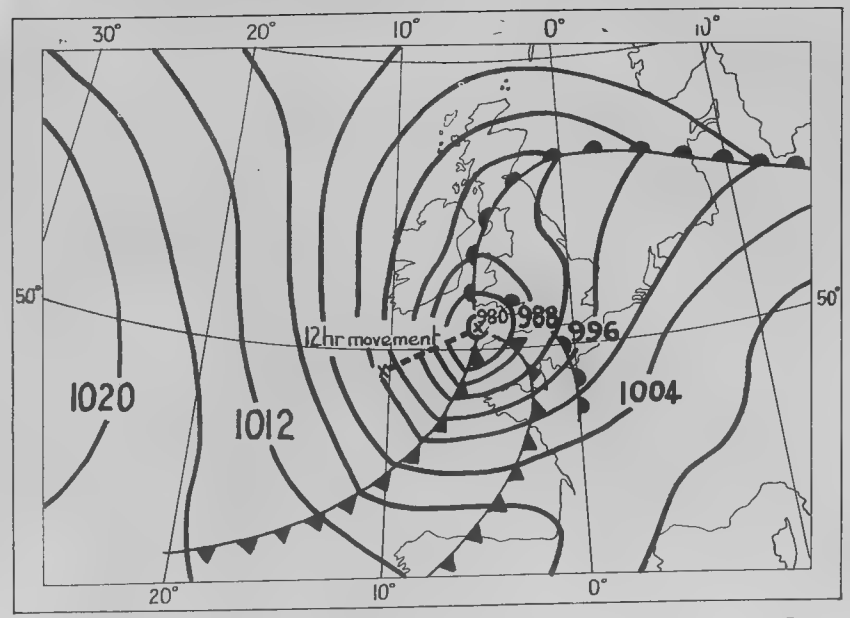

Fig.3(a) Sea level isobars 0300 G.M.T. 29:7:56

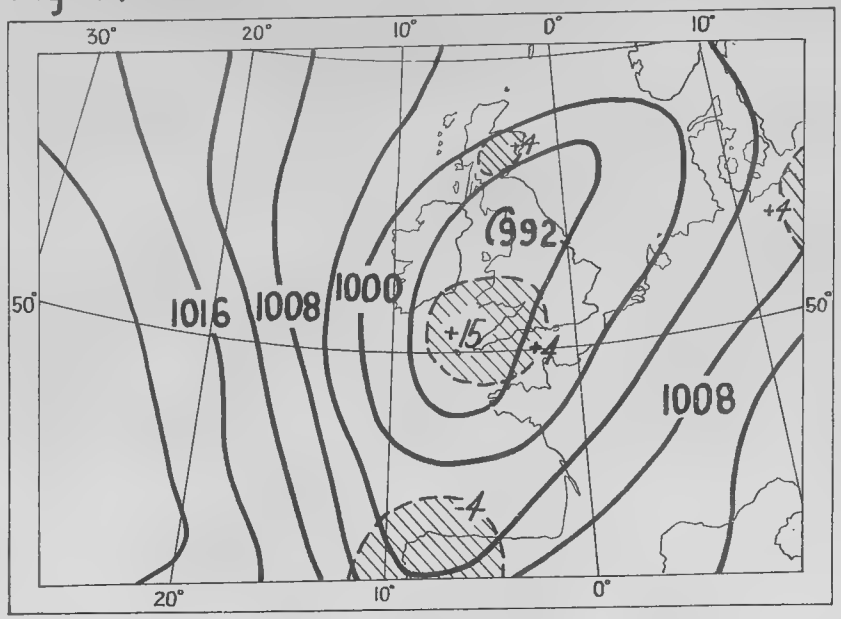

Fig.3(b) Calculated sea level isobars 0300 G.M.T. 29:7:56
(12 hr. prediction with simple two level model)

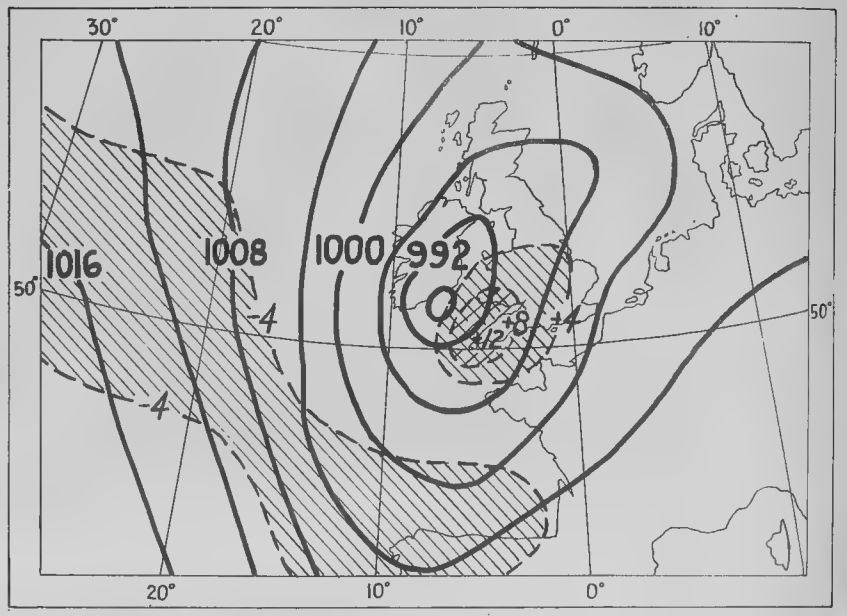

Fig. 3(c) Calculated sea level isobars 0300 G.M.T. 29:7:56 (12 hr. prediction - modified stability stream function used at two levels)

Error field

M.R.P. 1063

1 MAY 1958

M.R.P. 1064
S.C.11/241
26th August, 1957

A.M. 20871

Temperature, humidity and cloud near fronts in the middle and upper troposphere

by

J. S. Sawyer

(Meteorological Office)

AIR MINISTRY

METEOROLOGICAL RESEARCH COMMITTEE

MASTER FILE COPY
NOT TO BE REMOVED
FROM AWS TECH FILES

M.R.P.1064
S.C.II/241
26th August, 1957

AIR MINISTRY

METEOROLOGICAL RESEARCH COMMITTEE

Temperature, humidity and cloud near fronts in the middle and upper troposphere

by

J. S. Sawyer (Meteorological Office)

Introduction

Although from the initial introduction of the idea of a front into meteorology (Bjerknes, 1918) the concept has been three-dimensional, nevertheless until recent years the weather forecaster has not been accustomed either to take into account the observed structure of fronts in the middle or upper troposphere, or even to relate the distribution of cloud at these levels to the position of the front in the upper troposphere. The brilliant analysis techniques of indirect aerology introduced by T. Bergeron (1928) are three-dimensional in concept, but still only relate phenomena of the surface weather map, and it is this chart which has been, and still is, the forecaster's main tool in deciding the distribution of cloud and rain.

On the other hand the present network of upper air soundings enables reliable charts to be drawn for any selected level in the troposphere over much of the northern hemisphere, and attention has recently been directed to the well-defined nature of the frontal zone which can be identified upon these charts and, in particular, at the 500 mb level (Palmén, 1951). Godson, and others (Godson, 1950) have gone further and suggested that an analysis of the three-dimensional shape of frontal surfaces should be made regularly by means of frontal contour charts and should form part of the routine at major forecast offices.

It therefore becomes desirable to study the character of the frontal zone in mid-troposphere, and the relation of the mid-troposphere front to the cloud and rain of frontal regions. It is also desirable to have some idea regarding the means by which the frontal zone is created and maintained. It was with these objects in view that a series of flights was planned by the Meteorological Research Flight of the British Meteorological Office. Each flight was intended to cross the frontal zone at one or more levels in horizontal flight, and information on temperature, frost point and cloud were recorded.

In the present paper I wish to describe some of the observations, and discuss their interpretation in terms of the dynamics of the jet stream and frontal zone.

2. The observations

A Hastings aircraft was used for the flights and observations of temperature were made at half-minute intervals on a flat-plate electrical thermometer mounted beneath the nose of the aircraft. The error of the thermometer was probably about $\pm$ 0.2°F and some doubt (of the order of 1°F) attaches to the correction for airspeed which should have been applied when the aircraft was in cloud. However neither of these uncertainties can affect materially the temperature profiles shown in Fig. 1 and 2.

/Frost

Frost point was obtained by means of a manually operated Dobson-Brewer frost point hygrometer. The probable error of these observations is less than 3°F, but the records are not so complete as those of temperature because of the difficulty of maintaining a long series of readings at only $\frac{1}{2}$-minute intervals.

Visual observations of cloud were recorded on the flights.

3. Temperature profiles

In order to examine the thermal structure of fronts in mid-troposphere the temperature observations made during all horizontal traverses of fronts at (or near) the 500 mb and 600 mb levels have been collected in Fig. 1 and 2. In these diagrams the temperature has been plotted against time but since the aircraft speed was usually around 220 kt and the flight track roughly perpendicular to the frontal zone, the plotted temperatures may be regarded as displaying the horizontal profile of temperature across the front with the scale of distance indicated at the foot of the diagram. One point of the temperature profile has been identified as corresponding to the warm boundary of the frontal zone, and the temperature plots have been aligned for convenience with these points in a vertical line. (All flights which intersected an identifiable front in mid-troposphere on a cross-section based on radiosonde observations have been included). Data for some of the flights have already been published (Sawyer, 1955); other observations come from flights not yet fully analysed. On some occasions level runs were made near both the 500 mb and 600 mb levels, but on other occasions only one level in mid-troposphere was included.

At 500 mb, a well-defined frontal zone with quite sharp changes of temperature gradient can be identified on about half of the occasions. On the remaining flights the region of temperature change is more or less diffuse. The width of the frontal zone as observed on these flights varied between 35 and 170 n.m., and the temperature change from about 6 to 18°F. The strongest maintained temperature gradient was that on 29th November, 1954 which amounted to 10°F in 35 n.m.

At 600 mb the temperature profiles are similar but, on the whole, rather less clearly defined. On less than a third of the temperature profiles in Fig.2 can the frontal zone be identified unequivocably. This may be purely an accident of the sample but, more probably, there is a greater tendency to form a narrow frontal zone with clear-cut boundaries at 500 mb.

4. Distribution of humidity

Fig. 3 and 4 show the horizontal variation of frost point depression at the 500 mb and 600 mb level. With one exception for which no hygrometer observations are available, these correspond to the temperature observations in Fig. 1 and 2. The frost point plots are aligned with respect to the warm boundary of the frontal zone as defined by the temperature observations.

The most striking feature of these humidity observations is the very dry air which is frequently, but not always, found in and near the frontal zone. On seven out of the nine available frost point traverses at 500 mb, the frost point depression exceeds 30°F and on two occasions frost point depressions exceeding 60°F were measured. On the flights which failed to encounter this very dry air, the air is still not really moist. Frost point depressions less than 10°F seem to be the exception and cloud in the frontal zone was encountered only once. On two other occasions the aircraft flew through cloud some distance on the warm side of the frontal zone, and once on the cold side. Cloud would no doubt have been encountered more frequently if the flights could have been extended for greater horizontal distances into the warm air.

/The

The distribution of the frost point depression does not appear to be closely related to the frontal zone or its boundaries, except that when the frontal zone was very clearly defined by the temperature profile (e.g., 29th November, 1954, 3rd November, 1950, 3rd November, 1953, 27th April, 1951) the very dry air was present and the frost point depression reached its extreme near the warm boundary of the frontal zone.

At 600 mb the humidity distribution seems even more erratic than at 500 mb. Some very dry air (frost point depression greater than 30°F) occurred on 7 out of the 12 flights and on most of them frost point depression is greater than 10°F over considerable stretches of the flight. On three of the flights the very dry air was closely associated with the frontal zone but on the remainder it was irregularly distributed.

The aircraft passed through cloud on 9 out of the 12 flights. On six of these the cloud did not significantly enter the frontal zone, being mainly on the warm side. On three flights, however, there was extensive cloud in the frontal zone and on one of these solid cloud appeared to fill most of the transitional region. This occurred in a broad warm-front zone with a steep slope of 1 in 30 and might be regarded as exceptional.

5. Summary of the observations

In order to summarise the data average temperature and frost point profiles have been calculated (Fig. 5 and 6). This has been done using the position of the warm boundary of the frontal zone as a reference point, and the temperature at this point as a reference temperature. In view of the wide dis-similarity of individual profiles the resulting average cannot be regarded as particularly representative. However, it serves to emphasise that at 500 mb the air in and surrounding the frontal zone is normally dry and has the lowest relative humidity near the warm boundary of the frontal zone. The average frost point depression everywhere exceeds 15°F and reaches 35°F in the frontal zone. There is no sign of a rapid increase in water-content across the frontal zone or its boundaries and it seems quite clear that at this level the frontal zone does not represent a transition from a cold dry air mass to a warm moist one; nor is the idea of up-gliding of air immediately above the frontal zone substantiated.

At 600 mb the average structure is somewhat different. The average frost point depression is relatively small just on the warm side of the frontal zone (less than 10°F), while a dry region occurs in the frontal zone (on which the frost point depression exceeds 20°F). The moist region just in the "warm air" adjacent to the front is found on individual flights and saturation was reached in this region on several occasions with accompanying cloud.

6. Some theoretical considerations

Fronts are closely linked with depressions and with the jet stream, and any completely satisfying explanation of the character of fronts would probably have to start with a theory of depressions and the jet stream. Nevertheless there is value in more limited theoretical discussions, and in the following paragraphs I have attempted to show that some of the characteristics of fronts in the upper troposphere follow as consequences if we accept the existence of the jet stream, and the fact that it has a coherent and only slowly varying structure. Thus I wish to side-step the question "Why is the front there?", and merely consider why some of the properties which we observe are necessary for its self-consistency.

For this purpose it is useful to consider the conditions under which a jet stream can persist in the upper troposphere in only slowly varying form.

/It

It is a fact of observation that this occurs, and that the jet stream current is sinuous and that the velocity in the core varies along its length. The troughs and ridges and the velocity maxima move considerably more slowly than the wind. For simplicity, we may regard the flow pattern as stationary with respect to the flow at some level in mid-troposphere. To be specific, we regard the flow as steady relative to co-ordinates moving with the 600 mb flow, and we examine the changes of vorticity which occur at higher levels as the air flows through the pattern.

Cross-sections drawn through the jet stream draw attention to the narrow character of the velocity maximum and the high values of horizontal wind shear, more particularly on the cold side. A typical wind profile would be that represented in Fig. 7(a) and the corresponding vorticity profile based on the wind shear would be as represented in Fig. 7(b).

Changes in the intensity of the jet stream or changes of its curvature along its length will involve changes in the vertical component of vorticity, and it is useful to examine how these arise. The procedure which I shall adopt is to assume (1) that the jet stream intensifies without change of wind profile or alternatively (2) that from being straight the jet becomes curved downstream (again without change of form), and I shall examine the pattern of divergence and vertical motion which would be necessary to satisfy the vorticity equation. Regarded strictly this procedure is invalid because the wind profile may, and probably does, change along the stream but the only alternative appears to be to attempt the solution of the three-dimensional dynamical problem. The simpler approach is both more practical, and shows more clearly the interaction of the various dynamical processes.

The vorticity equation in isobaric co-ordinates can be used to describe the change of vertical component of vorticity as the air flows along the jet stream. Thus

$$\frac{D\zeta}{Dt} - \frac{\partial w}{\partial y}\frac{\partial u}{\partial p} + \frac{\partial u}{\partial x}\frac{\partial v}{\partial p} + (f+\zeta)\,\mathrm{Div}_p\,\underset{\sim}{v} = 0 \qquad (1)$$

where $w \equiv Dp/Dt$

If we choose the x axis along the direction of the jet stream, $\partial u/\partial$ is very much greater than $\partial v/\partial p$, and we can neglect the term $\frac{\partial w}{\partial x}\frac{\partial v}{\partial p}$

If, further, we assume that the flow is steady relative to some co-ordinate system moving with the general features of the flow at a speed corresponding to the wind at say 600 mb, and we ignore the local vorticity change in this moving co-ordinate system compared with the advective change, then

$$V\frac{\partial \zeta}{\partial s} + w\frac{\partial \zeta}{\partial p} - \frac{\partial w}{\partial y}\cdot\frac{\partial u}{\partial p} + (f+\zeta)\,\mathrm{Div}_p\,\underset{\sim}{v} = 0 \qquad (2)$$

where V is the wind velocity relative to the wind at 600 mb and $\frac{\partial \zeta}{\partial s}$ is the vorticity change along a horizontal projection of a stream line.

In order to make some general deductions about the character of the flow we will assume that $V\frac{\partial \zeta}{\partial s}$ can be roughly estimated from the fact that the

jet is assumed (1) to intensify downstream or, alternatively, (2) to acquire curvature along its length. We may also assume from the presence of relatively undistorted isentropic surfaces in the stratosphere only a little above the jet that there is a level of small vertical motion somewhere near the jet level. At such a level the principal terms of equation (2) must be $V\partial\zeta/\partial s$ and $(f+\zeta)\,\mathrm{Div}_p\, \underline{v}$. The divergence $\mathrm{Div}_p\, \underline{v}$ can be calculated from these two terms alone.

On this basis, the distribution of $\mathrm{Div}_p\, \underline{v}$ across the jet stream must be broadly as indicated in Fig. 7(c) and 7(d) for the two assumptions (1) of a jet stream intensifying along its axis and (2) of acquiring cyclonic curvature downstream. The particular conditions assumed in deriving Fig.7(c) and 7(d) respectively are (1) that the jet stream velocities increase by 10 per cent in 100 miles downstream $\left(V\frac{\partial\zeta}{\partial s} = \frac{V\zeta}{10^3}\ \text{hr}^{-2}\ \text{with}\ V\ \text{in kt}\right)$ and (2) that the jet stream acquires a curvature with 600 n.m. radius at a distance 1000 n.m. downstream from a straight section.

An interesting feature of these distributions of divergence is the strong gradients of divergence across the jet stream, and in particular the strong increase of convergence towards the jet axis from the cold side. If the vertical velocity is small near the jet stream level, then at lower levels towards mid-troposphere a strong gradient of vertical velocity must be expected with strong descent near to the jet stream axis and relatively weak descent only some 200 miles further towards the cold side of the jet. This differential subsidence can be expected to be effective in setting up a strong horizontal gradient of temperature in mid-troposphere as observed in the 500 mb frontal zone.

However the picture is more complicated, because the resulting values of the vertical velocity are large enough to make the second and third terms in equation (2) comparable in magnitude with the others. (The second and third terms represent respectively the vertical advection of vorticity and the vorticity change arising from the tilting of the vortex tubes). Were in fact the values of the divergence represented in Fig. 7(c) and 7(d) continued down to the 500 mb level then there would be values of ω and $\partial\omega/\partial x$ occurring at that level of as much as 10 mb/hr and 3.5×10^{-2} mb/hr^{-1}nm^{-1}. If we assume that the wind increases linearly from a uniform value of 40 kt at the 600 mb level up to the level of the jet stream at say 300 mb, then the order of magnitude of the terms in equation (2) would be as indicated in Table I. The crude assumption has been made that values of ω can be calculated from the divergence obtained ignoring terms $\omega\,\partial\zeta/\partial p$ and $-\partial\omega/\partial y \cdot \partial u/\partial p$.

Table I - Relative magnitude of terms in equation (2)

		$V\frac{\partial\zeta}{\partial s}$	$+\omega\frac{\partial\zeta}{\partial p}$	$-\frac{\partial\omega}{\partial y}\frac{\partial u}{\partial p}$	$+(f+\zeta)\mathrm{Div}_p V$
		(Units hr^{-2})			
400 mb	50 mi. from axis	1.6×10^{-2}	-0.4×10^{-2}	0	-1.2×10^{-2}
	150 mi. from axis	0.7×10^{-2}	-0.2×10^{-2}	-0.2×10^{-2}	-0.3×10^{-2}
500 mb	50 mi. from axis	0.4×10^{-2}	-0.8×10^{-2}	0	$+0.4 \times 10^{-2}$
	150 mi. from axis	0.2×10^{-2}	-0.4×10^{-2}	-0.4×10^{-2}	$+0.6 \times 10^{-2}$

/It

It is immediately clear that both the vertical advection of vorticity, $w\,\partial\zeta/\partial p$, and the "tilting term" $-\partial w/\partial y \cdot \partial u/\partial p$, are likely to be significant in the region immediately below and on the cold side of the jet stream. This has been confirmed, particularly as regards the latter term, by individual case studies by Reed and Sanders (1953), Reed (1955) and Newton (1954).

The values of w on which the preceding figures are based assume that the convergence can be calculated ignoring the two terms which we have seen to be important. This is clearly invalid. In fact we can deduce that the convergence rapidly decreases downwards, and may even be replaced by divergence. It is also clear that this reversal should take place more rapidly at 150 miles from the jet axis than closer to the axis because the stronger horizontal gradient of w at the former position gives rise to larger values of the "tilting term". The fields of divergence and of vertical motion in the region below and on the cold side of the jet must be roughly as indicated in Fig. 8(a) and (b).

The region of horizontal divergence below and to the cold side of the jet stream will bring about an intensification of the vertical gradient of potential temperature (i.e., it will increase the vertical stability) in this region as is observed in the 500 mb frontal zone. At the same time the tilting about a horizontal axis will increase the horizontal temperature gradient, and this will be accompanied by an increase in the cyclonic vorticity about a vertical axis apparently primarily as a result of the "tilting term" $-\partial w/\partial y \cdot \partial u/\partial p$, in equation (1).

It is not profitable to pursue the argument further without a more satisfactory treatment of the balance between the various dynamical factors involved. Nevertheless, the treatment has probably been adequate to show that a jet stream which has a strong shear on its cold side, and flows from a region of relatively low speed to one of higher speed, must develop a region of general subsidence on its cold side which is accompanied by an intensification of both horizontal and vertical gradients of potential temperature such as is observed in 500 mb frontal zones.

Similar conclusions would follow regarding regions where the jet stream flows into a slow-moving upper trough although the frontal zone would then be built up at a smaller horizontal distance from the jet axis.

This dynamical process provides no explanation as to why the boundaries of frontal zones should be so sharp and well-defined as is often observed. However, these rather abrupt changes of temperature gradient may well arise from the intensification and tilting of already existing boundaries to inversions or stable layers. The horizontal divergence will intensify the changes in vertical gradients of temperature and the tilting will introduce into the horizontal temperature gradients much stronger discontinuities than are normally present. Reed and Sanders (1953) describe a case in which the subsidence was sufficiently great to bring stratospheric air into the frontal zone, and the tropopause itself provided the initial discontinuity of lapse rate which became the boundaries of the frontal zone. I also examined a similar case which occurred over north France on 3rd November, 1950 and which appears in Fig. 1 and 3 (Sawyer, 1955). However, these cases are probably exceptional, and stable layers and inversions in the troposphere may also provide the initial discontinuities of lapse rate which are intensified into the boundaries of frontal zones.

So far, I have discussed the formation of a frontal zone in intense sections of the jet stream and in the regions of upper troughs. The arguments may be reversed to suggest a reverse circulation and frontolysis as the air passes into weaker sections of the jet and into upper ridges. No doubt detailed observations of the jet stream and studies of upper fronts have concentrated on regions where they are intense, but I think

/there

there is another reason why the structure which is built up in these intense regions of the jet and frontal zone should persist elsewhere. That is because it is unlikely that vertical circulation as the air enters a diffluence or a ridge will be the exact reverse of that in a preceding confluence or trough. It will not be the same air which descended in the confluence that ascends again in the diffluence - sufficient small changes in the relative position of front and jet will probably have taken place to mean that the air which rises most will not be precisely that which descended most. Thus in association with weaker sections of the jet and with upper ridges, we might expect to find some remnant, albeit less intense, of the dry frontal zone built up in preceding a confluence or trough.

Conclusions

The temperature observations on horizontal traverses beneath the jet stream confirm that a narrow "frontal zone" some 30 to 50 miles wide and with sharp boundaries is often present at the 500 mb level. ~~On other occasions the temperature changes are more diffuse.~~ Humidity observations indicate that the air in and near the "frontal zone" has undergone subsidence and make it seem unlikely that the "frontal zone" at this level owes its origin to the different geographical origin of the air on either side of it. Theoretical considerations suggest the horizontal temperature gradient arises from the differential subsidence of air on the cold side of the jet stream which leads to tilting of the isentropic surfaces. Dynamical considerations also explain the vertical stability and cyclonic vorticity associated with the front.

The front-forming processes in the upper troposphere only operate where the jet stream is intensifying or becoming more cyclonically curved along its length, but the characteristic structure is carried forward into other weaker sections of the jet and probably does not degenerate completely. ~~This may account for the variety of temperature and humidity profiles observed.~~

At 600 mb the temperature gradients at fronts are somewhat less well-defined than at 500 mb, and although dry subsided air is often found in the frontal zone, the air on the warm side of the warm frontal boundary is usually relatively moist. Saturation and cloud occur in this region and the structure corresponds more closely at 600 mb to the conventional front with upsliding warm air. ~~This conforms with previous findings (Sawyer and Dinsdale, 1955) that~~ the boundary of the frontal cloud mass slopes more steeply than the front itself and, on the average, intersects the warm boundary of the frontal zone around 600 mb.

References

Bergeron, T.	1928	Ober die drie-dimensional verknupfende Wetteranalyse. Geofysiske Publikationer, Vol. 5, No. 6.
Bjerknes, J.	1918	On the structure of moving cyclones. Geofysiske Publikationer, Vol. 1, No. 2.
Godson, W.L.	1950	The structure of North American weather systems. Centenary Proceedings, Roy. Met. Soc., p.89.
Newton, C.W.	1954	Frontogenesis and frontolysis as a three-dimensional process. J. Met., Vol. 11, p.449.
Palmén, E.	1951	The aerology of extra tropical disturbances. Compendium of Meteorology.
Reed, R.J. and F. Sanders	1953	An investigation of the development of a mid-tropospheric frontal-zone and its associated vorticity field. J. Met., Vol. 10, p.338.
Reed, R.J.	1955	A study of a characterictic type of upper-level cyclogenesis. J. Met., Vol. 12, p.226.
Sawyer, J.S.	1955	The free atmosphere in the vicinity of fronts. London, Met. Office, Geophysical Memoir No. 96, Vol. 12, No. 4.
Sawyer, J.S. and F.E. Dinsdale	1955	Cloud in relation to active warm fronts near Bircham Newton, 1942-46. London, Met. Office, Professional Note No. 115.

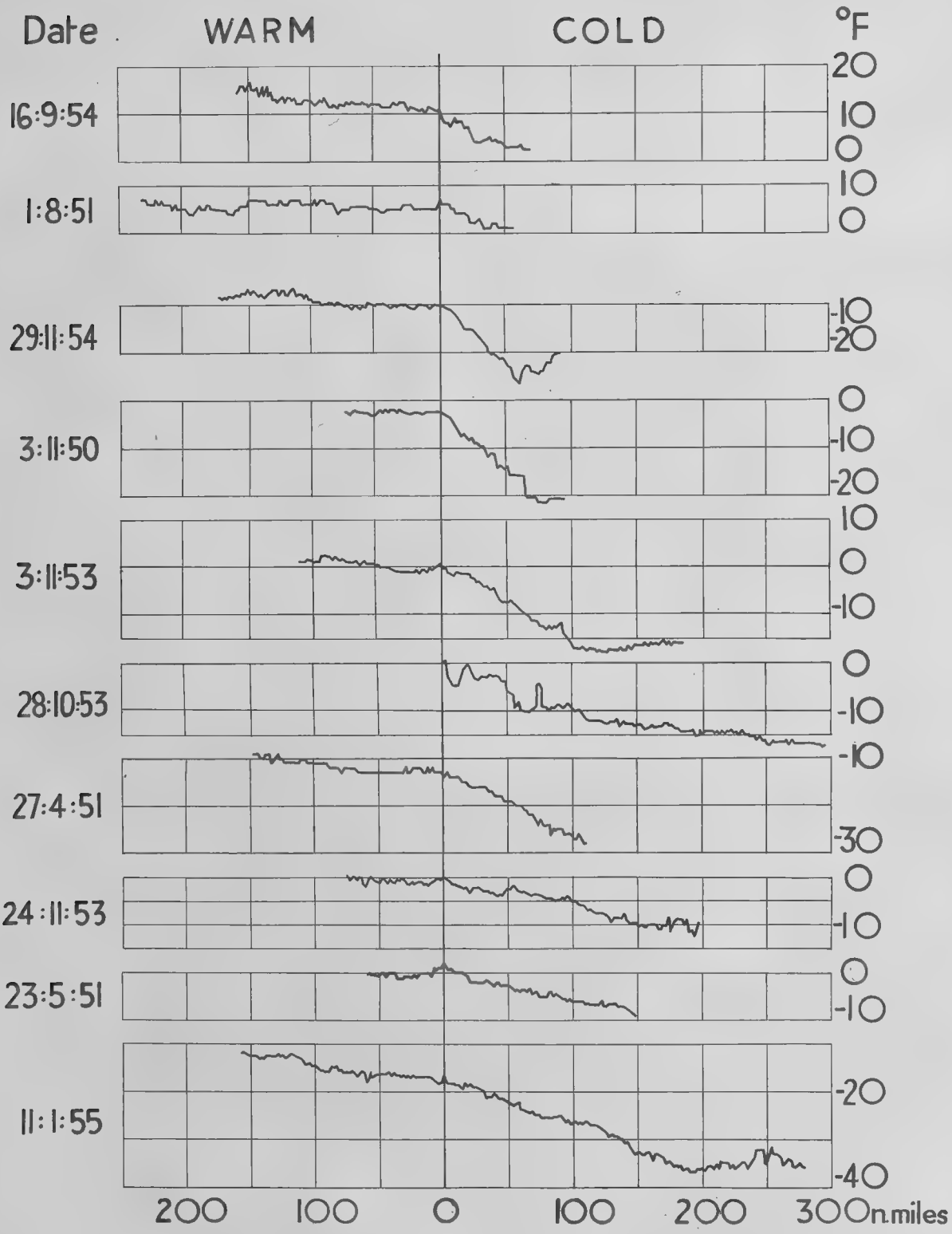

Approximate scale of distance

Horizontal distribution of temperature through frontal zones at 500mb.

Fig. 1

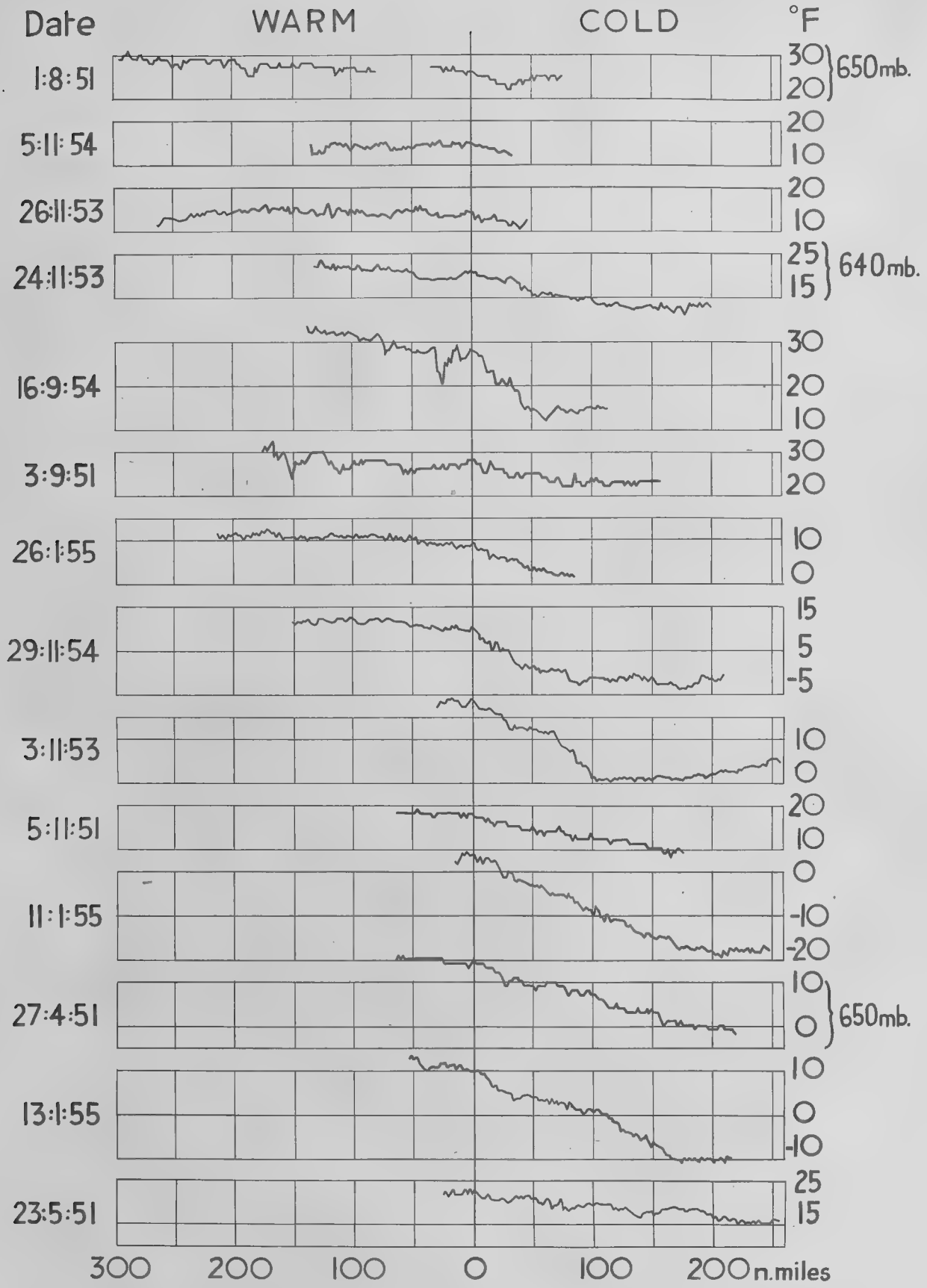

Approximate scale of distance

Horizontal distribution of temperature through frontal zones at 600mb.

Fig. 2

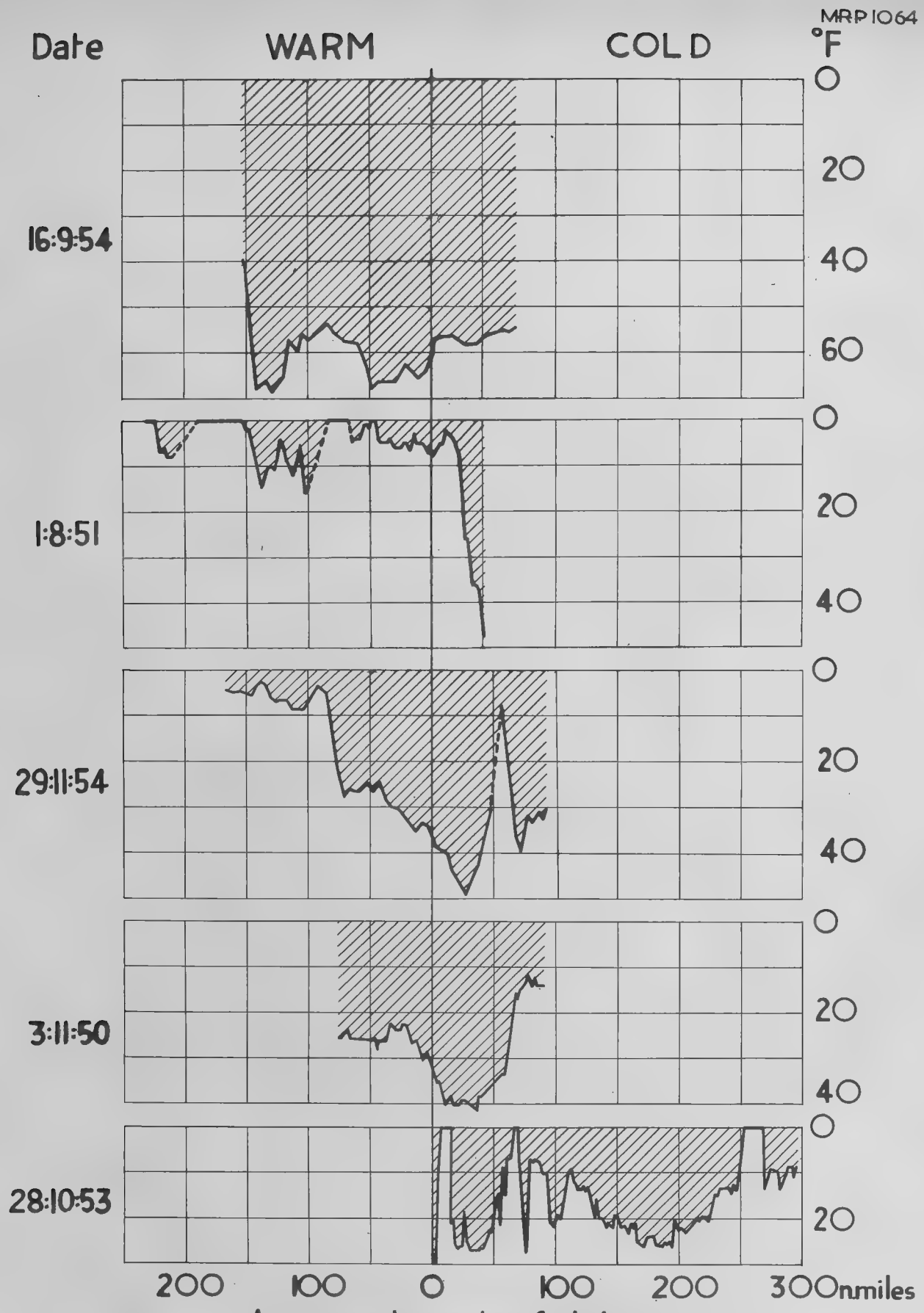

Horizontal distribution of frost point depression through frontal zones at 500 mb. (___ cloud)

Fig 3(a)

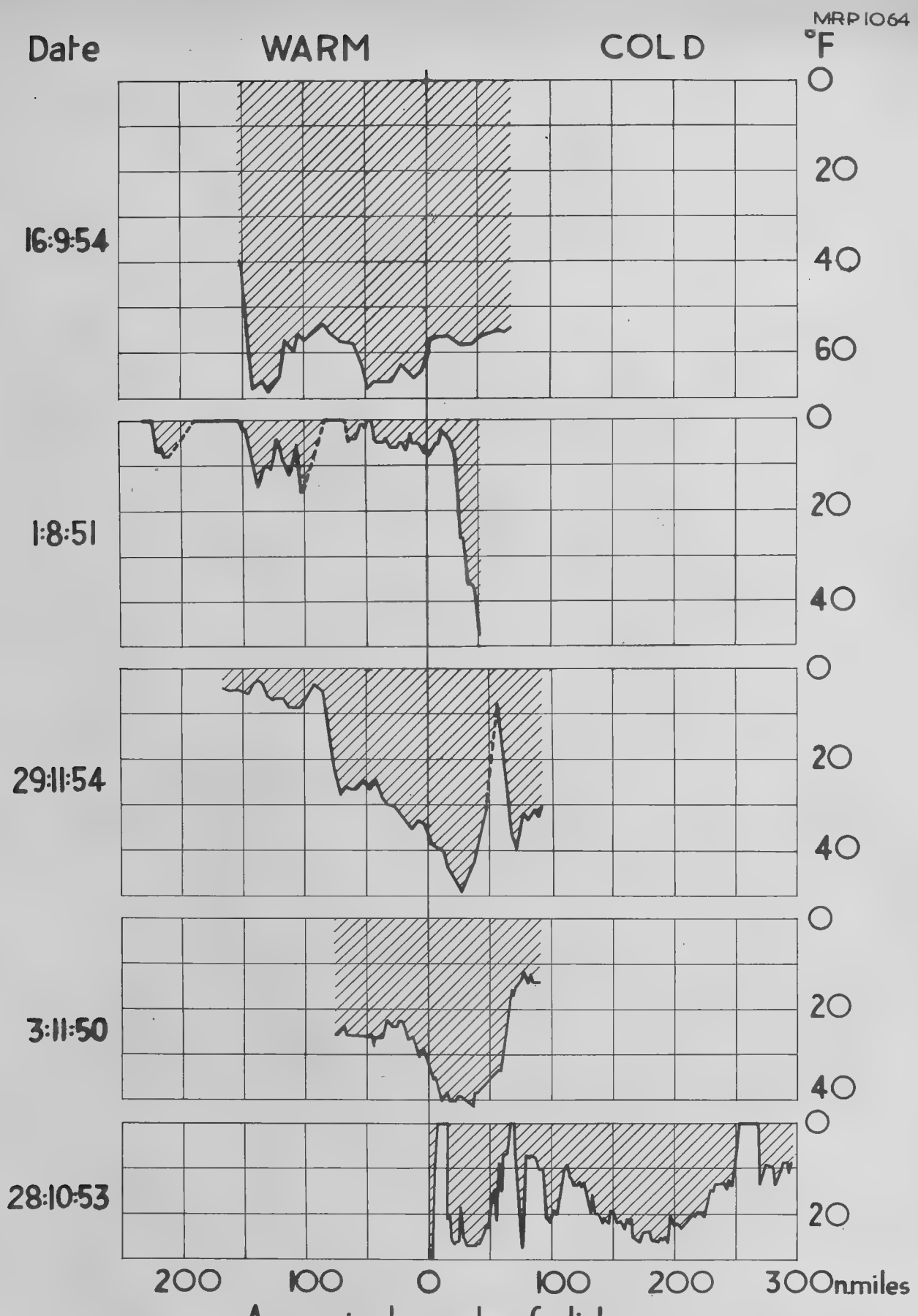

Horizontal distribution of frost point depression through frontal zones at 500 mb. (___ cloud)

Fig 3(a)

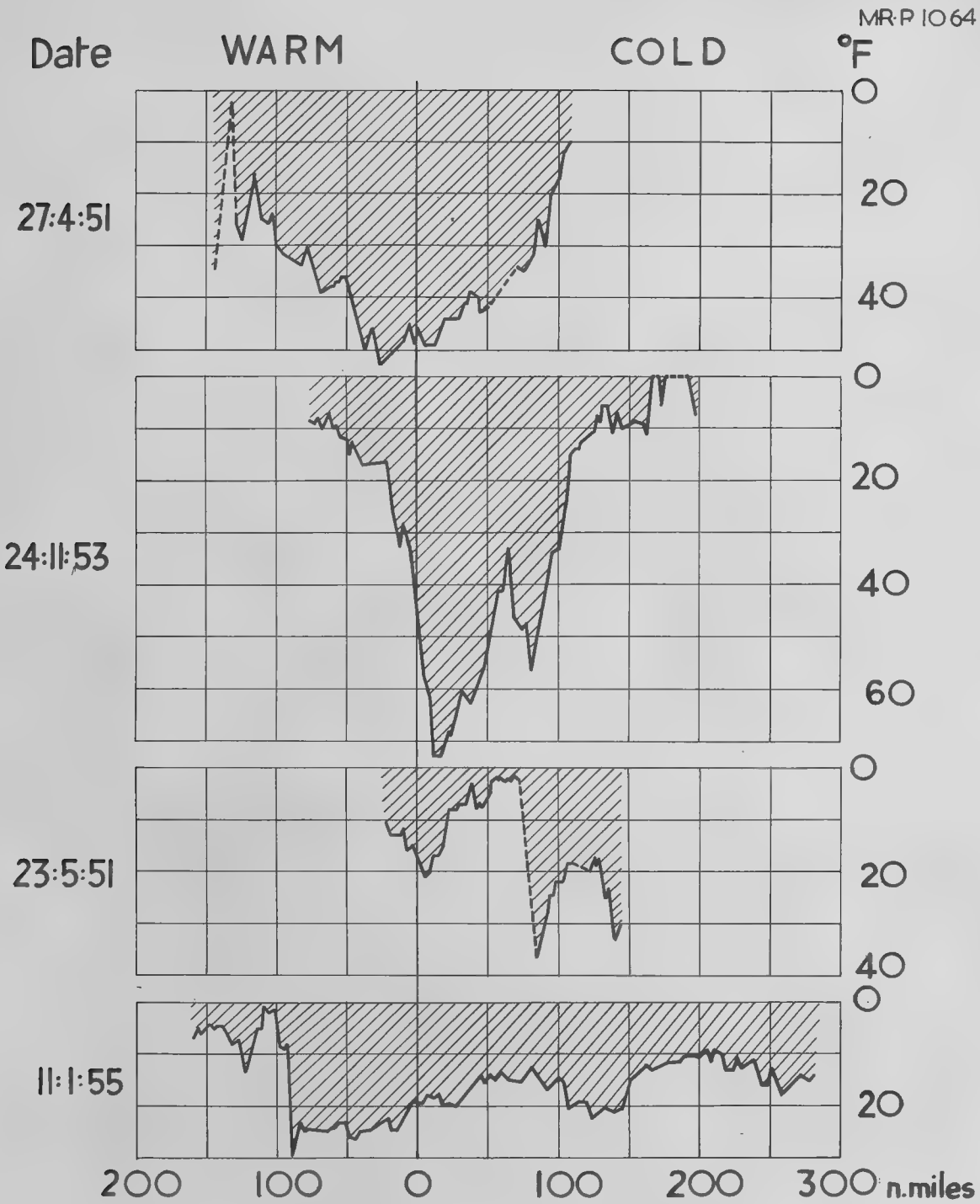

Horizontal distribution of frost point depression through frontal zones at 500 mb. (____ cloud)

Fig. 3(b)

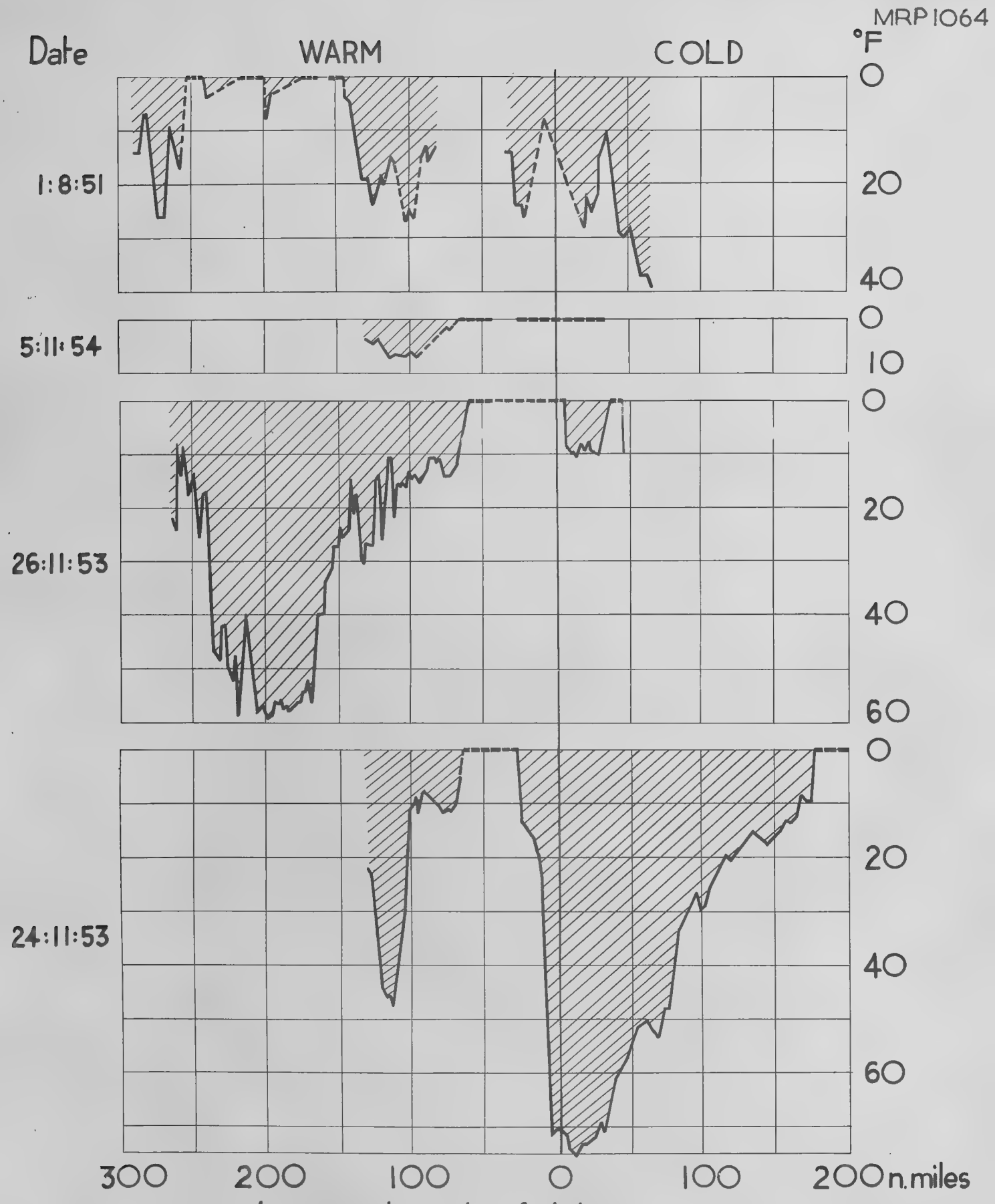

Horizontal distribution of frost point depression through frontal zones at 600 mb. (____ cloud)

Fig. 4 (a)

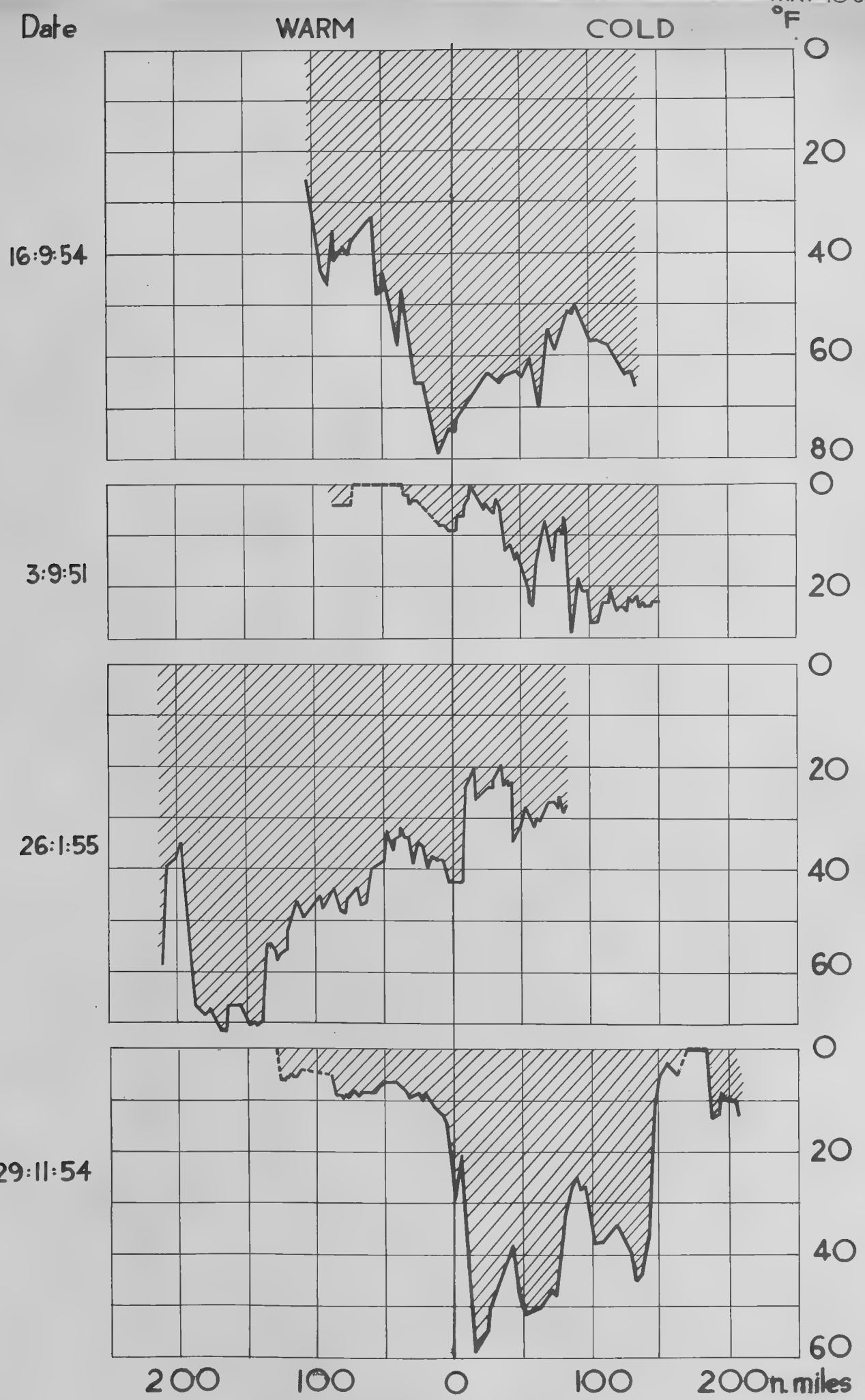

Horizontal distribution of frost point depression through frontal zones at 600 mb. (___ cloud)

Fig. 4(b)

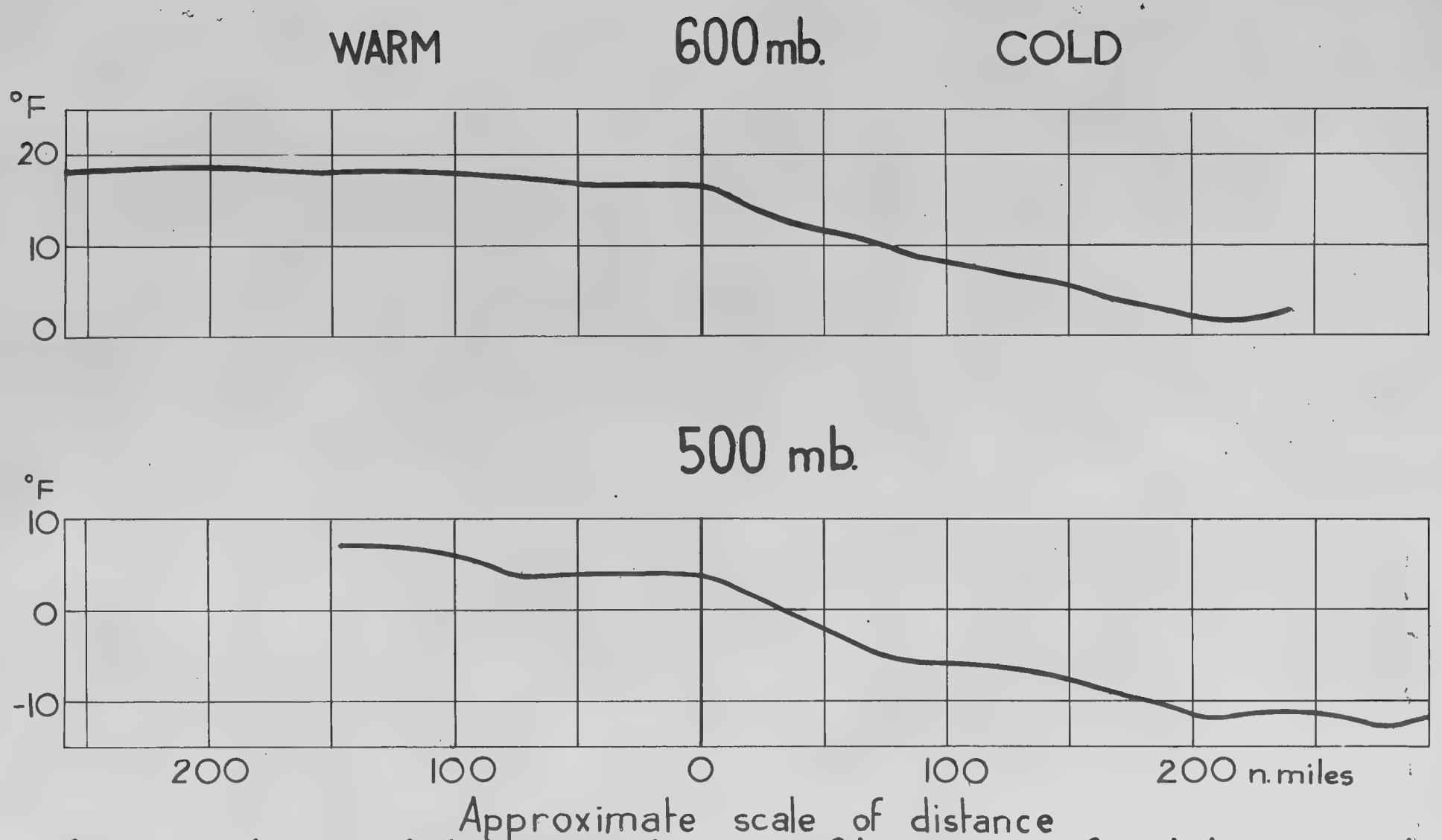

Average horizontal temperature profile across frontal zones at 500 mb. and 600 mb.

Fig. 5

MRP 1064

MRP1064

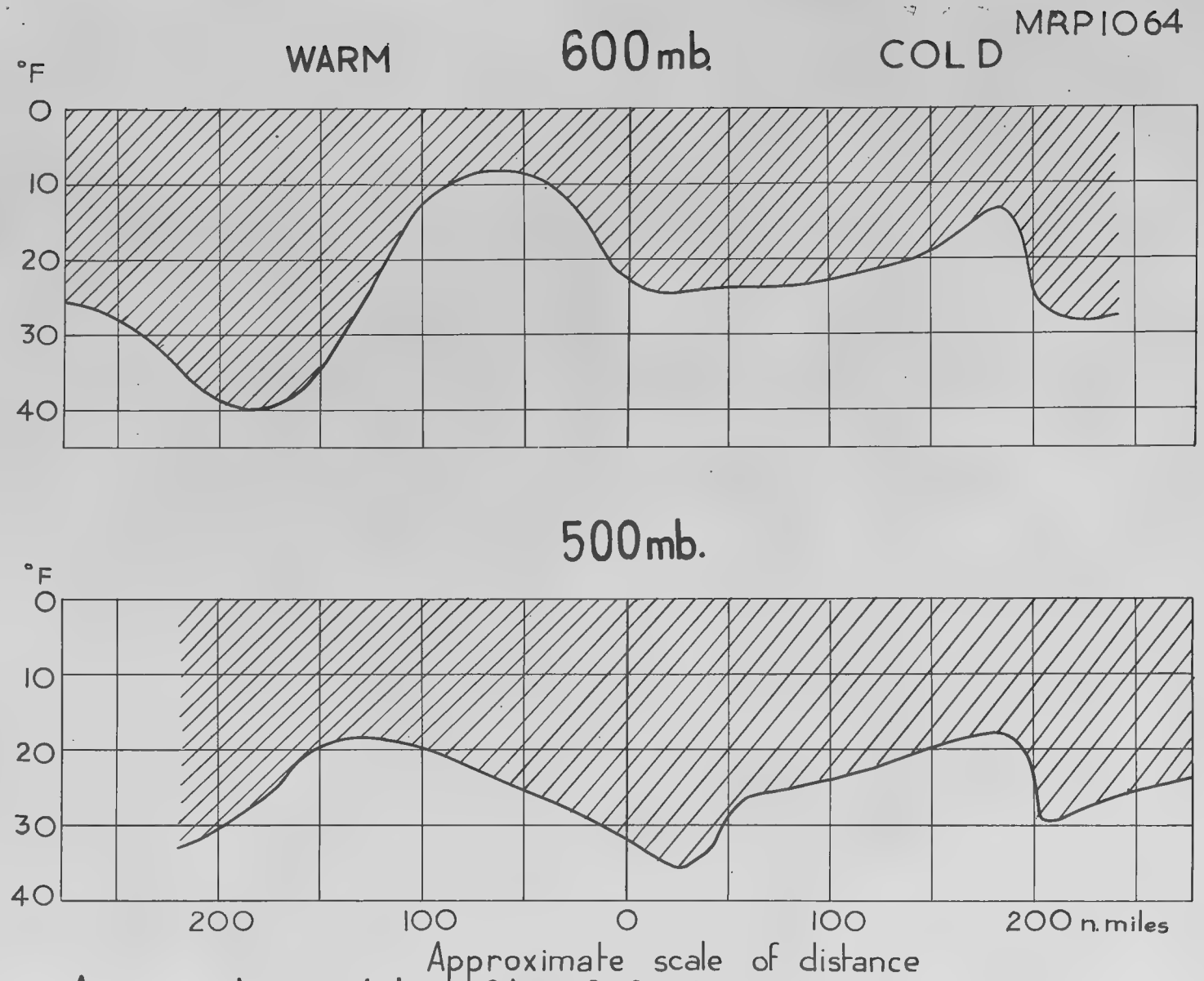

Average horizontal profile of frost point depression across frontal zones at 500mb. and 600mb.

Fig. 6

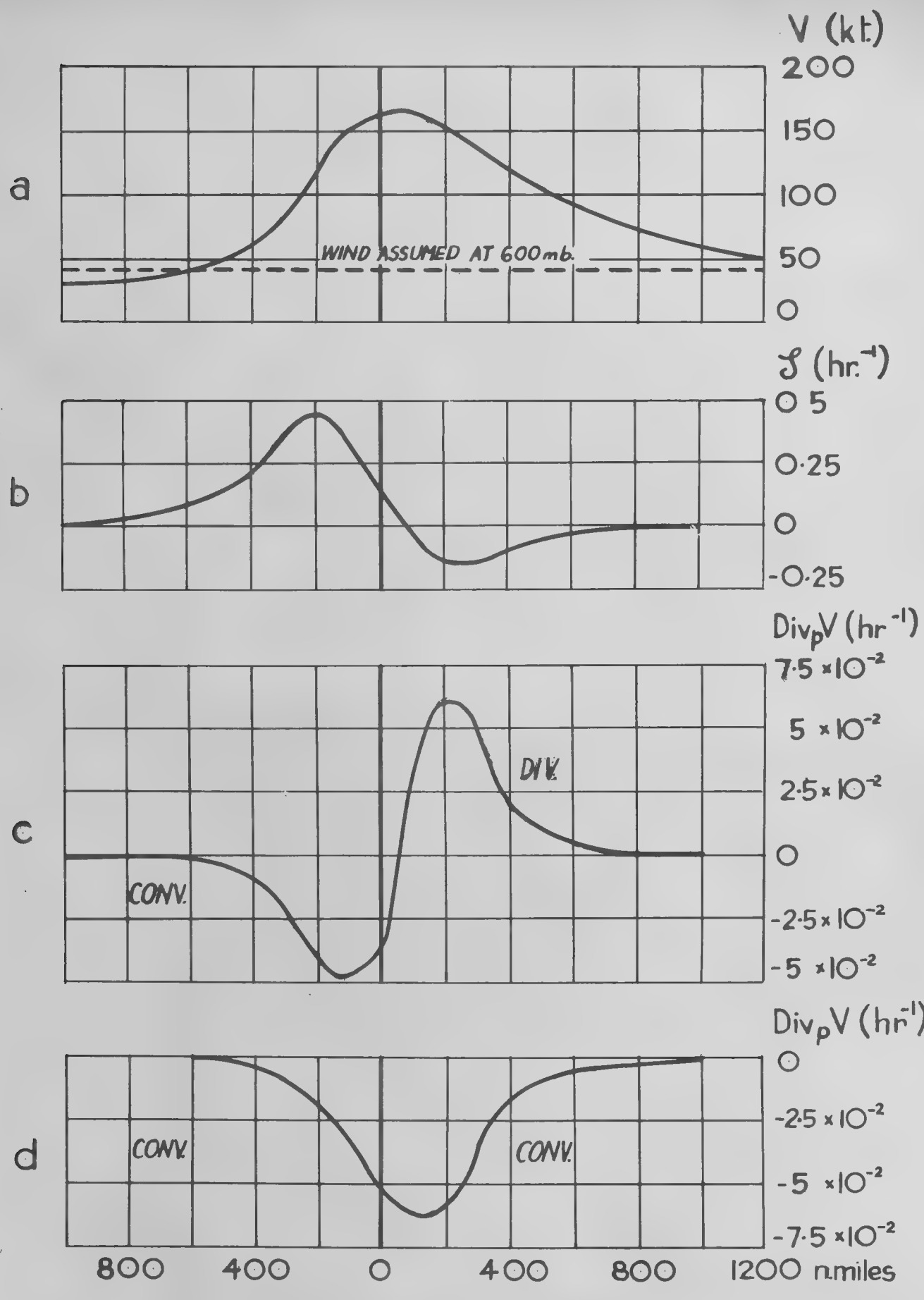

(a) Schematic profile of wind through a jet stream
(b) Corresponding profile of relative vorticity
(c) Distribution of divergence required if the jet stream intensifies along its length
(d) Distribution of divergence required if the jet stream is to acquire a curvation of 600 n. miles

Fig. 7

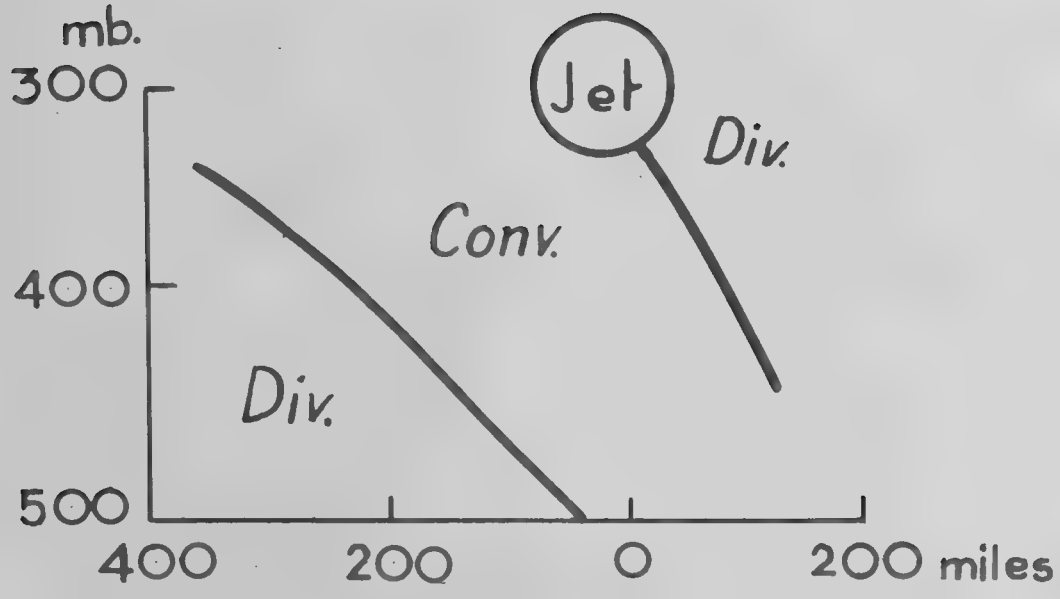

(a) Horizontal divergence

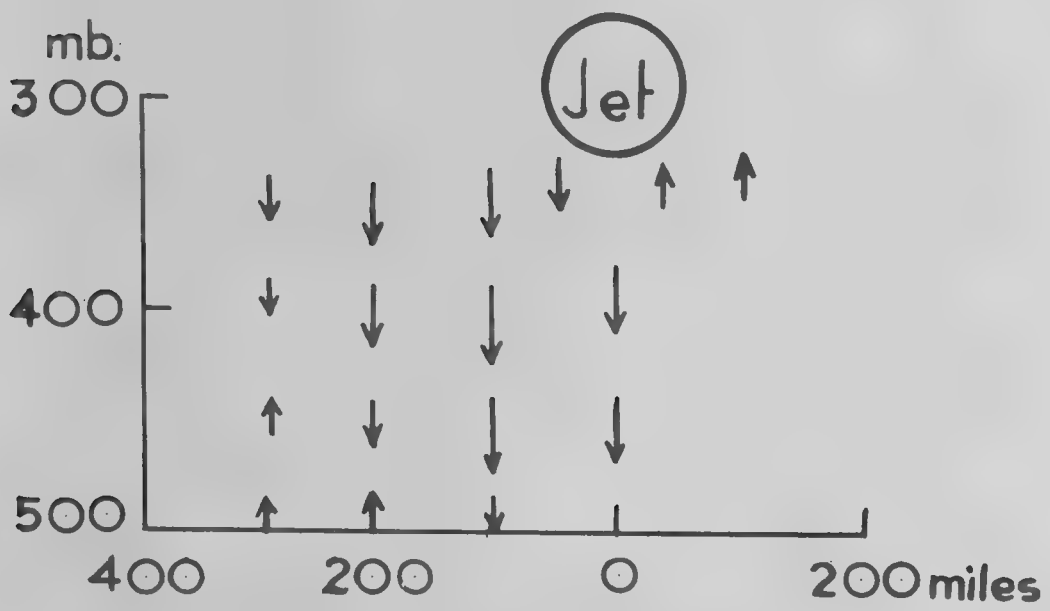

(b) Vertical motion

Distribution of horizontal divergence and vertical motion on the cold side of an intensifying jet stream

Fig. 8

M.R.P. 1065
S.C.11/242
14th August, 1957

2 MAR 1958
27 MAR 1958

The Southern Circumpolar Westerlies: broad characteristics and apparent associations

by

H. H. Lamb

(Meteorological Office)

AIR MINISTRY

METEOROLOGICAL RESEARCH COMMITTEE

At the time of issue this report has not been published. Any author desiring to quote this paper should refer to it as "A paper of the Meteorological Research Committee (London), M.R.P. No. 1065 by Mr. H.H. Lamb
A copy is available in the Library of the Meteorological Office."

M.R.P.1065
S.C.II/242
14th August, 1957

AIR MINISTRY

METEOROLOGICAL RESEARCH COMMITTEE

The Southern Circumpolar Westerlies; broad characteristics and apparent associations

by

H.H. Lamb (Meteorological Office)

Summary

The data available, which are admittedly and as yet unavoidably scanty, suggest that the southern hemisphere westerlies carry much more momentum than their northern counterparts, possibly by as much as a factor of nearly two over the year as a whole. In the northern summer-southern winter the factor is approximately four. The system appears to be the most energetic limb of the atmospheric circulation, and it may be useful to regard it as the "flywheel" and a sort of (partial) "governor".

Preliminary survey at the 500 mb level shows the main trough south of 40°S. in the Indian Ocean sector, centred about 100°-110°E. at most seasons of the year, and the main ridge in the western Pacific in the neighbourhood of the outer reaches of the Ross Sea. The mean troughs and ridges have notably smaller amplitude than in the northern hemisphere. The control of trough and ridge positions appears to be thermal rather than orographic, associated with the position of the broadest part of the Antarctic cooling surface, and, at certain seasons, perhaps, with the Eurasian monsoon. Little seasonal movement of the troughs and ridges in longitude is discerned and no very great change of circulation intensity, but there is an intensification of flow and increase of amplitude in the Indian Ocean trough from summer to late winter.

The pattern of glaciation, as well as available data on depression tracks and anticyclone distribution over the Southern Ocean, support the pattern of ridges and troughs at 500 mb here described and throw light upon the occurrence of blocking in various sectors of the southern hemisphere.

An important proposition suggests itself from this study, namely that it may be the momentum and energy of the southern westerlies which are ultimately responsible for maintaining the meteorological equator on average north of the true (geographical) equator, at least over the oceans. The marked deficit of pressure south of 50-60°S. by comparison with the rest of the world may be attributable to ageostrophic effects at the level of the most intense upper westerlies. In any climatic epoch when the southern westerlies were

(i) farther south than now,
and/
or (ii) weaker than now,

the meteorological equator should under this proposition be nearer the true equator than is now the case. (The work of other investigators has suggested that the equatorial low pressure belt should also be wider at times when the circumpolar westerlies weaken in either hemisphere.) These postulated changes appear to fit in with what is known of conditions around the culminating phase of the "Little Ice Age" in the northern hemisphere about a century and a half ago.

1. Introduction

Monthly mean maps of the 500 mb surface over the southern hemisphere for each month from December, 1951 to November, 1954 have been published in NOTOS (1). The network of upper air stations used has been given by Schmitt (2), and is repeated here for ease of reference. On fig. 1 have been added indications of the few points on and near the Antarctic continent for which upper wind and temperature soundings have been available at some time since 1945. In the same article Schmitt has described the methods used in the daily hemispheric surface and upper air analysis at Pretoria from which grid point values are derived to give the monthly mean 500 mb pattern. The method included derivation of a basic 1,000 mb topography and a map of 1,000-500 mb thickness, each chart once a day with all data for that day plotted which became available within the first six months after the event. The 500 mb topography was obtained by graphical addition, having regard also to the data plotted for that level and to the principle of continuity. The patterns of 1,000-500 mb thickness were completed with the aid of extrapolation of the movement of identified features eastwards, subject to the control imposed by passing over test stations such as the islands of Marion, Heard and Macquarie with their regular radio-sonde ascents. Also use was made of the discovery that at thoroughly oceanic stations the surface dew point in °F is nearly equal to the 1,000-500 mb thickness in dekametres with the 500 omitted. Corrections of 2 to 4 dekametres required in certain areas are systematic and the method appears sufficiently verified by internal controls, at least between South Africa and Australasia. For the eastern South Pacific, the broadest part of South America and the South Atlantic except between 40° and 60°S., the working hypotheses used in constructing the daily charts had to be carried on without available checks within the region.

Whatever doubts might be entertained about the adequacy of the observation network for the individual daily or monthly maps, confidence has been increased by subsequent verifications available in the case of the daily surface maps (3, 4); this must be attributed to some extent to the evident possibility of positioning correctly the large scale features of the main steering currents in the upper atmosphere over the great Southern Ocean. This appears to be also the view of the South African Weather Bureau which has published the monthly mean charts in the belief, expressed by Schmitt, that they "hold possibilities for the study of at least the broad scale features of the upper air flow patterns" (loc. cit.), which should be exploited for research.

The three-year mean pattern yielded by the 36 monthly NOTOS values of 500 mb height and presented here in fig. 2 can safely be used as a good approximation to the true picture. It has not been possible to complete the Pacific Ocean sector north of about 60°S: in this part of the southern hemisphere upper air data must unfortunately be considered quite inadequate. In fig. 2 random errors have certainly been reduced to a small order, and the network hardly allows systematic errors in the large scale features at least between 70°W. and 170-180°E. In any case we shall find it possible to confirm the main features from geographical evidence sufficient to eliminate any suspicion that they result from possible bias of the analyst.

Fig. 3a-d are approximate cross-sections from 90°N. to 90°S. of mean westerly velocity component in the four seasons. Fig. 3a, northern winter-southern summer, is for the sector 30-130°E, which contains nearly the strongest upper westerlies in both hemispheres and at roughly constant latitude throughout the sector. In the other seasons these considerations either do not apply or are less obvious, and therefore the cross-sections have been made to relate to the whole northern hemisphere and the widest sector of the southern hemisphere for which enough data are available. The sections have been constructed from published maps of upper winds over the world (5, 6, 7), amplified by the southern hemisphere maps here given at fig. 2, 6 and 7 as well as those for spring and autumn which are not shown. The mean cross-sections for the northern hemisphere given by Moore (8) have been extensively used.

It is immediately apparent that the southern circumpolar whirl must be considered as the biggest and most powerful limb of the atmospheric circulation over the year as a whole.

A tentative crude integration of the westerly angular momentum in either hemisphere between latitudes 0° and 70° and from the 1,000 mb up to the 100 mb level has been obtained by summing $m V \cos \phi$, where m stands for mass, V for the westerly component of velocity and ϕ for latitude, in 100 mb layers over each 5° zone of latitude. The sum for each zone was multiplied again by $\cos \phi$ to give appropriate weighting for the differing extent of the various latitude zones. The totals for each hemisphere suggest the following ratios (southern hemisphere ÷ northern hemisphere):-

	Angular momentum of the westerlies	Net westerly angular momentum
	Ratio	Ratio
S. summer - N. winter	0.7	0.6
S. autumn - N. spring	1.3	1.3
S. winter - N. summer	4.4	10.2
S. spring - N. autumn	1.6	1.9
Year (over-all average)	1.4	1.6

The figures for net westerly angular momentum in either hemisphere result from subtraction of the momentum of the easterlies. Experiments with extending the estimates to latitude 80° made no difference to the ratios, and because of the small extent of the high latitude zones it is likely that no significant difference to the ratios could result from incorporating them. Rather greater uncertainty is involved in the estimates of easterly and westerly momentum over the tropical oceans, and the entire Pacific sector of the southern hemisphere has had to be omitted; but these uncertainties are not likely to affect the ratios greatly. Indeed, different forms of computation, summing alternatively angular and linear momentum and estimates of these about a single meridian, were tried and found to have but little effect upon the ratios, since numerator and denominator alike were affected. It seems likely that the ratios are more trustworthy than the necessarily rough totals of momentum derived for either hemisphere: this is borne out by the results of repeated fresh estimates and computations. The most striking point was that some ratios hardly fall below unity even during the southern summer.

The figures point to overwhelming magnitude of the southern westerlies during a considerable part of the year, particularly during the northern summer-southern winter, and on balance over the year as a whole. The very high ratios for June-July-August result from a number of factors: (i) the seasonal weakening of the northern westerlies is particularly great, (ii) the northern westerlies move into relatively high latitudes, (iii) the momentum of the tropical easterlies becomes quite large in proportion to the momentum of the northern westerlies - this situation does not arise in the same degree in the southern hemisphere summer, partly because the southern climatic zones are nearer the equator.[*]

/It

---

[*] The following seasonal ratios of gross easterly to gross westerly angular momentum resulted from these calculations:-

Northern hemisphere	Southern hemisphere
Summer 0.58	Summer 0.18
Winter 0.09	Winter 0.02

It has long been appreciated that the southern westerlies were stronger than their northern counterparts, but these are believed to be the first numerical estimates of the ratio. It is to be noted that the overweight of momentum in the southern westerlies is plainly most marked in the lower troposphere, for which most data are available, between the surface and 500 mb; the result does not greatly depend on the (probably cautious) values here selected for 300 mb and higher levels, chiefly taken from Jenkinson (7). Revised values for high levels over the Southern Ocean would probably raise the ratios slightly, so that the best values of the ratio for the southern summer-northern winter are likely to be in the region of 0.8 and for the year as a whole in the range 1.5 to 2.

The seasonal change is greater in the northern than in the southern hemisphere, the respective winter/summer ratios of angular momentum in the westerlies being 4.1 and 1.5. Greater seasonal change of latitude as well as of intensity in the northern hemisphere contributes to this result.

Angular momentum in the southern westerlies appears to be greater than in the northern westerlies over the longitude ranges defined in fig. 3a and 3c, summer for summer in the ratio 2.9 and winter for winter in the ratio 1.1.

The over-all average southern hemisphere/northern hemisphere ratio of westerly linear momentum is two to two and a half.

Schell (9) has noted that G.T. Walker found more significant lag correlations between centres of action in the southern hemisphere and later conditions in the northern hemisphere than were found within the northern hemisphere itself. Lag correlations within the southern hemisphere were over three times more numerous. These discoveries may perhaps be regarded as expressions of the dominance of the momentum in the southern westerlies.

There is clearly a pressing need to survey the broad characteristics, probable associations and range of influence of the system.

2. Characteristics of the southern circumpolar whirl

The prominent characteristics of the southern hemisphere whirl (fig. 2) about which we can be sure may be described as follows:-

2.1. Smaller latitudinal amplitude of waves in the mean circumpolar westerlies than in the northern hemisphere

The mean pattern shows no troughs and ridges of comparable amplitude to those found between 50° and 90°N. (See for comparison the 3-year mean 500 mb contour pattern over the Arctic, fig. 4, given by Flohn (10).)

The apparent circularity of the over-all mean circulation in the southern hemisphere is not produced by any tendency for large amplitude oscillations to occur indifferently scattered over all longitudes in the Southern Ocean. There are preferred longitudes for the troughs and ridges, but these are for the most part of modest amplitude by comparison with those of the northern hemisphere, at least when averages are taken over a period of a month or longer.

To some extent the preferred longitudes for mean troughs or ridges result from successions of mobile features regularly attaining their greatest amplitude about these positions but stationary broad troughs and ridges of modest amplitude by northern standards also enter in.

2.2.1. Trough and ridge positions

Identification of the positions of the mean troughs and ridges is most easily seen from profiles drawn along the latitude parallels (fig. 5a). Similar profiles for the individual seasons (fig. 5b) repeat most features of the overall average.

The most striking points are:-

(i) In latitudes south of 45°S. the trough downstream from the Andes is less pronounced than the broad trough in the Indian Ocean sector with its axis about 100°-110°E.* Between 20° and 45°S. the trough in the western South Atlantic is possibly the biggest feature, in agreement with the deductions of J.A. Boffi from depression tracks and pilot balloon data (13).

(ii) There is a ridge over the Andes to about 50°S., but from 50° to 70°S. (and possibly even north of 50°S.) the ridge in the western Pacific (150°E.-150°W.) is a much more noticeable feature. The northern end of the latter ridge is close to New Zealand, but the situation in the zone of weaker flow over temperate latitudes here is out of phase and New Zealand itself appears rather in a trough.

(iii) There is a secondary ridge, unmistakable in 20°-50°S., between the longitude of South Africa and 40°- 60°E.

(iv) Any seasonal shifts of longitude of the troughs or ridges (fig. 5b) such as might imply lengthening or shortening wavelength appear rather ill marked apart from possible westward displacement of the broad Indian Ocean trough in summer to about 60°E. (Tentative estimates both of the mean and modal wind direction at 3,000 and 6,000 m. at Heard Island (53°S.,74°E.), based on seven months' radio theodolite wind data in 1953 and supported by several years' experience of pilot balloon data, were close to 270° in summer and close to 260° in the other seasons.) Few, if any, other seasonal shifts of trough position seem likely to prove authentic. By and large, there appears to be substantial constancy of the positions of the main troughs and ridges in different seasons. The prevailing direction shown by pilot balloons and cloud observations at medium and high cloud levels appears to be about 290° at all seasons at Macquarie Island (55°S., 159°E.).

The rather surprising weakness of the mean trough in the southern part of the South Atlantic is confirmed by the resultant mean wind for the 36 months from the Stanley, Falkland Islands (51.7°S., 57.9°W.) radiosonde ascents, namely 264°, 33 kt. This figure fits well with fig. 2 both as to direction and strength. The resultant mean winds at Stanley for the three summers, 259°, 38 kt., and for the three winters, 265°, 28 kt., fit equally well with fig. 6 and 7. It is a peculiar feature of this part of the hemisphere that the 500 mb winds as shown by maps and confirmed by the observed values are weaker in winter and spring than in summer and autumn. The summer maximum is believed to affect the winds at Stanley at all heights from the surface up to 200 mb: it is also seen in the surface winds at South Orkney (Signy Island). In some individual months at Stanley the mean 500 mb wind is reported to be from a point somewhat north of west, implying a ridge downstream from the longitude of the Andes.

/The

* That the main trough is a broad feature occupying the Indian Ocean sector agrees with the preliminary results reached by Schmitt (11). According to Schmitt, and also to Heastie (12) working independently, the axis of the trough in summer is rather in the western part of the Indian Ocean sector in longitudes 50°-70°E. The summer profiles at 40° and 60°S. here shown in fig. 5b tend to support this position. There are hints that in latitudes 30°-40°S. the trough may split in summer into two troughs near 50° and 100°E. The all-year profiles (fig. 5a) for the lower latitudes 20° and 30°S. also suggest a trough in the western part of the Indian Ocean sector (60°-90°E.).

The Andes, with peaks reaching 22,000 ft. (6,500 to 7,000 m.) at various latitudes between 9° and 33°S., are higher than the Rockies, but there are no peaks reaching 10,000 ft. (3,000 m.) south of 50°S. The New Zealand Alps exceed 12,000 ft. (3,700 m.) near 40°S., but their latitudinal extent is only about 5°. The main flow of the upper westerlies at 500 mb appears to pass south of both the Andes and the Southern Alps, though it is reported that the peaks of the Bolivian Andes near 23°S. are at times swept by violent westerly storms associated with the high-level subtropical jet stream (14).

The trough in the 500 mb flow in the Indian Ocean sector cannot be attributed to any orographic barrier in the mainstream of the upper westerlies between 40° and 60°S. This trough is not only the biggest on the 3-year mean map: it was also judged to be the biggest on about 70 per cent of the individual monthly maps. It may be plausibly associated with the eccentric position of the broadest part of the Antarctic continent, the effective centre of whose cold radiating surface is displaced from the pole towards this sector. The mean position of the centre of the whole region of Antarctic ice has been calculated as 86°S., 50°E.; the centre of the permanent icesheet of East Antarctica may be taken as about 81°S., 70°E.

The shape of Antarctica in eastern longitudes corresponds fairly well with that of the broad trough in the Indian Ocean sector, where the 3-year mean 500 mb isopleths run parallel with the general run of the coast. The ridge in the western Pacific also corresponds well with those longitudes where the coast of Antarctica lies farthest south. The average latitude of the edge of the permanent ice between 180° and 100°W. may be taken as 70°S., that of the coast as 75°S.

It is hard to avoid concluding that south of 45°S. the dominant control in determining the positions of troughs and ridges in the main atmospheric flow aloft is thermal.

2.2.2. Polar outbreaks

The paths of frequent outbreaks of polar air at the surface appear to fit the 3-year mean 500 mb pattern (fig. 2), and inasmuch as they have been known (for instance, to the whalers) for many years they tend to confirm the validity of this pattern over a much longer term of years.

Vowinckel (15) shows the maximum frequency of polar outbreaks revealed by analysis of 160,000 ships' observations near 64°S. (period 1920-1955) as occurring over a broad sector centred about 110°E. Frequencies were only slightly lower in all longitudes between 60° and 150°E. Apart from any possible loci of outbreaks in the Pacific sector (not investigated), only a much narrower region between 60° and 35°W. comprising the western and central parts of the Weddell Sea can compare with the Indian Ocean - Australian sector.*

Another preferred region for polar outbreaks just east of the northern tip of Enderby Land (66°S., 52°E.) has also been suspected, though this may be little more than a local effect superimposed on the general high frequency in the Indian Ocean sector.

The Weddell Sea outbreaks sweep north and northeast to affect all parts of the South Atlantic (16, 17) and sometimes turn east into the Indian Ocean.

/Cold

* The most northerly positions reached by occasional icebergs, under the combined influence of surface winds and water currents, are in the western South Atlantic and central Indian Ocean, in both cases about 35°-40°S.

Cold air from the South Polar Plateau and the vast interior of East Antarctica appears to flow out almost continuously over the Adélie Land coast and in a broad, generally ESE'ly, airstream over the fringe of Antarctica in the Indian Ocean sector between 150° and probably 50°E. This constancy is linked with the very great frequency of anticyclones centred near 80°S., 60°E. (cf. fig. 10-12). The common southerly blizzards near McMurdo Sound and in the western Ross Sea near 70°-75°S., 160°-170°E. may be seen as a branch of the same major outflow of cold air. Results from a few sample observational records from diverse periods, which bear witness to this quasi-permanent air current, are given in Table 1. Snow Hill (east side of Grahamland), Maudheim and Bay of Whales are included for comparison, to show the changes of dominant direction and rather greater scatter in other sectors.

Table 1. Frequencies per cent of various surface wind directions at open sites in East Antarctica and at certain other points for comparison

Position and period	N	NE	E	SE	S	SW	W	NW	Calms
Mawson (18) 67°S., 62°E. June-Oct. 1956	1	2	11	59	9	3	2	0.5	13
Gauss (19) 66°S., 90°E. 1902-3 (12 months)	0	2	57	11	5	3	9	2	11
(The Grottoes, 66°S., 95°E. 1912-13 (Shackleton Ice Shelf (20) (10 months)	0	0	35	48	3	2	4	1	4
Pionerskaya (18) 70°S., 95°E. June-Oct. 1956 2,700 m. a.s.l.	0.4	0.6	11	76	10	1	1	0.2	0
(Port Martin, (Adélie Land (21) 67°S., 141°E. 1950-51	1	2	4	58	23	2	1	1	8
Snow Hill (19) 64°S., 57°W. 1902-3 (1½ years)	3	13	5	1	15	38	7	1	17
Maudheim (22)* 71°S., 11°W. 1950-52 (22 months)	0	14	52	4	18	9	2	0	-
(Bay of Whales, (Ross Ice Shelf (19, 23) 78°S., 166°W. 1911-12, 1929-30, 1934-35, 1940-41. (4 years)	4	5	32	10	19	16	4	1	8

The outflow of cold air from East Antarctica is only partly katabatic in origin, and differs from the Greenland katabatic wind in giving rise to cold airmasses of great depth over the ocean.

/2.2.3.

* The data for Maudheim are provisional, being based upon occasions when the wind was $\geq$ 5 metres per second.

2.2.3. Intensity and breadth of the main belt of southern upper westerlies

The over-all range of yearly mean 500 mb height between the tropical and polar zones in the southern hemisphere, shown on fig. 2, materially exceeds the range in the northern hemisphere: this implies a greater total zonal circulation of the atmosphere over the southern hemisphere, as confirmed by fig. 4.

The greatest yearly mean 500 mb heights are believed to be about 5,900 m. (cf. (14)), over the high-level stations of the Bolivian Altiplano (la Paz 17°S., 68°W.) and 5,870 to 5,880 m. over the central African highlands. The nearest approach to these figures in the northern hemisphere, according to information supplied by the Upper Air Climatology Branch, appears to be in Mexico and the south-western United States - Mirida 21°N., 89°W., 5,883 m., Tacubaya 19°N., 99°W., 5,866 m., Mazatlan 23°N., 106°W., 5,852 m., Lake Charles 30°N., 93°W., 5,824 m. (It is probable (14) that the existence of the raised heating surface in low latitudes contributes to this result: raised surfaces of comparable extent in the northern hemisphere, e.g. Arizona and the Mexican highlands, Spain, Anatolia, Persia, Afghanistan and Tibet, are mostly well north of 25°N. and get too cold in winter to produce such high annual values of the 500 mb surface.

Heights over Cocos Is. (12°S., 97°E.), 5,870 m., and the equatorial zone of the South Pacific near the Gilbert and Ellice Islands (0-10°S., 170-180°E.) 5,850 m. also appear to exceed northern hemisphere equivalents: these places are remote from cold water currents and in or near the regions of warmest extensive ocean surfaces in the world (see (24), page 37).

The lowest yearly mean 500 mb heights over Antarctica, 4,920 to 4,990 m., indicated by the NOTOS charts with support from radio-sonde observations at Little America (1940-41), Maudheim (1950-52), and Port Martin (1951-52) are some 300 metres below the lowest in the Arctic (cf. fig. 4). Rather more than half of this disparity appears to be attributable to the prevalence of M.S.L. pressures about 15 to 25 mb lower in the Antarctic than in the Arctic: there is no obvious disparity between the prevailing pressures in the northern and southern subtropical high pressure belts, so that the surface circulation, like that aloft, shows a greater total of westerly momentum in the southern temperate zone than in the corresponding zone of the northern hemisphere. The rest of the disparity between the 500 mb heights over the Arctic and Antarctic is directly due to the colder Antarctic troposphere, especially in summer. The summer values of mean 1000-500 mb thickness over the Antarctic are 200 to 250 metres lower than over the Arctic. (South of 60°S. precipitation normally falls as snow at all seasons.) The winter thickness values are however similar in both northern and southern polar regions.

The steepest thermal gradient is in the Indian Ocean sector, between the trough in the higher latitudes and the particularly warm tropical zone of this ocean. That this thermal gradient must exceed any other in the world at the present epoch is confirmed by the fact that the islands in 50° to 80°E. exhibit climates ranging from fully tropical with tropical vegetation at Mauritius (20°S.) to ice age at Kerguelen (49°S.) and Heard (53°S.).

We should expect to find the strongest upper westerlies in this sector. This is instanced by an extreme wind observation of 300 kt. at 229 mb (11 km.) on 27 September, 1956 at Amsterdam Island (38°S., 78°E.) (25), and fits well with the distribution of average geostrophic speeds at 500 mb overprinted on fig. 2, 6 and 7. The strongest 500 mb gradient in the northern hemisphere on fig. 4 corresponds to a yearly resultant

mean wind of about 42 kt. over a restricted region of the Canadian maritime provinces between 45° and 50°N. This figure is exceeded over most of a 1,200 to 1,500 miles - wide zone between 40° and 60°S., 20-150°E. with peak values slightly over 50 kt. in the annual mean and probably 60 to 70 kt. or rather more in the means between June and October.

2.2.4. Polar front and subtropical jet streams

The maximum winds indicated by the mean 500 mb map correspond to the polar front jet streams over the Southern Ocean. As in the northern hemisphere the subtropical jet stream is at higher levels. It is clearly indicated at about 12 km. on the various published vertical cross-sections (26, 27, 28, 29, 30), but these all suffer severely from lack of data south of 40°-45°S. and do not show the maximum over the Southern Ocean associated with the polar front jet streams at all well.

The greatest average westerly component in the subtropical jet stream probably exceeds 100 kt. in winter in all the longitudes investigated. Over Australia and New Zealand its winter position is 25°-28°S.; in summer it moves south, perhaps as far as 40-45°S., and the maximum is thought to decline to 50-60 kt. The average latitude of this system over the eastern South Atlantic and western Indian Ocean is given rather further south than in the other sectors examined, namely at 35°-40°S. in winter and 40°-45°S. in summer, very much closer to the zone of the polar front jet streams than in the Australian sector.

The mean westerly components at 5 to 6 km. indicated by the published cross-sections for the Atlantic and Indian Ocean sectors agree well with fig. 6 and 7, both as to strength and position. Agreement between the 500 mb charts here illustrated and the published cross-sections in 150° and 170°E. is less obvious, but this is probably because the strongest 500 mb winds in these longitudes are further south - at 55° to 65°S., too far south for the observations used on the cross-sections. Nevertheless all the cross-sections indicate a secondary maximum of wind speed somewhere south of 45°S.

These comparisons suggest that, as in the northern hemisphere, the sub-tropical jet stream has a somewhat separate existence from the jet streams of higher latitudes moving about in association with the polar front though at times coalescences may occur, especially in the Indian Ocean (31, 32, 33). The latitudes of the zone (40°-60°S.) over which the mean winds at 500 mb are stronger than their northern hemisphere counterparts suggest that the disparity is principally associated with the polar front jet streams of the Southern Ocean. It remains to be determined how much of the difference is due to less variability of direction over the southern temperate zone. Since the polar front wanders all over the zone 40° to 60°S., the breadth of the belt with mean wind over 50 kt. at 500 mb may be taken to imply great frequency of high wind speeds at this level in the polar front jet streams.

2.2.5. Seasonal variation

The profiles in fig. 5b credibly indicate a shortening of the wave spacing of troughs and ridges at 40°S. from winter to summer in the South Atlantic and perhaps everywhere from the Andes to the Indian Ocean sector. It is also plain that the amplitude of the Indian Ocean trough is greatest in winter and spring: this feature becomes much less pronounced in summer,* though the great sweep of west-north-westerly

/winds

* During the southern summer the Eurasian winter monsoon forces the inter-tropical convergence south to a mean January position along an arc from 15°S. over Madagascar to 7°S. between 80° and 100°E. and 15° to 18°S. over north Australia. In approximately the same months the higher latitudes of the southern Indian Ocean are invaded by tropical storms, which, however, quickly occlude on their recurving tracks to the southeast.

winds between this and the western Pacific warm ridge is prominent at all seasons: the mean direction becomes almost NW. over the Ross Sea, as may be verified from Simpson's analysis of the frequency of different directions shown by the smoke from the Erebus volcano (4,000 m.) and by medium and high cloud at Cape Adare and McMurdo Sound (34). No regular longitudinal shift of this north-westerly steering current with the march of the seasons can be identified from the evidence here used. Depressions are steered east and southeast in the Australian sector and into the Ross Sea at all seasons.

The pronounced pressure minimum in late winter in the Ross Sea, culminating with normal October M.S.L. pressure about 973 mb (standard deviation circa 3 mb at Bay of Whales, based on 9 years' data for areas in the southern Ross Sea about 78°S.) is associated with depressions steered by the upper north-westerly winds in the Australian sector.

At the peak of this development in September and October low values of mean pressure seem regularly to spread across Antarctica (with the depression track) as far as southern Grahamland and the Weddell Sea. This phenomenon seems related to the seasonal maximum intensity of flow around the great Indian Ocean trough rather than to any noteworthy displacement of the latter.

The summer and winter 500 mb maps (see fig. 6 and 7) and those for spring and autumn (not reproduced) indicate some general northward shift of the zone of maximum wind from summer to winter. Speeds increase in the lower latitudes in winter, whereas in latitudes near 60°S. the maximum is in summer as appears to be the case even at Falkland (52°S.). In the South American sector the thermal gradient over quite a broad range of latitudes is actually stronger in summer than in winter. Meinardus (35) has considered this latter phenomenon, chiefly in terms of surface pressure and temperature gradients, but found supporting evidence in the prevailing speeds of depressions: apparently the combined effect of seasonal shift of latitude of the strongest westerlies and rather small overall seasonal change of strength in the southern hemisphere results in a fairly general summer maximum of the surface winds in 50°-60°S., especially in the South American, Australasian and Pacific sectors. There is however a general intensification of the flow around the broad Indian Ocean trough from summer through autumn to late winter and spring, followed by a rather rapid jump south and weakening of the maximum in early summer. The progression is clearly seen near 70°E., where the maxima in the mean 500 mb flow appear to be:-

Summer (Dec.-Feb.)	60 kt. near 58°S.
Autumn (Mar.-May)	55 kt. near 55°S.
Winter (June-Aug.)	60 kt. near 50°S.
Spring (Sept.-Nov.)	65 kt. near 50°S.

Although the overall seasonal change of maximum speed is not great, there is a noteworthy broadening of the belt of strong flow over the whole Indian Ocean sector from summer to late winter.

The seasonal movement appears to follow that of the ice limit, the maximum 500 mb wind lying some 8° north of the ice limit in this sector at each season.

3. Accompanying phenomena and independent verifications of the dominant upper air pattern

3.1. Incidence of blocking anticyclones

In the northern hemisphere investigators have found that, when the upper westerlies attain great strength over a considerable sector, large amplitude waves usually develop and lead to quasi-stationary blocking

patterns two to three days later with a great and rather persistent reduction of the zonal flow. Paradoxically, the mean speed of the 500 mb westerlies in 40°-60°S. for several months over a very wide sector reaches values that would be high for the northern hemisphere, yet stationary blocking situations are rare.

Fig. 10-12 show the distribution of once-daily positions of all surface anticyclones defined by at least one closed isobar (5 mb spacing) in the summer of 1946-7 (individual positions, half hemisphere) and (by frequency isopleths) in the three summers 1951-4 and three winters 1952-4.* Similar maps have been plotted for all seasons of the year and for other years, but are not reproduced. Numbers printed on fig. 13a and 13b show all cases south of 40°S. in the summer and winter of 1952-3 where a stationary anticyclone remained for four days or more centred within 600 nautical miles of the same position and record the number of days. It is found that quasi-stationary anticyclones south of 40°S. are limited to positions over Antarctica and to just three sectors of the surrounding ocean, namely:-

(i) From close to the south coast of Australia to a wider range of latitudes in the western Pacific probably as far as the region near 60°S., 120°-140°W.

(ii) Near the tip of South America and southeast thereof over the region of the Scotia Sea in 60°-65°S.; they are known to occur on rare occasions in longitudes farther east in the South Atlantic sector 50°-60°S.

(iii) The region southeast of South Africa about the Marion and Crozet Islands in 40°-50°S. in the west of the Indian Ocean sector.

Even in these regions the frequencies of stationary anticyclones do not appear to compare with the corresponding zone of the northern hemisphere, and the vast regions where virtually no anticyclones occur (fig.11 and 12), whether stationary or mobile, are unmatched in the north. An identical conclusion seems to have been reached in Pretoria by van Loon (36).

The daily positions of anticyclones over the Southern Ocean south of 40°S. show a preference for the same three sectors of the ocean. They almost entirely avoid the region of the great upper trough in the eastern part of the Indian Ocean sector, and are only really common in the western-central Pacific sector.

van Loon has remarked that, as in the northern hemisphere, blocking shows a pronounced maximum in late winter - early spring, but over the Southern Ocean the preferred positions are east, not west, of the major continents. He believes this means that the explanations favoured in the northern hemisphere in terms of an orographically produced pattern of ridges and troughs do not apply in the south. He prefers to associate the southern distribution with "easy access to warm air".

The present investigation strongly suggests that the three regions of principal occurrence of anticyclones over the ocean south of 40°S. are determined by

/(i)

* The consistency observed between the distribution indicated in the summers of 1946-7 (fig. 10) and 1951-4 (fig. 11) lends support to the belief that the observation network, which was much sparser south of 40°S. in the earlier year, has for some time been adequate for the purpose of this type of investigation. (The Pacific sector was not covered by the daily analyses from which fig. 10 was compiled.)

(i) anticyclogenesis occurring to the warm side of the strong west-north-westerly upper windstream in the Australasian sector well downstream from the great Indian Ocean trough. The latitude tends to increase eastwards and in the individual cases the surface anticyclone is presumably east of an upper ridge developing and travelling east into the Pacific.

(ii) and (iii) anticyclogenetic patterns just west of the South Atlantic and Indian Ocean troughs.

These preferred longitudes for anticyclones suggest a confirmation of the dominant upper air pattern.

The preference for the winter season is presumably linked with maximum amplitude of the troughs.

The Pacific sector, especially between 90° and 130°W., appears to be by far the most frequent location of occasional great quasi-meridional (usually NW.-SE.) ridges of high M.S.L. pressure linking the subtropical belt with the Antarctic. The writer has suggested elsewhere (3) that this is the normal mechanism and location both of renewal of anticyclones over Antarctica after relatively cyclonic periods and of the pressure surges which Simpson noted in the Ross Sea, apparently always coming from near 80°S., 120°W.

Blocking patterns do occur fairly frequently over certain parts of the Southern Ocean, and there is no reason to exclude the possibility that they follow periods of excessive zonal flow ("hydraulic jump"); but stationary situations seldom result. The anticyclones over the ocean nearly always tend to drift away east, no doubt because of the great over-all thermal gradient in the zone 40°-60°S. Cells do, however, split off over Antarctica, where there is little thermal gradient, and become stationary there.

Apparently, in the northern hemisphere the great continents in the temperate zone play an important part in permitting stationary patterns to develop, thanks to wide areas of slight thermal gradient often associated with the main winter snow-cover and the development of distorted thermal patterns between oceans and continents in the same latitude zone. In the southern hemisphere, geography does not generally permit large depressions or anticyclones to produce a thermal pattern capable of maintaining the system in a stationary position.

3.2. Depression tracks and the pattern of glaciation

Our knowledge of the commonest depression tracks over the Southern Ocean, supported by the observed distribution of glaciation, provides further confirmation of the general upper air pattern south of 40°S. and implies that the Indian Ocean trough has been dominant for a very long time.

Glaciation depends for its occurrence on sufficient precipitation, associated with cyclonic activity, at temperatures remaining near or below 0°C.

A sample map of the distribution of frequencies of depressions south of 30°S., originally published elsewhere (37), is reproduced as fig. 14 for ease of reference. The main frequency maxima are (i) near 65°S., 20°E. southeast of the South Atlantic trough; (ii) at 62°-65°S. in the Indian Ocean sector between 80° and 120°E.; (iii) along a broad depression path from near 50°S. in the Australian sector into the southeastern part of the Ross Sea; and (iv) in the Bellingshausen Sea near 65°S., 70°W. These positions show the expected associations with the troughs in the 500 mb flow (fig. 2, 6, 7). Depression frequencies all around the zone 60°-70°S. are kept high by the general, though often rather slow, eastward drift of occluded and decaying centres. Occasionally, in many longitudes, these

centres are swung south and west on looped tracks over the fringe of Antarctica under the influence of the circulations of more vigorous, younger depressions over the ocean to the north. The map also indicates several favoured paths and origins for frontal wave disturbances. Data available consistently indicate the lowest mean annual pressure at M.S.L. near 60° to 65°S. in the eastern part of the Indian Ocean sector in 90° to 110°E. where the value is possibly as low as 980 mb.

The long surface pressure trough with its characteristic SE.-NW. axis between the southern anticyclones in 40°-60°S. in the sector New Zealand to 140°W. and and quasi-permanent Easter Island anticyclones near 30°S. in the eastern Pacific is frequently prominent from latitude 70° to 20°S. The southerly winds in this system are the likely explanation of the northward bulge in the frequency of icebergs (fairly commonly reaching 50°S., occasional instances to 45°S.) in the central Pacific between 105° and 135°W. (38). There are some suggestions of a trough in the main flow at 500 mb in the central Pacific near 90°W. corresponding to this feature of the surface pressure patterns.

The most northerly island with many great glaciers - some of which reach the sea - is Kerguelen, an island 70 miles long near 49°S., 70°E., whose summit reaches over 6,000 ft. (1,865 m.). Heard Island, 25 miles long near 53°S., 74°E. with its summit a dormant volcano reaching 9,000 ft. (2,750 m.), is completely glaciated but for a few small ice-free areas on the lower slopes. Bouvet Island (54°S., 3°E.) is a volcanic cone, five miles across at sea level and reaching over 3,000 ft. (935 m.): the summit and the steep northern and western sides are free from ice but often snowcovered; the whole eastern side is under an ice-sheet. South Georgia is a much bigger and very mountainous island in about the same latitude, 100 miles long and 20 miles broad near 54°S., 38°W.: its highest summit reaches about 9,300 ft. (2,840 m.). There is much ice amongst the mountains of South Georgia and some glaciers reach sea level, but the permanent snow line is generally about 2,000 ft. falling to 1,000 ft. (300 m.) above sea level at the northwestern end where glaciation is relatively heaviest. In far eastern longitudes Macquarie Island, which is 18 miles long near 55°S., 159°E. and rises to a summit about 1,400 ft. (430 m.) above sea level, loses all its snow cover in summer. These islands, all in or near the zone 50°-55°S., support the diagnosis that a great, broad, quasi-permanent upper cold trough occupies the Indian Ocean sector, whereas South Georgia and Macquarie Island benefit to some extent from warm ridges, respectively some distance west and east of them.

The great ice-sheet of East Antarctica derives nourishment from snowfall in cyclonic situations all along its fringe, and there is evidence to suggest that depressions and frontal troughs pass inland with fair frequency across the sector between 120°-140°E. and the Ross Sea. The latter systems sometimes move in from the north or northwest and sometimes on recurving tracks from the Ross Sea in the east. However there is little doubt, either from the study of depression tracks or from the prevailing northwesterly winds at 500 mb in the Australian-Ross Sea sector, that the most frequent depressions over Antarctica are systems travelling southeast into the Ross Sea and occasionally crossing right over West Antarctica to the Bellingshausen and Weddell Seas. This means that, for the present, it remains a mystery why West Antarctica, which is very mountainous, with a highest reported peak 20,000 ft. (6,000 m.), appears much less heavily glaciated than East Antarctica; the ice-summits are believed to be about 5,000-7,000 ft. (2,000 m.) and 14,000 ft. (4,000 m.) respectively near 75°-80°S., 100-120°W. and 80°S., 50°E. (39). The depression tracks observed at the present epoch would suggest increasing glaciation in West Antarctica and possibly insufficient precipitation to maintain full nourishment of the East Antarctic ice dome.

Continental regions exceeding 1,500 nautical miles in longitudinal extent in high latitudes appear to have a critical importance in establishing a fixed cold trough in the upper air flow (40). A cold trough would presumably therefore be more readily established over East Antarctica than over West Antarctica which is scarcely 1,000 miles across.

3.3. World wide relationships; seasonal and secular variations

There is at all seasons an obvious deficit of M.S.L. pressure, and therefore of atmospheric mass, everywhere south of about 40°S. in comparison with the corresponding parts of the northern hemisphere. Over much of the region this disparity is of the order of 20 mb.

In more detail, calculations based on the best available world maps of average pressure at M.S.L. suggest that the deficiency as compared with the northern hemisphere begins about latitude 45° in the southern winter but extends to all latitudes in the southern summer. Over the year there is an apparent excess of mass over the northern hemisphere as a whole of about a half of one per cent, equivalent to about 5 mb of average M.S.L. pressure; the excess appears to range from about 0.9 per cent in the northern winter to 0.1 per cent in the northern summer.

When allowance is made for the intrusion of elevated land in either hemisphere, the apparent difference of one half per cent of atmospheric mass between northern and southern hemisphere is approximately cancelled out. (Much estimation is involved but the correction is clearly of the same order and seems to be close to the same value.) There is no doubt however of a disparity of over one per cent between latitudes south of 35°S. and north of 35°N. Between 5° and 30°S. the annual figures suggest a small excess over northern hemisphere equivalents. This excess must be at least partly associated with the further fact that the zone of subtropical maximum pressure in the southern hemisphere is about 5° nearer the equator than its northern counterpart when either the respective winter or summer positions are compared.

Various estimations of the mean latitude of the meteorological equator (intertropical convergence) based on latitudes of the subtropical anticyclone centres, limits given by various authors for the doldrums belt in different sectors, penetration of the NE. and SE. Trade Winds and even reported crossing of the geographical equator by old cold fronts principally of southern origin give corroborative figures about 3.5°N. for the over-all mean latitude of the intertropical convergence.* Only in the western Pacific sector, west of about 160°W., is the annual mean position south of the geographical equator (about 3°S.): it is perhaps significant that these are about the same longitudes as those of the main warm ridge in the southern upper westerlies.

It is not so easy on geographical grounds to make a direct comparison of the respective positions of the sub-Arctic and sub-Antarctic zones of minimum pressure, although a mean latitude 60°-65°S. is suggested as against rather north of 65°N.

There is an apparent paradox in the average northward displacement of all the climatic zones** in spite of an actual deficit of mass to the south of them. It seems that the likeliest clues to the physical explanation of this paradox are

/(i)

* The actual lines given by various authors for the intertropical convergence are also in general agreement with this figure.

** The latitudes of the ice-covered islands in the Southern Ocean mentioned on page 13 should also be compared with northern equivalents. In Chile the northernmost glacier (San Rafael) from the Patagonian ice-cap reaches the sea in 46° 40'S., ten degrees farther from the Pole than any Alaskan glacier.

(i) the latitudinal position of the main thermal gradient around the respective polar caps

(ii) the outstanding momentum and energy of the southern upper westerlies.

The latter appears to be the more fundamental.

Faust (41), Murray and Daniels (42) and others have noticed over Europe a net ageostrophic transport of air towards the warmer side of the jet stream, which is not confined to the jet stream exit but appears even in the middle of the jet stream and is believed to correspond to a net transport in this sense in the upper troposphere about the general level of maximum wind. Moreover, the ageostrophic transport away from the colder towards the warmer side appears to be in some senses proportional to the intensity of the maximum wind. The observed effect is associated with levels near the maximum wind level and winds at 500 mb probably cannot be used to demonstrate it.

Although this effect ("the Nullschicht effect") is not yet satisfactorily explained, it does suggest a northward transport of mass associated with the strength of the southern upper westerlies.

Comparison of the monthly mean pressure over the southern polar cap with the varying latitude and intensity of the upper westerlies suggests certain associations.

Mean M.S.L. pressures over the polar cap (70°-90°S.) and in the subpolar zone 60°-70°S. were compared with M.S.L. pressure, 1000-500 mb thickness and 500 mb heights and gradients in the zone of westerlies over the best covered longitudes 70°W.-170°E. from monthly data published in NOTOS over periods of up to 41 months. Higher than average pressure south of 60°S. was found, as would be expected, highly significantly correlated with weakened surface pressure gradients for westerly winds in all latitudes south of 45°S. ($r = -0.67$ to -0.77 for 29 to 41 months) and with equatorward displacement of the latitude of strongest surface westerlies ($r = -0.73$ for 29 months). Relatively high pressure south of 60°S. was significantly correlated with below-average values of 1000-500 mb thickness at 60°S. ($r = -0.50$ to -0.65 for 27 months) and showed weaker correlations with lowered thickness also at 50° and 40°S.: there was a suggested, though inconclusively demonstrated, association with increased thickness gradient between 40° and 60°S. ($r = +0.14$ to $+0.35$). There was a suggested association of high pressure everywhere south of 60°S. with weakened westerly flow at 500 mb in 50°-60°S. ($r = -0.11$ to -0.24 over 32 months), equatorward shift of the latitude of strongest flow at this level ($r = -0.27$ to -0.33 over 31 months) and strengthened flow in 30°-40°S. ($r = +0.23$ to 0.40 for 32 months), but none of these relationships was conclusively demonstrated. The most definite upper air correlations were with pressures in the subpolar zone rather than south of 70°S., where M.S.L. pressures are moreover largely fictitious and uncertain.

It appears inevitable that both seasonal and secular climatic trends associated with general strengthening or weakening of the zonal circulation and of the meridional temperature gradients affecting the position or intensity of the southern westerlies should have unlike effects south and north of this system and entail appreciable adjustments over the rest of the world.

Many years ago Meinardus (42) noticed that south of about 50°S. the highest M.S.L. pressures appeared to occur in summer (December-January), in spite of the complication of a double wave in the annual pressure curve in 60°-70°S. in the Weddell Sea-Atlantic sector with another maximum in May or June (44). The "anti-monsoonal" trend appears dominant in the highest southern latitudes, and about 78°S. in the Ross Sea the warm season maximum appears

/to

to be the only significant one; winter there is a season of low pressure, especially late winter. Meinardus made some calculations of the seasonal exchange of atmospheric mass involved. The null point in this exchange appeared to be approximately the latitude in which the strongest upper westerlies associated with the polar front jet streams are now seen to lie.

Willett (45) and others have noticed unlike climatic trends south of about 40°S. and over the rest of the world. During the period of great warming of the Arctic, for instance, culminating between 1900 and about 1938, latitudes south of 40°S. are believed by Willett to have been colder than formerly, and Kraus has suggested (46) that the westerly disturbances of the Southern Ocean were displaced north to affect Australia more in approximately those years than before or since. Since about 1945 there are signs (15) of an upward trend in surface temperatures over the Southern Ocean south of 60°S. and since about the 1920s of depression tracks keeping gradually farther south in the Australasian sector. This latest trend appears to coincide with a levelling-off of the warming trend over Spitsbergen and northern Europe, possibly the substitution of a rather colder regime with depression tracks somewhat farther south.

There are perhaps indications of opposite climatic trend over the southern polar regions from the rest of the world over a rather longer period: the farthest south positions reached by Cook near 40°E. in 1773 and near 110°W. in 1774 as well as by Bellingshausen in 1820 near the Greenwich meridian and Biscoe in 1831 between 0° and 30°E. were all 1° to 2° of latitude south of the normal limit of pack-ice in recent years at the end of the melting season (47), and in 1823 Weddell found the Weddell Sea almost free of ice - an experience never repeated since. When the frailty of the wooden ships of those days is remembered, it seems clear that the ice limit tended to be some degrees south of its supposed present normal position (as appears to be the view of the Scott Polar Research Institute). Dr. Herdman, however, doubts whether the modern normal is sufficiently determinate for this to be settled. There is nothing surprising in this since year to year variations are considerable and are liable to exceed the supposed change of long-period average position since the epoch 1770-1830.

The same over-all trend might be deduced from the present advanced state of the South Georgia glaciers, which are generally in contact with their side moraines down to sea level and are known to have advanced since the 1880s, but show erratic changes in the past 6 to 12 years. There is apparently no bare rock which has not obviously been exposed to the weather for decades or centuries.

Between 1770 and about 1840 the ice limit in the North Atlantic was near Iceland for much of the year, and it was a cold epoch all over northern Europe (48). The westerly winds on the North Atlantic and over western Europe were less strong, or less prevalent, than now and the climatic zones in this sector of the northern hemisphere were certainly displaced some degrees south from present day experience.

Superimposed upon any tendency for sympathetic shifting of all the climatic zones, it may be that there are periods of general weakening or intensification of the circulation, intensification being commonly held to entail a tendency for equatorward displacement of the main upper westerlies in both hemispheres. Kraus (46, 49, 50, 51) has postulated general intensification of the upper westerlies in both hemispheres from about 1895 to the 1920s or later, causing general intensification of the subtropical anticyclones and narrowing of the equatorial rain-belt. From about the mid 1920s to 1940 however the data seem more consistent with a general northward anomaly of the climatic zones in both hemispheres. Following an apparently sudden northward shift of the southern westerlies in 1893-4, by 1930 to 1940 the northward shift is believed to have affected most sectors of the northern hemisphere also and to have been noticeable in all seasons of the year.

It seems that changes in the southern upper westerlies might affect the general atmospheric circulation over the rest of the world in at least three ways:-

(i) changes of over-all intensity of the circumpolar whirl should be directly related to changes in intensity of the subtropical anticyclones in the southern hemisphere and therewith of the SE. Trade Winds. Such changes bring about changes in the supply of warm water to the Gulf Stream and in the value of Walker's "Southern Oscillation", which involves changes of mean pressure over much of the world. (It may be noted that changes of average M.S.L. pressure south of 50°S. would have about ten times the magnitude of any general compensatory changes of pressure level, if spread evenly over the rest of the world.)

(ii) changes in the mean latitude of the circumpolar whirl in the southern hemisphere are likely to be accompanied sooner or later by small, but probably appreciable, sympathetic shifts of other climatic zones.

(iii) changes of eccentricity of the southern whirl occur over short periods but any long-term changes might imply or require changes in the relative states of ice cover over East and West Antarctica. These can probably be ruled out within the period of our meteorological instrumental record, but might be important in considering the ice ages and epochs lasting several millenia.

G.24285/JB/9/57/65

Ministry, London, 1954. No. 823.

(8) MOORE, J.G. Cross-sections of the mean zonal component of geostrophic wind. Met. Mag., 85, pp. 167-171, London, 1956.

(9) SCHELL, I.I. The interdependence of weather and atmospheric circulations in the northern and southern hemisphere. Bull. Amer. Met. Soc., 20, pp. 332-333, Worcester (Mass.) 1939.

(10) FLOHN, H. Zur Aerologie der Polargebiete. Met. Rundschau, 5, pp. 81-87, 121-128, Heidelberg, 1952.

(11) SCHMITT, W. Preliminary mean absolute topography 500 mb southern hemisphere 70°W. to 120°E. Summer 1951-52. NOTOS, 1, pp. 7-17, Pretoria, 1952.

(12) HEASTIE, H. Average height of the standard isobaric surfaces over the temperate and tropical regions in January. Meteorological Research Papers, Air Ministry, London, 1957. No. 1045.

(13) BOFFI, J.A. Effect of the Andes mountains on the general circulation over the southern part of South America. Bull. Amer. Met. Soc., 30, pp. 242-247, Lancaster, Pa., 1949.

/(14)

REFERENCES:

(1) NOTOS — Vols. 2-4, published Weather Bureau, Pretoria, 1953-1955.

(2) SCHMITT, W. — Upper air analysis for the southern hemisphere. NOTOS, 2, pp. 20-27, Pretoria, 1953.

(3) LAMB, H.H. — Meteorological situations over the south polar regions and alimentation of the Antarctic ice-cap. Association d'Hydrologie Scientifique, Tome I, U.G.G.I., Brussels, 1951.

(4) LAMB, H.H. — Meteorological results of the Balaena expedition 1946-47. M.O. Geophysical Memoir No. 94, London, 1956.

(5) BROOKS, C.E.P.; DURST, C.S.; CARRUTHERS, N.; DEWAR, D. and SAWYER, J.S. — Upper winds over the world. M.O. Geophysical Memoir No. 85, London, 1950.

(6) BANNON, J.K. — Some aspects of the mean upper-air flow over the earth. Proceedings of the Toronto Met. Conference, September, 1953, pp. 109-121, published R. Met. Soc., London, 1954.

(7) JENKINSON, A.F. — Meteorological Research Papers, Air Ministry, London, 1954. No. 823.

(8) MOORE, J.G. — Cross-sections of the mean zonal component of geostrophic wind. Met. Mag., 85, pp. 167-171, London, 1956.

(9) SCHELL, I.I. — The interdependence of weather and atmospheric circulations in the northern and southern hemisphere. Bull. Amer. Met. Soc., 20, pp. 332-333, Worcester (Mass.) 1939.

(10) FLOHN, H. — Zur Aerologie der Polargebiete. Met. Rundschau, 5, pp. 81-87, 121-128, Heidelberg, 1952.

(11) SCHMITT, W. — Preliminary mean absolute topography 500 mb southern hemisphere 70°W. to 120°E. Summer 1951-52. NOTOS, 1, pp. 7-17, Pretoria, 1952.

(12) HEASTIE, H. — Average height of the standard isobaric surfaces over the temperate and tropical regions in January. Meteorological Research Papers, Air Ministry, London, 1957. No. 1045.

(13) BOFFI, J.A. — Effect of the Andes mountains on the general circulation over the southern part of South America. Bull. Amer. Met. Soc., 30, pp. 242-247, Lancaster, Pa., 1949.

/(14)

(14) FLOHN, H. Zur vergleichenden Meteorologie der Hochgebirge. Archiv für Met., Geophys. und Bioklimatologie Serie B, 6, pp. 193-206, Vienna, 1955.

(15) VOWINCKEL, E. Das Klima des antarktischen Ozeans, Teil II. Archiv für Met., Geophys. und Bioklimatologie Serie B, 7, pp. 342-369, Vienna, 1956.

(16) BRITTON, G.P. Pressure waves and their application to long range forecasting in the South Atlantic. Naval Weather Service, Circular No. 12/49, London, 1949.

(17) LAMB, H.H. Some special features of the climate of St. Helena and the Trade Wind Zone in the South Atlantic. Met. Mag., 86, pp. 73-76, London, 1957.

(18) New Zealand Meteorological Service Daily Weather Bulletins (Antarctic Section). Wellington (from June) 1956.

(19) MEINARDUS, W. Klimakunde der Antarktis, Köppen and Geiger's Handbuch der Klimatologie, 4 U., Berlin, 1938.

(20) Australian Antarctic Expedition 1911-14. Records of the Queen Mary Land Station. Scientific Reports, Series B, Vol. V, Part 1. Sydney (government printer) 1940.

(21) BOUJON, H. Les observations météorologiques de Port Martin en Terre Adélie, Fascicule I, Paris (Expéditions polaires françaises) 1954.

(22) SWITHINBANK, C. Ice Shelves. Geogr. J., 121, pp. 64-67, London, 1955.

(23) COURT, A. Meteorological data for Little America III. U.S. Monthly Weather Review, Suppt. 48, Washington (Weather Bureau) 1949.

(24) RIEHL, H. Tropical meteorology. New York (McGraw-Hill) 1954.

(25) SCHMITT, W. Record wind of 300 knots. News Letter No. 91, p. 7, Weather Bureau, Pretoria, 31st October, 1956.

(26) LOEWE, F. and RADOK, U. A meridional aerological cross-section in the S.W. Pacific. J. Met., 7, pp. 58-65, Lancaster, Pa., 1950.

(27) HUTCHINGS, J.W. A meridional atmospheric cross-section for an oceanic region. J.Met., 7, pp. 94-100, Lancaster, Pa., 1950.

/(28)

(28) FLOHN, H. Grundzüge der allgemeinen Zirkulation auf der Südhalbkugel. Archiv für Met., Geophys. und Bioklim. Serie A, 2, pp. 17-64, Vienna, 1950.

(29) van Loon, H. A note on meridional atmospheric cross-sections in the southern hemisphere. NOTOS, 4, pp. 127-129, Pretoria, 1955.

(30) GIBBS, W.J. A comparison of hemispheric circulations with particular reference to the western Pacific. Quart. J., R. Met. S., 79, pp. 121-136, London, 1953.

(31) PALMEN, E. Über die atmosphärischen Strahlströme. Met. Abhandlungen der Freien Universität Berlin, Band II, Heft 3, pp. 35-49, Berlin, 1954.

(32) BANNON, J.K. Note on the subtropical jet stream in January and April, 1951. Met. Mag., 83, pp. 257-263, London, 1954.

(33) LAMB, H.H.; FLEMING, J.; HOYLE, H.D. and ROBINSON, J. Jet streams over North Africa and the central Mediterranean: January and February, 1954. Met. Mag., 86, pp. 97-111, London, 1957.

(34) SIMPSON, G.C. British Antarctic Expedition 1910-13; Meteorology, Vol. I. (Discussion) pp. 133-135, Calcutta, 1919.

(35) MEINARDUS, W. Die jährliche Periode der meridionalen Luftdruckgradienten und der Windstärken auf der südlichen Halbkugel. Met. Rundschau, 1, pp. 134-137, Heidelberg, 1947.

(36) van LOON, H. Blocking action in the southern hemisphere. NOTOS, 5, pp. 171-3, Pretoria, 1956.

(37) LAMB, H.H. and BRITTON, G.P. General atmospheric circulation and weather variations in the Antarctic. Geogr. J., 121, pp. 334-349, London, 1955.

(38) SHAW, N. Manual of Meteorology, Vol. II, p. 19, Cambridge, 1936.

(39) SHARP, R.F. Antarctic Glaciological Research. Antarctica in the International Geophysical Year, pp. 27-35. American Geophysical Union, Geophysical Monographs No. 1, Washington, 1956.

(40) LAMB, H.H. Two-way relationship between the snow or ice limit and 1000-500 mb thicknesses in the overlying atmosphere. Quart. J., R. Met. Soc., 81, pp. 172-189, London, 1955.

(41) FAUST, H. Übergradientische Winde in der Nullschicht und das Problem der Strahlströme. Archiv für Met., Geophys. und Bioklim., Serie A, 8, pp. 45-71, Vienna, 1955.

(42) MURRAY, R. and DANIELS, S.M. Transverse flow at entrance and exit to jet streams. Quart. J., R. Met. S., 79, pp. 236-241, London, 1953.

(43) MEINARDUS, W. Die mittlere Höhe und Eisbedeckung der Antarktis. Nachrichten der Gesellschaft der Wissenschaften zu Göttingen, Math. - Phys. Klasse, 1927.

(44) SCHWERDTFEGER, W. and PROHASKA, F. Der Jahresgang des Luftdrucks auf der Erde. Met. Rundschau, 9, pp. 33-43, Heidelberg, 1956.

(45) WILLETT, H.C. Temperature trends of the past century. R.Met.Soc. Centenary Proceedings, pp. 195-206, London, 1950.

(46) KRAUS, E.B. Secular changes in the rainfall regime of S.E. Australia. Quart. J., R. Met. S., 80, pp. 591-601, London, 1954.

(47) MACKINTOSH, N.A. and HERDMAN, H.F.P. Distribution of the pack-ice in the Southern Ocean. Discovery Reports, Vol. XIX, pp. 285-296, Cambridge, 1940.

(48) KOCH, L. The East Greenland Ice. Meddelelser om Grönland, Bd. 130, Nr.3, Copenhagen, 1945.

(49) KRAUS, E.B. Secular changes of east-coast rainfall regimes. Quart. J., R. Met. Soc., 81, pp. 430-439, London, 1955.

(50) KRAUS, E.B. Secular changes of tropical rainfall regimes. Quart. J., R. Met. Soc., 81, pp. 198-210, London, 1955.

(51) KRAUS, E.B. Secular changes of the standing circulation. Quart. J., R. Met. Soc., 82, pp. 289-300, London, 1956.

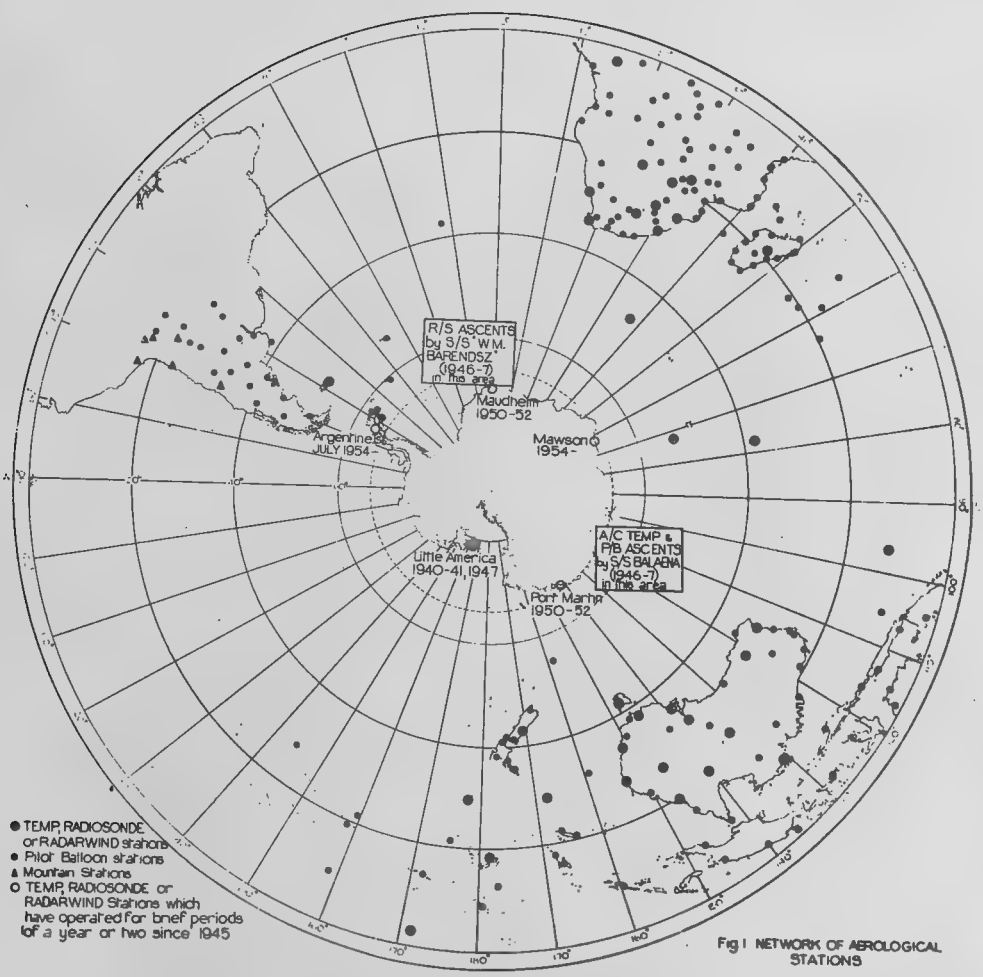

Fig 1 NETWORK OF AEROLOGICAL STATIONS

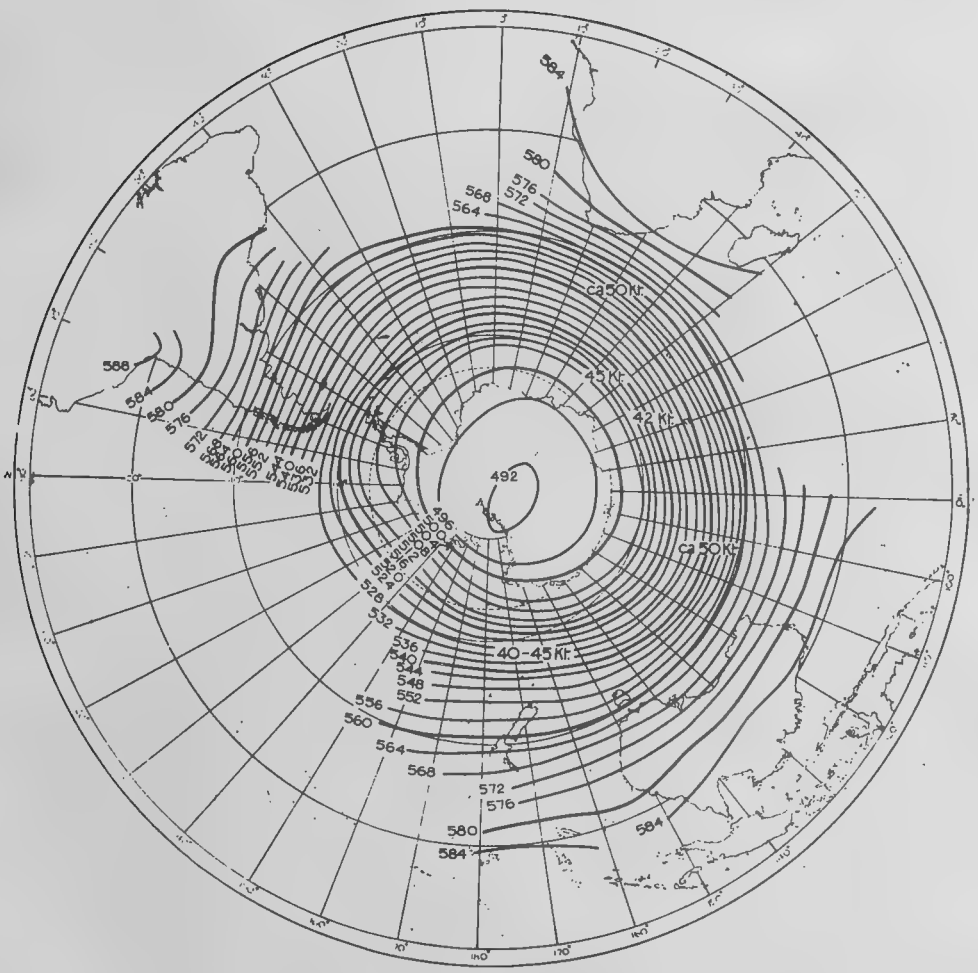

Fig.2. 3-YEAR MEAN HEIGHT OF 500 mb SURFACE IN DEKAMETRES DEC. 1951 - NOV. 1954

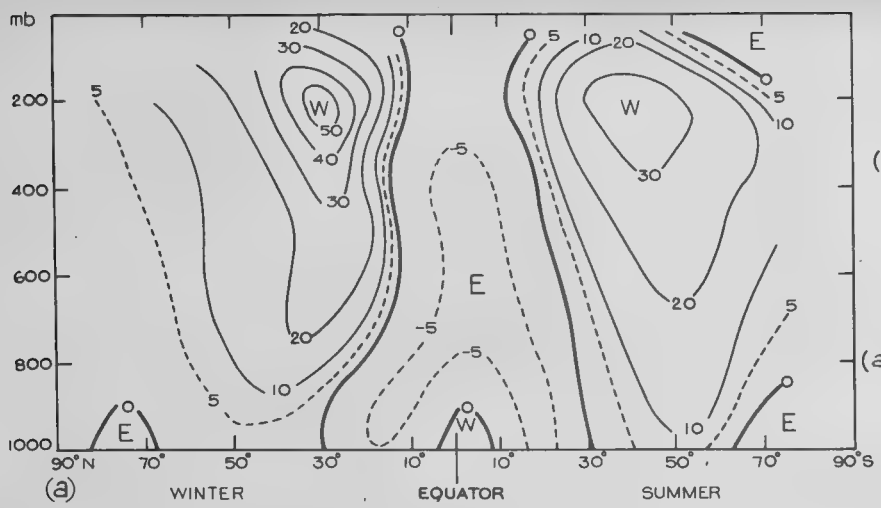

Fig. 3.
CROSS SECTIONS OF THE MEAN WESTERLY COMPONENT OF VELOCITY
(used in momentum ratio computations)

Velocities in metres per second

(a.) 30–130° E. in both hemispheres

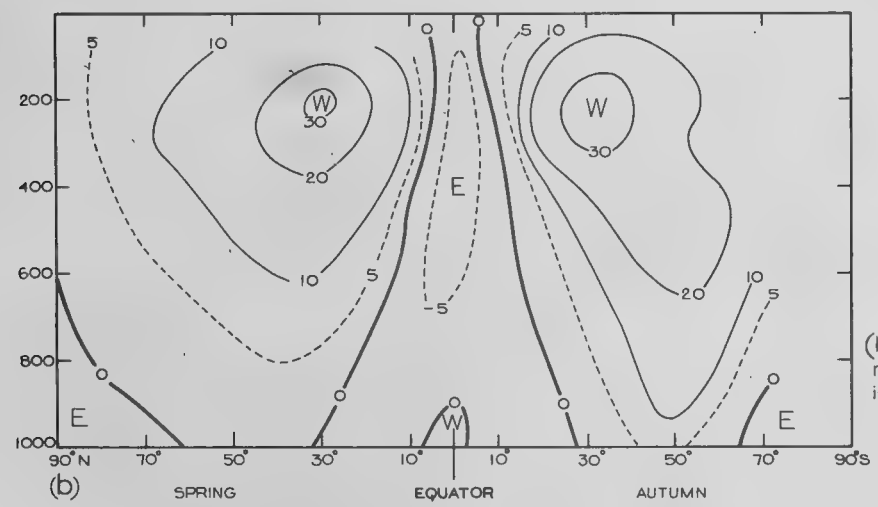

(b.) (c.) and (d.) all longitudes in northern hemisphere, 70° W–170° E. in southern hemisphere

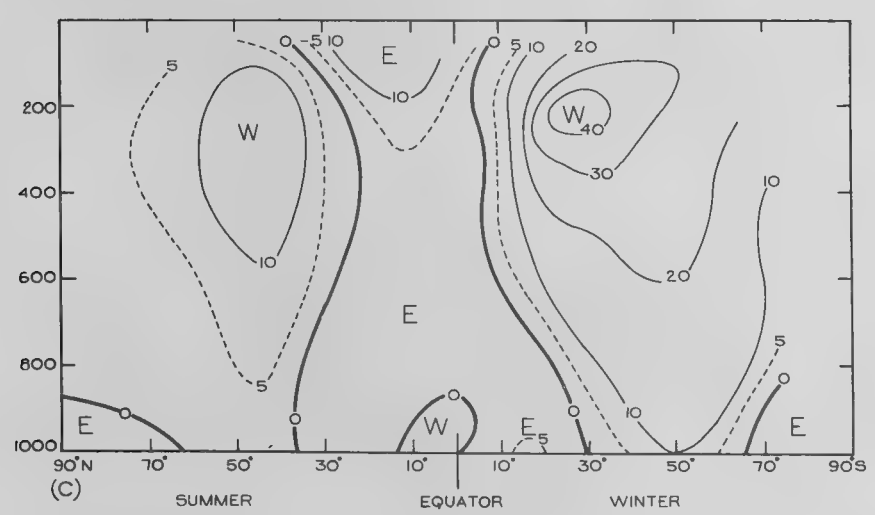

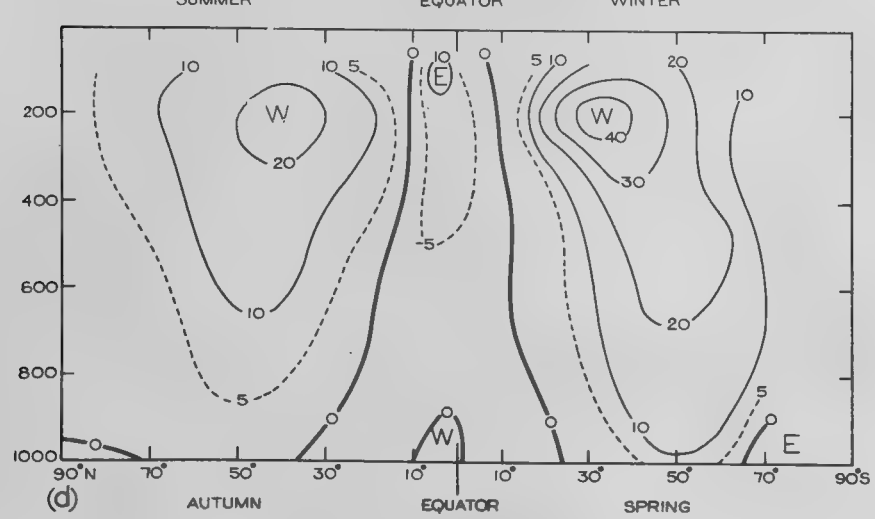

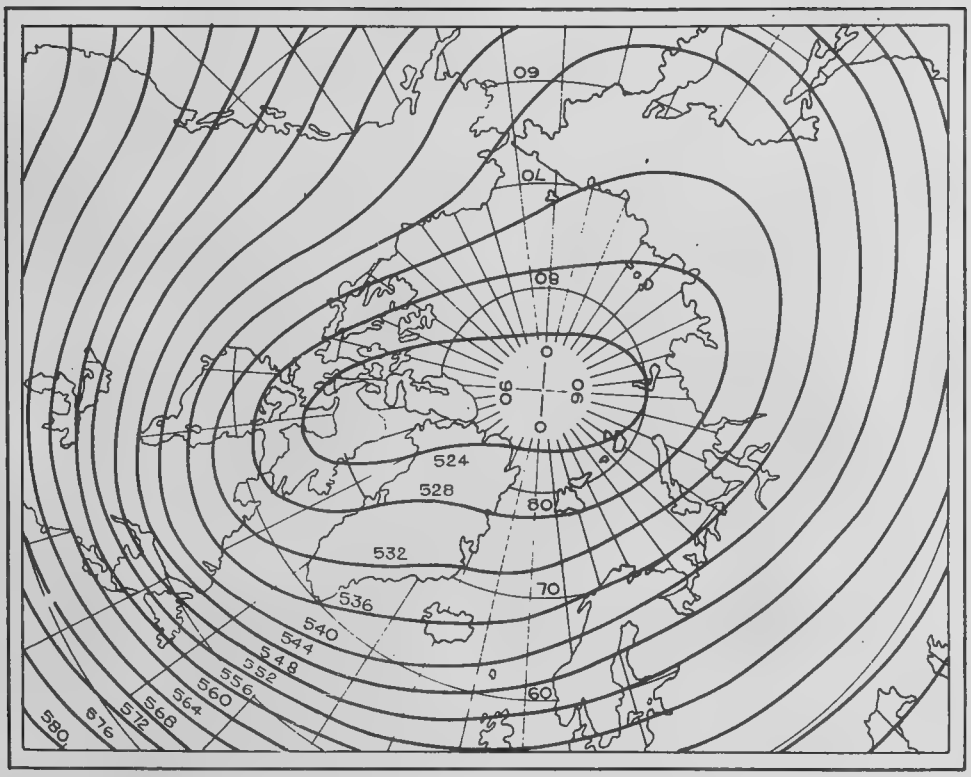

FIG. 4 3-YEAR MEAN 500 mb. HEIGHT, IN DEKAMETRES (1949-51) NORTHERN HEMISPHERE.

(AFTER FLOHN.)

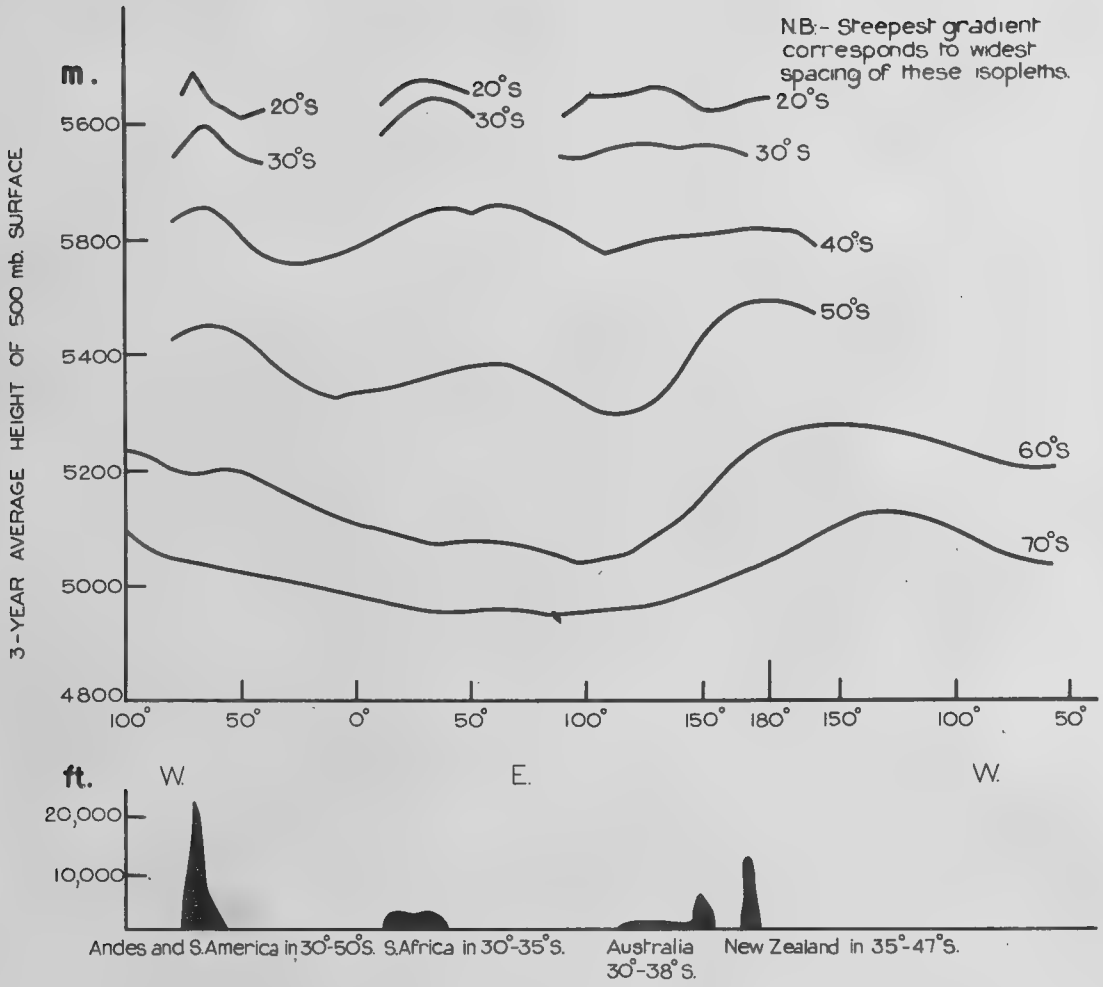

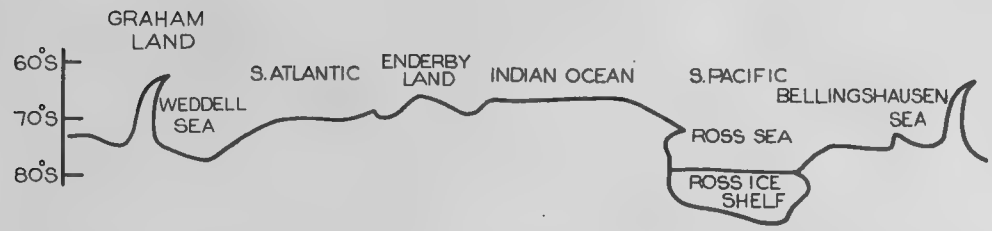

LATITUDE OF THE COAST OF ANTARCTICA.

Fig. 5a. 3-YEAR MEAN PROFILES OF THE 500 mb. SURFACE ALONG EACH 10° PARALLEL OF LATITUDE (DEC. 1951 - NOV. 1954)

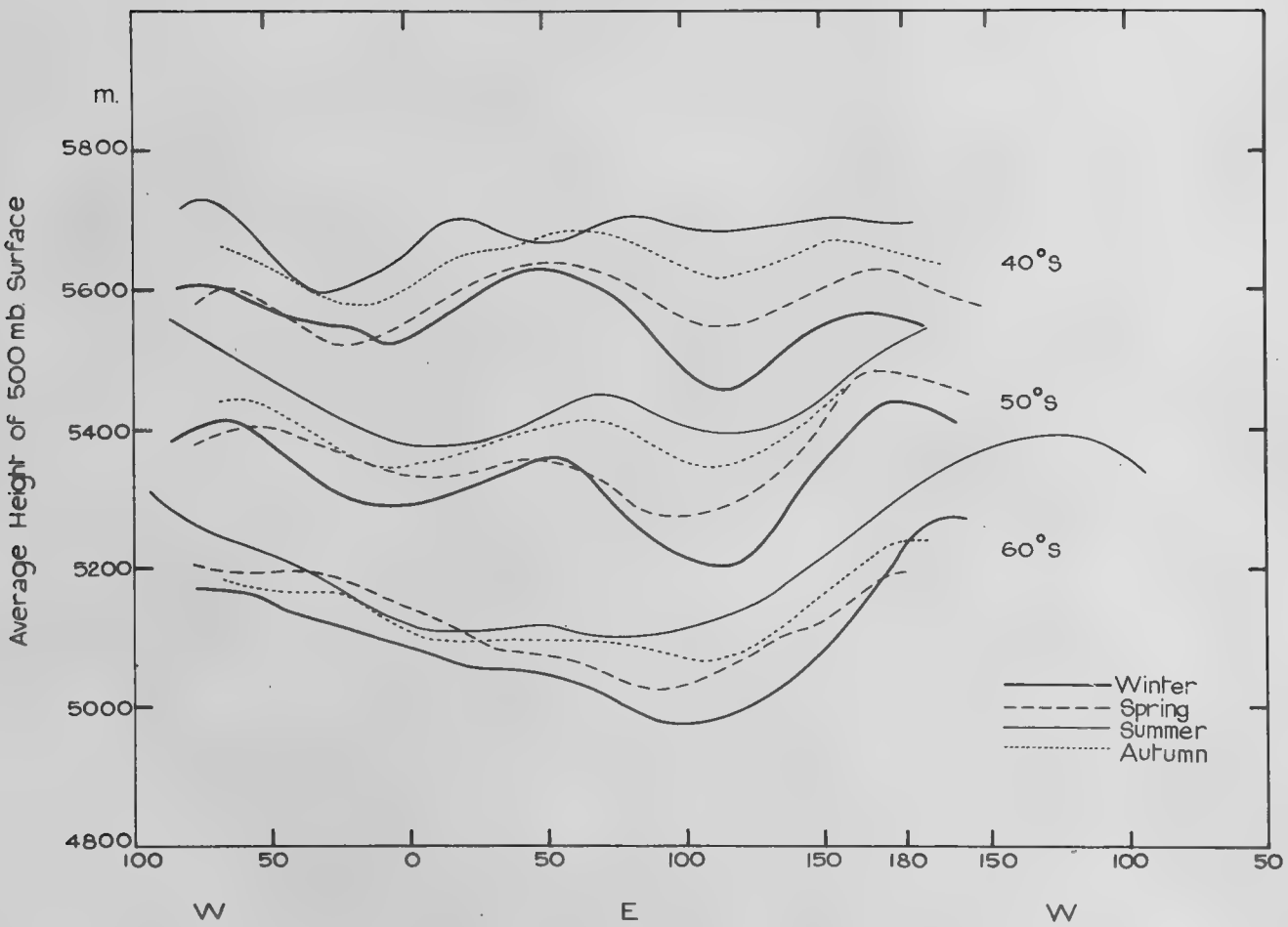

Fig. 5(b) SEASONAL PROFILES of 500 mb. HEIGHT ALONG 40°S, 50°S and 60°S. 1952-54.

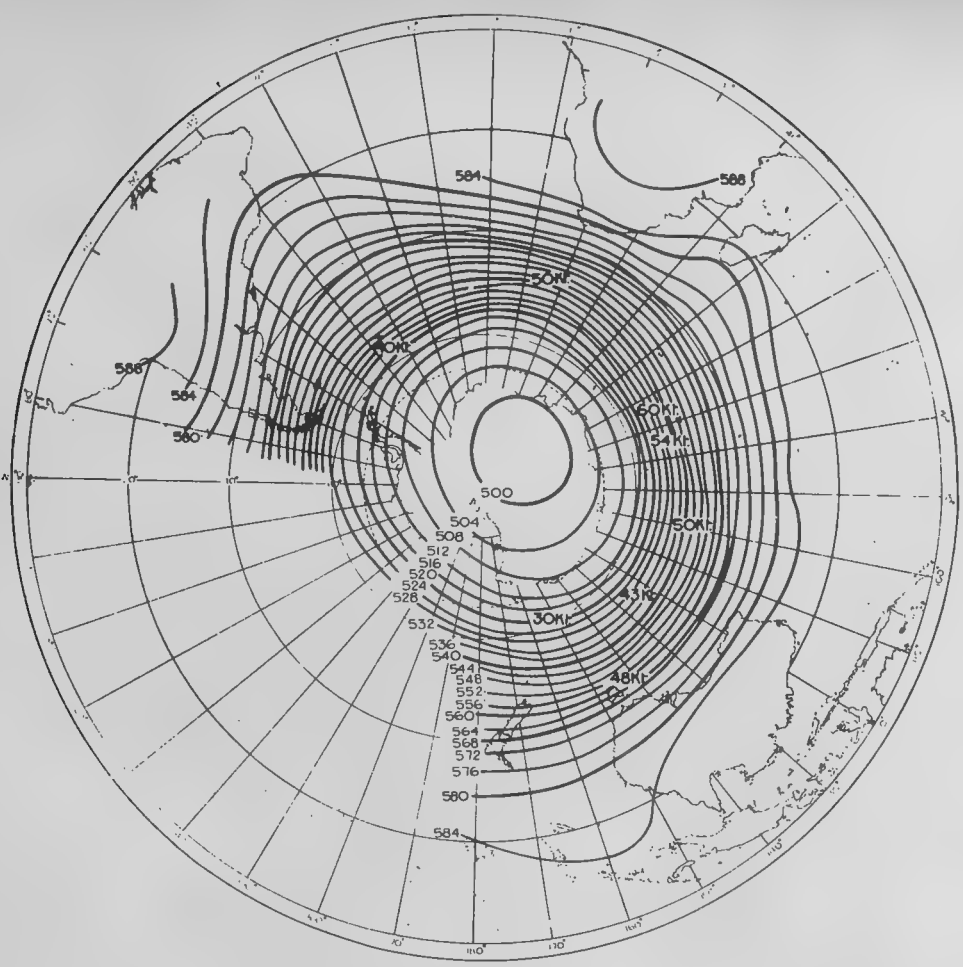

Fig 6. MEAN 500 mb. HEIGHTS (SUMMER)
(THREE SUMMERS)
1951-4

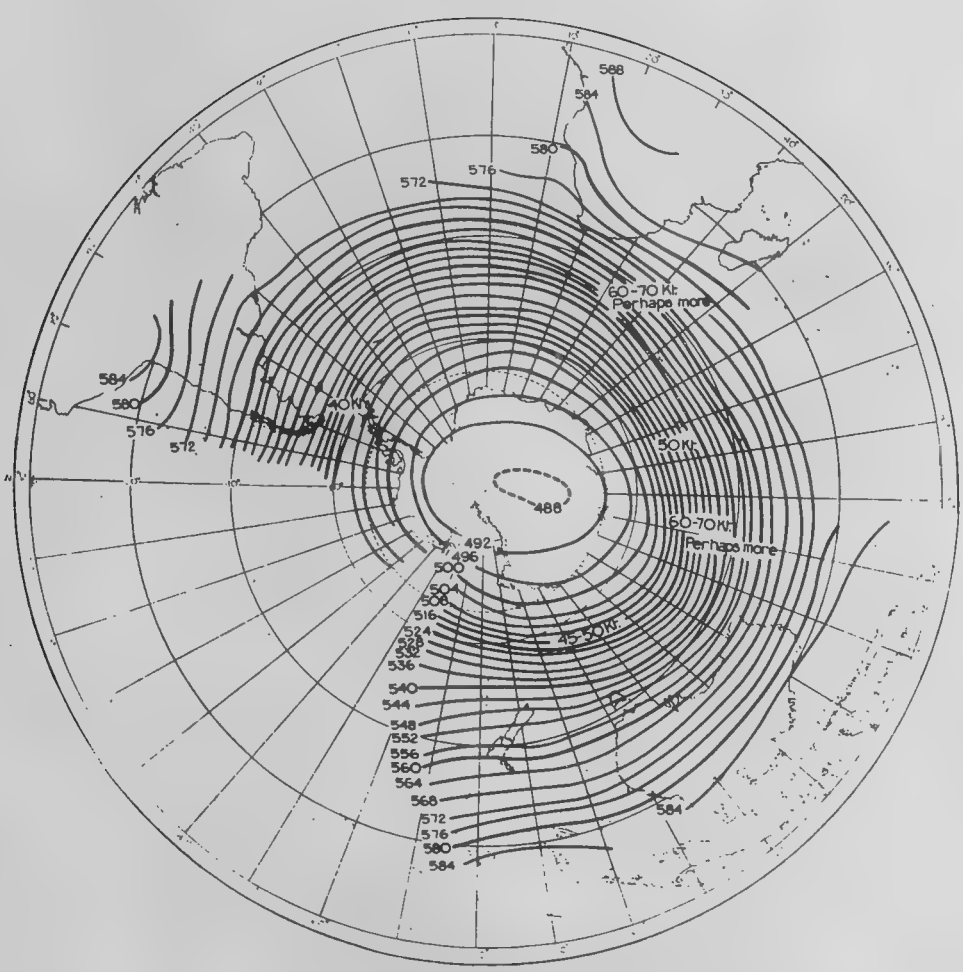

Fig 7. MEAN 500 mb. HEIGHTS (WINTER)
(THREE WINTERS)
1952-4

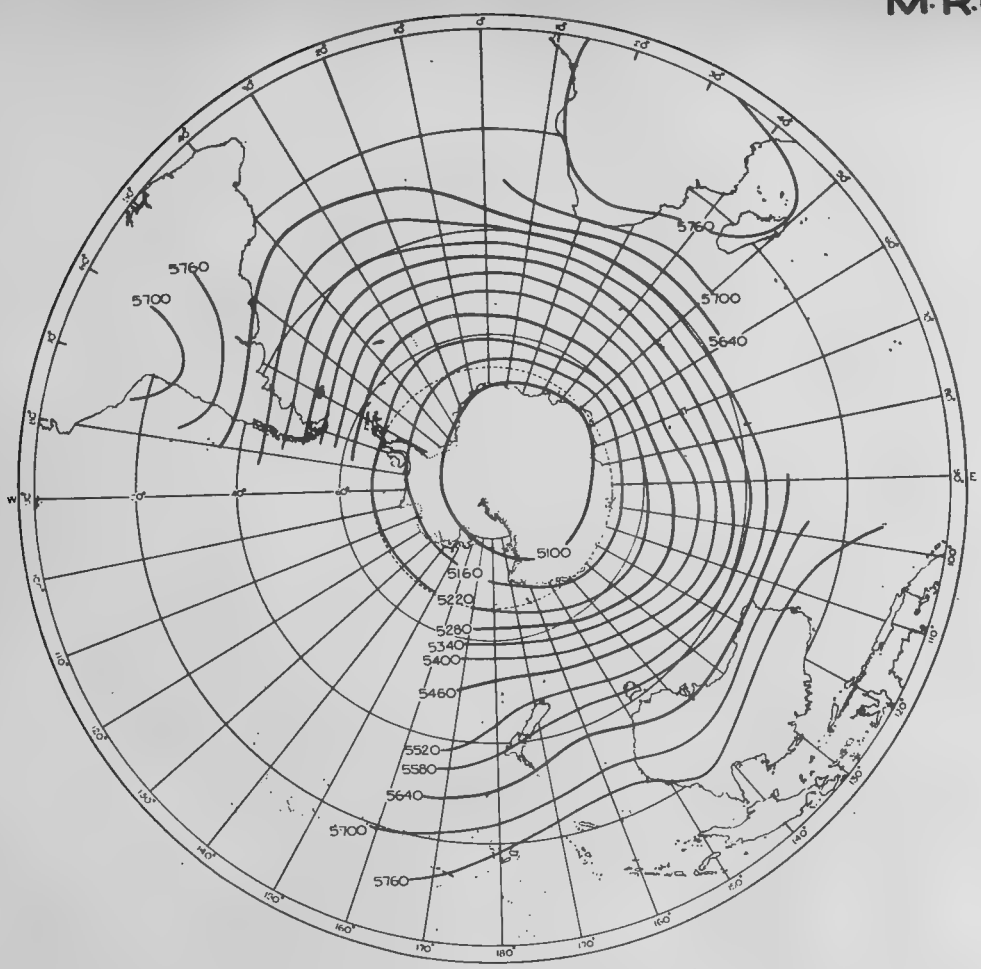

Fig 8 Mean 1000-500 mb Thickness (Summer)
in metres.
1951-4

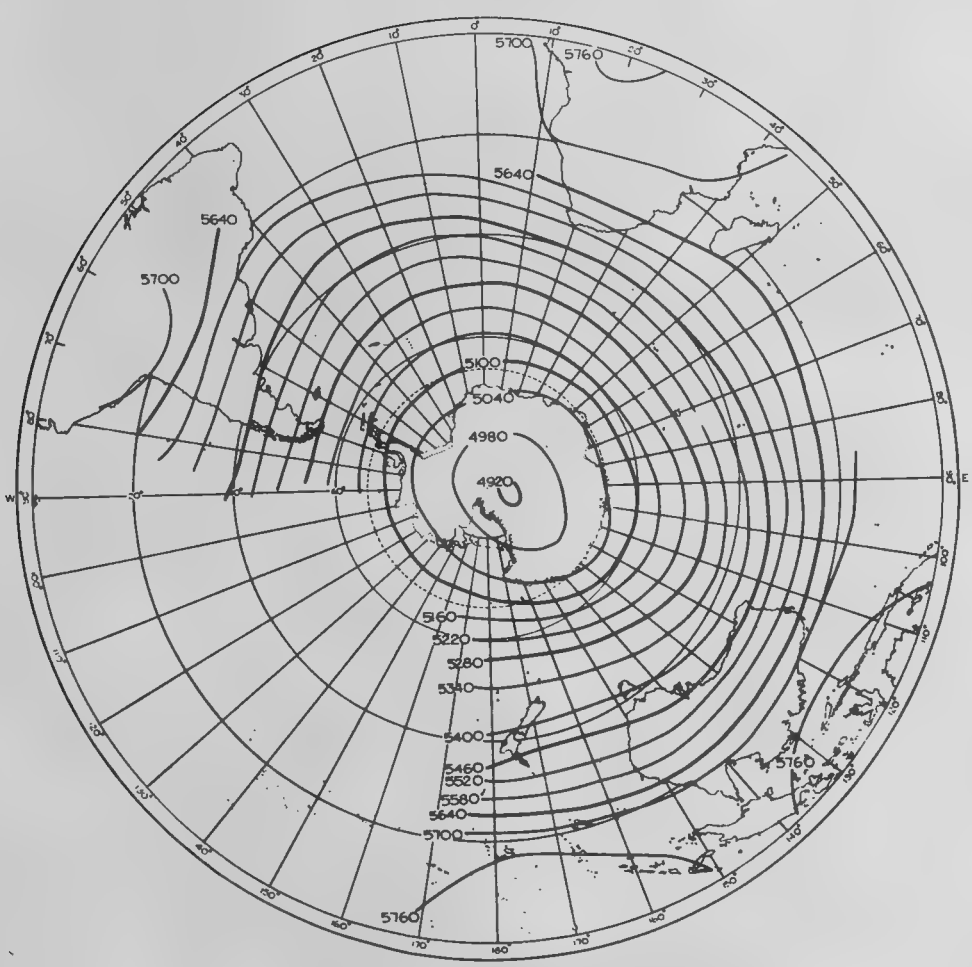

Fig 9 Mean 1000-500 mb Thickness (Winter)
in metres.
1952-4

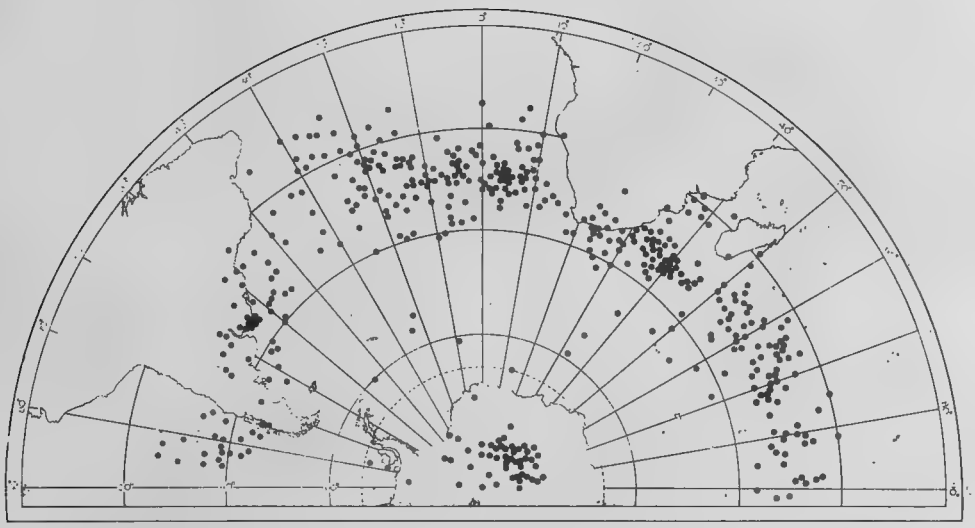

Fig 10. Distribution of once-daily positions of Anticyclone centres
SUMMER 1946-7 (Dec.-Feb)

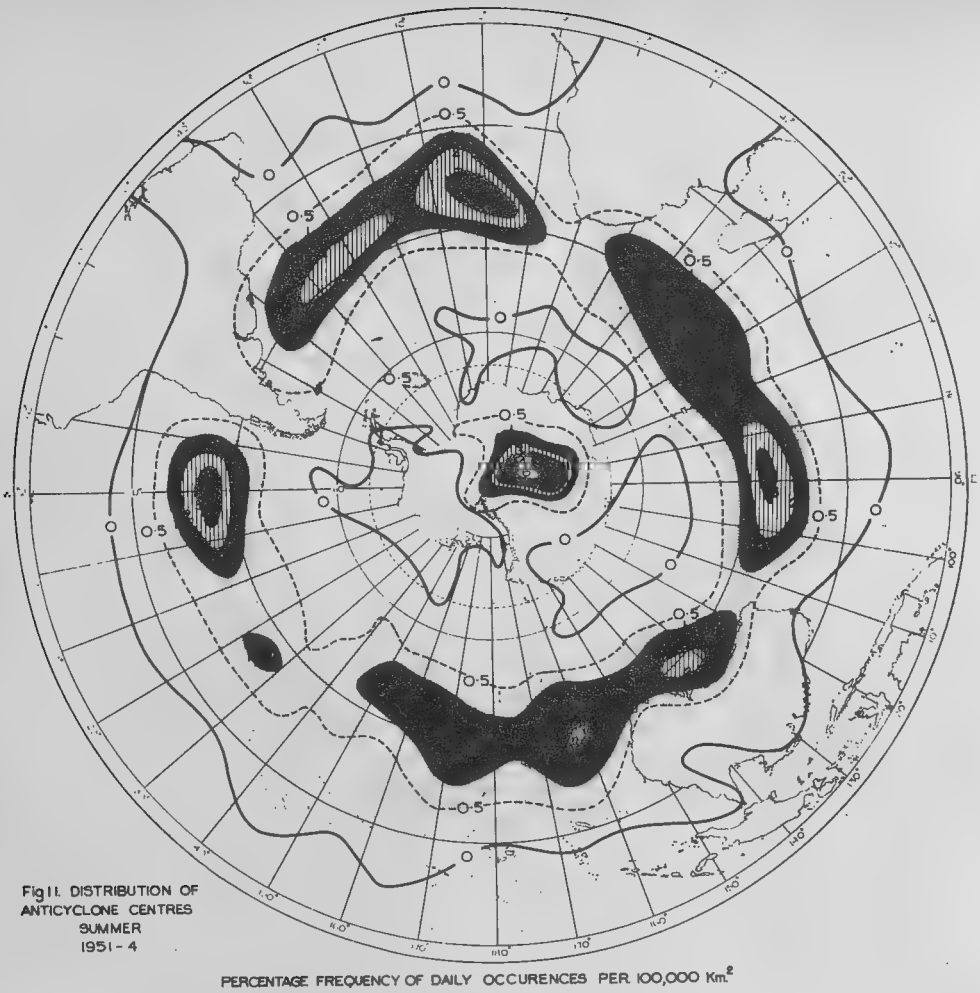
0
0·5
0·5
0·5

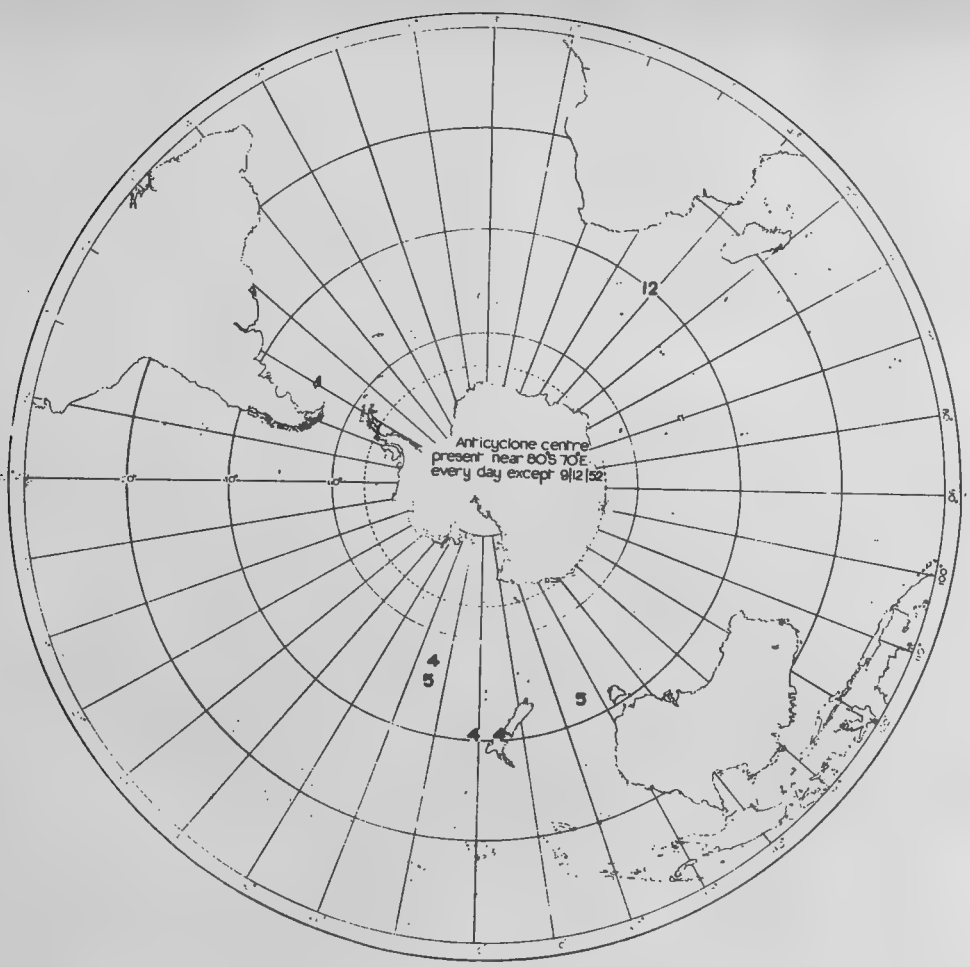

Fig 13a Occurrences of Quasi-Stationary Anticyclones South of 40°S. Summer (DJF) 1952-3
Centres which strayed x days within 600 n miles of the position marked by x, x plotted in all cases where x ≥ 4

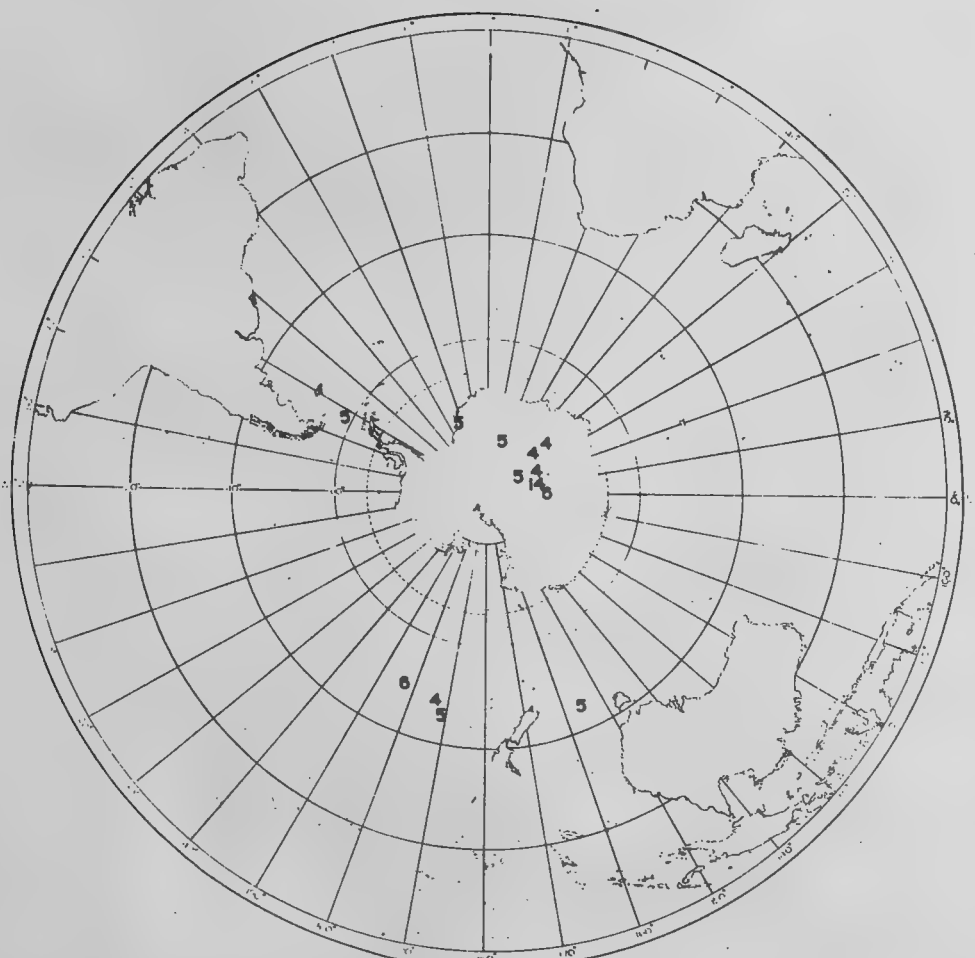

Fig 13b Occurrences of Quasi-Stationary Anticyclones South of 40°S Winter (JJA) 1952
Centres which strayed x days within 600 n miles of the position marked by x, x plotted in all cases where x ≥ 4

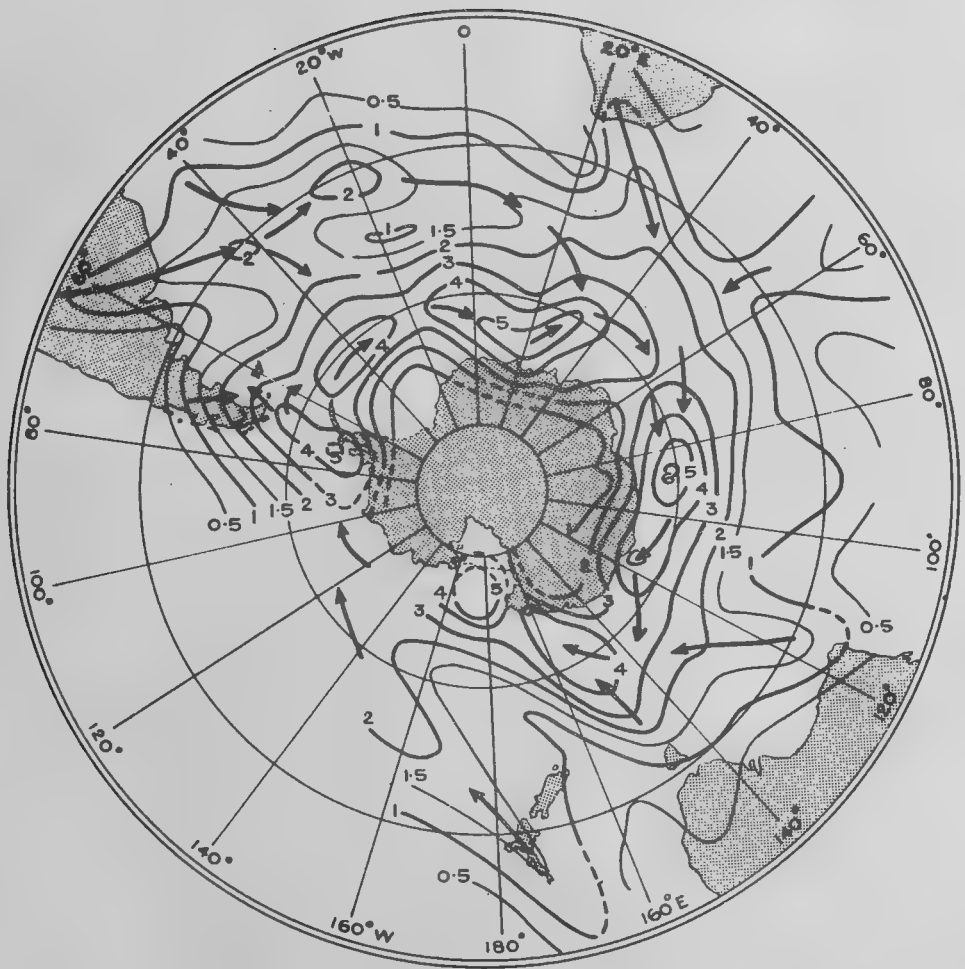

Fig. 14 Depression Frequencies: Jan.-Feb. 1947; mid March–mid April 1947; mid-March mid-April 1948.

Arrows indicate the general direction of movement.

(After Lamb and Britton)

M.R.P. 1066
S.C.11/243
27th August, 1957

Average height of the standard isobaric surfaces over the temperate and tropical regions in July.

by

H. Heastie

(Meteorological Office)

MASTER FILE COPY
NOT TO BE REMOVED
FROM AWS TECH FILES

AIR MINISTRY

METEOROLOGICAL RESEARCH COMMITTEE

MEMO ROUTING SLIP	NEVER USE FOR APPROVALS, DISAPPROVALS, CONCURRENCES, OR SIMILAR ACTIONS		
1 NAME OR TITLE Mr Lehr	INITIALS		CIRCULATE
ORGANIZATION AND LOCATION AWS55/TIPD	DATE		COORDINATION
2			FILE
			INFORMATION
3			NECESSARY ACTION
			NOTE AND RETURN
4			SEE ME
			SIGNATURE

REMARKS

M.R.P. 1066 herewith returned. Incidentally, should you ever need them, we have large photostat negatives of the height charts.

The history on these, so far, is:

MRP's 918, 981, 1020 Circumpolar maps to 55°N
Jan Jul Apr, Oct

MRP's 1045, 1066, ... Mercator world maps, 70°S - 75°N
Jan Jul Apr, Oct

FROM NAME OR TITLE Zuroy	DATE 16 May 58
ORGANIZATION AND LOCATION AWS Climatic Center	TELEPHONE

DD FORM 1 FEB 50 95 Replaces DA AGO Form 895, 1 Apr 48, and AFHQ Form 12, 10 Nov 47, which may be used.

☆ GPO : 1956—O-403461

At the time of issue this report has not been published. Any author desiring to quote this paper should refer to it as "A paper of the Meteorological Research Committee (London), M.R.P. No. 1066 by Mr. H. Heastie
A copy is available in the Library of the Meteorological Office."

M.R.P.1066
S.C.II/243
27th August, 1957.

AIR MINISTRY

METEOROLOGICAL RESEARCH COMMITTEE

Average height of the standard isobaric surfaces over the temperate and tropical regions in July

by

H. Heastie (Meteorological Office)

1. Introduction

This paper is a further step in the revision of Geophysical Memoir 85 - Upper Winds over the World. In a previous paper (1) the contours of the standard isobaric surfaces were mapped, on a Mercator projection, over the area from 75°N. to 60°S. for the month of January. The present paper shows similar charts for the month of July. The contour charts prepared in the course of the revision of this memoir are being presented as they are drawn for each month, with the object of making them quickly available to users, so avoiding the inevitable delay in publication.

2. The data

Data for the same period 1949-53 were used - the sources are listed in the previous paper (1). Whenever available, data from ascents made in darkness were used; no attempt was made to apply radiation corrections systematically to those data derived from daylight ascents, except in two cases for which corrections were readily available. The South African data were corrected in the light of a paper by Henry (2) as explained in the previous paper (1), and radiation and lag corrections, evaluated in the Upper Air Climatology Branch of the Meteorological Office, were applied to the data from overseas stations using the British radio-sonde. These corrections were based on a paper by Scrase (3). In addition a further correction was made to the 100 mb data from Nairobi and Bahrain where the temperature was below -90°F. (see ref. (1) para. 2). Wind data for British overseas stations and Hong Kong were again used. The period of these data was 1948-53 in general, though shorter periods only were available for some stations. All available data, irrespective of period, from Argentine Islands, Mawson and Terre Adélie in Antarctica were consulted as a guide to the drawing of the charts at the southern boundary. Stations for which data were available are shown in fig. 1, though in some cases data for individual years were missing.

3. Method of constructing the charts

The method of constructing the charts was almost the same as that described in the previous paper (1). Two minor differences may be mentioned here. For July, charts of average temperature were drawn for all levels from 700 mb to 100 mb, whereas for January the 700 mb and 500 mb temperature

/charts

charts were omitted. This procedure enables a slightly greater degree of consistency to be maintained between the contours at different levels and the full set of temperature charts is useful for the drawing of meridional cross-sections which it is proposed to include in the memoir at a later stage. For the January charts no "correction for tropopause" was applied in respect of the tropical tropopause. In July, however, this tropopause lies below the 100 mb surface over large areas of the chart. Moreover there is frequently a large temperature inversion just above it. Since the method of construction of the 150-100 mb thickness chart involves the calculation of the thickness from the temperature at 150 and 100 mb some correction had to be made for the presence of this tropopause. For each station the difference between the heights of the 100 mb and 150 mb surfaces was evaluated directly and the thickness of the 150-100 mb layer at a temperature equal to the mean of the 150 and 100 mb temperatures was calculated. The differences between these two thicknesses were plotted on a chart and isopleths drawn with the aid of a chart of tropopause pressure (4). Grid values of this parameter were then read off and interpolated as a "correction for tropopause" for places where direct data were not available.

4. The charts

It should be noted that, on the contour charts, the isopleth interval is 100 geopotential metres while, on the thickness charts, the interval is 50 geopotential metres. North of 55°N. the charts are merely the redrawing of the circumpolar charts on the Mercator projections, apart from some very minor amendments along the 55°N. parallel.

The seasonal contrast between summer and winter is much more marked in the northern than in the southern hemisphere. The very strong wind belts of the northern hemisphere which are such a feature of the upper troposphere in January have disappeared in July except over the eastern Mediterranean and northern United States where they appear with wind speeds much reduced. A belt of high contour height extends round the hemisphere at about 25-30°N. except over India and southern China in the lower levels where the monsoonal surface low is reflected by troughs in the 700 mb and 500 mb contours. At high levels this belt which is most marked over the Eurasian land mass leads to an easterly flow pattern over a large area south of about 25°N. in eastern longitudes. This area is too near the equator for the geostrophic relation to be used and no details of the flow can be deduced from the contours. The average wind at 100 mb at Aden is 090° 64 kt.

In the extratropical regions of the southern hemisphere there is mainly westerly flow with little meridional motion. This flow is generally stronger and extends further northward in July than in January. It seems probable that, in July, there are two strong wind belts corresponding to the temperate latitude and sub-tropical jet streams, but it is not possible to give details without drawing meridional cross-sections and isotach charts. The main trough which in January lies at about 40°E. appears at about 80°-90°E. in July.

References

(1) Heastie, H. Average height of the standard isobaric surfaces over the temperate and tropical regions in January. Meteorological Research Papers, Air Ministry, London, No. 1045, 1957.

(2) Henry, T. J. G. A comparison of mean temperatures obtained with Canadian and American types of radio-sonde. Department of Transport, Meteorological Division, Toronto, Circular 2041, 1951.

/(3)

(3) Scrase, F. J. Application of radiation and lag corrections to temperatures measured with the Meteorological Office radio-sonde. Met. Mag., London, 85, 1956, p.65.

(4) Goldie, N., Moore, J. G. and Austin, E. E. Upper air temperatures over the world. Geophys. Mem. No. 101, London (in the press).

G.H24324/MKR/9/57/65

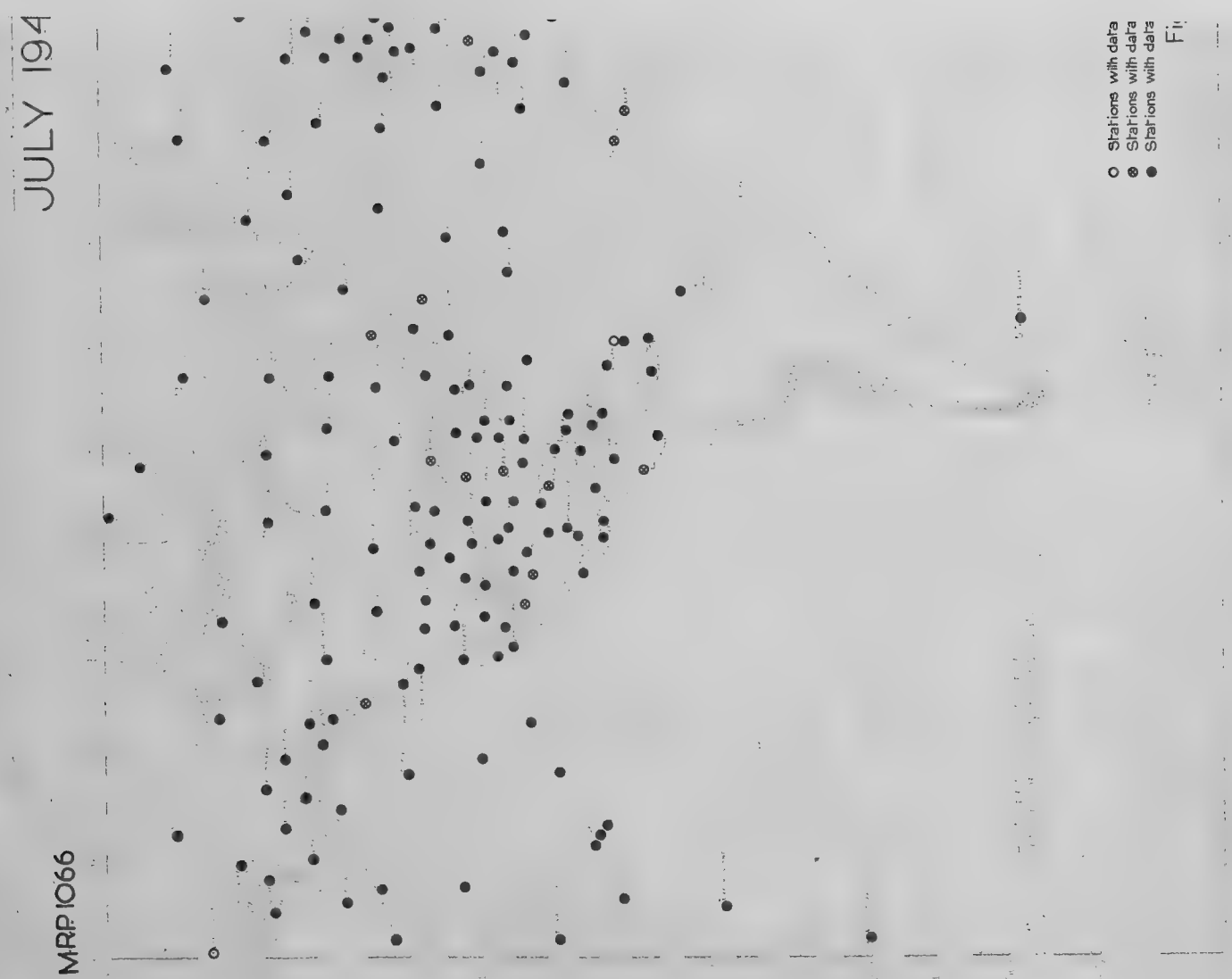

MRP 1066

JULY 1949-53

Fig. 1

M.O. 13

M.R.P 1066

Average 700 mb. Contour

JULY 1949-53

M. O. 13

MRP1066

Average 500mb. Contour JULY 1949-53

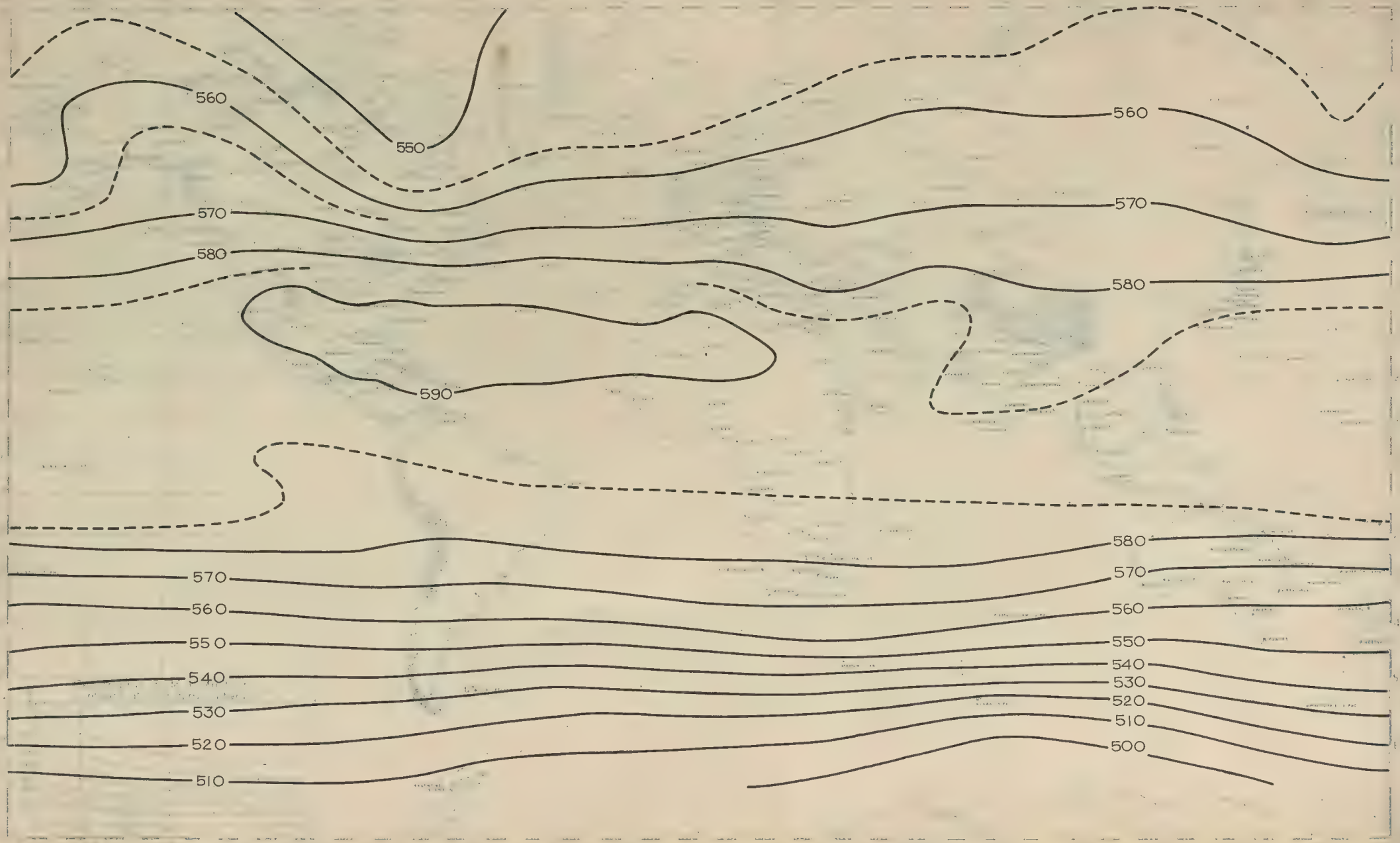

M.O. 13

M.R.P.1066

Average 300 mb. Contour

JULY 1949-53

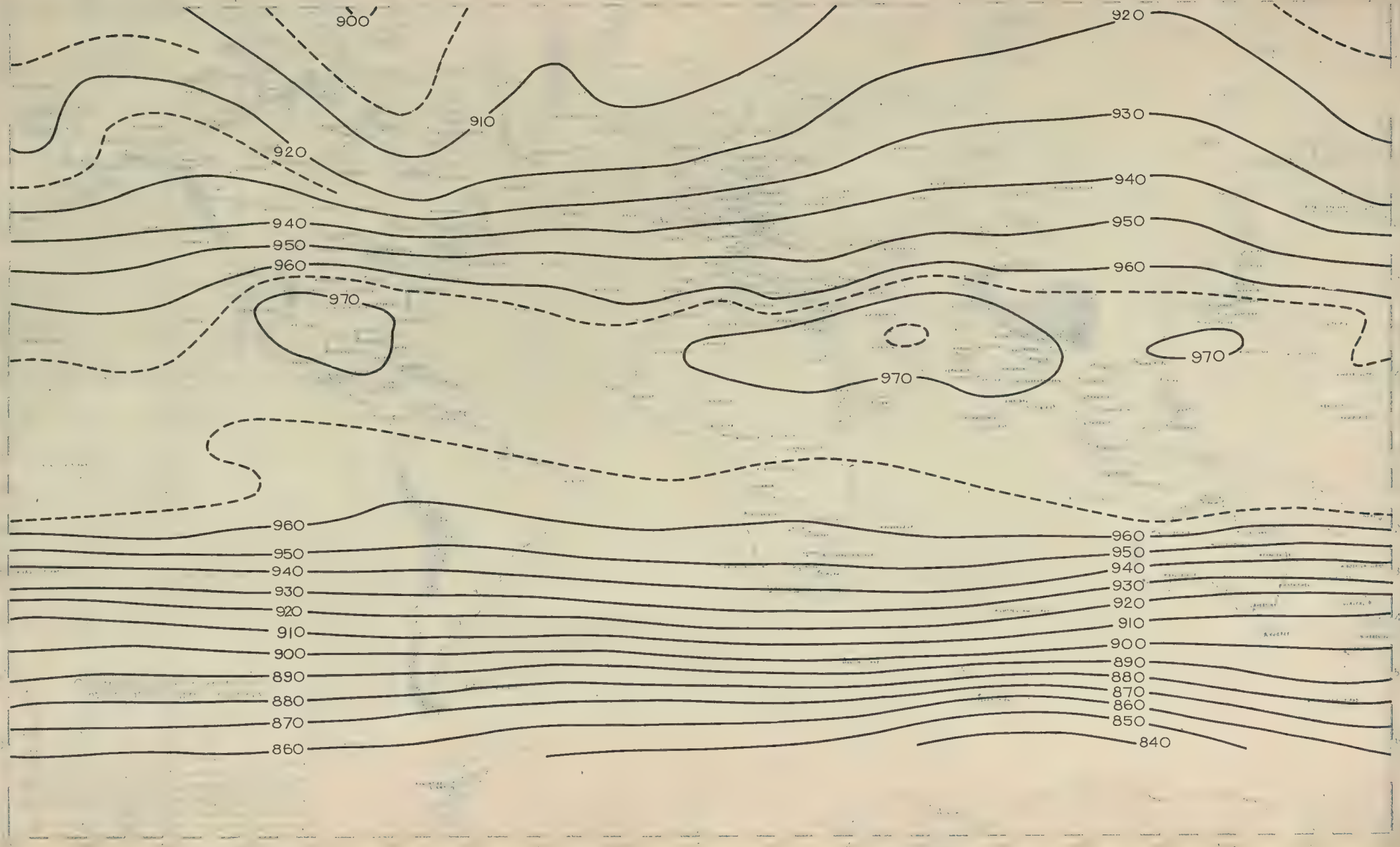

M. O. 13

M.R.P.1066

Average 200 mb. Contour

JULY 1949-53

M.O.13

M.R.P.1066

Average 150 mb. Contour

JULY 1949 - 53

M. O. 13

M.R.P.1066

Average 100 mb. Contour

JULY 1949-53

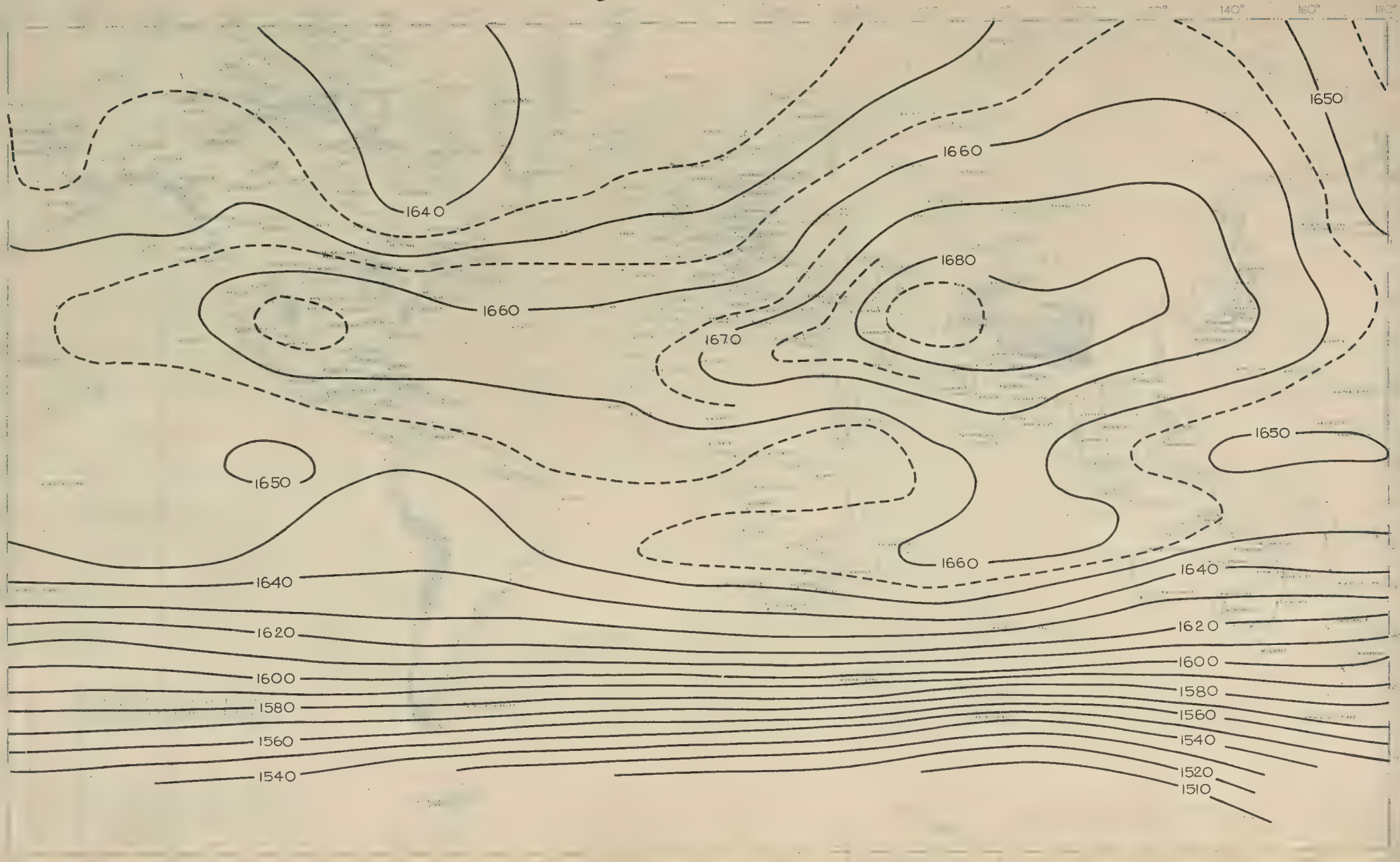

M.O. 13

M.R.P. 1066

Average 700-500mb. Thickness

JULY 1949-53

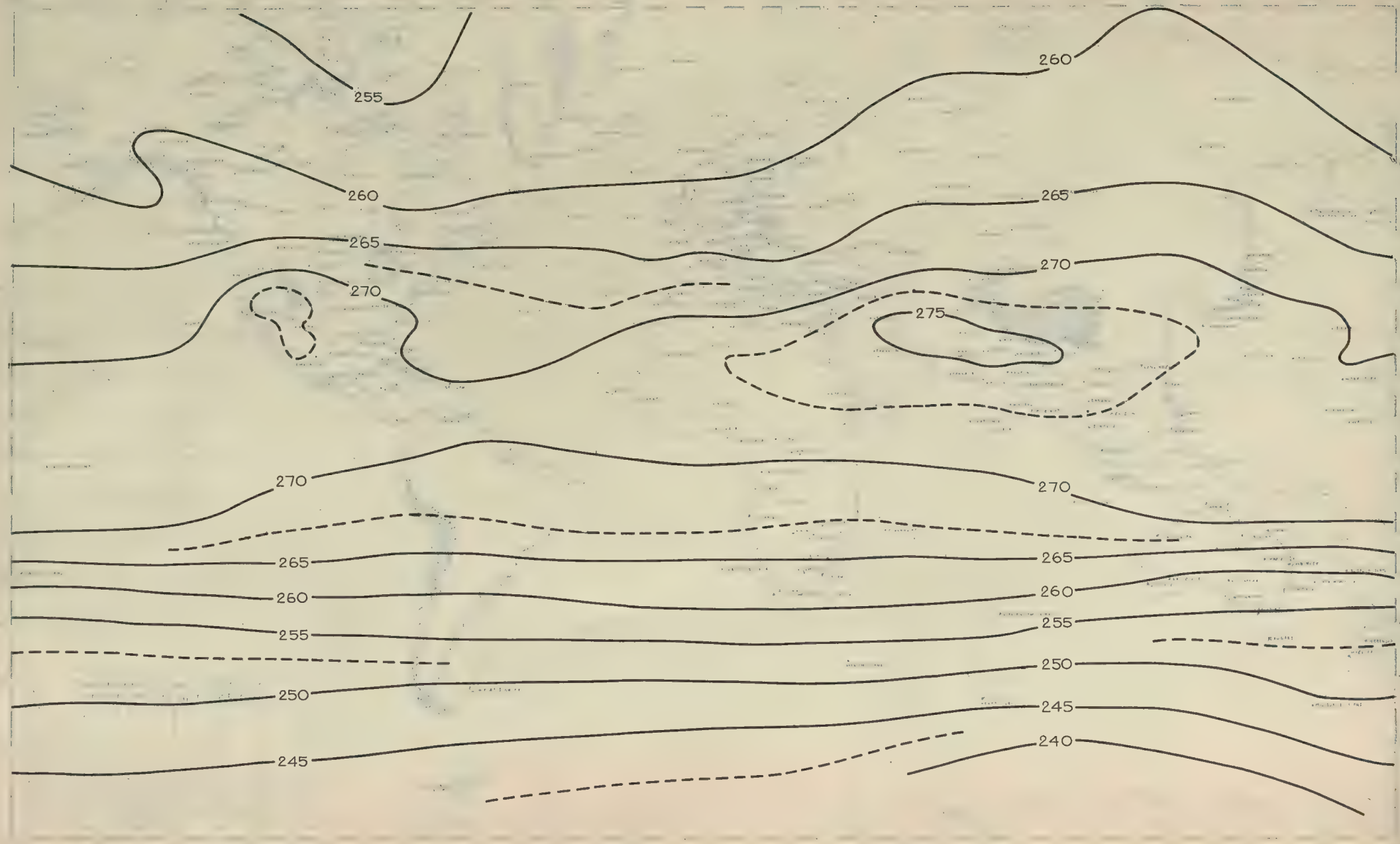

M. O. 13

MRP1066

Average 500-300 mb. Thickness

JULY 1949-53

M. O. 13

M.R.P 1066

Average 300-200 mb. Thickness

JULY 1949-53

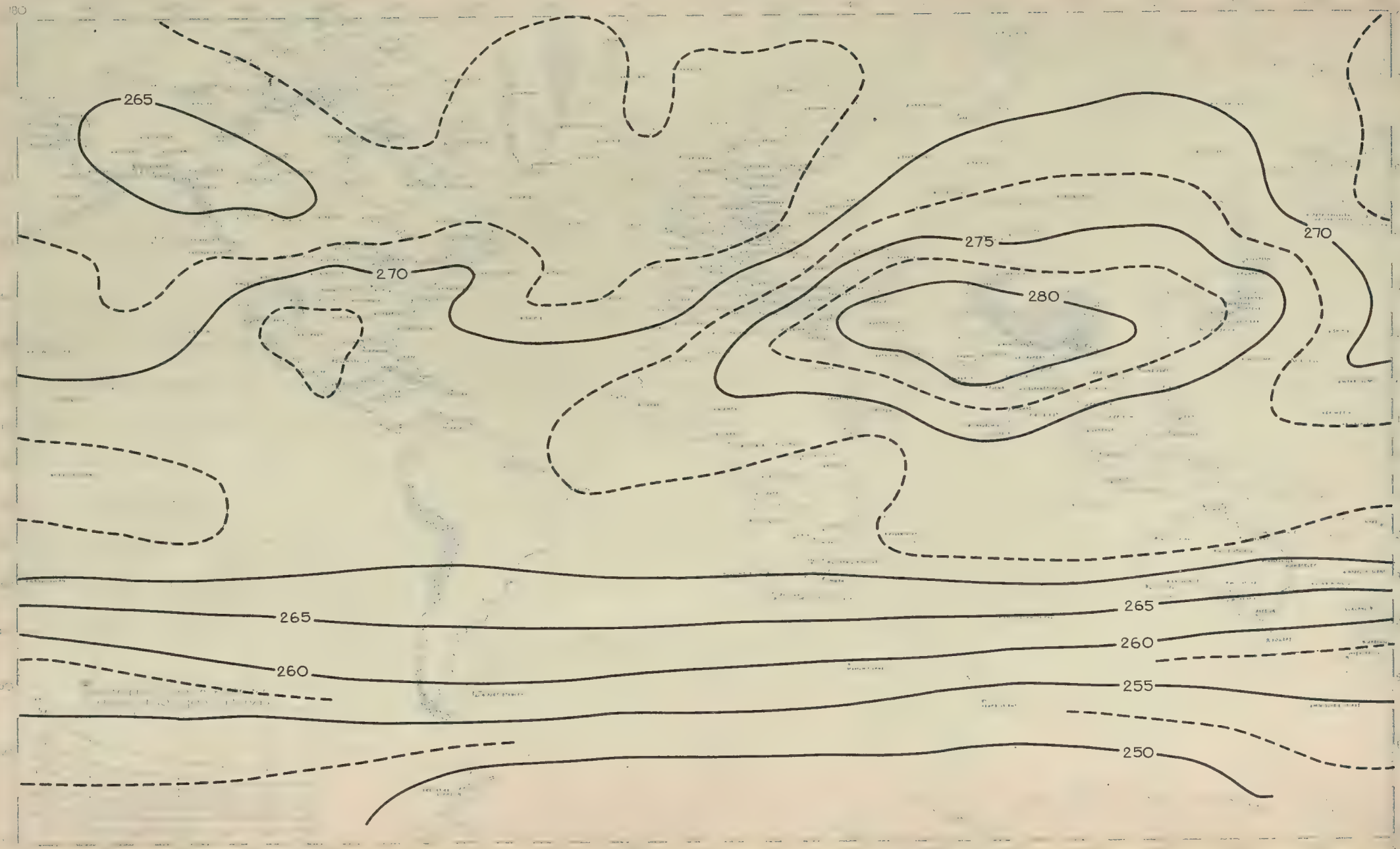

M.O.13

M.R.P. 1066

Average 200-150 mb. Thickness

JULY 1949-53

M. O. 13

M.R.P. 1066

Average 150-100 mb. Thickness

JULY 1949-53

M.O. 13

1 MAY 1958

M.R.P. 1068

S.C.111/241

28th August, 1957

The origin of radar 'angels'

by

W. G. Harper

(Meteorological Office)

AIR MINISTRY

METEOROLOGICAL RESEARCH COMMITTEE

MASTER FILE COPY
NOT TO BE REMOVED
FROM AWS TECH FILES

At the time of issue this report has not been published. Any author desiring to quote this paper should refer to it as "A paper of the Meteorological Research Committee (London), M.R.P. No. 1068 by Mr. W.G. Harper. A copy is available in the Library of the Meteorological Office."

M.R.P. 1068
S.C.III/241
28th August, 1957

AIR MINISTRY

METEOROLOGICAL RESEARCH COMMITTEE

The origin of radar 'angels'

by

W.G. Harper (Meteorological Office)

Summary

The remarkable nature and intensity of bird migration is shown to be adequate in explaining radar 'angels', which, as output powers have been increased, have come to present a hazard to airfield-control and military-type radars.

With a telescope mounted on the aerial of a target-tracking radar large numbers of birds have been seen when the radar was tracking angels, and it was clear that the radar was following their flight.

It would seem unnecessary to invoke any other mechanism to explain these phenomena, and it is suggested that there is little prospect of entirely eliminating their effects from airfield control radars.

1. Introduction

Since the inception of high-power centimetric radar unexplained echoes have been observed which for want of a valid explanation have been termed 'angels'. They appear as small blobs of echo on a plan-position (PPI) display, are usually indistinguishable from echoes received from point targets, and occasionally occur in immense numbers. As output powers have increased, in pace with the requirements of aviation, the range of detection of these extraordinary displays has also increased (we have reports of them being detectable to a range of 80 mi) until they have come to present a hazard to airfield-control and military-type radars.

As these effects have not been given wide publicity, some photographic records made at the Meteorological Office Radar Research Station at East Hill, which is in open country close to the Chiltern Hills, 30 mi north-west of London, are given:-

Fig. 1. Widespread display of angels on 10-cm PPI. Many appear as strong as echoes from aircraft. 1820 GMT, 13th March, 1957, 30 mi range. Range markers at 5 mi intervals.

Fig. 2. Permanent echo display of the East Hill PPI on the same range for comparison. No angels are present. The few stronger pip echoes beyond 10 mi are from aircraft.

Fig. 3. A locally dense display which masks most aircraft echoes, 1913 GMT, 11th March, 1957, 30 mi range.

Fig. 4. The most dense display of angels which has been recorded at East Hill. Permanent echoes and aircraft responses are completely masked. 2152 GMT, 5th March, 1952, 30 mi range. (After Jones(1)).

/Fig. 5.

Fig. 5. 10-cm range-height display (RHI) 1750 GMT, 13th March, 1957 (cf. Fig. 1). 008°M. Angels are broadly spread in height up to 5,000 ft, with one strong angel at 6,000 ft. Intense echoes on the baseline in the first 10 mi are permanent echoes caused by rising ground, trees, buildings, etc. Range markers at 5 mi intervals.

Fig. 6. 10-cm RHI display, 1915 GMT, 11th March, 1957, 002°M (cf. Fig. 3). Angels mainly concentrated at 2,500 ft, very frequent up to 5,000 ft, and scattered to 10,000 ft.

(The characteristics of the 10-cm radar equipment used are peak power 500 kw, pulse length 2 μ sec, beam widths to half-power: PPI $1\frac{1}{4}°$ x 6°, RHI $7\frac{1}{2}°$ x $1\frac{1}{2}°$.)

Lack and Varley(2) as early as 1945 reported that some point-target radar echoes were caused by large sea birds, but it has been generally held that birds could not cause the really dense displays such as Fig. 4, which are spread uniformly over large areas. Plank(3) more recently has calculated that large flying insects could account for many of the angels seen on his vertical-looking millimetric radar near Boston, Massachusetts, but he had no means of proving their presence, and it is inconceivable on theoretical grounds that wind-drifted insects could give echoes on long-range centimetric radars of sufficient intensity to cause difficulty in the control of aircraft. (It is hoped to consider some aspects of angel occurrence on millimetric radars in a separate paper, since they seem irrelevant to the aircraft control problem).

It is in fact widely held that radar angels are primarily of meteorological origin. Various theories have been developed invoking either reflection at an interface, or refraction by meteorological elements containing steep gradients of refractive index, but no single theory has managed to explain more than a few of the observed properties of angels, and the theoretical requirements have in each case been so stringent as to be difficult of acceptance.

In a search for another approach to the problem it was realised that the most intense occurrences of angels were at the times of spring and autumn bird migration, and this and other evidence is now presented suggesting that even the densest displays of angels observed in this country are caused by birds.

2. Seasonal distribution

The seasonal distribution of available East Hill records of angels, a total of 148 days spread over the period 1952-57, is shown in Fig. 7 with percentages of angel days with various degrees of activity as ordinate. Most assessments are from photographs, some are written records. The activity has been classed as light, moderate, etc., on the basis of the number of well-defined angels in the densest 20° azimuth sector of the PPI between the 10 and 15 mi range markers. This was convenient, being practically clear of permanent echo effects. Where only a written assessment was available the convention of Table 1 was adopted.

Table 1. Classification of angel activity

Density	No. in sample area	Alternative written assessment
Very light	< 5	Very few / one or two
Light	6 - 10	Some / scattered
Moderate	11 - 20	Fair number / fairly numerous
Heavy	21 - 40	Dense / numerous
Very heavy	> 40	Exceptional / very numerous

/This

This is obviously very imprecise, as even from photographs the numbers of angels cannot be stated with any certainty, and it is unlikely that visual estimates made by a number of observers over a period of years retain any precise standard. The heavy and very heavy occurrences would be more consistently reported than the lighter displays.

The 148 angel days are limited to occurrences of scattered or widespread dot echoes. A much smaller number of cases of lines of echo, usually lying up and downwind, and of arcs of echo, all of which appear to drift with the wind, seem capable of explanation in terms of birds, and indeed are of great interest, but because of their much slower speeds cannot readily be confused with aircraft responses. It is hoped to consider these in a separate account.

The interesting feature of Fig. 7 is that pronounced maxima of the general level of angel activity and of the frequency of occurrence of angels fall in March and October. The numbers of angel days in each month must of course be taken into account in studying the diagram. The percentage method used has the advantage of smoothing out to some extent any variations in the level of observing, but tends to over-emphasize the smaller numbers of occurrences, e.g., two heavy displays in January have resulted in a larger hatched area than nine 'heavy or greater' in March. It is a deficiency in the records on which Fig. 7 is based that angel activity occurring at sunset in the months May to August would not have been recorded, since radar observations were rarely continued after 1800 hr local time. The possible effect of this could only be determined by further observations. There is reason for thinking that if this occurred the numbers of angel days would be less affected than the levels of activity, since on most occasions in the dark months when an increase occurred at sunset a lower level of activity had already been recorded during the day, and a contribution to the numbers of days would have been made in any case.

The distribution of Fig. 7 seems to be reasonably related to the maxima of the spring and autumn bird migration movements in the British Isles, which comprise three important superimposed features (Witherby, Jourdain, Ticehurst and Tucker(4)),

(i) migration movements of British breeding birds,

(ii) the movement of great numbers of birds from north-central Europe, especially of rooks (Corvus frugilegus) and starlings (Sturnus vulgaris), which winter here, and

(iii) passage migrants through the British Isles which neither breed nor winter here.

Swallows and swifts are still arriving in May and commence their journey south in late July and August, but if these are excluded the overall migration periods are from late February to April, and from September usually well into December. The fact that occasional large movements of birds take place in winter is well-known to ornithologists. They refer to them as 'weather movements' (Thomson(5)), and infer that the causes are severe weather and failure of food supply. This would seem to provide adequate explanation for the occasional marked displays of angels in mid-winter.

3. Occurrences at night

Most of the angel occurrences which develop as really widespread displays start in the late afternoon and increase in intensity as darkness falls. This is consistent with the known facts of migration. Many species, especially the smaller passerines, must feed and rest during the day, and migrate mainly at night, mostly in small flocks. Exceptions to this are the aerial feeders such as swallows (Hirundinidae) and swifts (Apodidae), which are thought to migrate only by day.

/4.

4. Association with clear skies

The mechanism of migration is still largely a matter of controversy, but Matthews(6) has produced convincing evidence that the migratory urge in birds is strongly enhanced in fine sunny weather, and that many species have a preferred direction of flight which is in some way determined from the sun. Kramer(7) in some interesting experiments succeeded in re-orienting this directional urge in caged birds by displaying an artificial sun at an unnatural azimuth, and his results seem to be strong evidence for its reality.

This would seem to offer some reason for the association of the heavier angel displays with clear skies. Such movements set off by the late afternoon sun might well continue into the night. As a test case we have examined the weather conditions associated with the heaviest display of angels yet observed at East Hill, on 5th March, 1952. The Daily Weather Report shows that a frontal system cleared the east coast of England just before 1200 GMT on 5th, and that this was followed by a rapid clearance of cloud, with predominantly clear skies over the whole of England by 1700 GMT. The weather map for 1800 GMT is shown in Fig. 8. There is strong evidence that heavy migration movements take place in just such weather conditions. The winds were very favourable for migration towards the Baltic, averaging 255°/20 mph in the lower layers, but birds flying across the North Sea with this tailwind would in this instance have experienced bad weather before reaching the other side. It would be unreasonable to expect that they could have any foreknowledge of this, or that it could in any way affect their instinctive behaviour in undertaking migration flight. Some may turn back, but it is probable that most carry on. The arrival of migrating birds in an exhausted condition after a long sea crossing is regrettably common.

The really big increase in angel activity at East Hill occurred between 1730 and 2038, but there was some lighter activity during the day. Moderate activity was seen on the PPI when the equipment was switched on at 0955, to the rear of the frontal rainbelt, but it decreased to only 'one or two' by 1520. (Incidentally it was noted that there were "quite a number of birds about" at 1022). It had become light to moderate at 1730 just before sunset, when the equipment was switched off. There is no record as to just when the increase in activity occurred, but at 2038 when the equipment was switched on again the angels were very dense, and continued so to the end of observations at 2222 GMT (Fig. 4). If these were birds, as we suggest, they may have started their migration flights before sunset from points farther west. The direction and speed of movement of these angels (Jones(1)) was 255-285°/40-50 kt (46-57 mph). The RHI showed that the angels were mainly at around 2,000 ft in the morning, between 3,000 and 5,000 ft at 1730, but in the period of very heavy activity were densely concentrated in the layer from 2,000 to 5,000 ft, with scattered angels above to 10,000 ft. On one bearing at 2205 there were concentrations at two levels 2,500 and 6,500 ft. These records will be of interest in relation to the heights at which migrating birds are known to fly (para. 7), and to implications as to the numbers of birds involved in a movement of this intensity (para. 10).

5. Directions of movement

Perhaps the most striking evidence is that derived from study of the directions of movement of angels. Some of these measurements are from written records, but the majority are from time-lapse photographs, in which four to six rotations of the PPI at about minute intervals are recorded on the same negative. The clarity of this photographic method can be seen from Fig. 9, which is of six sweeps of the PPI, roughly every fourth rotation of the aerial. The PPI display is adjusted to give magnetic bearings. The azimuth markers are at 20° intervals, with magnetic north at the top of the display accentuated. Range markers are at 5 mi intervals.

/The

The faster moving objects at the top of the photograph are slow-flying aircraft. The angels are the weaker lines of dots scattered across the centre of the display. Directions and speeds of movement can readily be measured for many of the angels when the display is of moderate intensity, as in this case, but the method is not suitable with heavy and very heavy displays. While in these cases it can usually be seen that the great majority are moving in a consistent direction, it would rarely be possible to measure their speeds from time-lapse photographs because of superposition, and we have been dependent in these cases on individual measurements on the tube face and written records. As a result there are less of them than we would like. When the time-lapse method of recording was first used the sweeps were evenly spaced throughout, but we found we had to discard one day's records because we had not noted whether the angels were moving from east or west. The inclusion of one 3-rotation interval at the end of each sequence defines the direction of movement without ambiguity.

Many of the records which form the basis of the analysis of seasonal distribution of Fig. 7 are isolated photographs which allow an estimate of activity, but give no clue to the direction of movement, and we are reduced to 24 days with recorded directions in the months February to April, included without regard to their category of activity, which we shall refer to as the spring angel movements. They are shown in the inner zone of Fig. 10. Where the directions on any one day had a spread of values, say between 060 and 085°, a single vector is entered at 073°. It is seen that all but two lie in the sector 060 to 140°, and that 18 of the 24 lie in a 50° sector from 060 to 110°. The wind directions at the levels of most frequent occurrence of the angels derived from the nearest radar-wind soundings are shown in the outer zone (only 23 are given, one was a calm). They are seen to be almost exclusively the prevailing west to south-west winds, and to be in general agreement with the angel movements, but are spread through almost twice as big a sector in azimuth.

It might be thought that the angels only appear not to move with the wind because the radar-wind values are unrepresentative, but we have examined the individual pairs of directions and find convincing evidence that many of the angel movements have a substantial crosswind component. Fig. 9 is an instance of this. It is a time-lapse photograph centred at 0922 GMT on 13th March, 1957. The angels are moving from 270°T (260-280) with speeds measured from the photographs falling in the range 32 to 40 mph. Their heights were between 1,000 and 3,000 ft, at which levels the winds were in the azimuth range 180 to 210° (0800 hr radar winds - Hemsby 210/17, Crawley 210/14, Larkhill 186/21; the greatest veer at 1400 hr being to 230° at Hemsby. The wind measured at Cardington, 14 mi NNE of East Hill, at 1200 hr was south/26 at 2,000 ft. It seems unlikely that the low-level wind in the East Hill area at 0922 was of greater azimuth than 210°). Thus the general direction of movement of the angels diverges by at least 60° from the wind. Out of about 100 well-defined angel movements on this photograph only three show significant divergences from the main easterly movement, one at 310°M/16 mi is seen to be moving from 220°T, one at 015/13 from 225°T, and one at 225/11 from 290°T, i.e., only about 2 per cent were on this occasion moving with the wind. There are many similar instances in our records. In 5 of the 24 cases of Fig. 10, and in 7 of the 22 cases of Fig. 11 the great majority of the echoes were moving from directions diverging by at least 45° from the winds.

The two inconsistent movements of Fig. 10 are also of interest.

(i) The angels moving towards 168° occurred on 1st February, 1952, only just falling in the selected period. Only one time-lapse photograph was taken, showing about 30 angels scattered irregularly out to 30 mi, none diverging from this general direction by as much as 20°. The prevailing wind at the angel height of 3,000 to 4,000 ft was 310/30. To have made good the course and speed of the angels, birds would have had to head towards 210 at an airspeed of 28 mph. This date and direction suggest a 'weather movement' of wintering birds. (There are other winter

/records

records suggestive of weather movements, but angel directions and speeds have rarely been recorded. Several in the months of January and February are of angels ahead of belts of snow or associated with snow showers. One on 7th January, 1954 is of "a host of angels visible almost until noon, some out to 30 mi. Shower-type echoes on the display at the same time, but none in the angel zone. A line of scattered snow showers moving from 010/35-40 mph passed for most of the day, mostly 30 mi to the east of East Hill. Angels reappeared in great numbers by 1700". Observations then ceased. It is likely that the angels were moving from the north, for if their movement had been very different from that of the snow showers this would almost certainly have been noticed.)

(ii) The angels moving towards 015° were recorded between 1700 and 1830 GMT, just around sunset, at the height of the migration season, on 22nd March, 1957. Angels with an ENE movement had been recorded on each of the two preceding days. The most probable wind is that measured at Cardington only 12 mi distant, 145°/34 mph. To be drifted in direction 015° birds must actually have been heading towards 070°, a normal direction of migration, with airspeeds between 43 and 48 mph.

Analysis of the autumn angel movements is equally interesting. 22 movements are on record in the months September to December, and are displayed using the same presentation (Fig. 11). The movements are seen to be almost equally divided between south and west, and are limited to a 160° sector. The winds shown in the outer zone are however strikingly variable. There are no less than six days with winds between west and north-west, but no single case of angels moving with these winds (only 21 wind directions are recorded, one being light and variable). The evidence seems irrefutable that angels of this type are not wind-borne.

The movements of Fig. 10 and 11 are consistent with bird migration movements. The easterly movements in spring are mainly departures of flocks of wintering birds to their breeding grounds in north-central Europe, followed by passage migration through southern England. We suggest that the concentration of southerly angel movements (Fig. 11), which are spread evenly throughout the four months, are passage migrants bound for the Continent, and that the west-north-westerly movements are birds from northern Europe which winter in Ireland. Autumn movements of birds in southern England towards the west and west-north-west have been extensively reported (Lack(8)). A major part of this seems to consist of the October movements of chaffinches (Fringilla coelebs), skylarks (Alauda arvensis) and starlings, and these have even been observed at Oxford, only 35 mi west-south-west of East Hill (Lack and Lack(9)). It is interesting that five out of the six west-north-west angel movements of Fig. 11 took place in October, one in November.

We think that Fig. 10 and 11 alone are convincing evidence that widespread occurrences of angels on centimetric radars are caused by birds.

6. Speeds of movement

Jones(1) was, as far as we are aware, the first to draw clear attention to the fact that angels very commonly move at twice the speed of the wind or even more, but Baldwin(10) as early as 1948 had recorded that 3-cm and 10-cm angels do indeed move ".... in fairly level and straight courses, usually running a little faster than the surface wind, sometimes running across or against it. Once in a while one stops for a few seconds". Erratic behaviour such as this is quite inexplicable in terms of any proposed meteorological theory of angels, and it is almost certain that Baldwin was tracking birds.

It is unlikely however that the birds he was observing were on migration, because migration movements are characterized by a remarkable steadiness of flight, even amongst species which at other times are quite erratic in their movements.

/We

We are therefore able with confidence to subtract winds vectorially from these movements, and obtain 'flight speeds in still air' for comparison with published values of the speeds of bird flight.

On nine days in March, 1957, at the height of the spring migration, in a spell of unusually good weather (there is a press report in this period of jet fighter squadrons in western Germany reducing their flying for a few days because there had been so many collisions with birds - obviously heavy migration movements), we have 92 accurate measurements of height, speed and direction of angels which have been treated in this way, using the best available winds at their heights (the mean of the radar winds at Crawley and Hemsby where a Cardington wind was not available). They are presented as a histogram of still air flight speeds in Fig. 12. The highest and lowest speeds derived were 56 and 22 mph, and it can be seen that there is a pronounced maximum at 33 mph, and a secondary maximum at 44 mph.

Meinertzhagen(11) is the acknowledged authority in this field. He has collated reliable data measured in calm conditions, and has published the following speed ranges (mph):- smaller passerines 20-37, rooks 29-42, starlings 43-49, geese 42-55, ducks 44-59, while a few species achieve higher speeds. These values are in remarkable agreement with Fig. 12, and it can be seen that a judicious composition of smaller passerines, starlings and duck (common migratory birds in southern England - duck can be seen in considerable flocks at Tring Reservoirs 10 mi south-west of East Hill in migration times), could give a close fit to even the detailed structure of Fig. 12.

7. Heights

We find from RHI radar studies that on any one occasion the angels usually have a spread in height, but are most common around 2,000 to 3,000 ft, occasionally in concentrated layers, are scattered above 5,000 ft and very rare above 10,000 ft. We have seen isolated angels at different times at 13,000, 14,000 and 16,000 ft. (Compare the special case already described in para. 4).

Meinertzhagen(11) is again the source of the most reliable information of the height of migration of birds. He lists numerous instances, collected over many years, of birds observed and specified from aircraft at all heights up to 9,000 ft. On one occasion cranes were overtaken flying at 15,000 ft over France. He concludes that there is a growing volume of evidence to show that migratory movement does sometimes extend to extremely high altitudes.

From the physiological aspect there is evidence that some species of birds can live comfortably at great heights. Hunt(12) has reported that choughs followed the Everest climbers in 1953 to all camps up to the South Col at 26,000 ft, exhibiting quite normal behaviour around the tent sites, and a flock of small birds was seen flying over the Col.

Although the height ranges of aircraft sightings and of angel occurrences are seen to be in good general agreement, such sightings above 5,000 ft have been quite rare, making it uncertain whether migration occurs regularly at these heights. Yet with almost every widespread angel occurrence some angels are seen above 5,000 ft, occasionally large numbers, though never as numerous as in the concentrations below 5,000 ft. This is not as inconsistent as it may at first appear. An RHI search through all quadrants, taking only a few minutes, scans many hundreds of cubic miles of space. Even when angels are numerous above 5,000 ft (using the word 'numerous' rather more loosely than in the PPI assessments of Table 1) the density does not average as much as one per cubic mile. Pilots would be most unlikely to see birds in such concentrations.

/8.

8. Birds actually seen

In addition to the high-power PPI and RHI, angels are also detectable on the M.O. wind-finding radar type 1 (G.L.3, 10-cm, 250 kw, 1 μ sec, 6° beam), though the signal returns are much weaker than those from aircraft or balloon-borne reflectors. This radar uses a split-beam technique permitting accurate manual following of point targets, with probable error ±20 yd in range, ±0.1° in elevation and azimuth. It is only recently, since suspecting birds as the cause of angels, that we have mounted an 8x telescope on the paraboloid assembly, with its graticule aligned to the electrical and mechanical axes. We had immediate success. On 18th March, 1957, when a moderate display of angels lasted from 0900 to 1300 GMT, and redeveloped after 1700 GMT, angels were resolved quite clearly as birds. The technique adopted was to pick on an angel moving towards the radar at a range of about 5,000 yd and follow it in. Despite the fact that neither of the telescope observers was experienced in watching birds, 18 of 25 angels followed to within 2,000 yd were seen to be birds. In one additional case a momentary flash might well have been from a bird's plumage. The slant ranges and elevations placed two others above broken stratocumulus cloud where they could probably not have been seen. There was no doubt that the radar was following these birds. They remained in the graticule from the moment of detection until following ceased, often through considerable changes of azimuth and elevation. Most were flocks of from 5 to 30 small birds, one "about 40 birds". In a few cases they were described as "a small flock" with no estimate of numbers. One angel of greater than average signal intensity was identified while still at 3,000 yd, and was clearly seen as a V-formation of large birds flying steadily, probably geese.

We are equally convinced that the radar was following typical angels. The direction of movement agreed with the movement of the angels on the PPI display, and the range of heights of the birds seen (accurately derived from the wind-finding radar) and the average height 1,900 ft, were in good agreement with the RHI display.

9. Echo fluctuation

The persistence of angel echoes, and their fluctuation on range-amplitude display, are consistent with explanation as birds. Individual angels have been followed both on PPI and RHI for periods of half an hour, but even this cannot be regarded as their 'life', as they were well-defined when selected, and were only lost near maximum range of detection. Swingle(13) also has reported that during his observations of angels the echoes seemed to fluctuate very little, suggesting sharply localized sources. Admittedly reports of short-persistence angels have come from observers using vertical-looking millimetric radars, but this would naturally be so from birds flying through a beam whose width is measured in tens of feet, as against the 10-cm radar's beam which is measured in thousands of feet at normal working ranges.

The G.L.3, which can display the signal-amplitude of any selected range interval of 1,000 yd (R-scope) on a 6 in. tube, is well-suited to detailed study of the echoes. It confirms their persistent character, and that their fine-scale fluctuations of signal intensity are quite unlike either the rapid beating of rain echoes (incoherent scattering) or the slow variations of aircraft echoes (coherent scattering). They have a moderate and quite distinctive beat somewhere between the two.

10. Density of angels

It is inherent in PPI and RHI radars that a point target is displayed as a small patch of echo, of length half the pulse-length (300 m for our PPI and RHI), and of width in the plane of sweep approximately the beam width (240 m in azimuth at range 10 mi for the PPI, 280 m in the vertical at this range for the RHI). Thus if widespread angels had less than these separations a continuous diffuse echo would be displayed. It is almost continuous in

/Fig. 4

Fig. 4 at the shorter ranges (it appears rather less so on the original negatives, some detail having been lost in the printing process). The fact that the permanent echoes within 10 mi are masked is not of itself proof however that the masking echoes are of equal intensity. Signal limiting is introduced at an early stage in the receiver in order to cope with the tremendous range of received signals, and the true relative intensities can only be judged by reducing its gain. We find that most angel echoes on the East Hill display are removed by a gain reduction of 10 to 15 db, but permanent echoes are still very intense at this setting, requiring a further reduction of 30 to 60 db to remove them.

The intensity of the echo phenomena and their apparent spacing are thus somewhat misleading, but the latter can lead to a rough assessment of the numbers of birds required to give these displays. The obvious case to consider is the very dense display after sunset on 5th March, 1952 (Fig. 4 and para. 4) which has not been matched elsewhere in our records. The echo in Fig. 4 is very nearly continuous at 10 mi range. It will be assumed that it was in fact so, and that the angels were uniformly dense across the broad 60 mi front seen by the PPI. Since the angels on this occasion were moving at an average speed of 52 mph, the angels in an area 60 mi by 52 mi will pass in an hour. Taking the theoretical resolution given above we have that each angel occupies 300 m by 240 m of the display, which gives a figure of 7.7×10^4 angels per hour. The evidence of para. 8 suggests that one angel consists of from 5 to 30 birds, say 20. This gives a figure of 1.5×10^6 birds passing per hour on this 60 mi front, and we know that this very dense passage persisted for at least two hours.

In view of the assumptions which have been made it cannot be expected that this will be much more accurate than to the nearest order of magnitude, yet considered as an exceptional migration movement such numbers seem by no means impossible. As far as we are aware no assessment of the numbers of birds involved in migration movements has been made elsewhere (nor indeed have observers ever fully seen them), but we can make an indirect comparison with bird numbers. Fisher(15) has estimated that the total May land-bird breeding population of Britain is about 1.2×10^8. With young birds of the year this number would be roughly doubled. Most of these undertake migrations of shorter or greater length (many which were formerly classed as residents are now known to migrate regularly, e.g., from one part of Britain to another, and to be replaced by others), and the total numbers involved in movements of wintering birds, summer and passage migration may well be much greater. A passage of 3×10^6 birds does not seem impossible in relation to total populations of this magnitude, since all the evidence suggests that there are very few heavy migration movements in any one season, and the south-east of England may be a favoured area for these movements.

11. Discussion

The evidence which has been brought forward, especially of the directions and speeds of movement, strongly suggests that widespread displays of angels seen on centimetric radars in southern England are due to migration and weather movements of birds, and we can see no reason to invoke any other mechanism to explain them.

It would seem that PPI displays have not often been available as research tools in other countries, but Friend(14) has reported that the 10-cm PPI at the Cambridge Field Station, Massachusetts on occasions showed very large numbers of dot echoes, often when the sky was completely clear, and that "as many as perhaps 200,000 were sometimes noted within a 20 mi radius". This suggests that angels can be at least as dense in America as in England - indeed there are probably few countries in which airfield-control and other centimetric radars are not affected by them, since bird migration movements are world wide. Coastal radars are probably affected at least as much as inland radars, by directional migration and by coastal movements of seabirds and waders.

/There

There would seem to be little prospect of entirely eliminating angel effects from airfield-control radars. Responses from aircraft are normally of greater intensity, but gain reduction cannot be expected to commend itself to the aircraft controller, who may be responsible for several aircraft at one time, since continual gain adjustment would be necessary to convince oneself that nothing was being missed. Some alleviation can be expected from devices which suppress echoes from stationary and slow-moving targets electronically (MTI), but when flocks of fast-flying birds are travelling with a strong tailwind some difficulty seems inevitable.

To the ornithologist angels open a fascinating field of study, providing reliable evidence of a height and extent of bird migration which has been but dimly perceived or largely unsuspected.

References

1. Jones, R.F. 1952 Radar echoes from atmospheric inhomogeneities. Meteorological Research Papers, Air Ministry, London, No. 741.

2. Lack, D. and Varley, G.C. 1945 Detection of birds by radar. Nature, 156, 446.

3. Plank, V.G. 1956 A meteorological study of radar angels. Geophys. Res. Pap. No. 52, Air Force Cambridge Res. Centre, Bedford, Mass.

4. Witherby, H.F., Jourdain, F.C.R., Ticehurst, N.F. and Tucker, B.W. 1943 The handbook of British birds. Witherby, London.

5. Thomson, A.L. 1953 Visible migration of birds. Ibis, 95, 165.

6. Matthews, G.V.T. 1955 Bird navigation. Univ. Press, Cambridge.

7. Kramer, G. 1952 Experiments on bird orientation. Ibis, 94, 265.

8. Lack, D. 1957 The chaffinch migration in north Devon. Brit. Birds, 50, 10.

9. Lack, D. and Lack, E. 1949 Passerine migration through England. Brit. Birds, 42, 320.

10. Baldwin, M.W. 1948 Radar reflections from the lower atmosphere. Proc. I.R.E., 36, 363.

11. Meinertzhagen, R. 1955 The speed and altitude of bird flight. Ibis, 97, 81.

12. Hunt, J. 1953 The ascent of Everest. Hodder and Stoughton, London.

13. Swingle, D.M. 1952 Proc. Third Radar Weather Conf., McGill Univ., Montreal, F38.

14. Friend, A.W. 1948 Continuous tropospheric soundings by radar. Proc. I.R.E., 36, 501.

15. Fisher, J. 1951 Watching birds. Penguin, Harmondsworth, Middlesex.

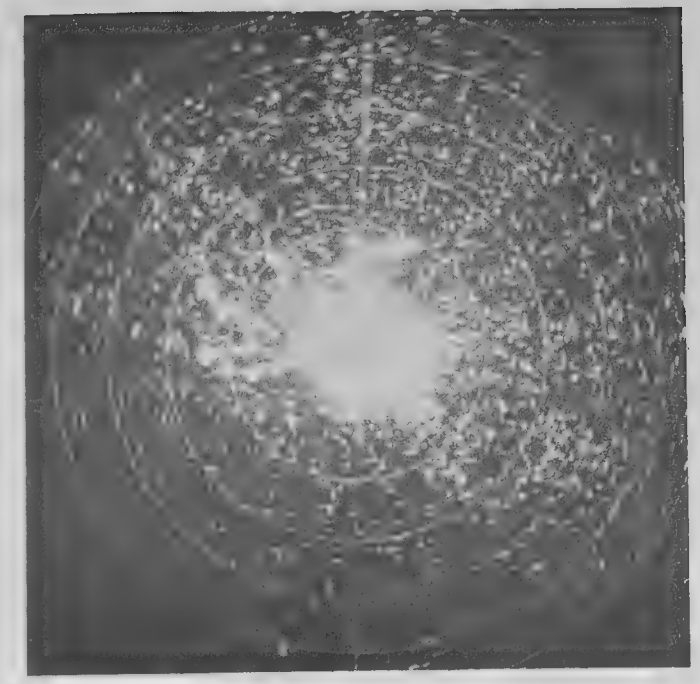

Fig. 1. Widespread display of angels on 10-cm PPI. 30 mi range, with range markers at 5 mi intervals. 1820 GMT, 13 March 1957. Many appear as strong as echoes from aircraft.

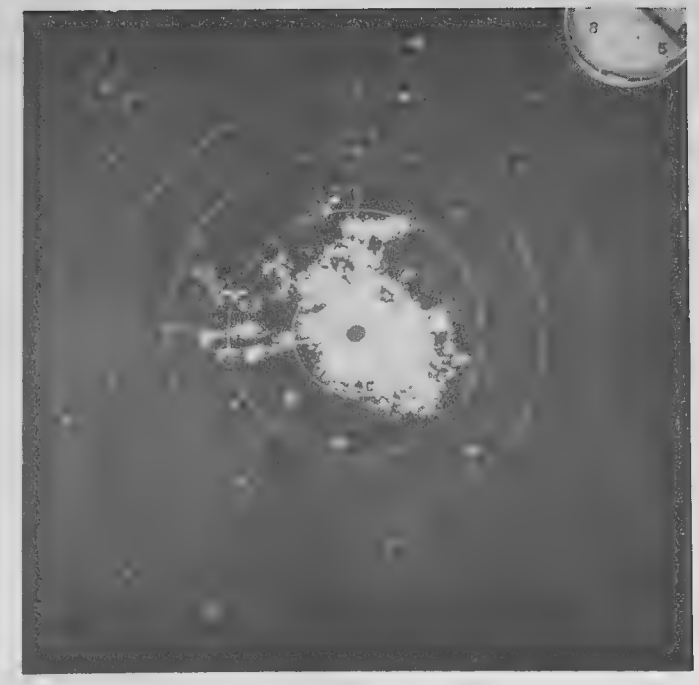

Fig. 2. Permanent echo display caused by rising ground, trees, buildings, etc. on the same scale for comparison. No angels are present. The pip echoes beyond 10 mi are from aircraft.

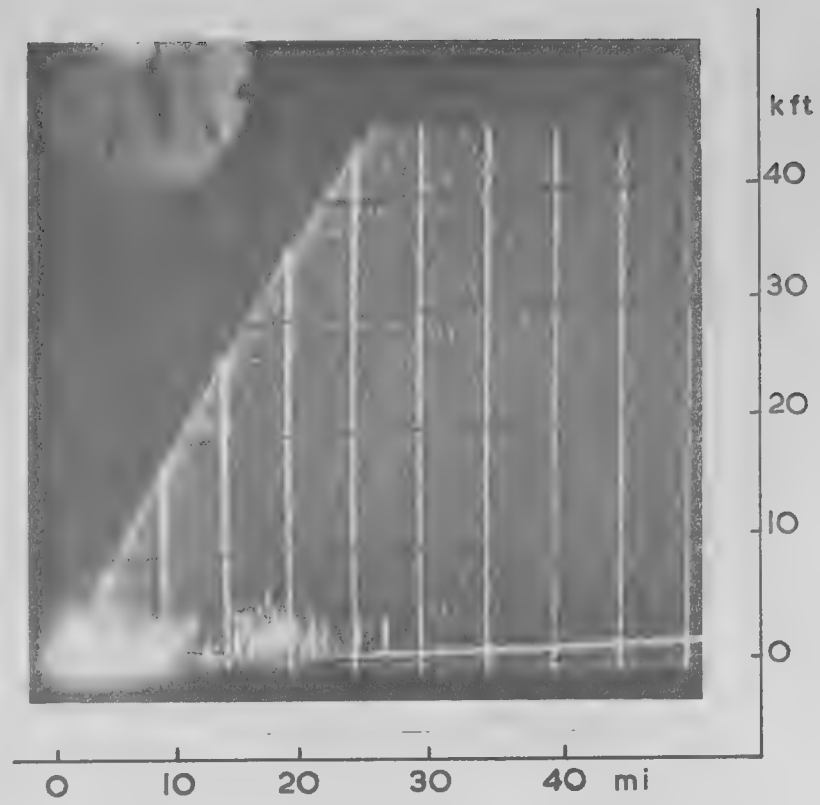

Fig. 5. Typical 10-cm range-height display of angels on occasion of fig. 1, taken at 1750 GMT, on 008°M. Angels are broadly spread in height up to 5,000 ft, with one strong angel at 6,000 ft. Intense echoes on the baseline in the first 10 mi are permanent echoes.

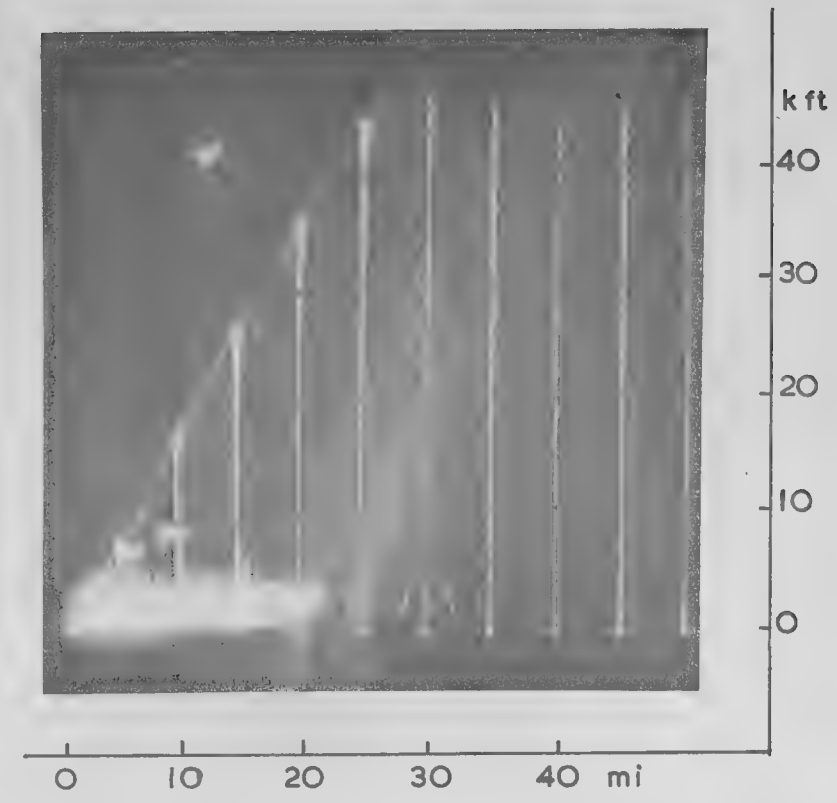

Fig. 6. Dense display of angels on occasion of fig. 3, taken at 1915 GMT on 002°M. Angels mainly concentrated at 2,500 ft, very frequent up to 5,000 ft, and scattered to 10,000 ft.

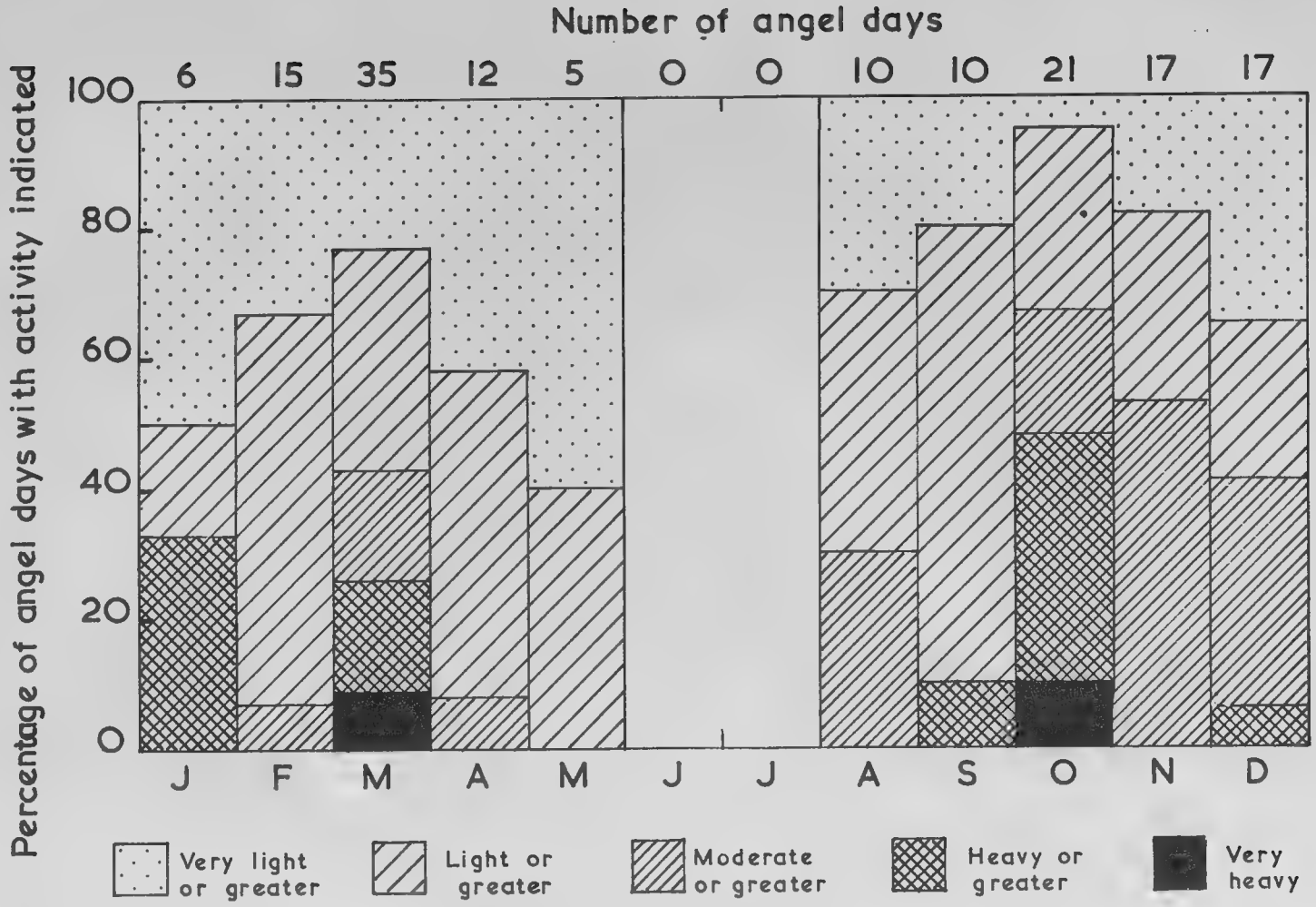

Fig. 7. Seasonal distribution of angel activity, with indication of degree of activity. All available records (148 occurrences) in the period 1952 - 57.

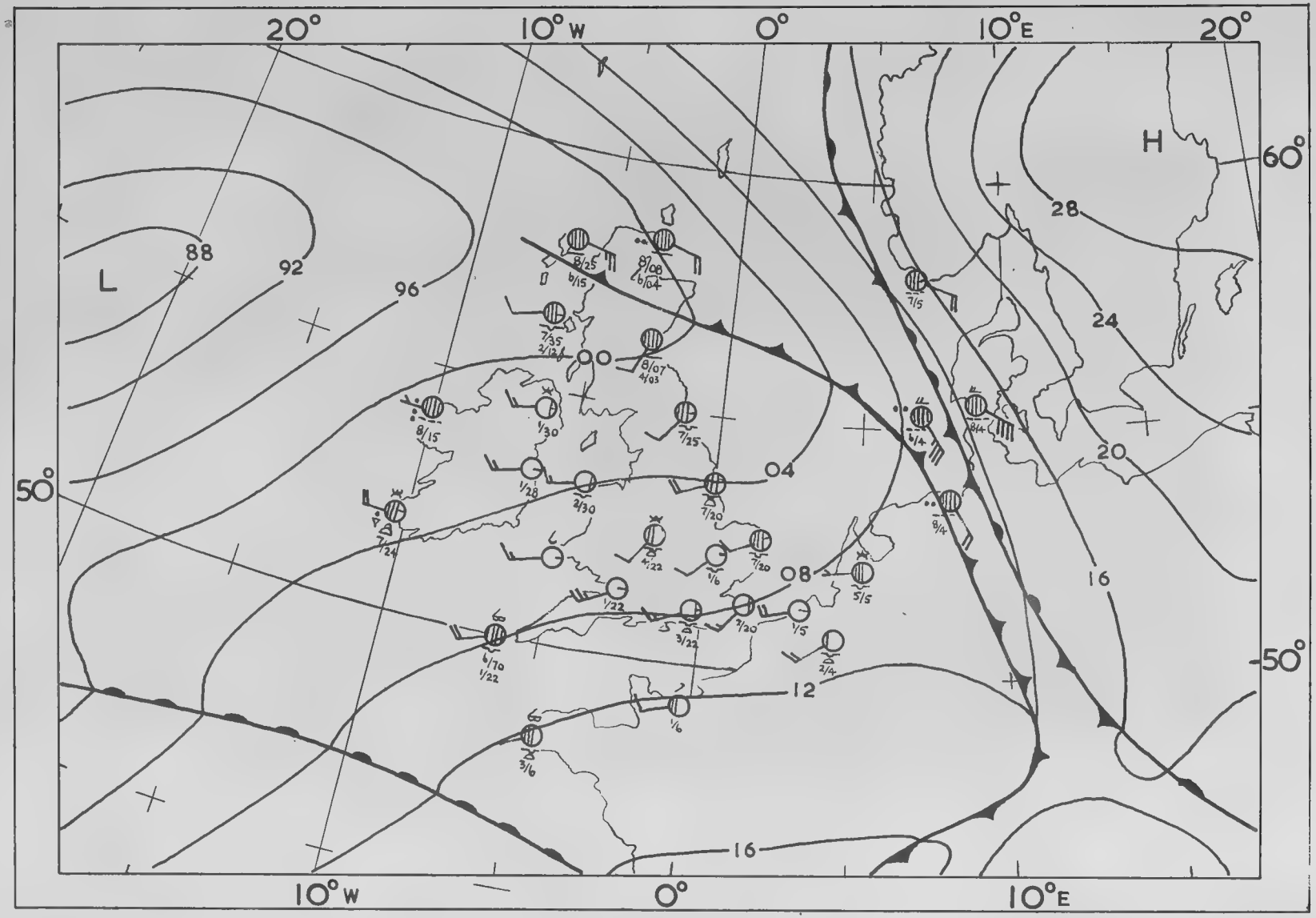

Fig.8. Weather situation associated with an exceptional display of angels, 1800 GMT, 5th March 1952.

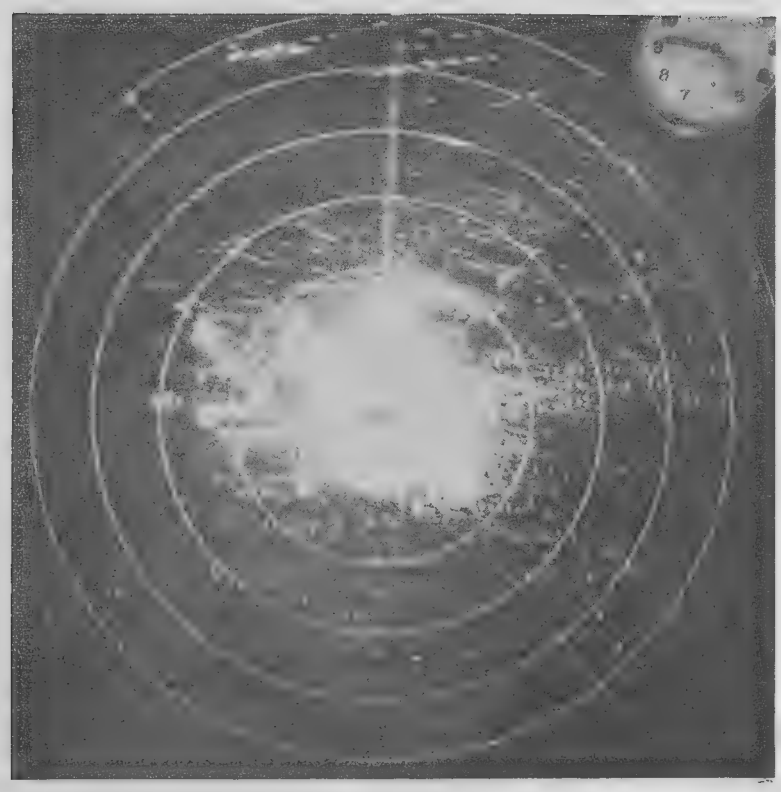

Fig. 9. Time-lapse photograph of six sweeps of the PPI at roughly minute intervals. Such records can give much information on the direction and speed of movement of angels. The fast-moving objects at the top of the photograph are aircraft.

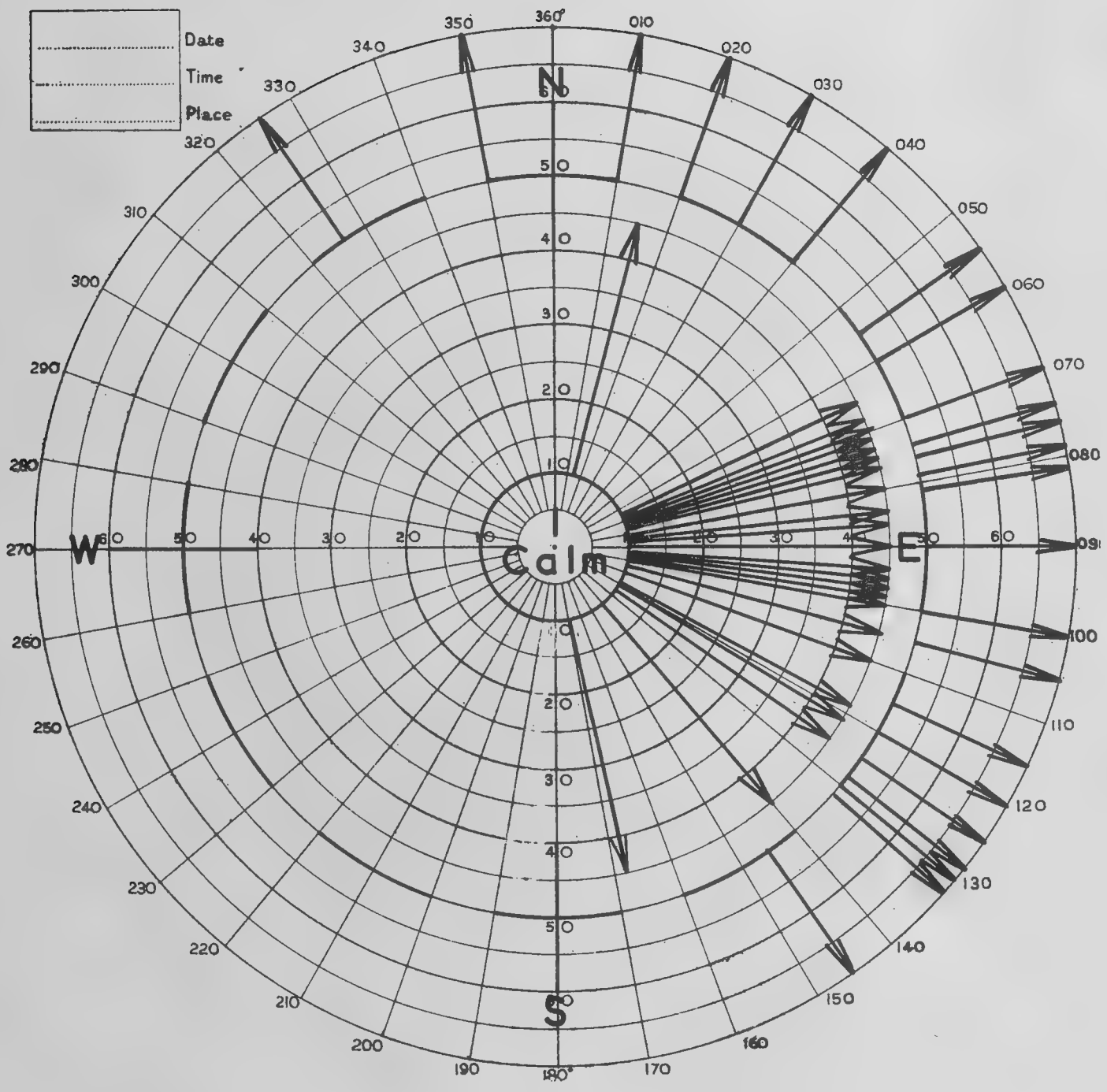

Fig. 10. Spring angel movements (February to April) in inner zone. All available East Hill records (24 days in period 1952 - 57). Wind directions in outer zone.

M.R.P. 1068

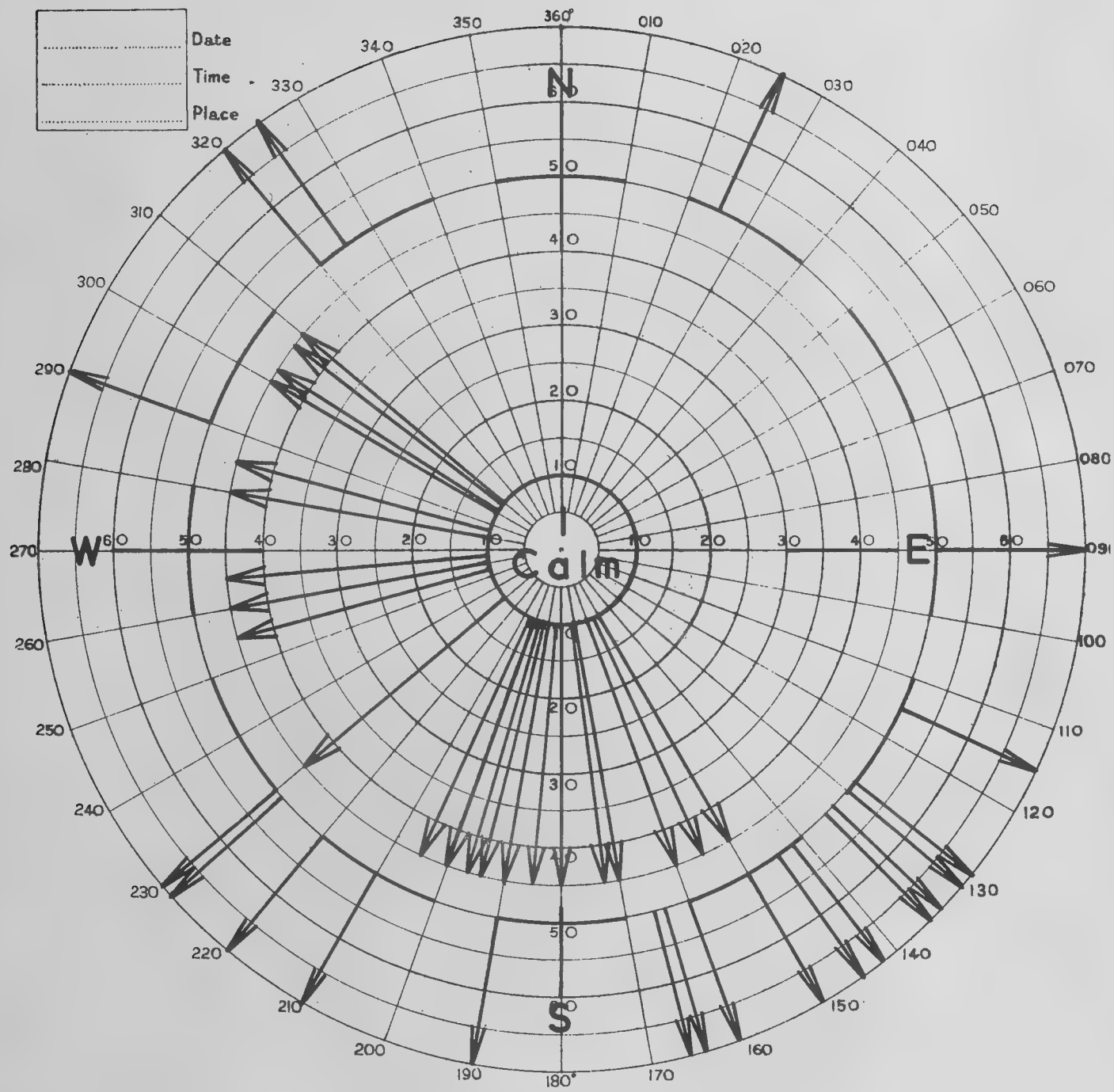

Fig. 11. Autumn angel movements (September to December) in inner zone. All available East Hill records (22 days in period 1952-56). Wind directions in outer zone.

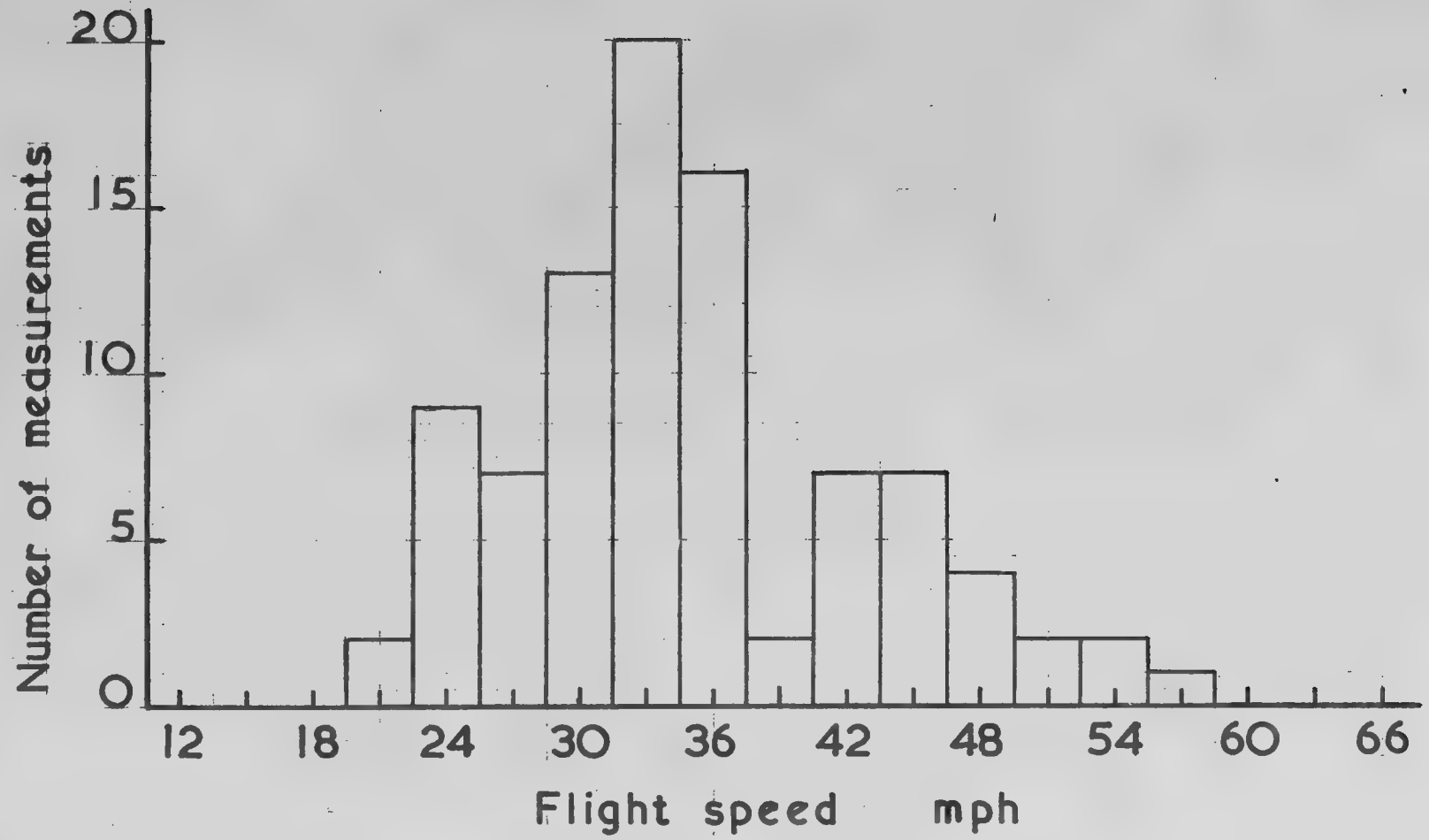

Fig. 12. Histogram of 92 measurements of flight speed of angels

5 MAY 1958

M.R.P. 1069
S.C.111/242
2nd September, 1957

Some airborne observations of condensation nucleus concentration

1. Variations in the vertical

by

G. J. Day

(Meteorological Office)

AIR MINISTRY

METEOROLOGICAL RESEARCH COMMITTEE

58-463

At the time of issue this paper has not been published. Any author desiring to quote this paper should refer to it as "A paper of the Meteorological Research Committee (London), M.R.P. No. 1069 by Mr. G.J. Day. A copy is available in the Library of the Meteorological Office."

M.R.P.1069
S.C.III/242
2nd September, 1957

AIR MINISTRY
METEOROLOGICAL RESEARCH COMMITTEE

Some airborne observations of condensation nucleus concentration

I. Variations in the vertical

by

G. J. Day (Meteorological Office)

1. Summary

Methods are discussed by which condensation nucleus concentration is customarily measured and attention drawn to the defects of these methods and to the present difficulty in investigating only that portion of the condensation nucleus population which participates in natural condensation processes.

An account is given of the Pollak photo-electric condensation nucleus counter and of its use in a Hastings aircraft of the Meteorological Research Flight in the investigation of the distribution in the vertical of condensation nuclei with radii greater than about 10^{-6} cm.

It was observed that over Southern England nucleus concentration attained a maximum value of 5000 cm^{-3} at 2000 ft with a regular decrease above to 500 cm^{-3} at 10000 ft.

Over a calm sea a maximum concentration of 1500 cm^{-3} was observed at 400 ft followed by a regular decrease to 100 cm^{-3} at 5000 ft. Over a moderately disturbed sea the maximum concentration increased to 3000 cm^{-3} at 600 ft, and over violently disturbed sea surfaces concentrations of 10000 cm^{-3} were observed up to heights of 2000 ft.

In general it was observed that the vertical stability of the air mass had a considerable influence on the local condensation nucleus population.

Proposals are made for further work and for the improvement of the equipment used.

2. Introduction

The concentration of condensation nuclei in the admosphere is a factor of importance in both theoretical and experimental cloud physics. Although extensive surveys have been made at ground level (1) and at mountain stations (2), there is very little information concerning the concentration in the free atmosphere. That which is available is limited to the balloon-ascents of Wigand (3) over Europe, and to the observation of sea-salt nuclei over the American continent (4) and over the Australian continent (5).

Attempts have been made by the Meteorological Research Flight to measure the concentration of condensation nuclei from an aircraft using a standard type of Aitken counter as used by e.g., Scrase (6). This instrument has several limitations; the chief of these is the small number of nuclei and the consequent necessity for several samples to be made in the establishment of a statistically reliable count. Each sample may require manipulation and

/observation

observation lasting about a minute and, as about twenty samples are usually required for each count, the observation is of the average condition over some tens of minutes. For some purposes such a rate of sampling is acceptable for ground level experiments, but in the case of experiments in aircraft it represents sampling on a scale of about fifty miles. Every atmospheric variable investigated so far has been notable for its extreme variability in space on a considerably smaller scale than this and there seems no reason to suppose that condensation nucleus concentration should be an exception. The coarse sampling obtained with an Aitken counter was, therefore, considered unacceptable and a more suitable instrument sought.

Consideration was given to recent variants of the basic Aitken counter, such as that of Pollak (7), but all suffered from the limitation noted above. Hence, it was decided to adopt the photo-electric condensation nucleus counter of Pollak (8) in which the sample volume is about a litre compared with about 10 cm^3 in the case of the Aitken counter and its variants.

A copy of the Pollak instrument was made in the workshops of the Meteorological Research Flight and calibrated in the laboratory of Senior Prof. L.W. Pollak at the Institute for Advanced Studies in Dublin. It was found to have a calibration identical with that of the original instrument within the working range of 10^2 to 5 x 10^5 nuclei cm^{-3} with a probable experimental error of $\pm 5\%$.

The instrument was installed in the Hastings aircraft of the Meteorological Research Flight and a preliminary series of observations made at different altitudes. These flights were principally over Southern England and are described in Part I of this report. Part II will discuss variations in the horizontal over the British Isles and Part III the variations at particular heights in the vicinity of Farnborough (Hants) during January, 1956.

Whilst the data so far obtained do not lead to a complete picture of the variations of concentration and the typical concentrations of condensation nuclei to be expected in all representative geographical and synoptic situations, it is considered that this is an appropriate stage to report on this work.

In all this work the question arises, what is counted by an instrument such as the photo-electric counter? The degree of supersaturation within the counter at the moment of operation is, perhaps, two or three hundred per cent compared with a maximum of, perhaps, 0.1% experienced during natural condensation processes. The counter samples all condensation nuclei having radii greater than 10^{-6}cm whereas natural condensation processes are probably concerned mainly with nuclei of radius greater than about 10^{-4}cm.

The view has been vigorously advanced by Dessens (9) and others that the selection of such a wide class of nuclei renders all observations with expansion-type instruments worthless for most purposes in the cloud physics context. As will be seen later in this report this view is at least open to question in the special circumstances of these flights. Further, it is suggested that, in the absence of more detailed and unassailable sources of information, the restricted information presented, in this report, is of value at the present time in providing an upper limit to the concentration of condensation nuclei available for natural condensation processes. Moreover, data with regard to source regions and distributions of nuclei in the vertical are of considerable interest in other branches of physical meteorology, e.g., air pollution, light scattering, radiative diffusion, etc. - in fact they are relevant to all work involving studies of aerosols.

3. The instrument

The instrument and its calibration have been discussed by Pollak (7). The Meteorological Research Flight version, though similar in essentials, differs considerably in constructional details from that described in (7), ease of maintenance and absolute rigidity under flight conditions being desired. An instrument very similar to that constructed at the Meteorological Research Flight was described by Pollak and O'Connor (10) recently.

/The

The instrument is mounted with its pump and filter units in the wardroom of a Hastings aircraft (Fig. 1). It is served by an air intake mounted about 3 m ahead of the propellers and about 15 cm away from the aircraft skin. A duct about 1 cm in diameter and 30 cm long connects the instrument to the intake.

Prior to an observation, air is allowed to flow through the instrument, under the ram pressure due to the aircraft motion, until about twenty volume changes have taken place. The instrument is then isolated and air is pumped through the filter unit into the fog chamber until a pressure of 1.22 x ambient pressure has been attained. The air in the fog chamber becomes saturated by evaporation from the moist, porous lining of the fog-chamber, and is then allowed to expand adiabatically to ambient pressure. The extinction coefficient of the fog thus formed is determined by comparison of the steady signals, before and after expansion, from a photo-cell mounted at one end of the chamber and illuminated by a parallel beam of light from an illuminator at the other end. Disturbing effects due to condensation on to the glass end plates of the fog-chamber are avoided by the use of electrically heated glasses.

The entire sequence of operations occupies about 1.5 min so that samples are conveniently taken every 2 min, i.e., every 5 mi. at the normal cruising speed of the Hastings aircraft. Proposals are made below by which it is thought that the sampling interval may be reduced to about 1.5 mi.

Calibration is achieved by comparing the instrument with a photographically recording, improved Aitken-type instrument, using air drawn from a large gas-holder, thereby ensuring the constancy of nucleus-concentration necessary for accurate measurements with the latter, absolute, instrument. The size-distribution of these nuclei, which are drawn from the heavily polluted air of the laboratory, probably differs from that of naturally occurring nuclei but work by Howell (11) suggests that this is not likely to affect the equilibrium value of fog-droplet size distribution and hence should not affect the calibration.

The accuracy quoted above is probably valid for comparisons between instruments of similar fog chamber design or for work with one instrument but the absolute accuracy is probably smaller. A defect of the instrument, which adversely affects its accuracy, is that the fog formed begins to disappear after a very short time - usually 2 to 3 sec. A method has been devised by Pollak (10) since this work, however, by which this defect may be overcome.

4. The investigations

An attempt was made to survey variations in condensation nucleus concentrations in the vertical and in the horizontal over the British Isles. Only variations in the vertical - which were studied mostly over Southern England - will be discussed here.

The flights fall into two main groups, which may be subdivided:-

A. Investigation of variations in the vertical over land

B. Investigation of variations in the vertical over:-

(i) Calm sea

(ii) Disturbed sea.

In these flights it was customary to make observations at nominally constant ground position and height. Over land, samples were taken at vertical intervals of 500 ft up to 10000 ft, and occasionally at irregular intervals thereafter to 20000 ft. Over the sea, samples were taken at 100 ft vertical intervals to 1000 ft, 200 ft intervals to 2000 ft, and occasionally at irregular intervals above this height.

/5.

5. The observations

A. Variations in the vertical over land

The ascents in this group total 29.

The observations are given in Table 1a which contains also the mean concentration at each height (all cases being considered), the maximum concentration at each height and a statement indicating the character of the air mass on each occasion. Where appropriate a further table, 1b, contains simultaneous observations of air temperature.

Considered individually, the ascents have little in common and are remarkable chiefly for their great variety. The work of Sagalyn and Faucher (12) suggests that some, at least, of this variation between apparently comparable cases may be due to a diurnal variation in the processes by which nuclei are dispersed. It would seem desirable that further flights, specifically concerned with this aspect, should be made.

Fig. 2a shows the variation of the mean concentration and of the maximum concentration with height. Generalisations are necessarily imprecise, but as far as can be judged from this series of observations, it appears that over Southern England:-

(a) Mean concentration of condensation nuclei decreased from between 7000 and 8000 nuclei cm^{-3} near the surface to about 1000 nuclei cm^{-3} at 10000 ft and 600 nuclei cm^{-3} at 20000 ft.

(b) On occasions the concentration reached 20000 nuclei cm^{-3} at heights up to 6000 ft but it was rare for the concentration to exceed 4000 nuclei cm^{-3} at heights above 10000 ft.

(c) The variation of concentration with height on individual occasions was by no means simple and appeared to be considerably influenced by the vertical stability of the air mass. Levels of increased vertical stability were usually accompanied by increases in nucleus concentration. On the macroscopic scale, increases in nucleus concentration were, in extreme cases, marked by haze layers.

The variation of both temperature and concentration in the vertical observed in certain typical flights is presented graphically in Fig. 2b.

(d) On rare occasions during this series of flights the concentration decreased regularly with height, usually from about a few thousand nuclei cm^{-3} near the ground to less than 100 nuclei cm^{-3} at 6000 ft. The ascent of 22.3.55 (Fig. 2b) was typical of such conditions. In general, variations with height of this form were observed on days of convective instability and, therefore, probably result from an efficient dispersal of nuclei from sources at ground level. The rarity of such cases in this series probably reflects the rarity of convective instability during the period of this investigation. An interesting occasion is that of 20.6.55 when several ascents were made at points around the centre of a small depression passing across the North Sea. One of these ascents, made over Holland, is illustrated in Fig. 2c and shows a marked change in variation of nucleus concentration with height at about 13000 ft. This may be identified with the penetration of the lifted warm sector of the occluded frontal depression and suggests that the different air masses were here characterised by nucleus concentrations differing by about a factor of four at medium altitudes.

B. Ascents over sea surfaces

These were made with two purposes in view:-

(i) To determine the nucleus concentration in relatively unpolluted air over the undisturbed sea and the variation of concentration with height.

(ii) To determine the effect of the production of sea salt nuclei by a disturbed sea surface on the nucleus concentration in the air above, and the variation of this effect with height. Flights were made over rapidly shoaling water, such as the Shingles Bank, or at places where tidal effects give rise to a locally disturbed sea surface, as in the vicinity of Portland Race.

Treating these two sections in turn:-

(i) Undisturbed sea. It was difficult to ensure that ascents were made over completely undisturbed water or in air unpolluted by land sources and the results are imprecise to this extent.

This group contains five sets of observations, two of which were made on the same flight. The results are given in Table 2a which also contains the mean concentration observed at each height and an indication of the vertical stability of the air mass. Fig. 3a illustrates the variation of the mean concentration with height and Fig. 3b represents the individual ascents.

The ascent of 6.4.55 made in the vicinity of the Scilly Isles and illustrated in Fig. 3b (iv) is typical of this group. The concentration of condensation nuclei rose from about 600 cm^{-3} at 100 ft to a maximum value of about 1400 cm^{-3} at 300 ft, above which there was an irregular decrease of concentration to a few hundreds per cm^3 at heights above 1000 ft. Stabilisation of the temperature lapse rate at 900 and 2000 ft was associated with maxima in the nucleus concentration variation with height.

In this series of flights the greatest concentration observed was about 3600 nuclei cm^{-3} at about 600 ft in the vicinity of the Scilly Isles, (Fig. 3b (iii)).

(ii) Disturbed sea. a. As a consequence of the synoptic conditions prevailing when an aircraft was available for this work, the data are weighted towards moderate wind speeds.

Five ascents were made and the observations are recorded in Table 2b, which also contains the mean concentration observed at each height and an indication of the vertical stability of the air on each occasion. In obtaining mean concentrations the exceptional case of 6.10.55 has been omitted and is dealt with separately in 5.B.(ii).b below.

The ascent of 11.11.55 is typical of this series and is illustrated in Fig. 3c (iii). Nucleus concentrations of about 1900 cm^{-3} were observed at about 100 ft and a maximum concentration of about 2900 cm^{-3} at 200 ft above which height there was a more or less regular decrease to slightly more than 1000 cm^{-3} above 1000 ft. The maximum concentration was observed in a layer of increased stability and similar increases in or below levels of increased stability were observed at 1200 and 1600 ft.

b. The ascent of 6.10.55 illustrated in Fig. 3c (v) was made over the Goodwin Sands on an occasion when the wind speed was between 25 and 30 kt and sea spray was observed to reach about 500 ft. Although observations were made downwind of Greater London it is not thought that there can have been any significant pollution since visibilities of about 10 mi were reported.

On this occasion condensation nucleus concentrations of more than 10000 cm^{-3} were observed in the layer between the surface and 2500 ft, a maximum concentration of about 12500 cm^{-3} being observed at about 1400 ft. At 4000 ft the concentration remained greater than 5000 nuclei cm^{-3}.

Once again maxima in the variation of concentration with height were found at, or immediately below, levels of increased stability, e.g., at 200, 600, 800 and 1400 ft.

/In

In this case there can be no doubt that there was production of a considerable number of nuclei at the sea surface, which was violently disturbed.

Considering the results from the nine flights of this group as a whole, it is possible to reach the following tentative conclusions:-

1. Concentration of nuclei over the sea, remote from land contamination, at levels where the bases of low clouds are usually found - say 2000 ft - is normally a few hundreds per cm^3.

2. Above seas which are moderately but not violently disturbed - say for wind speeds less than 15 to 20 kt in the absence of marked tidal or shoal water effects - concentrations appear to increase from between 1000 and 2000 nuclei cm^{-3} just above the surface to a maximum of between 2000 and 3000 cm^{-3} at about 600 ft and thereafter decrease to a few hundreds per cm^3 at about 3000 ft.

3. Comparison of Tables 2a and 2b suggests that there is a detectable production of condensation nuclei by moderately disturbed sea surfaces.

4. The unusually large concentrations of nuclei observed over a violently disturbed sea surface, in excess of 10000 cm^{-3}, must be ascribed to sea spray processes.

5. As in the case of ascents over the land, levels of increased vertical stability are usually marked by increases in condensation nucleus concentration.

These conclusions are based on a small, unevenly weighted sample and should not be regarded as firm. More ascents will be necessary to establish them securely. In particular it seems desirable that ascents should be made over the disturbed seas associated with vigorously developing Atlantic depressions at some distance from the land and in a wide range of wind speeds. It should then be possible to determine a critical wind speed for effective nucleus production by the sea spray mechanism.

6. Discussion

Squires (13) and Durbin (14) have reported droplet concentrations in cumulus clouds in maritime air of up to 300 cm^{-3}. It would appear, then, from the observations reported here that over the sea, and probably over the land away from pollution, the concentration of nuclei is comparable with that of cloud droplets, i.e., the indication is that probably a third of the nuclei sampled are operative in important meteorological processes. The validity of Dessens' (9) criticism, referred to in Section 2 above, then, may be questioned in these special circumstances. Indeed, over the sea at least, the inability of present droplet sampling systems to capture droplets of diameter less than about 3 μ may suggest that virtually all the nuclei sampled in this series of flights are active in natural condensation processes.

An outstanding feature of the concentrations observed up to medium altitudes was the inhomogeneity of the atmosphere, with respect to condensation nucleus concentration, in both time and space.

The results given above may be compared with those of previous workers. The only comparable European observations are those of Wigand (3) who made 14 balloon ascents in anticyclonic conditions over an industrial region of Central Europe. The mean concentrations determined by Wigand are plotted in Fig. 2a and will be seen to be consistent with the observations reported above. Observations by Amelung and Landsberg (18) during motor trips up the slopes of the Taunus Mountain in Germany show increases in concentration with increasing vertical stability of the atmosphere in a similar fashion to the aircraft ascents above. There appear to be no published ascents over sea surfaces adjacent to Europe.

/7.

7. Suggestions for further work

It is suggested:-

a. That further attention be paid to the conditions over disturbed sea surfaces under a representative range of wind speeds. In particular it is suggested that ascents should be made to greater heights, say 10000 ft, and in regions remote from possible polluting sources. The vicinity of vigorously developing Atlantic depressions would appear suitable.

b. That future work should be accompanied by direct sampling of sea salt nuclei, sampling by the Liesegang Ring (16) system for chemical identification of radicals, and by some attempt at size discrimination of the condensation nuclei sampled, as for instance, by the method of Rich (17).

c. That modifications be made to the equipment in use, as follows:-

(i) the manually-operated valves should be replaced by automatically controlled solenoid-operated valves thus permitting an economy in crew.

(ii) an attempt be made to humidify the sampled air during the passage to the fog chamber thus increasing the possible speed of operation.

An instrument embodying some of these proposals is in course of development for ground use and will be reported on at a later date.

/References

References

1.	Pollak, L.W. and Murphy, T.	1953	Archiv fur Meteorologie, Geophysik und Bioklimatologie, Serie A, p.10.
2.	Dessens, H	1947	La Meteor, pp.321-327, 328-340.
3.	Wigand	1919	Ann dor Physik, 59, pp.689-742.
4.	Reitan, Clayton, H. and Braham, R.R.	1954	Journal of Meteorology, Vol. 11, No. 6, p.503.
5.	Twomey	1954	Journal of Meteorology, Vol.11, No.4, pp.334-338.
6.	Scrase	1935	Geophysical Memoirs, No.64.
7.	Pollak, L.W.	1952	Geofisica Pura E Applicata, 22, pp.1-9.
8.	Nolan, P.J. and Pollak, L.W.	1946	Proc. Roy. Irish Academy, Dublin, 51, A2, pp.9-31.
9.	Dessens, H.	1956	Bulletin de L'Observatoire du Puy de Dome.
10.	Pollak, L.W. and O'Connor, T.C.	1955	Geofisica Pura E Applicata, 32, pp.139-146.
11.	Howell, W.E.	1949	Journal of Meteorology, Vol.6, No.2, April.
12.	Sagalyn, R. and Faucher, G.	1956	Journ. Roy. Met. Soc., 82, pp.428-445.
13.	Squires, P.	1956	Tellus, Vol.8, No.4, Nov.
14.	Durbin, W.G.	1956	Meteorological Research Papers, Air Ministry, London, No.991.
15.	Pearcey, T. and Hill, G.W.	1957	Journ. Roy. Met. Soc., Vol.83, No.355, p.77.
16.	Vittori, O.A. and Fedele, D.	1953	Rivista Met. Aero., 13, N4, 14.
17.	Rich, T.A.	1955	Geofisica Pura E Applicata, 31, pp.60-65.
18.	Amelung, W. and Landsberg, H.	1934	Meteor Z. Biokl. Beibl. 1, 49-53.

Table 1A Variation of concentration with height over land (Southern England)

Date	Concentration of condensation nuclei (Radii > 10^{-6} cm) - Nuclei cm^{-3}																				
Height (ft)	500	1000	1500	2000	2500	3000	3500	4000	4500	5000	5500	6000	6500	7000	7500	8000	8500	9000	9500	10000	10500	11000
21.3.55			13100	18200	17200	10700	7340	7080	9400	16300	15300	8050	580		250	100						
			17300	15300	17700	11400	10100	9760	12900	14000	18700	10400	1380									
a.m.				12900	16700	10100	8600	7560	15800	17200	10900											
25.3.55	6970	760	250		370	370	150	140	140	180	290	370										
p.m.										520			1070			100						
a.m.																						
28.3.55	4390	2380	2850	3490	1100	780	4700	5040	1070	120												
p.m.	8930	2690	1420	2570	2860	850		1300	700	1070	860	640	100	100	100							
22.3.55		3220		1080				3400		370			250						1110		840	270
	2680			2470		1820		2060		840		120		1330				280				100
		780			100		550		360	210	360					100				280		100
12.4.55		6800	6700	3830	6660	4740	1850	2420	100	100												
13.4.55			4400	6700	4700	1820	2040	2450														
14.6.55						260		440	880	2100	690	660	260	2150		140	120					
15.6.55				10300		1730		1480		160		540		480		650		360		1350		360
20.6.55			6000				6600					4320						2110			970	
			2340			970	640				490			540		760		780			540	
				4250	3700						880				850				660			
		3220			1930				2290		750		820			510	1930			650		
23.6.55		3430		690		100		810		790		220		430		410		5160				280
27.6.55			540	12800	8600																	
		11200	4060	5900	8000	1000	2230	890	1250	900	900											
a.m.		5120	6260					1950				800										
13.7.55		11300		15000		12900		7450		2470		2730		680		580		390		740		580
p.m.				2230	2780		1870	1770			470			800		200						
15.7.55		1040		1300		640		160		2100		110		100		100		100		100		400
20.7.55		16000		13300		5400		1840		1380		390		390		730		5400		13300		11000
25.7.55	12800	25000			16400	13600												210		100		
		24000		12700		12100		7080		5720		520		300		540		390		1840		1290
26.7.55		7700		5100		1900		800		300		300		360		1330		1080		1060		1290
4.8.55		9800		7560		9960		9200		3430		3290		1950		1860		970		500		390
9.8.55										1600						1720						
10.8.55		3800		2800		1560		1100		800		290		260		330		340		510		540
Mean) concen-	7150	7680	5440	7300	7260	4760	3590	3310	4070	3050	4220	1990	640	710	400	610	1030	1350	890	1860	710	1360
Max.) tration	12800	25000	17300	18200	17700	13600	10100	9760	15800	17200	18700	10400	1380	2150	850	1860	1930	5160	1110	13300	970	11000
Min.)	2680	760	250	690	100	100	150	140	140	< 100	290	110	250	< 100	< 100	< 100	< 100	< 100	660	< 100	540	< 100
No. of cases	5	18	12	22	15	22	13	23	11	23	12	17	7	14	3	17	2	13	2	11	3	12

G.24359(a)/AP/9/57/55

Contd.

Table 1A Variation of concentration with height over land (Southern England)

Date	Concentration of condensation nuclei (Radii > 10^{-6} cm) – Nuclei cm^{-3}																	
Height (ft)	11500	12000	12500	13000	13500	14000	14500	15000	15500	16000	16500	17000	17500	18000	18500	19000	20000	Vertical stability of air, etc.
21.3.55																		DALR to 5000 ft. Inversion above.
a.m.																		
23.3.55																		Inversion to 2000 ft. SALR to 10000 ft.
p.m.																		
a.m.																		DALR to 3500 ft. SALR above, no marked inversion. Inversion to 5500 ft, SALR to 10000 ft, inversion to 12000 ft.
28.3.55																		
p.m.																		
22.3.55		1090		100														
		100																
		100																
12.4.55																		DALR to 4000 ft, inversion of 7°F from 4000 to 5000 ft, DALR to 5000 ft, inversion above DALR.
13.4.55																		
14.6.55																		
15.6.55		1410		690		900		550		340		610		390		650	610	DALR to inversion at 4000 ft SALR with inversions at 6000 and 10000 ft.
20.6.55		1090										1480				1010	790	Stable to isothermal between
		1090	660	730	750	670		620		370	1140		1030	1300		860	550	5500 and 7500 ft. Further
	530			660														stable layer between 10000 and
	680			610		670		620										11000 ft.
23.6.55		500		540		610		210		610		1330		220		780	550	Inversion to 2000 ft, DALR above with inversions at 7500, 14000 and 16000 ft.
27.6.55																		DALR to inversion at 8500 ft. DALR above. Small stable layer at 7000 ft.
a.m.																		
13.7.55		470		680		470		800		680		390		350		530	920	DALR to an inversion at 4000 ft, DALR from 6000 ft with small inversion at 12000 ft.
p.m.																		
15.7.55		100																Stable to inversion at 11500 ft.
20.7.55		3050		1840		3430		2690										DALR, small inversion from 10500 to 11000 ft.

Contd.

Table 1A Variation of concentration with height over land (Southern England)

Date	Concentration of condensation nuclei (Radii > 10^{-6} cm) - Nuclei cm^{-3}																
Height (ft)	11500	12000	12500	13000	13500	14000	14500	15000	15500	16000	16500	17000	17500	18000	18500	19000	20000	Vertical stability of air, etc.
25.7.55	200	3170		1480		640		300		390		1380		1110		610	870	DALR to strong inversion at 6000 ft, isothermal from 8000 ft to 9000 ft.
26.7.55		1960		1700		2230		1970		1010		1960		730		840	730	DALR to inversion at 2000 ft. Stable above 4000 ft.
4.8.55		500		390		800		190		330		460		820		460	580	Stable to inversion at 8000 ft. SALR above 8500 ft.
9.8.55		420										350						Barely stable.
10.8.55																		Isothermal from 10000 to 10500 ft.
	470	1070		860		1160		880		530		990		700		790	700	Mean concentration
	680	3770		1840		3430		2650		1010		1960		1300		1010	920	Maximum concentration
	1200	< 100	660	< 100	750	470		210		330	1140	350	1030	220		460	550	Minimum concentration
	3	14	1	11	1	9		9		7	1	8	1	7		8	8	Number of occasions

Table 1B Air temperatures corresponding to data of Table 1A

Date	Air temperatures, degrees Fahrenheit																			
	500	1000	1500	2000	2500	3000	3500	4000	4500	5000	5500	6000	6500	7000	7500	8000	8500	9000	9500	10000	10500
21.3.55 a.m.			40.1	37.1	35.0	33.6	31.7	29.4	27.1	24.2	21.7	19.9	21.0		17.8	14.3					
25.3.55 p.m.		44.6	46.1	46.6 59.7	48.0 58.1	51.8 57.0	52.7 54.7	50.8 52.2	49.8 49.6	48.1 48.5	46.7 46.3	44.4 45.4	43.5	40.7	38.5	38.4	37.2	35.2			
28.3.55 a.m.	35.0	36.3	33.3	31.6	29.1	27.8	24.3	21.8	22.1	22.2											
22.3.55 p.m.		37.5 37.8	36.0	33.0 32.4	30.8	28.0 30.7		23.9 31.7	23.6	17.9 31.5	18.4	17.6 26.3	17.0	16.7 25.9	15.8			20.2		16.7	15.3
12.4.55		53.3	50.7	49.1	46.3	41.9	41.5	37.6	46.6	45.6											
13.4.55			54.2	51.5	48.3	46.0	43.7	41.7													
14.6.55			53.0			57.0		55.2	54.1	52.0	50.7	48.5	47.9	44.7		41.5	41.7				
15.6.55				58.0		54.0		48.0		50.0		45.1		44.8		43.2		39.5		36.0	
20.6.55					47.0					43.0	43.0	43.0	42.0		36.0						26.0
23.6.55		55.0		57.7		57.0		53.0		50.0		47.0		40.2		42.2		41.0		36.0	
27.6.55 a.m.					53.0						39.0		37.0					29.0	31.0		
13.7.55 p.m.		71.0	71.0	66.0	69.1	60.9 60.6	59.5	57.0		55.0 54.4		54.0	49.0	47.0		43.9 44.9		39.0		34.6	
15.7.55		72.0		66.0		62.0		57.5		54.9		52.0		48.1		46.1		41.5		48.9	
20.7.55		64.1		56.8		52.0		47.0		41.1		46.6		46.9		43.6		40.0		35.0	
26.7.55		55.0		49.5		45.9		50.0		46.9		44.1		40.0		34.4		32.1		30.2	
25.7.55	58.0		58.0	59.0	60.0	61.0	60.0	56.0	56.0	56.0	55.0		51.0		48.0					38.0	
4.8.55		61.4		58.0		53.1		48.2		43.9		39.0		35.9		34.2		38.6		35.4	
9.8.55										45.5											
10.8.55				56.0				48.0					38.0		35.0					23.0	

Contd.

Table 1B Air temperatures corresponding to data of Table 1A

Date	Air temperature, degrees Fahrenheit																	
	11000	11500	12000	12500	13000	13500	14000	14500	15500	16000	16500	17000	17500	18000	18500	19000	19500	20000	Height (ft)
21.3.55																			A
a.m.																			
25.3.55																			A
p.m.																			
a.m. 28.3.55																			A.
p.m.																			
22.3.55			9.9		6.6														A
12.4.55																			A.
13.4.55																			A
14.6.55																			A.
15.6.55	36.0		33.5		28.8		26.5			17.8		15.0		11.5		9.0			A
20.6.55				17.0						+1.0		-9.0			-18.0				R.S.
23.6.55	33.0		30.5		25.5		24.0		20.2	17.7		17.0		13.2		9.8		5.1	A
27.6.55						14.0		6.0				-11.0		-18.0	-20.0				R.S.
a.m.																			
13.7.55	31.1		27.5		26.0		22.0		19.0	14.1		11.4		8.0		2.8		-0.6	A
p.m.																			A
15.7.55	34.2		35.1																A
20.7.55	31.0		29.0		28.1		25.0		22.9										A
26.7.55	26.2		23.9		21 1		17.3		13.0	10.0		6.5		2.9		-2.0		-6.6	A
25.7.55				23.0	22.0	20.0				6.8		-3 0	-4.0						R.S.
4.8.55	33.0		31.0		26.9		25.0		21.6	18.1		13.7		9.1		6.9		3.0	A
9.8.55									20.6			9.0		5.5			-0.1	-2.0	A
10.8.55	23.0		19.0	14.0			6.0		-3.0			-13.0						-40.0	R.S.

A. = Simultaneous aircraft observation

R.S. = Most appropriate radio-sonde observation

Table 2A Variation of concentration with height over calm sea

Date	Concentration of condensation nuclei - Nuclei cm^{-3}																								
	100	200	300	400	500	600	700	800	900	1000	1200	1400	1600	1800	2000	2500	3000	3500	4000	4500	5000	5500	6000	6500	7000
28.3.55	790	850	1240	790	270	1240	1510		1210		1420	1620	1720	1540											
26.7.55	18700	19400	17500	18200	38000	2780	4020	7780	7450	7450	3070	4400	10300	16300	2470										
6.4.55	680		3580		940		400		210		220	120			150	180	100	830	250						
6.4.55	580		1190		810		990		270	120		280			330	150	150								
16.5.55	1200																	100		100	100		100	120	500
Mean concentration	810	850	2000	790	670	1240	960		560	120	820	670	1720	1540	240	165	125	470	250	100	< 100		< 100	120	500
Maximum concentration	1200	850	3580	790	940	1240	1510		1210	120	1420	1620	1720	1540	330	180	150	830	250	100	< 100		< 100	120	500
Number of cases	4	1	3	1	3	1	3		3	1	2	3	1	1	2	2	2	2	1	1	1		1	1	1

Contd.

Table 2A Variation of concentration with height over calm sea

Date	Remarks	Vertical stability, etc.
28.3.55	Shambles L.V. to Shingles L.V.	Stable lapse rate
26.7.55	Off Brighton, heavy pollution	
6.4.55	Off Scilly Isles	)DALR to 1000 ft. isothermal to)1200 ft. DLAR above
6.4.55	Off Scilly Isles	)
16.5.55	East of Tiree	Stable to inversions at 3000 and 4500 ft. DALR above to inversion at 6000 ft
		Mean concentration at height, excluding 26.7.55
		Maximum concentration at height, excluding 26.7.55
		Number of cases

Table 2B Variation of concentration over disturbed sea

Date	Concentration of condensation nuclei - Nuclei cm^{-3}																						
	100	200	300	400	500	600	700	800	900	1000	1200	1400	1600	1800	2000	2500	3000	3500	4000	4500	5000	5500	6000
25.3.55				2090	5910	7450	1270	6810	710	1050	910	540	720	370	460	290	280	370	120		140		
28.3.55	1130	860		940	820	1020	2070	1410		1950	1300	2490	1140	1380									
19.7.55	1550	1460	1980	1210	1550	1450	1760	1170	990	1050	1320	950			1050	1380							
11.11.55	1890	2260		2250		1670		1460		1200	1440	1050	1290	1130									
6.10.55	10450	12600	10400	9860	10100	11700	10400	11700	11500	10800		12700	12600	10900	11100	10200	9090	5960	5960				
Mean concentration	1530	1530	1980	1620	2760	2890	1680	2710	850	1310	1240	1160	1050	1050	760	840	280	370	120		140		
Maximum concentration	1890	2260	1980	2250	5910	7450	2070	6810	990	1950	1440	2090	1290	1380	1050	1380	280	370	120		140		
Number of cases	3	3	1	4	3	4	3	4	2	4	3	4	3	3	2	2	1	1	2		1		

Contd.

Table 2B Variation of concentration over disturbed sea

Date	Remarks	Vertical stability, etc.
25.3.55	Bournemouth to Needles, over Shingles Bank	Complex inversion to 1200 ft. Further inversions at 2500 and 3500 ft
28.3.55	Shambles L.V. to Portland Point	DALR above
19.7.55	Goodwin Sands, drying, sea moderate	Isothermals around 550 and 750 ft, stable lapse elsewhere
11.11.55	Portland Race	Inversion to 200 ft, DALR with stable layers elsewhere
6.10.55	Goodwin Sands, spray to 500 ft	Inversion to 200 ft and around 900 ft. Isothermal between 1600 and 2000 ft, DALR elsewhere
		Mean concentration at height, excluding 6.10.55
		Maximum concentration at height, excluding 6.10.55
		Number of cases

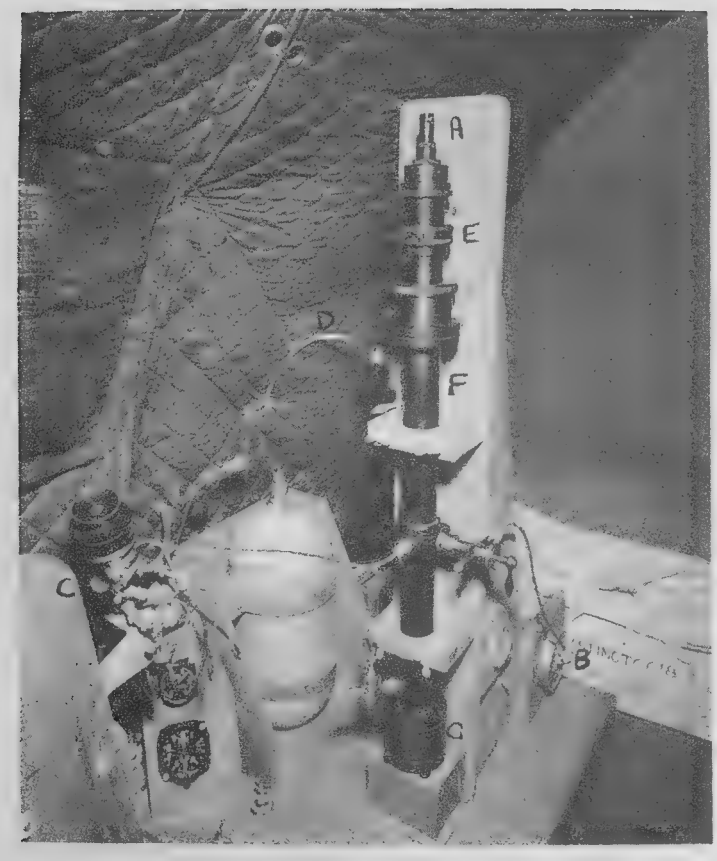

FIG. 1. PHOTO-ELECTRIC CONDENSATION NUCLEUS COUNTER MOUNTED IN WARD-ROOM OF HASTINGS AIRCRAFT

Nº MET. RES. FLT.
DR.
TR. O.W.H.
CH.
APP.

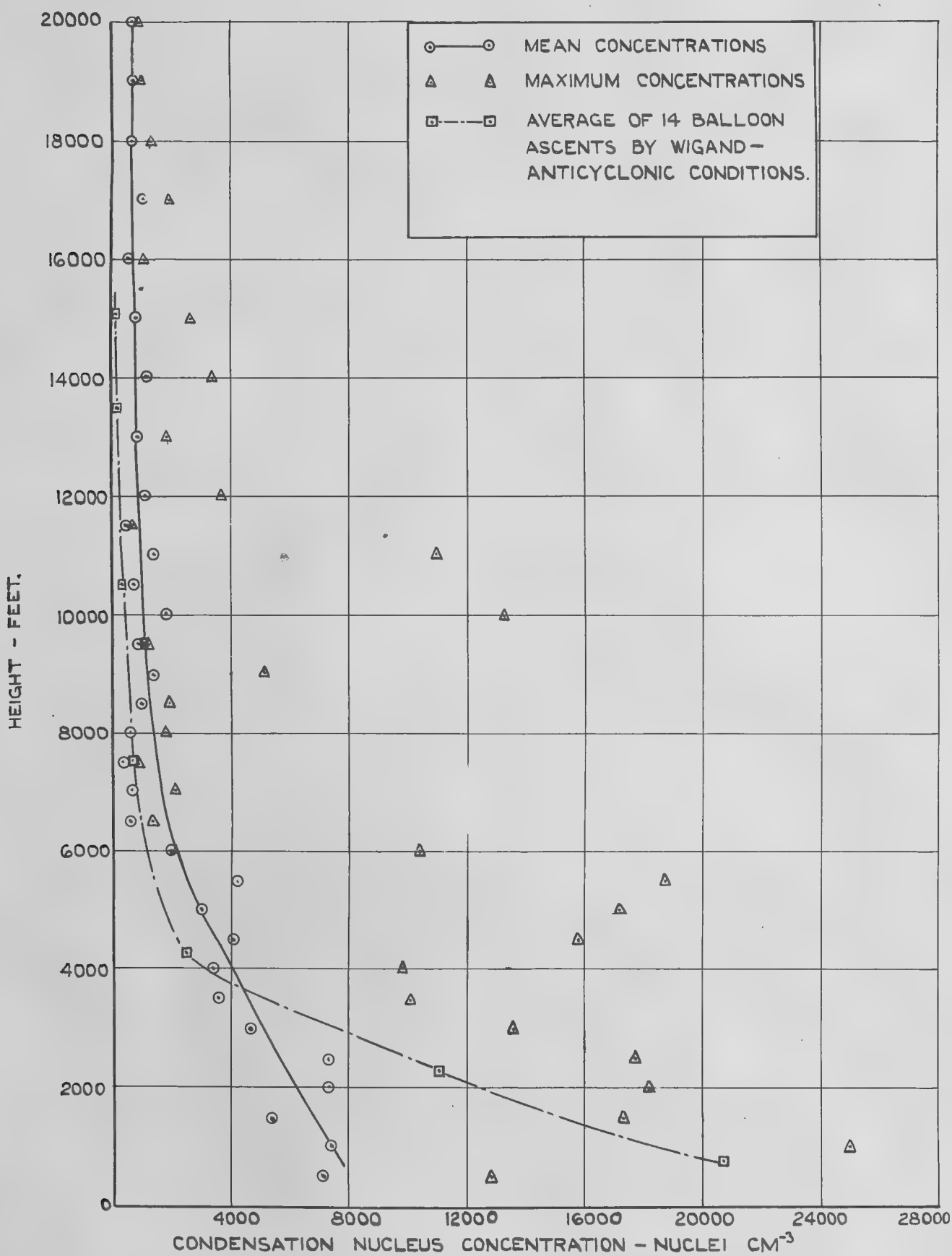

FIG. 2 a. VARIATION OF CONDENSATION NUCLEUS CONCENTRATION WITH HEIGHT OVER LAND.

Nº MET. RES. FLT.
DR.
TR. O.N.H.
CH.
APP.

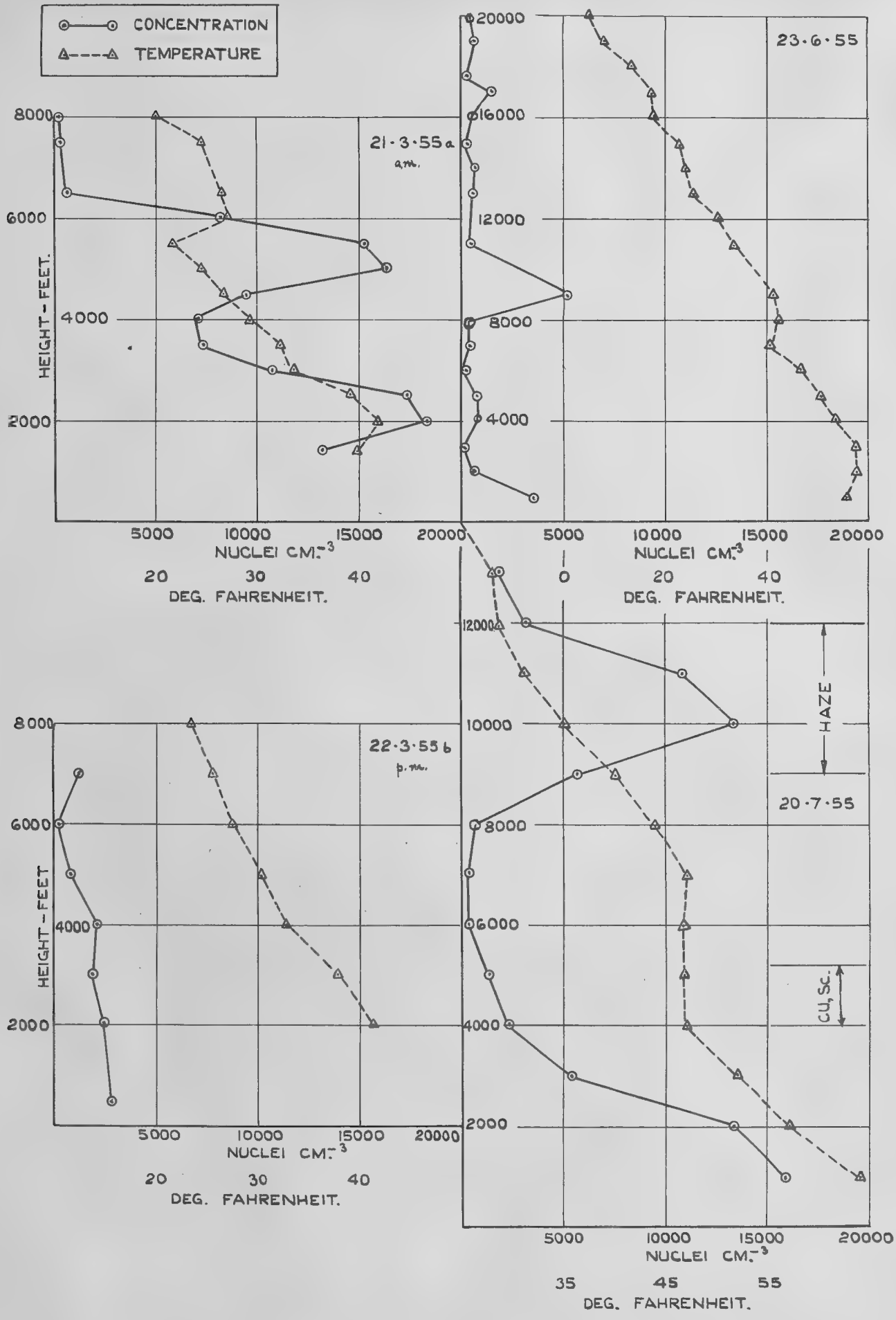

FIG. 2 b. INDIVIDUAL EXAMPLES OF VARIATION OF CONDENSATION NUCLEUS CONCENTRATION WITH HEIGHT.

No MET. RES. FLT.
DR.
TR. D.W.H.
CH.
APP.

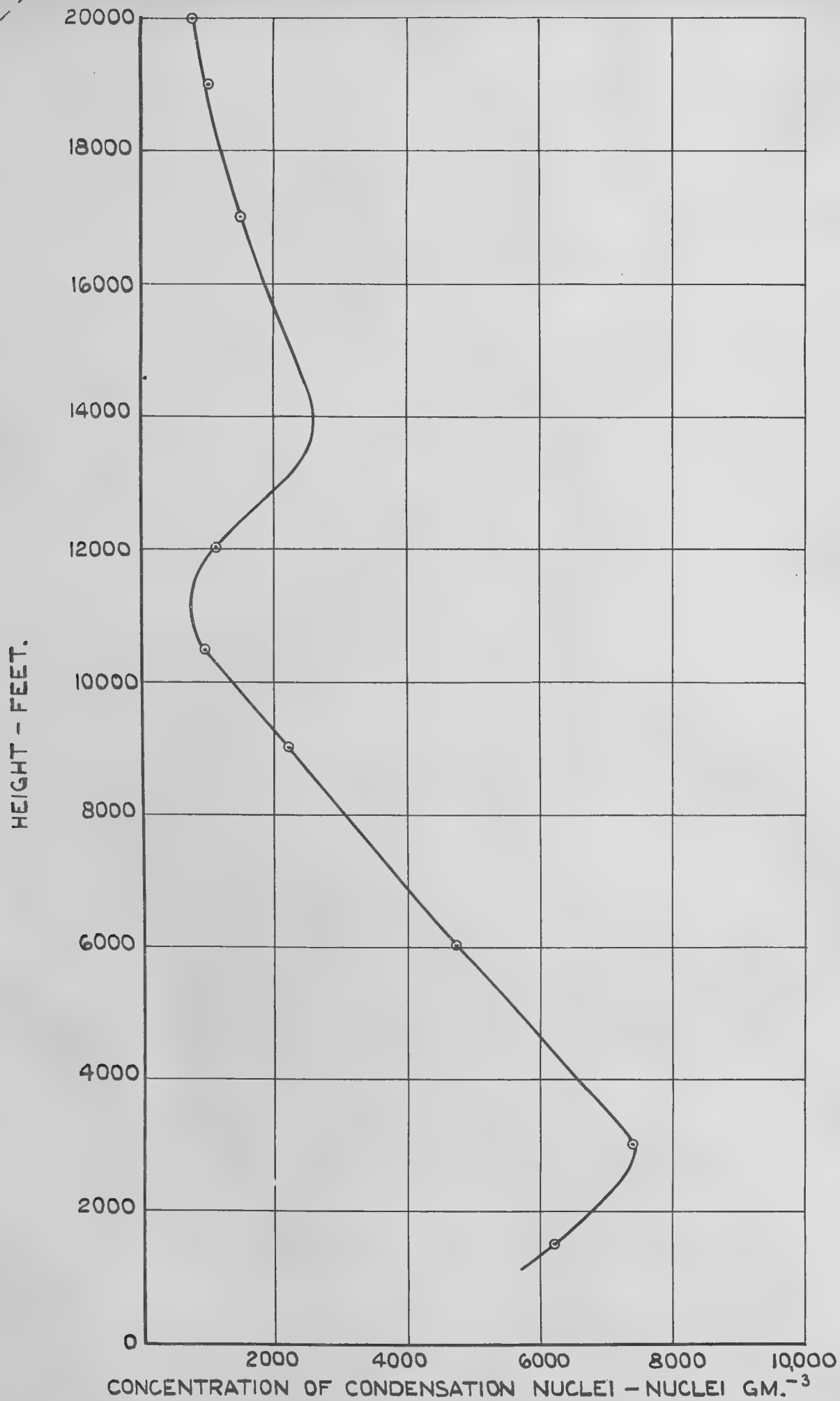

FIG. 2 c. ASCENT THROUGH A FRONTAL SURFACE, NEAR THE DUTCH COAST – 20·6·55.

No. MET. RES. FLT.
DR.
TR. O.W.H.
CH.
APP.

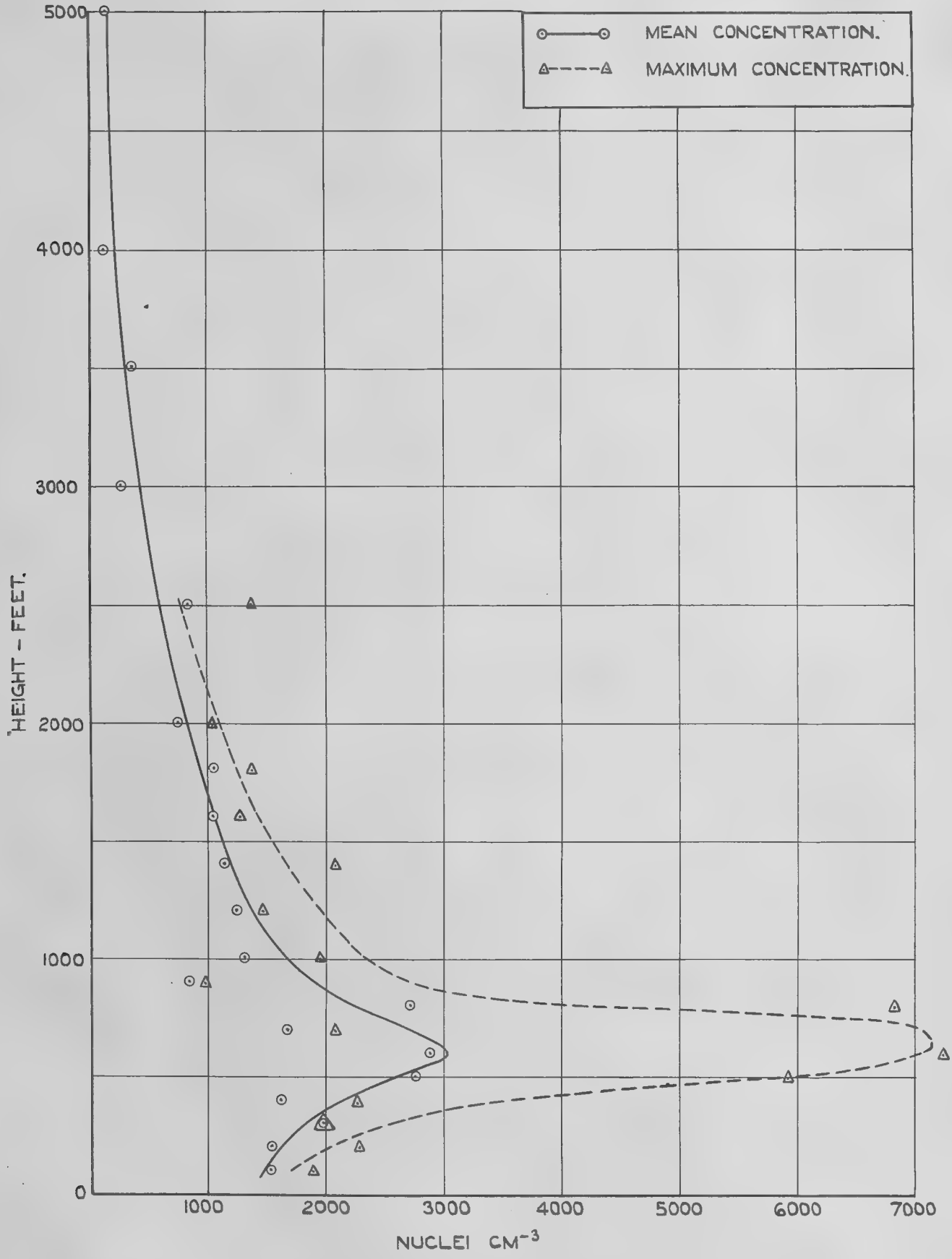

FIG. 3 a. VARIATION OF CONDENSATION NUCLEUS CONCENTRATION WITH HEIGHT OVER SLIGHTLY DISTURBED SEA.

No. MET. RES. FLT.
DR.
TR. O.W.H.
CH.
APP.

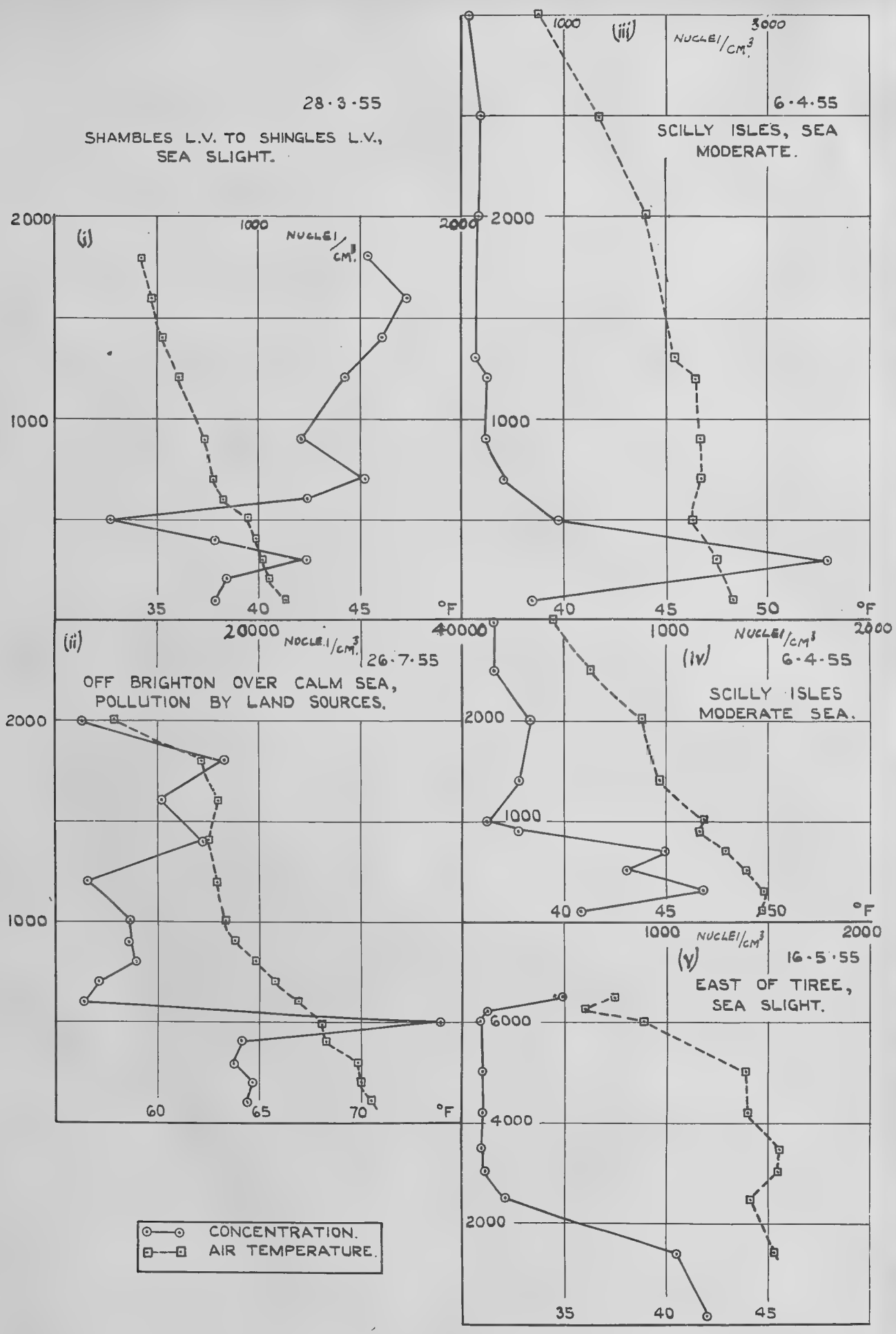

FIG. 3 b. VARIATION OF CONDENSATION NUCLEUS CONCENTRATION WITH HEIGHT OVER SLIGHTLY DISTURBED SEA.

Nº MET. RES. FLT.
DR.
TR. O.W.H.
CH.
APP.

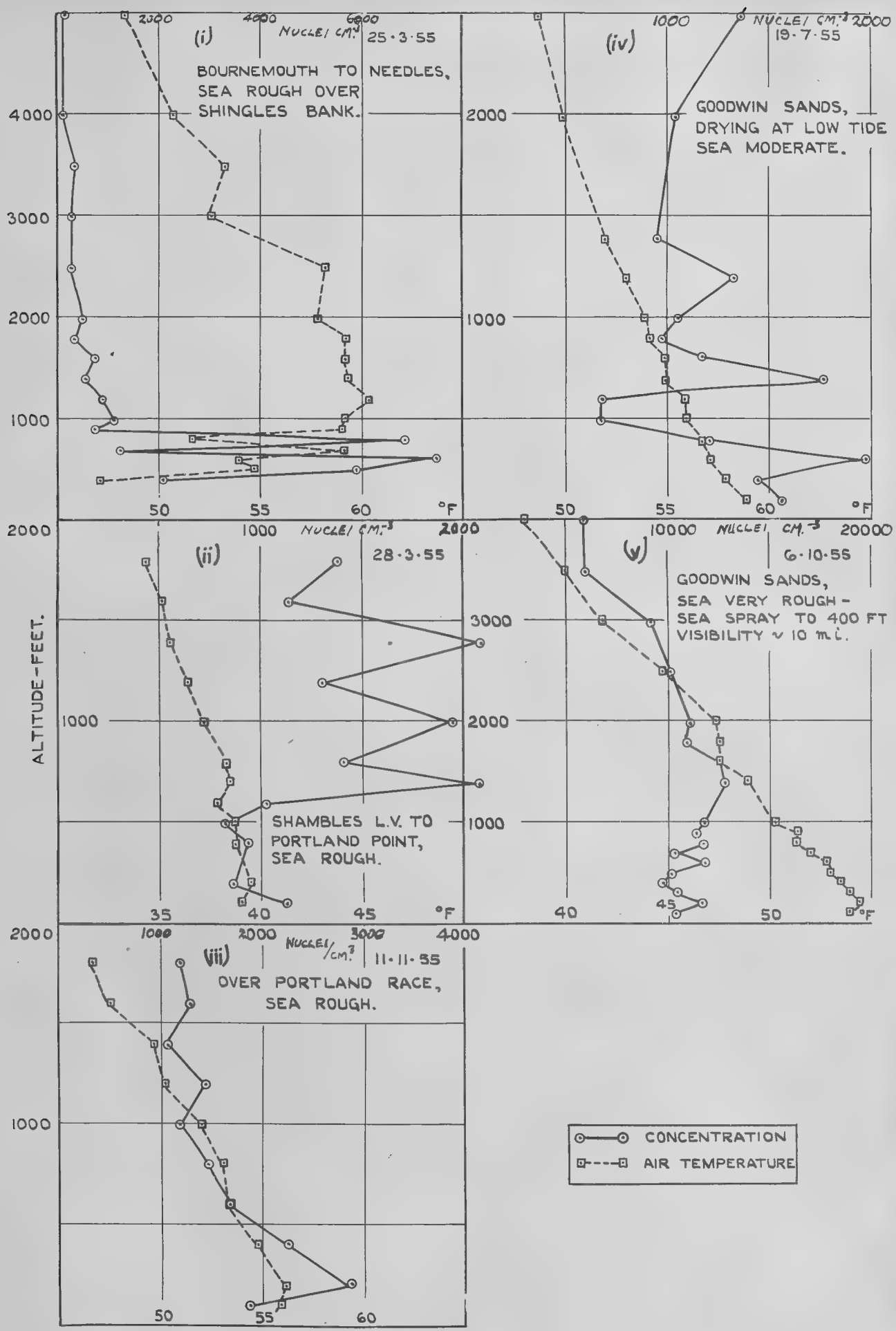

FIG. 3c. VARIATION OF CONDENSATION NUCLEUS CONCENTRATION WITH HEIGHT OVER DISTURBED SEA.

M.R.P. 1070
S.C.1/128
S.C.111/243
27th September, 1957

The measurement of wind at altitude by airborne instruments

by

R. J. Murgatroyd and N. C. Helliwell

(Meteorological Office)

AIR MINISTRY

METEOROLOGICAL RESEARCH COMMITTEE

58-464

As the time of issue this report has not been published. Any author desiring to quote this paper should refer to it as "A paper of the Meteorological Research Committee (London), M.R.P. No. 1070 by Mr. R.J. Murgatroyd and Mr. N.C. Helliwell. A copy is available in the Library of the Meteorological Office."

M.R.P. 1070
S.C.I/128
S.C.III/243
27th September, 1957

AIR MINISTRY

METEOROLOGICAL RESEARCH COMMITTEE

The measurement of wind at altitude by airborne instruments

by

R.J. Murgatroyd and N.C. Helliwell (Meteorological Office)

1. Introduction

1.1. In 1955 a Marconi navigational system based on the Doppler principle was installed in a jet aircraft of the Meteorological Research Flight. This system enables the ground speed and the angle of drift between the ground speed vector and the airspeed vector to be evaluated to high accuracy by means of radio techniques. The purpose of this investigation was to determine the errors involved when this equipment is used to measure the wind.

1.2. With this equipment, a wind measurement requires the determination of four basic quantities, (a) the heading of the aircraft, (b) the true airspeed (i.e., the speed of the aircraft relative to the air which, in turn, can only be derived from the indicated airspeed, pressure altitude and true air temperature), (c) the ground speed as measured by the radio equipment and (d) the drift angle as measured by the radio equipment. The wind is the vector difference between the airspeed vector given by (a) and (b) and the ground speed vector given by (a), (c) and (d). The method used to determine the wind is given in Appendix I which also includes the calculation of errors. Each of the measured quantities is considered below.

1.2.1. Provided the heading is kept constant the error in the wind direction is equal in magnitude to the error in the heading and the error in the wind speed is a second order effect. It is, however, necessary to ensure that the heading is not varied substantially during any series of measurements and for this reason the best possible measurement of heading was always obtained. This was achieved by installing a completely separate additional gyro compass and taking photographs of its master compass presentation. This can be read to half a degree compared to the one or two degrees of the repeater compasses. Random reading errors of 0.25° in heading arising in this way can be regarded as similar errors in drift angle and will be treated as such.

1.2.2. Of all the necessary measurements, that of airspeed is the least accurate. It is subject to all the errors in the pressure indicating instruments (e.g., static and pitot position errors), instrument errors, and temperature errors including variations of the speed correction coefficient. Using the best available data and laboratory calibrations of the various instruments, both systematic and random residual errors can still be expected. The first object of the calibration was to obtain values of these residual errors which could be used to correct and interpret the observations made in subsequent flights.

1.2.3. The quoted maximum error of the ground speed indicator is 0.3 per cent and the instrument is calibrated electronically before flight to be within this tolerance.

/1.2.4.

1.2.4. The measurement of drift is susceptible to both systematic and random errors; the former arise from minor misalignments of the aerials and the latter are due to sideslip, yaw, etc. It was decided, therefore, that the second part of the calibration should be an attempt to find the systematic errors in the measurement of drift.

1.3. The most direct method of obtaining calibrations is to use simultaneous independent wind measurements and probably the best practical approach is to fire smoke puffs from the aircraft and to track the motion of the smoke visually from the ground, readings being taken in the aircraft at the same time. Unfortunately, owing to unsuitable weather conditions, this has not yet been done, but it has been possible to obtain a calibration using two other methods which are not so direct in that they assume constancy of wind in time and space over periods of up to one hour and distances up to 50 miles compared with the 5 minutes or so and distances up to 10 miles involved in the measurement by the smoke puff technique.

1.3.1. Various geometrical air tracks were flown and a theory is derived below enabling a correction factor K to be evaluated for the airspeed modulus and a systematic error γ in the angle of drift to be computed. These flights are discussed below under the heading "Geometrical Flights".

1.3.2. Seven flights were made near the time of release of a radiosonde balloon and in the region of a radiosonde station. Interpolations from the displacement winds of the radiosonde were then used to evaluate the same two constants K and γ by resolution of these winds along and at right angles to the heading of the aircraft. These flights are referred to below as "Comparison Flights".

2. List of Symbols used

Symbol	Definition	Units
α	the angle of drift	degrees
$\beta = \alpha + \gamma$	the corrected angle of drift	degrees
γ	the correction to the angle of drift	degrees
Δx	the error in the quantity x	-
θ	the heading of the aircraft	degrees true from North
ϕ	the wind direction	degrees true from North
a	the speed correction coefficient of the thermometer	-
K	true airspeed correction factor	-
$\underline{n}$	unit vector normal to the course	-
p	I.C.A.N. pressure height	mb
q	true airspeed uncorrected	kt
$\underline{q}$	true airspeed vector uncorrected	-
$\underline{s}$	unit vector along the course	-
T_i	indicated air temperature	°C
T	true air temperature	°C
t	time	min

/u

Symbol	Definition	Units
$\underline{u} = K\underline{q}$	the corrected true airspeed vector	-
$U = Kq$	the corrected true airspeed	kt
$\underline{V}$	the ground speed vector	-
V	the ground speed	kt
V_i	the indicated airspeed	kt
V_e	the equivalent airspeed	kt
$\underline{w}$	the wind vector	-
W	the complex wind vector	-
w	the wind speed	kt
w_1	the component of the radiosonde wind along θ	kt
w_2	the component of the radiosonde wind perpendicular to θ	kt
var (x)	the variance of the quantity x	
$\bar{x}$	the mean value of the quantity x	

3. Instruments and their accuracy

3.1. The observations were taken in two ways:-

(1) By visual methods in the pressure cabin of the aircraft.

(2) By photographic methods.

3.2. Visual method

The observer took readings at stated intervals (usually one minute in the Geometrical Flights and three to five minutes in the Comparison Flights) of the following quantities and to the stated accuracy:-

(a)	Time	assumed exact.
(b)	Altitude in feet	probably, when corrected for all known errors, $\pm$100 ft maximum error using a pressure altimeter.
(c)	Heading	assumed exact by standard aircraft master compass, (see para. 1.2.1.).
(d)	Temperature	$\pm$ 2°C maximum error, measured by standard flat plate thermometer and bridge. (Ref. 1).
(e)	Ground speed	assumed exact, using electronic equipment.
(f)	Drift angle	to be found.
(g)	Airspeed	to be found after correction for existing errors.

/3.3.

3.3. Photographic method: auto-observer readings

A specially designed mounting was made for the following instruments:- clock (time), altimeter (altitude), aircraft master compass independently synchronised (heading), airspeed meter (airspeed) and duplicates of those instruments in the pressure cabin from which drift and ground speed are read. Photographs of the meters were taken at intervals of about 50 seconds (or about six miles of flight) by a camera controlled from the pressure cabin. This camera was fitted with a special heater muff to prevent icing.

3.4. Care was taken to synchronise the clock on the auto-observer with the observer's watch. In general it would be expected that the results from the visual readings would agree with those obtained by the photographic methods as both depend on indications from similar instruments. This is so except when the readings are varying rapidly and the visual readings become a subjective mean over an interval of time whilst the photographic values remain those at a given instant. In this work this effect did not give rise to any difficulties except in the case of the drift meter. In flight, this instrument, which is calibrated in degrees, did not generally show a steady reading but varied slowly and irregularly by 1° to 2° about a mean value. This is probably due to either instrumental hunt or variation in pitch, yaw, etc., not reflected in the compass readings, or possibly a combination of both. The exact cause is unimportant to the text of this paper which is concerned only with the standard error in measurements made up to date using the meter. However, it should be noted that the observer must necessarily take a mean value over some interval (usually about one minute in duration) and that his readings can only be made to 0.25° at best and 0.5° at worst. In all flights readings were taken visually to the nearest 0.5°. In the auto-observer the camera takes an instaneous photograph and so the individual readings may be in error by as much as 2° in the worst possible case: if the error is random this will be reflected in the statistics as a large standard deviation for the error in drift angle (i.e., the standard error of the error in drift angle obtained using the photographic data would be larger than that obtained by visual methods although the means would not differ greatly).

3.5. Recently a modification has been introduced to reduce the instrumental hunt by increasing the servo-damping in the drift unit and preliminary results indicate that the hunt is now about ±0.5° so that further work using the auto-observer is likely to present less variability than that examined up to date.

3.6. In each case, the readings of heading, ground speed and drift were directly available; that of true airspeed was obtained from the indicated temperature, airspeed and height using standard expressions in the form:

$$q = V_e \left\{ \frac{3.53\ (T+273)}{p} \right\}^{\frac{1}{2}} \qquad (1)$$

$$T = T_i - \frac{V_e^2}{100^2} \cdot \frac{a\ 3.53\ (T+273)}{p} \qquad (2)$$

where V_e is the equivalent airspeed obtained by correcting the indicated airspeed V_i for instrumental calibration, compressibility and pressure error.

/4.

4. Geometrical Flights

4.1. Providing the wind can be assumed constant over reasonably short intervals of space and time, measurements of wind and airspeed can be obtained directly from the readings of the ground speed meter by flying various geometrical paths through the air. The simplest of these paths is to fly at constant airspeed on reciprocal compass readings of equal time duration using headings such that the drift is zero. In this case it is assumed that the two legs have equal following and head winds so that the airspeed is equal to the mean of the ground speeds and the wind speed is the difference between the ground speed and the airspeed. These ideas can be elaborated by flying in other patterns (e.g., squares or triangles). In all, six flights of this type were made. The theory of the method is given in Appendix II. Another method which can be used for this type of investigation (although it was developed for another purpose) has been suggested by C.S. Durst (unpublished) and using the same data he has obtained results in good agreement with those quoted below.

4.2. Provided the heading of the aircraft is maintained at constant altitude there is no necessity for it to perform any special turns at the corners of any geometrical flight. The theory merely requires equal times in any two reciprocal directions and constancy of wind. The aircraft therefore climbed to the height at which the pattern was to be flown, and when level, carried out the requisite number of legs (two, three, or four) in the requisite number of directions performing shallow banks at the end of each leg so that the equipment did not become unlocked. The duration of each leg was usually four minutes or about 25 miles of flight.

4.2.1. Flights in a square

Four legs were flown in the form of a square. If the mean airspeed at the jth minute was q_{ij} on the ith leg and the ground speed was V_{ij}, the drift angle α_{ij}, then the formulae (11) and (12) of Appendix II become:

$$\tan\gamma = -\frac{\sum_i \sum_j V_{ij} \sin\alpha_{ij}}{\sum_i \sum_j V_{ij} \cos\alpha_{ij}} \qquad \begin{matrix} i = 1, 2, 3, 4 \\ j = 1, 2, 3, 4 \end{matrix} \qquad (3)$$

$$K = \frac{\sum_i \sum_j V_{ij} \cos(\alpha_{ij} + \gamma)}{\sum_i \sum_j q_{ij}} \qquad (4)$$

4.2.2. Flights in an equilateral triangle

Similar equations can be proved to hold as in 4.2.1. with $i = 1,2,3$ and $j = 1,2,3,4$.

4.2.3. Flights on reciprocal headings

Here, equations (3) and (4) hold with $i = 1$ and 2 and $j = 1,2,3,4$.

/4.3.

4.3. Table I gives values of K and γ calculated for squares, a triangle and reciprocal flights.

Table I

Values of K and γ derived from Geometrical Flights

Date	Height ft	Pattern	Observer		Photographic method		Pilot	Observer
			K	γ deg	K	γ deg		
17.11.55	25,000	Triangle	1.034	-0.23	1.020	-0.29	A	X
	35,000	Triangle	1.028	-0.27	1.026	-0.40	A	X
8.11.55	20,000	Square	1.025	+0.43	1.023	+0.12	B	Y
	40,000	Square	1.027	+0.08	1.025	+0.11	B	Y
9.11.55	10,000	Square	1.024	-0.20	1.015	+0.21	A	Z
	30,000	Square	1.042	+0.21	1.033	+0.31	A	Z
1.11.55	5,000	Reciprocal	1.016	+0.65	1.028	+0.75	B	Y
	10,000	"	1.018	+0.55	1.020	+0.72	B	Y
	20,000	"	1.012	+0.43	1.018	+1.19	B	Y
	25,000	"	1.025	+0.48	1.020	+0.74	B	Y
	30,000	"	1.026	+0.56	1.025	+0.75	B	Y
7.11.55	30,000	"	1.025	+0.58	1.023	+0.10	B	Y
	35,000	"	1.037	+0.39	1.039	+0.25	B	Y
	40,000	"	1.033	+0.50	1.027	+0.60	B	Y
	45,000	"	1.016	+0.82	1.014	+1.28	B	Y
21.10.55	15,000	"	1.025	+0.75			B	X
	20,000	"	1.029	+0.82			B	X
	30,000	"	1.027	+0.82			B	X
	40,000	"	1.031	+0.33			B	X

Mean value of K from:-		Variance
visual readings	1.026	$0.54 \cdot 10^{-4}$
photographic readings	1.024	$0.39 \cdot 10^{-4}$
all readings	1.025	$0.62 \cdot 10^{-4}$

Mean value of γ from:-		Variance (rad^2)
visual readings	+0.41 deg.	$0.35 \cdot 10^{-4}$
photographic readings	+0.43 "	$0.68 \cdot 10^{-4}$
all readings	+0.42 "	$0.49 \cdot 10^{-4}$ (0.40 deg^2)

5. Comparison Flights

5.1. As already mentioned, these were comparisons between mean winds determined by radiosonde and winds determined by the aircraft. The opportunity was taken at the same time to make similar comparisons of frost points and temperatures, but only the comparisons of winds will be considered here.

/5.2.

5.2. Since the balloon ascends at 1,200 ft per minute and also changes its plan position irregularly due to changes of wind it was evidently useless to attempt synchronous readings. The procedure adopted was to time the aircraft's flight so that, when the balloon left the ground, the aircraft observer had already taken several measurements of frost point at standard levels. These standard levels are at 5,000 ft intervals from 5,000 ft to 30,000 ft and then at 2,000 ft intervals from 32,000 ft to 48,000 ft with one extra reading at 35,000 ft. Before and after the frost point was measured, readings were taken of all the other parameters:- temperature, airspeed, ground speed, heading, drift and height. The flight usually ended about an hour after the balloon had reached 50,000 ft. The auto-observer was again used to duplicate the readings and there were many more readings available from this instrument than the two taken visually at any level.

5.3. Theory

Consider components of the wind, airspeed and ground speed along and perpendicular to the heading: let w_1 be the radiosonde wind component along the heading and w_2 be the radiosonde wind component perpendicular to the heading, so that:-

$$V \cos(\alpha + \gamma) = U + w_1 \qquad (5)$$

$$V \sin(\alpha + \gamma) = w_2 . \qquad (6)$$

Equation (6) can be solved for γ since all the other quantities are known.

$$\gamma = -\alpha + \sin^{-1}\frac{w_2}{V} . \qquad (7)$$

Using this value of γ, put $U = Kq$ in equation (5) and solve for

$$K = \frac{V \cos(\alpha + \gamma) - w_1}{q} . \qquad (8)$$

5.4. Analysis

The radiosonde wind is a mean over an interval of one minute and it was resolved into north and east components using the raw data. These components were taken at the mean height of the layer through which the balloon travelled during the time interval. Graphs of north and east components against geometric height were plotted and the radiosonde temperatures were used to convert these heights into I.C.A.N. pressure heights. The corrected I.C.A.N. height of each observation taken in the aircraft is known and so a wind can be estimated in the form of north and east components at the height of each aircraft observation. These components were resolved along and perpendicular to the indicated heading of the aircraft giving w_1 and w_2. Formulae (7) and (8) were then used to derive values of K and γ for each observation.

5.5. Values of K and γ were plotted against height, indicated airspeed, drift angle and against each other. No relationship was found. Table II gives mean values of K and γ obtained on flights by both the visual readings and the photographic readings together with the variance about these means. Separate overall means and variance are listed for visual and photographic values irrespective of date and the gross means and variances (visual plus photographic readings) are also listed. The total number of values is 432.

/Table II

TABLE II

Values of K and γ derived from Comparison Flights

Date	Pilot	Readings taken visually					Readings taken photographically					Observer
		No. of observations	Mean K	Variance of K x 10^4	Mean γ deg	Variance of γ deg^2	No. of observations	Mean K	Variance of K x 10^4	Mean γ deg	Variance of γ deg^2	
28.10.55	A	19	1.027	11.7	+0.50	1.50	80	1.026	5.2	+0.71	1.64	X
31.10.55	B	19	1.033	0.1	+1.20	0.79	41	1.034	4.0	+0.86	0.58	X
1.11.55	A	17	1.017	5.6	+0.87	0.46	55	1.019	4.0	+1.11	0.79	X
8.11.55	A	19	1.030	3.4	+0.70	1.20	66	1.025	2.3	+0.71	1.15	X
22.11.55	B	17	1.025	6.5	+0.60	0.92	21	1.012	8.1	+0.43	1.11	X
28.11.55	C	15	1.021	4.8	+0.83	0.80	50	1.025	1.4	+0.72	1.81	X
29.11.55	B	13	1.017	5.0	+0.40	1.96	-	-	-	-	-	X
Mean		TOTAL 119	1.025	5.9	+0.74	1.18	TOTAL 313	1.024	8.2	+0.71	1.30	
Gross Mean		TOTAL 432	1.025	7.5	+0.72	1.25 = 3.84 x 10^{-4} radians^2						

Mean value of means for each flight $\overline{K}$ = 1.025 Variance of $\overline{K}$ = 0.39 . 10^{-4}
$\overline{\gamma}$ = +0.72 Variance of $\overline{\gamma}$ = 0.23 . 10^{-4} radians^2

6. Discussion

6.1. It is very difficult to separate the sources of error and apportion the magnitudes in this type of work and so the first step in the analysis was to construct Table III which shows mean values of K and γ for each height obtained on all flights but separated into four classes as shown in the headings. Means of each column and corresponding variances are also given.

/Table III

Table III

Variations of K and γ with height

(Number of observations in brackets)

Height ft	Geometrical Flights				Comparison Flights			
	Visual K	Photo K	Visual γ deg	Photo γ deg	Visual K	Photo K	Visual γ deg	Photo γ deg
5,000	1.016(1)	1.028(1)	+0.65	+0.75	1.026(5)	1.016(4)	+0.43	+0.91
7,000	-	-	-	-	1.049(1)	1.016(1)	+0.73	+0.30
10,000	1.021(2)	1.017(2)	+0.17	+0.46	1.029(7)	1.021(6)	+0.64	+1.09
15,000	1.025(1)	-	+0.75	-	1.017(7)	1.020(6)	+0.53	+0.88
20,000	1.022(3)	1.020(2)	+0.56	+0.66	1.024(7)	1.018(6)	+0.66	+0.70
25,000	1.029(2)	1.020(2)	+0.13	+0.22	1.037(6)	1.030(6)	+0.55	+0.20
30,000	1.030(4)	1.027(3)	+0.54	+0.39	1.031(7)	1.029(5)	+0.79	+0.17
34,000	-	-	-	-	1.005(1)	1.067(1)	+1.95	+1.49
35,000	1.032(2)	1.032(2)	+0.06	-0.07	1.040(5)	1.013(1)	+0.84	+1.45
36,000	-	-	-	-	1.022(2)	1.027(4)	+0.14	+0.76
38,000	-	-	-	-	-	1.012(1)	-	-1.80
40,000	1.030(3)	1.026(2)	+0.31	+0.36	1.013(6)	1.012(4)	+0.65	+0.65
42,000	-	-	-	-	-	1.017(2)	-	+1.70
43,000	-	-	-	-	-	1.030(1)	-	+1.89
44,000	-	-	-	-	-	1.037(2)	-	+1.52
45,000	1.016(1)	1.014(1)	+0.82	+1.28	-	-	-	-
46,000	-	-	-	-	1.019(7)	1.028(5)	+0.63	+1.01
48,000	-	-	-	-	1.018(7)	1.032(5)	+0.81	+0.57
Mean	1.025(9)	1.023(8)	+0.44	+0.51	1.025(13)	1.025(17)	+0.72	+0.78
Variance x 10^4	0.336	0.332	0.216 (rad^2)	0.43 (rad^2)	1.016	1.74	0.48 (rad^2)	2.11 (rad^2)

At first sight there would appear to be a correlation of K with height but the mean values of γ are so variable that no correlation with height is apparent. In order to find the correlation of K with height (expressed in thousands of feet), the Geometrical Flight data were used and gave the following results:-

(a) Visual readings

Correlation coefficient +0.39

Regression line $K - 1.025 = (1.88).10^{-4} \times (\text{height} - 25)$.

(b) Photographic readings

Correlation coefficient -0.03

Regression line $K - 1.023 = (1.44).10^{-5} \times (26.25 - \text{height})$.

The probable error of the value of correlation coefficient was 0.2 in each case, and it is considered that no significant variation with height has been shown by the above analysis. The correlation of Comparison Flight data with height would be heavily masked by errors to be discussed later. It was decided therefore to find the best values of K and γ without regard to variation with height for both types of flight.

/6.2.

6.2. In the Geometrical Flights, the values of K and γ obtained at any level on a given day are necessarily mean values and any such values can be considered as a separate flight in the analysis. In the Comparison Flights, however, the values of K and γ on each flight are found from isolated readings and so, besides the separation into heights, it is possible to find means for a flight irrespective of height. There are, therefore, several means involved in the analysis and these will be discussed before being applied to the data available.

(a) Geometrical Flights

(1) Mean K and γ can be found for each height (Table III) and for all days and finally means of these for all heights can be found.

(2) Mean K and γ can be found for all the determination in Table I. The means are differently weighted from those in para. (a)(1) in a manner which depends on the number of evaluations at each height.

(3) Variances can be found for both K and γ about the overall mean values in para. (1) and (2) above.

(4) Since there are two separate sets of observations - visual and photographic - these can be combined before operation (a)(1) is carried out and this will give values for mean K and mean γ. This smoothing of the data, however, will introduce observational errors which cannot be assessed, and for this reason it was considered that this process is not justified.

(5) Student's t-test can be used when operations described in para. (2) and (3) have been performed separately on the visual and photographic values of K and γ to discover whether they are significantly different.

(b) Comparison Flights

(1) Mean values can be found for each day without regard to height and variances about these means can be computed. (Table II).

(2) Mean values can be found for each height on each day and then the mean value for all days at each height can be derived. Variance can be computed about each of these means. (Table III).

(3) Student's t-test can be used to examine the statistical difference between the values of K and γ derived from visual readings and those derived from photographic readings in both para. (b)(1) and (b)(2).

6.3. Since it seems very doubtful from para. 6.1. whether K and γ vary with height, the meaning process described in para. 6.2.(a)(2) was used for both sets of observational data (visual and photographic) on the Geometrical Flights. Student's t-test showed that at the 5 per cent level of significance there was no difference between these two observational methods. Variances of K and γ corresponding to these means were also found. These variances are in part due to (a) time and space variations of the wind during the period of measurement and in part due to (b) instrumental variations. If (a) could be estimated (b) would be determinate. In order to do this, the mean values of K and γ found above were used to find individual winds $\underline{w}_i$ and mean winds $\underline{\bar{w}}$ for each flight. The root mean square differences between each individual wind and these means were found and summed in the form $\sum \frac{1}{n} (\underline{w}_i - \underline{\bar{w}})^2$ Results are given in Table IV.

/Results

Table IV

Geometrical Flights

Comparison of root mean square differences with probable variation of wind

Height ft	Date	Track	Root mean square diff. kt	Mean wind kt	Variability of wind (Durst) kt	
					Distance	Time
20,000	8.11.55	Square	6.33	33.6	12	2.5
40,000		"	6.36	39.5	11	3.5
10,000	9.11.55	"	8.76	34.5	7.5	2
30,000		"	13.01	31.1	15	6
25,000	17.11.55	Triangle	8.31	51.3	12.5	4
35,000		"	8.32	72.4	12	4
30,000	7.11.55	Reciprocal	5.72	68.1	12	4
35,000		"	6.35	61.8	11	4
40,000		"	4.85	58.9	9	3.5
45,000		"	6.36	33.9	7.5	2.5
5,000	1.11.55	"	3.14	11.1	6	2
10,000		"	4.12	4.7	7	2
20,000		"	5.48	14.4	10	2.5
25,000		"	3.24	21.7	11.5	3.5
30,000		"	3.96	24.8	12	4
15,000	21.10.55	"	5.95	30.9	7.5	2
20,000		"	5.60	17.9	10	2.5
30,000		"	8.63	33.4	12	4
40,000		"	7.13	4.2	9	3.5

Also included in this table are estimates of the distance and time variation to be expected from Fig.5 of Geophysical Memoir 93(2) using representative flight durations and distances. It can be seen that the root mean square differences found above are in all cases less than the expected time and distance variations. Hence it is impossible to separate the two sources of variance. However, it is evident that the standard errors of wind measurements cannot exceed, and may be considerably less than, the values indicated in column 4 of Table IV.

An estimate of the standard error of a wind reading may be given using equation (9) of Appendix 1 with the results in Table I, i.e., $\mathrm{var}(K) = 0.54.10^{-4}$, $\mathrm{var}(\gamma) = 0.35.10^{-4}$ rad^2 for visual readings and $\mathrm{var}(K) = 0.39.10^{-4}$, $\mathrm{var}(\gamma) = 0.68.10^{-4}$ rad^2 for photographic readings. With $K = 1.025$ and $\gamma = +0.5$, typical values using the data of the example in Appendix I, shows, for visual readings, the standard error is 4.5 kt, and for photographic readings 5.0 kt.

/6.4.

6.4. The Comparison Flights were analysed in both of the ways outlined in para. 6.2.(b). The results of para. 6.2.(b)(1) are shown in Table II and those of 6.2.(b)(2) in Table III. Non-weighted means were used in all cases. It will be seen from these tables that, for any particular day or any particular height, the mean K is 1.025 by both methods of analysis and for the two different types of observation and that the mean γ is near $+0.75^{\circ}$. An attempt was also made to separate space and time variations from instrumental effects. The effects of space and time variation involved here are much larger than in the Geometrical Flights since the compared values may be at a time difference of one hour and 50 miles apart. Table V(a) shows the expected vector variation in time and space of the wind (based on Geophysical Memoir No. 93)(2). For comparison purposes, the values of var(K) and var(γ) were taken from Table II and inserted into equation (9) of Appendix I as in 6.3.

Table V(a)

Wind Errors in Comparison Flights

Height ft	Variability of wind (Durst) kt	
	50 mile distance	1 hour time
5,000	7.0	4.0
10,000	7.5	4.5
15,000	8.5	5.0
20,000	12.0	6.5
25,000	14.0	8.0
30,000	15.0	8.5
35,000	13.0	8.0
40,000	10.5	6.5
45,000	8.0	5.0
50,000	6.5	4.0

Table V(b)

Date	Wind error (kt)	
	Visual	Photographic
28.10.55	17.36	14.42
31.10.55	7.86	10.40
1.11.55	11.16	11.15
8.11.55	12.07	11.15
22.11.55	13.19	14.63
28.11.55	11.74	12.73
29.11.55	15.14	

The specimen errors produced, shown in Table V(b), are of the same magnitude as the vector variation in Table V(a) or slightly larger. In view of the failure in 6.3. above to produce any adequate discrimination of the two types of errors by using the data of Geophysical Memoir No. 93(2) in this way it was not considered worthwhile to attempt to assign quantitative values to the instrumental error in this case.

6.5. From the various values of standard variance shown in Tables I, II and III it is difficult to choose the one which should be used finally in estimating the error of the wind. The most useful figures to apply in practice to visual observations are var$(\gamma) = 0.4.10^{-4}$ rad^2 and var$(K) = 0.5.10^{-4}$ these figures being reasonable estimates allowing for the variation in experimental methods and averaging processes. As discussed in para. 6.3. and 6.4. above the cause of the scatter is not known although it appears likely that the major cause is not instrumental.

/6.6.

6.6. Whatever the averaging process employed in the analysis of the visual observations the results in the mean suggest a value of $K = 1.025$ and this will, in general, be the nearest practical estimate of the airspeed correction factor. Table VI gives suggested corrections for the speed ranges shown which should be added to the true airspeed.

Table VI

Corrections to true airspeed

True airspeed (kt)	Correction (kt)
280 to 299	+7
300 to 339	+8
340 to 379	+9
380 to 419	+10
420 to 459	+11
460 to 499	+12

This rough correction is not suggested for accurate wind finding in which the factor 1.025 should be applied directly to the data, but can be of value to the navigator in routine work using this particular installation.

6.7. The value of γ is subject to various calibration errors but it is suggested that $+0.5^\circ$ is a reasonably practical quantity which could be added to all drift readings when starboard drifts are counted positive.

6.8. The error is shown to be 11 kt for any single wind reading in Appendix I when no special corrections are applied. Using $K = 1.025$ $\gamma = +0.5^\circ$ and $\mathrm{var}(K) = 0.5.10^{-4}$ and $\mathrm{var}(\gamma) = 0.4.10^{-4}$ rad^2 the error of a wind determination is shown to be 4.5 kt approx. and in a continuing series of observations it is probably much less than this. More recent work on long flights using the above values of K and γ with readings at intervals of one minute, suggests that errors in continuing sequences may be as small as one knot when used comparatively, although the absolute value of the wind vector may have a considerably larger error.

6.9. For the photographic readings, although the mean values of K and γ can be applied as for the visual readings, it is desirable to assume larger variances since the errors are somewhat larger due to the fact that the drift meter varies in a random fashion. It seems from the tables that values $\mathrm{var}(K) = 0.4.10^{-4}$, $\mathrm{var}(\gamma) = 0.7.10^{-4}$ rad^2 should be used. This gives the error of a wind reading taken photographically to be 5 kt. In the case of photographic readings, however, this is the resolution of the system since in any continuing series of observations it is unlikely that greater accuracy can be obtained because of the variations on the drift meter.

7. Conclusions

7.1. The equipment giving ground speed and drift has now been in regular use at the Meteorological Research Flight for about 18 months; during this period its serviceability has been extremely good but there are some limitations. Over calm seas and in steep banks or turns this equipment sometimes gives erroneous values since the basic radio principle involved requires straight and level flight with good surface reflections. To the observer this "unlocking" can be detected by indicators on the display panel but some selection of the photographic observations is occasionally necessary. This limitation has caused little trouble in routine meteorological work.

7.2. When a fault occurs on the apparatus and the maintenance has been carried out, there sometimes appears to be a change in calibration and calibration checks of the type described in section 4 are necessary before any large scale investigation is undertaken.

/7.3.

7.3. The reduction of the data obtained is straightforward but laborious particularly when auto-observer techniques are used. There is a requirement for some form of automatic computer which will give direct presentation of the wind data in flight.

7.4. In the comparative type of work for which this instrumental system will be used, e.g., jet streams, the errors involved will be fairly small and can be estimated roughly by the methods shown in Appendix I. In work of a more absolute nature, e.g., variation of wind in time and space, some further improvement is desirable but this improvement should be attempted in the pressure indicating instruments not in the electronic system.

8. Summary

An extremely useful equipment is now available for measurement of wind from aircraft for meteorological investigations.

It is suggested that (with the present installations on the aircraft of the Meteorological Research Flight) if the true airspeed is multiplied by a factor of 1.025 and +0.5° is added to all drift angles - starboard drift angles being positive - the error in a wind measurement using this system will be less than 5 kt.

9. Bibliography

1. Durbin, W.G. 1955 Meteorological Research Papers, Air Ministry, London, No. 930.

2. Durst, C.S. 1955 Geophysical Memoirs No. 93, Air Ministry, London.

APPENDIX I

The calculation of the wind from ground speed, airspeed, drift angle and heading and the effect of errors in these quantities

A.1.1.

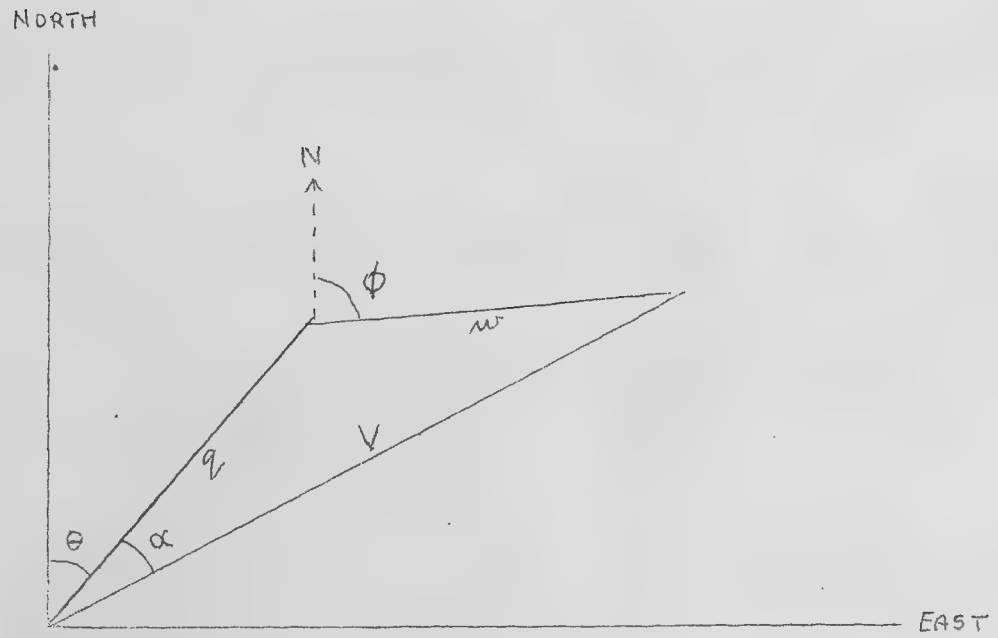

Referring to Fig.1, in vector notation:-

$$\text{the wind} \qquad \underline{w} = \underline{V} - \underline{q} \qquad (1)$$

or in cartesian co-ordinates

$$w \cos \phi = V \cos (\theta + \alpha) - q \cos \theta \qquad (2)$$

$$w \sin \phi = V \sin (\theta + \alpha) - q \sin \theta \qquad (3)$$

w and ϕ can be calculated using measured independent values of V, q, θ and α from (2) and (3).

A.1.2. Rewriting (2) and (3) in complex form

$$W = w e^{i\phi} = V \exp i (\theta + \alpha) - q \exp i\theta . \qquad (4)$$

/If

If errors ΔV, Δq, $\Delta \theta$ and $\Delta \alpha$ occur in the respective measured values, the total mean square vector error in W is given by

$$|\Delta W|^2 = \left|\frac{\partial W}{\partial V}\right|^2 |\Delta V|^2 + \left|\frac{\partial W}{\partial q}\right|^2 |\Delta q|^2 + \left|\frac{\partial W}{\partial \theta}\right|^2 |\Delta \theta|^2 + \left|\frac{\partial W}{\partial \alpha}\right|^2 |\Delta \alpha|^2 \qquad (5)$$

Differentiating (4) with respect to V, q, θ and α in turn and substituting in (5)

$$|\Delta W|^2 = |\Delta V|^2 + |\Delta q|^2 + w^2 |\Delta \theta|^2 + V^2 |\Delta \alpha|^2 \qquad (6)$$

which can be used to examine the contribution of the various errors. If

$\Delta \theta \simeq$ 0.01 radians - the compass reading error;

w = 100 kt - the calculated wind speed;

$\Delta V \simeq$ 0.003 V = 1.5 kt if V = 500 kt. This error is the maximum error by an electronic calibration;

$\Delta q \simeq$ 0.025 q = 10 kt if q = 400 kt - determined experimentally in the text above;

$\Delta \alpha \simeq$ 0.008 radians - determined experimentally in the text above;

then

$$|\Delta W|^2 = 1 + 2.25 + 100 + 16 = 119.25.$$

So $|\Delta W|$ = 11 kt when no special corrections are made. If those due to Δq and $\Delta \alpha$ could be eliminated by calibration, $|\Delta W|$ could be reduced to about 2 kt in the most favourable circumstances. In practice this will not be achieved due to reading and random errors and these are considered further below.

A.2.1. The object of the calibrating flights was to find mean corrections K to q and γ to α, where

$$u = Kq \quad \text{and} \quad \beta = \gamma + \alpha \qquad (7)$$

where u is the corrected airspeed and β the corrected drift angle, if K and γ can be found exactly $\Delta u = 0 = \Delta \beta$ and the equation (6) reduces to

$$|\Delta W|^2 = |\Delta V|^2 + w^2 |\Delta \theta|^2$$

A.2.2. If the determination of K and γ involves errors ΔK and $\Delta \gamma$

$$\Delta u = K \Delta q + q \Delta K \quad \text{and} \quad \Delta \beta = \Delta \gamma + \Delta \alpha$$

/and

and $\Delta q = 0 = \Delta\alpha$ since these quantities have already been corrected by K and γ. Hence $\Delta u = q\Delta K$ and $\Delta\beta = \Delta\gamma$ and (6) becomes

$$|\Delta W|^2 = |\Delta V|^2 + w^2|\Delta\theta|^2 + q^2|\Delta K|^2 + V^2|\Delta\gamma|^2 \qquad (8)$$

where w is the value of the wind using the corrected values for airspeed and drift angle.

A.2.3. Since $(\Delta K)^2$ and $(\Delta\gamma)^2$ were examined as variances about the mean and $(\Delta V)^2$ and $(\Delta\theta)^2$ are known as maximum errors, using variances (8) becomes

$$\text{var}(W) \simeq \left|\frac{\Delta V}{3}\right|^2 + w^2\left|\frac{\Delta\theta}{3}\right|^2 + q^2\,\text{var}(K) + V^2\,\text{var}(\gamma). \qquad (9)$$

A.3. It would not be worthwhile at the present stage to attempt to carry this analysis further since variations of wind with time and space have been unavoidable in the experimental procedure used so far.

APPENDIX II

Theory of the geometrical flight calculations

A.2.1. Consider a path in the air whose unit normal vector is $\underline{n}$ and whose unit tangent vector is $\underline{s}$. The wind equation is

$$\underline{V} = \underline{U} + \underline{w}.$$

In time dt the distance moved along the path is

$$\underline{U} . \underline{s}\ dt = \underline{V} . \underline{s}\ dt - \underline{w} . \underline{s}\ dt \qquad (1)$$

and the distance moved perpendicular to the path is

$$\underline{U} . \underline{n}\ dt = \underline{V} . \underline{n}\ dt - \underline{w} . \underline{n}\ dt \qquad (2)$$

Now $\underline{qs}$ is the uncorrected airspeed vector. Put $\underline{U} = K\,\underline{qs}$ where K is some correcting factor.

$$\therefore \quad \underline{U} . \underline{n} = Kq\,\underline{s} . \underline{n} = 0$$

and equations (1) and (2) become

$$\underline{V} . \underline{s}\ dt = (Kq + \underline{w} . \underline{s})\ dt \qquad (4)$$

$$\underline{V} . \underline{n}\ dt = \underline{w} . \underline{n}\ dt \qquad (5)$$

and if

$$\int_0^t \underline{w} . \underline{n}\ dt = 0 = \int_0^t \underline{w} . \underline{s}\ dt \qquad (6)$$

and $\underline{w}$ is constant, (4) and (5) on integration with respect to t

$$\int_0^t V . s\ dt = \int_0^t Kq\ dt \qquad (7)$$

$$\int_0^t \underline{V} . \underline{n}\ dt = 0. \qquad (8)$$

Reverting to Cartesian co-ordinates, equation (6) means that the flight plan has to be such that the time spent flying an easterly component must be balanced by an equal time spent flying a westerly component and similarly with the north-south directions, e.g., reciprocal headings, squares and equilateral triangles with equal times of flight on each leg. If constant airspeed is maintained, any closed circuit which returns to the original air position satisfies the conditions.

/A. 2. 2.

A.2.2. If there is an error γ in the angle of drift α and V is the modulus ground speed

$$\underline{V} \cdot \underline{n} = V \sin(\alpha + \gamma) = V \sin\alpha \cos\gamma + V \cos\alpha \sin\gamma \quad (9)$$

$$\underline{V} \cdot \underline{s} = V \cos(\alpha + \gamma) \quad (10)$$

using the expanded form of (9) and allowing γ to be independent of time, equation (8) becomes:

$$\int_0^t V \sin\alpha \cos\gamma \, dt = - \int_0^t V \cos\alpha \sin\gamma \, dt$$

$$\therefore \quad \tan\gamma = - \frac{\int_0^t V \sin\alpha \, dt}{\int_0^t V \cos\alpha \, dt} \quad (11)$$

This enables a value of γ to be calculated for each complete geometrical pattern and when this value is known and equation (10) is substituted in equation (7)

$$\int_0^t Kq \, dt = \int_0^t V \cos(\alpha + \gamma) \, dt$$

and if K is independent of t

$$K = \frac{\int_0^t V \cos(\alpha + \gamma) \, dt}{\int_0^t q \, dt} \quad (12)$$

M.R.P. 1071
S.C.1/129
10th October, 1957

A diagram for obtaining true air temperatures from indicated air temperatures for aircraft resistance thermometers

by

W. G. Durbin

(Meteorological Office)

AIR MINISTRY

METEOROLOGICAL RESEARCH COMMITTEE

58-465

At the time of issue this report has not been published. Any author desiring to quote this paper should refer to it as "A paper of the Meteorological Research Committee (London), M.R.P. No. 1071 by Mr. W.G. Durbin. A copy is available in the Library of the Meteorological Office."

M.R.P. 1071
S.C.I/129
10th October, 1957

AIR MINISTRY

METEOROLOGICAL RESEARCH COMMITTEE

A diagram for obtaining true air temperatures from indicated air temperatures for aircraft resistance thermometers

by

W. G. Durbin (Meteorological Office)

1. Theory

The correction, due to kinetic heating, to be applied to the indicated reading of an aircraft resistance thermometer is given by the equation

$$\Delta T_K = K \frac{V^2}{2JC_p} \quad \ldots\ldots\ldots\ldots\ldots\ldots\ldots\ldots (1)$$

where ΔT_K is the temperature correction in °C appropriate to a recovery factor K, V is the true airspeed in cm sec^{-1}, J is the mechanical equivalent of heat (4.18×10^7 erg cal^{-1}) and C_p is the specific heat of air at constant pressure (0.24 cal gm^{-1} $°C^{-1}$). (1). The recovery factor, K, represents the proportion of the kinetic energy of the air that is given up to the thermometer and theoretically lies between 0 and 1. If the quoted values of J and C_p and the conversion factor from cm sec^{-1} to kt be substituted in equation (1), it becomes

$$\Delta T_K = 1.322\, K \left(\frac{V}{100}\right)^2 \quad \ldots\ldots\ldots\ldots\ldots\ldots\ldots\ldots (2)$$

where V is now in kt.

The recovery factor depends on the design of the thermometer, the position in which it is mounted on the aircraft and, to some extent, the height at which the aircraft is flying. The quantity 1.322K is called the "Speed Correction Coefficient". It is usually denoted by α and the method of obtaining it is described in reference (2).

An airspeed indicator does not, in general, give readings of true airspeed because the density of the air at the level of flight is usually different from that obtaining when the instrument was calibrated. In the absence of any other errors the airspeed indicator will give readings of what is called the "Equivalent Airspeed". The equivalent airspeed is related to the true airspeed by an equation whose first approximation is

$$V^2 = V_E^2 \left(\frac{\rho_0}{\rho}\right) \quad \ldots\ldots\ldots\ldots\ldots\ldots\ldots\ldots (3)$$

where V and V_E are the true and equivalent airspeeds and ρ_0 and ρ are the densities of air at the base of the I.C.A.N. atmosphere and at the level of flight respectively.

/Equation

Equation 3 may be rewritten as

$$V^2 = V_E^2 \frac{P_o T'}{T_o' P}$$ where P_o, T_o', P and T' are the air pressures

and temperatures (°K) respectively corresponding to ρ_o and ρ. Substituting 1013.2 mb for P_o and 288°K for T_o', these representing conditions at the base of the I.C.A.N. atmosphere, the above equation becomes

$$V^2 = 3.518 V_E^2 \frac{T'}{P}$$ where T' is the true air temperature in °K and

P is the true air pressure in mb at the level of flight, or,

$$V^2 = 3.518 V_E^2 \frac{(T + 273)}{P}$$

where T is the true air temperature in °C.

Substituting this value for V^2, equation (2) becomes

$$\Delta T_K = 4.65K \frac{(T + 273)}{P} \left(\frac{V_E}{100}\right)^2 \quad \ldots\ldots\ldots\ldots\ldots\ldots \quad (5)$$

The true air temperature, T, is, of course, not known and must be written as $T = T_i - \Delta T_K$ where T_i is the indicated temperature.

Equation (5) therefore becomes

$$\Delta T_K = \frac{4.65K(T_i - \Delta T_K + 273)}{P} \frac{(V_E)^2}{(100)} \quad \ldots\ldots\ldots \quad (6)$$

Rearranging, equation (6) reduces to

$$\Delta T_K = (T_i + 273) \frac{K\phi}{(1 + K\phi)} \quad \ldots\ldots\ldots \quad (7)$$

where ϕ is $\frac{4.65 V_E^2}{100^2 P}$.

In the particular case for which K = 1, equation (7) becomes

$$\Delta T_{K=1} = (T_i + 273) \frac{\phi}{(1 + \phi)} \quad \ldots\ldots\ldots \quad (8)$$

so that $\frac{\Delta T_K}{\Delta T_{K=1}} = \frac{K(1 + \phi)}{(1 + K\phi)} = \frac{K(1 + 1/\phi)}{(K + 1/\phi)}$

or $\Delta T_K = f(K)\ \Delta T_{K=1} \quad \ldots\ldots\ldots\ldots\ldots\ldots \quad (9)$

where $f(K) = \frac{K(1 + 1/\phi)}{(K + 1/\phi)}$

Equation (9) is the basic equation used for the construction of the temperature - correction diagram.

2. Construction of the diagram

The principle behind the diagram is to draw isopleths of $\Delta T_{K=1}$, f(K) and the product of these. The first step in the preparation of the diagram was to derive isopleths of $\Delta T_{K=1}$ for the limits of indicated height, airspeed and temperature required. These limits were chosen to be from -2,000 ft to +53,000 ft on the I.C.A.N. scale, from 60 kt to 500 kt and from -67°C to +35°C respectively. The maximum indicated airspeed that can be catered for

falls off with increasing height but the diagram incorporates all conditions of height, airspeed and temperature likely to be encountered by aircraft whose performances are not significantly greater than those of conventional Canberra aircraft.

From equation (8),

$$\Delta T_{K=1} = (T_i + 273)\frac{1}{(1 + 1/\phi)} \quad \text{and} \quad \phi = \frac{4.65V_E^2}{100^2 P}$$

The first isopleths plotted were those for constant values of the indicated airspeed V_i, in steps of 5 kt, on a graph having $1 + 1/\phi$ along the ordinate and P along the abscissa. The indicated airspeed differs from the equivalent airspeed due to calibration compressibility error and position error. Details of these errors are given elsewhere (e.g., appendix B of reference (2)). It suffices here to say that the former error increases with height and airspeed in a manner which can be determined exactly by theory. It is independent of the aeroplane and can therefore be allowed for in these isopleths. Position error, however, although generally comparatively small, depends on the design and position on the aircraft of the pitot tube and static vent and cannot be allowed for.

Allowance for compressibility was therefore made and the curves were plotted on paper which was logarithmic both along the ordinate and the abscissa. This has the advantage of greatly reducing the crowding of the curves compared with that which would be obtained by plotting on linear graph paper. It also has the advantage that, since the pressure - height relationship is logarithmic, the pressures along the abscissa can be converted to I.C.A.N. heights which are conveniently spaced. These isopleths therefore allow values of $1 + 1/\phi$ to be obtained for different values of indicated height and airspeed.

The second step in the construction of the diagram was to draw isopleths of $\Delta T_{K=1}$, this being obtained from equation (8) as the quotient $\frac{T_i + 273}{1 + 1/\phi}$. These were drawn on a second sheet of graph paper, this time logarithmic along the ordinate and linear along the abscissa. Values of $1 + 1/\phi$, between the same limits as for the first graph, were plotted along the ordinate and values of the indicated temperature, between +35°C and -67°C were plotted along the abscissa. From the values of $1 + 1/\phi$ obtained from the first graph and the values of the indicated temperature, this second graph allows values of $\Delta T_{K=1}$ to be obtained.

The third step was to superimpose isopleths of f(K) on the second graph. Values of f(K) ($= \frac{K(1 + 1/\phi)}{(K + 1/\phi)}$) were computed for the same limits of $1 + 1/\phi$ as before and for values of K between 0.5 and 1.5. For these isopleths, values of $1 + 1/\phi$ were again taken along the ordinate and values of K were taken along the abscissa. The value of K = 1.5 is greater than that theoretically possible (i.e., 1.0) but in cases where the mounting of the thermometer is such that the airspeed over it is greater than the speed of the aircraft, apparent values of K greater than 1.0 can result. To give one example, the mean value for all heights of the recovery factor for the navigator's thermometer on the Canberra aircraft of the Meteorological Research Flight was found to be 1.06. This corresponds to the value of 2.53 given for speed correction coefficient in reference (2). The value found at 40,000 ft, for the same thermometer, was 1.23, the corresponding value of the speed correction coefficient being 2.94.

The curves of f(K) were plotted in steps of 0.1 in K giving a total of 11 curves between the chosen limits of K. It is unnecessary to have more than this number since it is a simple matter to interpolate between successive curves and errors which might arise due to poor interpolation are negligible.

/The

The next step in the construction of the diagram was to draw isopleths of ΔT_K on the second graph. These were obtained by a gridding process as the product of the curves for $\Delta T_{K=1}$ and those for f(K) and were drawn in steps of 0.5°C for values of ΔT_K between 2°C and 40°C.

The final step was to superimpose the first and second graphs, retaining a background graph and the completed diagram is shown in Fig. 1. From the manner of construction of the diagram it is unnecessary to know the ordinate values and these have been omitted. Furthermore, it is more suitable to retain a linear than a partly or fully logarithmic background graph and this has been done.

3. Use of the diagram

The full instructions for the use of the diagram are as follows:-

(1) Obtain the point on the diagram corresponding to the indicated values of height (corrected for instrument error, static pressure error and converted to an altimeter setting of 1013.2 mb) and airspeed (corrected for instrument error and static pressure error).

(2) Move from the point obtained in (1) parallel to the abscissa to the value of the indicated temperature (corrected for instrument error) and obtain a second point.

(3) Move from this second point parallel to the pecked lines to a third point at the junction with the appropriate curve for f(K), i.e., the f(K) curve corresponding to the required value of K.

(4) At this third point read off the required temperature correction, interpolating between the curves for ΔT.

4. Discussion of the diagram

Although first impressions of the diagram may be that it is complicated and difficult to use, this is really not so and it should not take the average person long to become proficient in its use.

Theoretically it gives the temperature correction exactly and this represents an advantage over the method previously used at the Meteorological Research Flight and probably used in modified forms by many other establishments. This previous method uses the equation

$$\Delta T = \frac{3.5344\,\alpha\,(T + 273)}{P}\,\frac{V_E^2}{(100)^2}$$ where α is the speed correction coefficient. Tables of $3.5344\,\alpha\,(T + 273)$ were prepared for a range of values of T and for each required value of α. It has been usual to use, as the value of α for an aircraft, the mean of the values obtained at different levels by the method of speed runs. While this is probably not seriously in error, it does involve the assumption of a speed correction coefficient which is invariant with height. This is contrary to experience with both the Meteorological Office flat plate thermometer and most commercial types of aircraft thermometer, even though different experimenters have disagreed on the manner in which the speed correction coefficient does vary with height. In computing the temperature correction by this method it is first assumed that the indicated temperature is a first approximation to the true temperature and a value of $3.5344\,\alpha\,(T + 273)$ may be obtained from the appropriate table. After allowing for instrument and position error corrections, the indicated airspeed V_i has to be converted to the equivalent airspeed V_E and a first approximation of ΔT is obtained by a slide rule operation. A second approximation to the true temperature T is then obtained by subtracting the first approximation to ΔT from the indicated temperature and the process is then repeated. This gives a second approximation to ΔT which differs from the true value of ΔT by a much smaller amount. In practice, this second approximation may be taken as the true value.

/The

The temperature - correction diagram makes allowance for variations in the recovery factor, K, and renders the computation of tables unnecessary. Compressibility errors are allowed for in the airspeed isopleths, again avoiding the need for a correction table. No slide-rule computations are necessary and, since the diagram is theoretically exact, the temperature corrections obtained from it are as correct as the user can obtain them. The error in using the diagram is not likely to be more than about 0.1°C at the lower airspeeds or about 0.5°C at the higher airspeeds. Errors of these magnitudes are, however, equally likely by the method which involves using the slide rule.

The absolute accuracy of the obtained temperature correction depends, of course, on the validity of the underlying theory and on the reliability of the airspeed indicator, altimeter and temperature indicator. Furthermore, values of the recovery factor, K, obtained from pairs of speed runs, carried out at different times but under apparently the same conditions, usually exhibit a large scatter which increases with height. Uncertainties in the accuracy of the measuring instruments and in the value of the recovery factor lead to probable temperature errors which are substantially larger than those likely to result from using the diagram. For example, the probable error of the flat plate thermometer fitted to the Canberra aircraft of the Meteorological Research Flight was found to vary at 40,000 ft from about 0.4°C at 200 kt to about 2°C at 450 kt.

It is possible to produce temperature-correction diagrams of the type presented to include any aircraft performance characteristics. Such diagrams could be presented on an enlarged scale to make for greater accuracy in reading them.

It is also possible to devise an instrument based on this diagram. Such an instrument would use sliding scales for parallel movements and would render some of the isopleths unnecessary. It is hoped to produce a prototype computer in the near future.

5. Acknowledgements

The work of devising this diagram was undertaken following a suggestion by Mr. F. H. Ludlam, during a joint M.R.F. - Imperial College investigation, that for slow speed aircraft an approximation to the temperature correction might be obtained diagrammatically.

The author is grateful to Mr. M. P. Gladstone who assisted in the computations while attached to Meteorological Research Flight as a vacation student.

6. References

(1) Meteorological Air Observer's Handbook, M.O. 470, p.15.

(2) Durbin, W.G. 1955 Some further determinations made by the M.R.F. of the speed correction coefficients of aircraft thermometers. Meteorological Research Papers, Air Ministry, London, No. 930.

M.R.P 1071

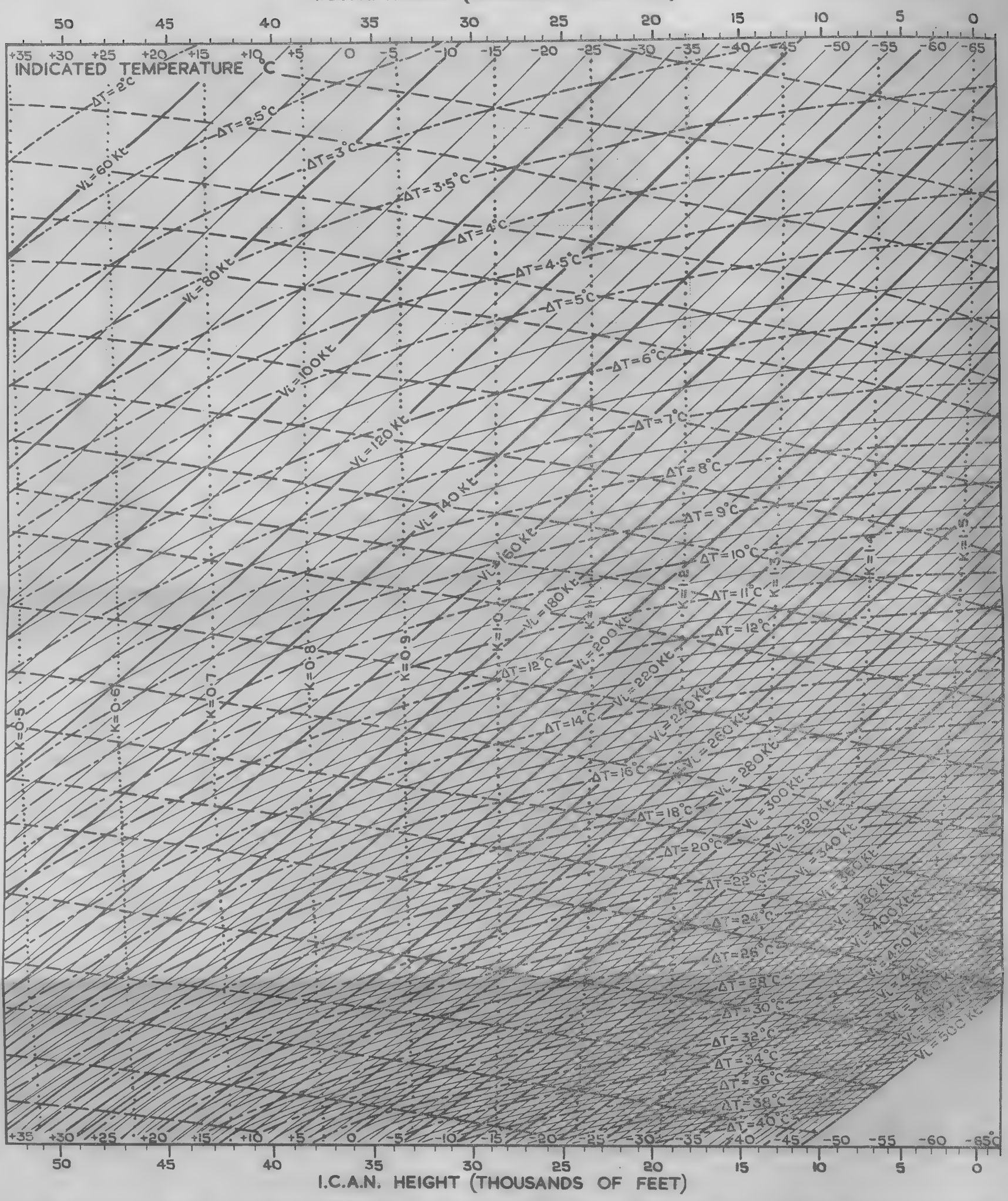

TEMPERATURE–CORRECTION DIAGRAM FOR AIRCRAFT THERMOMETERS.

M.R.P. 1073
S.C.111/245
9th October, 1957.

FILE (29) S

Convection - diffusion processes below a stable layer - Part 11

by

F. B. Smith.

(Meteorological Office)

AIR MINISTRY

METEOROLOGICAL RESEARCH COMMITTEE

M.R.P. 1073
S.C.III/245
9th October, 1957

AIR MINISTRY

METEOROLOGICAL RESEARCH COMMITTEE

Convection-diffusion processes below a stable layer - Part II

by

F.B. Smith

SUMMARY

Part of a previous paper* (I) dealt with the dual effect of convection and normal turbulent diffusion on the dispersal of an emittant from a ground level crosswind line source into an atmosphere of finite depth. The convection was represented directly in an independent way from that of turbulent diffusion. The latter was represented by the usual diffusion coefficient $K(z)$.

The model given below is an extension of (I), it being improved in two main respects. Firstly, the possible forms that $K(z)$ can take is altered from the previous form $K = k(H-z)$ to the family $K = kz^{-\alpha}$. Suggestions are made for generalizing possible values of $K(z)$ still further. Secondly, entrainment from the environment into the ascending convective motions is accounted for by an empirical relation for the velocity of environmental subsidence. A comparison between the improved model and the previous one is made for $K(z) = k(H-z)$.

1. INTRODUCTION

The effect of free convection on the statistical distribution of light particles emitted from a crosswind line source at ground level into a turbulent atmosphere of finite depth has been discussed in an earlier paper (Smith 1957: referred to herein as I). In this, a model was devised which accounted for many of the important properties of the convection-diffusion process yet which at the same time could be mathematically solved.

The model's most serious defect was that it assumed that the ascending elements of the convection process are completely generated at the ground, thereby ignoring any entrainment of the air and emittant after they have left the ground in their ascent to the top of the layer. In the present paper, this property, previously ignored, is taken into account and the solution is carried through for a more general set of diffusion coefficients.

The elements of the convection process may take the form of discrete bubbles or they may be more like continuous jets - their precise nature is a matter of controversy. In this paper and in (I) the actual nature is not relevant - the knowledge of the mechanics of the convective process needed in this analysis does not rely on such details.

In this model, as in (I), we shall generally consider $K(z)$ to decrease with height. The form taken is

$$K = kz^{-\alpha} \qquad (1)$$

Thus, although unrestricted, the value of the parameter α will most often be taken as positive, even though this implies infinite K at the ground. Except at very small distances from the source, this is not thought to be a very serious drawback since, remembering that $\frac{\partial C}{\partial z}$ is zero on $z=0$, all that

/it

* M.R.P. 1048

it means is that concentration will vary somewhat more slowly at first with height than with a K which ideally falls to zero at the ground.

The conception of the free-convection process is the same as in (I) except that here account is taken of entrainment of environmental air into the convective elements. These elements grow in size with height and collect emittant not only from the ground but from all levels. To compensate for this upward flux of matter the environment must subside. If the mean velocity of subsidence is $v(z)$ then the mean rate of entrainment into the convective elements is $\frac{dv}{dz}$ per unit volume of environment. But the relationships between rate of entrainment and the other features of the convection (such as the mean size, velocity etc., of the elements) can, at present, only be guessed at and it seems that more experimental evidence is needed before suitable relations can be established (although several theoretical attempts have been made to tackle problems related to this, a completely satisfactory solution is not yet available). We must therefore fall back on hypothesis. This analysis is based on the hypothesis that the mean velocity of subsidence decreases linearly to zero at the ground.

$$v = \lambda z \qquad (2)$$

Such an assumption, not only being physically plausible, considerably simplies the mathematical analysis. In fact, the experimental evidence would have to show that it is very much in error before one would feel justified in rejecting it, since rejection would almost certainly increase the analytical complexity.

Equations (1) and (2) represent the major assumptions. These give sufficient information regarding the entrainment process and the diffusion process needed to determine the statistical properties of the concentration, provided it can be assumed that the volume of the convective elements relative to the remainder of the atmosphere is fairly small (say not more than 10%). This requires the horizontal dimensions to be in the ratio of not more than about 1:3. If this were not so then it is clear that because of difficulties arising from relating the velocity of subsidence to the total flux into the elements when this ratio of relative volumes is appreciable, more detailed information regarding the nature of the convective elements would be required. The convective elements on reaching the top of the layer spread out over the top of previous elements causing them to subside. In this process they completely lose their former identity and become part of the general subsiding environment. As such they again become liable to re-entrainment into the convective motions. After reaching the top they act, statistically speaking, as a succession of plane sources subsiding with velocity $v = v(z)$ and at the same time diffusing one into the other at a rate determined by (1).

The emittant may be considered in three parts. Firstly, that which has not been entrained into the convective motions will belong to what is called the source-centred plume. Secondly, there is that contained in the convective elements and thirdly, that which has previously been brought up to the top of the layer and is in a state of subsidence. The last belongs to what shall be called the convected plume. These parts may be treated separately except in so far as the flux of matter into one must be balanced by an equal loss by the others. Section 2 deals with the source-centred plume, Section 3 with the convective motions and the convected plume. Section 4 discusses the deductions that should be made from data obtained in experiments designed to test the model. Section 5 briefly suggests how the model may be extended to more general forms of K. Examples are given. In particular the analysis is carried out for $K(z)$ varying as in (I) $k(z) = k(H-z)$, (H is the height of the convective layer). The result is then compared with the previous one at two distances. 10km. and 30km. for certain reasonable values of the parameters. It is noted that although there are differences, these are capable of qualitative explanation on grounds of the different assumptions in the two models. These differences are small, thereby suggesting that the solutions are not over-sensitive to the precise nature of the convection process.

/2.

2. EFFECT OF CONVECTION ON SOURCE-CENTRED PLUME

Now, without convection, diffusion coefficients of the form $K = kz^{\alpha}$ result in similarity - profile solutions. That is, the shape* of the concentration profile in the vertical is the same at all values of x, although the actual profile will differ from one value of x to another in scale (i.e. the scale height is a function of x). Mathematically, if at $x = x_1$, for given z_1,

$\frac{C(z)}{C(z_1)} = \chi\left(\frac{z}{z_1}\right)$ for all z, then at any other x, $x = x_2$ there exists a z_2 such that $\frac{C(z)}{C(z_2)} = \chi\left(\frac{z}{z_2}\right)$ for all z. The ratio of z_1 to z_2 will be equal to the ratio of the scale heights of the plume at x_1 and x_2 respectively.

This can be deduced from the solution (for zero convection):

$$C = \frac{Q}{u}\,\frac{(2\nu)^{2n-1}}{(-n)!}\left(\frac{Kx}{u}\right)^{n-1} e^{-\frac{uz^{2\nu}}{4\nu^2 kx}} \qquad \ldots\ldots\ldots (3)$$

where $n = \frac{1+\alpha}{2+\alpha}$, $\nu = \frac{2+\alpha}{2}$, $2\nu(1-n) = 1$

Consider now the effect of the particular form of convection represented by equation (2): $v = \lambda z$, on the shape of the source-centred plume. This convection process has two main properties, entrainment and subsidence. In considering their effect on the plume it is useful to think of them separately.

Firstly, the volume of air-plus-emittant being lost per unit time, per unit volume of atmosphere, through the action of entrainment into the convective elements is $\frac{dv}{dz}$, and this is an absolute constant, equal to λ. Thus entrainment acts as a uniform volume-sink throughout the whole region removing equal volumes of air from all layers in equal times. And in so doing it removes some of the emittant, the amount being in absolute proportion to the concentration of that level and to the constant rate of entrainment. Thus entrainment results in a percentage loss of emittant equal to all heights. This can be summarised in the following results:

Result (i): The loss of emittant by entrainment does not in itself alter the shape of the concentration profile in the source-centred plume; it makes a uniform percentage reduction in the quantity of emittant in each layer.

Secondly, the downward velocity of subsidence of the environment has a linear increase with height. This results in a uniform 'compressive' action, meaning that the vertical separation between any two horizontal layers is continually decreasing at a rate proportional to their separation, and from this the second result may be deduced.

Result (ii): The compression resulting from subsidence is uniform and does not depend on z. Thus the ratio of the heights of any two points A and B (see figures (i)) does not change with time.

Let the heights of B, B', A and A' be z_1, z_1', z and z' respectively. Then result (i) gives

$$\frac{C(z)}{C(z_1)} = \frac{C(z')}{C(z_1')}$$

and result (ii) states that $\frac{z}{z_1} = \frac{z'}{z_1'}$

Taken together these add up to the condition of similarity given at the beginning of the section. Moreover, since the above results do not depend on the magnitude of λ, so that λ could be slowly and uniformly increased from zero to any desired value without changing the shape of the profile (although the scale would be changed), we deduce that the shape of the profiles is dependent only on K and not on λ.

/We

---

*Two profiles have the same shape if they are related by a linear change in scale

We thus have the following theorem:

Theorem. If, without convection, the source-centred plume from a ground level continuous infinite cross-wind line source has the property of similarity (as defined above) the additional effect of convection, defined by $v = \lambda z$, is

(i) similarity is preserved

(ii) the shape of the profiles is conserved, i.e. for equal scale heights and equal z, the function χ is unaltered.

(iii) the scale height of the plume varies in a different way with distance downstream (x).

All the results which follow are deductions from this theorem. The first deduction is that, with convection, the profile of the source-centred plume must have the form

$$C = g(x)\ e^{-z^{2\nu}/f(x)} \qquad \ldots\ldots (4)$$

where $g(x)$ and $f(x)$ are functions of x to be determined.

One of the important properties of similarity profiles is that, as the shape is constant, the profile at any value of x is determined solely by one parameter μ - which we may call the scale height.

This may be defined as the mean m

$$m = \frac{\int_0^\infty zC\,dz}{\int_0^\infty C\,dz}$$

or as the standard deviation σ, where

$$\sigma^2 = \frac{\int_0^\infty z^2 C\,dz}{\int_0^\infty C\,dz}$$

or by any other convenient length-scale. There will always exist a constant relation connection μ with m and σ, independent of x. Consequently, knowledge of how μ changes with x, gives complete understanding of the concentration profile of the source-centred plume at all position.

The rate of change of μ with x is governed by the dual action of diffusion and subsidence. Since both these processes are shape-preserving they can be considered independently (see fig. (ii)).

Diffusion tends to increase μ and at a rate equal to that if there were no convection. This is represented by the first term on the R.H.S. of equation (5): $\left(\frac{d\mu}{dx}\right)_{\lambda=0,\ x^M}$, meaning the rate of change of μ with x with no convection ($\lambda = 0$) at the distance downstream equal to x^M (where μ takes the same value as at x with convection). Comparing (3) and (4) x^M is given by

$$4\ \nu\ K x^M = uf(x)$$

Subsidence on the other hand is tending to decrease μ. Since the velocity of subsidence at height μ is λ/u, the contribution of this effect in (5) is $-\frac{\lambda}{u}\mu$. Thus

$$\left(\frac{d\mu}{dx}\right)_{\lambda,x} = \left(\frac{d\mu}{dx}\right)_{\lambda=0,x=x} + \frac{\lambda}{u}\mu \qquad \ldots\ldots (5)$$

This equation can be deduced from the equation of diffusion

$$u\frac{\partial C}{\partial x} = \frac{\partial}{\partial z}\left[K\frac{\partial C}{\partial z}\right] + \lambda z\frac{\partial C}{\partial z}$$

The other important property of convection relevant to the source-centred plume is that given in Result (i), namely, that the overall concentration in theplume is reduced at a rate proportional to the concentration itself and to the rate of entrainment λ

$$\frac{d}{dx}\int_0^\infty C\,dz = -\frac{\lambda}{u}\int_0^\infty C\,dz \qquad \ldots\ldots (6)$$

This solution of which is

$$\int_0^\infty C\,dz = \frac{Q}{u}e^{-\frac{\lambda}{u}x} \qquad \ldots\ldots (7)$$

where Q is the source strength.

Equations (5) and (7) are the operational manifestations of the theorem, and are sufficient to determine the hitherto unknown functions $f(x)$ and $g(x)$ in (4).

As $\lambda \longrightarrow 0$, that is, the convection reduced to zero, then

$$f(x) \longrightarrow 4\nu^2 Kx$$

$$g(x) \longrightarrow \frac{(2\nu)^{2n-1}}{(-n)!}\frac{Q}{u}\left(\frac{u}{Kx}\right)^{1-n}$$

so that form (4) reduces to (3).

To determine $f(x)$ we apply (5). Take μ as the standard deviation σ. For (3) it is given by

$$\sigma^2 = \frac{(\frac{1}{\nu}-n)!}{(-n)!}\left[4\nu^2 Kx/u\right]^{2(1-n)} \qquad \ldots\ldots (8)$$

whereas for (4) it is

$$\sigma^2 = \frac{(\frac{1}{\nu}-n)!}{(-n)!}\left[f(x)\right]^{2(1-n)} \qquad \ldots\ldots (9)$$

Inserting these in (5)

$$\sqrt{\frac{(\frac{1}{\nu}-n)!}{(-n)!}}\,(1-n)\left[f(x)\right]^{-n}\frac{df}{dx} = \left(4\nu^2\frac{K}{u}\right)\sqrt{\frac{(\frac{1}{\nu}-n)!}{(-n)!}}\,(1-n)x^{-n} - \frac{\lambda}{u}\sqrt{\frac{(\frac{1}{\nu}-n)!}{(-n)!}}\left[f(x)\right]^{1-n}$$

$$\text{i.e.}\quad \frac{df}{dx} + \frac{\lambda}{u(1-n)}f = 4\nu^2\frac{K}{u} \qquad \ldots\ldots \quad (10)$$

The solution of (10), which is zero at $x = 0$, is

$$f(x) = \frac{2\nu K}{\lambda}\left[1 - e^{-2\frac{\lambda}{u}x}\right] \qquad \ldots\ldots \quad (11)$$

Thus $f(x)$ is determined, and it is noted that since $f(x)$ tends to a constant for large x the source-centred plume will not fill the whole layer but will reach an equilibrium height when the tendency to increase due to diffusion is balanced by the tendency to decrease on account of the subsidence.

The function $g(x)$ is determined from (4) and (7)

$$g(x) = \frac{Qe^{-\frac{\lambda}{u}x}}{u(1-n)!\left[f(x)\right]^{1-n}} \qquad \ldots\ldots \quad (12)$$

thereby giving the complete solution

$$C(x,z) = \frac{Q}{u(1-n)!}\left(\frac{\lambda}{2\nu K}\right)^{1-n}\left[1 - e^{-2\nu\frac{\lambda}{u}x}\right]^{n-1} e^{-\frac{\lambda x}{u}} \exp\left[-\frac{\lambda z^{2\nu}}{2\nu K(1-e^{-2\nu\frac{\lambda}{u}x})}\right]$$

$$\ldots\ldots \quad (13)$$

3. CONVECTED PLUME

It has been seen that some of the emittant becomes entrained in the ascending convective elements of warm air. In balance with this upward flux there exists an environmental subsidence. In accordance with our hypothesis, the velocity of subsidence is λz downwards. The path of an element after having reached the top of the layer is given by

$$z_m = H\,e^{-\frac{\lambda}{u}(x-x')} \qquad \ldots\ldots \quad (14)$$

where H is the height of the layer and x' is the distance downwind of the source at which the convective element reached the top.

Each element will be diffusing relative to this path but because K (as given by (1)) is small at such heights, this diffusion will be fairly slow. Eventually, of course, they will subside sufficiently far for them to reach the more turbulent layer near the ground, but by this time practically uniform concentration will have been achieved across the layer and what happens to the individual elements will be no longer of any interest. Therefore, in the region of interest the spread of each elemental plume will be small and it will suffice to assume that the rate of increase of this spread with distance downstream will be governed by a diffusion coefficient, K, effectively constant across its width, and taking the value given by (1), z being the value at the centre of the plume $z = z_m$.

Then the distribution of concentration across each of these elemental plumes will be normal

$$C = \frac{A}{\sqrt{2\pi}\,\sigma(x)} \exp\left[-\frac{(z - z_m)^2}{2\sigma^2(x)}\right] \qquad \ldots\ldots(15)$$

where (x) is the standard deviation of the plume, and is to be determined. Locally, the spread of a plume in a region of constant K is given by

$\sigma^2 = \frac{2K}{u}(x-a)$ where $x = a$ is the virtual origin of the plume.

The rate of change of the spread due to K is therefore given by

$$\frac{d\sigma}{dx} = \frac{K}{\sigma u} \qquad \ldots\ldots(16)$$

Thus a plume whose spread is σ, in an atmosphere with quasi-uniform K and u will increase in width at a rate given by (16) if no other phenomena are influencing it. There is, however, the additional effect of entrainment and subsidence.

Because of the latter, the magnitude of K, which varies with z, will vary with distance downstream at a rate depending on the rate of fall of the element. By (1) and (14)

$$K = \frac{k}{H^\alpha} e^{\frac{\lambda}{u}(x-x')} \qquad \ldots\ldots(17)$$

Also because of the entrainment, the elemental paths tend to converge. This implies that, as before, the rate of change of σ has to be modified by a term proportional to the entrainment

$$\frac{d\sigma}{dx} = \frac{1}{\sigma}\frac{K(x)}{u} - \frac{\lambda}{u}\sigma \qquad \ldots\ldots(18)$$

Putting $y = \frac{1}{2}\sigma^2$ and substituting for K from (17), this transforms to

$$\frac{dy}{dx} + \frac{2\lambda}{u}y = \frac{k}{uH^\alpha} e^{\frac{\lambda}{u}\alpha(x-x')} \qquad \ldots\ldots(19)$$

the solution of which is

$$\sigma^2 = \frac{2k}{H^\alpha \lambda(\alpha+2)}\left[\left(\frac{z_m}{H}\right)^{-\alpha} - \left(\frac{z_m}{H}\right)^2\right] \qquad \ldots\ldots(20)$$

The standard deviation σ in equation (15) is therefore determined. The coefficient A may be found as follows:

The total integral expectation concentration in the depth H is Q/u. Therefore $\frac{\lambda Q}{u}$ is being entrained into the convective elements every second over unit horizontal surface area. This then is the flux of emittant arriving at the top of the layer every second. Similarly the volume of air arriving in the elements over the same area is λH. The concentration in the elements is therefore

$$A = \frac{\lambda Q}{u} \cdot \frac{1}{\lambda H} = \frac{Q}{uH} \qquad \ldots\ldots\ldots (21)$$

That is, the elements arrive at the base of the inversion with a concentration equal to that of the final concentration a long distance downstream when the emittant is uniformly spread throughout the layer. These arguments are essentially unaffected by the intermittancy of the convection process.

The convected plume is made up of the sum of the elemental plumes, given by (5) where σ and A are given by (20) and (21)

$$C(x,z) = \int_{z_{mo}}^{H} \frac{Q}{Hu\sqrt{2\pi\sigma(z_m)}} \exp\left[-\frac{(z-z_m)^2}{2\sigma^2(z_m)}\right] dz_m \qquad \ldots\ldots (22)$$

$$\text{where } z_{mo} = H e^{-\frac{\lambda}{u}x}$$

It is clear from the nature of the process involved that $C(x,z)$ will approximate very closely to $\frac{Q}{uH}$ for z greater than $z_{mo} + \sigma(z_{mo})$. For z less than this value, the concentration will fall below $\frac{Q}{uH}$ until for z less than $z_{mo} - (z_{mo})$, the concentration is sensibly zero.

Hence it is only necessary to consider the integral (22) in this narrow range. Moreover, if $\sigma(z_{mo})$ is not too large, $\sigma(z_m)$ can be taken as constant inside the integral, its value being taken as $\sigma(z_{mo})$.

For $-\sigma(z_{mo}) < z - z_{mo} < \sigma(z_{mo})$

$$C(x,z) = \int_{z_{mo}}^{H} \frac{Q}{Hu\sqrt{2\pi\sigma(z_{mo})}} \exp\left[-\frac{(z-z_m)^2}{2\sigma^2(z_{mo})}\right] dz_m \qquad \ldots\ldots (23)$$

$$C(x,z) = \frac{Q}{2uH} \operatorname{erfc}\left(\frac{z_{mo} - z}{\sqrt{2\sigma(z_{mo})}}\right) \qquad \ldots\ldots (24)$$

In a field experiment in which convection plays a significant role in the dispersion of the emittant the sampling instruments would not only be recording the concentration of the environment but would also be spasmodically sampling concentrations in the ascending convective elements. To determine what proportion of the whole is due to these elements requires more information than we have already. It is possible to anticipate what the concentration in the elements will be (see (25) below) but one also requires to know the proportion of the atmosphere filled by the elements. This can be found if some property such as their vertical velocity is known. But without this information it will be impossible to predict fully the total catch of the sampler, although generally, except when the environmental concentration is small compared with Q/uH, the contribution from the convective elements will only represent a small proportion of the whole.

The concentration in the elements at height z is

$$C = \frac{1}{\lambda x} \cdot \lambda \int_0^z g(x) \exp\left[- \frac{z^{2\nu}}{f} \right] dz$$

$$C = \frac{Q}{uz} e^{-\frac{\lambda}{u}x} I\left(\frac{z}{f}^{2\nu}, -n\right) \qquad \ldots\ldots \quad (25)$$

where I is the incomplete Γ-function. This is the concentration before the elements reach the subsiding emittant. At the line $z_{\infty o} = H e^{-\frac{\lambda}{u}x}$

$$C(x, z_{\infty o}) \simeq \frac{Q}{uH} \qquad \ldots\ldots \quad (26)$$

since $I \simeq 1$ for large z. Above this the element will remain at the same concentration, since the air it is entraining is the same concentration as itself. Therefore above $z = z_{\infty o}$ the sampler should record the correct environmental concentration Q/uH, the proportion of the atmosphere filled with convective elements is irrelevant.

4. TESTING TECHNIQUE

At present no really satisfactory evidence can be brought forward in support of this theory. It would be interesting to see if the predictions are, in fact, borne out in practice under conditions we have tried to simulate in this model, and in particular if a significant increase in the concentration could be detected as one approaches the top of the convective layer. In the event of these predictions being confirmed by future experiments, it should then prove possible to determine from (14) the magnitude of λ by measuring the depth of the quasi-uniform convected plume.

An alternative approach would be to take a series of samples at ground level in the downwind direction (although this might be rather difficult and expensive to do properly). Since over a fairly wide range of large x (and yet not so large that the convected plume has begun to interfere with the ground level concentrations), (13) gives $C \propto \exp\left[- \frac{\lambda}{u}x \right]$, there should exist a flat part of the curve of the logarithm of concentration against x whose slope is $- \lambda/u$ (see figures (iii)).

5. EXTENSION TO MORE GENERAL K

If K differs significantly in form from those given in equation (1), then part of the above analysis will not be valid and some of the predictions must be altered. Provided K is still small in the upper regions of the layer, these alterations are restricted to the quantitative predictions relating to the source-centred plume, the qualitative picture and the results of 3 remain sensibly unaltered.

In most circumstances the equation of diffusion without convection

$$u \frac{\partial C}{\partial x} = \frac{\partial}{\partial z}\left[K \frac{\partial C}{\partial z} \right] \qquad \ldots\ldots \quad (27)$$

is more likely to be solved than that with convection

$$u \frac{\partial C}{\partial x} = \frac{\partial}{\partial z}\left[K \frac{\partial C}{\partial z} \right] + \lambda z \frac{\partial C}{\partial z} \qquad \ldots\ldots \quad (28)$$

In these circumstances (that is, when (27) is solved but not (28)) an estimate of the shape of the source-centred plume (with convection) can be arrived at by application of some feasible hypothesis, suggested perhaps by the physics or by the results of the analysis in 2, linking the two solutions together.

The following is suggested:

Hypothesis

Since the primary parameter determining the concentration profile of the plume from one value of x to another is the first moment $m = \int_0^\infty zCdz / \int_0^\infty Cdz$, we suppose there exists a link relating the rates of growth of m, with distance downstream, with convection and without convection. This link is assumed to be that given by equation (5) (putting $\mu = m$)

$$\left(\frac{dm}{dx}\right)_{\lambda,x} = \left(\frac{dm}{dx}\right)_{\lambda=0,x^*} - \frac{\lambda}{u}m \qquad \ldots\ldots \quad (29)$$

(the notation has the same meaning as before). Naturally, having chosen this equation none of the other moments will be expected to satisfy (5) - the concentration profile for general K is not a similarity profile. Thus if the solution of (27) is determined, then m is found. To find the relation between x and x^* we use (29):

$$\frac{dx^*}{dx} = 1 - \frac{\lambda}{u}m\frac{dx^*}{dm} \qquad \ldots\ldots \quad (30)$$

$$\text{i.e. } x = \int_0^{x^*} \frac{ds}{1 - \frac{\lambda}{u}m(s)\frac{ds}{dm}} \qquad \ldots\ldots \quad (31)$$

from which we deduce $x^*(x)$ $\ldots\ldots$ (32)

Also since (11) is independent of K, the total concentration in the source-centred plume is known, so that the approximate form for the plume is

$$C(x,z,\lambda) = e^{-\frac{\lambda}{u}x} C(x^*,z,0) \qquad \ldots\ldots \quad (33)$$

Briefly, as an example of this take $K = kz(H-z)$ the solution of which, without convection, is given in (I). Firstly determine m(x): The equation of diffusion is

$$u\frac{\partial C}{\partial x} = k\frac{\partial}{\partial z}\left[z(H-z)\frac{\partial C}{\partial z}\right] \qquad \ldots\ldots \quad (34)$$

Multiply by z and integrate between z = 0 and z = H

$$u\frac{\partial}{\partial x}\int_0^H zCdz = k\int_0^H z\frac{\partial}{\partial z}\left[z(H-z)\frac{\partial C}{\partial z}\right]dz$$

Integrating by parts $\frac{\partial m}{\partial x} + \frac{2k}{u} m = \frac{k}{u} H$ ..... (35)

Thus
$$\left.\begin{aligned} m &= \frac{H}{2}\left(1-e^{-\frac{2k}{u}x}\right) \\ \frac{\partial m}{\partial x} &= k\frac{H}{u} e^{-\frac{2k}{u}x} \end{aligned}\right\} \quad \ldots\ldots \quad (36)$$

Inserting these into (31)

$$x = \frac{2k}{2k+\lambda} x^{*} - \frac{u}{2k+\lambda} \log\left[1 + \frac{\lambda}{2k}\left(1-e^{\frac{2k}{u}x}\right)\right] \ldots\ldots \quad (37)$$

From this $x^{*}(x)$ may be obtained graphically. The solution is then obtained from the known solution by (33). Equation (37) shows that the centre of gravity of the plume is depressed by convection, when x is large, from $H/2$ to $\frac{kH}{2k+\lambda}$. The convected plume is treated in the same way as in 3, and the final solution is the sum of the two plumes.

6. COMPARISON WITH MODEL OF PAPER I

In paper I in which $v(z)$ was constant and equal to λ_1, and the diffusion coefficient decreased linearly with height:

$$K = k(H-z) \quad \ldots\ldots \quad (38)$$

an evaluation was given for $\lambda/k = \frac{1}{2}$, corresponding to weak convection.

With the method suggested in the previous section it is possible to carry through a similar evaluation for the present model using the same K as (38) and the same average value of the velocity of subsidence:

$$v = \frac{2\lambda_1 z}{H} .$$

The equation for m in the corresponding zero-convection problem is given by

$$\frac{dm}{dx} = \frac{k}{u}\left(\frac{uH}{Q} C(o) - 1\right)$$

Putting $\frac{m}{H} = M$ and $\frac{k}{uH} x = X$ this becomes

$$\frac{dM}{dX} = \left(\frac{uH}{Q} C(o) - 1\right) = F(X) \quad \ldots\ldots \quad (39)$$

Now $\frac{uH}{Q} C(o)$ is known ((I) equation (20)) and therefore $\frac{dM}{dX}$, and, by integration, M. The function $G(X) = \frac{1}{1-M\frac{dX}{dM}}$ is then formed from which we can deduce, using (31), the corresponding value of X with convection

$$X = \int_0^{X^{*}} G(X)\,dX \quad \ldots\ldots \quad (40)$$

For the purposes of comparison let us take the convenient figures:

$$K(o) = 5 \times 10^5 \text{ cm}^2/\text{sec}, \quad u = 4.5 \text{ m/sec}, \quad H = 1\text{km}, \quad x = 10 \text{ km}$$

Then $X = 0.111$ and $X^{*} = 0.1$. The profile of the source-centred plume is thus given by (I) - (20) and by (33) above

$$C(x, z, \lambda) = e^{-X} C(X^{*}, z, o)$$

The convected plume is found in a similar way as before. Also

$$\frac{Z_{*}}{H} = e^{-X} \qquad \ldots\ldots \qquad (41)$$

Putting $Y = \frac{1}{2}\frac{\sigma^2}{H^2}$ the corresponding equation to (19) is

$$\frac{dY}{dX} + 2Y = 1 - e^{-X} \qquad \ldots\ldots \qquad (42)$$

The solution of which is

$$\frac{\sigma^2}{H^2} = 1 + e^{-2X} - 2e^{-X} \qquad \ldots\ldots \qquad (43)$$

Assuming (24) to be still valid, equations (41) and (42) give the solution to the convected plume. The two solutions can now be added to give the complete environmental concentration. The result at 10 km is compared with the solution of (I) in figure (iv). The result for 30 km shows that the variations from the uniform concentration Q/uH are negligible, as they were in the previous model.

Comparison of these solutions with those obtained as a result of using a form of $K(z)$ given in equation 0 indicate that agreement is not good if the form of $K(z)$ is in error.

Recordings of vertical wind velocity fluctuations in vigorous convective conditions suggest that v is something of the order of tens of centimetres per second, corresponding to upward velocities of the convective elements of several metres per second. Figure (v) is a comparison of the concentration profiles in what might very well be typical weak and vigorous convective conditions respectively. The chosen values of the parameters are given in the legend to the figure. It is seen that in the case of vigorous convection almost complete uniformity has been achieved at this distance (10 kms) whereas for the weak convection case only about half the layer contains any appreciable amount of the emittant.

It should be noted, in conclusion, that the above evaluations are purely formal in that we are still without sufficiently realistic data on the functional form of $K(z)$ and the magnitude of λ. But one thing is clear, this present model is to be preferred to that given in (I) both on theoretical grounds and also because of the comperative simplicity of the computations involved.

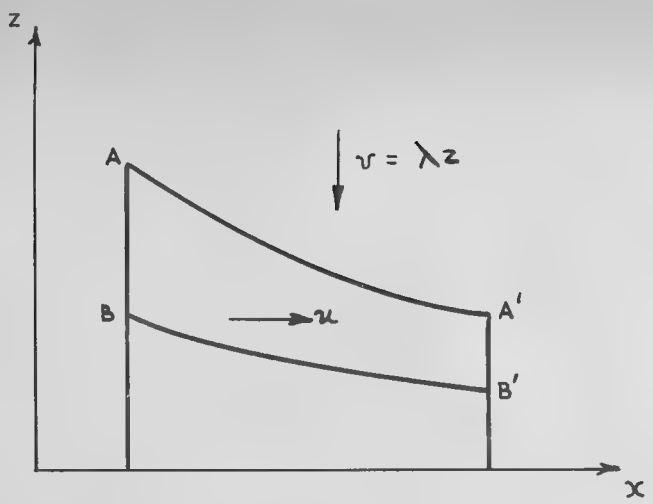

FIGURE (i) DIAGRAMMATIC REPRESENTATION OF THE EFFECT OF SUBSIDENCE IN UNIFORMLY COMPRESSING THE SOURCE-CENTRED PLUME THE RELATIVE HEIGHTS OF A & B REMAIN UNALTERED.

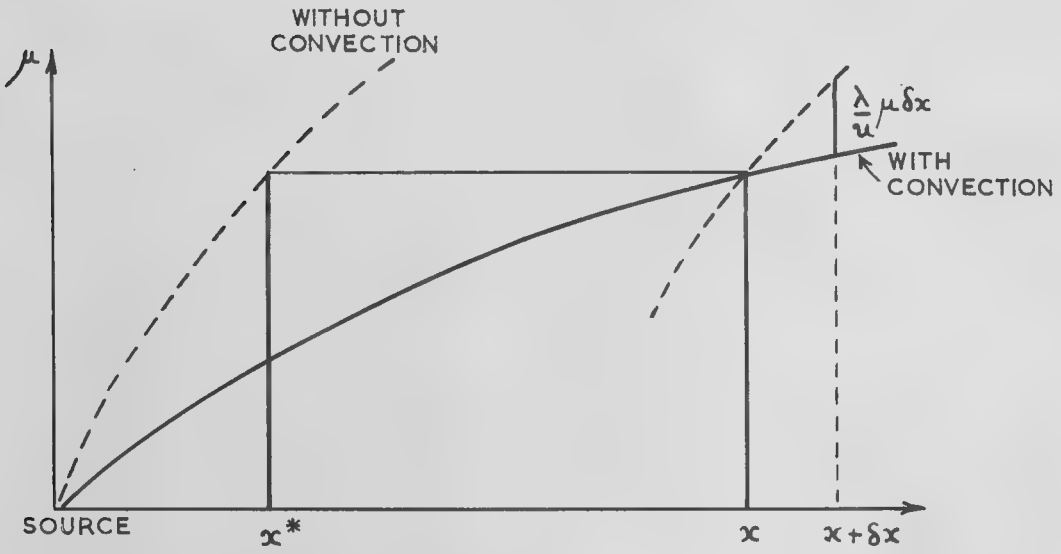

FIGURE (ii) THE RATE OF GROWTH OF μ AT x, WITH CONVECTION, IS THE SAME AS AT x^*, WITHOUT CONVECTION, EXCEPT FOR A TERM $\frac{\lambda}{u}\mu$ ARISING FROM THE COMPRESSIVE EFFECT OF SUBSIDENCE.

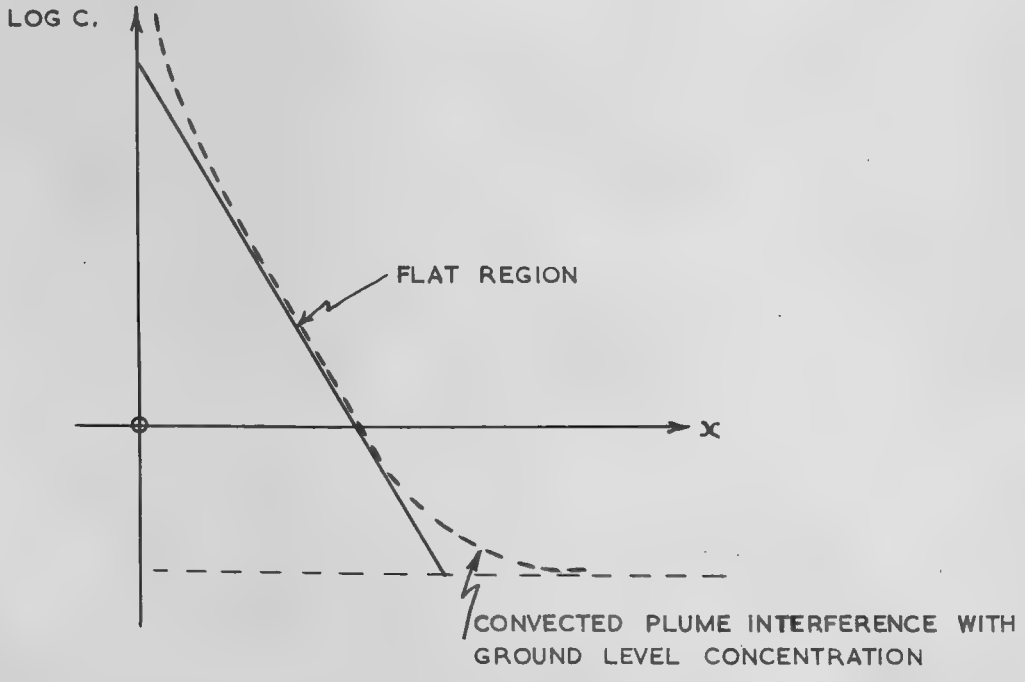

FIGURE (iii) THE PLOT OF THE LOGARITHM OF CONCENTRATION AGAINST DISTANCE DOWNSTREAM x SHOWS A FLAT REGION OVER A CONSIDERABLE RANGE OF x. THE SLOPE OF THIS REGION IS $-\frac{\lambda}{u}$

FIGURE (IV)

MRP 1073

COMPARISON OF MODELS AT 10 km.

$$K = k.\ (H - z.)$$

K IS THE COEFFICIENT OF DIFFUSION, H THE HEIGHT OF THE CONVECTIVE LAYER, Z IS THE HEIGHT ABOVE GROUND, x IS THE DISTANCE DOWNSTREAM OF THE SOURCE, u IS THE CONSTANT WIND SPEED, v THE VELOCITY OF SUBSIDENCE IN THE ENTRAINMENT MODEL, λ_1 IN THE NON-ENTRAINMENT MODEL; C IS THE CONCENTRATION AND Q THE SOURCE STRENGTH.

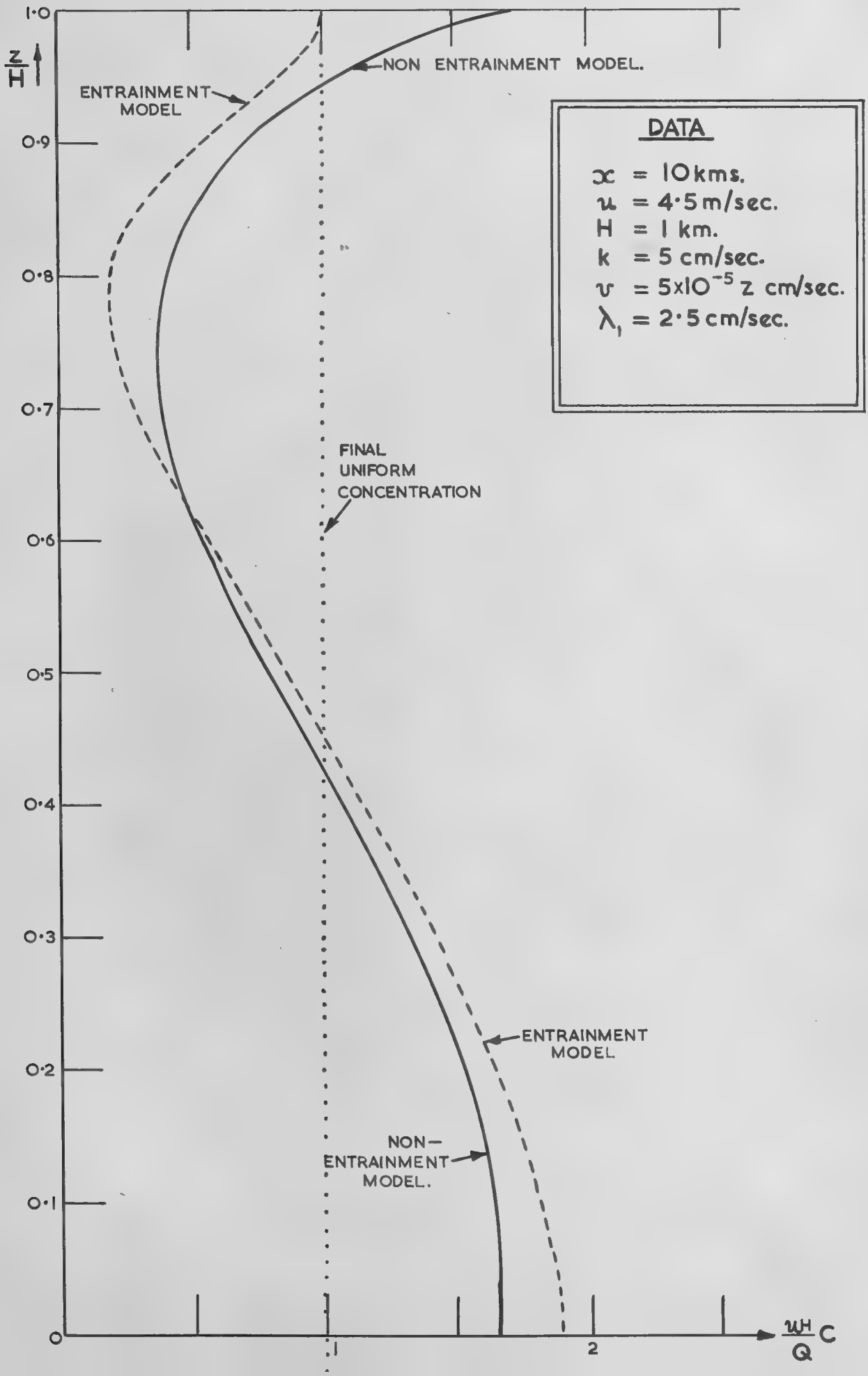

FIGURE (V)

COMPARISON BETWEEN CONCENTRATION PROFILES FOR WEAK AND VIGOROUS CONVECTION.

THE SYMBOLS HAVE THE SAME MEANING AS IN FIGURE (IV)

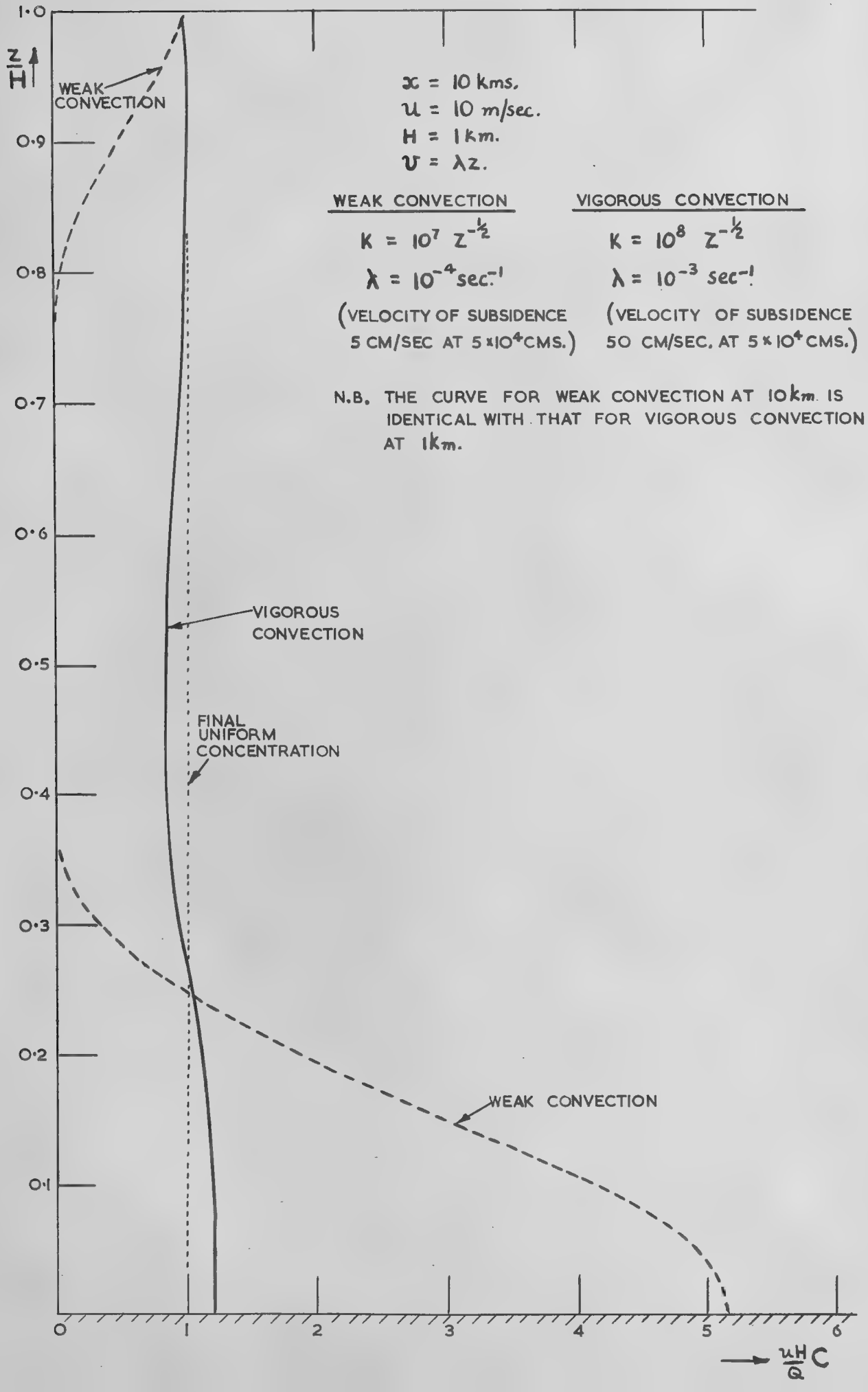

M.R.P. 1074
S.C.111/246
S.C.1/130
28th October, 1957

Some observations on the composition of fogs

by

K. H. Stewart

(Meteorological Office)

AIR MINISTRY

METEOROLOGICAL RESEARCH COMMITTEE

MASTER FILE COPY
NOT TO BE REMOVED
FROM AWS TECH FILES

At the time of issue this report has not been published. Any author desiring to quote this paper should refer to it as "A paper of the Meteorological Research Committee (London), M.R.P. No. 1074 by Dr. K.H. Stewart. A copy is available in the Library of the Meteorological Office."

M.R.P. 1074
S.C.III/246
S.C.I/130
28th October, 1957

AIR MINISTRY

METEOROLOGICAL RESEARCH COMMITTEE

Some observations on the composition of fogs

by

K.H. Stewart (Meteorological Office)

1. Introduction

A knowledge of the number of droplets of different sizes in a fog is essential to the understanding of many of the physical processes involved in its formation, persistence and dispersal. It was therefore decided to include the measurement of drop size distribution in the general programme of research on fog being carried out at Cardington. It was at first thought that the measurements could be made relatively simply, but unexpected difficulties arose and the problem of devising satisfactory measuring techniques was transferred to Kew Observatory. The techniques devised at Kew are still under development and do not yet give drop size distributions in great detail, but the results already obtained differ so much from previous ideas on the composition of fog as to seem worth reporting.

2. Observations with a cascade impactor

Samples of many fogs were taken with the "cascade impactor" described by May (1945). The fog drops were caught on microscope slides coated with Napthol Green B in gelatine (Wootten, 1955) and the resulting ring-shaped stains were counted and sized under a microscope. Fuller details of the sampling technique are given in Appendix I.

The results are summarized in table I which gives, for each size-range of drops, the sum of the cross-sectional areas (πr^2) of all the drops in unit volume of air whose diameters lie within the size-range. This quantity is denoted by S_i (for the i th size-range); its dimensions are area/volume and it is conveniently expressed in units of Km^{-1}. It is convenient to use S_i rather than the number (n_i) or mass (m_i) of drops of given sizes per unit volume because S_i is more closely related to the optical properties studied in the present work. In particular, the contribution of the drops of the i th size-range to the optical attenuation coefficient, σ_i, is given by $\sigma_i = K_i S_i$ where K_i is the appropriate value of the "scattering area coefficient" K calculated by Houghton and Chalker (1949) and others as a function of r/λ (r = radius of drop, λ = wavelength of light). For drops larger than about 5μ in diameter, the only ones of importance in table I, K is found to be equal to 2.0. The contribution of all the drops of a sample to the attenuation coefficient is therefore given by $\sigma_d = 2 \Sigma_i S_i$ which is included in table I.

The values of σ_d are to be compared with observed values of attenuation coefficient, σ, given in the next column of table I. Most of the values of σ were derived from observations of visibility, V, by Koschmieder's formula $\sigma V = 3.91$, but others were obtained, independently of visibility observations or Koschmieder's formula, from measurements of attenuation made with a Gold or photoelectric visibility meter. (Despite their names, these instruments measure attenuation not "visibility").

It will be seen that there are enormous discrepancies between the values of σ_d and σ . A part of the discrepancy can be attributed to the effect of smoke particles on the attenuation, but rough estimates of their contribution (σ_s) to the attenuation coefficient can be made from the measurements of smoke pollution made with the Owens automatic pollution recorder and it will be seen that in most of the cases tabulated σ_s can account for only a small fraction of the discrepancy.

A careful investigation of the operation of the cascade impactor (see Appendix I) showed that it was very unreliable as a sampler of water drops smaller than about 10μ in diameter. Many of these drops seem to be lost by evaporation in their passage through the impactor, the fraction lost increasing rapidly with decreasing size. For drops between 10 and 20μ the impactor seems reasonably accurate (though random errors of sampling lead to an uncertainty factor of the order of 2 in the true drop concentrations) but for larger drops sampling errors due to inertia effects begin to be important. These are rather worse in the conditions of fog sampling (when a quite small volume of air has to be sampled from an almost calm atmosphere) than in the conditions in which the impactor was originally tested (with relatively large volumes drawn from a wind blowing into the instrument), but for drops up to 50μ the average losses probably do not exceed 75 per cent.

We conclude, therefore, that the results of table I can be taken as approximately correct for the size range 10-20μ ; for sizes of 5-10μ and 20-50μ the impactor results give some qualitative indication of the presence or absence of drops, while drops smaller than 5μ or larger than 50μ may be missed entirely.

An independent rough estimate of the numbers of drops larger than about 10μ was made on several occasions by the very simple method of exposing Napthol Green-coated slides face upwards on the ground for a few minutes and then examining the stains produced by drops that had settled under gravity on to the slides. The numbers of drops of different sizes per unit volume of air were calculated from the numbers of stains per unit area of slide, the times of exposure and the theoretical terminal velocity of the drops. The results are included in table I. It will be seen that these "sedimentation" samples agree tolerably well with simultaneous impactor samples in the 10-20μ size range but contain fewer smaller drops and more larger ones. Presumably drops smaller than 10μ are prevented from settling by local eddies or evaporate on contact with the slide, without leaving a stain, while larger drops are sampled correctly by the sedimentation method and the excess over impactor results above 20μ is due to inertial losses in the impactor. The chief value of the sedimentation results, however, is that they indicate that in most of the fogs sampled there were no appreciable numbers of drops larger than 50μ and relatively few between 20 and 50μ , so that the inertial losses of the impactor for large drops affect only the upper tail of the drop size distributions of Kew fogs and are certainly not the prime cause of the wide discrepancies between σ and σ_d in most cases of table I. It is clear that the discrepancies must be attributed to the presence of large numbers of drops too small for the impactor to sample properly, i.e., below 5-10μ .

The results of table I have been considered in the light of these ideas on the performance of the impactor. The samples fall roughly into two classes; in the denser fogs (visibility less than 100 metres) there are quite large numbers of drops, mostly 5μ and above, enough to account for about 1/5 of the observed attenuation coefficient, but in the thinner fogs (with visibilities 100-400 metres) the numbers of drops in the samples are extremely small and never account for more than 1/20 of the attenuation. In these thinner fogs it seems very unlikely, even making maximum allowance for evaporation losses in the impactor, that drops bigger than 5μ can be numerous enough to contribute more than a very small fraction of the attenuation; the bulk of the attenuation must be due to smaller drops, possibly to drops so small that they should be classed as "nuclei" rather than as "true" water drops.

In the thicker fogs it is just possible, by supposing rather large inertial and evaporative losses in the impactor, to explain the observed attenuation in terms of a distribution of "large" drops ($> 5\mu$), but it seems more likely that in these fogs too, small drops below 5μ contribute an important part, probably more than half, of the total attenuation.

The liquid water contents suggested by the data in table I are also of interest. In the thicker fogs the values calculated from the impactor samples range from about 0.1 gm/m^3 down to 0.01 gm/m^3. These values have, of course, to be increased to allow for the relatively small number of large drops lost by inertial effects and the large number of small drops lost by evaporation. The former can be estimated roughly from the sedimentation measurements, and an upper limit to the latter can be found from the attenuation attributed to the small drops. The result is that the measured water content should be increased by a factor of roughly 2, so that we obtain a maximum liquid water content of about 0.2 gm/m^3 for Kew fogs, with 0.1 gm/m^3 as a typical value for fogs of about 30 metres visibility. In the thinner fogs the measured values are extremely low, from nil up to about 0.001 gm/m^3. An upper limit for the contribution from small drops lost by evaporation can again be found from the attenuation; it is about 0.05 gm/m^3 for a fog with 100 metres visibility, but the actual value may be well below this limit. These liquid water contents are at least ten times smaller than the much-quoted values given by Houghton and Radford (1938); their figures referred to coastal fog and cloud rather than to the suburban radiation fogs sampled at Kew.

The cascade impactor results are obviously very unsatisfactory and the deductions drawn from them must be regarded as speculative. In view of the idea that drops smaller than 5μ, and perhaps even those below 1μ, are an important component of fogs it seemed unlikely that the cascade impactor, or indeed any other impaction device, could be made to give satisfactory results and other methods of studying fogs were investigated.

3. Optical methods of studying fog

The idea of obtaining information about the drop size distribution in fog from optical measurements (including those using infra-red radiation) is attractive because it is possible to make measurements in almost undisturbed fog, giving average values over quite large volumes. The disadvantage of optical methods is that there is no property which varies in a simple manner with drop size (over the range encountered in fogs) and it is consequently difficult to determine size distributions uniquely from the optical measurements. Two types of measurement seem to offer the best hope of obtaining useful results. The first is the measurement of attenuation as a function of wavelength; as a very rough approximation the attenuation should be independent of wavelength for short waves but fall to zero for waves longer than the drop diameter, so that measurements at a given wavelength indicate the contribution from drops larger than that length. The more exact dependence of attenuation on drop size and wavelength, as calculated by Johnson and Terrel (1955) is not so simple, and the construction of drop size distributions from attenuation measurements is correspondingly difficult and uncertain. Nevertheless Arnulf, Bricard and Veret (1954) have found fairly close agreement between experimental and theoretical attenuations in natural fogs and Eldridge (1957) has applied the method to the estimation of drop size distributions in cloud on Mount Washington. The range of sizes for which the method is effective is roughly the same as the range of wavelengths employed, so it is desirable to extend the measurements as far into the infra-red as possible.

The second type of measurement is of the fraction of an incident beam scattered at small forward angles. This is an extension of the familiar "corona" method in which a mean size of cloud drops is deduced from the angular position of the first minimum in the scattered light. The corona method fails in most fogs because the spread of drop sizes is so great that no minimum is discernible. By quantitative observations of the intensity of scattered

light as a function of angle a good deal more information about the drop size distribution can be obtained. The relation between drop size and scattered light is again not simple, so that interpretation of the results is difficult and uncertain. The relations are simplest and the discrimination between drops of different sizes best when the drops are large compared with the wavelengths used and when the observations are made at angles of order λ/r, so that fog measurements are best made with visible light and at angles from a fraction of a degree to several degrees.

Both types of optical measurement have been attempted at Kew, using crude forms of apparatus intended to give some idea of the type of result to be expected and so to permit the design of improved measurements. Neither method leads to great experimental difficulties, unless very high accuracy is required, but both lead to the same type of problem in the interpretation of results, the construction of drop size distributions whose optical properties would fit the observed results, and the determination of the limits within which these distributions must lie. (There will always be more than one distribution fitting the data to any required degree of accuracy).

Details of the methods of measurement are given in the appendices. Observations were made in five broad bands of wavelength in the attenuation method and at four angles in the scattering method. In the attenuation method the "sample" was a 40 metre stretch of fog about 4 ft above the lawn at Kew, disturbed only by the apparatus at the two ends of the stretch; in the scattering method the sample was a small volume of fog about 1 cm x 2 cm x 20 cm, 5 ft above the lawn and practically undisturbed by the apparatus. The results are given in table II, expressed as attenuation coefficients (Km^{-1}) for the five wavebands or as angular scattering coefficients (beam candlepower/unit volume for each lumen/unit area in the incident beam) in Km^{-1} for the four angles of observation.

The first stage in finding drop size distributions that would fit these observations is to find the contribution that a drop of any particular size would make to the attenuation or scattering coefficients at the selected wavelengths or angles. This was done by drawing graphs of the coefficients as functions of drop size from the data of Johnson (1955) and of Gumprecht et al (1952), obtained by numerical computations from the Mie theory. The scattering coefficients are given directly by the numerical data, for the four selected angles, for certain values of drop size, but to cover the full range of drop sizes required it was necessary both to interpolate between the data and to extrapolate them to larger sizes (using simple diffraction theory). The curves so obtained are probably accurate enough for use with the present observations but some closer approximation to the full Mie theory may have to be used in the future. The attenuation coefficients given by Johnson for a series of values of drop size and wavelength had to be suitably averaged to allow for the distribution of energy over each of the wavebands for which observations were made.

The curves obtained in this way show the broad features that would be expected. The attenuation produced by drops larger than 12μ diameter is about the same for all the wavebands used; smaller drops give maximum attenuation for wavelengths of about twice their diameter falling to a constant, slightly smaller value for shorter wavelengths and to very small values for larger wavelengths; drops smaller than about 0.5μ affect only the shortest waveband used. The scattering produced by drops smaller than 2μ is approximately constant for all four angles of observation but as the drop size increases the scattered light becomes more and more concentrated at small angles. Both sets of curves contain many minor oscillations, but these would only be important in fogs with remarkably uniform drop size.

/Given

Given the curves of attenuation or scattering coefficients against drop size, we have to find drop size distributions which will give rise to the observed values of the coefficients set out in table II. Since there are only four or five observations to be fitted, it is unlikely that we shall be able to determine distributions in much detail; at best we can hope to estimate about four parameters defining the distribution. The results of table II have therefore been fitted by taking groups of drops of sizes 0-1.25, 1.25-2.5, 2.5-5, 5-10 and 10-20 μ and finding the number in each group required to give a distribution whose attenuation or scattering coefficients would match the observed values. It is, of course, necessary to make some assumption about how the drops are distributed within each of the groups, and the convenient and reasonably plausible assumption made here is that the number of drops, dN, with radius between r and r + dr is given by

$$\frac{dN}{d \log_{10} r} = \frac{C_i}{r^2} \quad \text{or} \quad \frac{dN}{dr} = \frac{C_i}{2.3r^3} \qquad \ldots\ldots (1)$$

where C_i is a constant for the i th size range. The effects of different assumptions about the distribution will be discussed later. From (1) and the curves for attenuation and scattering coefficients as functions of drop size, we can calculate the contribution, for unit value of C_i, which each group would make to the coefficients. These contributions are set out in table III. To find a distribution, then, we have to find sets of values of C_i by which the contributions in table III have to be multiplied in order that the sums of the contributions for each waveband or angle may match the observations. This of course involves solving a set of four or five simultaneous linear equations, with the proviso that negative values of C_i are not allowed. The values of C_i given in table II have, in fact, been found by a process of trial and error, usually intuitive but in some cases a systematic relaxation process.

These values of C_i, together with equation (1), define the distributions which fit the observations, and can readily be converted into mass - or number - distributions if required. The most direct conversion is into the area-distribution used in presenting the cascade impactor results; it can easily be shown from equation (1) that the value of C_i for a given size-range of drops is proportional to the total cross-sectional area of those drops per unit volume of air, i.e., to the quantity S_i used in table I. For a size range whose limits are in the ratio two to one, as in tables I and II, we find $S_i = (\pi \log_{10} 2) C_i$ or, to the accuracy of the present results, $S_i \doteq C_i$. This does not apply, of course, to the smallest size group of the tables, which, if equation (1) applied down to the very small sizes, would contribute an infinite amount to the cross-sectional area. Factors for converting the tabulated C_i values into the number, mass or contribution to opacity in each size group are given at the foot of the table.

Because the observations cannot be taken as exact, there is a certain amount of latitude in choosing values of C_i to match the observations. Some lines of table II show alternative sets of values of C_i all leading to agreement with observation within the limits of experimental error. It will be seen that fairly big variations in distribution are possible but that the general balance between "big" and "small" drops seems fairly well fixed.

A more detailed study of how well the distributions given in table II can be expected to represent the true distributions is illustrated in fig. 1 and 2. These show, for occasions when observations were made nearly simultaneously by more than one method, distributions of several different types, all calculated to fit the optical observations and, in addition, the distributions given by cascade impactor measurements. The distributions are shown as graphs of $\log_{10} (dN/d \log_{10} D)$ vs $\log_{10} D$ (D = diameter of drop). Distributions of the type used in table II are therefore represented by a set of lines of slope -2 whose vertical positions depend on the values of C_i. In addition to the C_i

calculated for the standard groups of drops used in table II, values calculated for a different set of groups, with limits at 3.3, 6.6, 13.3 and 26.7μ are shown, to illustrate how far the distribution depends on the (arbitrary) choice of size-limits for the groups. Further distributions shown are ones calculated with a different distribution law ($dN/dr = C_i\ r^{-4}$) within each group, and one consisting not of four broad groups of drops, but of only two groups of almost uniform drops, the sizes and number of drops in the two groups being chosen to fit the observations; the fit obtained from this type of distribution is usually not as good as from the four-group type, but can be brought within the limits of experimental error in most cases.

The distributions of table IIA and fig. 1 were calculated from the angular scattering coefficients alone. They can be checked by calculating the total (i.e., "mean spherical") scattering coefficient that would be given by each distribution and comparing it with the observed attenuation coefficient for visible light. In the absence of absorption these coefficients should be equal. Exact agreement is not to be expected because the scattering measurements were made on a small sample of fog and the attenuation measurements on an extended one, but the last two columns of table IIA show that fairly good agreement is, in fact, obtained. The calculated values of total scatter for the various distributions of fig. 1 are given on the figure, and comparison with the observed attenuation shows that some distributions are in better agreement than others; the distribution with two isolated groups of drops gives particularly bad agreement. The distributions of table IIB, deduced from transmission measurements cannot, of course, be checked in this way as the attenuation coefficient for visible light was one of the quantities used in calculating distributions.

The cascade impactor results, included in fig. 1, show that some drops larger than 20μ were present, so that arbitrary cutting off of the calculated distributions at 20μ, as in table II, is unjustified. It is shown, however, that the inclusion of a group of drops of 20-40μ has no very drastic effect on the calculated distribution; the larger drops are provided, as might be expected, at the expense of the slightly smaller ones.

Fig. 1k and 2f show the best estimates of the drop size distributions in the two fogs that can be made from the present measurements. The curves have been drawn using the earlier curves as a guide, but smoothing out physically unlikely discontinuities and adjusting the final curves by trial and error until the calculated optical properties of the distributions agreed with the observations. The probable accuracy of these smoothed distributions is to be assessed by comparison with the discontinuous distributions, all of which fit the observations within the experimental accuracy. For the thicker fog, curve 1k is thought to be reasonably accurate throughout, but for the thinner fog the right-hand part of curve 2(f) is not drawn with much confidence. The group of larger drops indicated by the bump in the curve at about 10μ is so small relative to the large number of small drops that it contributes very little to the opacity or other optical properties of the fog and was revealed in the measurements only by a high intensity of scattered light at the smallest angle of observation (1°). This single observation could be explained as well by a smaller number of still larger drops as by the actual size and number shown in fig. 2. The cascade impactor result, on the other hand, suggests a group of drops at about 4μ with very few larger than 10μ.

Accepting the final curves as the best estimates of drop size distribution in their respective fogs, we can deduce the following quantities for the two fogs:

/Time and date

Time and date Visibility	2130,13.11.56 55	2320,20.12.56 330	metres
Mass of drops	0.14	0.014	gm/m^3
Number > 7μ diam.	100	1.0	cm^{-3}
Number 1-7μ diam.	5,200	1,150	cm^{-3}
Number < 1μ diam.	> 20,000	> 10,000	cm^{-3}
Mean diameter	indefinite	indefinite	
Median diameter	indefinite	indefinite	
Mass median diam.	12	11	microns

Fig. 1 and 2 illustrate the range of variation possible in drop size distributions fitting the optical data. We can set some quantitative limits on possible distributions by considering the ratios of the contribution to attenuation at different wavelengths or to scattering at different angles made by drops of various sizes. If, for example, the attenuation is high in the 0.6 and 1.2μ bands and very low in the 10μ band, it is clear that very little attenuation is provided by drops larger than 5μ. Results can best be expressed in terms of the contribution of drops smaller or larger than certain sizes to the attenuation in the visible, the "opacity". Contributions to the total mass or number of drops are uncertain because a large mass in the form of very big drops or a large number in the form of very small drops might pass undetected by the optical methods.

For the thick fog (55 m visibility) at 1025 on 19/12/56 we find from the attenuation measurements:

drops	smaller	than	10 μ	diameter	contributed	at	least	60%	of the	observed opacity
"	"	"	2.2μ	"	"	"	"	40%	" "	" "
"	larger	"	0.5μ	"	"	"	"	45%	" "	" "
"	"	"	2.2μ	"	"	"	"	21%	" "	" "
"	"	"	5 μ	"	"	"	"	19%	" "	" "
"	"	"	7 μ	"	"	"	"	13%	" "	" "

and for the thinner fog (135 m visibility) at 1445 the same day

drops	smaller	than	8 μ	diameter	contributed	at	least	90%	of the	observed opacity
"	"	"	2μ	"	"	"	"	75%	" "	" "
"	"	"	1.5μ	"	"	"	"	45%	" "	" "
"	larger	"	0.5μ	"	"	"	"	15%	" "	" "
"	"	"	1.5μ	"	"	"	"	5%	" "	" "

Similar deductions can be made from the scattering observations.

4. Discussion of results

Tables I and II contain data on most of the thick fogs at Kew in the past two winters and may be taken as reasonably representative of such fogs. They contain little information about fog or haze with visibility greater than 300 m. Cascade impactor samples were taken at all stages of fog development, but most frequently in the morning, before and during the clearance of fog. Scattered light measurements were necessarily made at night, mostly some hours after fog formed. Attenuation measurements come chiefly from the one long spell of fog (December, 1956) that has occurred since the apparatus was completed.

The most striking feature of the results is the preponderance of very small drops. The optical results, like the impactor ones, suggest that the fogs fall into two fairly distinct classes, with visibilities above and below 100 yards. In the thinner fogs practically all the drops fall into the smallest (or next-to-smallest) size-group, which contributes almost all the opacity and a large part of the liquid water content of the fog. In the thicker fogs the contribution from small drops is increased several times but

in addition there is an important component of larger drops which provides almost all the liquid water and up to half of the opacity of the fog. In most cases the division into "small" and "large" drops seems to be significant, in the sense that there is an intermediate range of size, usually around 5μ, in which drops are relatively rare. As fig. 1 and 2 suggest, the methods of observation used so far can indicate the approximate position and size of these two groups in the drop size distribution, but cannot determine the distribution of drops within each group with any precision.

It is natural to enquire how much the results reflect the situation of Kew and the influence of pollution from London. No measurements have so far been made by the optical methods except at Kew, but cascade impactor fog samples have been taken by many workers at different places, including places as remote from sources of pollution as Cornwall, Wick, Rye and the Isle of Man and in all cases (with the exception of one recently reported from Porton) the opacity deduced from the samples has been smaller by a factor of at least five (and often by a much larger factor) than the opacity deduced from visibility observations. It is thus certain that most fogs contain some components not properly sampled by the impactor as normally used; it is not possible to say, without further observations, whether the chief missing component consists of large drops lost by inertial effects or of smaller drops lost by evaporation, as at Kew.

The contribution of dry smoke particles to the Kew results has been estimated, as mentioned in section 1, from the records of the Owens automatic air filter and found to be quite small. This does not mean, of course, that the "small drops" found in Kew fogs may not consist of water condensed around particles of smoke; it does mean that the condensed water contributes much more to the opacity than the original smoke particles. No accurate measurements of humidity were made at the site of the fog measurements. The Observatory records from the North Wall screen give relative humidities of over 90% on all occasions but seldom exceeded 97% and only once reached 100%, even though many of the fogs were obviously "wet".

The simplest interpretation of the size distributions observed at Kew is that the fogs consist of a mixture of drops of the two equilibrium sizes suggested by the familiar curve of drop size against relative humidity; the "large" drops have grown so far that the effects of surface tension and dissolved substances are unimportant and their size is controlled only by the available water, with the result that they act as a regulator maintaining the humidity at almost exactly 100%; the "small" drops are the remaining nuclei grown to a size determined by this humidity and by the amount of hygroscopic matter they contain. This is a very natural picture of a fog, but its unexpected feature is the large contribution, particularly to the opacity, made by the small-drop component. The pioneer work of Wright (1939 etc.) had suggested that condensation occurred almost exclusively on large "sea salt" nuclei, that smoke particles were unaffected by condensation and that small "industrial nuclei" scarcely affected the visibility even at high humidities. More recent work by Junge (1955) and others shows that condensation is possible on a wide range of sizes of nuclei. Samples taken at humidities below about 70% show that the nuclei are usually distributed according to the law

$$\frac{dN}{d \log r} = \frac{C_1}{r^3}$$

As humidity increases the larger nuclei grow more than the smaller ones and Junge calculates that the distribution law should change to

$$\frac{dN}{d \log r} = \frac{C_2}{r^2}$$

when the air is just saturated. If supersaturation occurs the extra water will be taken up by the larger nuclei of the distribution, which will pass beyond the condensation point in their growth curve and then serve to maintain the

humidity very close to 100%. The resulting distribution would clearly be of the general form suggested by fig. 1. The actual values of C (i.e., the number of nuclei of a given size) suggested by table II are from 3 to 30 times higher than those obtained by Junge from measurements at Frankfurt; the difference can be attributed to the heavier pollution of the Kew atmosphere in foggy conditions. If the curves of fig. 1 are extrapolated down to a radius of 10^{-5} cm, we can estimate the total number of nuclei greater than this size as rather less than 10^5 per cm^3, which is of the order of magnitude suggested by Aitken counter results.

If this interpretation of the present results is correct, most of the opacity of Kew fogs is simply the result of bringing dirty air very close to saturation, and we have to enquire why thick fog is always accompanied by an appreciable concentration of "large" drops; they seem to be essential to the formation of thick fog even though they contribute only a fraction of its opacity. Two explanations seem possible. One is that the large drops play an essential role in the production of saturated air; air cooled by contact with cold ground tends to lose water faster than it loses heat and it has been suggested (Stewart, 1955) that radiative cooling not only of the air itself but also from the larger suspended particles or drops is necessary before saturation can be reached. Alternatively the large drops may appear simply because it may be inevitable that in a very nearly saturated atmosphere local fluctuations will occasionally lead to local supersaturation and the growth of some nuclei beyond their condensation point. In either case the large drops act an an indicator that saturation has been achieved.

The "thin fogs" of tables I and II contain far fewer "large" drops. In most cases there are indications (quite definite indications when a few drops are caught by the impactor or seen as specks of light in the beam of the scatter apparatus) that a few large drops are present, but in others they cannot be detected at all. The "small" drops are also less numerous (for a given size) in the thin fogs, but only by a factor comparable with the increase in visibility. The thin fogs studied at Kew have all developed from thick fogs, mostly as the fog was clearing during the morning. The development of a thick fog from a thin one has not been studied and seems to be an unusual occurrence or, if it occurs, a very rapid process. The typical sequence of events is a slow fall in visibility to values of the order of 1000 metres followed by a very rapid fall to "thick fog" conditions with visibility of perhaps 50 metres and then a long period of fairly steady conditions ending, usually after dawn, with a slow and irregular rise in visibility through "thin fog", which may persist for many hours, particularly in midwinter, to complete clearance. There is a striking difference between the rapid formation of fog and its slow clearance, in polluted regions. The fact that the "thin" clearing fogs consist almost entirely of small drops suggests that falling humidity has evaporated the big drops and that the remaining small drops are, for some reason, less sensitive to changes in humidity than in the early stages of fog formation. It may be that coagulation of nuclei or the effects of dissolved gases and chemical changes play important parts here.

The methods used so far are not very suitable for following changes in fog; even a hurried observation takes about five minutes and one with careful checks at least a quarter of an hour, while any change in scattering or attenuation properties during the observation may lead to misleading results. Nevertheless there are two periods when fairly good observations are available during clearance of fog.

Between 0830 and 1300 on 19.12.56 there was a fairly slow change from thick fog with visibility 40 metres to a thin fog with visibility about 150 metres, which persisted for the rest of the day. In the same period there was a 2°F rise in temperature (in the North Wall screen) and a fall in relative humidity from 100% to 97%. The observation at 0930 shows a more or less uniform distribution of drops, in the sense that equation (1) is followed with nearly the same value of C for all size groups; the apparent

excess of drops in the largest groups may be due to the arbitrary cutting-off of the distribution at 20μ . The next two observations show little change in the smallest groups but a marked decrease in the drops in the largest group and signs of a "gap" in the distribution between the large and small drops. The visibility increased from 45 to 60 metres, a change which is accounted for roughly by the loss of large drops. Between 1025 and 1245 there were more marked changes; the drops in the largest group disappeared altogether and relatively few remained in the 5-10μ group. The smallest group changed little but the next two groups vanished, so that by 1245 there was a typical "thin fog" with a large component of very small drops and a quite small component of larger ones. These changes were confirmed by the cascade impactor samples at 0955 and 1300; the former shows a substantial component of large drops, the latter a very small number of drops in the region of 5μ .

A somewhat similar sequence of changes occurred between 2245 on 21.12.56 and 0030 on the 22nd., when there was an increase of wind and thick fog cleared almost completely. Between 2245 and 2340 conditions were rather unsteady so that the observations may be a little unreliable, but there seems to have been a tendency for the number of drops in the large groups to increase at the expense of the smaller groups. By 0010 the wind and visibility had increased and the fog drops separated into distinct groups of large and small drops with the contribution from each group distinctly less than in the thick fog. By 0030 the fog was clearing rapidly, the contribution from the larger drops had become very small and that from the small drops had also become much smaller (in contrast to its relative constancy on 19.12.56).

5. Applications of results

Although the present results give little detail of drop size distributions, they bring out clearly the importance of the small and very small drops in determining the visibility in fog, and it is interesting to examine some of the more practical consequences of this fact.

The dominating influence of small drops suggests that in attempting to forecast visibility in fog attention should be directed towards the number, size and nature of the nuclei present in the air rather than to the amount of liquid water expected to be condonsed. The fact that quite small amounts of water are needed to form a thick fog implies that the mixing of nearly saturated air at different temperatures may be more important in producing fog than is sometimes suggested. Apart from this the present results give little help with the main problem of fog forecasting, that of predicting when true saturation of the air will be attained. It is possible that the radiative and hygroscopic properties of the nuclei play an important part here, but the present techniques would require considerable modification before they could be used to study the early stages of the growth of nuclei.

In connection with the artifical dispersal of fog, the low values of liquid water content now obtained emphasize how little of the energy found necessary in the thermal method is actually used in evaporating water drops; the bulk of the energy must be devoted to lowering the humidity of the air to induce the drops to evaporate in a short enough time. The gap between the theoretical efficiency of the process and that achieved in practice thus seems even larger than had been thought and is all the more worth investigating. Similar considerations apply to the idea of drying the air by hygroscopic materials. Mechanical methods of clearing fog have hitherto been considered mostly in relation to the removal of "large" drops. If consideration is given to the "small" drops, the simple methods of dropping large drops or particles through the fog seem unpromising, because of the very low collision efficiencies expected with small drops, but the electrical and acoustic methods of inducing coagulation seem more promising because of the higher mobility of small drops. It might be well worth while to investigate the electrical state of the small drops in fogs.

/Finally,

Finally, the drop size distributions or more directly the attenuation measurements themselves, show that the use of infra-red devices should give signalling or seeing ranges appreciably greater than the "visibility"; in fogs of the type found at Kew. In the thick fogs the attenuation was found to decrease fairly slowly with increasing wavelength and at 10μ was $\frac{1}{2}$ to $\frac{1}{4}$ of that in the visible region. This increased transmission might be of use in some special circumstances but bearing in mind the limitations and complexity of the available sources and detectors, it is unlikely to have any great importance. In the "thin" fogs, however, which account for a quite large proportion of all fog at Kew, transmission increases much more rapidly with wavelength and by working at about 2μ it should often be possible to get ranges five or ten times the visual range. The greatest use for such an increase of range - from one or two hundred yards to perhaps half a mile - would be in the landing and taking off of aircraft, but it seems rather doubtful if infra-red seeing devices of sufficient simplicity and reliability for general use could be developed, bearing in mind the limited number of occasions on which they could be used.

6. Future work

The two obvious limitations of the work done so far are the uncertainty and inaccuracy of the drop size distributions that are obtained and the fact that it has been done only in a rather heavily polluted atmosphere. It therefore seems desirable to develop improved methods of measurement and to use them both at Kew and at some station relatively free from pollution.

Possible developments of the optical methods are mentioned in the appendices. It is thought that it should be relatively simple to develop either of them to give approximate drop-size distributions, analysed into five or six size groups, with a good deal less uncertainty than the distributions obtained from the present apparatus. The precision of the results, however, depends a good deal on the type of fog studied; a fog with very uniform drops will give simple and unambiguous results but there will always be some doubt as to the exact form of a broad distribution. The most effective size ranges of the two methods are not the same. The scatter method could be made to give accurate information about the largest drops of a distribution, but cannot easily discriminate between different sizes among the smaller drops. The attenuation method is more satisfactory for small drops but has poor discrimination for large ones, at any rate if measurements are confined to wavelengths below about 13μ, as is almost inevitable. It therefore seems necessary to continue to use both methods together if complete results are to be obtained.

The cascade impactor is a very convenient instrument to use and gives direct and detailed results, though the counting of drops is laborious. In its present form it certainly gives inaccurate results. Proposals have been made (May, private communication) that would probably make it an effective sampler down to at least 5μ, but at the cost of a considerable increase in complexity. It seems unlikely that any device of this type would be satisfactory as a sampler of the smallest drops.

It is suggested that the most economical line of development would be to improve the scatter method in the direction of increased accuracy, range of angles, sensitivity, ease of operation and portability and to use it at various places. The attenuation method should be retained and improved at Kew and the cascade impactor, in its simple form but with any precautions that can be suggested to avoid error, should be used as a general check on the size distribution of the large drops.

This programme should give results of the type of table II but with less uncertainty and greater precision, and for fog in clean as well as dirty air.

If still greater precision in drop size distributions is required considerable development of the optical techniques (and of the associated calculations) would be necessary and it would be desirable to examine other

possible techniques such as photography for the larger drops and electrostatic or spider-web capture for the smaller ones. For most purposes, however, relatively crude approximations to the drop size distribution seem sufficient and any further extension of the present work could probably be made more profitably in the direction of exploring the connection between the fog drops and the nuclei present before fog forms. There are obviously many other interesting lines of enquiry such as the electrical state of the drops, their interaction with polluting gases, their distribution with height and possible collisions between drops of different sizes, but present resources are likely to be fully occupied with the development and use of the scatter and attenuation methods as outlined above.

7. References

Arnulf, A., Bricard, J. and Veret, C. 1954 Rev. Optique (Paris), 33, p.658.

Eldridge, R.G. 1957 Journ. Met., 14, p.55.

Gumprecht, R.O., Sung, N.L., Chin, J.H. and Sliepcevich, C.M. 1952 J.Opt. Soc. Amer, 42, p.226.

Houghton, H.G. and Radford, W.H. 1938 Papers in Oceanography and Phys. Met., No. 4, (M.I.T.).

Houghton, H.G. and Chalker, W.R. 1949 J. Opt. Soc. Amer., 39, p.955.

Johnson, J.C. and Terrel, J.R. 1955 J. Opt. Soc. Amer., 45, p.451.

Junge, C. 1955 Journ. Met., 12, p.13.

Liddell, H.F. and Wootten, N.W. 1957 Q.J.R. Met. Soc., 83, p.263.

Linke, F. 1933 Meteor. Taschenbuch, Vol.2, p.305.

May, K.R. 1945 J.Sci. Inst., 22, p.187.

May, K.R. 1956 A.M.A. Arch. of Indust. Health, 13, p.481.

Middleton, W.E.K. 1952 Vision through the Atmosphere (Univ. of Toronto) p.177ff.

Stewart, K.H. 1955 Meteorological Research Papers, Air Ministry, London, No. 912.

Wootten, N.W. 1955 Porton Tech. Pap. No. 506.

Wright, H.L. 1939 Q.J.R. Met. Soc., 65, p.411.

Appendix I

Measurements with a Cascade Impactor

1. Sampling technique

The instrument has been fully described by May (1945), with details of the method of taking and examining samples. In the present work the only major departure from the methods described by May was the use of the Naphthol Green-in-gelatine coating on the slides (Liddell and Wootten, 1957), but the following minor points may be worth noting. Aspiration was provided not by an air pump but by a simple water aspirator fitted with a large-bore quick-acting tap. The head of water was adjusted so that the rate of aspiration was close to the value of 17.5 l/min recommended by May. In use, the water run out of the aspirator was collected and measured as a convenient way of finding the volume of air sampled, without the need to measure short intervals of time. In most fogs samples of a few hundred cm^3, taken in times of one or two seconds, gave drop deposits of convenient density. Most of the samples were taken in very light winds (1-2 ft/sec) and at first they were taken with the bell-mouth adaptor fitted to the impactor and with the intake aperture facing vertically upwards. This method often produced a rather irregular-shaped deposit on the first slide, and later samples were taken with the aperture facing into what wind there was and inclined slightly upwards; this produced much more even deposits of drops.

2. Examination of samples

The slides were examined under a good-quality microscope with objectives of 16, 8 and 4 mm. The drop stains were sized with the help of an eyepiece graticule calibrated against a 1/100 mm scale. The stains on the first and second slide were normally easy to see and there was little difficulty in sizing and counting them, provided the slides were not overexposed. Several "traverses" across the deposit on the slide were usually made, to obtain a good estimate of the numbers of drops. On the second slide there was usually a considerably higher concentration of drops at the ends than in the middle of the trace of drops. Although this limits the accuracy of estimates from the slides, the limitation is not important in the present work.

3. The third slide usually had a fairly even deposit, slightly denser towards the end of the trace, but the distinctness of the stains was rather variable. On some slides they were quite plain but on others they were barely visible and very hard to size and count. Presumably some slides were better prepared than others, though no conscious changes in technique were made. The third slide often had a fairly sparse deposit of opaque particles of irregular shape in addition to (and apparently not connected with) the drop stains. On the fourth slide these particles were smaller and much more numerous. On none of the fourth slides was it possible to identify drop stains with any certainty. On some there were quite small numbers of ring shaped stains that may have been due to water drops, but it was impossible to be sure that they were genuine stains and not out-of-focus images of opaque particles or diffraction rings surrounding them. It is felt that if stains equivalent to those made by the smaller drops (1 μ diam.) on the third slides had been present on the fourth slides, they could have been identified fairly confidently.

4. Tests in artificial fog

When it was realized that the impactor samples were quite incapable of accounting for the observed opacities of Kew fogs, experiments to check the operation of the impactor were started. These were done in a small (8 $ft.^3$) heat-insulated, waterproofed room, the "fog chamber", in which artificial fogs could be produced and maintained. The opacity of the fogs was measured by measuring the attenuation of a beam of light in the chamber with a simple photoelectric meter; with a small chamber it was difficult to measure attenuation coefficients of less than about 100 km^{-1} with much accuracy. Most of the results to be quoted are therefore only semi-quantitative.

5. The first method of making artificial fogs at Kew was by using an ordinary paint spray, with air pressures of 20-50 lb/sq.in. Samples of fogs made in this way were very similar to natural fog samples. Drops were caught on the first three slides, but their total area was far too small to explain the observed attenuation coefficient. It was suspected that very small drops were responsible for the extra attenuation.

6. Apparatus was made for measuring the light scattered at small angles (1° - 5°) by fog. From these measurements it was possible to deduce, within fairly wide limits, the size distribution of the drops responsible for the attenuation. It was found that most of the attenuation in the spray fog was, in fact, due to small drops, though the predominant size was 1-3μ rather than below 1μ, as had been guessed.

7. Changes in spraying technique were tried in an attempt to produce fogs not containing small drops, the size being checked by the light scatter method. It was found that by using air pressures below 10 lb/sq. in. and a low rate of water flow the desired type of fog could be made. Samples of these fogs gave drops mostly in the range 15-30μ and the attenuations deduced from the drop samples agreed well with those observed directly - the first time such agreement had been obtained.

8. Attempts were next made to produce fogs with drops predominantly in the range 5-10μ, which should be caught on the second slide. Spray methods were unsuccessful but steam fogs produced by boiling water inside the fog chamber were found to have a very suitable drop size distribution, sharply peaked at about 7μ. Most samples from these fogs contained enough drops to account for the observed attenuation (if the fog was at all dense the second slide was flooded) but a few contained far too few drops, perhaps because the fog was not uniform. All slides were found to have a "crazy paving" pattern on the green gelatine and the drop stains were often hard to see. Some stains were in focus at the same level as the crazy paving pattern but others seemed to be at a lower level and were diffuse and partly obscured by the out-of-focus crazy paving. The effect was attributed to the high humidity of the warm fog relative to the impactor and, in order to avoid it, the impactor (with its slides inside) was warmed over an electric stove before being taken into the fog. This procedure entirely eliminated the crazy paving effect and gave very well defined drop stains, but it also resulted in much less dense samples so that the attenuation deduced from the samples was much less than that observed directly. It seems clear that with a warm impactor the drops evaporate to a considerable extent, in the space outside and above the impactor, during their passage through it or after impinging on the slide. The amount of warming required to produce the effect is not large, though it has not yet been investigated thoroughly. The impactor was usually heated about 20°C above room temperature, then taken into the fog where it was kept for about 10 minutes before sampling. The temperature difference between impactor and its surroundings was found to fall by half in about 6 minutes. At the time of sampling the impactor was probably about 5°C warmer than the fog.

9. In the light of these experiments, further samples of small-drop spray fogs were taken, first with the impactor at about fog temperature, then with the fog chamber warmed, so that the impactor was cooler than the fog. With equal temperatures, drops were found on the second and third slides, but in far too small numbers to explain the observed attenuation. No drops were found on the fourth slide, but there was a fairly dense deposit of opaque particles. With the fog warmer than the impactor the second and third slides were not much changed (though showing "crazy paving") but the trace on the fourth slide was "flooded", the dye being almost completely washed away from a rather well-defined area about equal to that of the jet. The light-scatter observations in these fogs indicated that they were composed mainly of drops below 5μ, with (less certainly) a predominant size of 2-3μ.

/10.

10. Another way of avoiding evaporation is by using fogs of salt solution rather than of water. Somewhat different spray arrangements were used and the light-scatter measurements suggested that most drops were between 2 and 10μ, with few larger or smaller ones. A sample in a moderately dense fog gave flooding on second, third and fourth slides (in conditions where a water fog would have given only thinly covered slides) and a sample in a thin fog gave about half the number of drops required to explain the attenuation. The drop stains were not well defined and usually irregular in outline, suggesting that the salt interacted with the dye. These experiments, though not at all precise, suggest that if evaporation is avoided the impactor gives a much more nearly true sample.

11. The general result of the various tests is thus that the impactor gives a roughly correct sample if it is a few degrees cooler than the fog and a decidely incorrect one if it is a few degrees warmer. If it is at nearly the same temperature as the fog (i.e., prepared in a room at the same temperature, then left in the fog for some time) drops large enough to appear on the first slide are sampled correctly, those appearing on the second slide are probably somewhat underestimated and those on the third and fourth slides are very seriously underestimated. Whether a true sample could be obtained by very accurate control of the temperature (either to the fog temperature or to one a degree or two lower) is not known, but it is quite clear that for ordinary fog samples serious underestimation of the smaller drops would be expected.

12. The explanation of these results is not obvious. If air passing through the impactors undergoes "adiabatic" expansion it will be cooled and its relative humidity raised. If it undergoes "throttled" expansion it will be cooled to a much smaller extent and the effect of the expansion will be to lower the relative humidity (by nearly 4% at the fourth jet). The actual flow process is complicated and probably does not fit any simple model, so that it is almost impossible to say what the actual changes of relative humidity are. In any case, however, it is hard to see how they could exceed about 5%, and changes of this amount would not be expected to cause appreciable growth or shrinkage of fog drops in the very short time of their passage through the impactor. On the other hand, there is the observed fact that changes of humidity of about this size brought about by warming the impactor do actually result in loss of drops. It may be that evaporation can go on after the drops have reached the slides.

13. The results obtained in natural fogs were reviewed in the light of the artificial fog experiments. The first point noticed was that none of the slides showed the "crazy paving" effect that is characteristic of an impactor below fog temperature. The second point concerns the relative numbers of drops of different sizes appearing on the different slides of a sample. We define the "halfway size" for two successive slides as the size that appears with equal frequency on the two slides. According to Casella's curves the halfway size is about 12μ for slides 1 and 2, 4μ for slides 2 and 3, and 1.5μ for slides 3 and 4. (Sampling unit density drops at 17½ l/min.) The halfway sizes actually found in the natural fog samples are about 10μ for slides 1 and 2, 2.5μ for slides 2 and 3 and less than 1μ for slides 3 and 4. The fact that these halfway sizes are smaller than those found in tests with non-volatile drops (i.e., Casella's curves) and that the difference is, in proportion, greatest for the smallest drops suggests strongly that drops are being lost in each stage of the impactor, as would happen if evaporation were occurring. The suggestion is supported by details of the drop size distributions; there is a fairly consistent tendency for minima to occur in each of the size ranges for which drops are shared between two slides. This can hardly be a regular natural phenomenon and is much more likely to be due to losses in the impactor. The effect could, however, be produced by relatively small systematic errors in the microscopic sizing of drops and could, by itself, only provide clear evidence for or against the evaporation hypothesis after careful statistical examination.

/14.

14. The possibility that drops might be lost by deposition on the walls of the impactor was investigated by May, but a few additional tests with water fog were made in the Kew chamber by inserting very small pieces of dye-coated cover glass in various positions in the impactor. The results confirmed that wall losses were negligible.

15. Losses of large drops

The artificial fog experiments show that the impactor samples "large-drop" fogs correctly within a factor of about two, but are not accurate enough to detect smaller errors and have not been extended to drops larger than about 30 μ. Experiments by May (1956) have shown that errors of up to 50% may arise when sampling large drops in light winds because drops larger than 20 μ may not follow the air streamlines closely enough to enter the impactor. Another type of error seems likely with the very small air samples found necessary in fog work; it can be calculated that if 500 cc of air are drawn into the impactor, starting with the air at rest, some 30% of 30 μ drops and 70% of 50 μ drops will fail to reach the first slide of the impactor, being left behind as the air accelerates. These inertial errors have not been studied experimentally at Kew.

16. Size of sample; overlapping of stains

Although the samples taken in natural fogs do not contain nearly enough drops to account for the observed opacity, the number of drops in many samples from thick fogs was large enough to cause a serious overexposure of the slides, even though the volume of air sampled was kept as small as possible. This implies that if the impactor sampled all the drops correctly, the problem of obtaining satisfactory exposures would become very serious. Experience shows that the best slides are those where the drop stains cover about 1/50 of the area of the "exposed" part of the slide; if the coverage is greater than about 1/20, counting and sizing becomes very difficult because of overlapping of the stains. The area of the stains is proportional to the cross-sectional area of the drops and hence, approximately, to the product of the attenuation coefficient and the volume of fog sampled. We find, for the area, A, of the stains from the drops in C cm^3 of fog with attenuation coefficient σ,

$$A = 3.1\, C\, \sigma$$

or

$$A = \frac{12.5\, C}{V}$$

where σ has been taken as $4/V$, V being the visibility in the fog. The fractional coverage of the slides is therefore

$$\frac{A}{S} = \frac{12.5\, C}{VS}$$

where S is the area of the slides exposed in the impactor. If A/S is to have the desired value 1/50 we find that the volume of fog that should be sampled is given by

$$C = \frac{1}{50}\,\frac{V.S}{12.5}$$

The total area of slides exposed in the impactor is about 2.5 cm^2, so that

$$C = \frac{V}{250}\ \text{cm}^3 \quad (V \text{ in cm})$$

or

$$C = 50\ \text{cm}^3 \text{ if } V = 125\ \text{m}.$$

If therefore, the impactor was to sample correctly all the drops which affect the visibility in a fog with visibility 125 m, it would be necessary to restrict the volume of air sampled to 50 cm^3. The impactor itself has a volume of at least 100 cm^3, so that it seems quite impracticable to take such a small sample. The situation is even worse if the smaller drops contribute most of the opacity of fog because then the sample is concentrated on the very small exposed area of the later slides (less than 0.5 cm^2 for the third and fourth slides together).

17. Possible modifications to impactor technique

Proposals for overcoming the limitations of the cascade impactor as a fog sampling device have been made by May (private communication.) He suggests that loss of large drops could be avoided by mounting the impactor inside a wind tunnel, through which fog would be drawn at the optimum sampling speed for the impactor (~ 8 m.p.h.); that the problem of overexposure of the slides could be met by moving the slides past the sampling slits of the impactor and thus spreading the deposit over a greater area; and that evaporative losses could be avoided by using only the first and third stages of the impactor (May believes that little evaporation can occur before the second slide, in normal use) and applying corrections to the number of small drops recorded, to allow for those that would slip past the third stage. The drawback to these proposals is that they would convert the impactor from a simple and handy device into a quite large and complicated installation. Also, while they seem likely to overcome the errors for large drops and so should lead to quite good estimates of the distribution of the bulk of the water in fogs, it seems far from certain that they would really be effective in avoiding or allowing for losses of small drops, so that the opacity - producing components of fogs might still not be measured adequately.

Appendix II

Scattered light measurements

1. The apparatus is shown schematically in fig. 3 (not to scale). The slits S_1 and S_2 select a narrow beam of light from the 12 volt 48 watt filament lamp C. The lenses L_1 and L_2 help to illuminate S_1 evenly and the various auxiliary screens reduce stray light. These components were all mounted on a single 10 ft beam which could be set up on a light framework indoors or out. Light scattered from a portion of the beam at O was measured by a photometer P which pivoted about O to receive light scattered at different angles. The photometer P was a Salford Electrical Instruments photographic exposure photometer modified by substituting a 10 cm focus objective lens for its own short-focus one so that brightness could be measured for a field of only about 1/10 degree rather than for the 1 degree field of the original instrument. The photometer contains a Lummer-Brodhun head with a small oval comparison spot illuminated through variable filters by a small electric bulb standardized against a photocell. Auxiliary filters are provided for covering a wide range of brightness and for colour correction. The aperture of the objective lens was restricted to a slit 0.9 cm x 2.0 cm by a screen fixed just outside the lens. The screen extended for about 15 cm on each side of the lens and was marked with a scale in centimetres, so that the angular position of the photometer with respect to the light beam could be found by observing the position of the beam on the scale. The photometer head and its objective lens were adjusted so that parallel light from the direction of the pivot O was brought to a focus on the comparison spot of the photometer cube. The photometer was carried in a light but rigid metal frame; the end nearest the observer rested on a small table and could be slid from side to side by the observer, while the other end consisted of a metal beam extending to the pivot O which was carried on a theodolite tripod. The fog under observation at O was therefore relatively free from interference; it was about 3 metres from the light source C, about 1 metre from the final slit S_2 and its supporting frame, and about 1 metre from the photometer head and the observer. In the immediate neighbourhood of O the only interference was from the tripod and the beam of the photometer resting on its pivot; these were several centimetres below the point from which the light was scattered.

2. Measurements were made by turning the photometer to each of the desired angles of observation in turn and adjusting the brightness of the comparison spot until it matched the surrounding field provided by light scattered from the fog. The photometer scale was marked in logarithmic units of brightness and it was found that settings could usually be repeated to within 0.1 $\log_{10}$ units, though in some cases the fog was patchy and less accurate readings were obtained. The matching was done with white light, using the "artificial light" colour correction filter in the photometer. There was often a tendency for the scattered light to appear rather too blue at small angles and rather too red at large angles, but not sufficiently to cause serious errors in matching (the readings were scarcely affected if the "daylight" filter was used rather than the "artificial light" one). Readings were normally taken to one side of the incident beam only, but checks on a number of occasions showed that readings on the other side were very nearly the same.

3. At the end of each series of scattered light readings a piece of white card was placed at the pivot O, normal to the incident beam, and the photometer was swung right round to view the patch of light from a direction close to that of the beam. Brightness readings were taken, just as for the scattered light, to provide a measure of the flux in the beam. The reflectivity of the card (ρ) was later measured by comparison with a magnesium oxide surface.

4. The relative values of the scattering coefficient of the fog at different angles (b_θ) were taken as proportional to the brightness readings on the photometer scale, B_θ , multiplied by the sine of the scattering angle θ , because the depth of the illuminated fog seen through the photometer was inversely proportional to the sine of the angle of observation. The absolute values were calculated from the formula

$$b_\theta = \frac{B_\theta}{B_o} \frac{\rho\theta}{\pi a}$$

/where..

where B_o is the brightness reading obtained with the beam of light incident on the white card and a is the width of the aperture in front of the photometer lens. (It is necessary to use this width in the calculations rather than the actual width of the beam of light at O to allow for the fact that the measurement of B_o is made on a patch smaller than the photometer aperture and with a photometer focussed for infinity).

5. The accuracy of the measurements was limited primarily by the accuracy of the photometer wedge, by the difficulty of matching the comparison spot in view of its small size and low brightness and by the variability of the fog from moment to moment. Errors due to secondary scattering of light, to misplacement of the pivot O or to bad alignment or focussing of the photometer were small by comparison. One correction which had to be applied was for incorrect density of one of the range-changing filters of the photometer, which was found to have a density of about 2.2 instead of the nominal 2.0 ($\log_{10}$ units); the calibration of the main wedge filter of the photometer was checked roughly by an inverse square law method and found to be correct within about 0.1 $\log_{10}$ units. Quite erroneous results were obtained in the early stages through condensation of water on the photometer lenses. This was avoided by keeping the photometer in a heated hut except for fairly brief periods of observation. The onset of condensation is easy to detect.

6. The main defects of the method just described are that it depends on visual photometry, which is slow and not very accurate in the circumstances, and that it uses white light. It is planned to construct a more accurate and convenient apparatus, sketched in fig. 4.

A narrow beam of monochromatic light is provided by the high pressure mercury lamp S, filter F and circular aperture A. The main beam is absorbed in the light trap T but scattered light is collected by the lenses L_1 and L_2, and the aperture B allows light from a small section of the beam to pass on the photomultiplier P. This light is further restricted, by the movable annular aperture C, to that which has been scattered within a narrow range of angles; the mean angle of scattering can be varied by sliding C along the axis of the system. It is not certain that this system of apertures will eliminate unwanted light sufficiently. It may be necessary to employ pairs of annular slots close to each lens to define the length of beam and range of angles more closely.

Appendix III

Attenuation measurements

1. The experimental arrangement is sketched in fig. 5. Four sources of radiation were provided, mounted in line about 3 ft apart on a light framework 4 ft above the ground. The sources were

W. A 100 watt electric lamp run at full voltage

X. A 2000 watt electric lamp run at a much reduced voltage giving a temperature of about 1200°C

Y. An electric hotplate of 20 cm diameter with a well oxidised surface, run at a very dull red heat

Z. A similar hotplate painted with optical black and run at a surface temperature of about 100°C.

The radiation from these sources was received through the open window of a hut 46 m distant, with the arrangement shown. The front silvered spherical mirror M, of aperture about 20 cm and focal length 60 cm, reflected radiation through the apertures and on to the thermopile of a Linke-Feussner radiometer, I. The mirror was tilted slightly from a vertical plane and the radiometer mounted below its axis, so that a horizontal beam of radiation falling on the mirror was not obstructed by the radiometer. M and L were mounted on a framework with one end pivoted, so that it could turn about a vertical axis, and the other end free to slide on a rigid table. The receiver assembly could thus be turned to accept radiation from each source in turn. The mirror M was just large enough to fill the field of view of the radiometer. The thermopile had a diameter of 1 cm so that the cone of radiation accepted by the receiver had a half-angle of just under 0.5 degrees. An experimental test of the angular response curve of the receiver showed that it was reasonably flat-topped and that the response fell to half its full value at about 0.3° off the axis. The radiometer was connected to a sensitive moving-coil galvanometer whose voltage sensitivity (with radiometer in circuit) was checked from time to time by an auxiliary circuit and found to vary by less than 3 per cent.

2. Measurements were made on the four sources with the following filters in position in the radiometer:-

W. RG2 filter 1.55 mm thick, passing radiation between about 0.63 and 2.8 μ

X. The same

Y_1. The same

Y_2. Quartz filter 1.60 mm thick passing radiation up to about 4 μ

Z. No filter.

It was assumed that the sources radiated as black bodies at temperatures of 2750, 1500, 850 and 373°K respectively, and from the theoretical variation of radiated energy with wavelength, the filter characteristics tabulated by Linke (1933) and, for the longer wavelengths, the approximate atmospheric absorption spectrum, the curves shown in fig. 6 were calculated, giving the effective distribution of energy in wavelength for the bands in which measurements were made. The short-wave measurements V, were made on source W with a "photoelectric visibility meter, Mk.II", as receiver, placed alongside the radiometer receiver. The energy curve for V is determined by the radiation curve of the source and the response curve of the selenium cell in the receiver.

/3.

3. Measurements were made by fitting the appropriate filter, turning the receiver to view the space between two sources or beyond the line of sources, reading the galvanometer, turning the receiver to view the desired source and again reading the galvonometer. The readings were normally repeated several times in an attempt to eliminate drifts, which were always troublesome, and to reduce the effects of random variations. Measurements were made daily in clear weather (visibility greater than 1 Km) for about three months and as often as possible in fog. The clear weather measurements were taken to represent 100 percent transmission in the wavebands concerned, and the attenuation due to fog was calculated by expressing the signal received in fog as a fraction of that received in clear conditions. The clear air measurements had standard deviations of about 10% for sources X and Z, 13% for Y and 20% for W. These variations probably come from several causes; the source temperatures were not controlled and may have varied because of mains voltage variations and the effects of wind and air temperature; background radiation received in the zero positions between the sources may have varied; mechanical imperfections in the receiver probably led to errors in alignment on the sources. The large deviations for source W may have been due to variations in contact resistance of the lamp holder, as most of the variance came from a fairly small number of highly irregular readings. In the conditions of fog measurements most of these errors were probably smaller and it is thought that the 100 percent transmissions values, taken from clear air observations just before and after the fog rather than from the mean of the whole set of clear air observations, were accurate to rather better than 10 percent for all wavebands. The fog measurements themselves were presumably subject to a similar error. The combined effect of these errors of observation of the attenuation coefficients given in table II varies with the amount of the attenuation; for very low attenuations (< 10 Km^{-1}) the standard error of the values in the table is about 2 Km^{-1}, at 20 Km^{-1} it is about 3 Km^{-1} and for the highest values (about 100 Km^{-1}) it is about 6 Km^{-1}.

4. The effects of water vapour absorption (as distinct from scattering and absorption by water drops) were studied by examining the clear air observations in relation to vapour pressure. Dividing the observations into two groups, with high and low values of vapour pressure (means of 9.7 and 6.9 mb respectively), no significant difference in the radiation received from source Z (which should be most affected by water vapour absorption) could be detected. It was concluded that the values of table II represent the effects of suspended drops or particles and are only negligibly affected by water vapour.

5. It has been pointed out by Middleton (1952) that all transmission measurements of this type may underestimate the attenuation coefficient because a certain amount of scattered light will enter the receiver in addition to the unscattered direct beam which is supposed to be measured. The error is small provided the cone of radiation accepted by the receiver is small and provided the attenuation being measured is not too large. Rough estimates suggest it is negligible in the present work except in the thickest fogs, where it might lead to slight underestimation of the attenuation coefficient at the shorter wavelengths. The measurements at the shortest wavelength of all, however, (waveband V) would be less affected than the others because the photoelectric receiver had a rather narrower field of view than the radiometer.

6. The main defects of the present method of measurement are the great width and poor definition of the wavebands used and the general low accuracy of measurement, chiefly attributable to the variability of the sources used and the impossibility of checking their outputs during fog. It will clearly not be possible to overcome these defects without using considerably more elaborate apparatus. For the isolation of reasonably narrow wavebands (a bandwidth of about 0.1 λ at wavelength λ would be suitable) it will be necessary to use a simple form of infra-red spectrometer, at any rate for the longer wavelengths; for wavelengths below about 2μ it might be preferable to use filters. To achieve satisfactory accuracy, it will be necessary to arrange the optics of the measurement so that transmission over long and short paths can be compared and variations in source and receiver allowed for.

Table I. Data from cascade impactor (C) and sedimentation (S) samples (all in Km^{-1})

Date	Time G.M.T.	Visibility metres	Type of sample C or S	Cross-sections of drops in diameter ranges 0-1.25μ S_1	1.25-2.5μ S_2	2-5-5μ S_3	5-10μ S_4	10-20μ S_5	> 20μ S_6	$\sigma_d = 2\sum S_i$	$\sigma = 3.91/V$	σ_s
1955												
30. 8	11.00	360	C	0	0	0	0.01	0.01	0	0.04	11	1.0
24. 9	09.30	220	C	-	-	0.03	0.1	0.2	0.05	0.76	18	4.5
11.10	09.20	75	C	0.02	0.03	0.4	0.5	0.9	1.2	5.4	55	1.0
11.10	18.15	20	C	0.001	0.003	0.8	3.8	3.9	0	17.0	200	1.0
12.10	10.20	360	C	0	0	0.1	0.04	0.03	0.04	0.4	11	1.0
1.11	10.00	135	C	0	0	0	0	0	0	0	30	4.5
1.11	10.30	200	C	0	0	0	0	0	0	0	20	4.5
30.11	09.15	55	C	0.03	0.19	0.53	1.1	3.2	2.7	15.4	75	3.0
30.11	09.15	55	S	-	-	-	0.7	2.1	2.0	9.6	75	3.0
30.11	10.45	75	C	0.03	0.21	0.29	0.21	0.50	0.27	3.0	55	3.0
30.11	10.45	75	S	-	-	-	0	0.6	0.4	2.0	55	3.0
30.11	12.00	220	S	-	-	-	0	0	0	0	18	4.5
30.11	21.15	220	C	0	0	0	0	0	0	0	18	4.5
1.12	18.00	45	C	0.005	0.07	0.6	2.9	2.2	0	11.6	90	4.0
1.12	21.40	90	C	0.03	0.07	0.04	0.002	0	0	0.3	45	4.0
1.12	23.00	90	C	0.03	0.1	0.05	0	0	0	0.3	45	6.2
2.12	09.20	45	C	0.02	0.2	0.9	1.6	2.4	2.9	16.0	90	3.0
2.12	10.10	45	C	0.02	0.2	1.0	1.5	2.5	2.5	15.4	90	4.0
2.12	10.45	360	C	0	0	0	0	0	0	0	11	4.5
17.12	09.45	40	C	0.03	0.12	0.5	1.4	4.3	2.5	17.6	100	2.0
17.12	10.00	40	S	-	-	-	1.8	5.0	2.8	19.2	100	2.0
17.12	11.00	90	C	0.01	0.12	0.3	0.5	1.0	0.5	4.6	45	3.0
17.12	11.20	100	S	-	-	-	0.34	0.65	0.72	3.5	40	3.0
19.12	10.45	90	C	0.01	0.09	0.19	0.12	0	0	0.8	45	-
19.12	12.10	200	C	0	0	0	0	0	0	0	20	-
1956												
4. 1	11.55	20	C	0.07	0.23	1.05	0.36	0.15	0	3.7	200	7.5
5. 1	12.40	60	C	0.15	0.29	0.68	0.07	0	0	0	65	4.5
5. 1	15.30	16	C	0.17	0.34	1.5	1.0	0.75	0.3	7.1	250	7.5
5. 1	16.30	15	C	0.18	0.86	0.50	0.2	0.9	0.4	6.0	270	10.0
5. 1	17.00	18	S	-	-	-	1.6	0.8	0.33	5.5	225	10.0
12.10	01.25	33	C	0.01	-	-	2	5.0	0.3	15	120	3.0
12.10	01.33	33	S	-	-	-	1.1	9.0	1.1	22.4	120	3.0
16.10	00.16	30	C	-	-	-	2.0	9.9	2.7	29	135	2.0
16.10	00.16	30	S	-	-	-	12.5	13.6	1.2	54.6	135	2.0
13.11	21.50	50	C	0.07	0.32	0.25	0.53	2.6	2.6	12.8	80	4.0
19.12	09.55	45	C	0.01	0.09	0.4	1.3	1.7	0.6	8.2	90	2.0
19.12	10.25	55	S	-	-	-	0.3	0.4	0.2	1.8	75	3.0
19.12	13.00	135	C	0.02	0.03	0.06	0.09	0	0	0.4	30	6.0
19.12	15.25	135	S	-	-	-	0	0	0	0	30	6.0
20.12	12.15	220	C	0.02	0.05	0.05	0.1	0	0	0.4	18	3.0
20.12	16.20	180	S	-	-	-	0	0	0	0	22	3.0
20.12	23.25	330	C	0	0	0.01	0.02	0	0	0.06	12	1.5
21.12	23.45	75	C	0.07	0.15	0.4	0.8	1.5	0.8	7.4	55	1.0
21.12	23.45	75	S	-	-	-	0.6	2.9	2.1	11.2	55	1.0
22.12	00.20	330	C	0	0.01	0.05	0.3	0.7	0	2.2	12	1.0

Table IIA. Results of optical measurements: scattered light measurements

Date	Time	Visibility	Observed scattering coefficients (Km^{-1})				Values of C_i (Km^{-1}) for drop size distributions which fit the observations: Range of drop diameters				Calculated total scatter coefficient	Observed attenuation coefficient
	G.M.T.	metres	1^0	2^0	3^0	5^0	0-2½ μ	2½-5 μ	5-10 μ	10-20 μ		
1956							$C_{1,2}$	C_3	C_4	C_5	Km^{-1}	Km^{-1}
12.10	00.25	33	8900	2250	760	450	13	0	9.0	18.5	159	120
12.10	00.35	33	6300	1120	480	350	12	0	0	21	137	120
14.10	00.25	20	5100	1600	610	320	10	0	9.3	12	122	195
14.10	01.50	33	4700	1130	610	250	0	13	1.8	13	62	120
							2.2	9.0	7.3	11	77	
15.10	22.45	20	14900	2850	860	400	12	0	7.3	48	205	195
							9.3	1.9	9.3	45	191	
16.10	00.15	30	10400	2230	560	230	16	0	14	29	215	130
13.11	21.30	55	3500	1000	540	260	5.1	5.1	5.1	8.3	80	71
19.12	17.40	200	172	102	84	86	3.2	0	0	0.3	26	19
							3.2	0	0.06	0.19	25	
19.12	18.45	300	66	47	38	50	1.7	0	0	0.05	13	13
20.12	17.45	160	101	80	80	50	1.2	1.2	0	0	12	24
							1.4	0.9	0.06	0		
20.12	23.15	330	75	45	38	43	1.5	0	0	0.09	12	12
21.12	22.45	70	2340	1170	700	465	12	8.0	2.9	0.4	119	56
21.12	23.05	80	1780	1000	680	400	5.9	14	0	2.9	86	49
21.12	23.35	75	2860	1440	770	320	5.9	8.6	9.9	3.2	95	52
21.12	23.40	75	4040	1810	970	570	21	0	12	5.9	200	52
22.12	00.30	350	357	143	108	114	4.2	0	0	0.7	34	11
1957												
2. 1	05.20	45	3870	1440	615	322	9.3	3.2	11	6.7	117	87
2. 1	06.55	110	100	80	85	80	3.0	0	0	0	23	36
2. 1	07.05	80	324	178	151	126	3.8	1.6	0	0.4	34	49
To obtain number/cm^3 of drops in each size group, multiply values of C_i (in Km^{-1}) by the factors:-							(∞)	104	26.1	6.5		
To obtain liquid water content (mgm/m^3) due to drops in each size group, multiply values of C_i (in Km^{-1}) by the factors:-							2.28	2.28	4.55	9.11		
To obtain opacity (in Km^{-1}) due to drops in each size group, multiply values of C_i (in Km^{-1}) by the factors:-							7.75	2.40	2.12	2.09		

Table IIB. Results of optical measurements; measurements of transmission of radiation

Date	Time	Visibility	Observed attenuation coefficients (Km^{-1}) in wavebands centred on:					Values of C_i (Km^{-1}) for drop size distributions which fit the observations:- Range of drop diameters				
	G.M.T.	metres	0.6 μ	1.2 μ	2.0 μ	3.4 μ	10 μ	0-1.25 μ	1.25-2.5 μ	2.5-5 μ	5-10 μ	10-20 μ
								C_1	C_2	C_3	C_4	C_5
1956												
13.11	20.00	15	260	*	-	-	75					
13.11	22.10	45	90	-	-	-	33					
19.12	08.30	35	100	75	67	-	-					
	09.30	45	88	75	67	60	37	7.0	1.6	9.5	1.6	16
								6.4	6.4	3.2	6.4	16
	09.45	45	88	60	-	53	34					
	10.25	55	74	58	40	46	21	6.4	8.0	0	9.5	4.8
	11.10	60	64	43	35	27	15	8.6	3.2	3.8	3.2	6.4
	12.45	135	30	9	7	4	0	6.4	0	1.6	0	0
	14.45	130	32	11	4	7	0	8.0	0	0	1.4	0
	16.10	110	37	9	3	6	0	8.0	0	0	1.4	0
	18.15	180	22	5	0	0	0	5.4	0	0	0	0
20.12	11.30	150	28	10	2	-	0)					
	14.30	160	25	9	2	6	0)	6.0	0	0	1.3	0
	16.40	170	23	10	4	6	0)					
	22.30	290	14	6	0	-	0	2.5	1.6	0	0	0
	23.30	320	12	5	0	1	0	2.4	1.1	0	0	0
21.12	23.00	80	49	46	24	36	10	4.8	8.0	0	8.0	0
	23.25	65	64	46	47	44	28	8.0	0	3.2	6.4	9.5
22.12	00.10	175	23	17	12	14	6	1.6	3.2	0	2.5	1.6
1957												
2. 1	06.15	200*	70	23	-	64	14	Observations cannot be fitte				
	06.40	225*	31	11	14	6	2	4.8	0	3.2	0	0
	07.35	225*	48	31	17	14	4	6.4	7.7	0	1.9	1.0
To obtain number/cm^3 of drops in each size group multiply values of C_i (in Km^{-1}) by the factors:-								(∞)	416	104	26.1	6.5
To obtain liquid water content (mgm/m^3) due to drops in each size group, multiply values of C_i (in Km^{-1}) by the factors:-								1.14	1.14	2.28	4.55	9.11
To obtain opacity (in Km^{-1}) due to drops in each size group, multiply values of C_i (Km^{-1}) by the factors:-								4.7	3.0	2.40	2.12	2.09

* These figures give the general visibility. The transmission measurements were made in a denser layer of ground fog within the Observatory enclosure.

Table III

A. Contributions which groups of drops with $C_i = 1\ Km^{-1}$ make to scattering coefficients at four angles of observation for light of wavelength 0.525 μ

Km^{-1}		Size ranges: diameters in microns			
		0 - 2.5	2.5 - 5	5 - 10	10 - 20
Angle of scattering	1°	31	49	132	294
	2°	30	42	77	35
	3°	28	33	30	7
	5°	25	17	2	2

B. Contributions which groups of drops with $C_i = 1\ Km^{-1}$ make to attenuation coefficients in five wavebands (see fig. 6)

Km^{-1}		Size range: diameters in microns				
		0 - 1.25	1.25 - 2.5	2.5 - 5	5 - 10	10 - 20
Waveband	V	3.95	2.50	2.13	2.13	1.91
	W	1.00	2.29	2.72	2.26	2.22
	X	0.34	1.22	2.86	2.32	1.82
	Y	0.03	0.72	2.22	3.14	2.13
	Z	0.00	0.02	0.31	1.10	1.88

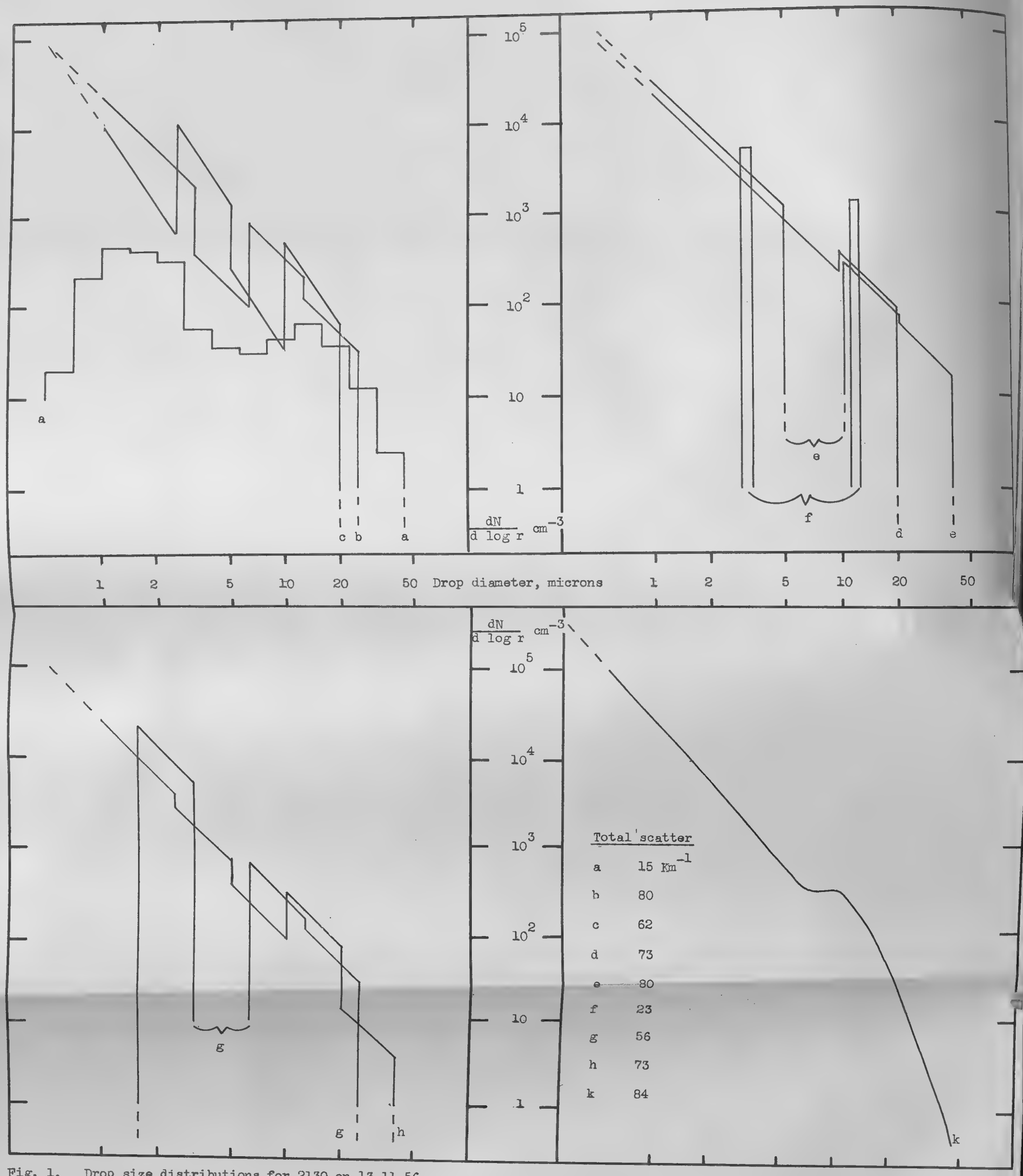

Fig. 1. Drop size distributions for 2130 on 13.11.56

a - cascade impactor results; b-h - various distributions giving results in agreement with scattered light observations; k - final "best estimate" of distribution. Figures on last diagram give calculated total scatter (Km^{-1}) for the various distributions; observed total scatter (i.e. attenuation) was 71 Km^{-1}.

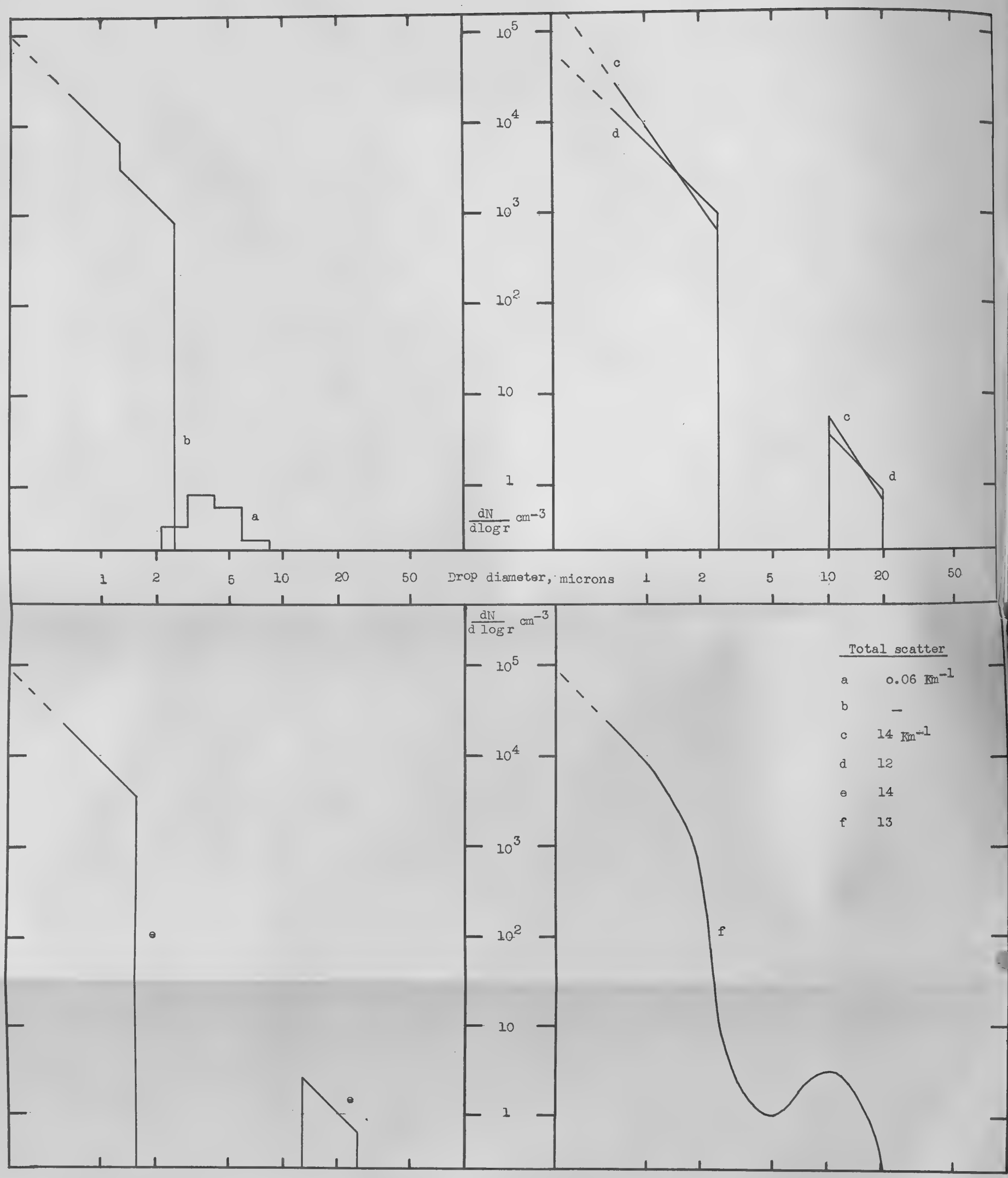

Fig. 2. Drop size distributions for 2320 on 20.12.56 . a – cascade impactor results: b – distribution fitting attenuation observations: c,d,e, – distributions fitting scattered light observations: f – final "best estimate" of distribution. Figures on the last diagram give calculated total scatter (Km^{-1}) for the various distributions; observed total scatter (i.e. attenuation coefficient for visible light) was 12 Km^{-1}.

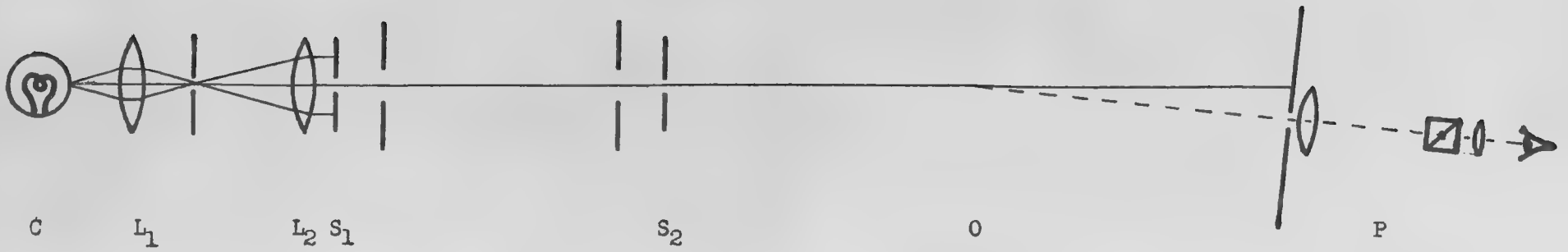

Fig. 3. Schematic diagram of apparatus used for the measurement of scattered light

MRP 1074

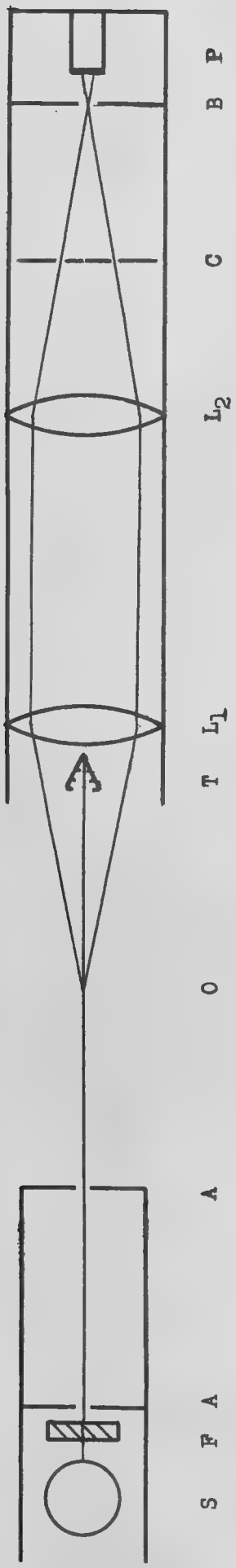

Fig. 4. Schematic diagram of proposed apparatus for measurement of scattered light

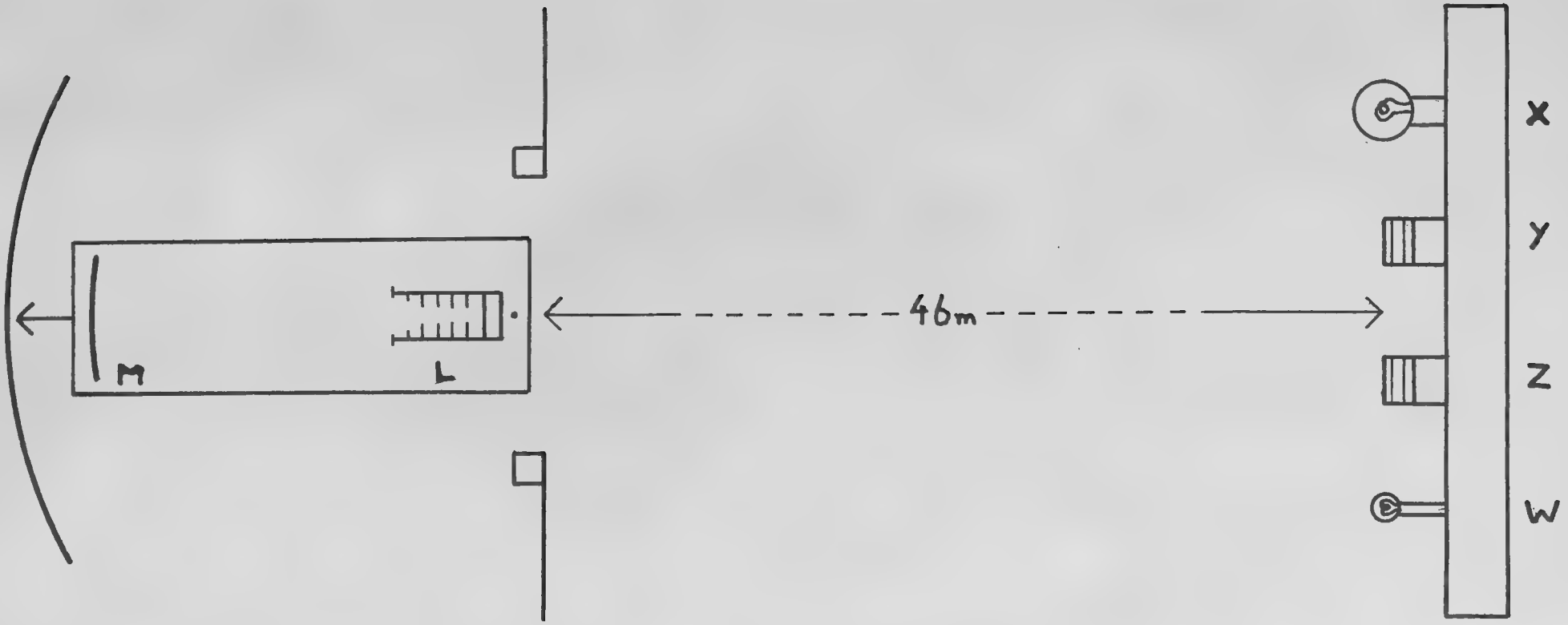

Fig. 5. Schematic diagram of apparatus for measurement of attenuation

MRP 1074

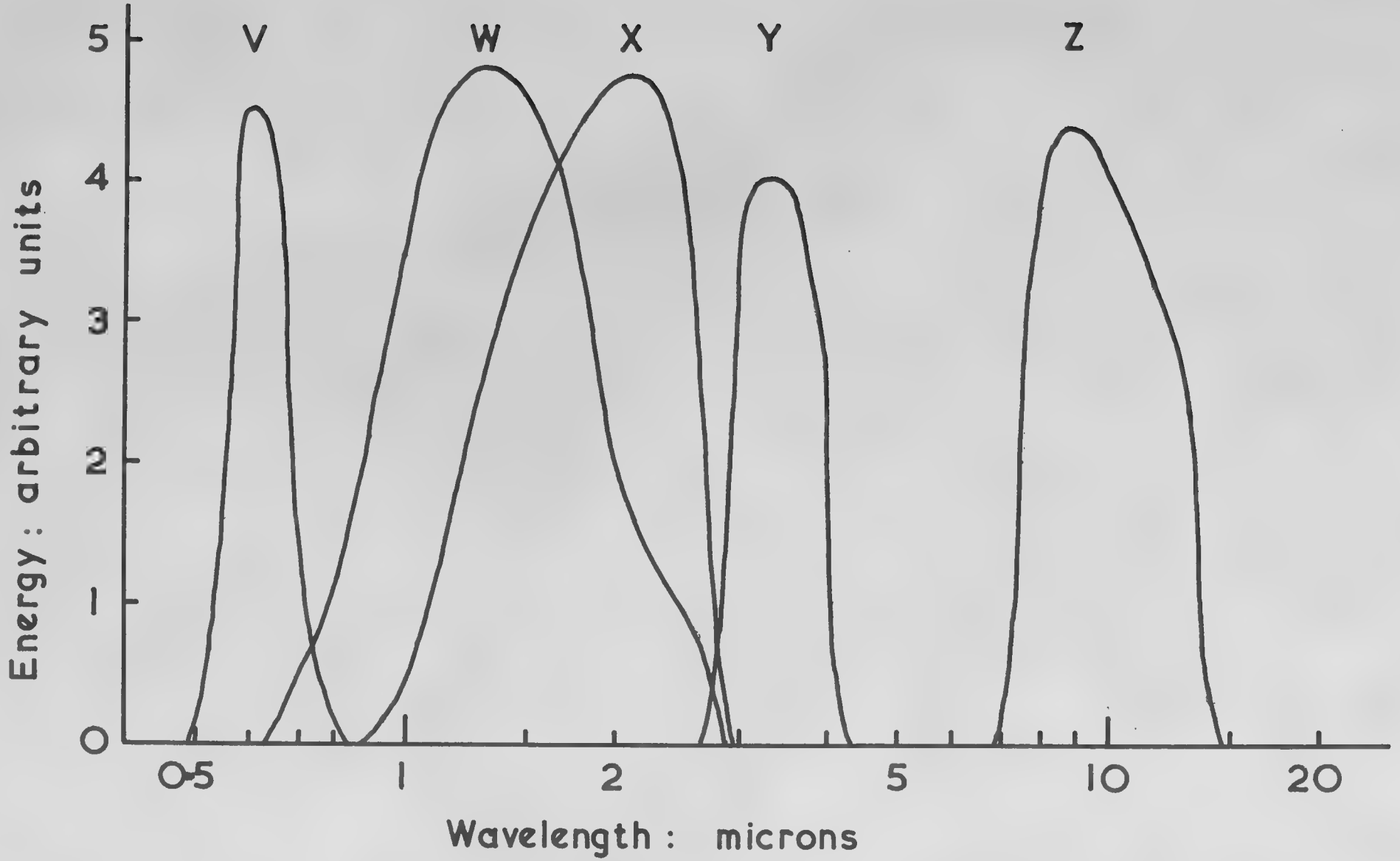

Fig. 6. Effective distribution of energy in wavebands used for attenuation measurements.

MRP 1074

M.R.P. 1075
S.C.11/245
30th October, 1957

MATS (1)

Average water - vapour content of the air.

by

J. K. Bannon and L. P. Steele

(Meteorological Office)

AIR MINISTRY

METEOROLOGICAL RESEARCH COMMITTEE

5f-1048

At the time of issue this report has not been published. Any author desiring to quote this paper should refer to it as "A paper of the Meteorological Research Committee London.
M.R.P. No. 1075 by Messrs.J.K.Bannon
L.P.Steele
A copy is available in the Library of Meteorological Office."

M.R.P.1075
S.C.II/245
30th October, 1957

AIR MINISTRY

METEOROLOGICAL RESEARCH COMMITTEE

Average water-vapour content of the air

by

J. K. Bannon and L. P. Steele (Meteorological Office)

Summary

Charts are presented of the average water-vapour content above 1cm^2 at the earth's surface and the levels 850, 700 and 500 mb for each of the months January, April, July and October based mainly on data for 1951-1955. The area covered by the charts is approximately 70°N - 52°S.

1. Introduction

Water-vapour in the atmosphere is usually described by the relative humidity, vapour pressure or some other measure applicable to one level or place. For some purposes, e.g. in studies of the absorption of radiation, it is necessary to know the amount of water vapour in various layers of the atmosphere. Observations of humidity in the upper air obtained by radio-sonde are now sufficient to attempt to chart the water-vapour content and this paper presents charts of the amount (mass) of water vapour above 1cm^2 at the earth's surface and above each of the levels 850, 700 and 500 mb over most of the earth except the Antarctic for the months January, April, July and October. No account is taken of water held in suspension by the air in solid or liquid form.

2. Data

The main source of data was the series of Climat Temp messages. These messages give among other things mean dew-point at the levels 850, 700, 500 and 300 mb for each month and are broadcast soon after the month to which they refer. The messages are confirmed or corrected in the publication (1). The Climat Temp messages began in 1949 but data for the first two years were considerably fewer than for subsequent years. Accordingly, as far as possible the data used were for the period 1951-1955 inclusive. The Climat Temp data were supplemented by data supplied specially by the United States Weather Bureau for another purpose (2), for 1951 and 1952 for some of the Pacific Islands. Data for a few stations were also taken from publications (3) and (4) to supplement the Climat Temp network. Data for stations in the British Isles were available in the form of monthly mean humidity mixing ratios. Surface data were obtained from Climat messages in most cases but some stations which broadcast Climat Temp messages did not broadcast corresponding Climat messages for the surface and for these stations values had to be interpolated between nearby observations; in a few cases in the Arctic such interpolation was impossible.

Climat Temp messages were not broadcast for stations in the U.S.S.R. Radio interception of daily upper air observations from this region are published in (5), and Mr. G. A. Tunnell put at our disposal mean dew-points

/at

at surface, 850, 700 and 500 mb worked from such data for a large number of stations for each mid-season month of the period 1949-1952 and for a few stations also for 1946 or 1947. The number of humidity observations for a particular month and station was in many cases small especially in January, and Mr. Tunnell has attempted to correct his mean values making allowance for the presence of temperature inversions and bias towards high temperatures and using the analogy of observations from similarly situated stations in Canada. These corrected mean values were accepted for the present purpose as the best estimates available. It is emphasized that the period of the observations is not the same as for the remaining observations and that the averages are in some cases based on small numbers of observations.

Figure 1 shows the distribution of stations from which observations of humidity in the upper air were available and utilised for this study. In many cases data were missing for one or more years.

3. Method of construction

The mass of water-vapour in the layer of air between pressures p_1 and p_2 is

$$\frac{1}{g}\int_{p_1}^{p_2} q\, dp$$

per cm^2 of horizontal area. Where

q = specific humidity (gm of water-vapour per gm of air and water vapour) and

g = acceleration of gravity.

q was calculated from the humidity mixing ratio, r (gm of water-vapour per gm of dry air) which is a convenient parameter as it is tabulated for British stations. The difference between q and r is small and is less than 0.05 gm/Kg for r less than 7 gm/Kg so that the calculation of q from r only involved the application of a small correction for larger values of r. Over the British Isles r is less than 7 gm/Kg at 850 mb and higher levels throughout the year and also at the surface in winter and spring.

Most of the data were in the form of average dew-points and these were converted into average humidity mixing ratios. Average humidity mixing ratios so calculated will underestimate the true average humidity mixing ratio but the error is not large. (See Section 4). Mean humidity mixing ratios for a few American and Japanese stations were calculated from mean relative humidities as published in (3) and (4); this method was also used for the observations from some Pacific Islands. Again there will be a small systematic error because the relation between relative humidity and humidity mixing ratio is not linear.

The integrations of the water-vapour content were made using the simple trapezium rule, for the layers (a) above 500 mb, (b) 700-500 mb, (c) 850-700 mb and (d) surface to 850 mb. Errors involved in this method are discussed in Section 4.

Usual methods of measuring humidity by radio sonde in the upper air do not work at low temperatures, about -40°C and below. Observations are lacking therefore for levels above 300 mb and in many cases for lower levels also. However, the saturated water-vapour content of the air at low temperatures in the high atmosphere is very low and, moreover, available evidence indicates that relative humidity is often very low in these layers also. Accordingly when temperatures were low and water-vapour content at 300 mb was not measured it was assumed to be zero.

/The

The average surface pressure was used in the integral for the lowest layer; if there is a significant correlation between humidity mixing ratio and surface pressure this could lead to error but such a relation is unlikely.

This method of evaluating the integral of q with respect to p was compared with the more accurate method of taking the distribution of q with pressure as defined by values at 100 mb intervals of pressure and also at 850 mb. This was done for 27 different distributions of q with p covering different months at stations in Britain and overseas. It was found that when q falls sharply between surface (near 1000 mb) and 850 mb the "short" method over-estimates the true value of

$$\int_{850}^{\text{surface}} q \, dp$$

An empirical rule for correcting water-vapour content of the layer surface-850 mb in such cases was devised by plotting the necessary correction against the lapse of specific humidity, surface to 850 mb, when surface pressure was near 1000 mb. This rule shows correction (to be subtracted) is equal to $2.6 \times 10^{-2}(q_s - q_{850} - 3.5)$ gm where q_s, q_{850} are specific humidities (gm/Kg) at surface and 850 mb respectively.

The water-vapour contents of the layers above the levels 500, 700, 850 mb and surface, calculated as above, were then plotted on charts for each of the months January, April, July and October. The units were tenths of gm/cm^2. As seen from Figure 1 there was only one observing station in the South American Continent. Accordingly values of surface humidities were used tc make rough estimates of the total water-vapour contents. Long period average humidity mixing ratios for a few stations in South America (see Figure 1) were compared with similar values for stations in other parts of the world with similar climates for the particular season. For example values in the Amazon Basin in the most rainy season compared with values over parts of India in the SW. Monsoon. In this way estimates of water-vapour content above 700 mb were obtained for three high level stations in the Andes and for 12 low level stations elsewhere. The charts were then drawn to the observations as far as possible and using normal rainfall maps and analogies with similar regions with good observations as guides over areas without observations. The chart for 500 mb and above was drawn first, then the 700 mb and above chart followed by those for 850 mb and the surface. Account was taken of the major mountain masses; thus the water-vapour content shown over the Himalayas is small on the charts for every level. On the surface charts there are areas of low water-vapour content over all the large mountain regions. It is emphasized, however, that it was only possible to take account of the more important areas of high ground and then only in a rough manner. More detail would be undesirable on world charts and would also be misleading, remembering the crude nature of some of the material from which the charts were prepared. The horizontal gradients of total water-vapour content are large in regions of steeply sloping mountains and the isopleths therefore run together in many places on the charts.

The charts for January are in Figure 2; Figure 2A shows the water-vapour content above $1 cm^2$ at the earth's surface; Figure 2B that above 850 mb; Figure 2C above 700 mb and Figure 2D above 500 mb. Figures 3, 4 and 5 show corresponding charts for April, July and October respectively.

4. Accuracy of the data and charts

Measures of humidity are perhaps the least reliable of those made by radio sonde and there are probably considerable differences in the typical errors of different types of sonde (6).

/Apart

Apart from this heterogeneity in the observations there are the following possible sources of systematic error in the water-vapour contents calculated from various data and used in the construction of the charts. Casual errors of measurement of humidity are assumed to be unimportant in the mean.

(a) Lag errors of the radio sonde

(b) Calculation of mean humidity mixing ratio from mean dew-points

(c) Calculation of mean specific humidity from mean humidity mixing ratio

(d) Errors in performing the integration with respect to pressure.

(a) Lag errors

All forms of humidity-measuring in routine use on radio sondes are subject to lag errors. These errors result in the mean in a slight over-estimation of humidity in the upper air over Britain in summer (7) and it is likely that this is a general fault as the middle troposphere is often dry even over the tropics. This over-estimation may amount to perhaps 2 per cent (7) on the average in mid troposphere, but is probably very much smaller in the layer below the 850 mb level where most of the water-vapour lies.

Errors from this source will be positive (i.e. over-estimation) and will probably be considerably less than 1 per cent for the total water-vapour content above the surface.

(b) Errors in mean humidity mixing ratios calculated from mean dew-points

This is a more serious source of error. Since for low relative humidities there is a much larger range in dew-point than in the corresponding humidity mixing ratio, the relation between the two variables being non-linear, the humidity mixing ratio corresponding to the mean dew-point will be lower than the true mean humidity mixing ratio. The errors will be greatest for those stations with the largest variability in humidity.

Monthly mean humidity mixing ratios for 850, 700 and 500 mb for four months for each of the years 1951-1955 inclusive for Lerwick, Aden and Gibraltar were compared with corresponding values computed from the mean dew-points. Results were as follows. If r^1 is the average humidity mixing ratio for one month for five years, calculated from the average dew-point, and r is the true average humidity mixing ratio then

$$r^1 = 0.96r$$

fits most observations at 850 mb for Aden and Lerwick and for two of the four months for Gibraltar; the fit is especially good for the high water-vapour contents at Aden. For 700 and 500 mb

$$r^1 = 0.92r$$

fits most months but the higher water contents at Aden and also the values for one or two other months at Lerwick are better described by the former relation. From a quick glance at daily values, humidity appears to be more variable at Gibraltar than at Aden or Lerwick.

It would seem therefore that there may be a systematic under-estimation of mean water-vapour content of 4 per cent over most of the charts and up to 8 per cent in regions of great variability of humidity. This error will not apply to observations over Britain which are true mean humidity mixing ratios. It should be noted however that in drawing the charts the observations from Lerwick, Leuchars and Larkhill/Crawley did not seem consistently higher than neighbouring observations from the weather ships and Western Europe but often the reverse.

/(c)

(c) Errors in mean specific humidity calculated from mean humidity mixing ratio

Errors from this source are very small. It can be shown that the difference between the value of the specific humidity obtained from the mean humidity mixing ratio and the true value is approximately the mean square of the humidity mixing ratio. (Humidity mixing ratio must of course be expressed as gm/gm; the mean square is then of order $(5 \times 10^{-3})^2$ or less at low levels in the atmosphere i.e. 25×10^{-6} or less. Humidity mixing ratios are commonly of order 10×10^{-3} or less at low levels).

(d) Errors in integration with respect to pressure

The crude trapezium rule applied to thick layers of 150 mb or more may lead to error in the calculation of the total water-vapour content. Typical variation of water-vapour content with height is shown in Figure 6 (Larkhill). The curve is usually concave upwards. The "short" method of integrating the water-vapour content will therefore tend to over-estimate. The integrals for 27 different mean distributions of water-vapour content with pressure, covering different months at stations in Britain and overseas, were calculated using values of specific humidity at 100 mb intervals and also at the levels of 850 mb and the results compared with the "short" method of computation actually used in the preparation of the charts. This comparison showed that there was a small error in the "short" method above the 850 mb level. After correcting the surface-850 mb integral (see Section 3) the over-estimate in the total water-vapour content above the earth's surface was of the order of 2 per cent over Britain and 5 per cent in the Mediterranean-Middle East region.

The errors from the sources (a), (b), (c) and (d) in the total water-vapour content above the earth's surface are thus of the order

(a) less than 1 per cent over-estimate

(b) 4-8 per cent under-estimate

(c) negligible

(d) 2-5 per cent over-estimate

The net error would appear to be an under-estimate of 1-3 per cent.

Apart from the above systematic errors the errors in drawing up the charts from the observations may be considerable. The observations showed considerable scatter and were difficult to reconcile among themselves especially over Europe and the U.S.S.R. In many regions there were no observations. The average distribution of water-vapour shown in Figures 2-5, is, it is hoped, correct in broad outline but cannot be accurate in detail.

5. Discussion

The charts in Figure 2-5 show few surprising features. In winter the continents have least and the oceans most water-vapour above them, the reverse being the case in summer except over Australia. This is no doubt associated with the similar temperature distribution. The charts for April and October (Figures 3A and 5A) are more like those for January in the Northern Hemisphere than those for July over the oceans.

The low values of water-vapour content over North Africa and the Near East are interesting.

Although there are few island observing stations in the tropics what observations there are show that the water-vapour content of the air over the tropical oceans is less than over land. Again this is doubtless associated with the higher temperatures over land and the more regular and effective

/convection

convection there to transport water-vapour upwards. The greatest water-vapour contents appear to be over the Ganges Valley in July (6.5 gm/cm^2) and the greatest value over the sea is also in July over the Western Pacific, south of Japan (5.6 gm/cm^2).

REFERENCES

(1) U.S. Weather Bureau — Monthly Climatic Data for the World.

(2) Hoyle, H.D. — The sub-tropical jet stream of the Eastern North Pacific Ocean, in January and April, 1952. Prof. Notes No. 126, Met. Off., London, 1957.

(3) U.S. Weather Bureau — Climatological Data. National Summary.

(4) Central Meteorological Observatory, Tokyo. — Aerological Data for Japan.

(5) U.S. Weather Bureau — Daily Series Synoptic Weather Maps.

(6) Hooper, A.H. — Heterogeneity in the measurements of humidity made by the radio sonde network of Europe. Met. Mag., 86, 1957, p.13.

(7) Hutchings, J.W. — Water-vapour flux and flux-divergence over Southern England: Summer, 1954. Quart. J. R. Met. Soc., 83, 1957, p.30.

MRP 1075

OBSERVING STATIONS

Fig. 1

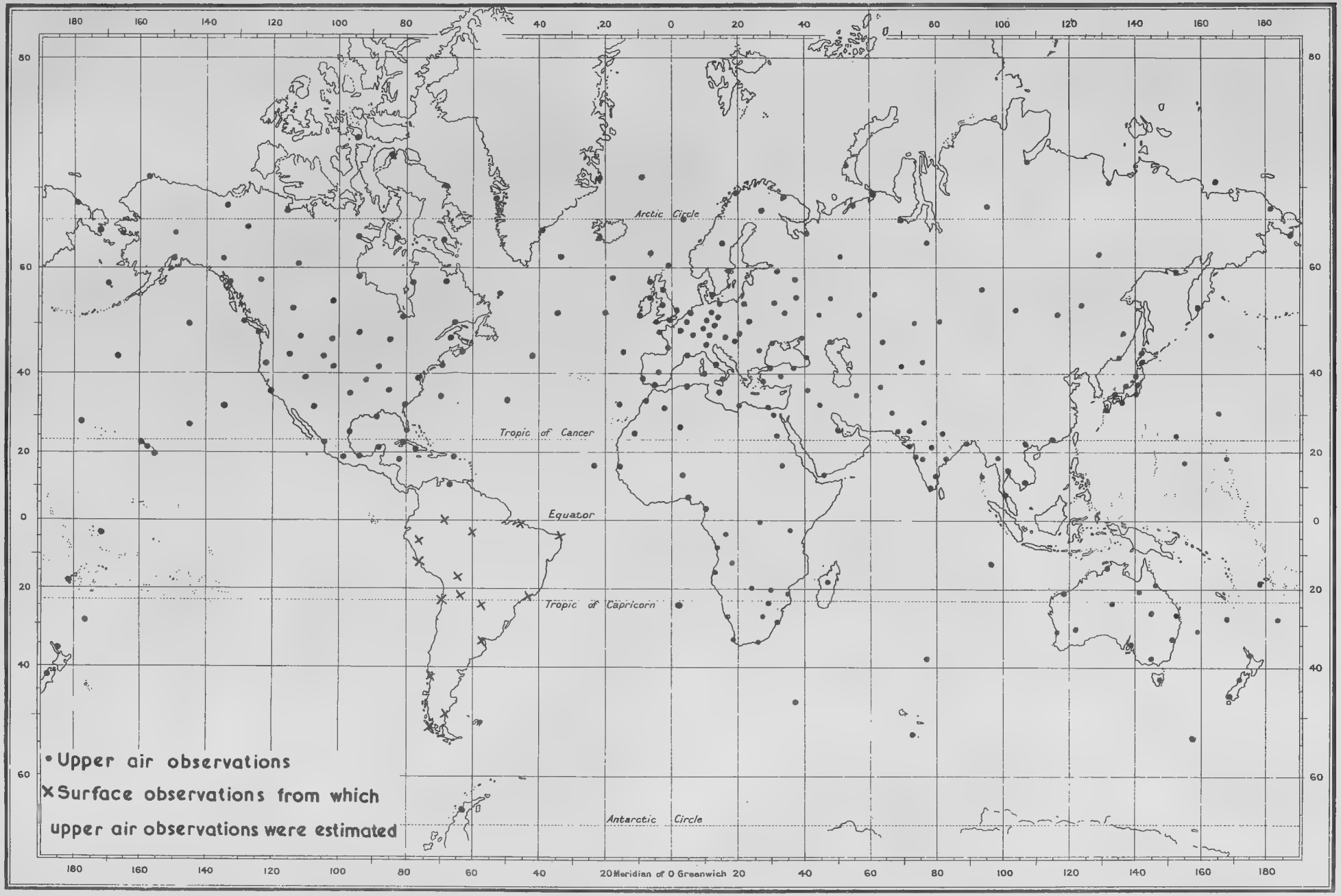

Water Vapour (⅛ of gm.) above 1 cm² at surface January 1951–55

M.R.P. 1075

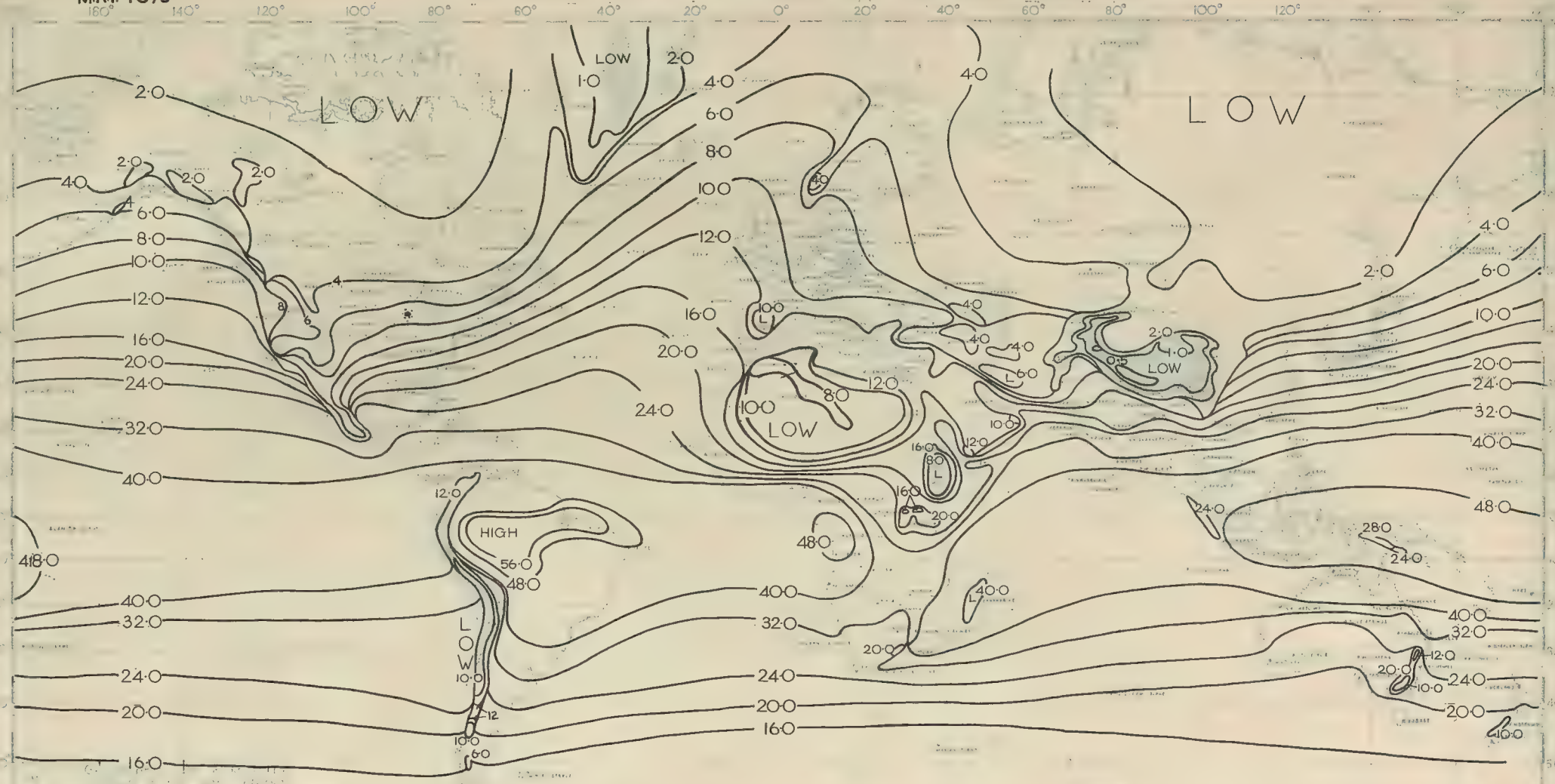

M.R.P. 1075

Water Vapour (⅛ of gm.) above 1 cm.² at 850 mb. January 1951–55

Fig. 2(b)

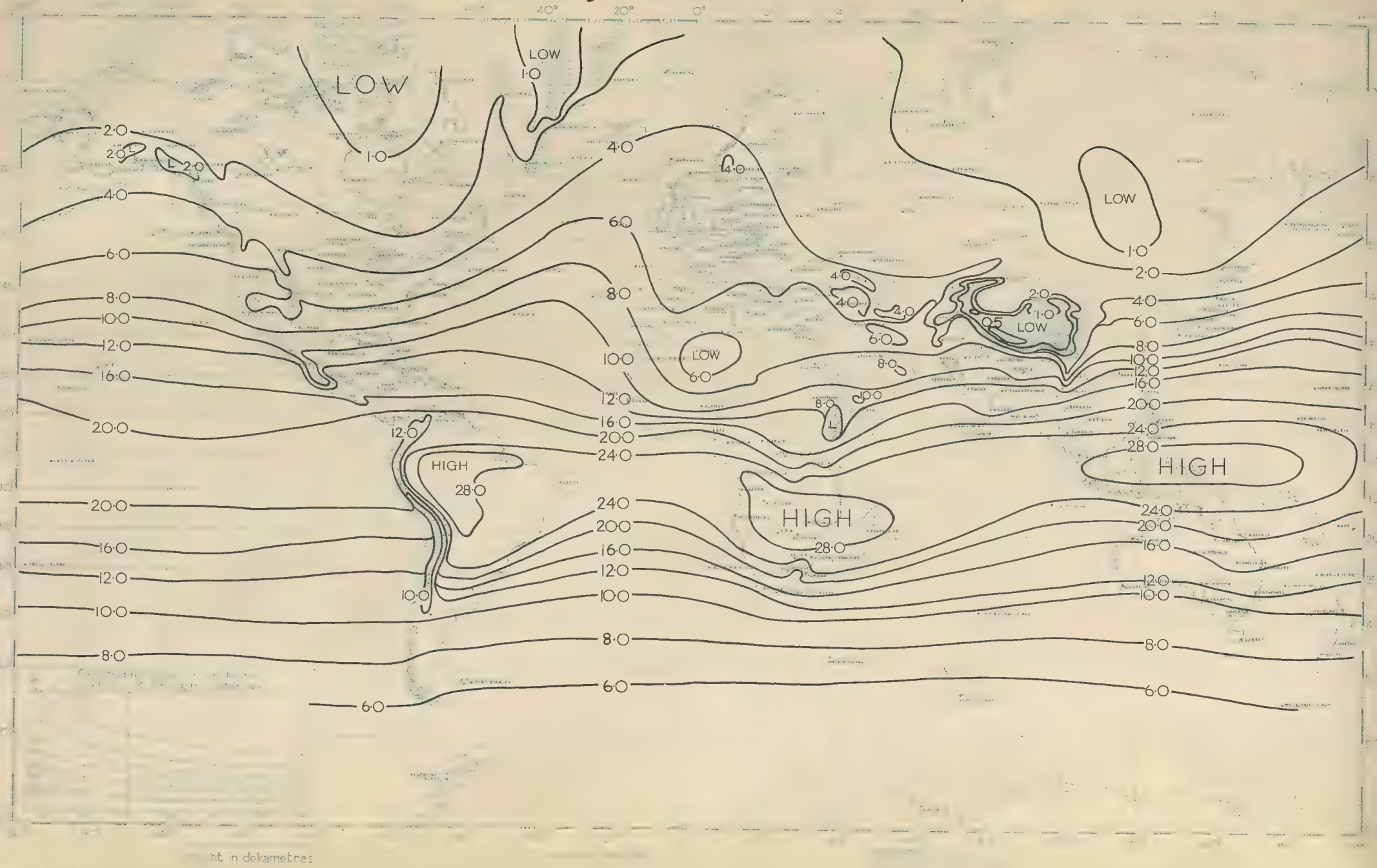

M.R.P. 1075

Water Vapour (1/10 of gm.) above 1 cm² at 700 mb. January 1951–55

Fig. 2 (c)

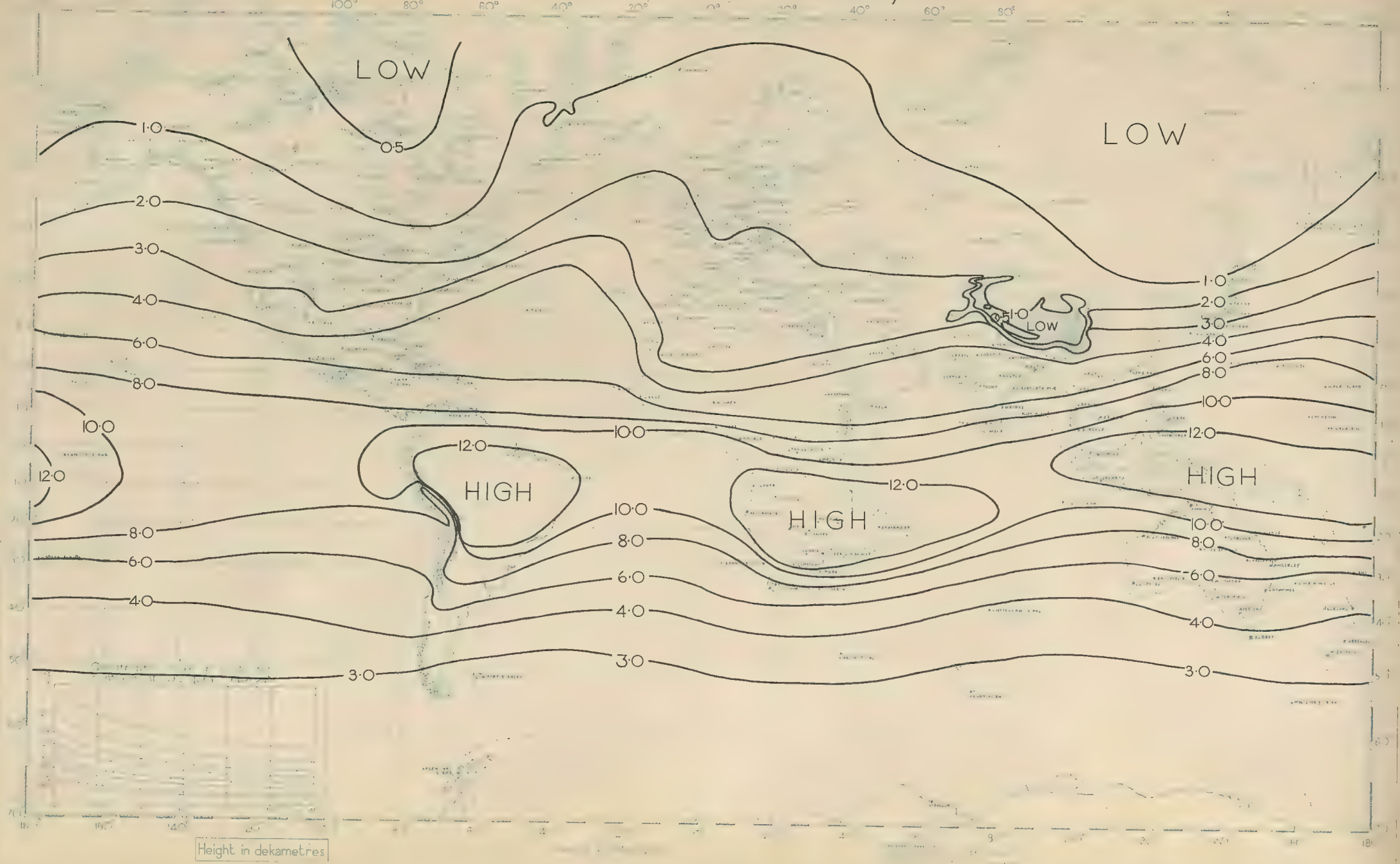

M.R.P. 1075

Water Vapour ($\frac{1}{100}$ of gm.) above 1 cm.^{2} at 500 mb. January 1951-55

Fig 2(d)

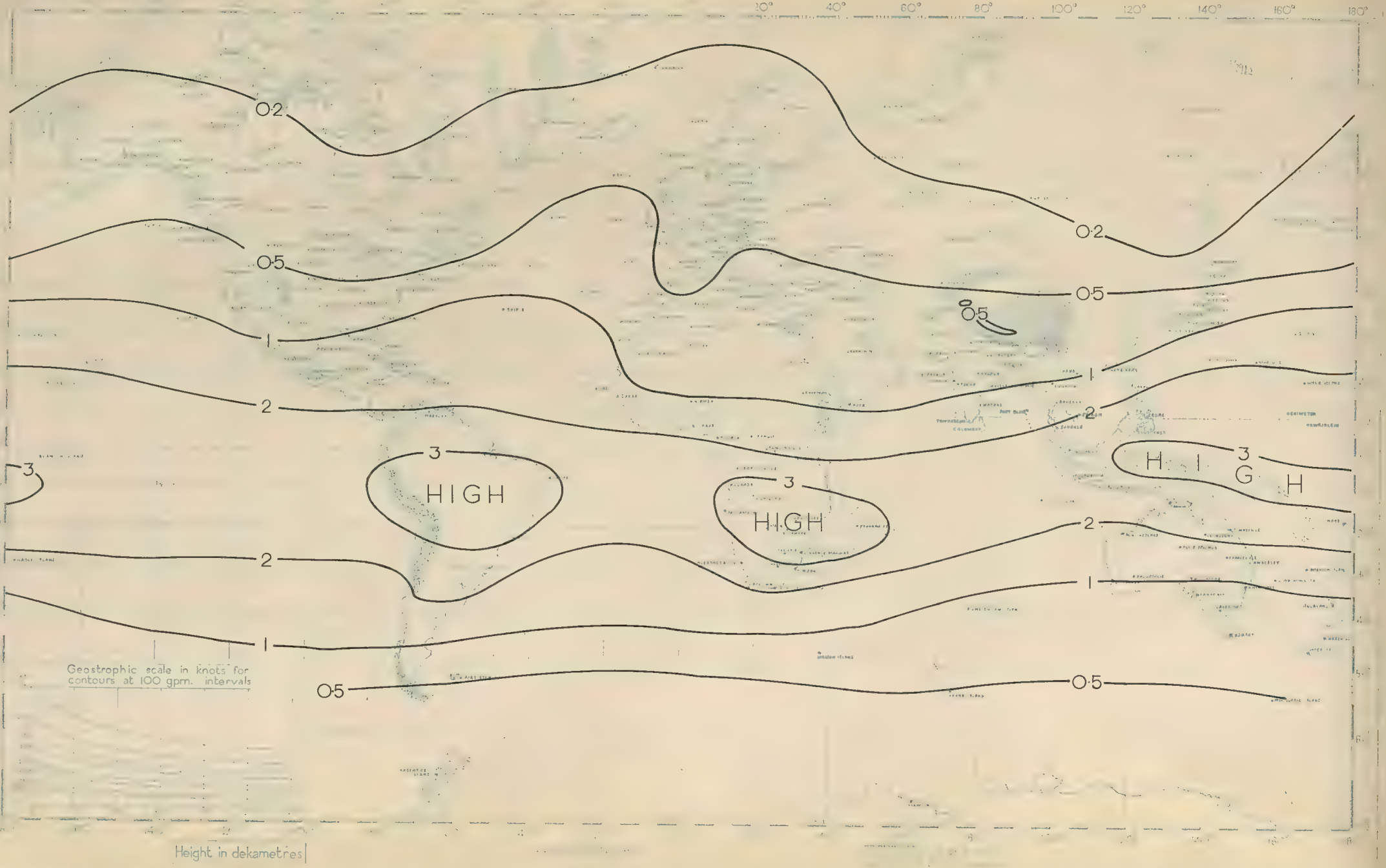

Water Vapour (1/10 of gm) above 1cm² at surface April 1951-55

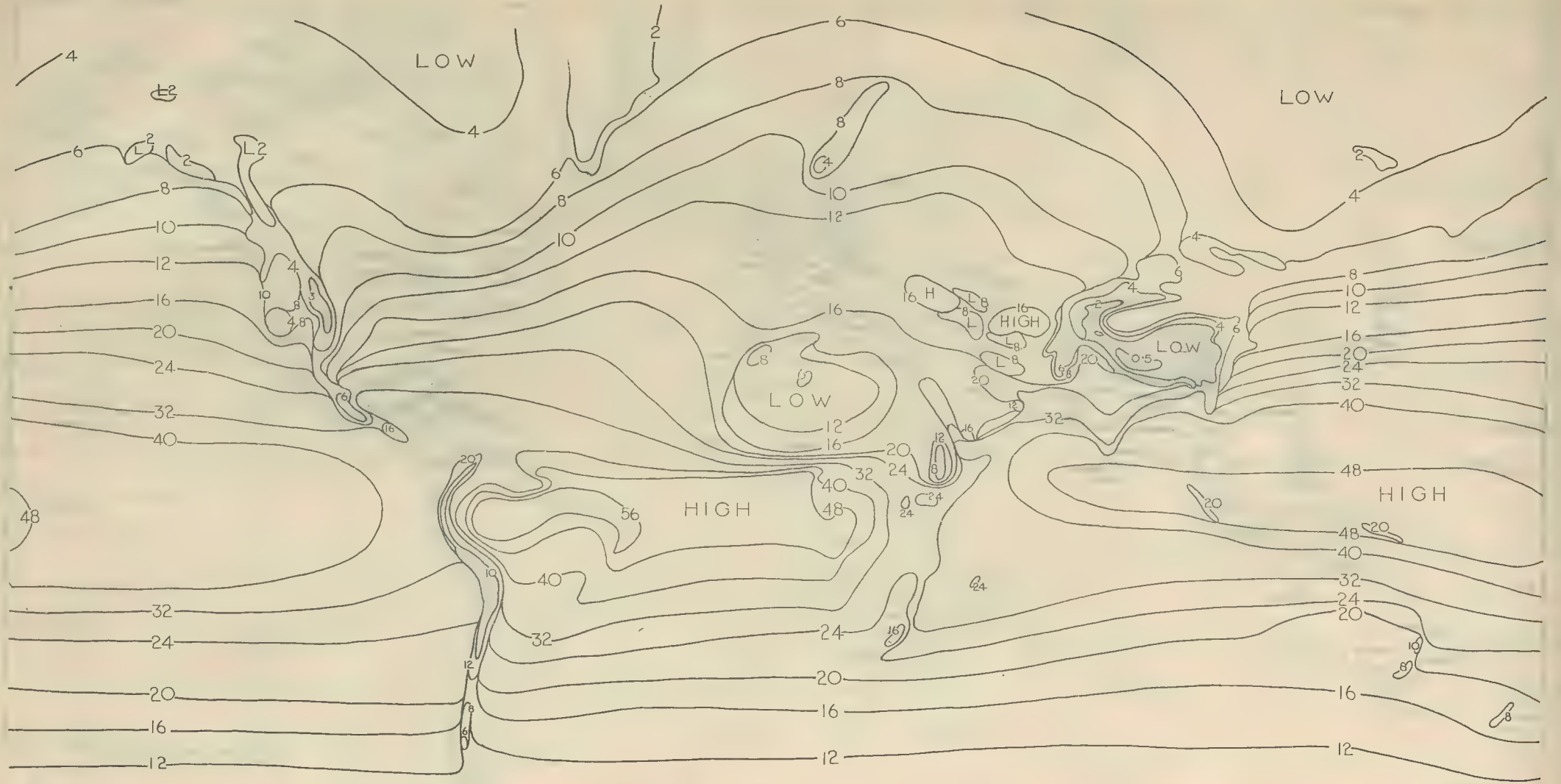

M.R.P. 1075

Water Vapour (1/10 of gram) above 1cm² at 850mb. April 1951–55

Fig.3(b)

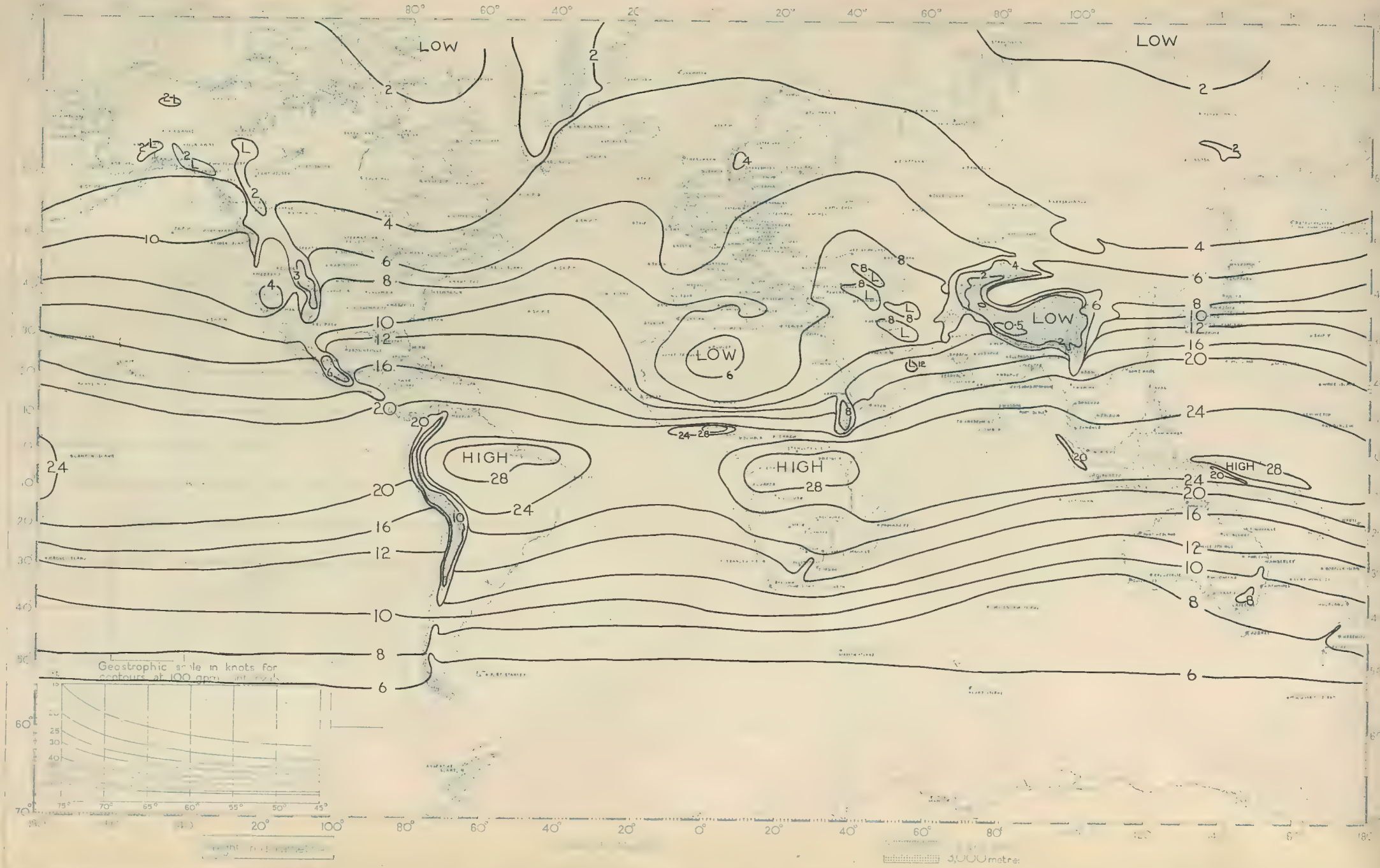

Water Vapour (1/10 of gm) above 1cm² at 700 mb. April 1951-55

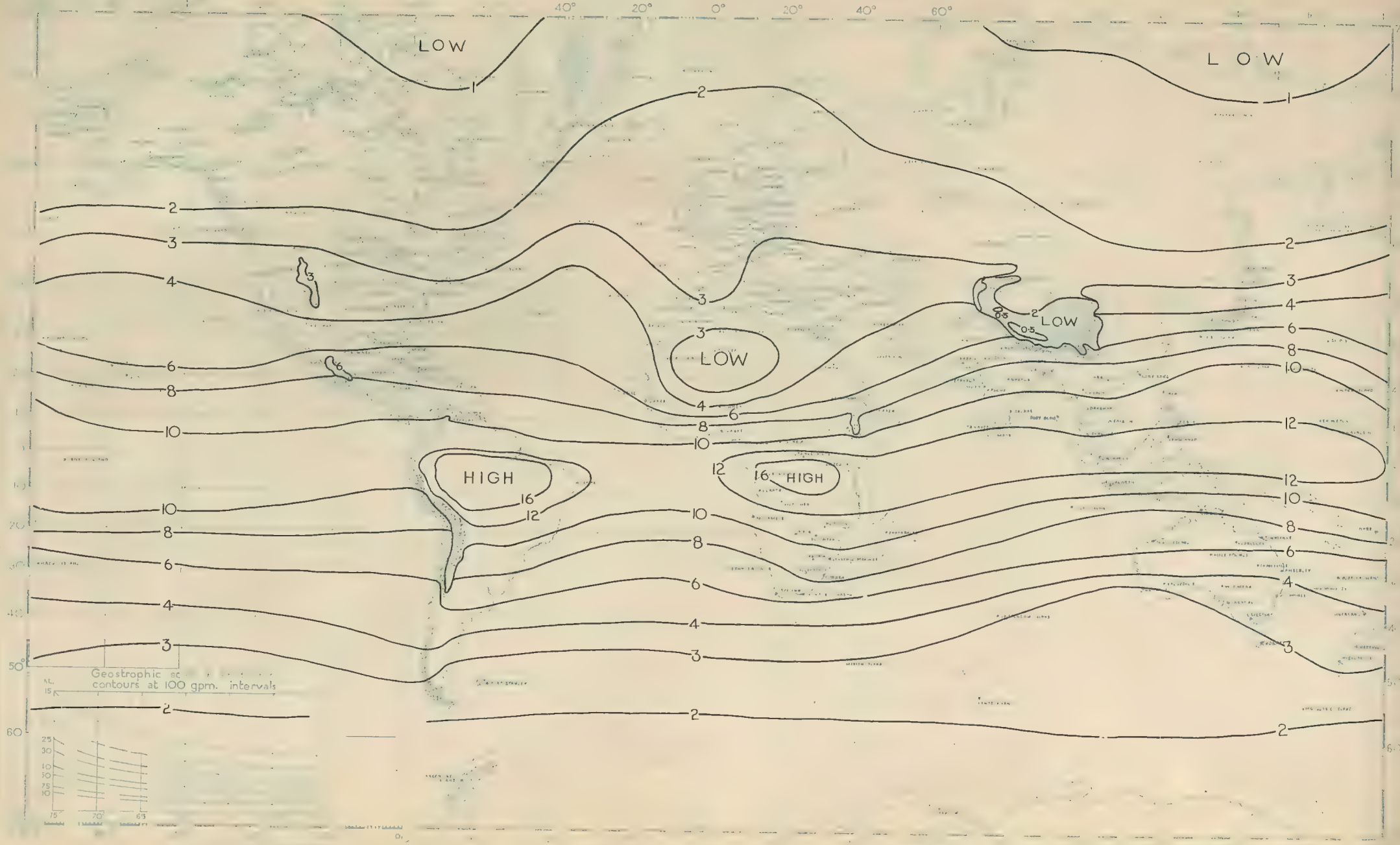

M.R.P. 1075

Water Vapour (% of gm) above 1cm² at 500mb. April 1951-55

Fig.3(d)

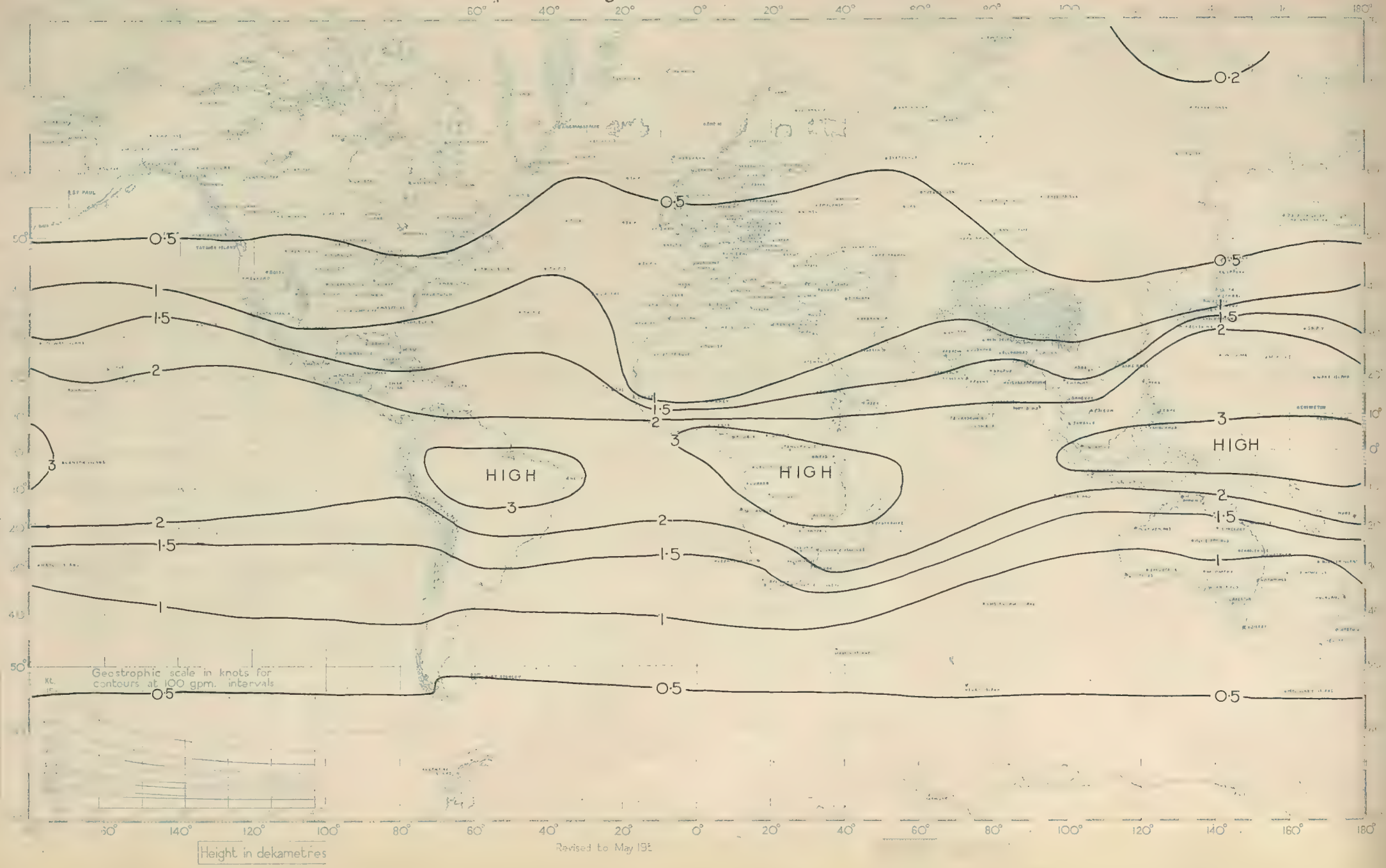

M.R.P 1075

Water Vapour (1/10 of gm) above 1cm.² at surface July 1951–55

Fig. 4(a)

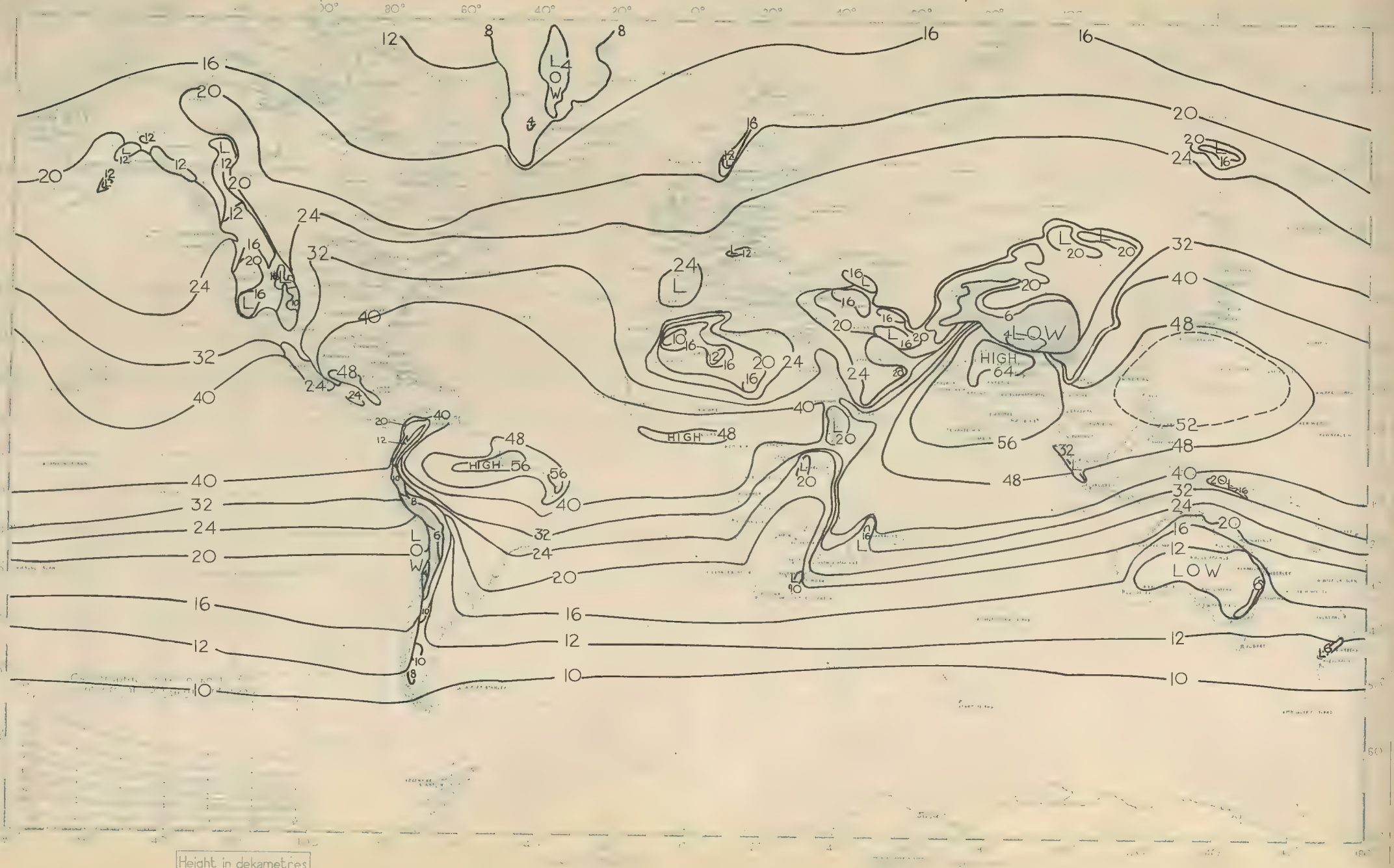

M.R.P. 1075

Water Vapour (% of gm) above 1 cm² at 850 mb July 1951-55

Fig.4(b)

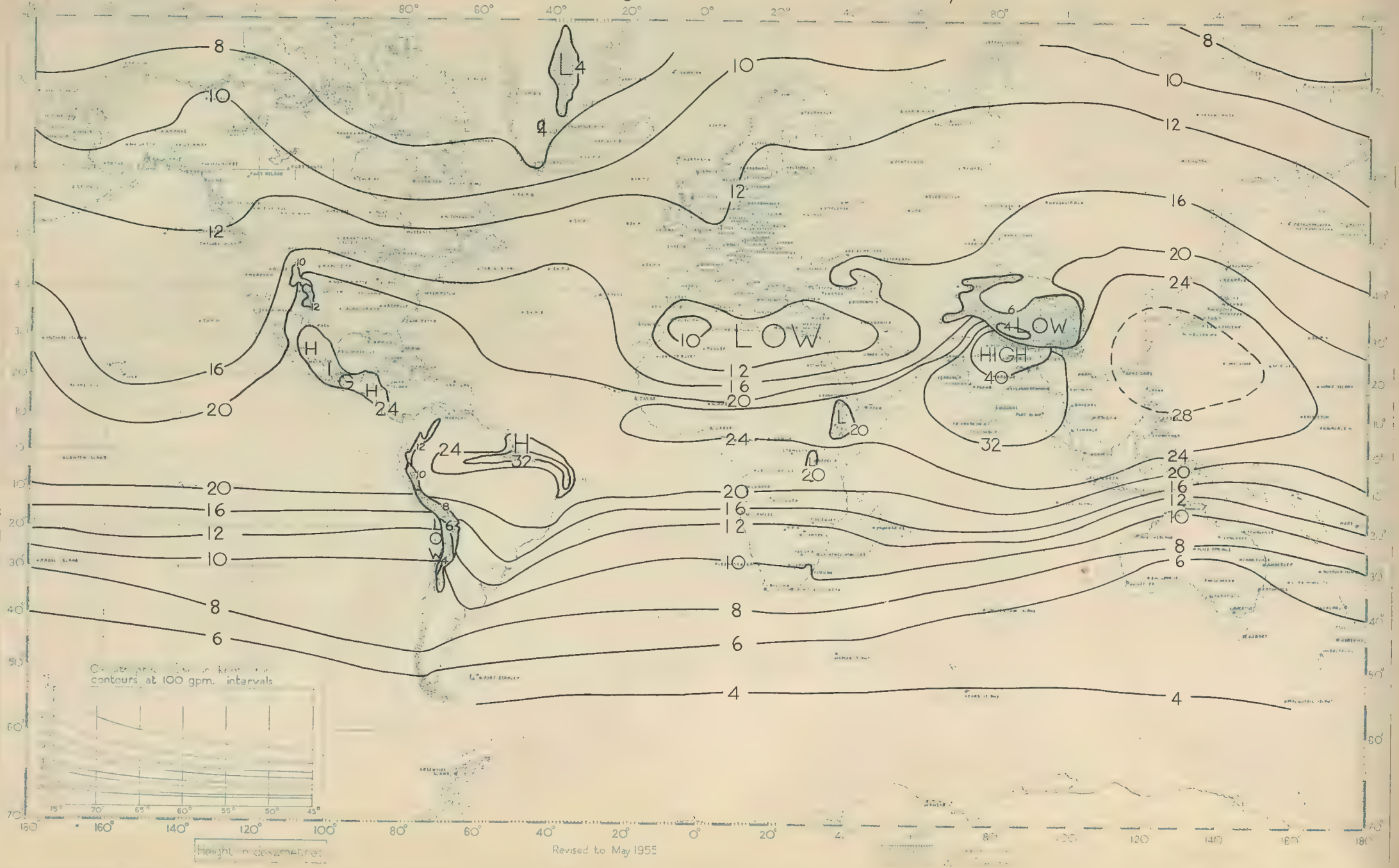

M.R.P. 1075

Water Vapour (1/10 cm gm) above 1 cm² at 700 mb. July 1951-55

Fig.4(c)

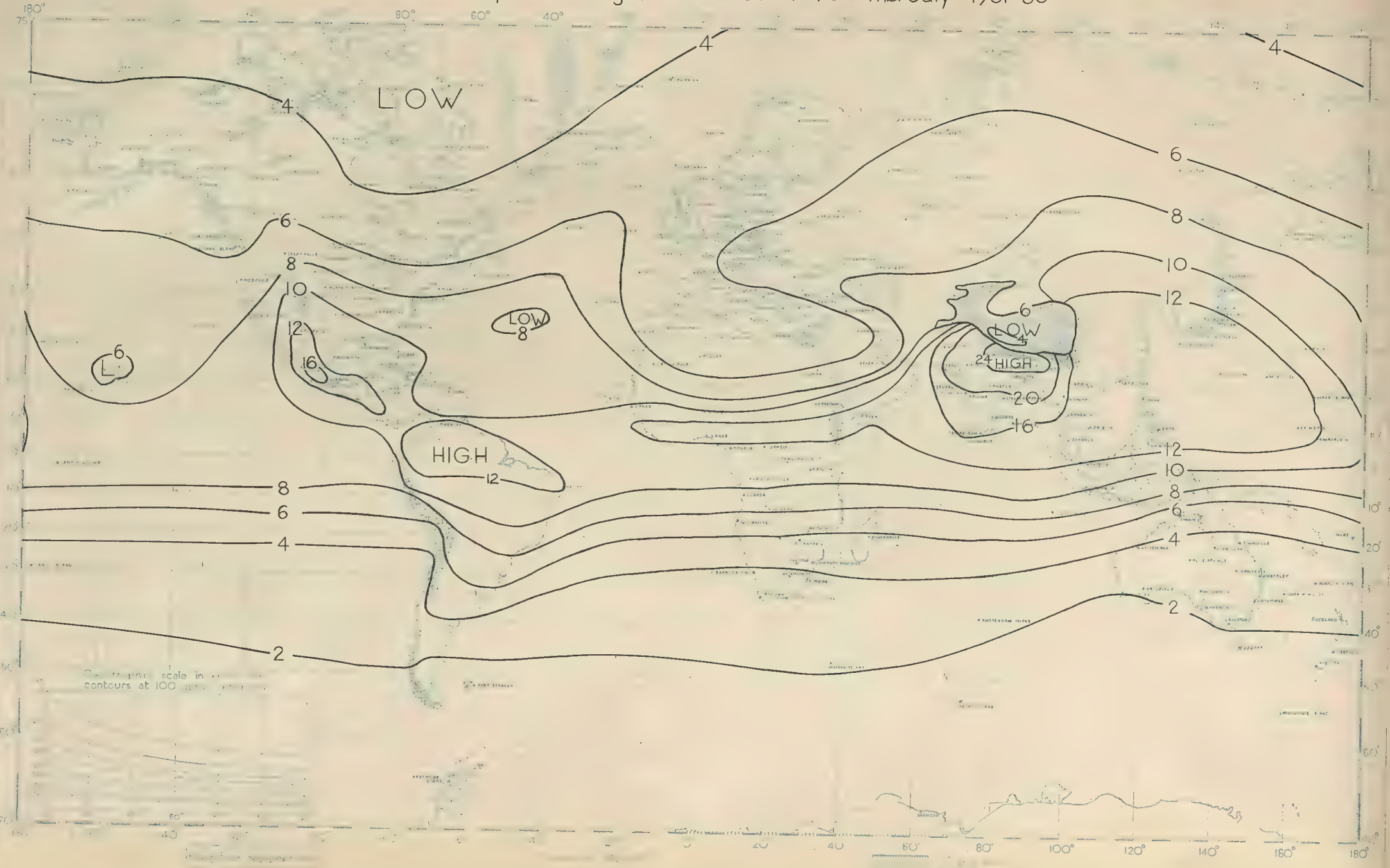

M.R.P. 1075

Water Vapour (⅛ of gm) above 1 cm² at 500 mb July 1951-55

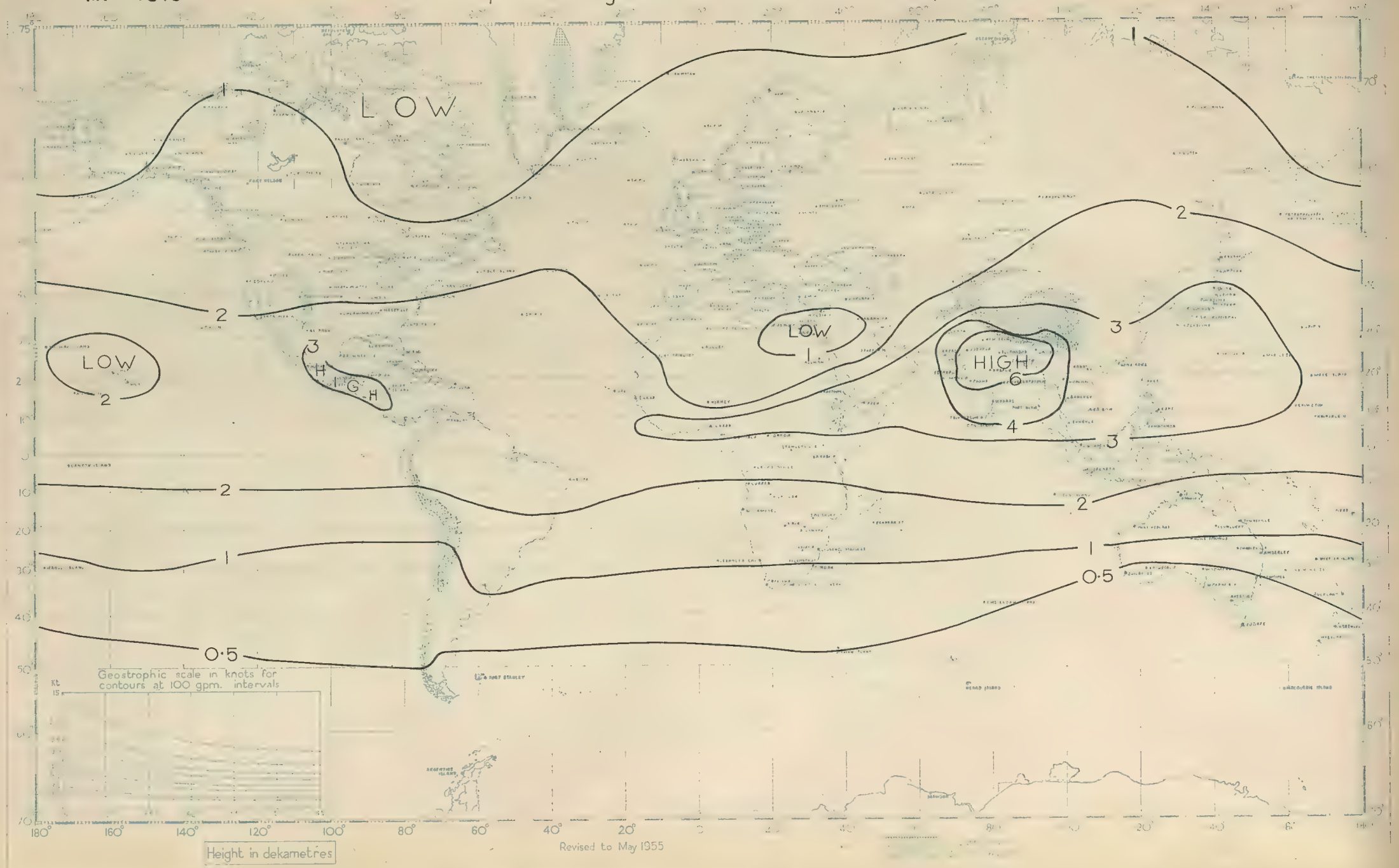

Water Vapour (1/10 of gm.) above 1cm² at surface October 1951-55

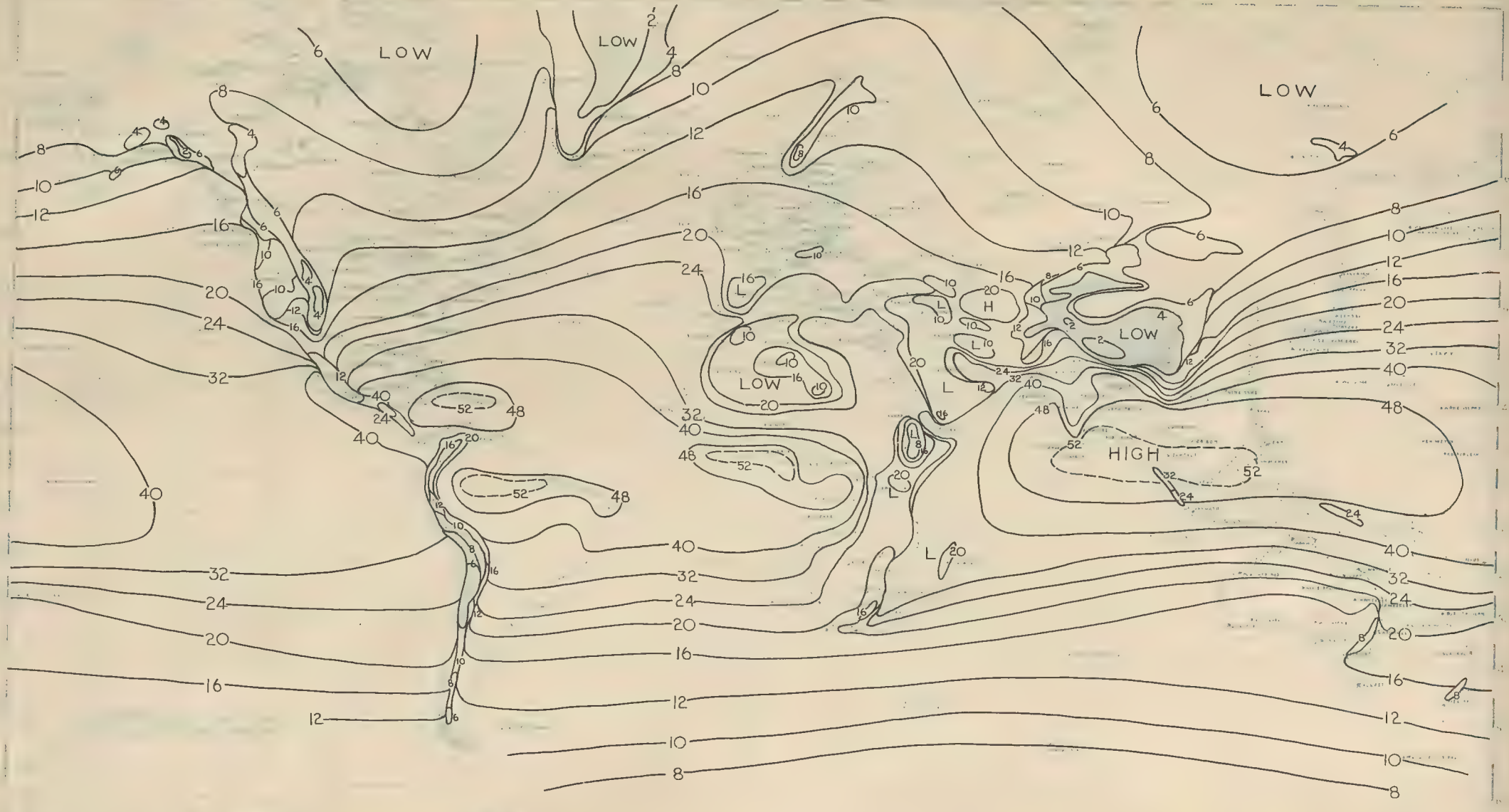

MRP1075

Water Vapour (1/10 of gm) above 1cm² at 850mb. October 1951-55

Fig. 5(b)

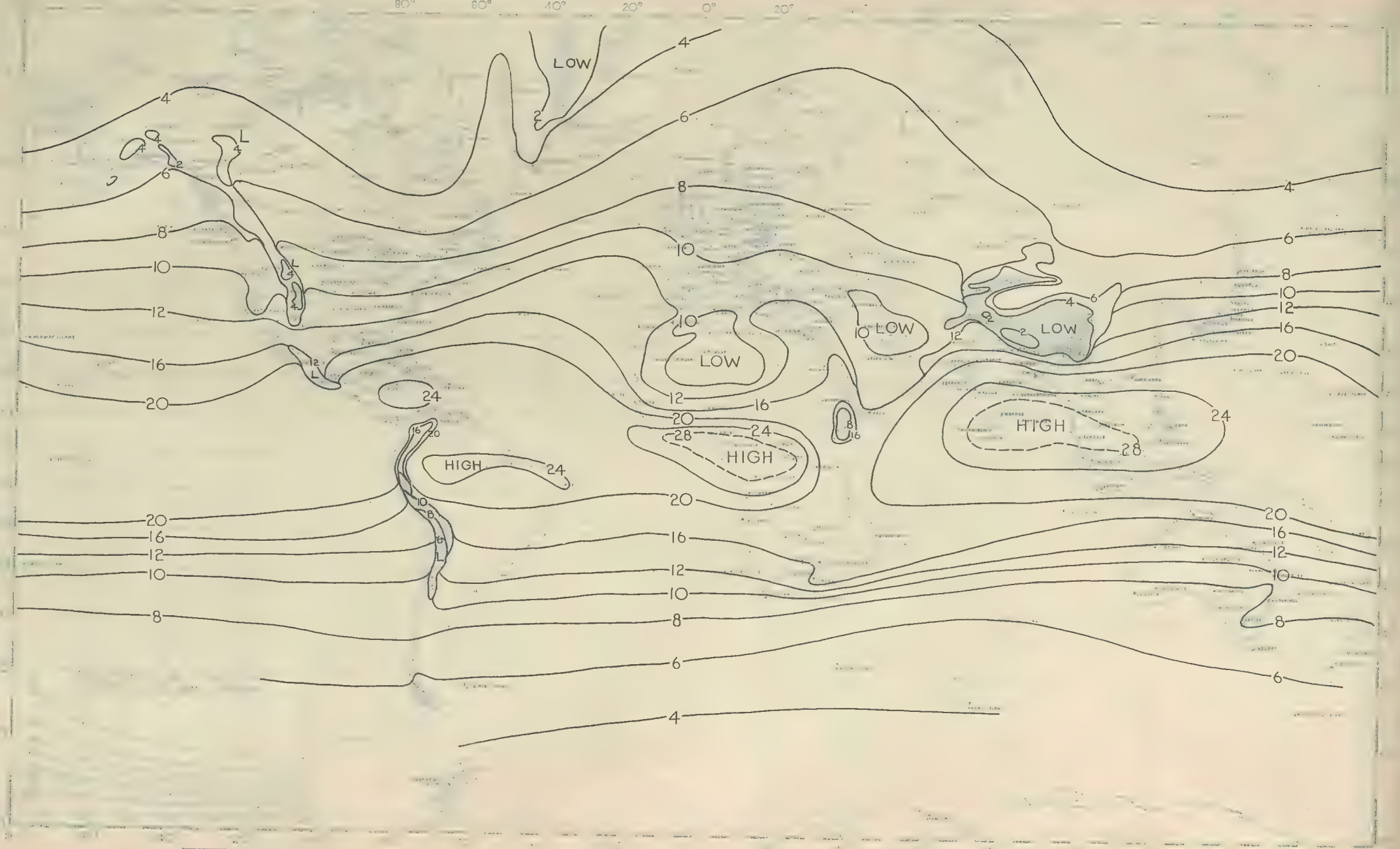

M.R.P. 1075

Water Vapour (1/10 of gram) above 1 cm² at 700mb. October 1951-55

Fig. 5(c)

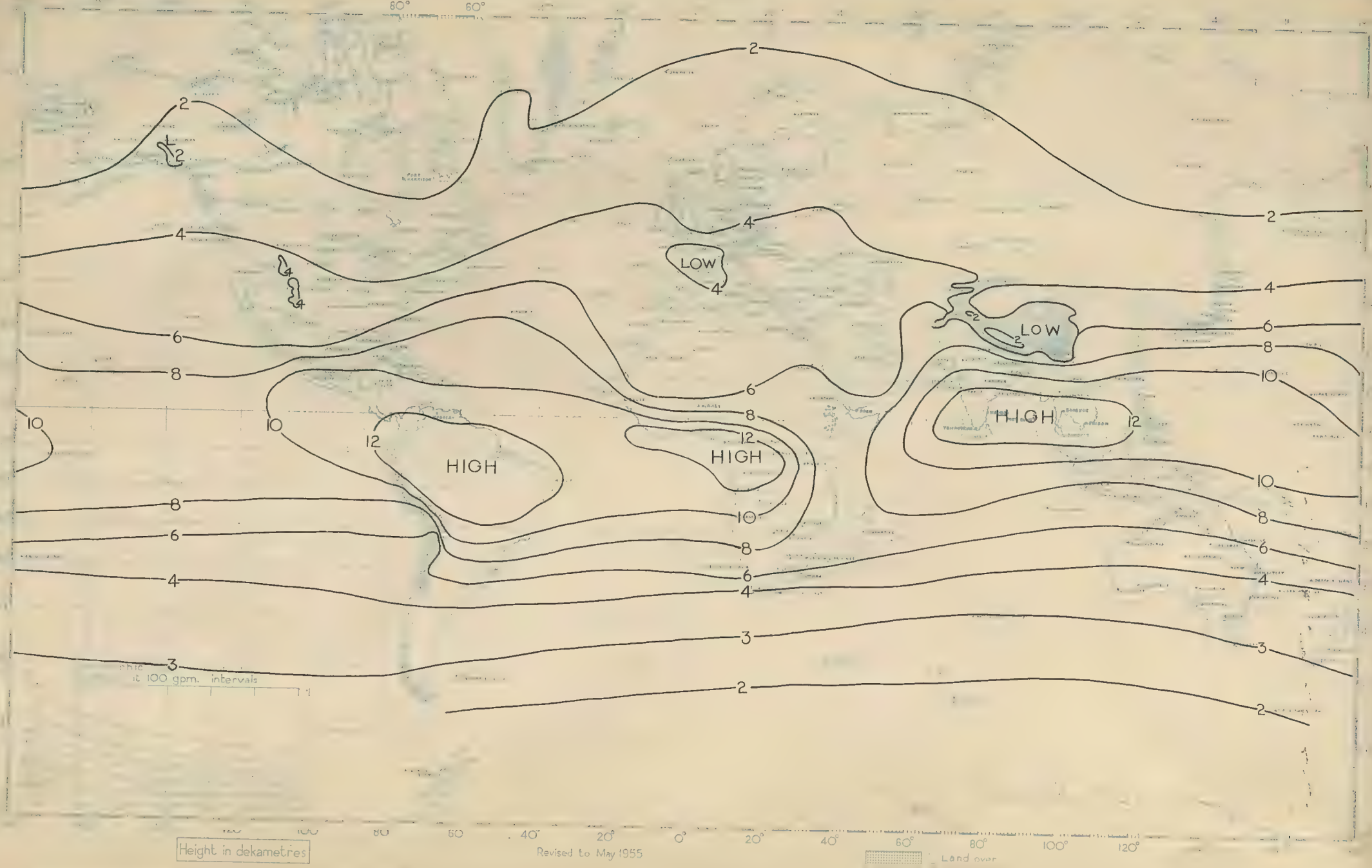

MRP1075

Water Vapour (1/10 of gm) above 1cm² at 500mb. October 1951-55

Fig. 5(d)

MRP 1075

Fig. 6

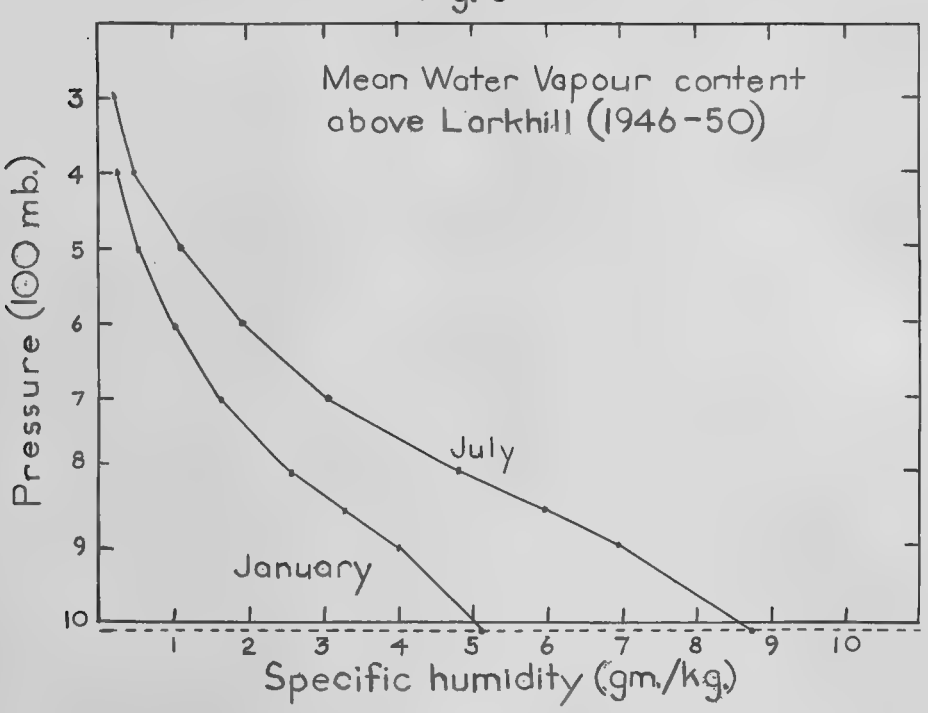

M.R.P. 1077
S.C.1/131
19th November, 1957

The development of precision aneroids - interim report

by

R. Frith

(Meteorological Office)

AIR MINISTRY

METEOROLOGICAL RESEARCH COMMITTEE

At the time of issue this report has not been published. Any author desiring to quote this paper should refer to it as "A paper of the Meteorological Research Committee (London). M.R.P. No. 1077 by Dr. R. FRITH A copy is available in the Library of the Meteorological Office."

M.R.P. 1077
S.C.I/131
19th November, 1957

AIR MINISTRY
METEOROLOGICAL RESEARCH COMMITTEE

The development of precision aneroids - interim report

by

R. Frith (Meteorological Office)

Introduction

Late in 1956 the Meteorological Office received three aneroids (G.1, G.2 and G.3) made to our Specification of Requirements No. 429 (General Purpose Precision Aneroid Barometer) and two aneroids (H.1 and H.2) made to our Specification No. 430 (High Precision Aneroid), all made by the same firm.

The instruments were not tested for robustness but in all other respects, as far as could be judged, they satisfied the requirements of the Specification. The robustness test (Clause 11 in the Specification) has not been made because the instruments are so heavy that a quite unreasonably large "strong wooden crate" would be required to give the protection needed to pass this test. The makers state that this defect could be overcome in future by building the mechanism into a light fabricated case instead of the present, very heavy, cast iron case. For a period of six months these instruments have been read every working day and the readings compared against a mercury barometer (except that Aneroid H.2 was lent to Prestwick after four months for special work there). The readings have now been analysed and the results are presented and discussed. The results of a similar analysis made some years ago on an earlier High Precision Aneroid (B) made for us by the same maker and on a commercially available aneroid (A), made by a different maker are included for comparison.

The basic data

The aneroids were left undisturbed throughout the period. They were sheltered from the sun and were tapped before reading. Two mercury barometers were in the same room. These never differed between themselves by more than 0.3 mb and rarely by more than 0.2. One of the mercury barometers was chosen as the 'standard'.

As far as could be determined, none of the aneroids had any scale error - that is to say, the errors appeared to be the same at all points of the scale. The temperature error, over the range of temperatures experienced, was very small.

The differences (aneroid-mercury barometer) for every reading are shown in Figure 1, and the frequency distribution of these errors is shown in Table 1, (only the period up to the first "jump" is used for Aneroid B)*.

Long-term stability

Figure 2 shows the errors plotted as running means of 10. With the possible exception of G.3, all the new aneroids show a tendency to secular drift in the sense of positive errors increasing, as indicated by pecked lines. This is in the same sense as drifts caused by a gradually weakening spring;

/and

*Until the present series of tests, sudden and persistent changes of 'zero' of this type were found in all aneroids tested.

and in the opposite sense to that caused by a leaking capsule. Instrument A might show the same tendency but there is no sign of it in B.

This drift is large enough to be important where the aneroids could be checked only, say, once a year and where, at the same time, accuracies of 0.5 mb or better are needed.

Accuracy

The effect of secular drift can be reduced to negligible proportions by checks against an accurate barometer at intervals of about two months. Table 2 indicates the accuracy which would have been achieved during the test period if the instruments had been adjusted on the basis of spot checks every two months. In order to make the most of the available data, every (overlapping) group of 40 observations (approximately two months) was separately analysed. The table shows also the accuracy which would have been achieved if the adjustments had been based on the mean of five consecutive (daily) observations instead of a single reading.

Discussion

These results may be discussed in the light of known requirements. The most obvious requirement is for use at sea, both in Selected Ships and in Ocean Weather Ships. Aneroids used in Selected Ships could normally be checked against a mercury barometer on shore at least once every second month without difficulty but the check would probably have to be based on a single reading. If we assume that the performance at sea would be no worse than the performance under laboratory conditions (and this has to be verified) then Table 2 indicates that, with all save one of the aneroids tested, there would be very few errors greater than 0.5 mb. This accuracy is considered to be sufficient for ordinary synoptic purposes at sea. (It should be noted that, where the accuracy aimed at is ±0.5 mb, there was little to choose between the relatively inexpensive commerical Aneroid and the more expensive specially made instruments.)

A rather higher accuracy is desirable on Ocean Weather Ships. Aneroids on Ocean Weather Ships could be checked before every voyage on the basis of five (or even more) daily readings. Assuming, again, that the accuracy at sea is no worse than has been found during these tests, then a 90 per cent accuracy of better than ±0.3 mb would be achieved with all save G.2. One, but only one, of the High Precision Aneroids, has an accuracy very much better than that. Apart from this High Precision Aneroid, the cheaper commercial instrument appears to be just about as good as any of the others.

Conclusions

It seems likely that an available commercial aneroid would be suitable for routine use at sea both on Selected Ships (checked every second month or so) and on Ocean Weather Ships (checked before every voyage).

The performances of the new aneroids were variable. It does not appear worthwhile to have aneroids specially made for us unless we could be sure that they would be as good as H.1 (the only one which was significantly better than A). This matter is being discussed with the makers.

(Note. We are also having made, and delivery is expected at any time, an aneroid which uses an ordinary capsule but, instead of the usual delicate magnification system of levers or chains, uses a robust electronic contact device. This instrument will also be tested for stability and accuracy.)

/Table 1.

Table 1. Percentage frequency distribution of errors over a period of about six months

	Error (aneroid - mercury barometer) - mb																				Mean error
	$\bar{0.5}$	$\bar{0.4}$	$\bar{0.3}$	$\bar{0.2}$	$\bar{0.1}$	0	0.1	0.2	0.3	0.4	0.5	0.6	0.7	0.8	0.9	1.0	1.1	1.2	1.3	1.4	1.5	
G.1									1	5	9	14	23	27	15	7						+0.75
G.2									1	2	0	2	8	8	12	14	16	14	13	8	3	+1.1
G.3						1	7	12	14	28	14	7	7	2								+0.4
H.1							2	6	8	23	27	25	8	1	1							+0.5
H.2									3	1	6	18	30	21	16	3	1					+0.75
A			2	8	12	18	15	20	10	5	6	3	1									+0.15
B	2	2	3	10	20	25	13	20	3	1	0	2										+0.0

/Table 2.

Table 2. Percentage number of observations with errors not greater than specified amounts when aneroids are checked against a mercury barometer once every two months.

	Errors not greater than			
	± 0.3	± 0.5	± 0.3	± 0.5
	(Check based on a single reading)		(Check based on mean of 5 consecutive readings)	
G.1	90	99	94	100
G.2	74	91	78	98
G.3	84	97	91	99
H.1	93	100	100	100
H.2	90	99	94	100
A	80	97	92	98
B	84	98	93	99

M.O. Specification No. 429
Issue 1.
October, 1954.

METEOROLOGICAL OFFICE, AIR MINISTRY

Specification of Requirements for General Purpose Precision Aneroid Barometer

A. Materials

The best material for tropical and Arctic use commercially available for the purpose shall be used. Wherever possible, metals used shall be non-corrosive; if corrosive materials are used they shall, wherever possible, be adequately protected from corrosion by plating, lacquer, baked enamel, or other suitable covering or finish. Finishes which will crack, chip or peel under normal usage and ageing, or when subjected to changes of temperature and humidity, shall not be employed. Wear surfaces of gear teeth, pivots, bearing faces, etc. which cannot be protected with finishes shall be made of a material which will not appreciably tarnish or form oxydisation films.

B. Construction

1. The instrument shall be suitable for use at sea and in the field and it shall not be affected by the sort of vibration and movement experienced on a ship. It shall be sufficiently robust to withstand all ordinary transit risks when packed in a transit case (which shall be supplied with the instrument).

2. Means shall be provided for mounting the instrument vertically on a panel.

3. The dial shall cover the range of at least 930 - 1055 mb. and shall be graduated every millibar.

4. The distance between graduation marks shall be not less than .04 in.

5. The face of the dial shall be white, or matt silver.

6. The width of the pointer at the end extending over the graduations shall be not wider than 0.01".

7. There shall be some anti-parallax device.

8. The readings at any point shall not differ by more than 0.5 millibar when the instrument is used in a horizontal or in any vertical position.

9. A screw adjustment shall be provided, for setting the instrument, and it shall be possible to set the instrument accurately to 0.3 millibar. It shall be possible to make this adjustment whilst the instrument is mounted vertically on a panel.

10. The case of the instrument shall be airtight and fitted with a static connection in the side of the case. It should be possible to close this static connection.

11. With the static connection open the instrument shall be capable of withstanding pressures of 500 millibars and 1200 millibars without damage or change of calibration.

C. Accuracy

Random errors shall not exceed 0.5 millibar. (This includes hysteresis). Calibration (scale) errors shall not exceed 0.5 millibar.

/D.

D. Temperature Errors

The instrument shall be compensated for temperature: the reading at any point shall not change by more than 0.5 millibar for a change of temperature of 20 degrees C.

E. Drift

During the course of a year the scale error at any point shall not change by more than 1.0 mb.

Note

No relaxation of Clauses A, B.1, B.2, B.3, B.9, B.11, C and E can be tolerated. Manufacturers may, if they wish, quote for instruments not satisfying B.4, B.5, B.6, B.7, B.8, B.10, and D, but the extent to which these clauses will not be met must be stated in the quotation.

F. Tests

1. Visual and mechanical inspection

The instrument will be given a visual and mechanical inspection to determine the quality of materials, workmanship and general compliance with the requirements of this specification.

2. Vibration

There shall be no change in the reading when the instrument is subjected to vibration similar to that experienced on board ship.

3. Pressure seal

With the static connection closed and pressure reduced to 500 mb. the indicated pressure shall not change by more than 1 millibar in 10 minutes.

4. Calibration

The instrument will be calibrated in a pressure chamber at a temperature of about 20°C. The error at any point shall not exceed 1.0 millibar. During this calibration the pressure shall be changed at a rate not exceeding 10 millibars per minute and shall be held constant for at least one minute before any reading is taken. Readings shall be taken at about 10 millibar intervals over the whole range of the barometer.

5. Looseness and Backlash

The pressure shall be decreased from atmospheric to 930 mb. in 10 millibar steps and read at each step. The process shall be repeated for increasing pressure to 1050 mb. and then decreased again to atmospheric. The average difference in reading for increasing and decreasing pressure shall not exceed 0.5 millibar and at no point exceed 1.0 millibar.

6. Movement

The movement of the indicating hand shall be noted in tests 4 and 5. When the pressure is changing uniformly the indicating hand shall move uniformly. Irregular motion of the indicating hand shall be a cause for rejection of the instrument.

7. Friction

The aneroid shall be held in the hand and read without jarring or rotating, the instrument shall then be slowly and carefully lowered 3 feet. There shall be a perceptible movement of the indicating hand. The barometer shall then be raised 3 feet. There shall be a perceptible movement of the indicating hand.

8. Random Errors

The test specified in section 4 shall be repeated. The mean error shall not differ from the mean error obtained from the original calibration by more than 0.5 millibar and the difference shall not exceed 1.0 millibar at any point.

9. Change in error at 40°C.

The instrument shall be kept at 40°C. for at least 2 hours before testing. The test described in section 4 shall be carried out at a temperature of 40°C. The average error shall not differ from that found in the original calibration by more than 1.0 millibar.

10. Change in error at 0°C

The instrument shall be kept at 0°C. for at least 2 hours before testing. The test described in section 4 shall be carried out at a temperature of 0°C. The average error shall not differ from that found in the original calibration by more than 1.0 millibar.

11. Shock

The instrument, packed in its carrying case, and this, in turn, packed in a strong wooden crate and protected by wood wool (or similar) shall be dropped from a height of 3 feet on to a concrete floor on each corner, and each face in turn. The instrument shall then be tested as in sections 4 and 5: the mean change shall not exceed 0.5 millibar and the error shall not exceed 1.0 millibar at any point.

Note

Failure to pass this test will result in rejection of the instrument. The manufacturer will be notified when the test is to take place and he may, if he wishes, be represented at the test.

Annex 2 to M.R.P. 1077

M.O. Specification No. 430
Issue 1.
October, 1954

METEOROLOGICAL OFFICE, AIR MINISTRY

Specification of Requirements for High Precision Aneroid Barometers

A. Materials

The best material for tropical and Arctic use commercially available for the purpose shall be used. Wherever possible metals used shall be non-corrosive; if corrosive materials are used they shall, wherever possible, be adequately protected from corrosion by plating, lacquer, baked enamel, or other suitable covering or finish. Finishes which will crack, chip or peel under normal usage and ageing, or when subjected to changes of temperature and humidity, shall not be employed. Wear surfaces of gear teeth, pivots, bearing faces, etc. which cannot be protected with finishes shall be made of a material which will not appreciably tarnish or form oxydisation films.

B. Construction

1. The instrument shall be suitable for use at sea and in the field and it shall not be affected by the sort of vibration and movement experienced on a ship. It shall be sufficiently robust to withstand all ordinary transit risks when packed in a transit case (which shall be supplied with the instrument).

2. Means shall provided for mounting the instrument vertically on a panel.

3. The dial shall cover the range of at least 930 - 1055 mb. and shall be graduated every millibar.

4. The distance between graduation marks shall be not less than 0.1 in.

5. The face of the dial shall be white or matt silver. The graduation marks shall be black, clean-cut, clear and of uniform width between 0.004" and 0.007".

6. The width of the pointer at the end extending over the graduations shall be not wider than 0.01".

7. There shall be some anti-parallax device.

8. With the pressure held constant the readings shall not differ by more than 0.5 millibar when the instrument is used in a horizontal or in any vertical position.

9. A screw adjustment shall be provided for setting the instrument, and it shall be possible to set the instrument accurately to 0.1 millibar. It shall be possible to make this adjustment whilst the instrument is mounted vertically on a panel.

10. The case of the instrument shall be airtight and fitted with a static connection in the side of the case. It should be possible to close this static connection.

11. With the static connection open the instrument shall be capable of withstanding pressures of 500 millibars and 1200 millibars without damage or change of calibration

/C.

C. Accuracy

Random errors shall not exceed 0.2 millibar. (This includes hysteresis). Calibration (scale) errors shall not exceed 0.4 millibar.

D. Temperature Errors

The instrument shall be compensated for temperature: the reading at any point shall not change by more than 0.5 millibar for a change of temperature of 20 degrees C.

E. Drift

During the course of a year the scale error at any point shall not change by more than 0.5 mb.

Note

No relaxation of Clauses A, B.1, B.2, B.3, B.6, B.7, B.9, B.11, C and E can be tolerated. Manufacturers may, if they wish, quote for instruments not satisfying A.4, A.5, A.8, A.10 and D, but the extent to which these clauses will not be met must be stated in the quotation.

F. Tests

1. Visual and mechanical inspection

The instrument will be given a visual and mechanical inspection to determine the quality of materials, workmanship and general compliance with the requirements of this specification.

2. Vibration

There shall be no change in the reading when the instrument is subjected to vibration similar to that experienced on board ship.

3. Pressure seal

With the static connection closed and pressure reduced to 500 mb. the indicated pressure shall not change by more than 1 millibar in 10 minutes.

4. Calibration

The instrument will be calibrated in a pressure chamber at a temperature of about 20°C. The error at any point shall not exceed 0.6 millibar. During this calibration the pressure shall be changed at a rate not exceeding 10 millibars per minute and shall be held constant for at least one minute before any reading is taken. Readings shall be taken at about 10 millibar intervals over the whole range of the barometer.

5. Looseness and Backlash

The pressure shall be decreased from atmospheric to 930 mb. in 10 millibar steps and read at each step. The process shall be repeated for increasing pressure to 1050 mb. and then decreased again to atmospheric. The average difference in reading for increasing and decreasing pressure shall not exceed 0.2 millibar and at no point exceed 0.4 millibar.

6. Movement

The movement of the indicating hand shall be noted in tests 4 and 5. When the pressure is changing uniformly the indicating hand shall move uniformly. Irregular motion of the indicating hand shall be a cause for rejection of the instrument.

/7.

7. Friction

The aneroid shall be held in the hand and read; without jarring or rotating, the instrument shall then be slowly and carefully lowered 3 feet. There shall be a perceptible movement of the indicating hand. The barometer shall then be raised 3 ft. There shall be a perceptible movement of the indicating hand.

8. Random Errors

The test specified in section 4 shall be repeated. The mean error shall not differ from the mean error obtained from the original calibration by more then 0.2 millibar and the difference shall not exceed 0.4 millibar at any point.

9. Change in error at 40°C.

The instrument shall be kept at 40°C. for at least 2 hours before testing. The test described in section 4 shall be carried out at a temperature of 40°C. The average error shall not differ from that found in the original calibration by more than 0.5 millibar.

10. Change in error at 0°C.

The imstrument shall be kept at 0°C. for a least 2 hours before testing. The test described in section 4 shall be carried out at a temperature of 0°C. The average error shall not differ from that found in the original calibration by more than 0.5 millibar.

11. Shock

The instrument, packed in its carrying case and this, in turn, packed in a strong wooden crate and protected by wood wool (or similar) shall be dropped from a height of 3 feet on to a concrete floor on each corner, and each face in turn. The instrument shall then be tested as in sections 4 and 5: the mean change shall not exceed 0.2 millibar and the error shall not exceed 0.4 millibar at any point.

Note

Failure to pass this test will result in rejection of the instrument. The manufacturer will be notified when the test is to take place and he may, if he wishes, be represented at the test.

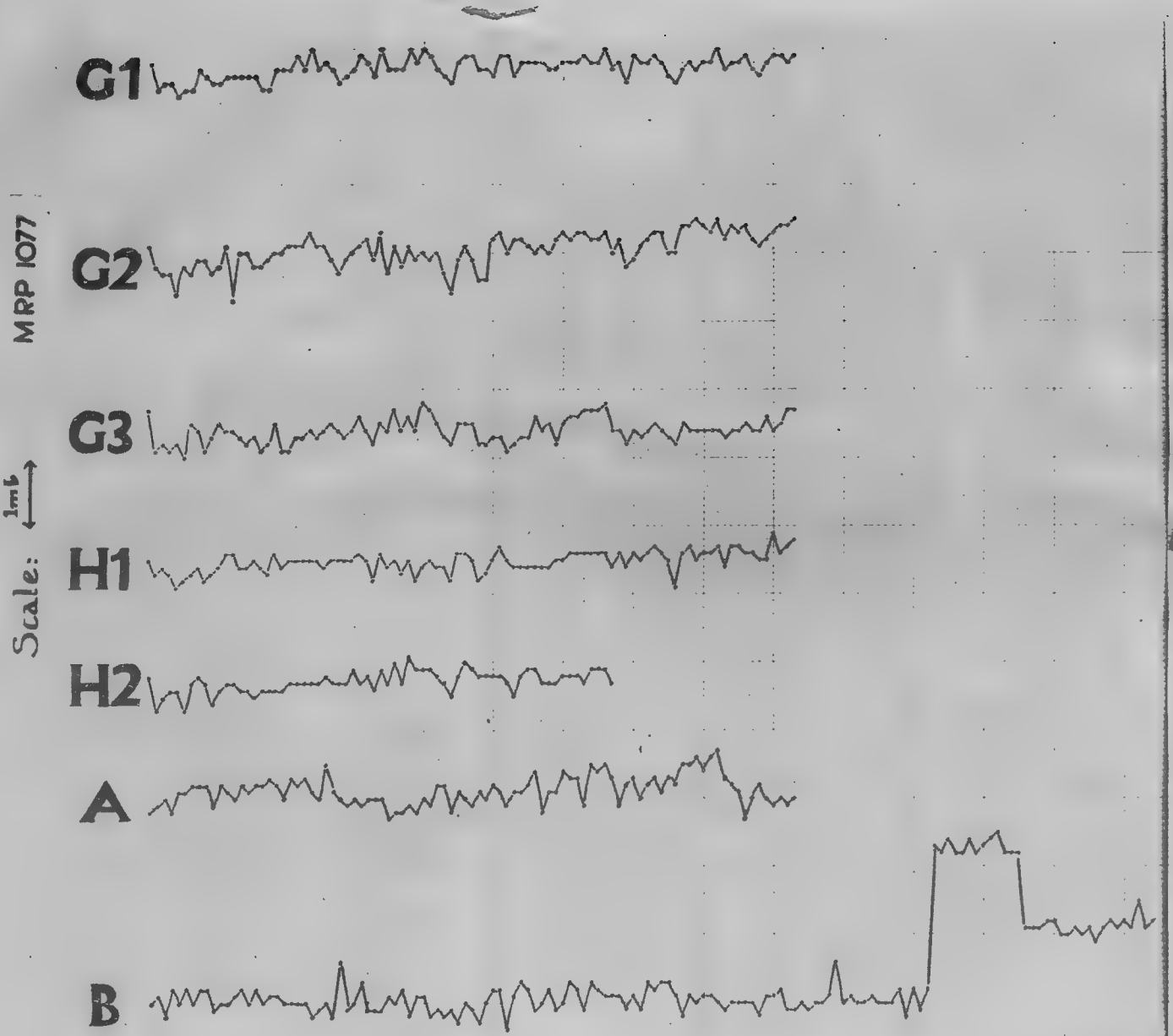

Fig. 1.

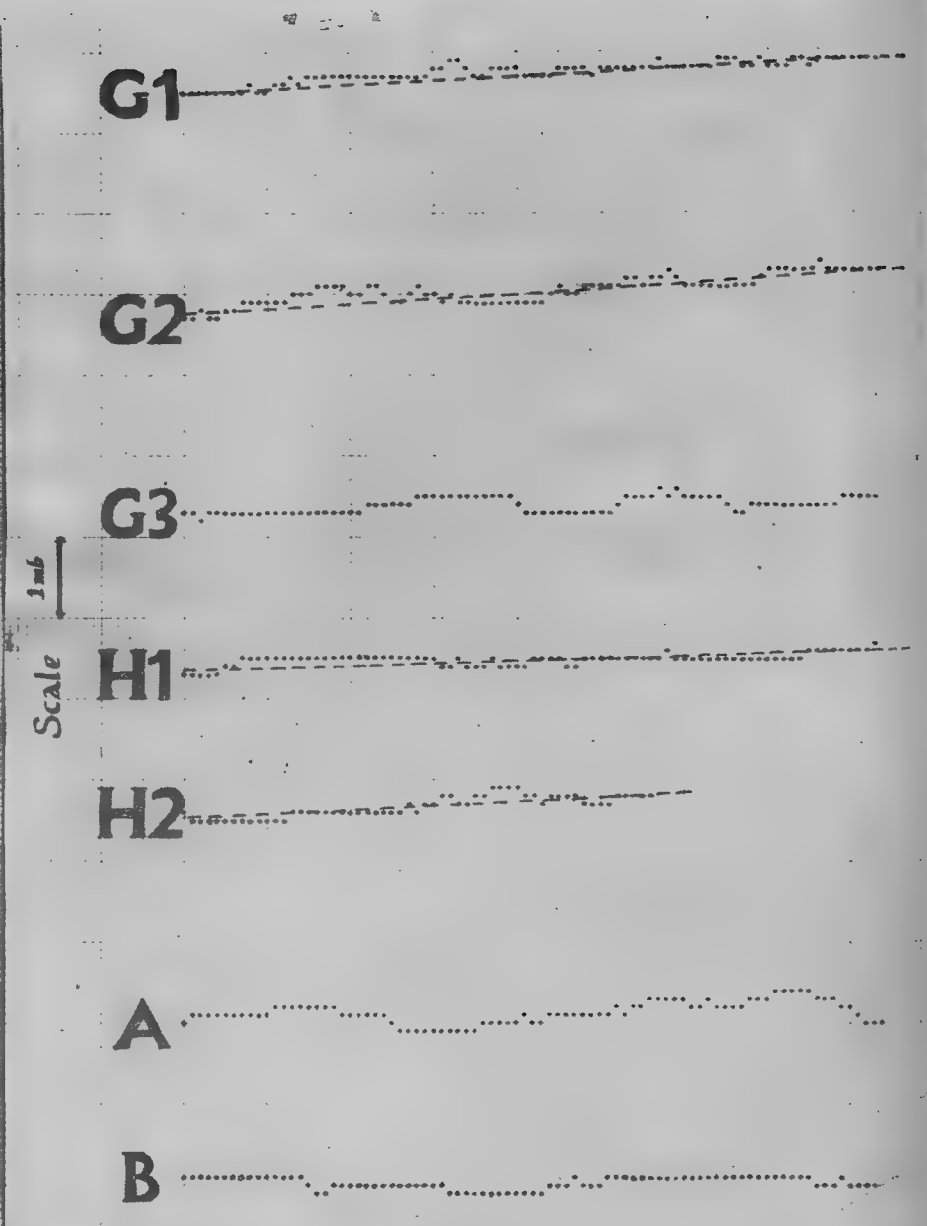

Fig. 2

M.R.P. 1078
S.C.11/246
15th November, 1957

Conservation of Vorticity at 100 mb

by

J. R. Probert-Jones

(Meteorological Office)

AIR MINISTRY

METEOROLOGICAL RESEARCH COMMITTEE

At the time of issue this report has not been published. Any author desiring to quote this paper should refer to it as "A paper of the Meteorological Research Committee (London), M.R.P. No. 1078 by Mr. J.R. PROBERT-JONES A copy is available in the Library of the Meteorological Office."

M.R.P.1078
S.C.II/246
15th November, 1957

AIR MINISTRY

METEOROLOGICAL RESEARCH COMMITTEE

Conservation of Vorticity at 100 mb

by
J. R. Probert-Jones (Meteorological Office)

1. Introduction

The purpose of the experiment described in this report has been to ascertain whether the flow at 100 mb can be treated as essentially non-divergent. The method of attack has been to determine whether sequences of 100 mb charts can be so drawn that (geostrophic) absolute vorticity is conserved in the motion. The graphical technique developed by Fjortoft (1) has been used.

2. Theory

The vorticity equation in non-divergent flow, neglecting vertical motion, is

$$\frac{\partial \eta}{\partial t} + \underline{V} \cdot \underline{\nabla} \eta = 0, \qquad (1)$$

where η is the absolute vorticity.

If we consider geostrophic motion in an isobaric surface,

$$\eta = \frac{g}{l} \nabla^2 z + l$$

and $\underline{V} = \frac{g}{l} \underline{k} \wedge \underline{\nabla} z$, where 'z' is the height of the isobaric surface, 'l' is the Coriolis parameter, and 'k' the unit vertical vector, equation (1) becomes:

$$\frac{\partial}{\partial t} \nabla^2 z = -J(z, \eta) \qquad (2)$$

If Z_i are the values of z at the four points of a square mesh of side 2h surrounding a point 0, a simple finite difference approximation to $\nabla^2 z$ is

$$\nabla^2 z = \frac{1}{h^2} \left(\sum_{i=1}^{4} Z_i - 4 Z_0 \right) = \frac{4}{h^2} \left(\bar{Z} - Z_0 \right),$$

where $$\bar{Z} = \frac{1}{4} \sum_{i=1}^{4} Z_i .$$

/Equation

Equation (2) gives:

$$\frac{\partial}{\partial t}\left(Z-\bar{Z}\right) = -\frac{l}{m^2}\,\underline{V}\cdot\underline{\nabla}\left\{\frac{m^2}{l}\left(Z-\bar{Z}\right)\right\} + \underline{V}\cdot\frac{lh^2}{4gm^2}\underline{\nabla}l, \quad (3)$$

where m is the scale factor of the map projection used. Putting:

$$G = \int_0^{\theta} \frac{l^2h^2}{4gm^2}\cot\theta\, d\theta,$$

θ being the latitude, and neglecting $(Z - \bar{Z})\underline{\nabla}\frac{m^2}{l}$ in comparison with $\frac{m^2}{l}\underline{\nabla}(Z - \bar{Z})$, equation (3) becomes:

$$\frac{\partial}{\partial t}\left(Z-\bar{Z}-G\right) = -\frac{g}{l}J\left(z, Z-\bar{Z}-G\right)$$

$$= -\frac{g}{l}J\left(\bar{Z}+G, Z-\bar{Z}-G\right). \quad (4)$$

Equation (4) shows that in non-divergent geostrophic flow the vorticity approximation $Z - \bar{Z} - G$ is conserved in the space-mean field $\bar{Z} + G$. This latter field is known from experiment to be more conservative than the Z field, and is assumed sufficiently constant to warrant displacement of the vorticity field in a single time-step of 12 hrs.

Contours of G are shown in Fig. 1.

It can be shown that the maximum value of $(Z - \bar{Z})\underline{\nabla}\frac{m^2}{l}$, the term neglected above, is about one-fifth of $\frac{m^2}{l}\underline{\nabla}(Z - \bar{Z})$.

3. Design of the experiment

It has been shown above that if the flow at 100 mb is non-divergent a certain function $Z - \bar{Z} - G$, representing the vorticity, will be conserved in the $\bar{Z} + G$, or smoothed flow, field. For convenience throughout this report the $Z - \bar{Z} - G$ field will be referred to as the vorticity field, although it is only a graphical approximation to this field.

Johnson (2, 3) finds that the root-mean-square random error of observation of height of the 100 mb surface over the British Isles is 150 ft, and that the vector root-mean-square error for wind observations is less than 6 kt. These errors and the scarcity of observations, particularly of wind, at this level, allow considerable latitude in the drawing of 100 mb contours. Therefore it was decided to examine a few sequences of routine 100 mb charts and to attempt to redraw them to be consistent with the hypothesis that absolute vorticity was conserved following the motion and yet retain consistency with the observations. Thus the vorticity given by any one chart should not differ, by more than a stipulated amount at any point, from the vorticity obtained by advection, forwards or backwards in time, from its immediate neighbour. It was anticipated that more than one modification to any one chart might be necessary.

If the charts could be so redrawn, a comparison could subsequently be made between the fitting of the wind and height reports in the original and modified drawings.

4. Method

100 mb charts for the six months November to April for the winters 1953-54,

/1954

1954-55 and 1955-56 were examined for sequences in which a fairly strong flow existed in the neighbourhood of the British Isles together with a well-marked feature in the flow pattern which would provide significant vorticity variations. A reasonable cover of observations was also sought. Five sequences were extracted and are detailed below.

1. 1500Z 16/12/55 to 1500Z 19/12/55. A trough to the west of the British Isles in the strong flow moved east and was replaced by a quasi-stationary ridge over the Atlantic.

2. 1500Z 5/2/54 to 1500Z 8/2/54. A trough developed to the west of Ireland and moved east slowly to lie over Central Europe.

3. 0300Z 4/11/55 to 1500Z 6/11/55. A deep trough with its axis from Iceland to the Azores remained quasi-stationary and developed a closed vortex.

4. 0300Z 14/2/54 to 0300Z 17/2/54. In the strong flow a ridge from the Azores to Iceland and a trough over the east of America moved east to cover the British Isles and the central Atlantic respectively.

5. 0300Z 8/11/55 to 1500Z 12/11/55. A trough to the west of Ireland decreased in amplitude while a ridge off Labrador moved east slowly.

A preliminary inspection of routine working charts suggested that too much emphasis had been placed on height values and too little on winds and that some alteration was allowable. This was therefore carried out for all sequences, care being taken to ensure continuity in time throughout each sequence. In the remainder of this report these redrawn charts will be referred to as 'original' charts. These charts for sequences (2) and (3) are shown in the Figures.

Estoqué (4) has detailed the method of obtaining graphically the required vorticity and advection fields. A grid-length of 600 mi. was used, and isopleths drawn at 100 ft intervals. One alteration was made to his procedure in the present case. Instead of forming the $\overline{Z} + G$ field by adding the G field to the $\overline{Z}$ field, a vary inaccurate process at the 100 mb level, the Z - G field was formed as an intermediate step. From this the $Z-\overline{Z}-G$ field and thence the $\overline{Z} + G$ field is easily obtained.

The field of $-(Z-\overline{Z}-G)$, corresponding to the vorticity, for the first chart of each sequence, was advected for a period of 12 hrs. On comparing this with the pattern of $-(Z-\overline{Z}-G)$ for the second chart it was apparent that significant differences existed, of the order of 300 ft in places, and the patterns definitely did not resemble each other. Since the $Z-\overline{Z}-G$ ispoleths were drawn at 100 ft intervals, it was decided to attempt to achieve correspondence within a tolerance of 100 ft which is equivalent to a divergence of about 2×10^{-6} sec^{-1}.

An attempt was then made to modify the second chart within the limits of the accuracy of the observations by altering the shear and curvature, to give a vorticity pattern similar to the advected one and within the 100 ft tolerance. In the first two sequences this was not possible in one step, and changes in the first chart in each sequence had to be made, using advection of vorticity backwards in time from a modified second chart, in order to keep within the 100 ft tolerance.

The vorticity of the modified second chart was then advected in the space-mean flow field and the third chart modified to give a vorticity pattern similar to the advected one. This procedure was continued for the rest of the sequence. The original and modified height charts, and the original, modified and advected vorticity charts, for sequences (2) and (3) are shown in Fig.3 to 30 and 31 to 52 respectively.

The method requires that the advective field can be treated as constant

/over

over the period of advection. Examination of these fields at 12 hr intervals showed that this was satisfied to a high order of accuracy.

5. Results

It was found possible to redraw the five sequences of 100 mb charts so that the change in each 12 hr period implied a divergence of less than 2×10^{-6} sec^{-1}, which is negligible on the synoptic scale. A visual comparison of the original, advected, and modified vorticity fields, shown for sequences (2) and (3) in the Figures, clearly reveals the great improvement given by the modified fields in comparison with the original fields in corresponding with the advected fields.

An indication of the relative accuracy of the two sets of 100 mb charts is given by a comparison of their smoothness in time. Values of height and geostrophic wind were read off at points of a grid shown in Fig.2 covering that part of the chart where the drawing was considered most reliable. Values of the statistics $(Z_{12} - Z_o)$, the modulus of the twelve-hour height change, and $(V_{12} - V_o)$, the modulus of the twelve-hour vector wind change, are given in Table I, where $\overline{|V|}$ is the mean of the wind-speeds.

Table I

Time variation in height and geostrophic wind from grid

Sequence	$(Z_{12} - Z_o)$		$(V_{12} - V_o)$			
	Average value ft.	r.m.s. value ft.	Average value kt.	r.m.s. value kt.	$\overline{\lvert V \rvert}$ kt.	No. of cases
I Original	184	241	16	20	44	72
I Modified	160	206	12	14	48	
II Original	167	211	14	18	39	72
II Modified	176	217	9	10	37	
III Original	158	183	12	15	29	60
III Modified	154	171	8	9	30	
IV Original	203	261	17	19	42	72
IV Modified	165	222	11	13	40	
V Original	178	207	10	12	29	108
V Modified	157	183	6	7	29	

A comparison between reported winds and heights, and those read off the two sets of charts at the seventeen stations O.W.S. 'A', 'B', 'C', 'D', 'E', 'I', 'J', 'K', Stornoway, Aldergrove, Hemsby, Camborne, Flensburg, Wiesbaden, Munich, Gibraltar and Malta, is given in Table II, where Zr, Vr refer to the heights and geostrophic winds read off the charts, and Zo, Vo the observed or reported values from the radiosonde ascents.

/Table

Table II

Comparison between observed and measured winds and heights

Sequence	(Zr - Zo) Average value ft.	(Zr - Zo) r.m.s. value ft.	No. of cases	(Vr - Vo) Average value kt.	(Vr - Vo) r.m.s. value kt.	$\overline{(Vo)}$ kt.	$\overline{\lvert Vr \rvert}$ kt.	No. of cases
I Original	114	157	98	11	14	45	43	73
I Modified	158	196		10	12		42	
II Original	131	174	92	10	12	39	38	38
II Modified	167	210		11	12		34	
III Original	83	120	85	9	11	27	28	62
III Modified	98	134		9	11		26	
IV Original	101	148	78	13	15	40	40	48
IV Modified	136	187		11	12		38	
V Original	95	129	137	9	12	25	26	99
V Modified	109	145		8	10		24	

No deterioration in the fitting of the observations during the course of any sequence was found.

Johnson (2) shows that the root-mean-square random error of observation of height at 100 mb from British radiosondes is 150 ft, and this figure probably applies to the radiosondes of the other stations used in Table II. The results of the Payerne trials, however, show a significant systematic error between the radiosondes of different countries. Errors due to chart drawing and reading off the charts are small in comparison, and the expected value of (Zr - Zo) can be taken as greater than 150 ft by perhaps 20 to 30 ft.

Upper limits to the root-mean-square error of wind observations from British and British Ocean Weather Ship stations of 6 kt and 9 kt are given by Johnson (3). Errors due to chart drawing, a geostrophic motion and estimation of the geostrophic wind are not negligible, but it is probable that the expected value of (Vr - Vo) does not exceed 10 kt.

6. Conclusions

The twelve-hour root-mean-square variation of height and geostrophic wind of the original set of 100 mb charts is 222 ft and 17 kt respectively; for the set modified to be consistent with vorticity advection the figures are 200 ft and 11 kt. The observations of height and wind have been fitted with root-mean-square errors for the original set of 146 ft and 13 kt. and for the modified set of 175 ft and 11 kt respectively. The modified set is therefore smoother in time with respect to height and significantly smoother with respect to wind than the original set. The observed winds are fitted better by the modified drawings, and although the heights are fitted better by the original set, the discussion of the errors in the height values given above would seem to indicate that the fit of the original set is too good. On the basis of these figures it is suggested that the modified set provides a more realistic approximation to the true flow than the original set.

Any generalisation to conditions at the 100 mb level at other times is not strictly justified. Since, however, the sequences selected show very varying conditions and probably contain representative types of flow found at this level, it can be concluded that the evidence supports the hypothesis of approximate non-divergent flow at the 100 mb level.

/REFERENCES:

REFERENCES:

1. Fjortoft, R. 1952. "Numerical Method of Integrating the Barotropic Vorticity Equation." Tellus 4, No. 3.

2. Johnson, D.H. 1954. "Accuracy of 100 mb Contour Heights." Met. Mag., Vol. 83, p.37.

3. Johnson, D.H. 1953. "Accuracy of 100 mb Winds." Met. Mag. Vol. 82, p.44.

4. Estoqué, M.A. 1956. "A Prediction Model for Cyclone Development Integrated by Fjortoft's Graphical Method." J. Met., Vol. 13, No.2.

MRP 1078

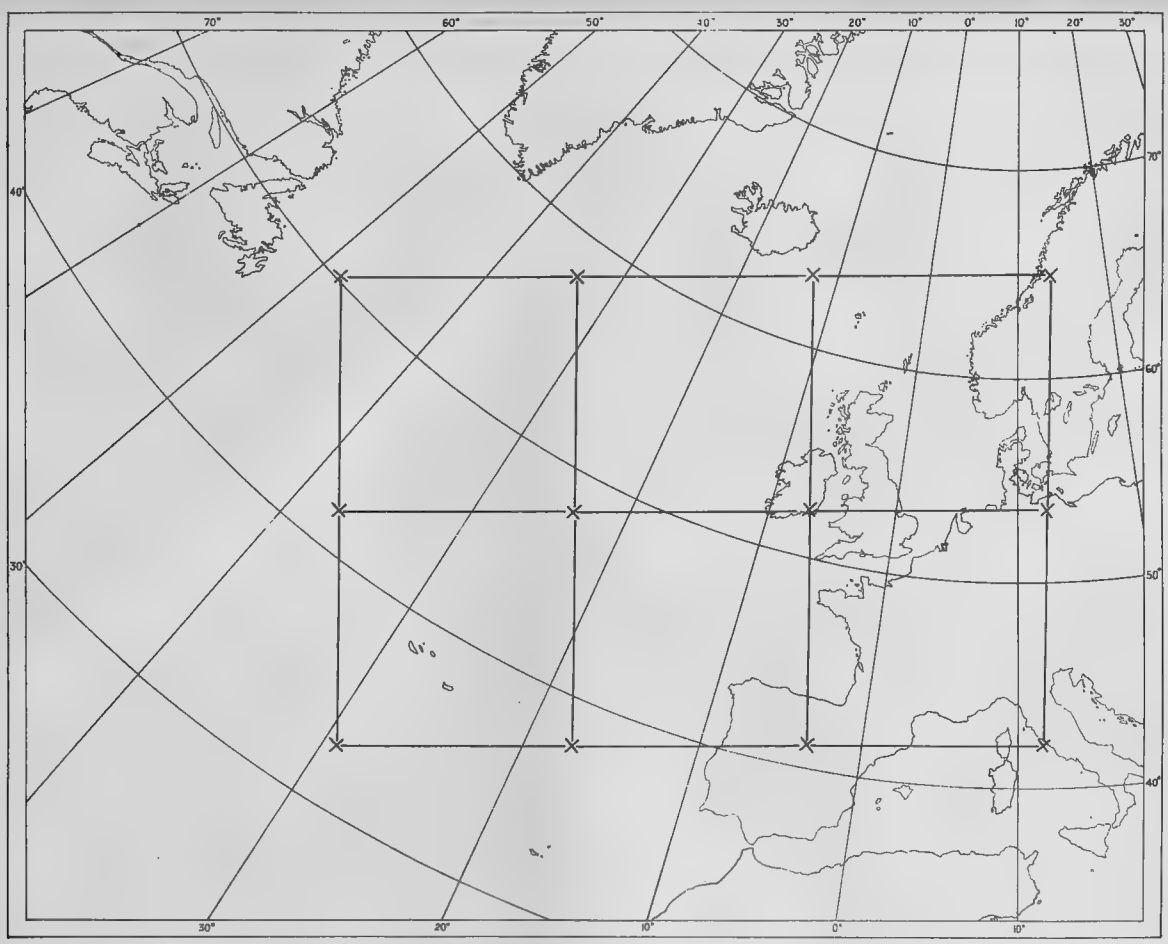

Fig.2. Grid used in testing the time variations of contour height and geostrophic wind

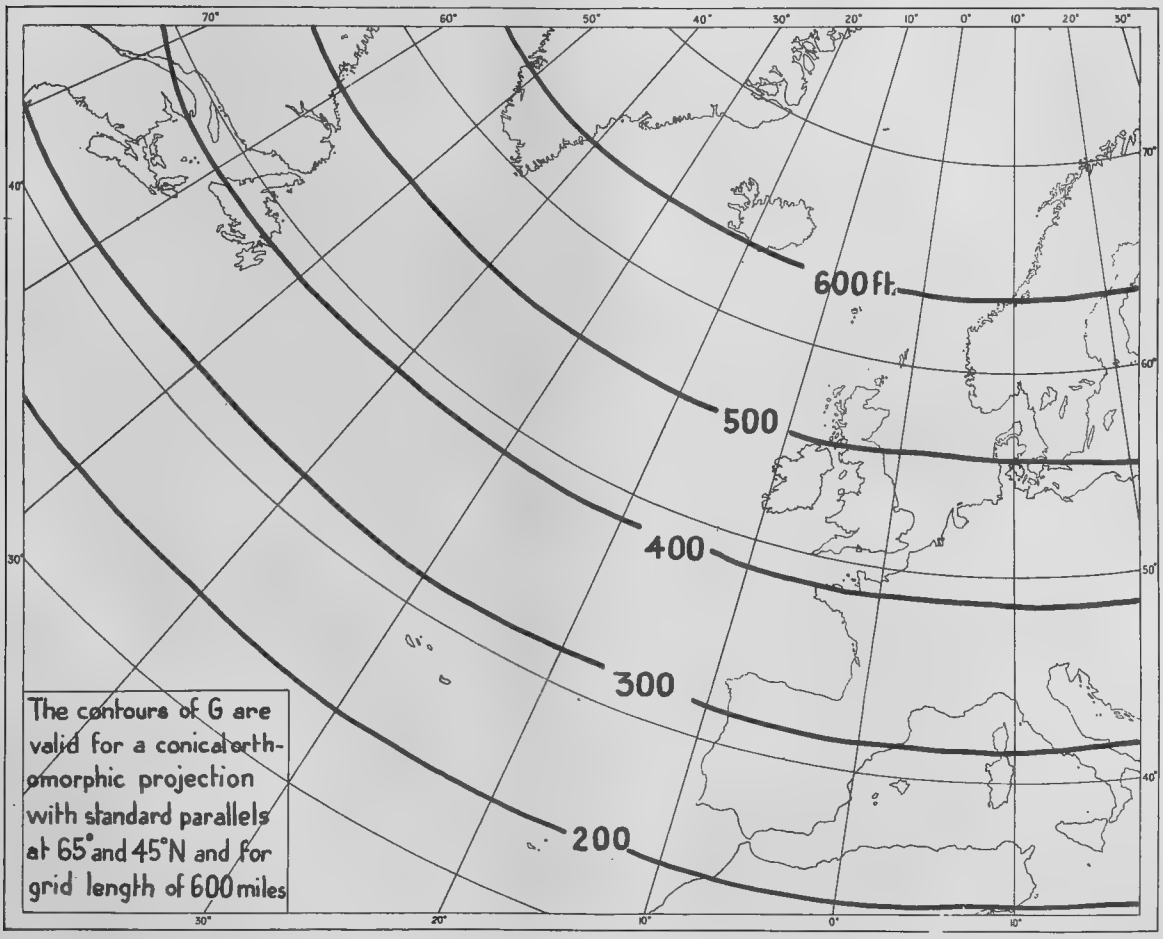

Fig.1. Contours of the G field

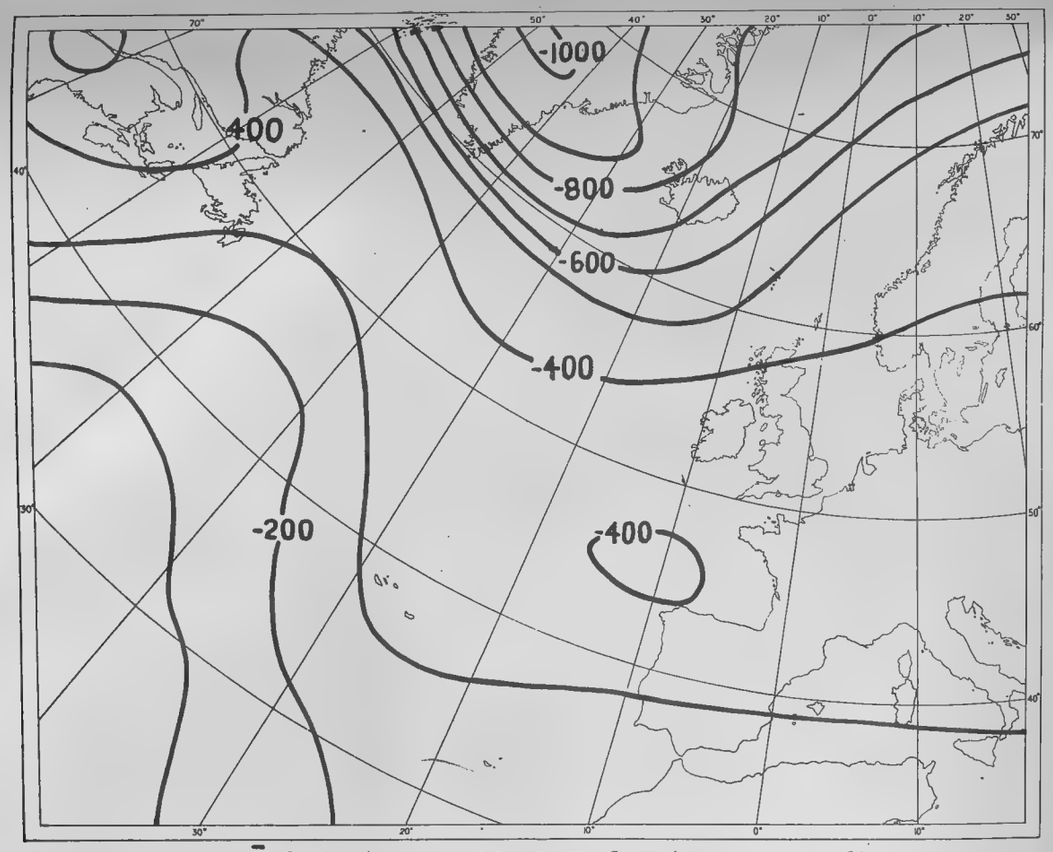

Fig.4 Original Z-Z̄-G field 1500 G.M.T. 5:2:54 Units: ft.

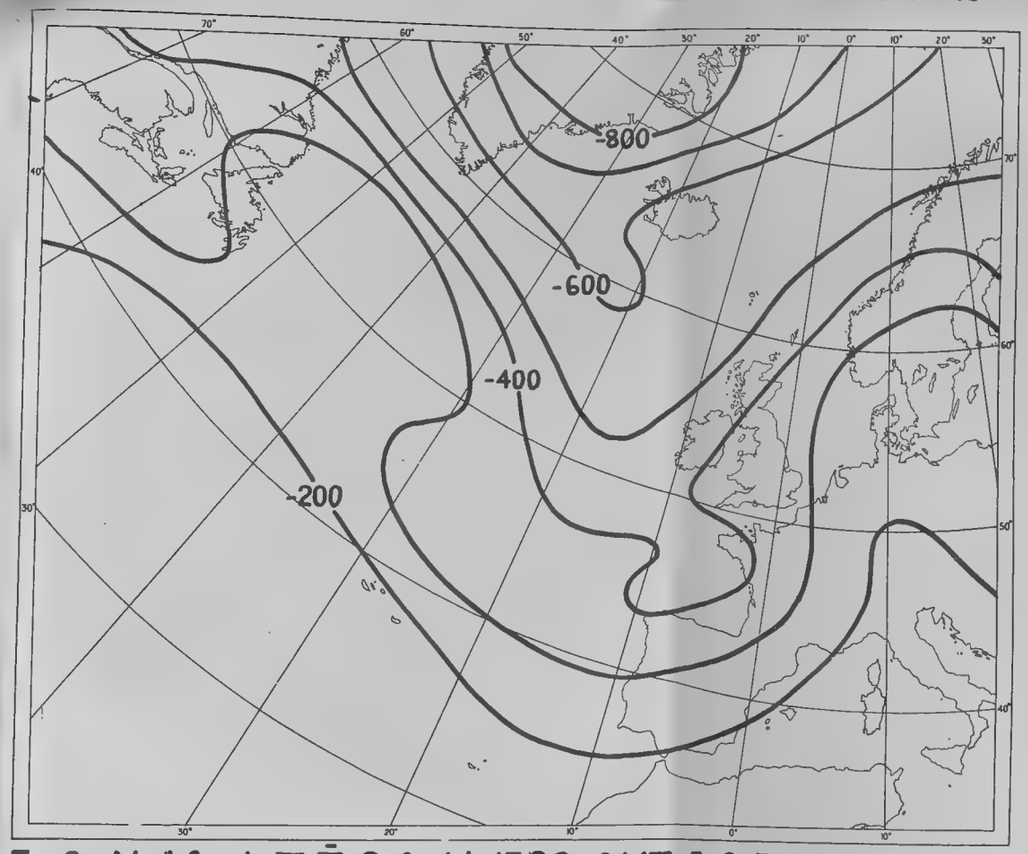

Fig.6. Modified Z-Z̄-G field 1500 G.M.T. 5:2:54 Units: ft.

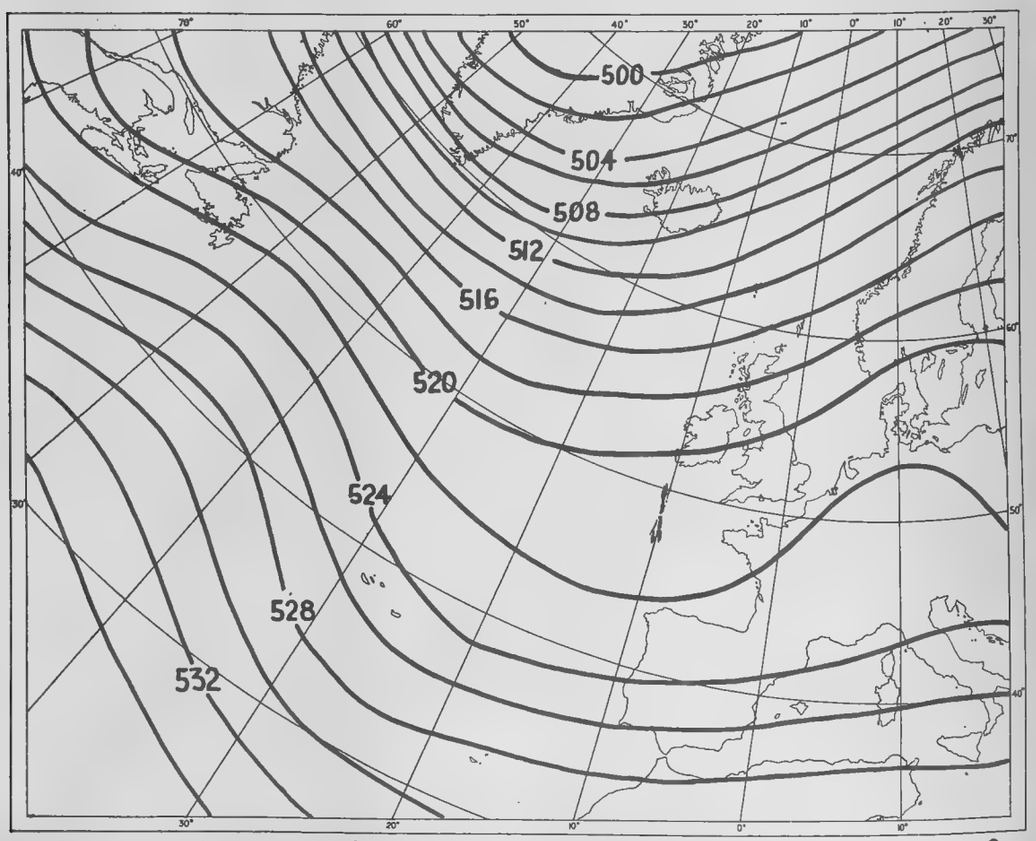

Fig.3 Original Z field (100 mb. contours) 1500 G.M.T. 5:2:54 Units 10^2 ft.

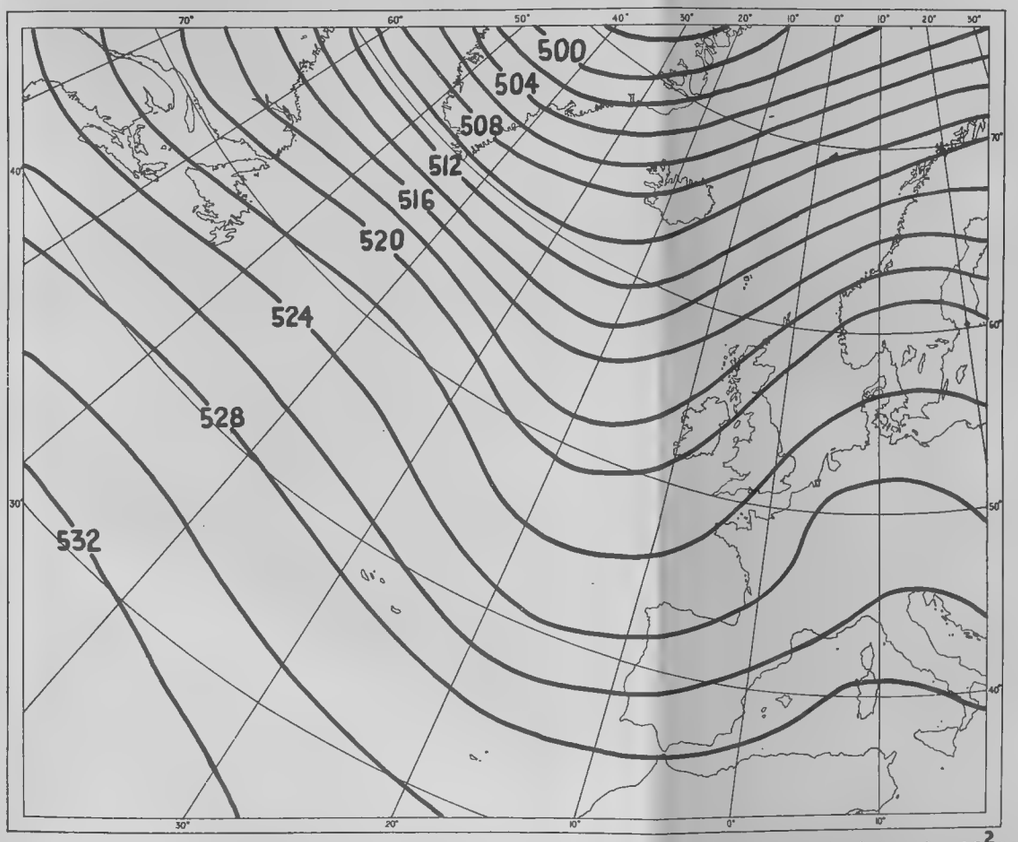

Fig.5. Modified Z field (100 mb. contours) 1500 G.M.T. 5:2:54 Units: 10^2 ft.

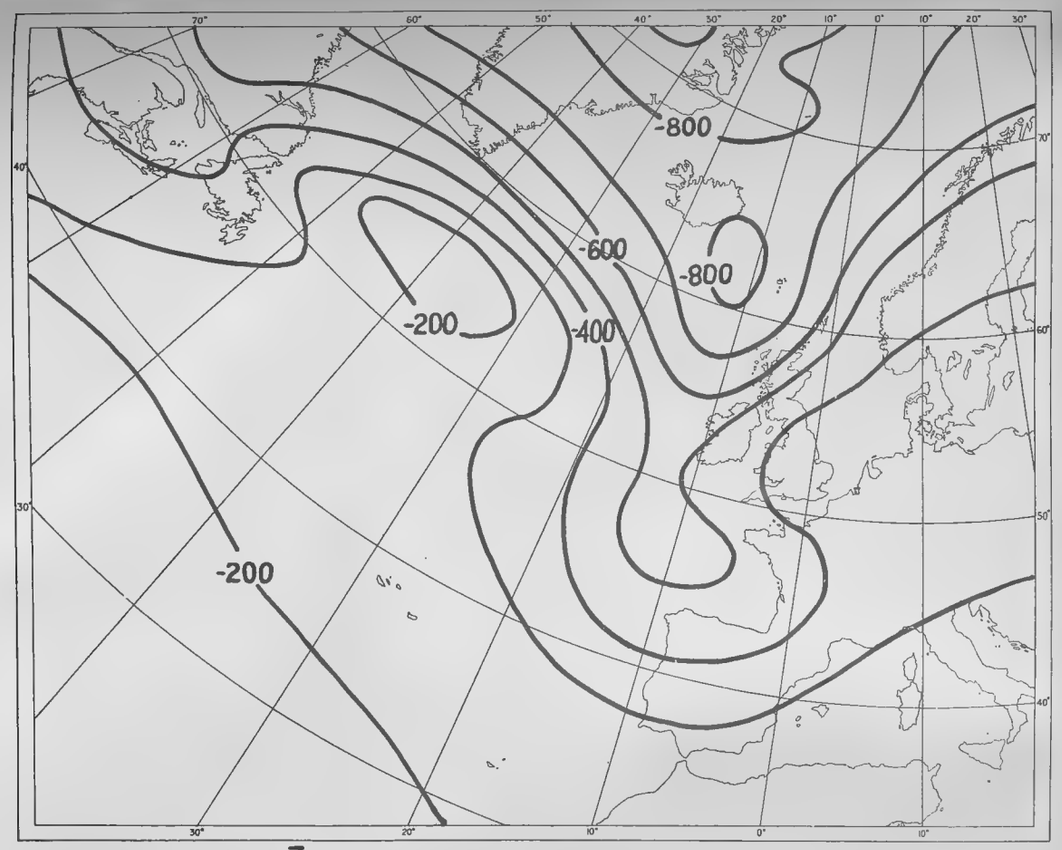

Fig.8. Original Z-$\bar{Z}$-G field 0300 G.M.T. 6:2:54 Units : ft.

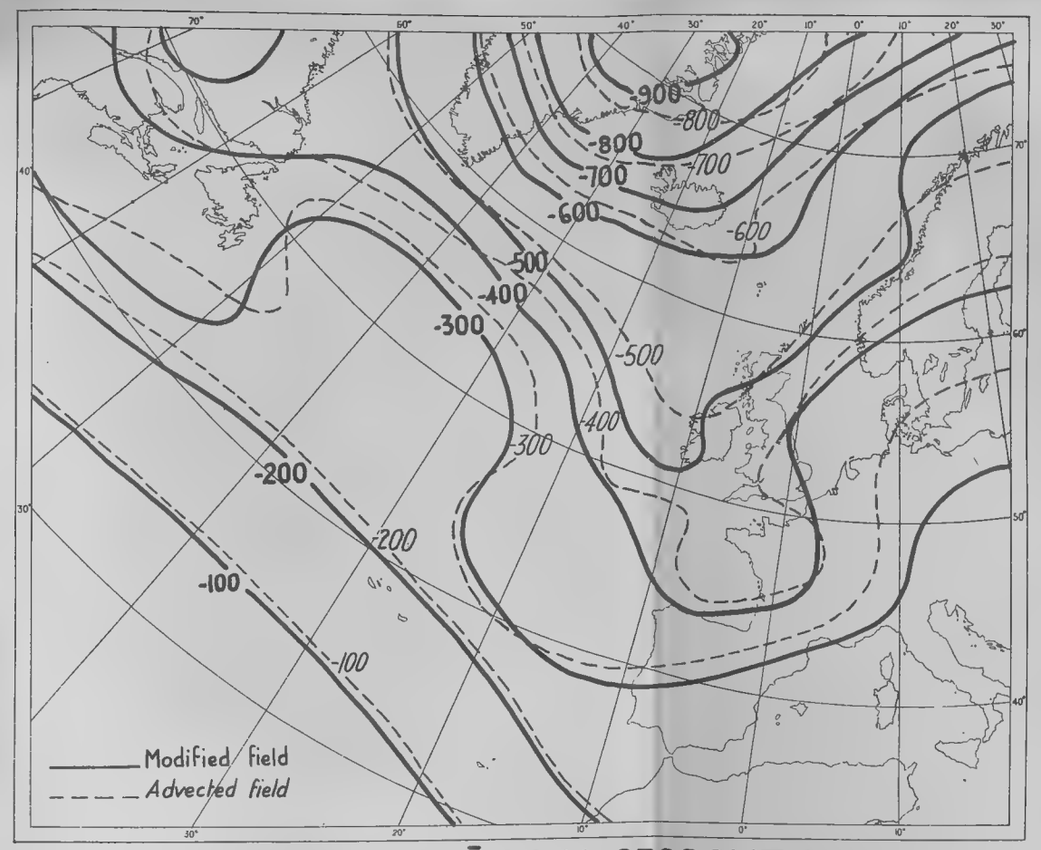

Fig.10. Modified and advected Z-$\bar{Z}$-G fields 0300 G.M.T. 6:2:54 Units: ft

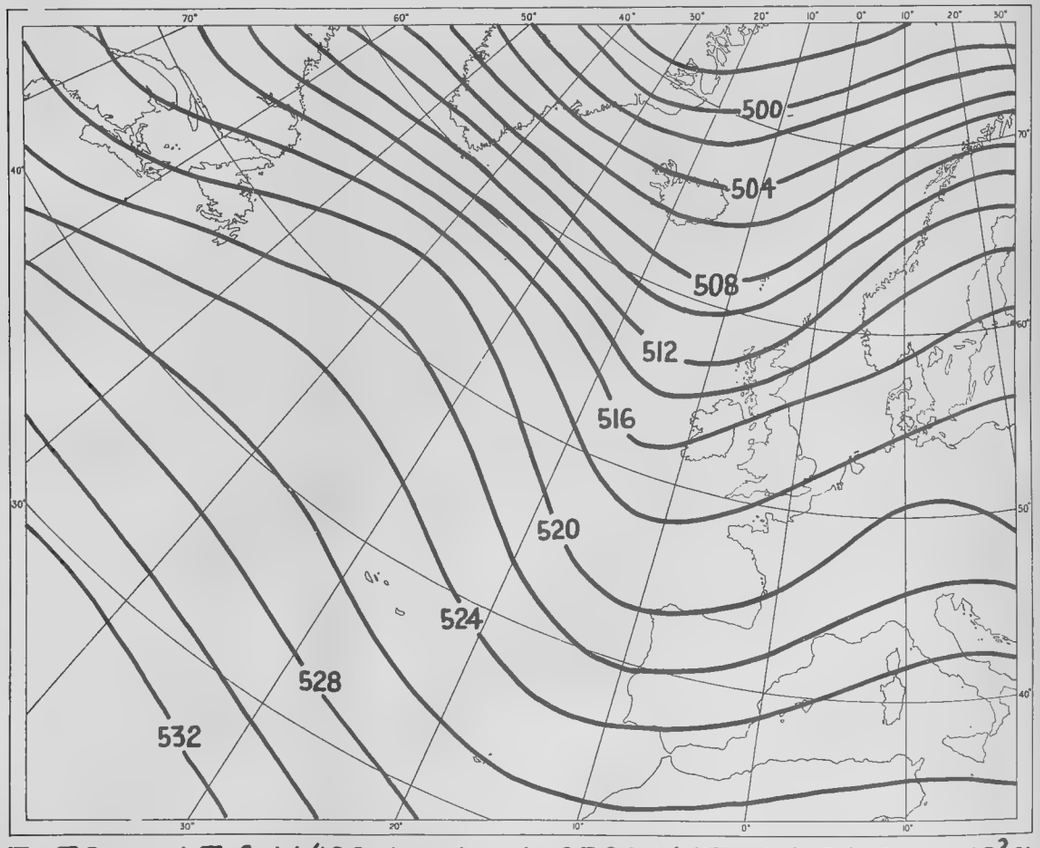

Fig.7. Original Z field (100 mb. contours) 0300 G.M.T. 6:2:54 Units 10^2 ft.

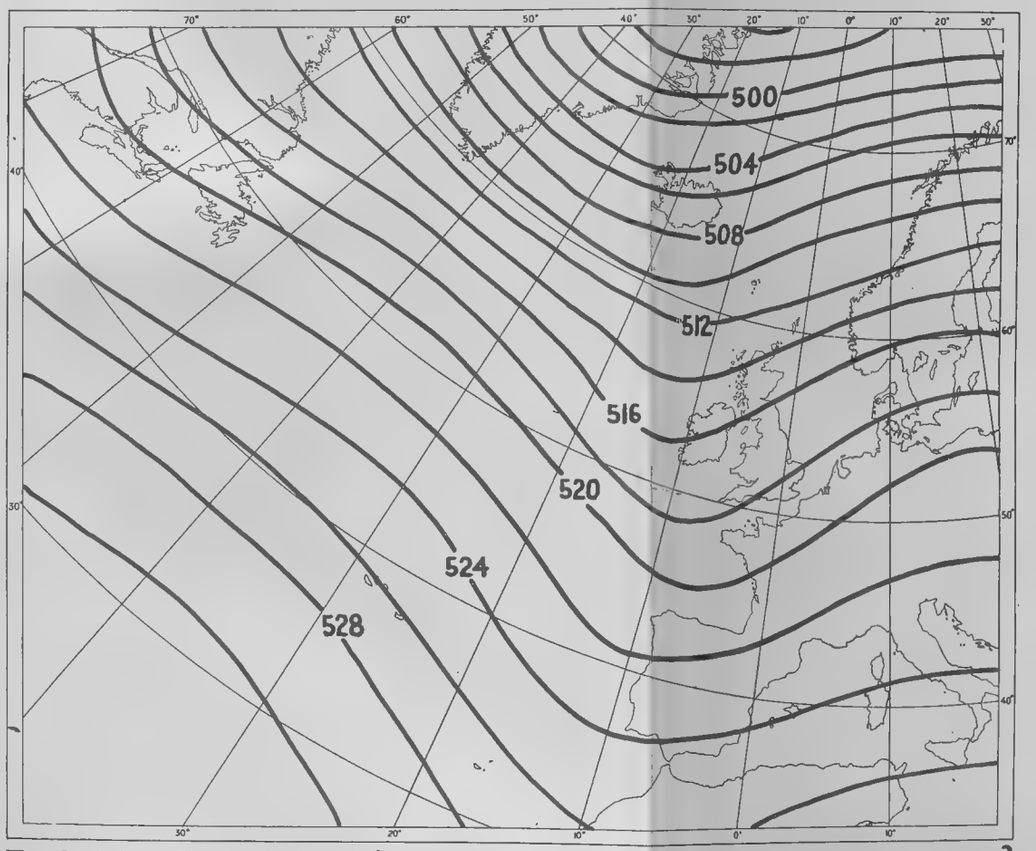

Fig.9. Modified Z field (100 mb. contours) 0300 G.M.T. 6:2:54 Units: 10^2 ft.

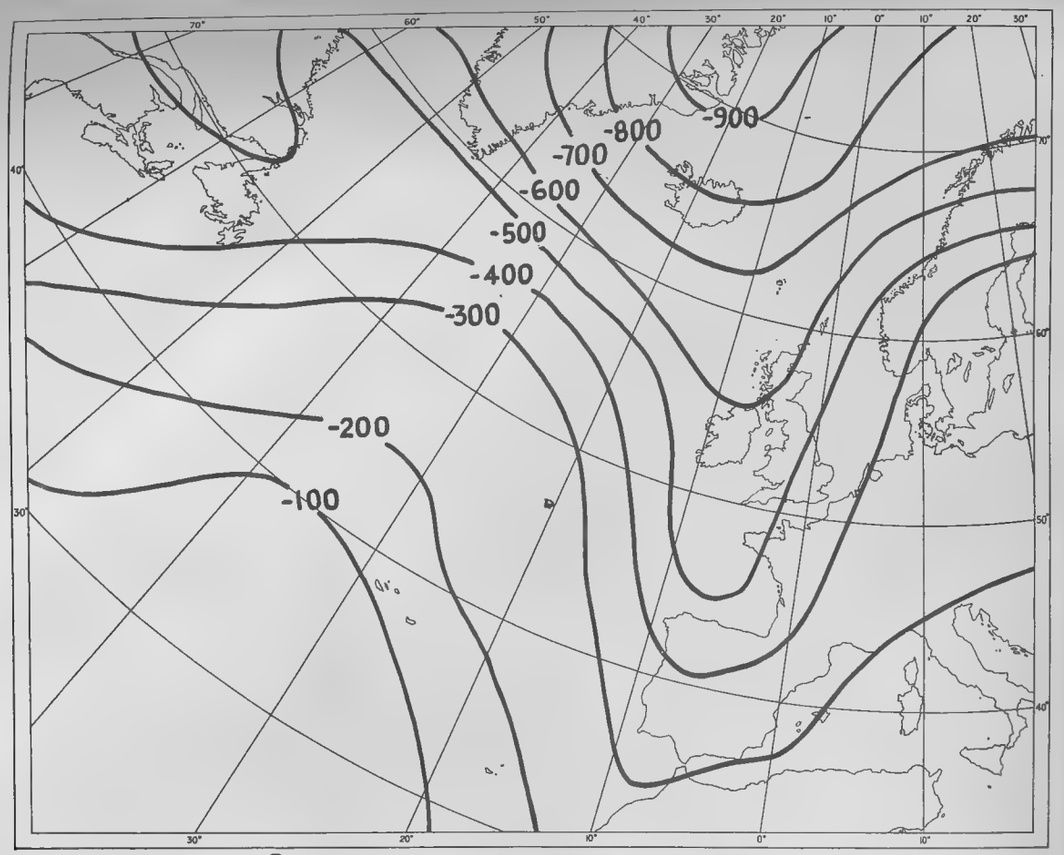

Fig 12. Original Z-Z̄-G field 1500 G.M.T. 6:2:54 Units: Ft

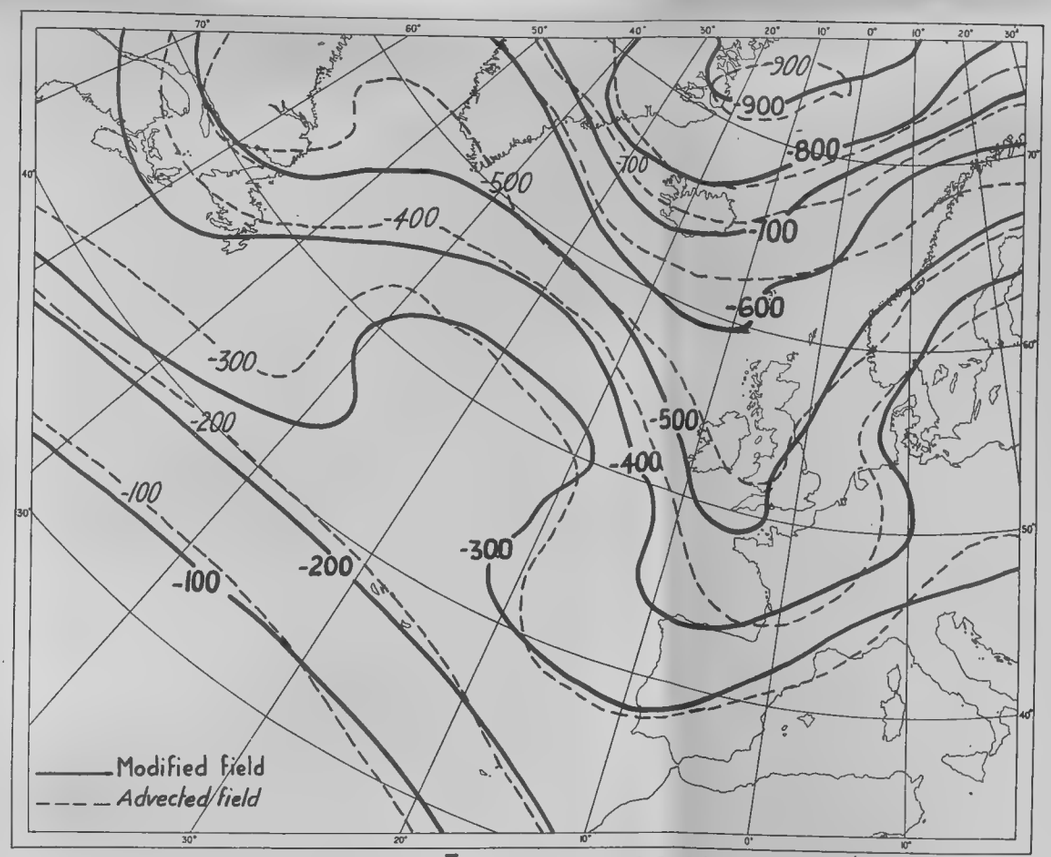

Fig 14. Modified and advective Z-Z̄-G fields 1500 G.M.T. 6:2:54 Units: Ft

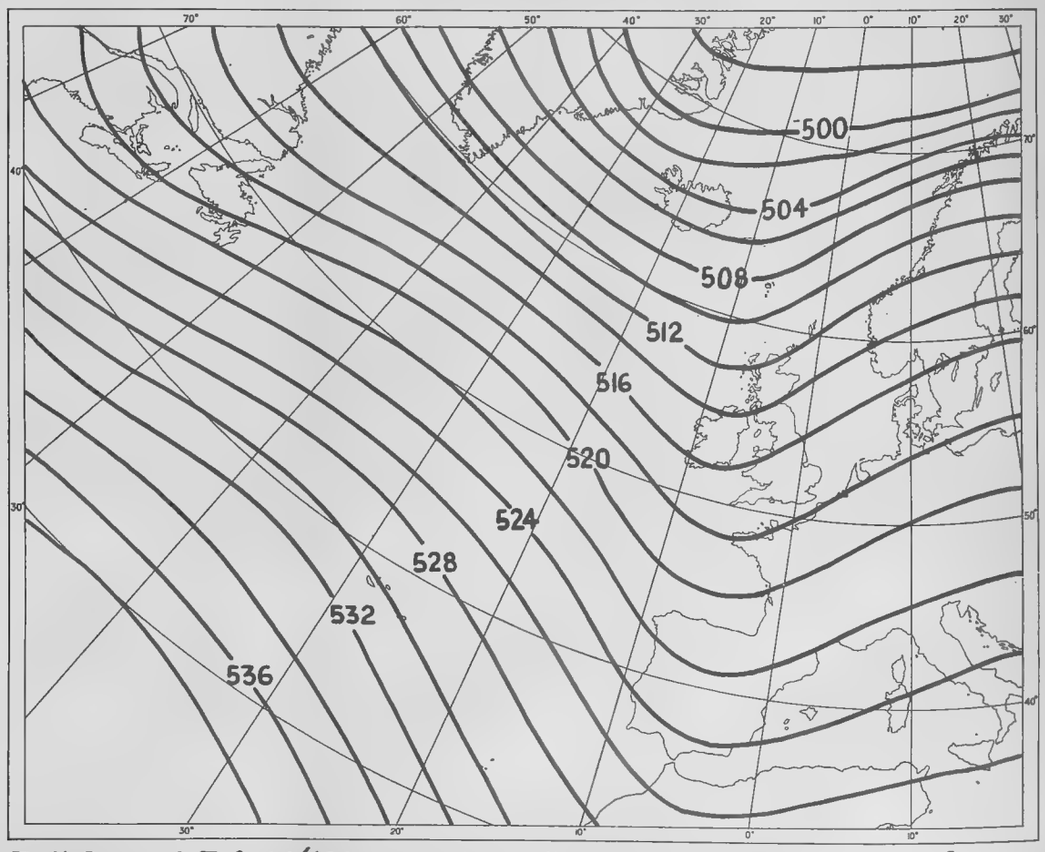

Fig 11. Original Z field (100 mb. contours) 1500 G.M.T. 6:2:54 Units: 10^2 Ft.

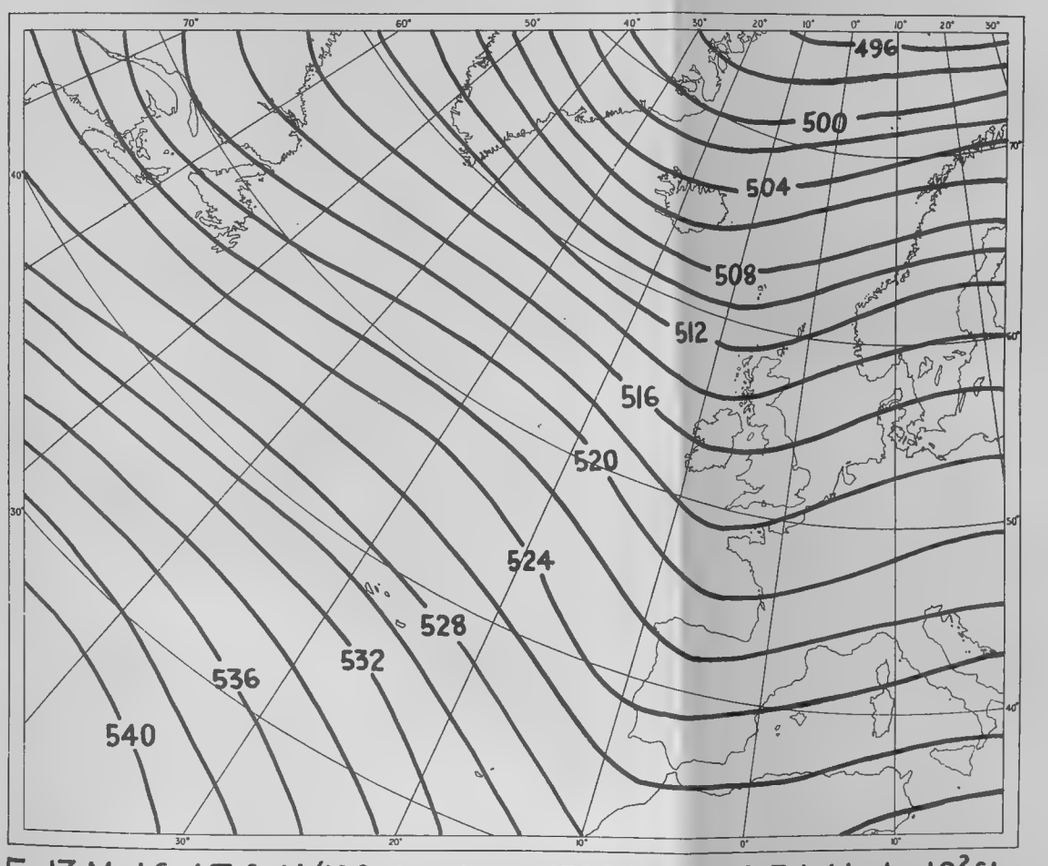

Fig 13. Modified Z field (100 mb. contours) 1500 G.M.T. 6:2:54 Units 10^2 Ft.

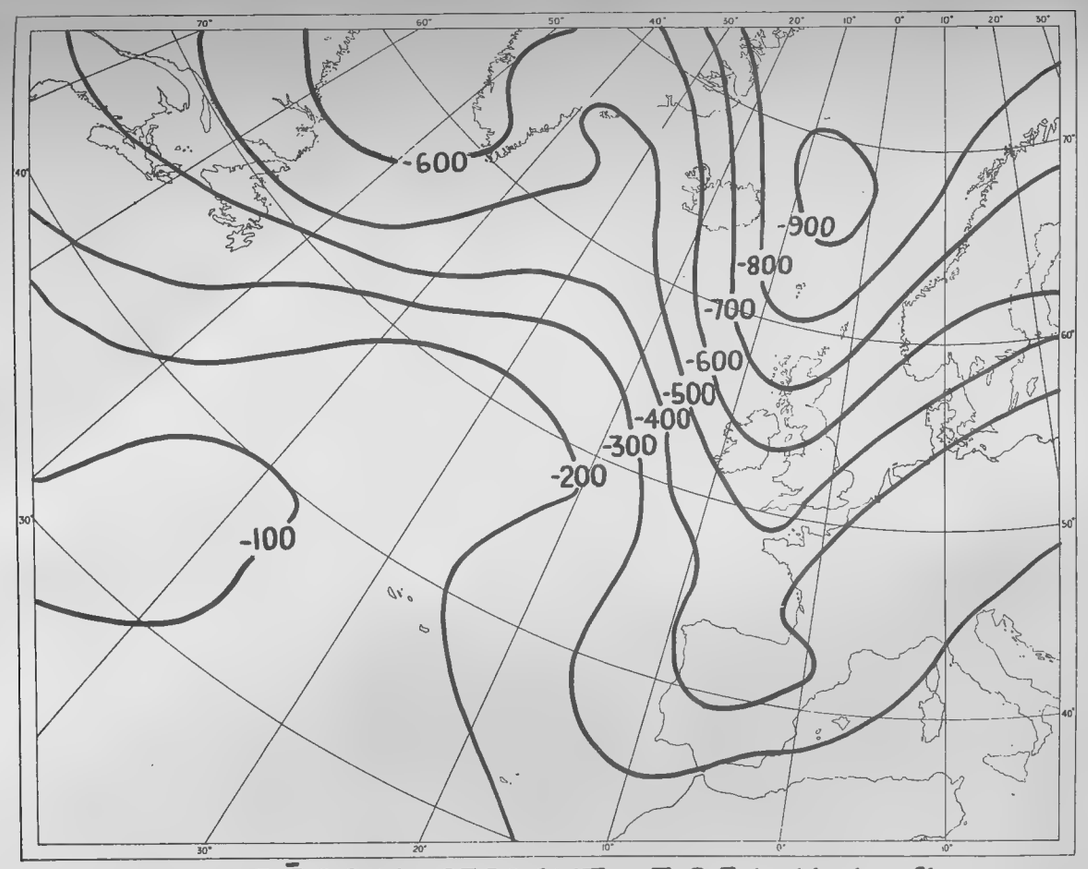

Fig.16 Original Z-Z̄-G fields 0300 G.M.T. 7:2:54 Units: Ft.

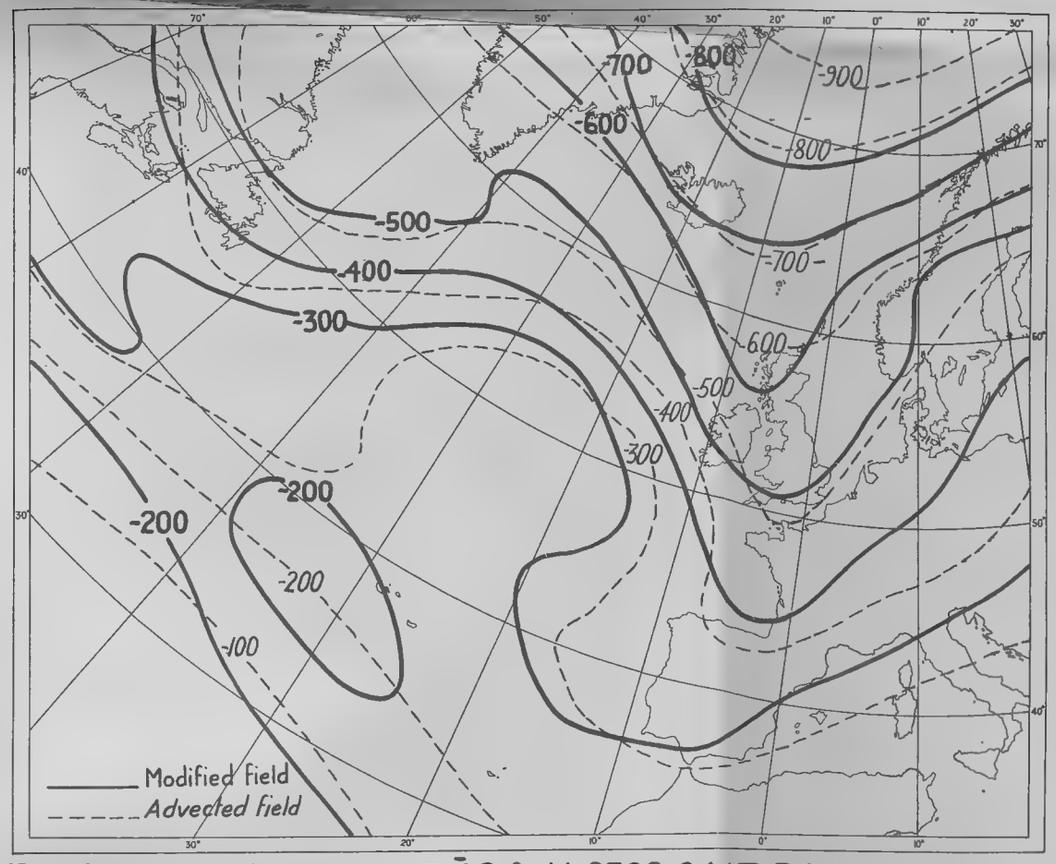

Fig.18 Modified and advected Z-Z̄-G field 0300 G.M.T. 7:2:54 Units: Ft.

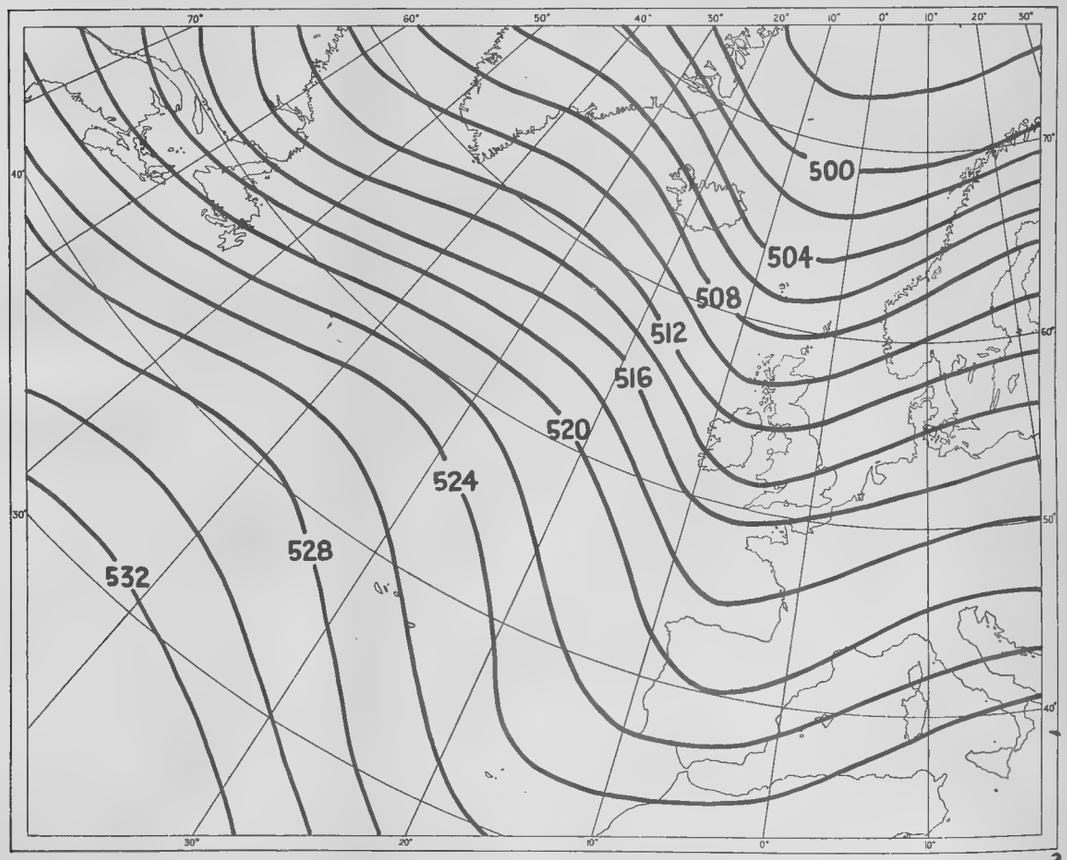

Fig.15 Original Z field (100 mb. contours) 0300 G.M.T. 7:2:54 Units: 10^2 ft.

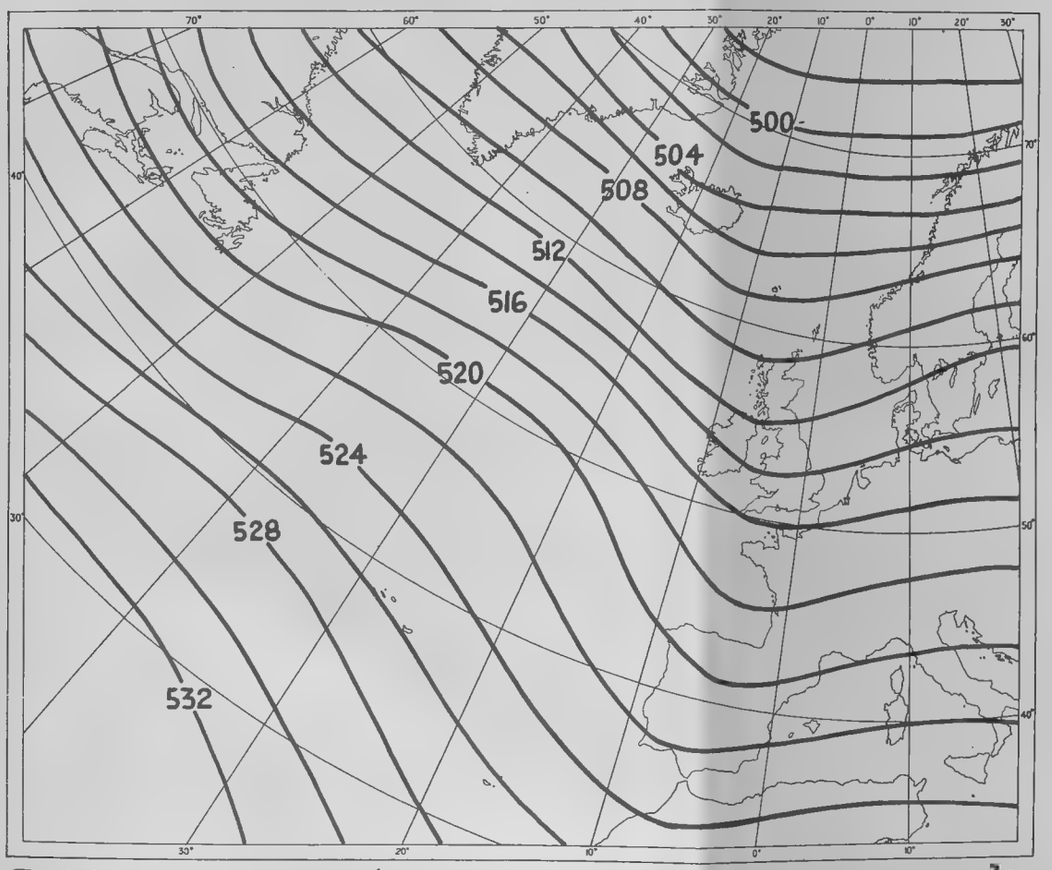

Fig.17 Modified Z field (100 mb. contours) 0300 G.M.T. 7:2:54 Units: 10^2 ft.

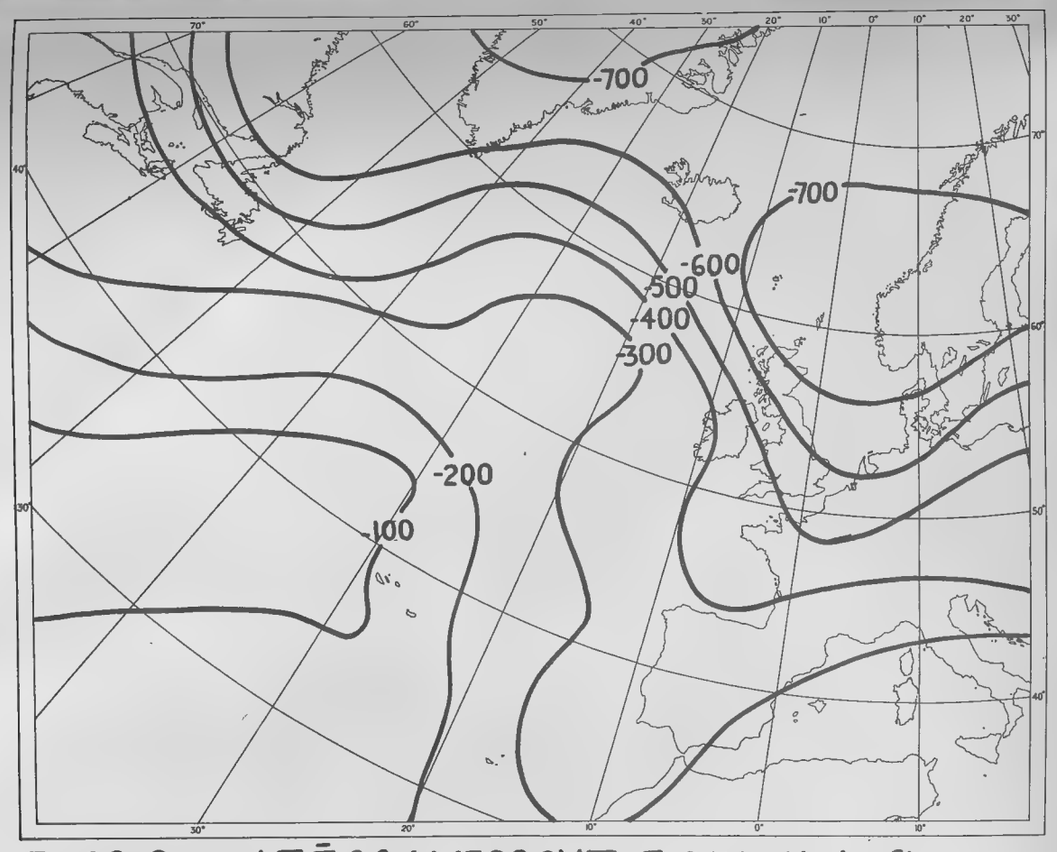

Fig. 20. Original Z-Z̄-G field 1500 G.M.T. 7:2:54 Units: ft.

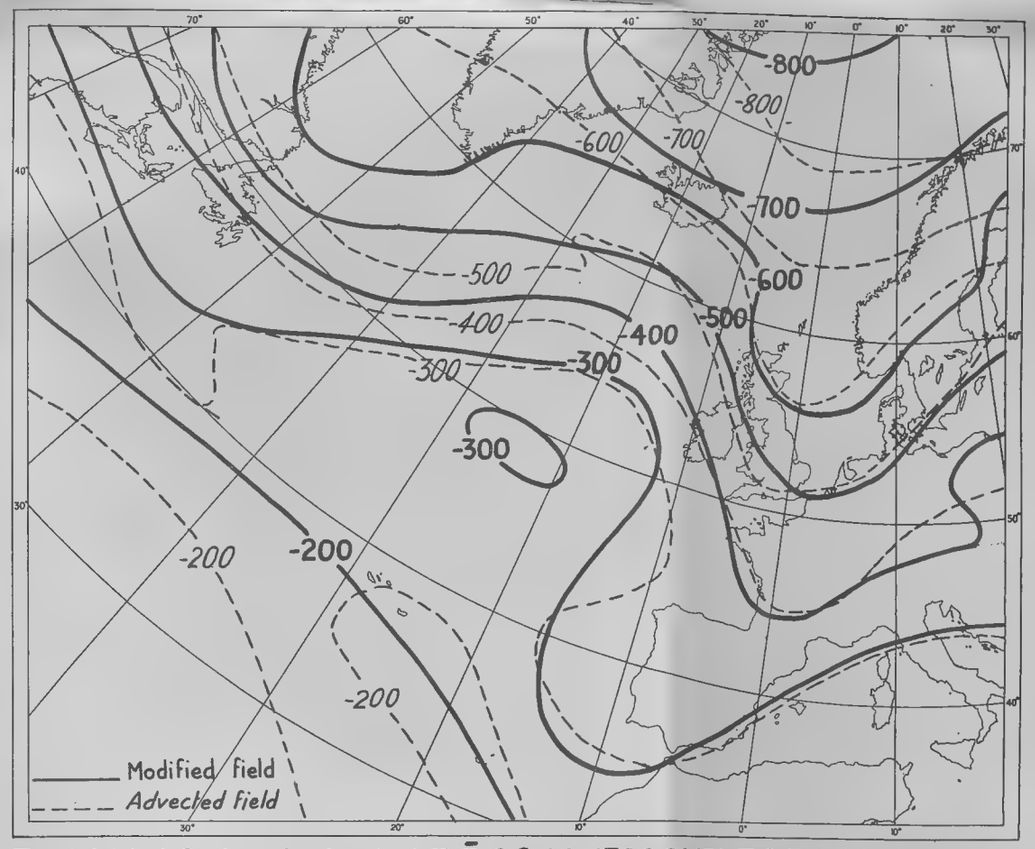

Fig. 22. Modified and advected Z-Z̄-G fields 1500 G.M.T. 7:2:54 Units: ft.

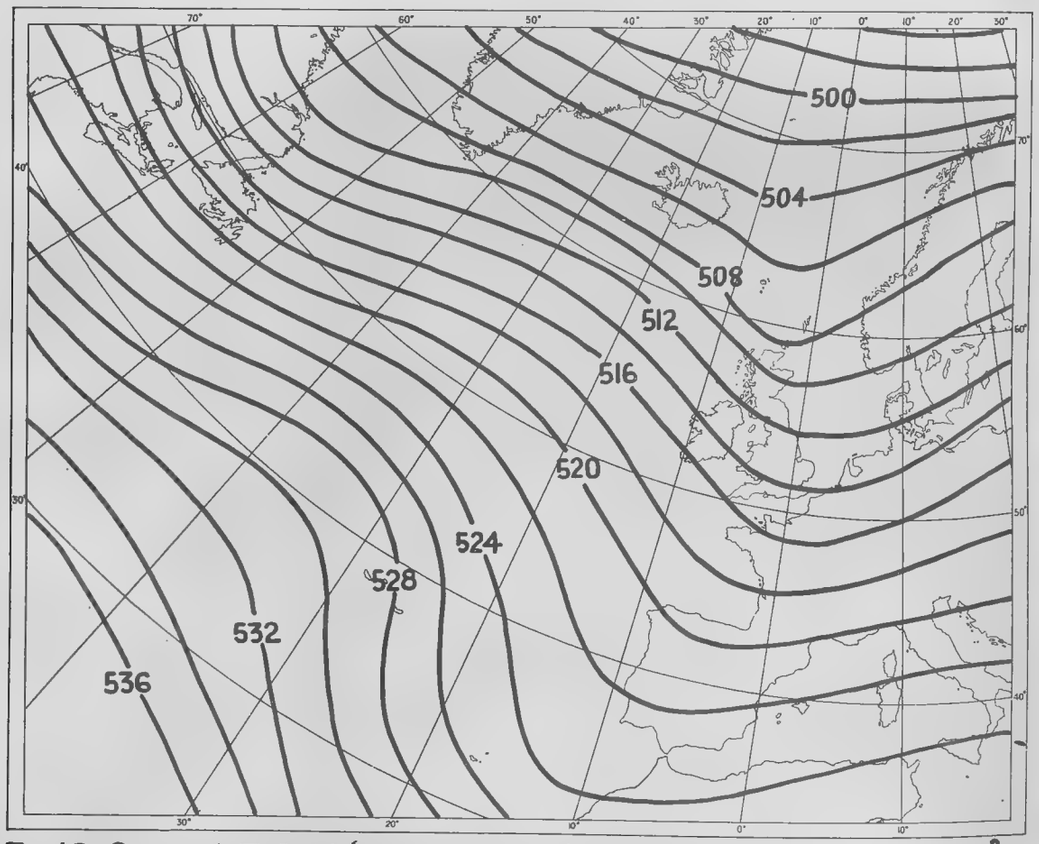

Fig. 19. Original Z field (100 mb. contours) 1500 G.M.T. 7:2:54 Units: 10^2 ft.

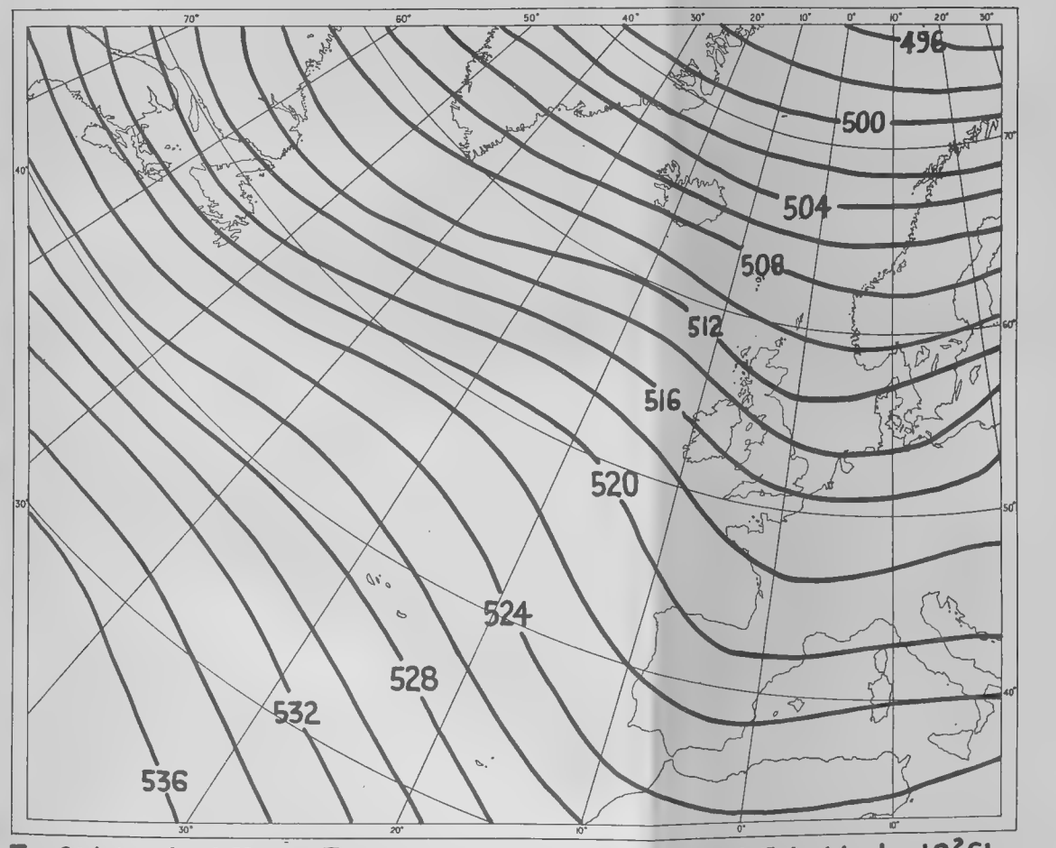

Fig. 21. Modified Z field (100 mb. contours) 1500 G.M.T. 7:2:54 Units 10^2 ft.

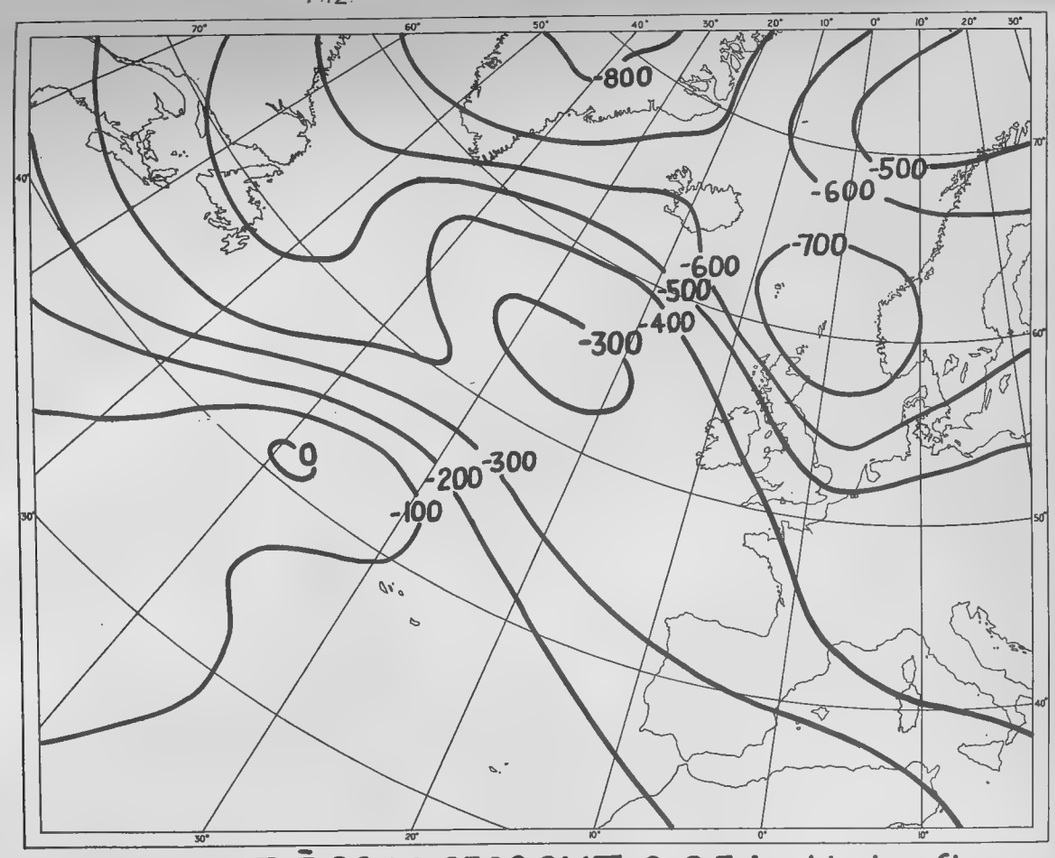

Fig.24. Original Z-$\bar{Z}$-G field 0300 G.M.T. 8:2:54 Units: ft.

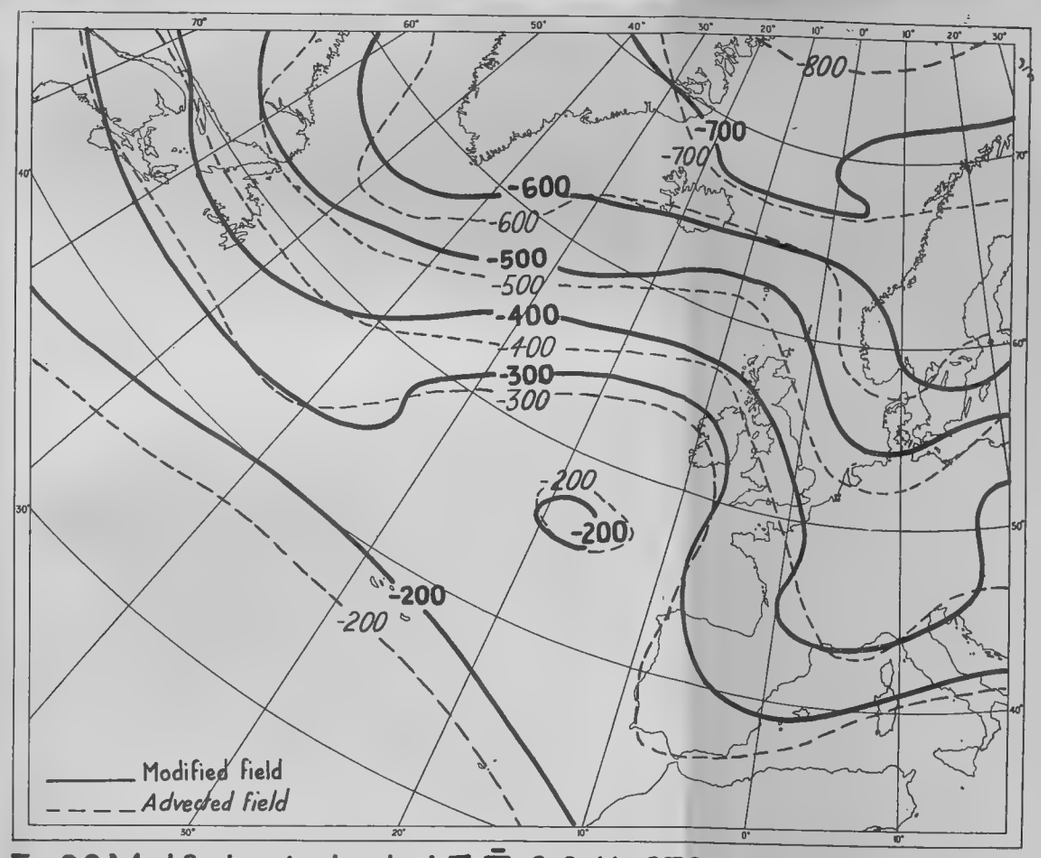

Fig.26. Modified and advected Z-$\bar{Z}$-G fields 0300 G.M.T. 8:2:54 Units ft.

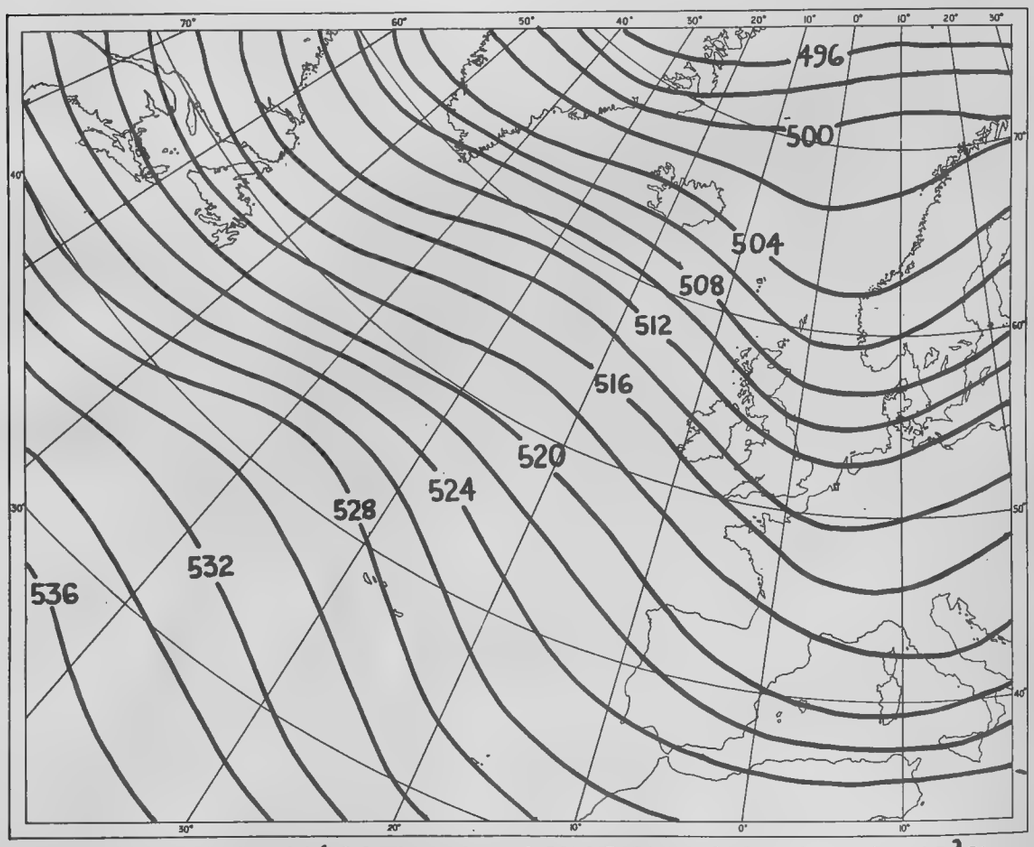

Fig.23. Original Z field (100mb. contours) 0300 G.M.T. 8:2:54 Units: 10^2 ft.

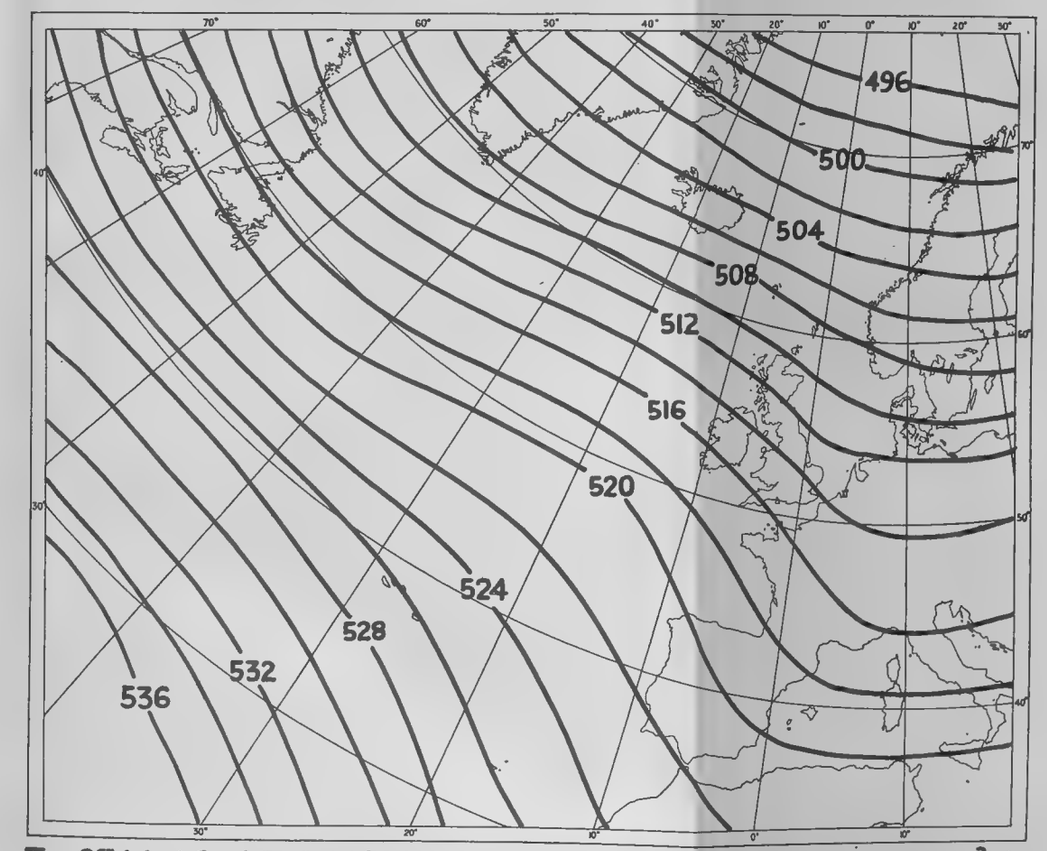

Fig.25. Modified Z field (100mb. contours) 0300 G.M.T. 8:2:54 Units 10^2 ft

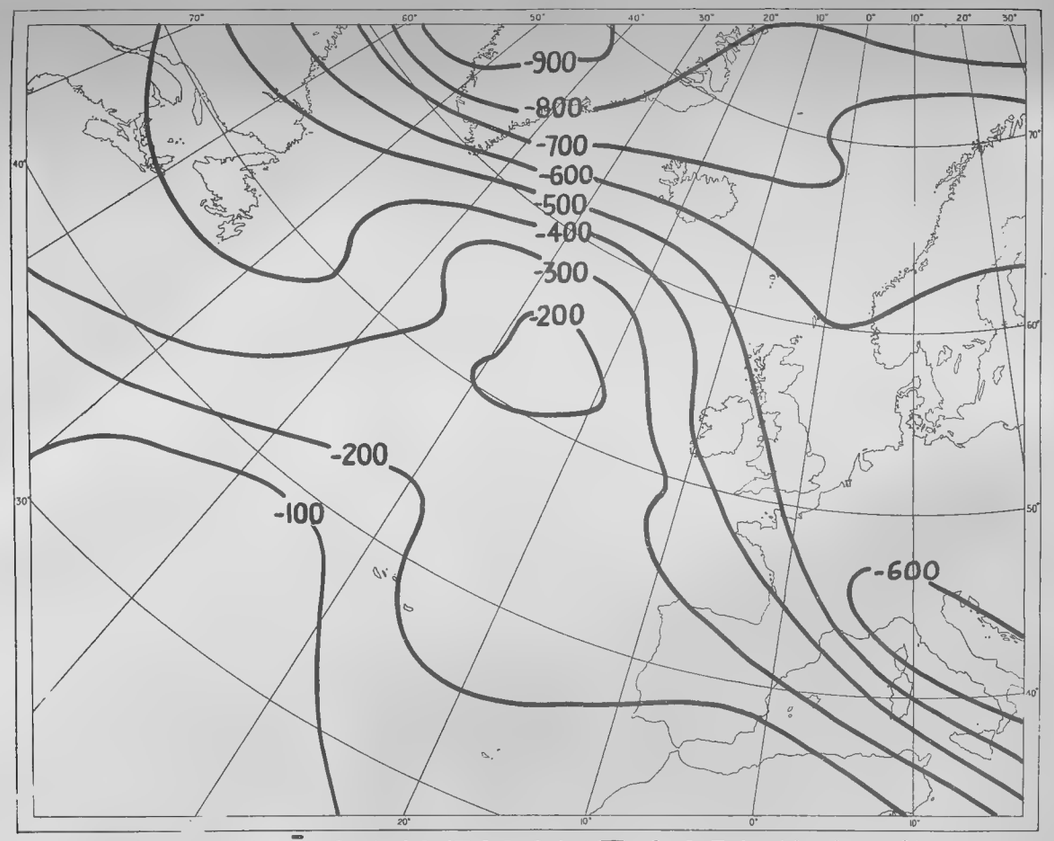

Fig. 28. Original Z-Z̄-G field 1500 G.M.T. 8:2:54 Units : ft

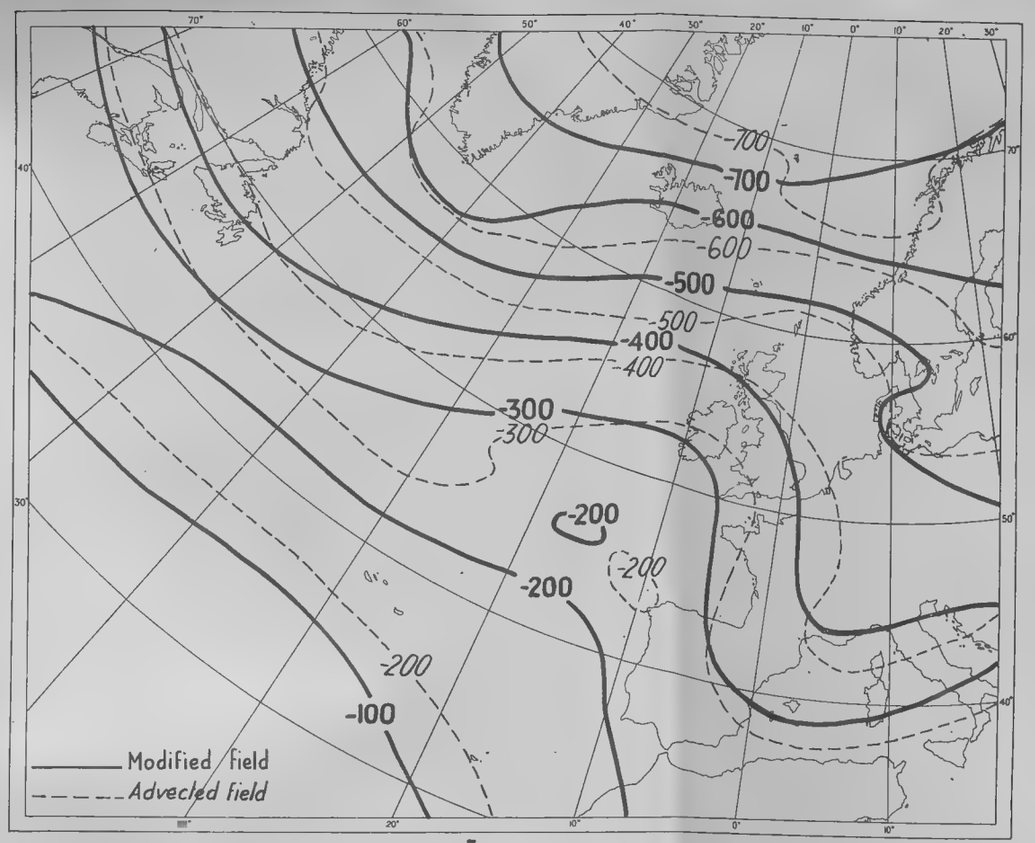

Fig. 30. Modified and advected Z-Z̄-G fields 1500 G.M.T. 8:2:54 Units : ft

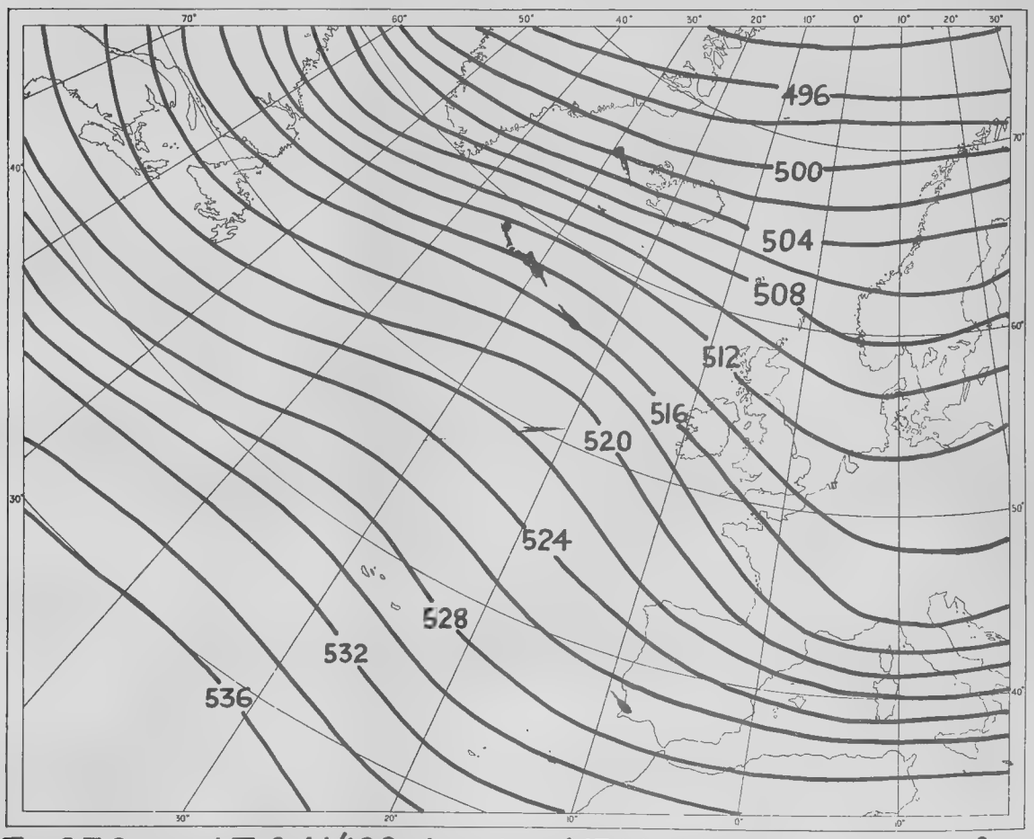

Fig. 27. Original Z field (100mb. contours) 1500 G.M.T. 8:2:54 Units 10^2 ft.

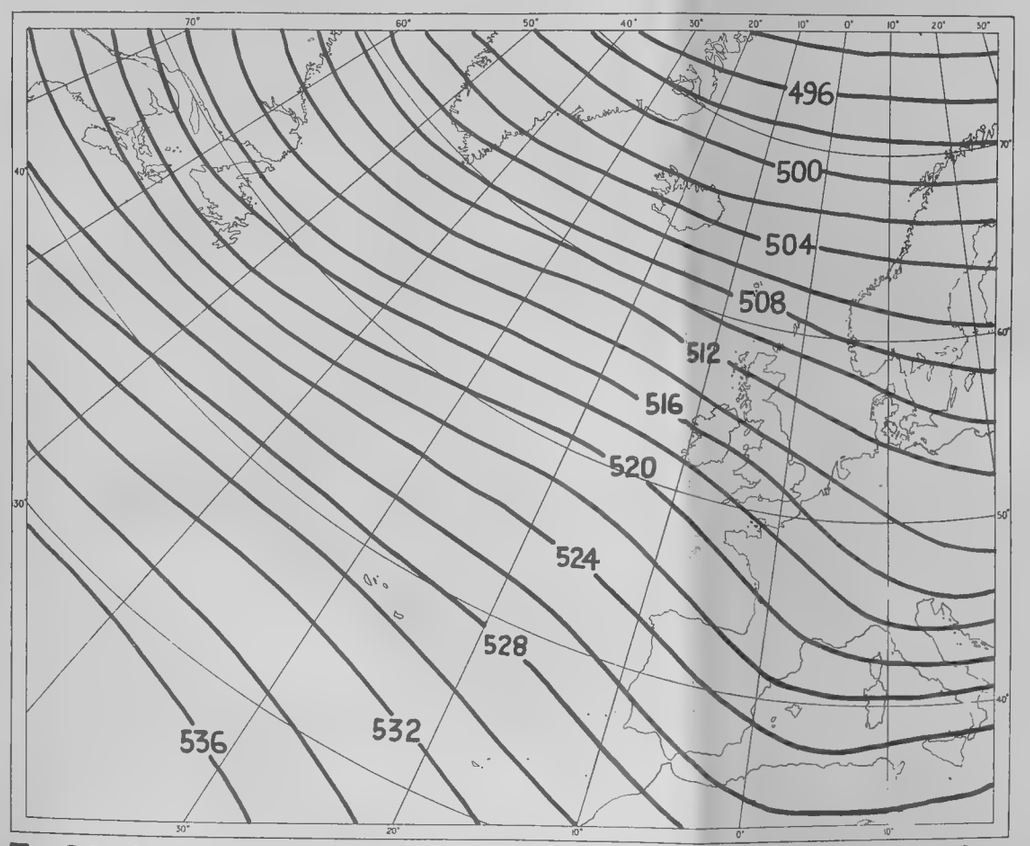

Fig. 29. Modified Z field (100mb. contours) 1500 G.M.T. 8:2:54 Units 10^2 ft.

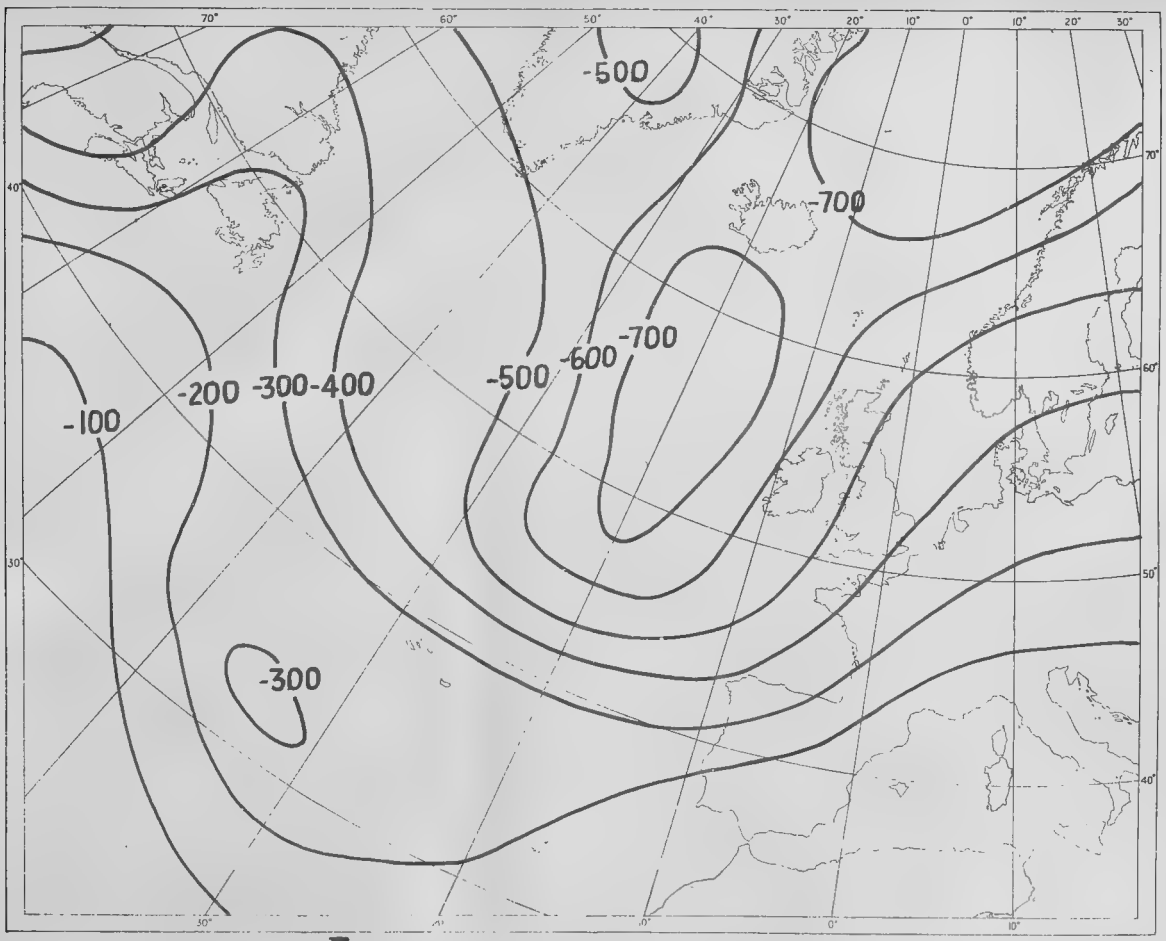

Fig.32. Original Z-$\bar{Z}$-G field 0300 G.M.T. 4:11:55 Units: Ft.

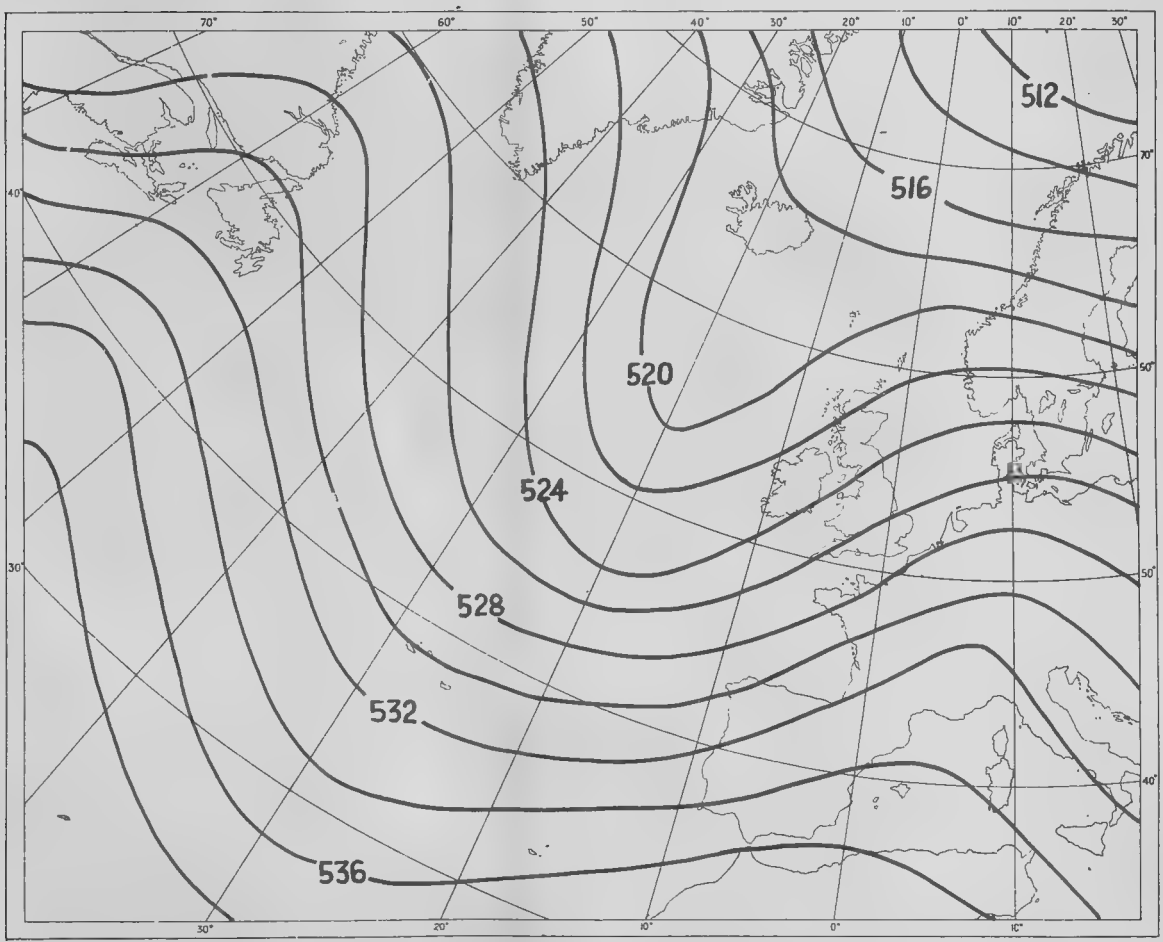

Fig.31. Original Z field (100 mb. contours) 0300 G.M.T. 4:11:55 Units: 10^2 ft.

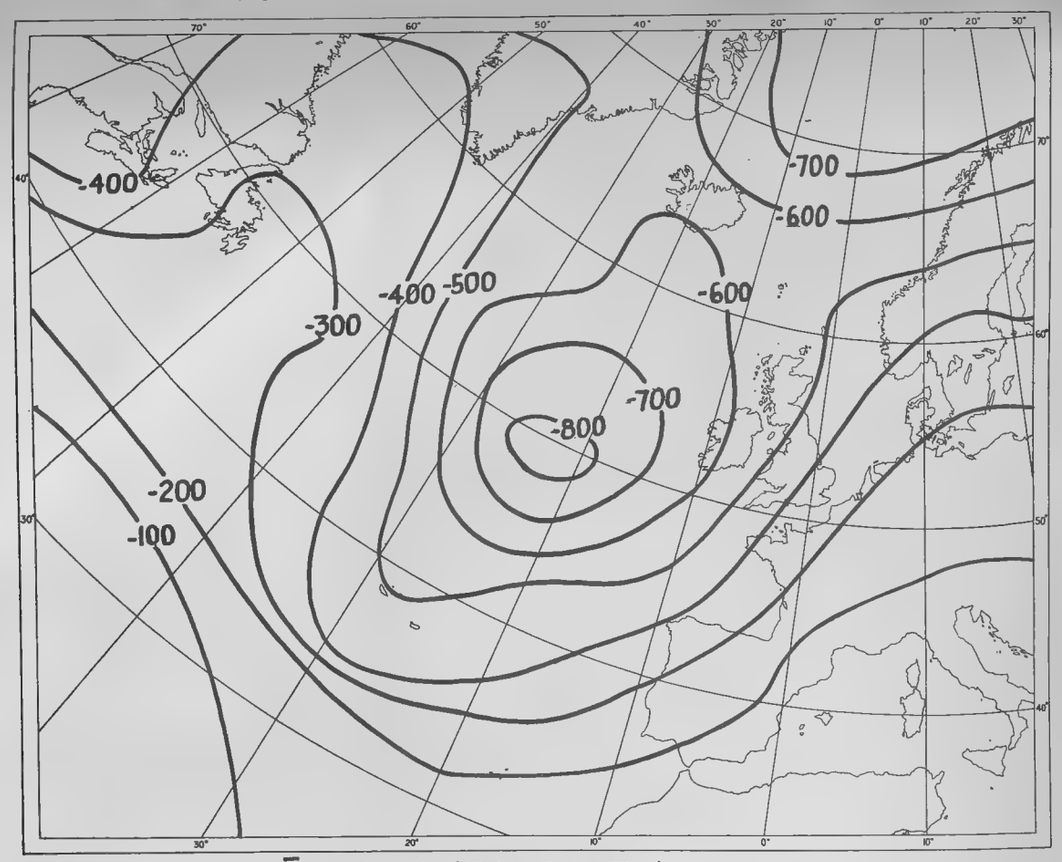

Fig.34. Original Z-$\bar{Z}$-G field 1500 G.M.T. 4:11:55 Units: ft

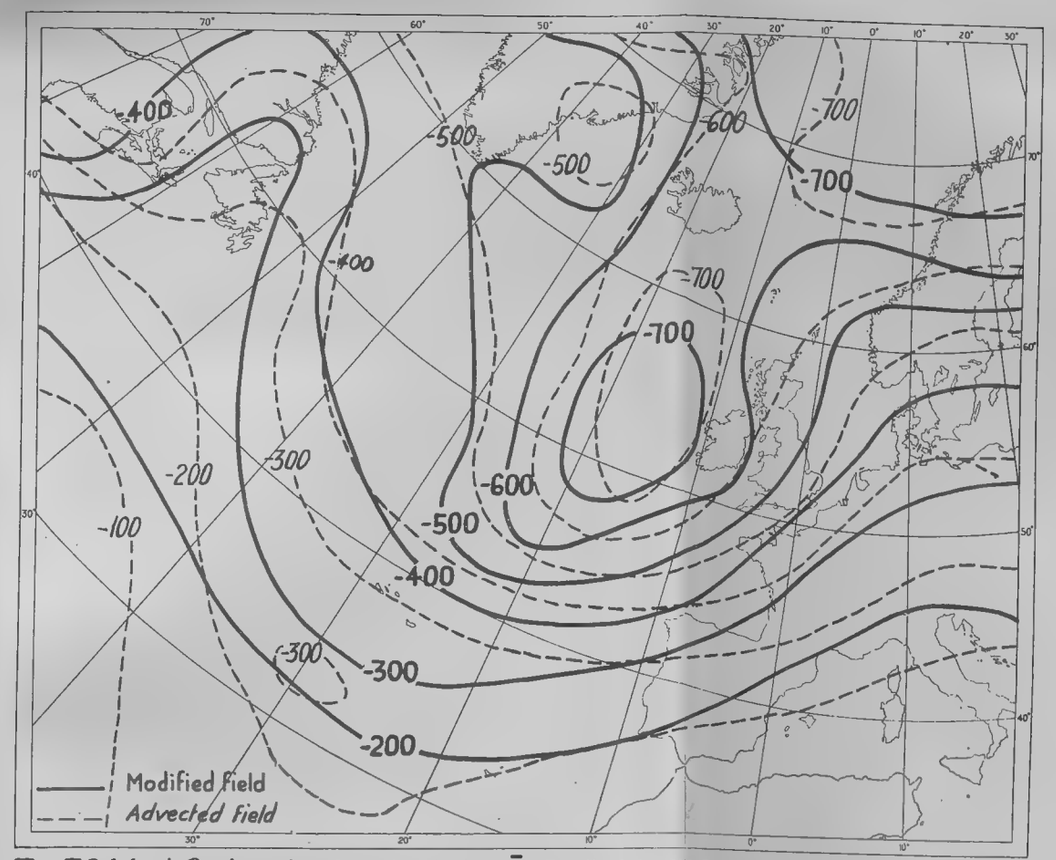

Fig.36. Modified and advected Z-$\bar{Z}$-G fields 1500 G.M.T. 4:11:55 Unit: ft

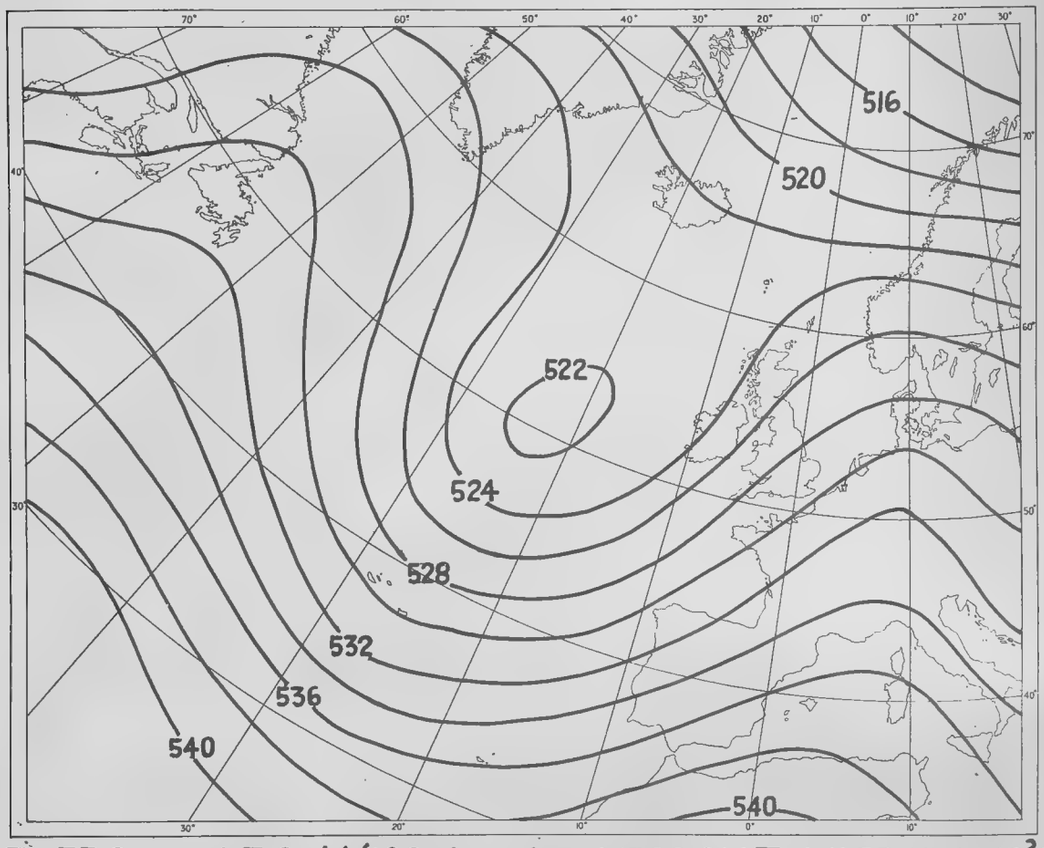

Fig.33. Original Z field (100mb contours) 1500 G.M.T. 4:11:55 Units: 10^2 ft.

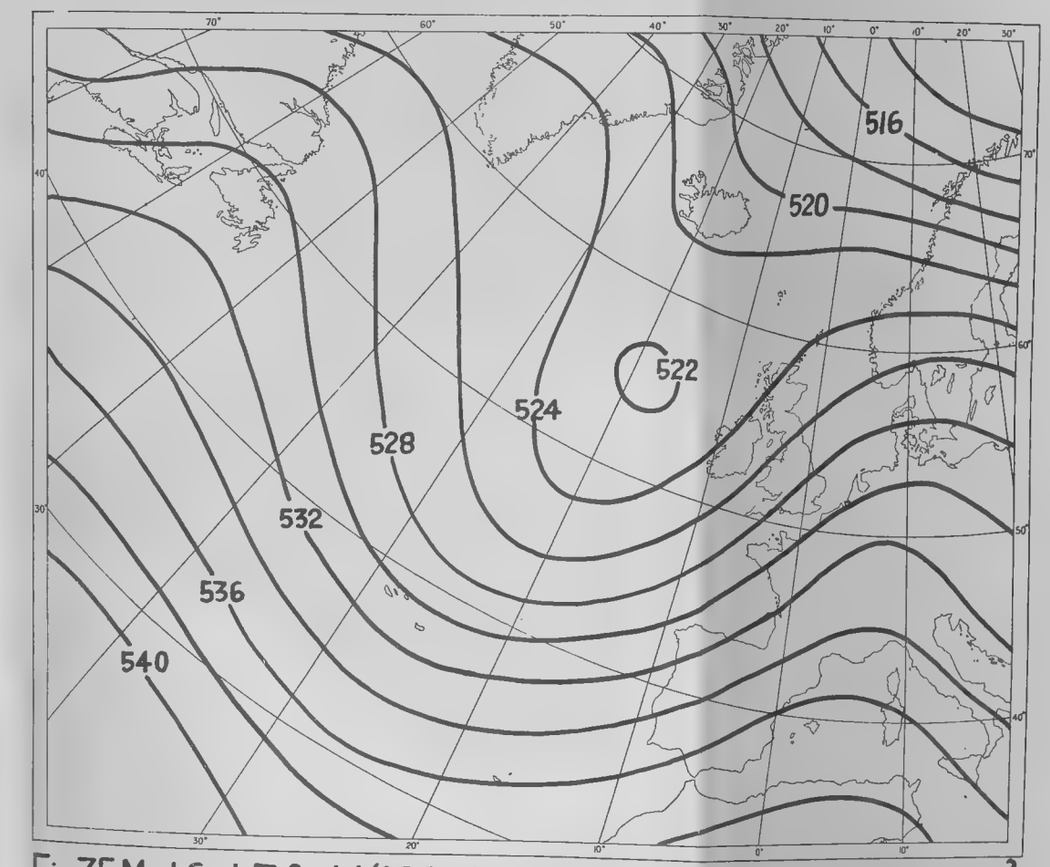

Fig.35. Modified Z field (100mb contours) 1500 G.M.T. 4:11:55 Units: 10^2 ft.

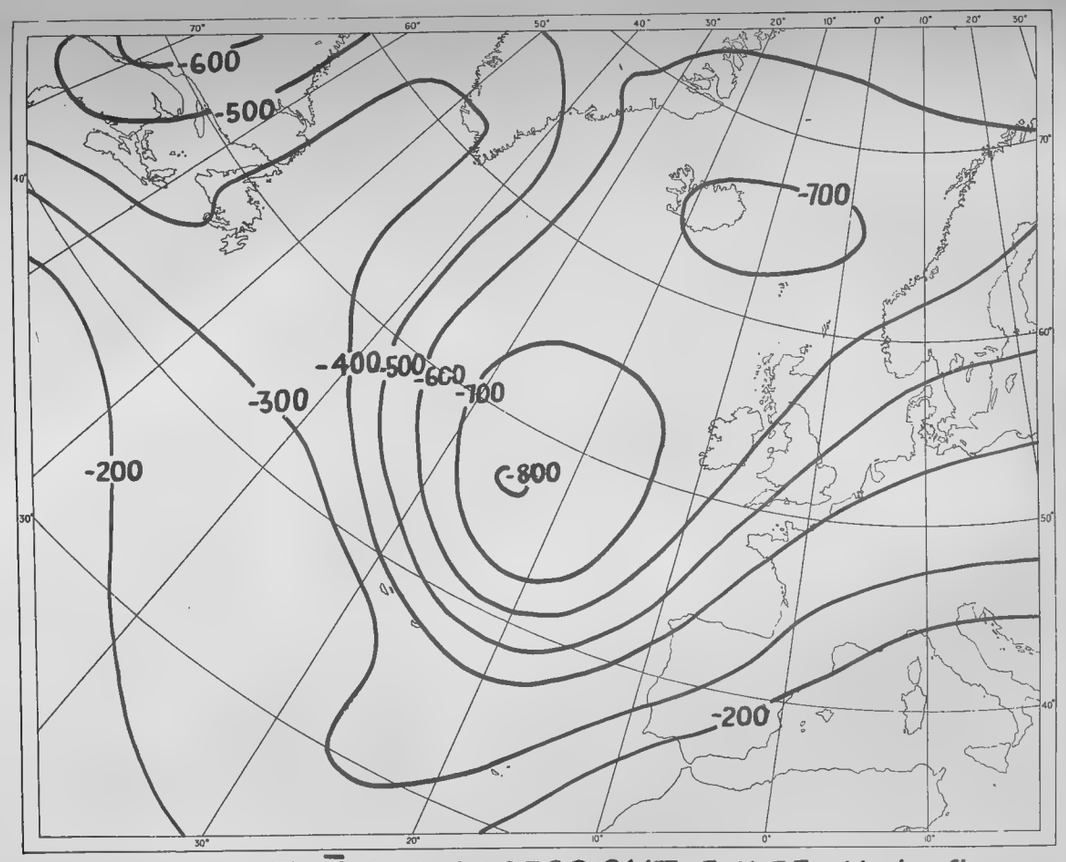

Fig.38. Original Z-$\bar{Z}$-G field 0300 G.M.T. 5:11:55 Units: ft.

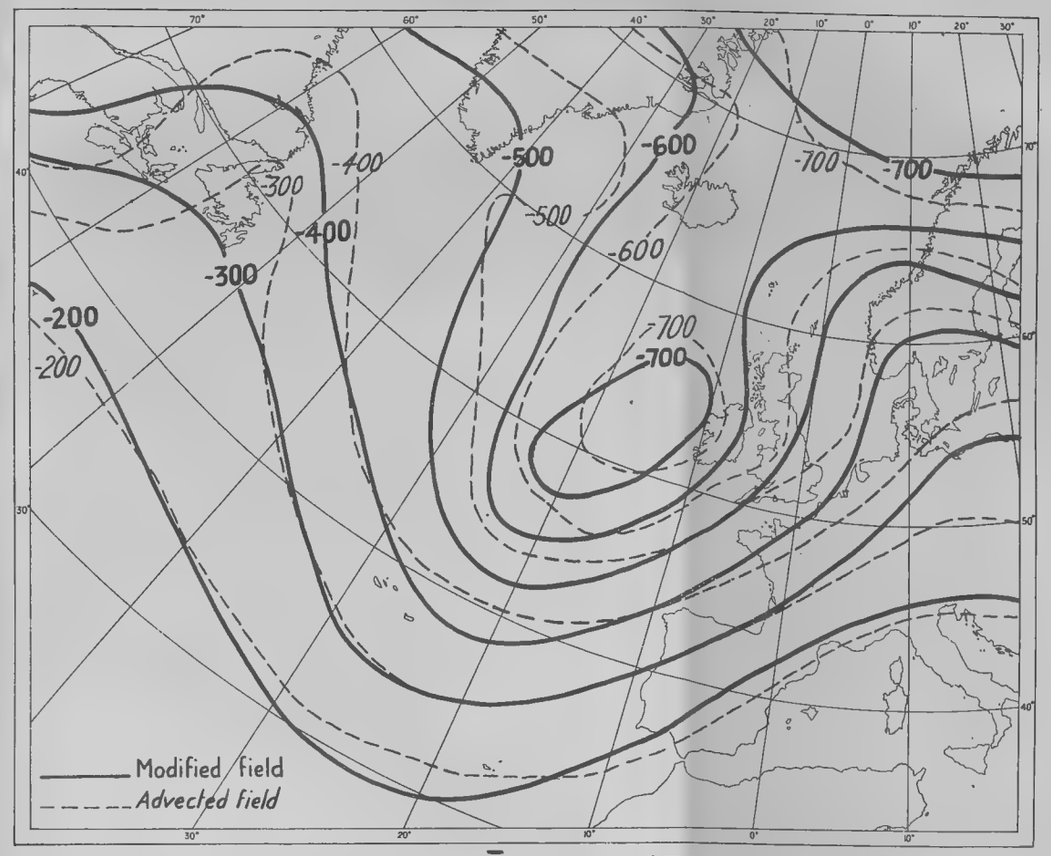

Fig.40. Modified and advected Z-$\bar{Z}$-G fields 0300 G.M.T. 5:11:55 Units: ft.

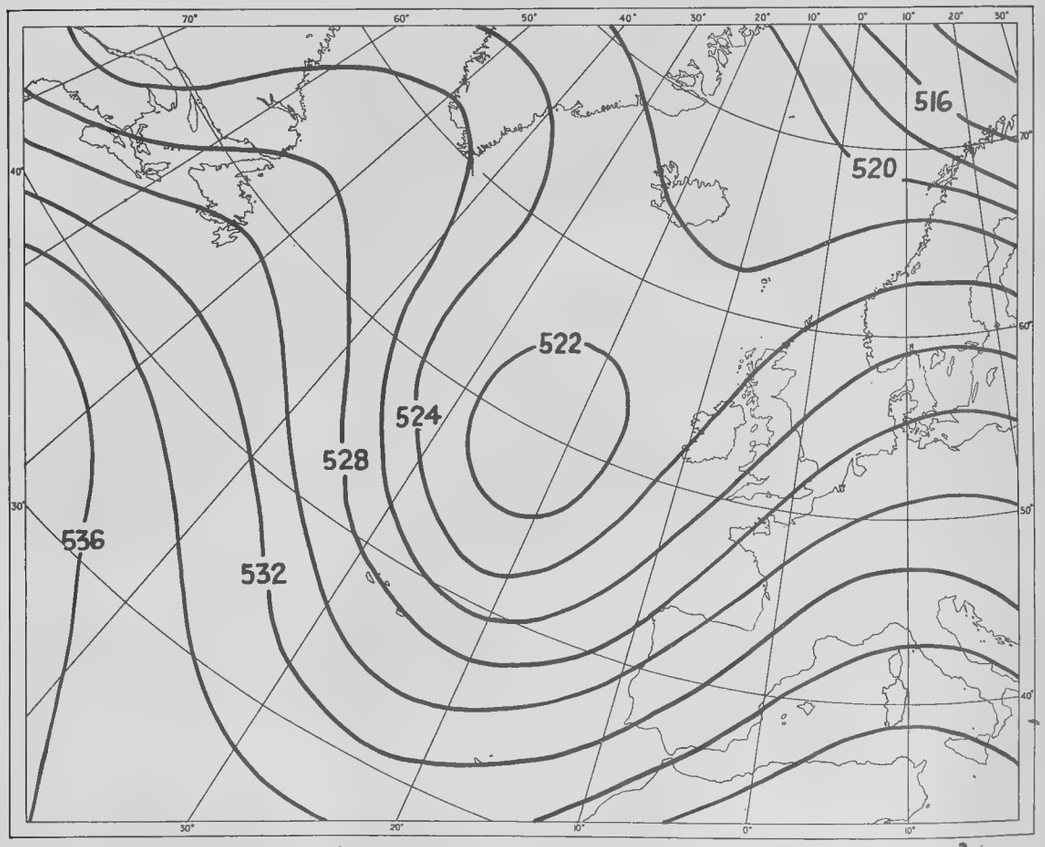

Fig.37. Original Z field (100 mb. contours) 0300 G.M.T. 5:11:55 Units: 10^2 ft.

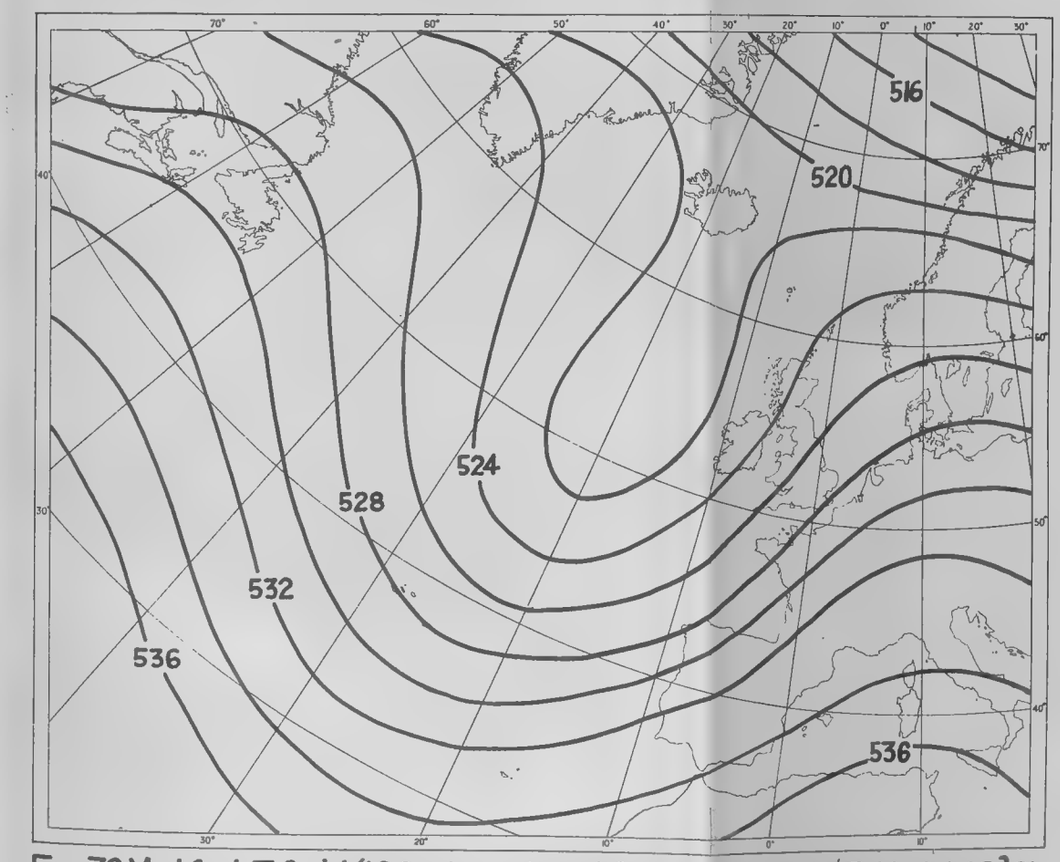

Fig.39. Modified Z field (100 mb. contours) 0300 G.M.T. 5:11:55 Units: 10^2 ft

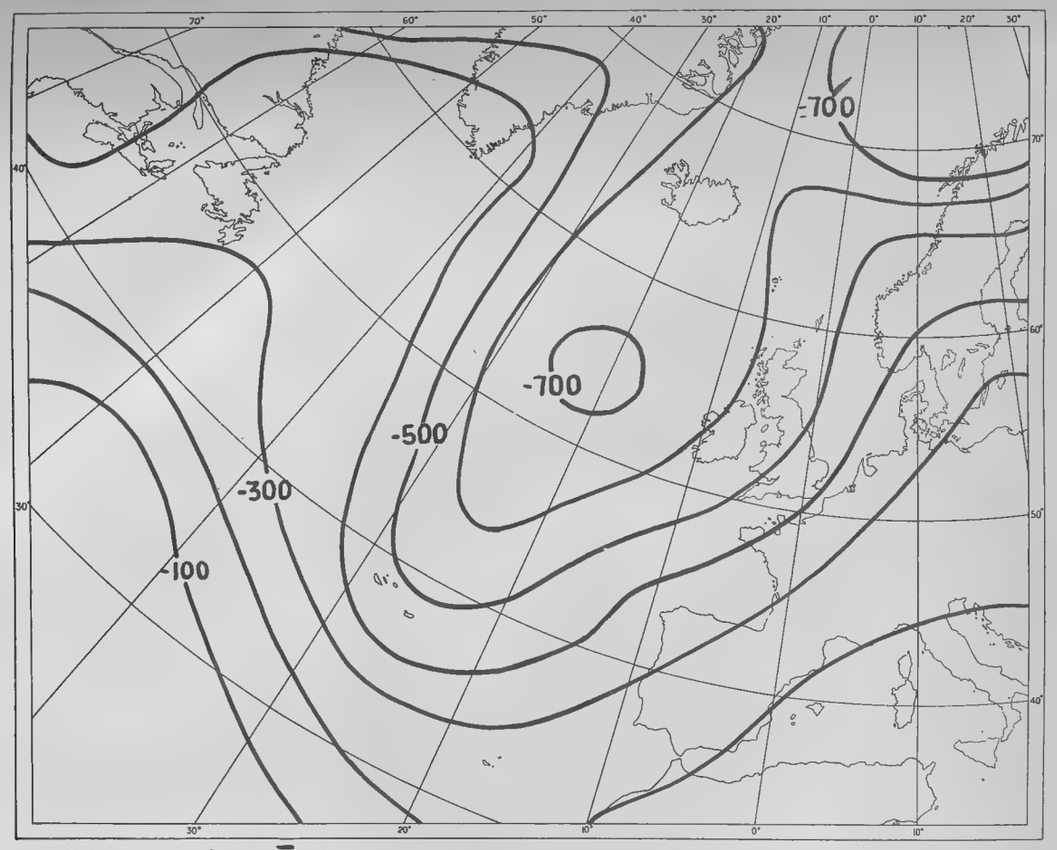

Fig.42. Original Z-$\bar{Z}$-G field 1500 G.M.T. 5:11:55 Units: Ft.

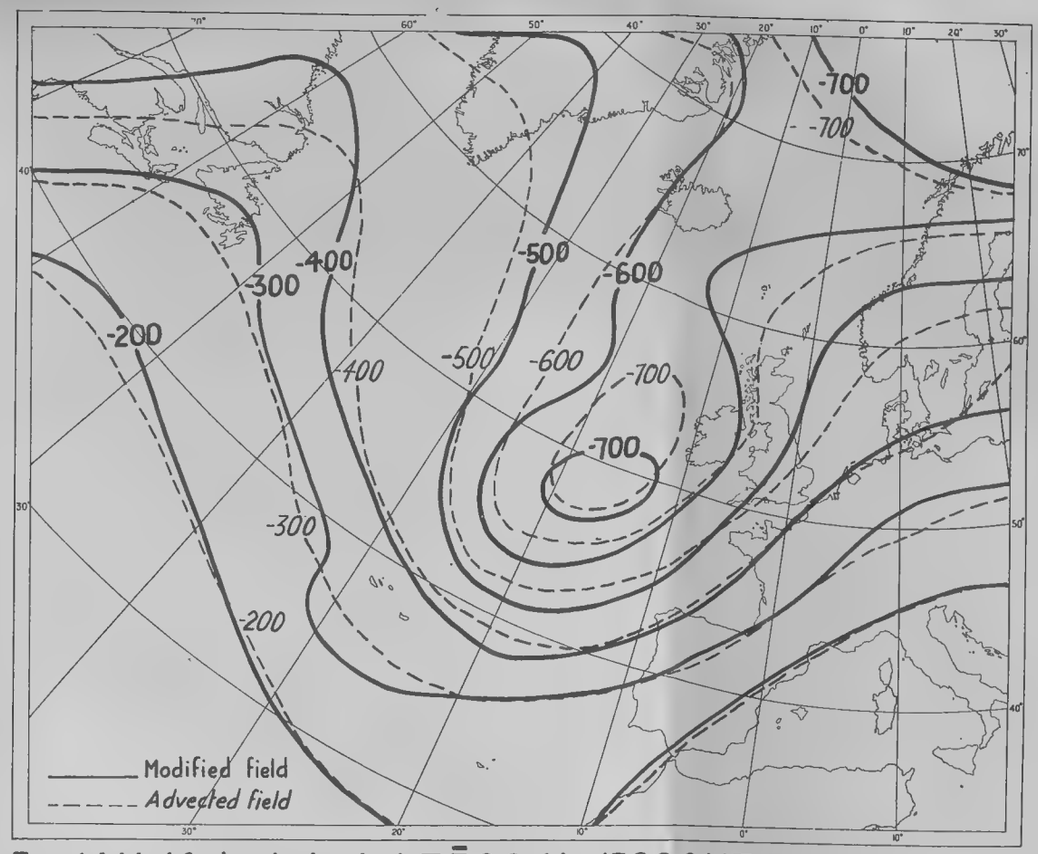

Fig.44. Modified and advected Z-$\bar{Z}$-G fields 1500 G.M.T. 5:11:55 Units: Ft.

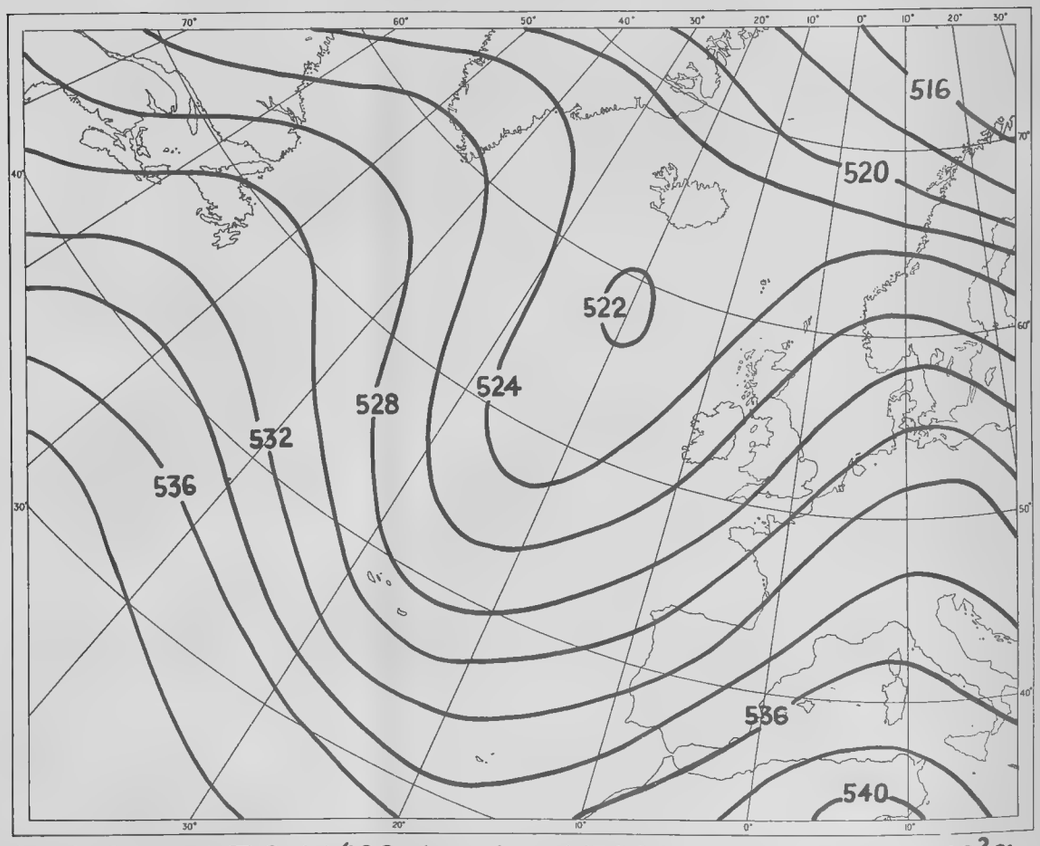

Fig.41. Original Z field (100mb. contours) 1500 G.M.T. 5:11:55 Units 10^2 Ft.

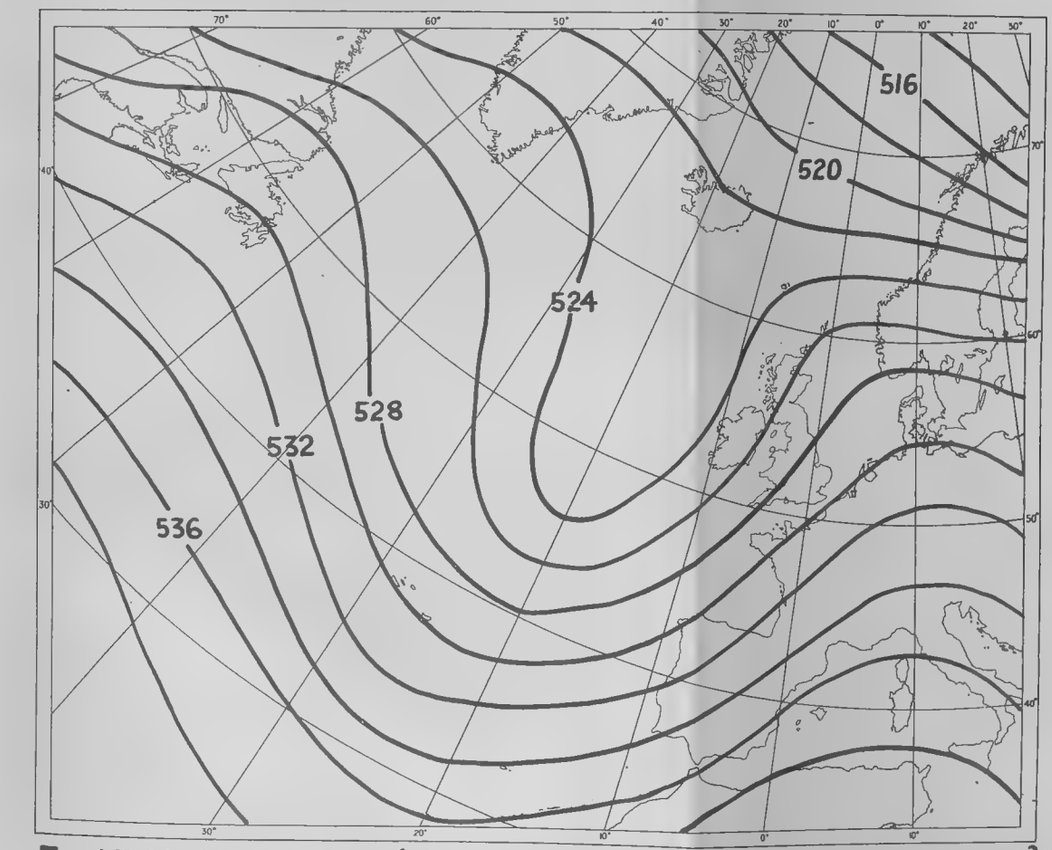

Fig.43. Modified Z field (100mb. contours) 1500 G.M.T. 5:11:55 Units: 10^2 Ft

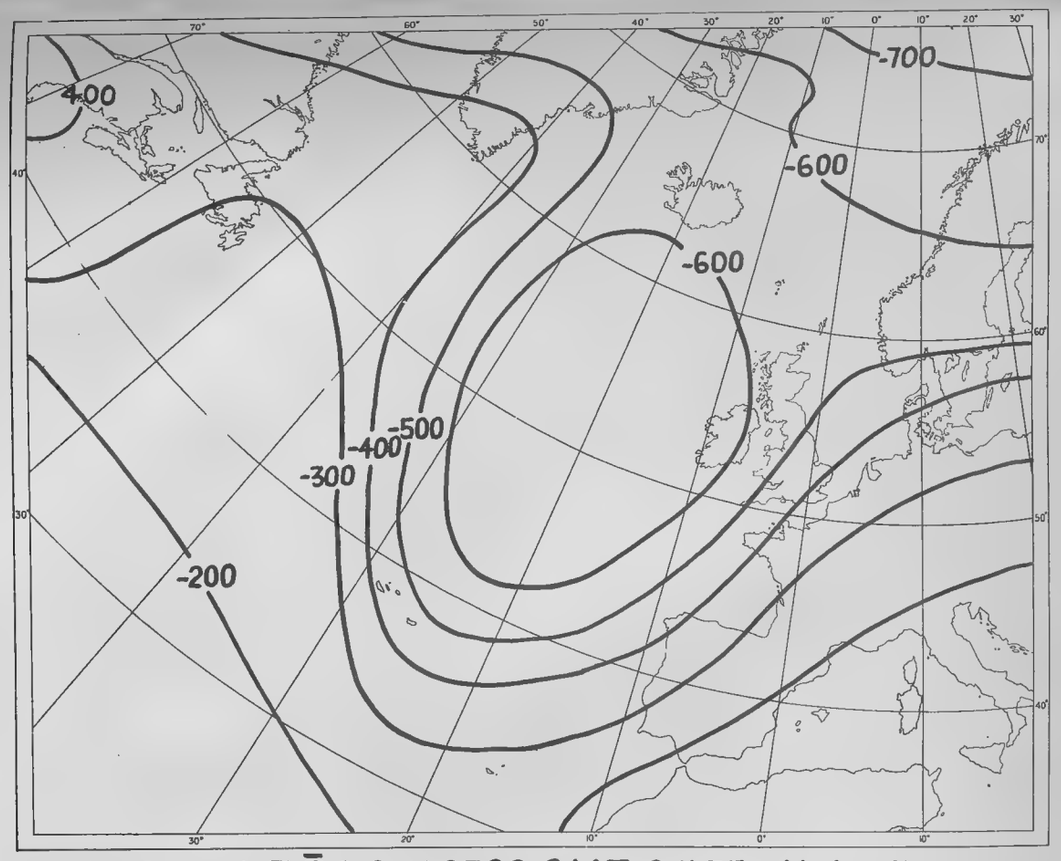

Fig.46. Original Z-$\bar{Z}$-G field 0300 G.M.T. 6:11:55 Units : ft.

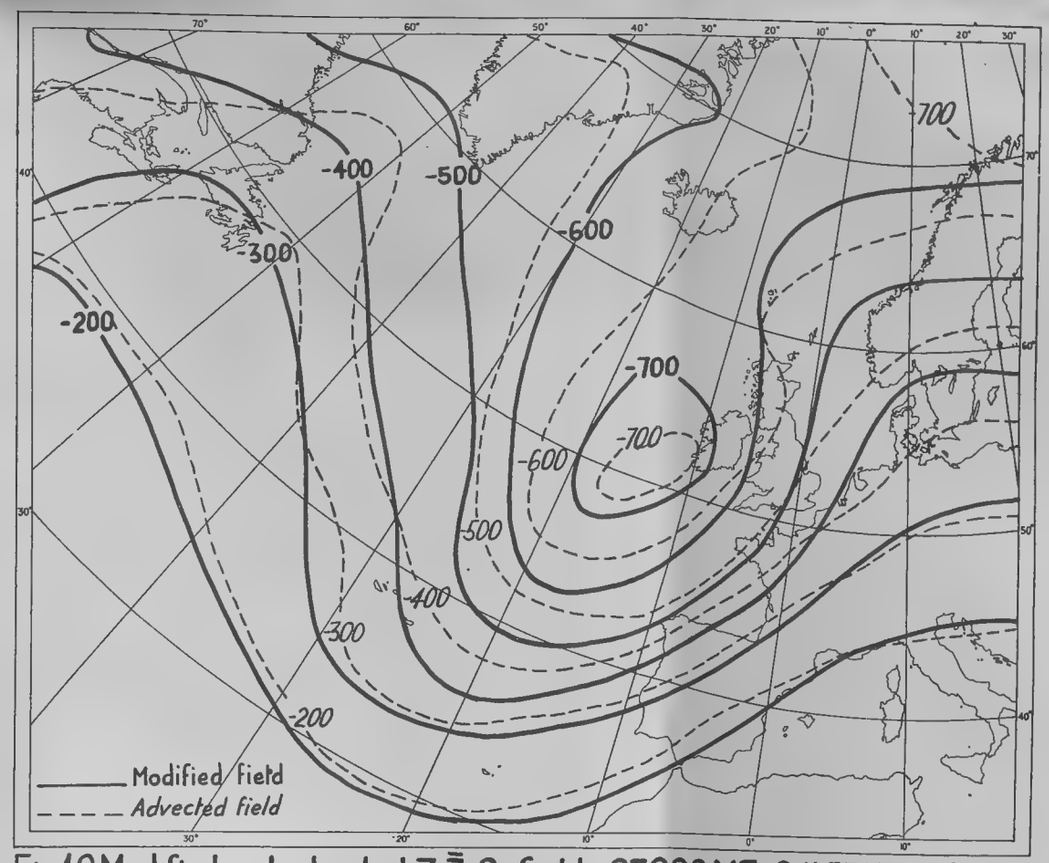

Fig.48. Modified and advected Z-$\bar{Z}$-G fields 0300 G.M.T. 6:11:55 Units : ft

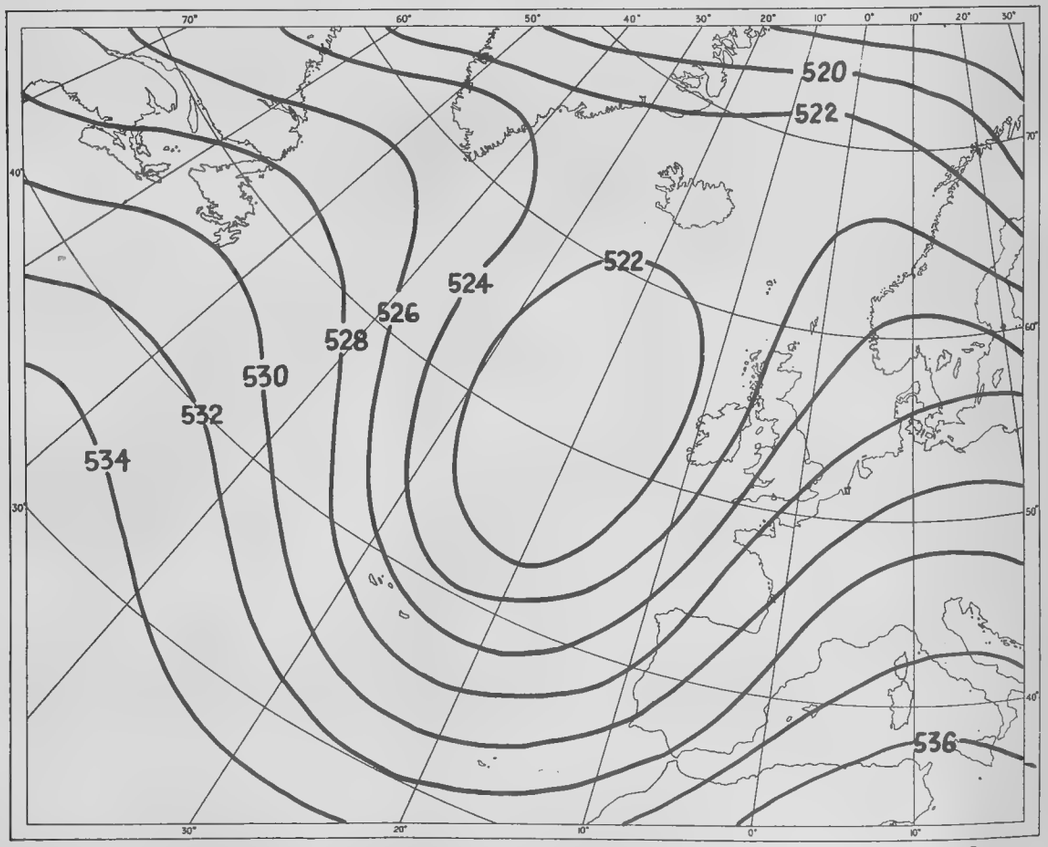

Fig.45. Original Z field (100mb. contours) 0300 G.M.T. 6:11:55 Units : 10^2 ft.

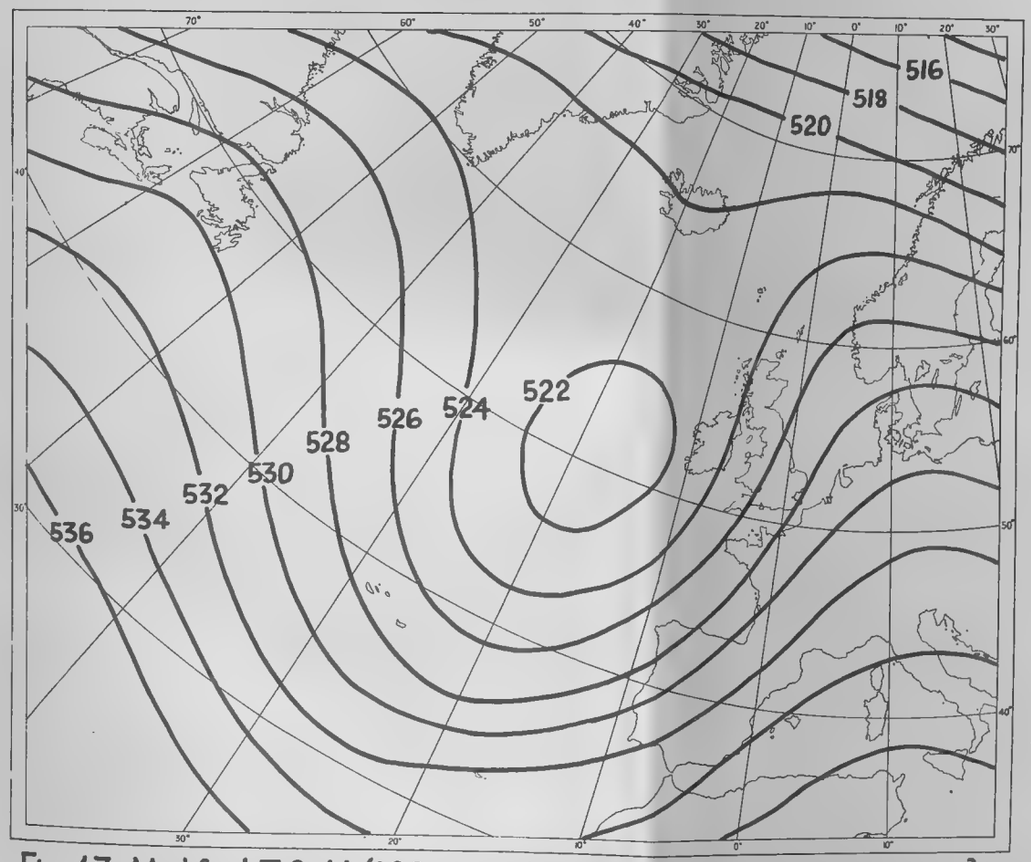

Fig. 47. Modified Z field (100mb. contours) 0300 G.M.T. 6:11:55 Units 10^2 ft.

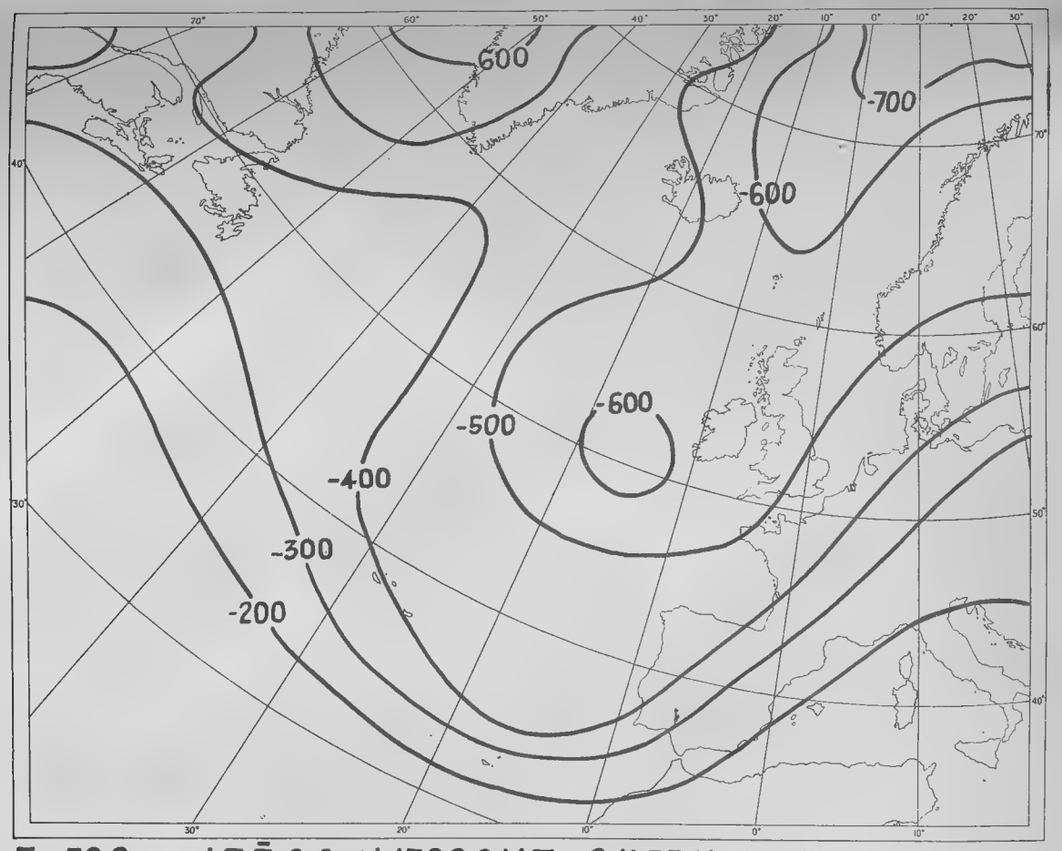

Fig.50 Original Z-Z̄-G Field 1500 G.M.T. 6:11:55 Units : Ft.

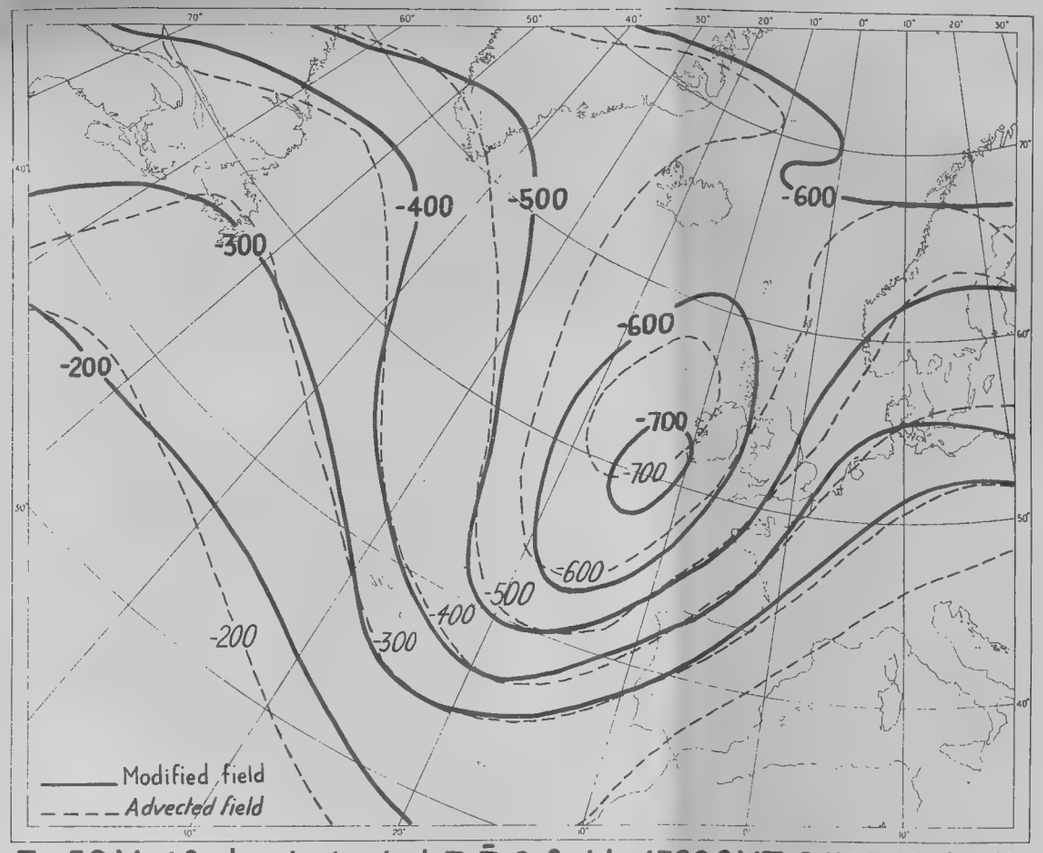

Fig.52 Modified and advected Z-Z̄-G fields 1500 G.M.T. 6:11:55 Units : Ft.

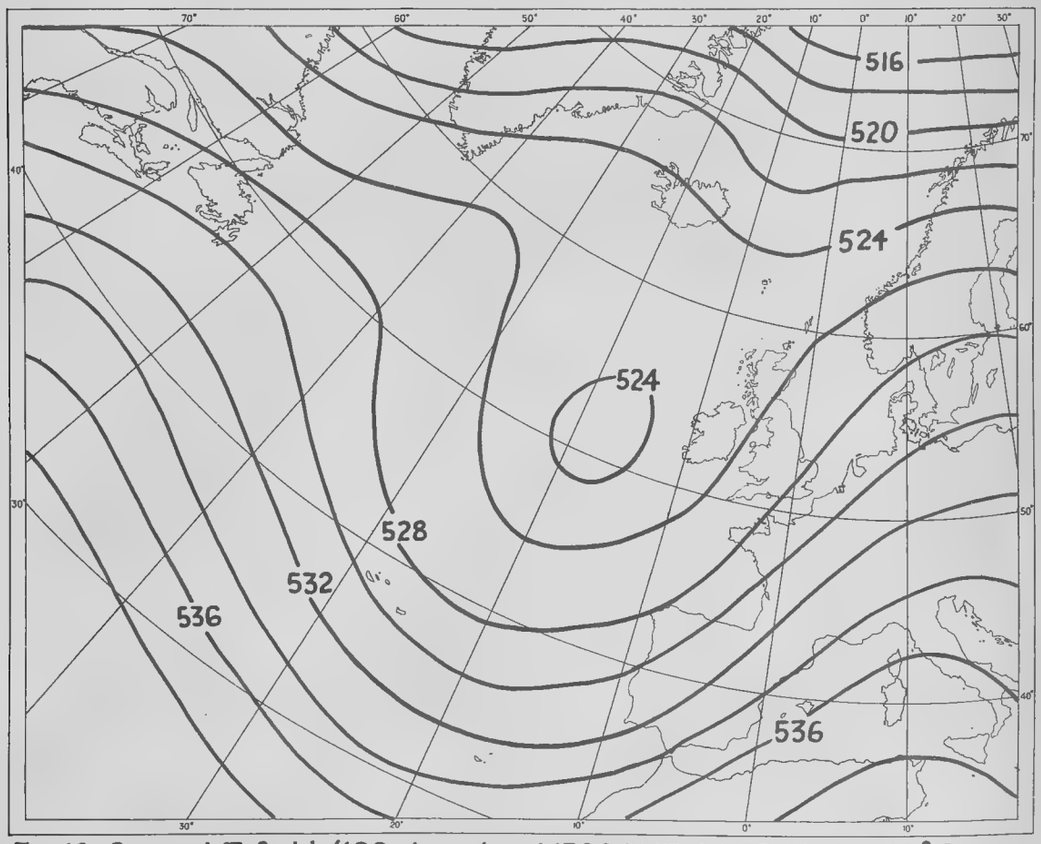

Fig.49 Original Z field (100mb. contours) 1500 G.M.T. 6:11:55 Units : 10^2 Ft.

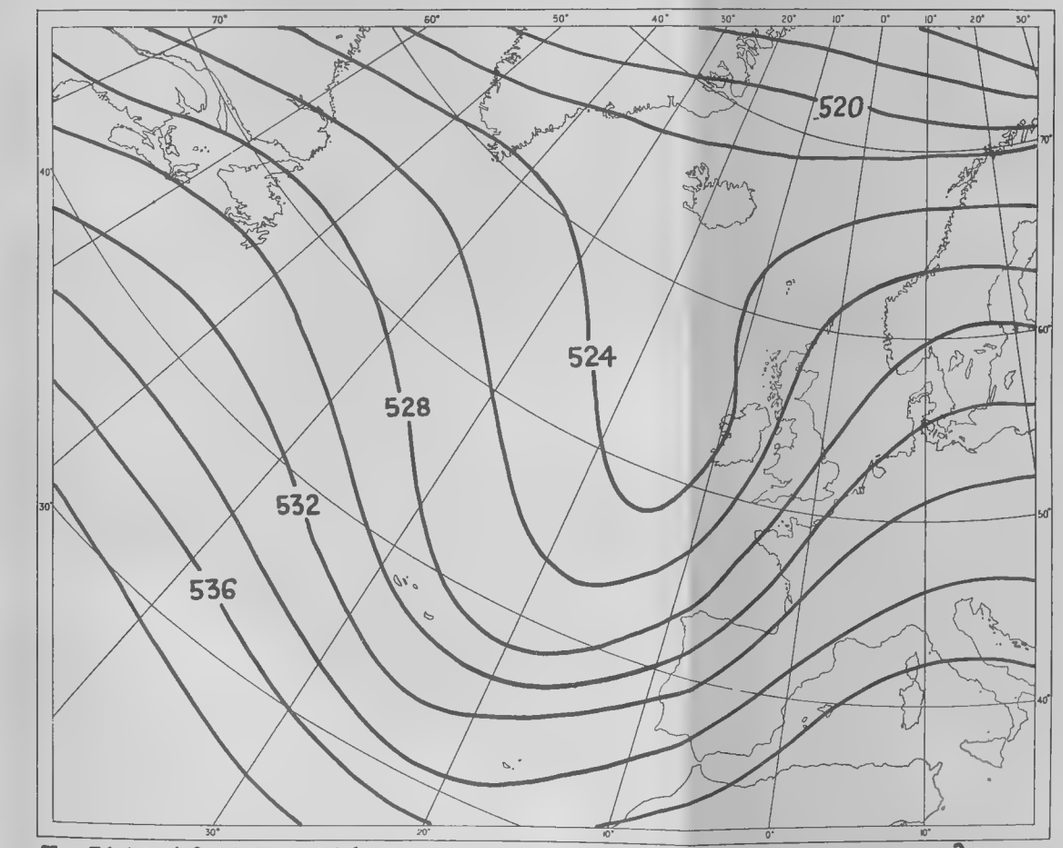

Fig.51 Modified Z field (100 mb. contours) 1500 G.M.T. 6:11:55 Units : 10^2 Ft.

M.R.P. 1079
S.C. 1/132
S.C. III/247A
26th November, 1957.

MAFF

Some measurements of temperature and humidity near the sea surface

BY

H. C. Shellard.

(Meteorological Office)

AIR MINISTRY

METEOROLOGICAL RESEARCH COMMITTEE

3-8-1046

At the time of issue this report has not been published. Any author desiring to quote this paper should refer to it as "A paper of the Meteorological Research Committee (London), M.R.P. No. 1079 by Mr. H.C. SHELLARD A copy is available in the Library of the Meteorological Office."

M.R.P. 1079
S.C.I/132
S.C.III/247A
26th November, 1957

AIR MINISTRY

METEOROLOGICAL RESEARCH COMMITTEE

Some measurements of temperature and humidity near the sea surface

by

H. C. Shellard (Meteorological Office)

1. Introduction

Because of the large proportion of the earth's surface that is covered by the oceans it is clear that the energy transferred from the oceans to the atmosphere must be an important factor in many meteorological problems. It is therefore desirable that our knowledge concerning the processes by which this transfer of energy occurs should be increased as much as possible. It is fairly certain that the form of the equations representing the vertical distributions of temperature and humidity overland will not usually apply over the open sea and information is lacking concerning the extent to which conditions over the oceans can depart from those of neutral stability. The importance of attempting to make actual measurements of the vertical profiles of temperature and humidity over the ocean is therefore obvious. More extensive discussion of this subject has been given by Charnock (1951).

The object of this paper is to describe a method of making such measurements and to indicate its possibilities by presenting a few results. The instrument used, for which Mr. J. MacDowall was mainly responsible, is described in some detail, although it might well be modified in the light of further experience. This account has been written without waiting for further observations because the instrument became unserviceable and, owing to pressure of other work in the Instruments Division, it may not be possible to make any further measurements for some considerable time.

2. Instrumental

(a) The apparatus

One of the major difficulties in measuring temperature and humidity at sea is that the presence of a ship introduces errors in the readings so that they are to some extent unrepresentative. If it is desired to make accurate measurements of the gradients of temperature and humidity near the sea surface such errors become prohibitive. It is therefore necessary to devise an apparatus with which the desired measurements can be made in the free air some distance away from and preferably to the windward of the ship. Such equipment has been developed in the Meteorological Office and is illustrated in Fig.1. It consists of a modified danbuoy the spar of which has been replaced by a hollow aluminium pole. This pole carries five aspirated dry and wet bulb thermoelectric psychrometers fixed at various distances above the waterline and four single thermocouples, for measuring sea temperature, at different levels below the waterline. A 60 lb. ballast weight is attached to the bottom of the pole to assist in keeping it vertical in the water. Each psychrometer is encased in a tufnol housing, painted white to reduce radiation effects (see Fig.2), each wet bulb element having a wick leading to a water

/reservoir.

reservoir. The thermocouple elements are similar to those used by Pasquill (1949). Ventilation is provided by two blowers driven by electric motors mounted in a watertight housing below the danbuoy and exhausting downwind through a rubber "snort" tube. Water traps are provided at the bottom of the mast and the "snort". The ventilation rate is controlled by a butterfly valve in each housing, the valves being set to give the same ventilation rate to each psychrometer. This rate is about 2.2 m./sec., when the lag coefficients of the dry bulb and wet bulb elements are about 70 seconds and 45 seconds respectively. Suitable cables, supported by floats, are used to carry power from the ship for the motors and to connect the various thermocouples to a switch which enables them to be connected in sequence on board to a potentiometer, an ice-junction being used as a reference. The heights of the elements above the water line in the 1956 trials of the equipment, the results of which are here presented, were 56, 89, 135, 195 and 287 cm. and the depth of those below the water-line 13, 30, 66 and 122 cm. There had been some earlier experiments in which thermisters were used as thermometer elements but difficulties were experienced due to calibration shifts.

(b) Operation and exposure

The complete apparatus, which has become known as a "thermobuoy", is launched from the stationary weather ship, to which it is attached by mooring lines as well as by the above-mentioned cables. It is allowed to float some 100 feet or so upwind of the ship and readily takes up this position as the ship drifts away from the thermobuoy under the action of the wind. The general arrangement is shown in Fig. 3. It has been found that the thermobuoy, as at present designed, floats in a vertical position in the open sea provided the wind is not much above force 3. It will be noted that although the buoy is upwind of the ship, the water in which it floats may well have been previously affected by the ship. It seems probable that this difficulty could be overcome by steaming slowly at right angles to the wind direction while observations are being made.

3. Observations

The apparatus was tried out successfully at sea from the O.W.S. "Weather Recorder" at station 'India' in July, 1956. Two sets of profiles which are believed to be reliable, and which have a number of points of interest, were obtained on the mornings of 6th and 9th July, 1956. Further sets were obtained on the 10th and 18th but during the first of these, conditions became unsuitable owing to increasing wind and sea and during the second some of the wet bulb readings were doubtful, dry patches afterwards being found on the wicks. The fact that at the next trial of the equipment, from the same weather ship on her next voyage in August 1956, both the cable and the electric motors were found to have become unserviceable also suggests that it is as well to reject the fourth set of observations made in July.

Having launched the thermobuoy and got it into position upwind of the ship, readings were taken as follows. Potentiometer readings were noted as pairs of thermojunctions were switched into the circuit in a fixed order, viz., first dry bulb junction at 287 cm. against reference junction in melting ice, then each of the other dry bulb junctions in turn against the first, then each wet bulb junction in turn against its corresponding dry bulb junction and finally each sea temperature junction in turn against the first dry bulb junction, proceeding in each case from the highest level to the lowest one. The cycle was then repeated. On 6th July the complete cycle was repeated eight times and took about 90 minutes and on 9th July it was repeated ten times and occupied about 115 minutes.

It was found that there were appreciable fluctuations of air temperature with time at all levels. The best way of dealing with the readings, which could not in any case have been taken simultaneously at all levels, was therefore to take mean values at each level over the whole run and regard these as giving approximate mean temperature and humidity profiles during the period of the observations. The results could be checked to some

/extent

extent by comparison with the routine observations being taken on the ship for synoptic purposes and with the air and sea thermograph charts.

The results of the first set of observations with the thermobuoy are given in Table 1. Readings taken from the ship's meteorological logbook and as interpolated from the ship's air and sea thermographs are given in the bottom part of the table. It will be seen that the thermobuoy results are in general agreement with the observations taken on the ship and this consistency indicates that the equipment was working satisfactorily. A marked fluctuation in air temperature during the experiment was also clearly shown on the ship's air thermograph. The waves and swell varied the height of the buoy in the water over a range of about 25 cm. but it floated in the correct vertical position. After the experiment the ice standard and wet bulbs were in perfect condition.

The second set of results is given in the same way in Table II. On 9th July weather conditions were somewhat similar to those in the first experiment but the wind was lighter and recording conditions were much better because there was hardly any roll of the ship and the potentiometer could be read more accurately.

4. Discussion

The results set out in Tables I and II have been plotted against a linear scale of height in Fig.4 to show how the dry bulb, wet bulb, dew point and sea temperatures varied with distance from the sea suface. On both days the sea temperature was higher than the air temperature, as measured at the highest level, by between a half and one degree Fahrenheit and it would be expected that there would be an increase both in temperature and humidity as the sea surface was approached. It will be noted that the temperature rise is very slight; there is in fact a slight inversion between 56 cm. and 135 cm. in Fig.4(a) while in Fig.4(b) the whole increase amounts to less than two tenths of a degree. On both occasions the mean temperature at 56 cm. was considerably closer to the temperature at screen height on the weather ship (about 25 ft or 760 cm.) than it was to the sea surface temperature. The dew point profiles, however, show a more significant increase as the sea surface is approached. The increase is more marked in Fig.4(b) and this is consistent with the somewhat lighter winds on this day. It will also be noted that the observations are less scattered under the better recording conditions of 9th July.

The most striking feature of the results, perhaps, is the fact that the difference between the sea surface temperature and the dew point temperature only 56 cm. from the surface is a large fraction of that between the sea surface temperature and the dew point at the 287 cm. level (which is itself not greatly different from the dew point at the level of the ship's screen). On 6th July the dew points at 56 cm. and in the ship's screen were, respectively, 5.4 and 5.7 degrees below the sea surface temperature and on 9th July the corresponding figures were 6.6 and 7.7 degrees, so that even as near to the sea surface as 56 cm., 95 and 86 per cent, respectively, of the difference (sea surface temperature - dew point at about 25 ft) still existed.

It will be noted that on both days the sea temperature profiles to a depth of 122 cm. were almost exactly isothermal. This is a little surprising because Houghton (1956) measured two profiles of sea temperature at station J during the summer of 1950 in somewhat similar weather conditions and found that the temperature at 122 cm. was appreciably colder than that near the surface, but the fact that his observations were made later in the day, at about 1430 G.M.T., may partly account for this and the somewhat doubtful exposure of the thermobuoy so far as sea temperatures are concerned may also be relevant.

In Fig.5 are shown, plotted on a logarithmic height scale, the profiles of $(t_o - t_z)$, where t_o is the sea surface temperature and t_z the temperature at height z cm., both for dry bulb and wet bulb temperature, and also of $(e_o - e_z)$, where e_o = .98 x the saturation vapour pressure in millibars at the sea

/surface

surface temperature, .98 being a correction for salinity, and e_z the vapour pressure at height z. It is clear that the profiles are reasonably logarithmic, the fit of the second set being particularly good. The straight lines were fitted by the method of least squares and their equations found to be as follows:-

6.7.56

Dry bulb	$t_o - t_z = .174 (\log_{10} z + 1.46)$
Wet bulb	$t_o - t_z = .233 (\log_{10} z + 11.98)$
Vapour pressure	$e_o - e_z = .192 (\log_{10} z + 9.53)$

9.7.56

Dry bulb	$t_o - t_z = .218 (\log_{10} z + 2.07)$
Wet bulb	$t_o - t_z = .866 (\log_{10} z + 2.78)$
Vapour pressure	$e_o - e_z = .621 (\log_{10} z + 2.65)$

It is well known that in neutral conditions the wind profile immediately over an aerodynamically rough surface can be expressed as

$$\frac{u}{u_*} = \frac{1}{k} \log \frac{z}{z_o}$$

where u_* is the friction velocity (defined by $u_* = \sqrt{\frac{\tau_o}{\rho}}$, where τ_o is the surface drag and ρ the air density), 'k' is von Karman's constant, and z_o is the roughness parameter which characterises the geometry of the boundary. Values of z_o for smooth sea at low wind speeds are now usually thought to be of order 0.02 cm. (Sutton 1955). Application of the general equation suggested by Charnock (1955) for the vertical profile of mean wind over a water surface to the mean wind speed of 6th and 9th July, respectively, gives values of z_o of about $10^{-2.8}$ and $10^{-3.4}$ cm.

If we refer to the intercept of the temperature or humidity profile on the log z axis as Z_o, by analogy with z_o, it is seen that there is some evidence that the values of Z_o and z_o were of the same order in these experiments over the ocean (e.g. on 9th July, 1956, Z_o was $10^{-2.1}$ cm. for temperature and $10^{-2.7}$ cm. for vapour pressure), and that in these near-neutral conditions the profiles of wind, temperature and humidity are roughly similar. Rider and Robinson (1951) demonstrated that profiles of temperature and humidity over land are roughly similar and it is of importance to test their conclusion over the sea surface under various conditions.

5. Conclusions

The thermobuoy apparatus is capable of giving valuable observations of temperature and humidity profiles near the sea surface, certainly if the wind speed is not much above 12 knots.

The accuracy of the measurements appears to be just about adequate but in view of the small gradients that have to be measured some improvement in this direction is desirable. On the other hand greater lag in the thermometer elements could probably be tolerated and might be helpful in reducing the effects of fluctuations and the need for so many readings.

Preliminary results indicate that profiles of temperature, humidity and wind are roughly similar. This is a matter of some importance and further observations are needed to confirm these results and to extend them to other wind and stability conditions. This could be done by similar measurements at ocean weather stations A, J, K and I. Simultaneous observations of the wind profile would be valuable but the difficulty in ensuring adequate exposure for the anemometers would be considerable.

/REFERENCES

REFERENCES

Charnock, H.	1951	Science Progress No.153, p.80.
Pasquill, F.	1949	Q.J.R. Met. Soc., 75, p.239.
Houghton, D.M.	1956	Q.J.R. Met. Soc., 82, p.515.
Sutton, O.G.	1955	Atmospheric Turbulence, Methuen, p.107.
Charnock, H.	1955	Q.J.R. Met. Soc., 81, p.639.
Rider, N.E. and Robinson, G.D.	1951	Q.J.R. Met. Soc., 77, p.375.

Total 776

(c) Air and sea thermographs indicated the following hourly values (corrected)

Hour	0900	1000	1100	1200	1300	G.M.T.
Dry-bulb temp.°F.	51.2	51.3	50.1	51.3	51.3	
Wet-bulb temp.°F.	48.8	48.6	48.4	48.3	48.2	
Sea temp. °F.	52.0	52.3	52.2	52.3	52.3	

TABLE I - Observations taken at Station 'India' (59°N. 19°W.) on 6th July, 1956, 1040-1210 G.M.T.

(a) Thermobuoy observations

Height above sea, cm.	Mean dry-bulb temperature, °F.	Mean wet-bulb temperature, °F.	Mean dew point temperature, °F.	Mean sea temperature, °F.
287	51.23	48.55	46.18	
195	51.25	48.57	46.21	
135	51.41	48.63	46.18	
89	51.32	48.68	46.36	
56	51.23	48.70	46.48	
-13				51.91
- 30				51.91
- 66				51.89
-122				51.90

(b) Synoptic observations at 0900 and 1200 G.M.T. included the following:-

G.M.T.	Dry-bulb	Wet-bulb	Dew point	Sea temp.	Cloud	Visibility	Wind	Waves	
0900	51.2	48.8	46.3	52.0	3/8 Cu 2,000 ft. 4/8 Sc 4,500 ft. Some Ac. Total 7/8	Over 12 mi.	200°/10 kt.	Direction Period Height	220° 7-9 sec. 5 ft.
1200	51.3	48.3	45.0	52.4	1/8 Cu 2,200 ft. 4/8 Sc 4,500 ft. 6/8 Sc 5,900 ft. Total 7/8	Over 12 mi.	200°/12 kt.	Direction Period Height	220° 7-9 sec. 5 ft.

(c) Air and sea thermographs indicated the following hourly values (corrected)

Hour	0900	1000	1100	1200	1300	G.M.T.
Dry-bulb temp.°F.	51.2	51.3	50.1	51.3	51.3	
Wet-bulb temp.°F.	48.8	48.6	48.4	48.3	48.2	
Sea temp. °F.	52.0	52.3	52.2	52.3	52.3	

TABLE II - Observations taken at Station 'India' (59°N. 19°W.) on 9th July, 1956, 1025-1220 G.M.T.

(a) Thermobuoy observations

Height above sea, cm.	Mean dry-bulb temperature, °F.	Mean wet-bulb temperature, °F.	Mean dew point temperature, °F.	Mean sea temperature, °F.
287	52.18	48.64	45.48	
195	52.18	48.74	45.69	
135	52.24	48.89	45.94	
89	52.26	49.06	46.26	
56	52.33	49.24	46.56	
- 13				53.15
- 30				53.16
- 66				53.15
-122				53.13

(b) Synoptic observations at 0900 and 1200 G.M.T. included the following:-

G.M.T.	Dry-bulb	Wet-bulb	Dew point	Sea temp.	Cloud	Visibility	Wind	Waves	
0900	52.2	49.0	45.6	53.5	3/8 Cb 2,000 ft. 6/8 Sc 5,000 ft. Total 6/8	Over 30 mi.	330°/3 kt.	Direction Period Height	340° 7-9 sec. 5 ft.
1200	52.7	49.0	45.0	53.6	2/8 Cb 2,000 ft. 4/8 Sc 5,800 ft. Some Ac. Total 5/8	Over 30 mi.	310°/9 kt.	Direction Period Height	330° 7-9 sec. 5 ft.

(c) Air and sea thermographs indicated the following values:-

Hour	0900	1000	1100	1200	1300	G.M.T.
Dry-bulb temp. °F	52.2	52.1	-	52.7	52.7	
Wet-bulb temp. °F.	49.0	49.0	-	49.0	49.4	
Sea temp. °F.	53.5	53.5	53.5	53.6	53.7	

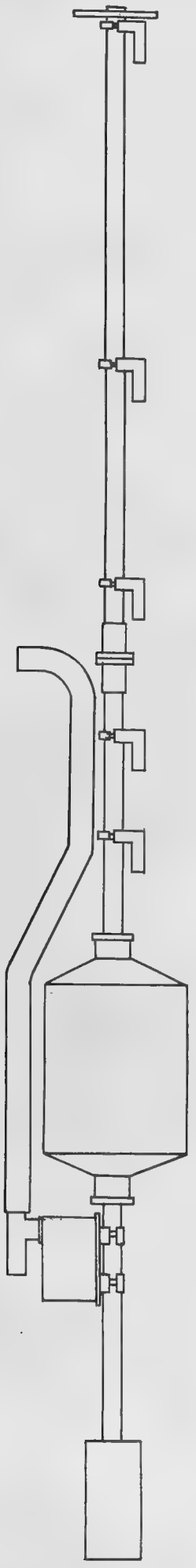

FIG. 1 SKETCH OF "THERMOBUOY"

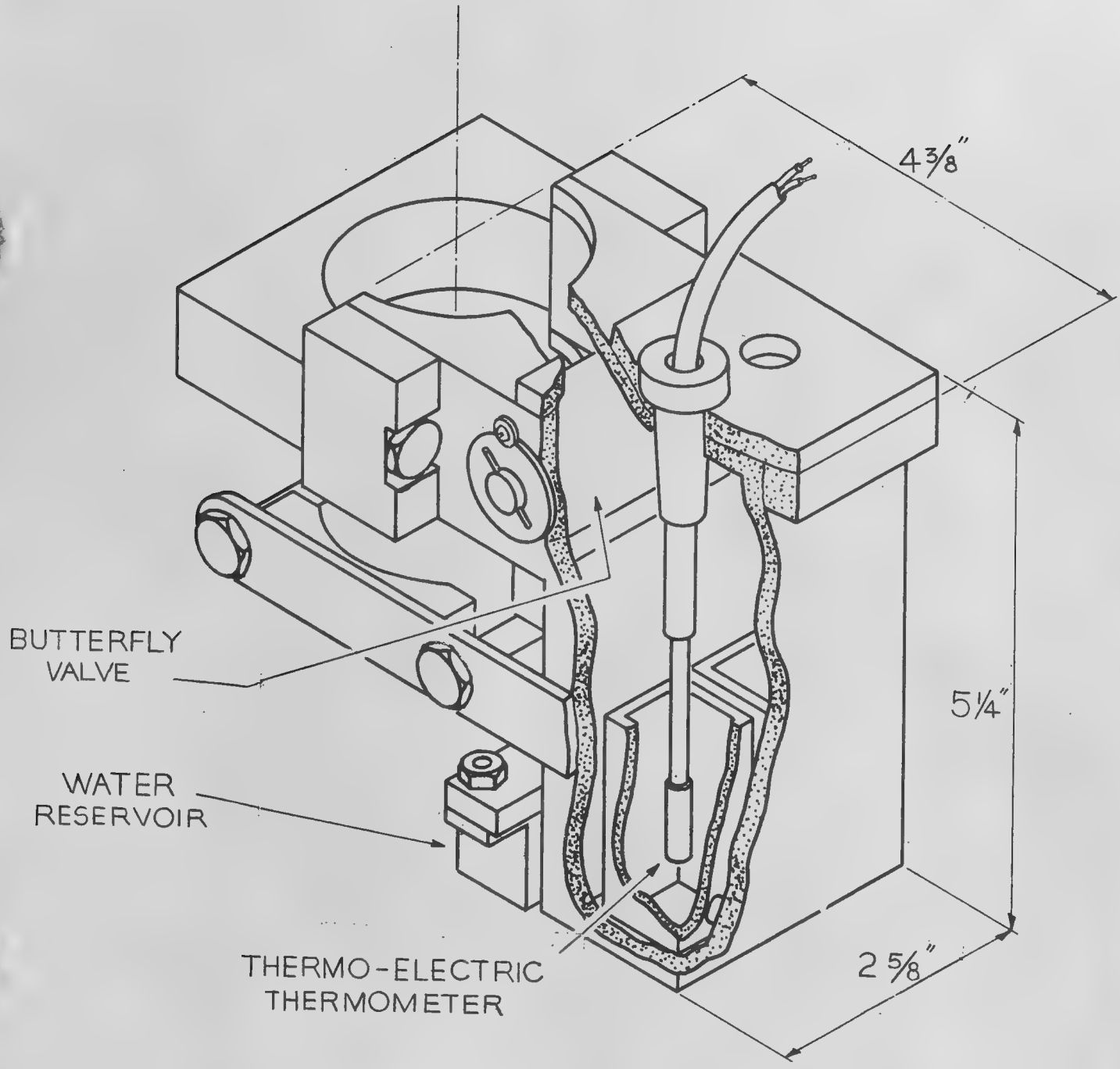

FIG. 2 DETAILS OF PSYCHROMETER HOUSING

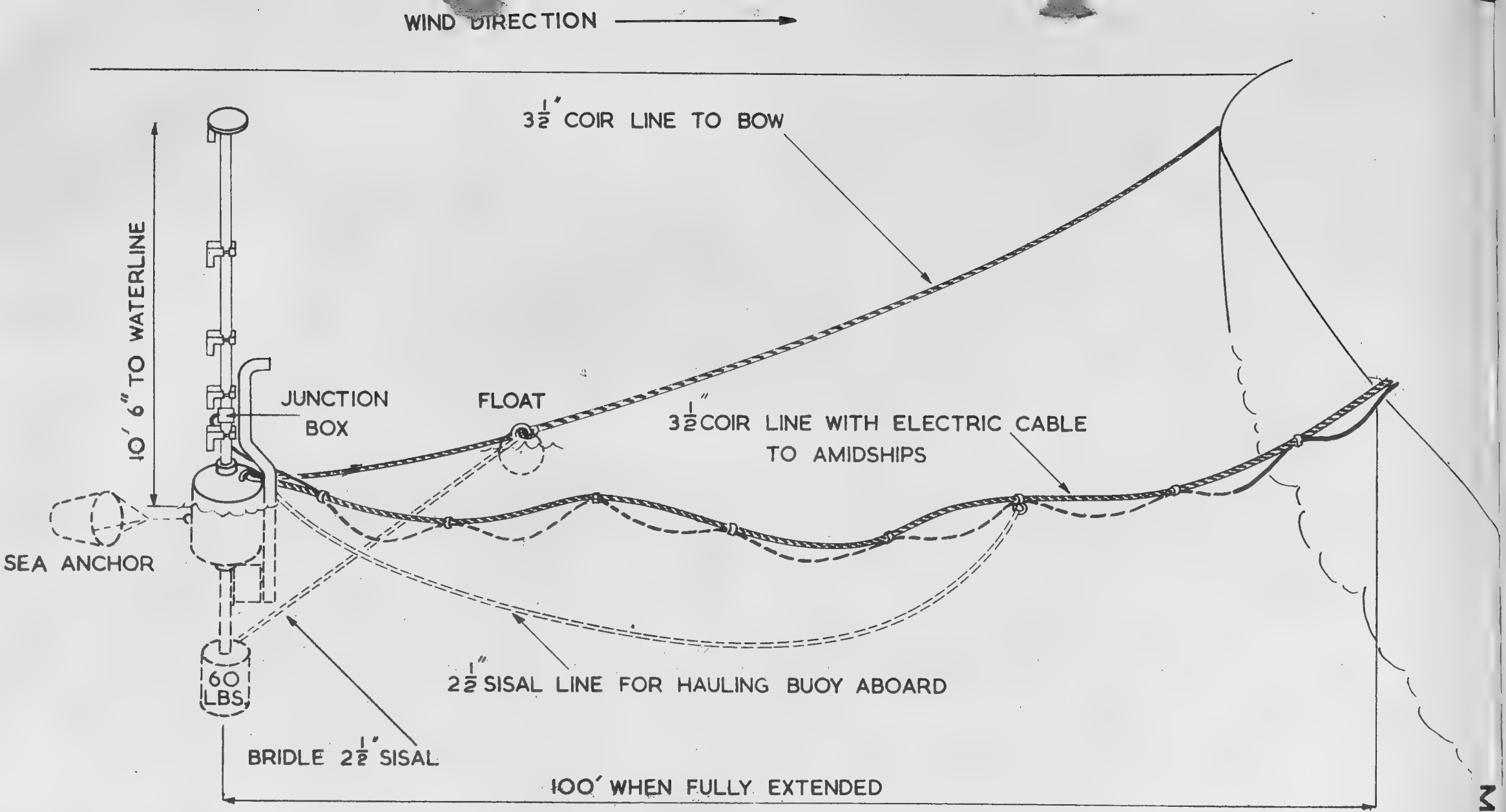

FIG. 3 GENERAL ARRANGEMENT OF "THERMOBUOY" IN OPERATION

FIG. 4 PROFILES MEASURED AT O.W. STATION I ON 6TH AND 9TH JULY 1956

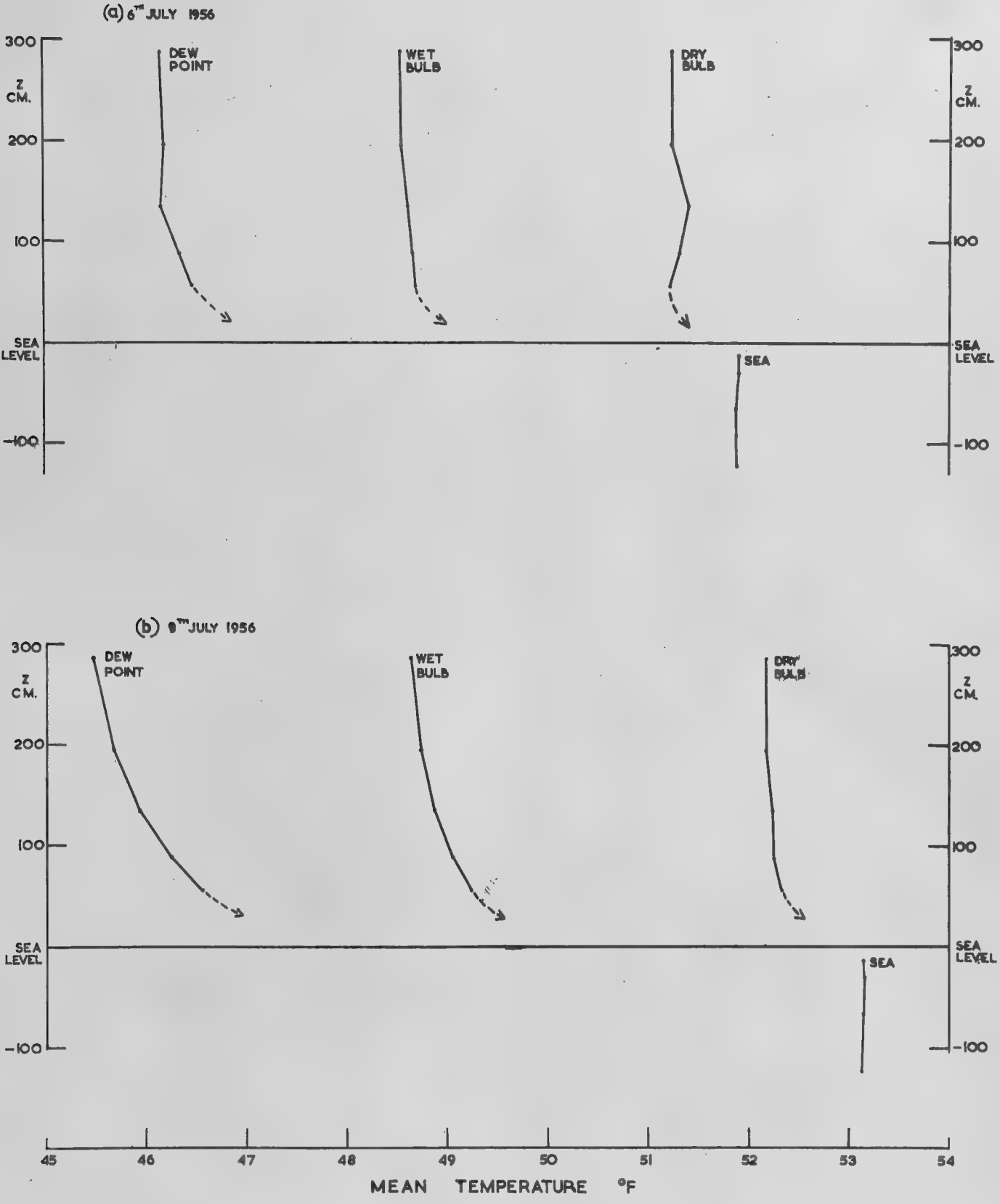

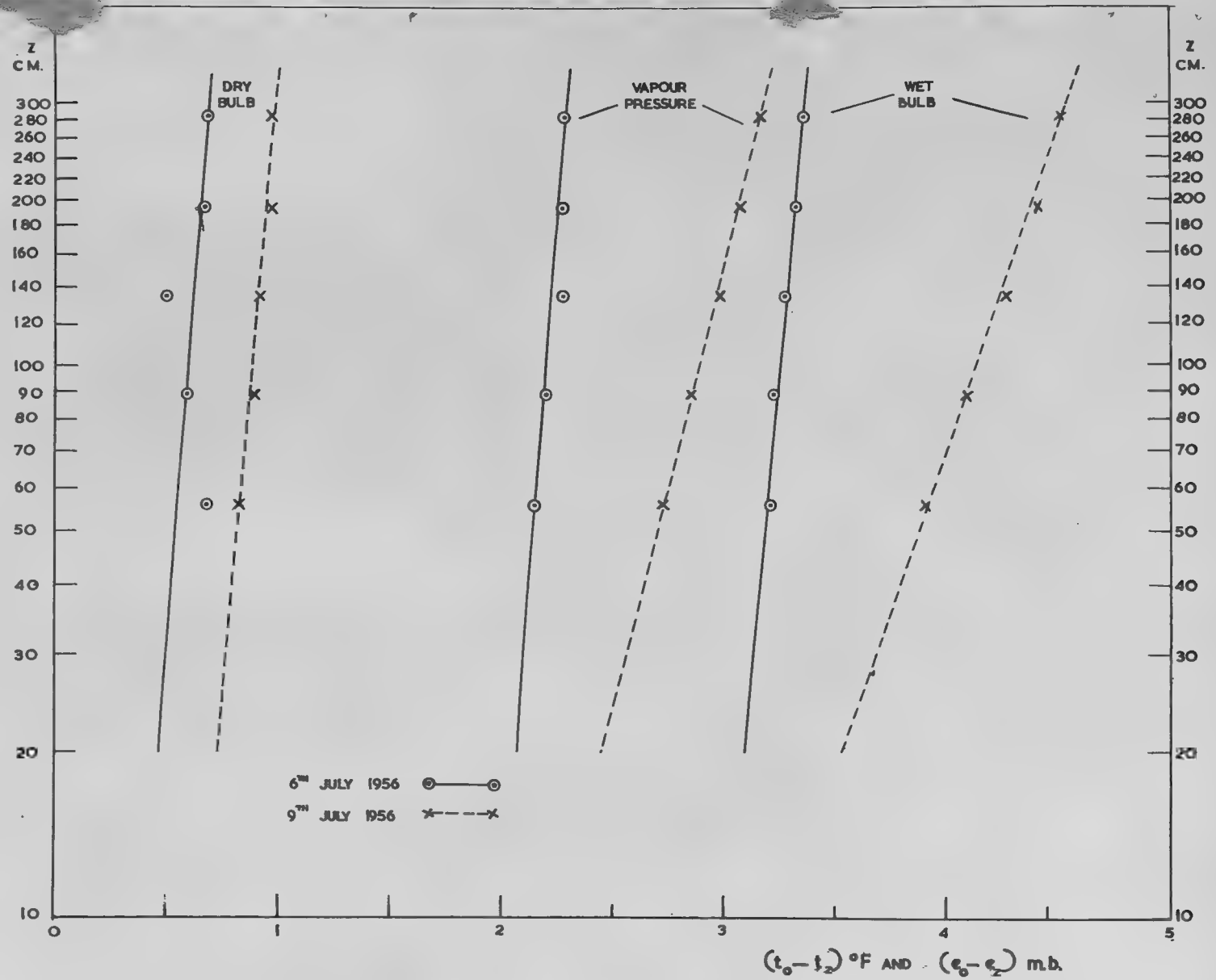

FIG. 5 PROFILES OF $(t_o - t_z)$ AND $(e_o - e_z)$ ON LOGARITHMIC HEIGHT SCALE

AD 216168

M.R.P. 1080
S.C.11/248
20th November, 1957

The relation between anomalies of surface air temperature and of 1000-500 mb thickness over the Atlantic sector of the Northern Hemisphere

by

C. A. S. Lowndes

(Meteorological Office)

AIR MINISTRY

METEOROLOGICAL RESEARCH COMMITTEE

At the time of issue this report has not been published. Any author desiring to quote this paper should refer to it as "A paper of the Meteorological Research Committee (London), M.R.P. No. 1080 by Mr. C.A.S. LOWNDES A copy is available in the Library of the Meteorological Office."

M.R.P.1080
S.C.II/248
20th November, 1957

AIR MINISTRY

METEOROLOGICAL RESEARCH COMMITTEE

The relation between anomalies of surface air temperature and of 1000-500 mb thickness over the Atlantic sector of the Northern Hemisphere.

by

C.A.S. Lowndes (Meteorological Office)

Summary

The preparation is described of two series of charts, covering the Atlantic sector of the Northern Hemisphere, one giving the monthly mean surface temperature anomaly and the other the monthly mean 1000-500-mb thickness anomaly for each month of the year 1956.

From a comparison of the charts month by month, it is evident that the main features of the thickness anomaly patterns are reflected in the surface temperature anomaly patterns. The importance of this relationship to a long-range forecasting method is discussed. In the Appendix, charts are produced to show how the temperature anomaly patterns are affected by the choice of the period used to obtain the normal from which the anomalies are measured.

1. Introduction

Since May 1955, the work of the Forecasting Research Division has included the construction of 5-day mean temperature anomaly charts covering the Atlantic half of the Northern Hemisphere. The preparation of these charts is described by Craddock and Lowndes (1956). Many of the temperature anomaly patterns are large, slow-moving and long lived, suggesting a relation with the character of the general circulation.

From August 1955, charts of monthly mean temperature anomaly were derived from the 5-day charts and were used to forecast the general character of the weather in South-east England during the following month by choosing an analogue for the anomaly chart from past years, an experiment which met with some success.

The present work was undertaken to clarify the relationship between the temperature anomaly patterns and the general circulation. The 1000-500 mb thickness was chosen for comparison with the mean surface temperature because it was regarded as characterising the upper air circulation.

2. The preparation of monthly mean thickness anomaly charts

The work of the Forecasting Research Division has included since 1949 the construction of monthly mean thickness charts for the whole Northern Hemisphere based on 0300Z synoptic charts. From these data, 5-year mean charts have been prepared for the Northern Hemisphere based on the period 1949-53 for the months June to December and on 1950-54 for January to May.

/The

The thickness anomaly charts were obtained by graphical subtraction from each monthly mean thickness chart of the appropriate 5-year mean chart. Isopleths are drawn at intervals of 20 metres, with the zero isopleths shown as pecked lines. Assuming a standard I.C.A.O. atmosphere, a thickness anomaly of 20 metres corresponds to an anomaly of 0.99°C in the mean temperature of the 1000-500 mb layer. The isopleths of thickness anomaly thus closely correspond to isopleths of mean upper air temperature anomaly drawn at 1°C intervals. On the same assumption, the maximum values at the centres of the patterns are shown to the nearest whole degree celsius. This facilitates comparison with the surface temperature anomaly charts.

3. The preparation of monthly mean surface temperature anomaly charts

The 5-day charts from which the monthly mean temperature anomaly charts were derived were based on long period means mostly obtained from data for the period 1921-1940. To make them comparable with the thickness anomaly charts it was necessary to refer the values to a 5-year mean based on the period 1949-53 (1950-54). The 5-year mean was evaluated for the network of stations shown on the key chart (see Appendix). The network was restricted to an area westward of 30°E because monthly temperature data for Eastern Europe were not available. The difference between the 20-year and the 5-year mean* was obtained for each station and was added to the value of the monthly mean temperature anomaly, thus referring it to the 5-year mean. Revised charts of monthly mean temperature anomaly were prepared in this way for each month of 1956. Isopleths are drawn at 1°C intervals with the zero isopleths shown as pecked lines. The maximum value at the centre of each area is shown to the nearest whole degree.

4. A comparison of the surface temperature and thickness anomaly patterns for each month of 1956

January (Fig. 1A, 1B)

The patterns in January show a marked similarity. The two main features, the warm area centred over Hudson Bay and the cold area near Iceland, are very similar in position, extent and intensity. An exception occurs over the Atlantic where the extension southwards of the cold thickness anomaly is not reflected to the same extent at the surface.

/February

Note. *Charts of the differences between the long period means for each month are reproduced as an appendix to this paper. Large differences occur over America and Greenland, in particular during the months January to March. A value of about 7°C occurs in January near the west coast of America. For all stations, one mean was based on a 5-year period; for the months June to December on 1949-1953 and for January to May on 1950-1954. The other mean was for the majority of stations based on the 20-year period, 1921-1940. For a few stations in Canada, it was based on a 30-year period, 1921-1950. These stations are indicated on the key chart by the figure 30. For a number of stations, particularly over Northern Canada and Greenland, it was based on various numbers of years within the period 1921-1940. The number of years used is shown on the key chart next to the name of the station.

Isopleths are drawn at 1°C intervals with the zero isopleths shown as pecked lines. The maximum value at the centre of each area is shown to the nearest whole degree.

February (Fig. 2A, 2B)

The patterns are very similar in February with the maximum values at the centre of each area comparable in magnitude. The main differences occur over Eastern America where the warm area extends further southward and the Newfoundland cold area further northward on the surface chart.

March (Fig. 3A, 3B)

The main feature of the March chart is a cold area which is centred over Eastern Canada and is of the same intensity on both charts. The Rockies warm area, though of similar intensity on both charts, extends further northward and eastward on the surface chart. The main difference is associated with the warm area near Iceland which extends further southward in the region of the British Isles on the surface chart. This difference seems to have been associated with surface warmth in persistent south-easterly advection with cooler air aloft.

April (Fig. 4A, 4B)

The patterns in April are much weaker and although the general distribution and intensities are similar, the extent and shape of the areas are much less comparable than in the earlier months. The main differences are associated with the warm area near Greenland which is centred further west and extends further west on the surface chart. The cold area over Eastern Greenland on the surface chart was associated with persistent northerly advection in the lower layers on the east side of a warm anticyclone over Greenland.

May (Fig. 5A, 5B)

The well-defined pattern over America in May is very similar on both charts, with the cold area extending somewhat further westward towards the Rockies on the thickness chart. The extension of the cold area to the east of Iceland on the thickness chart is not reflected at the surface where a warm area is situated over the Norwegian Sea. The patterns over Europe are very weak and show little similarity.

June (Fig. 6A, 6B)

The thickness chart for June shows an extensive cold area stretching from Greenland across the Atlantic to Western Europe and a warm area over central America. These features are generally similar on the surface chart but differ considerably in detail. The extension of the warm area northward across Canada on the thickness chart is not reflected in the surface chart where a weak cold area is centred over Hudson Bay.

A further difference occurs to the east of Greenland where the thickness chart shows an extension of the cold area but the surface chart a weak warm area.

July (Fig. 7A, 7B)

In July, the well-defined patterns over America, a weak cold area near Iceland and a warm area over Scandinavia are similar on both charts. The weak warm area to the North-west of the Azores does not appear on the thickness chart. The most remarkable difference occurs over South-west Europe where a cold area centred over Northern Italy on the surface chart does not appear on the thickness chart.

August (Fig. 8A, 8B)

The patterns in August although mainly weak, show a marked similarity of position and intensity on both charts.

/September

September (Fig. 9A, 9B)

The patterns over America in September are similar on both charts and the mainly rather weak patterns elsewhere are similarly positioned. The main difference occurs over Greenland where the cold area on the thickness chart is more intense and centred further north than on the surface chart.

October (Fig. 10A, 10B)

The main feature of the October charts is a warm area over America centred to the south of Hudson Bay on the thickness chart but further south-west on the surface chart. The extension of the warm area across the Atlantic to Spain and the cold area over Western Europe are similar on both charts. The main differences are associated with the area west of Hudson Bay where a cold area on the thickness chart does not appear on the surface chart, and to the west of Greenland where the cold area extends much further south on the surface chart.

November (Fig. 11A, 11B)

The patterns in November are very similar with the exception of the area south of Hudson Bay where a weak warm area at the surface does not appear on the thickness chart.

December (Fig. 12A, 12B)

The large patterns in December are very similar in position and extent on both charts. The charts differ from those of all the other months in that the maximum values at the centre of all the areas are much larger on the surface chart.

5. Discussion

The patterns, especially the more intense ones, are in the main similar on both charts throughout the year. Assuming a standard I.C.A.O. atmosphere, the maximum values of temperature anomaly are of the same order of magnitude on both charts.

Thickness patterns with a maximum anomaly of 2°C or more are, with three exceptions, reflected in a similar manner on the surface chart. In most cases a similar geographical area is covered but there is often some difference in the position of the centre, especially with the less intense patterns.

The exceptions occur (1) in April over Greenland, (2) in June to the north-west of Hudson Bay and (3) in September over Northern Greenland, suggesting that in these regions, and probably in other localities with peculiar surface characteristics, the surface pattern may not, under certain conditions, reflect the thickness pattern.

Surface patterns with a maximum anomaly of 3°C or more are, with two exceptions, reflections of similar patterns on the thickness chart. The exceptions occur (1) in April near Greenland and (2) in July over the Mediterranean area.

The close association between the two sets of patterns suggests that it is in general justifiable to use the more intense surface patterns as indicators of the character of the horizontal temperature field in the troposphere.

As mentioned already, Craddock and Lowndes (1956) have shown that the field of temperature anomaly at the earth's surface may show very persistent features lasting up to a month or two. The present work makes it seem very probable that the same persistent features would be found by examination of any other measure of the horizontal temperature field in the troposphere.

/If

If these features are indicators which can be used as a basis for successful forecasting it does not matter much whether they are identified by means of the surface temperature patterns, which are available in detail over a long period of years, or by means of patterns of the 1000-500 mb thickness which are available for only about a decade. However, the clear relation between the surface temperature anomalies and the upper air circulation may assist us in interpreting their cause.

Reference

Craddock, J.M. and Lowndes, C.A.S. 1956. A synoptic study of anomalies of surface air temperature over the Atlantic half of the Northern Hemisphere.

G.27940/PO/1/58/65

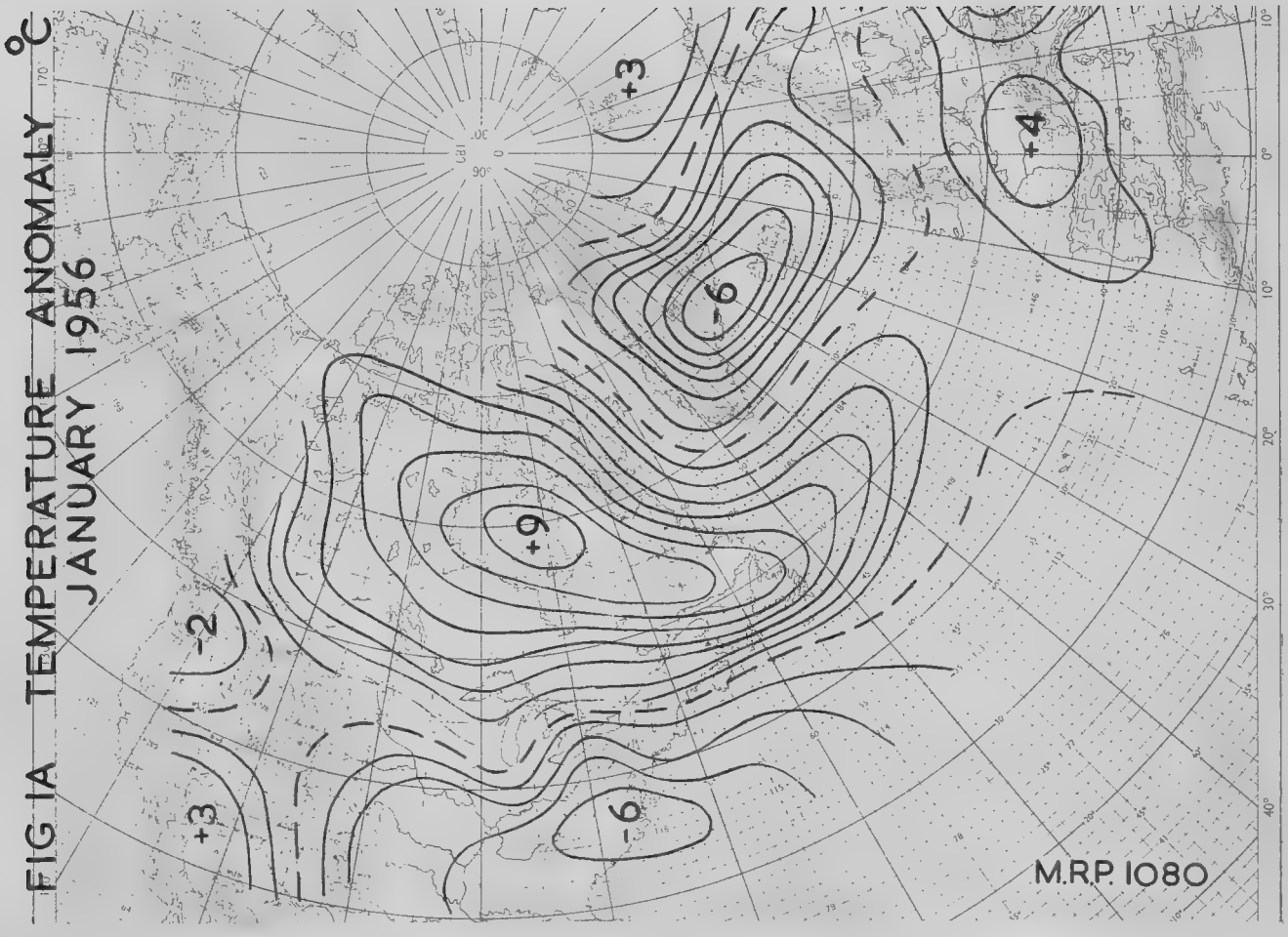

FIG IA TEMPERATURE ANOMALY °C
JANUARY 1956

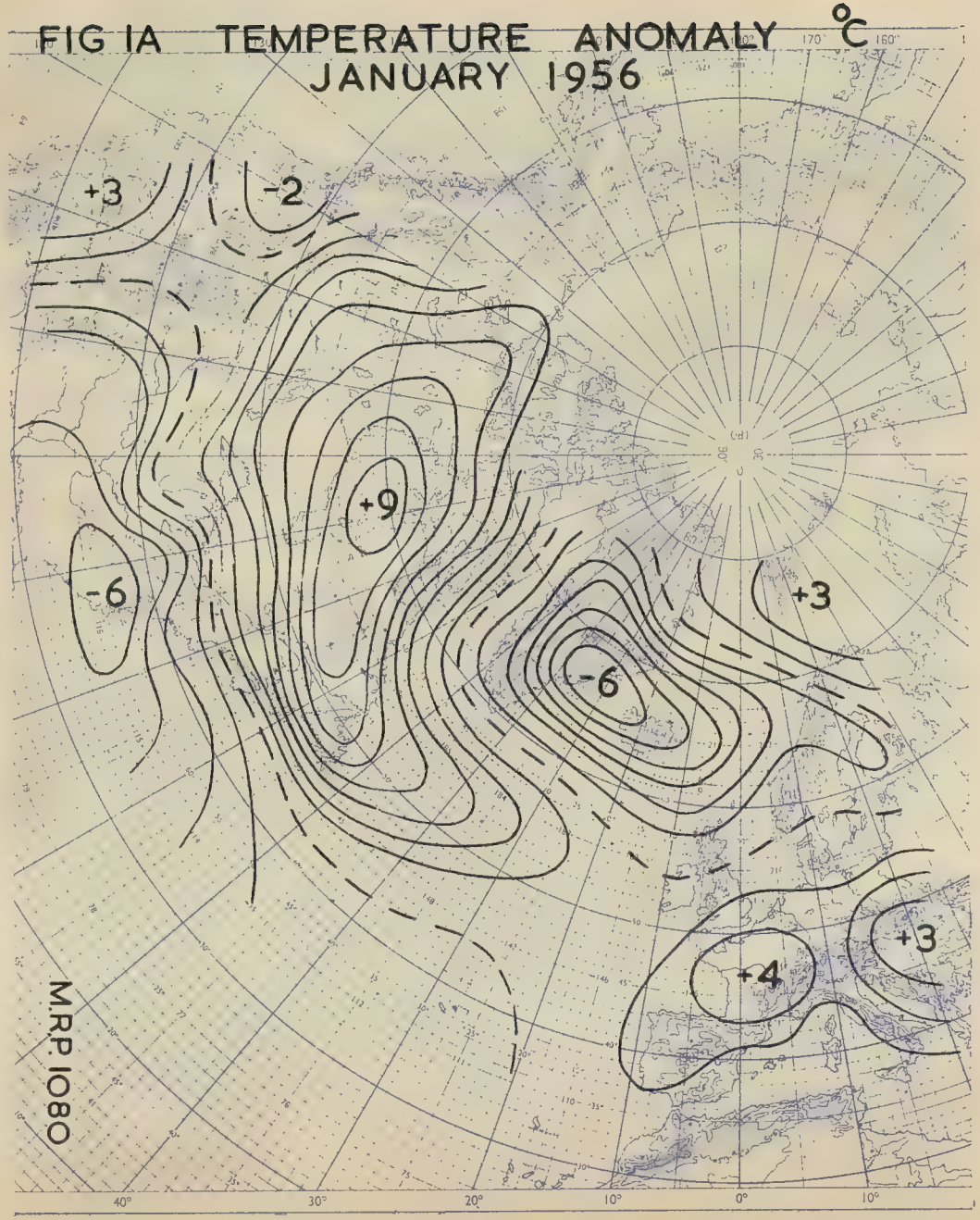

FIG 1B THICKNESS ANOMALY M. °C
JANUARY 1956

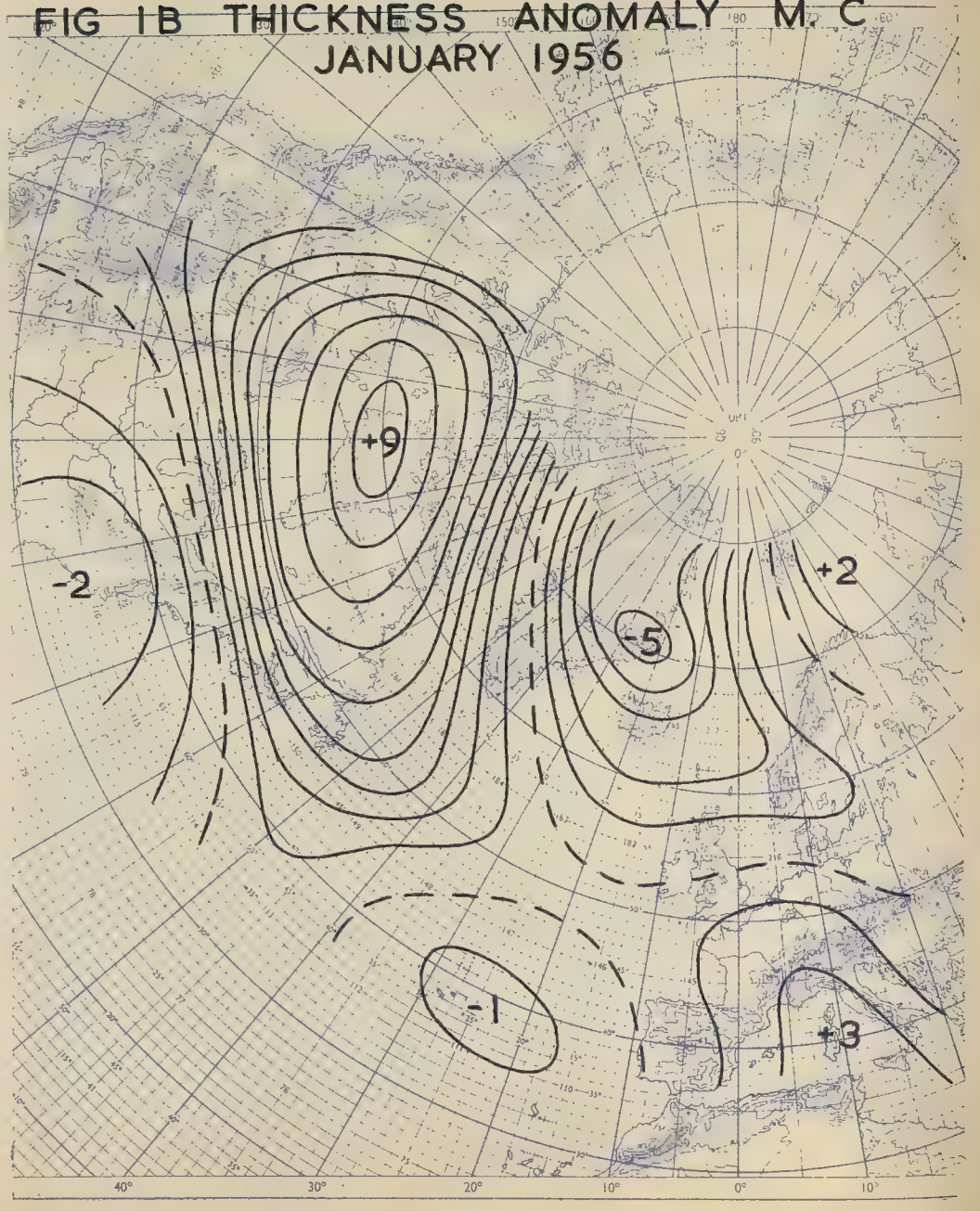

FIG 2A TEMPERATURE ANOMALY °C
FEBRUARY 1956

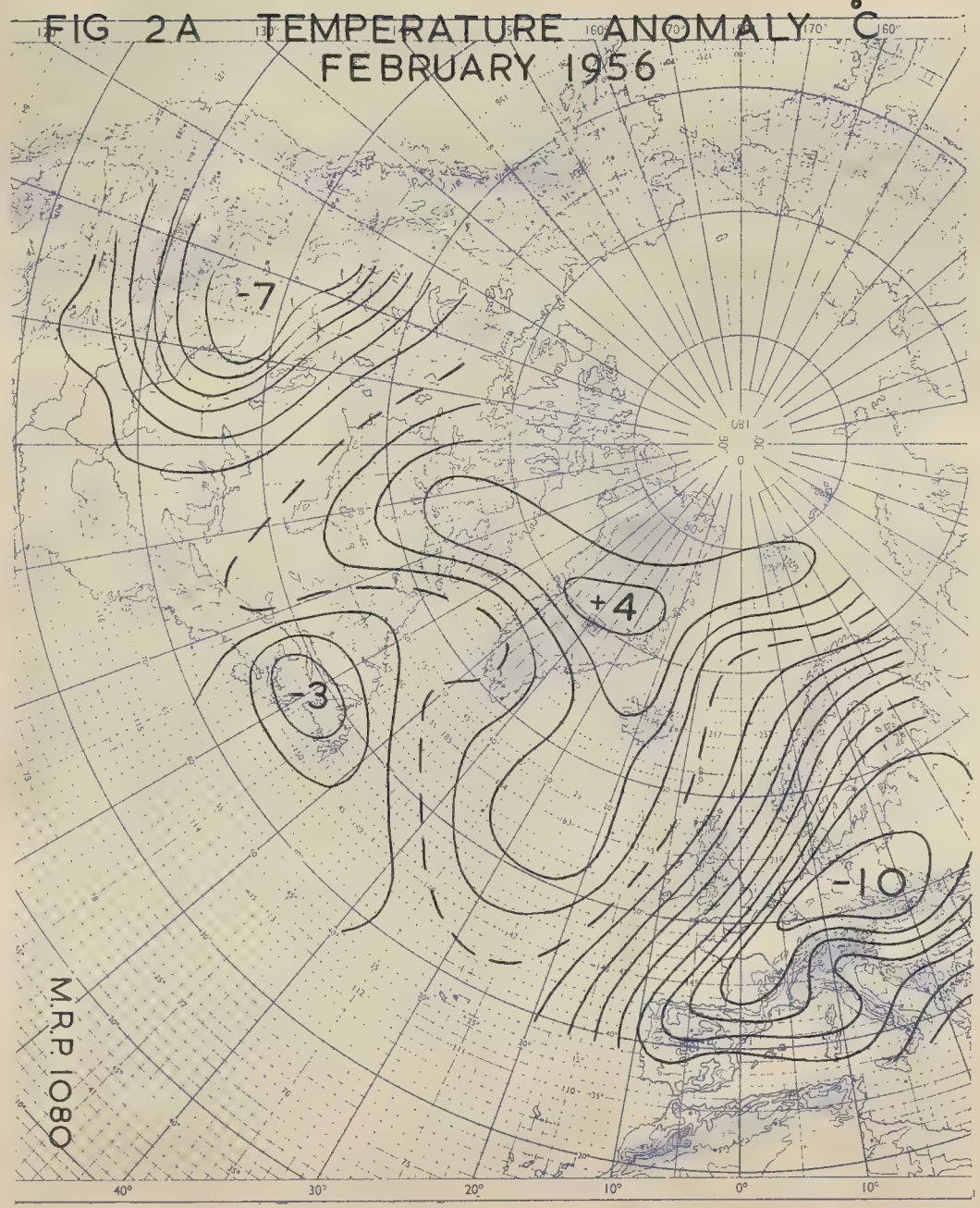

FIG 2B THICKNESS ANOMALY M.°C
FEBRUARY 1956

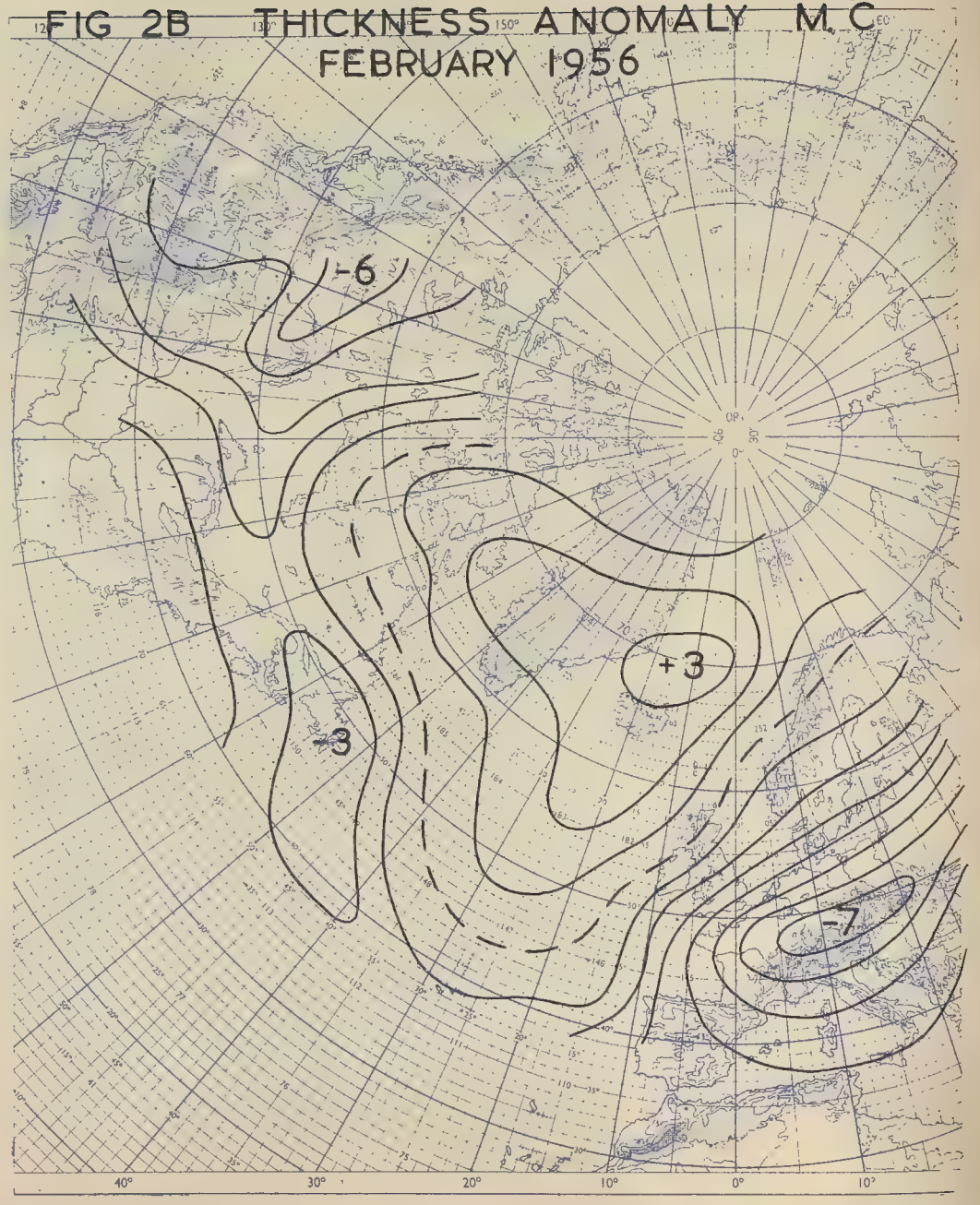

FIG 3A TEMPERATURE ANOMALY °C
MARCH 1956

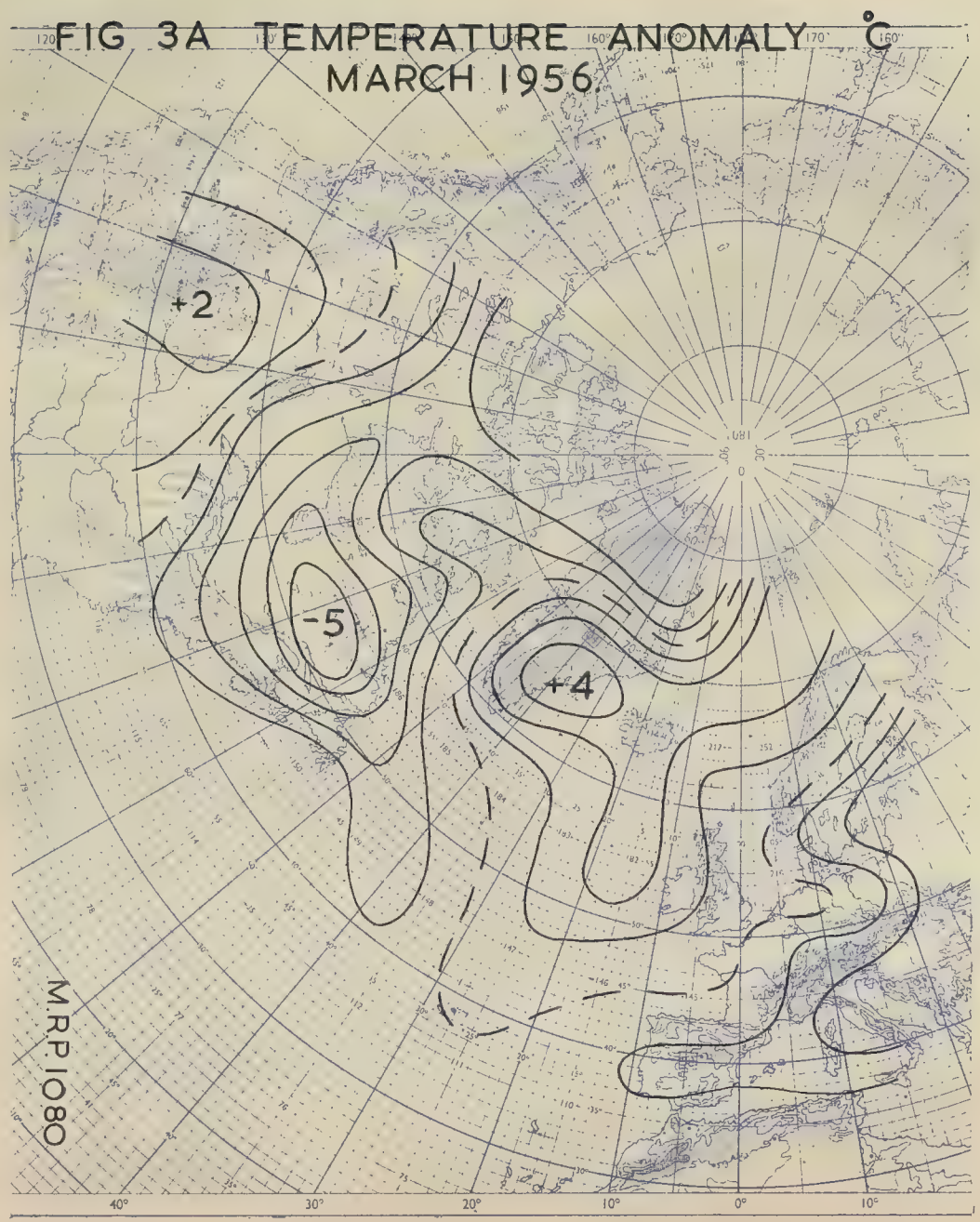

FIG 3B THICKNESS ANOMALY M. °C
MARCH 1956

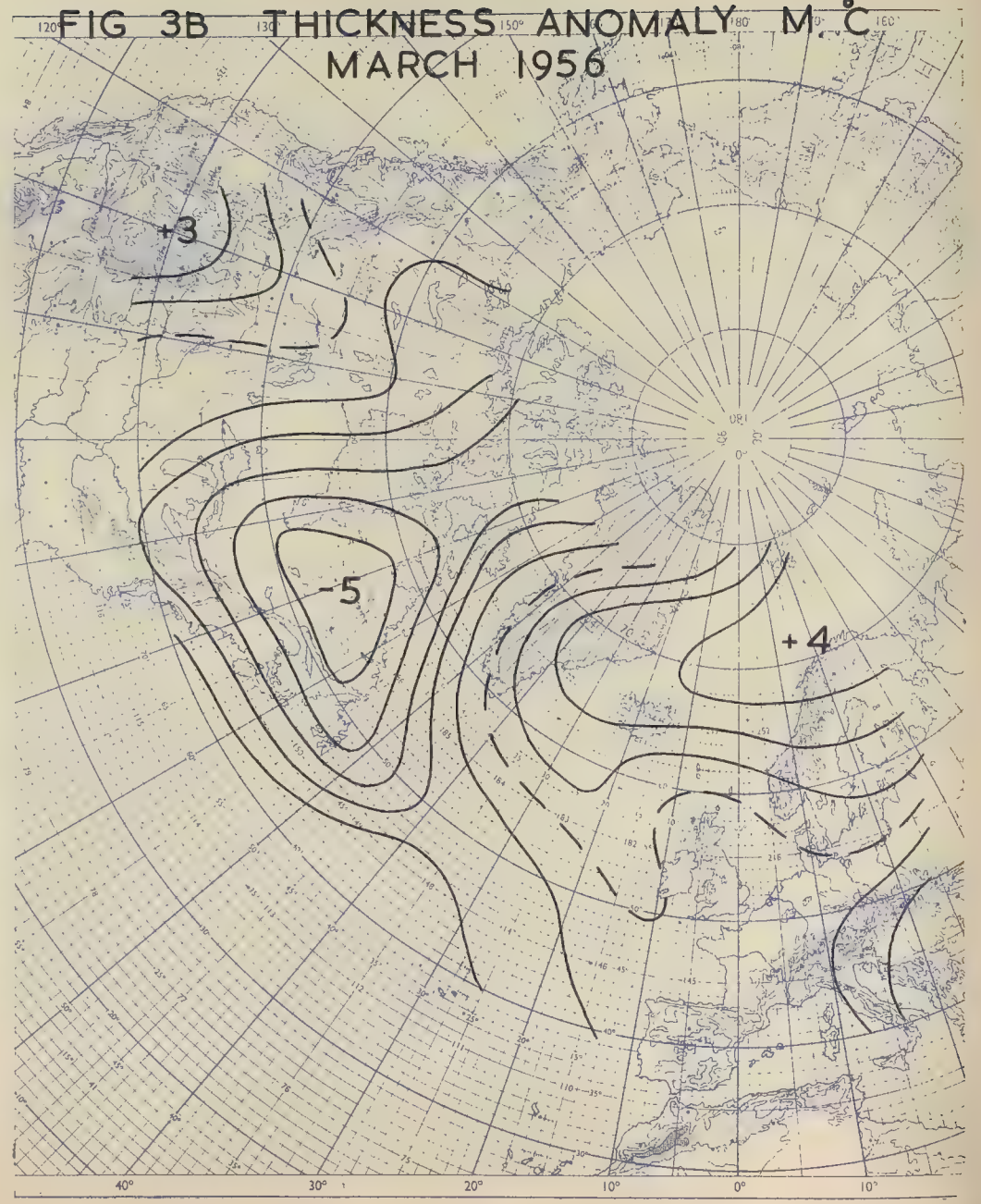

FIG 4A TEMPERATURE ANOMALY °C
APRIL 1956

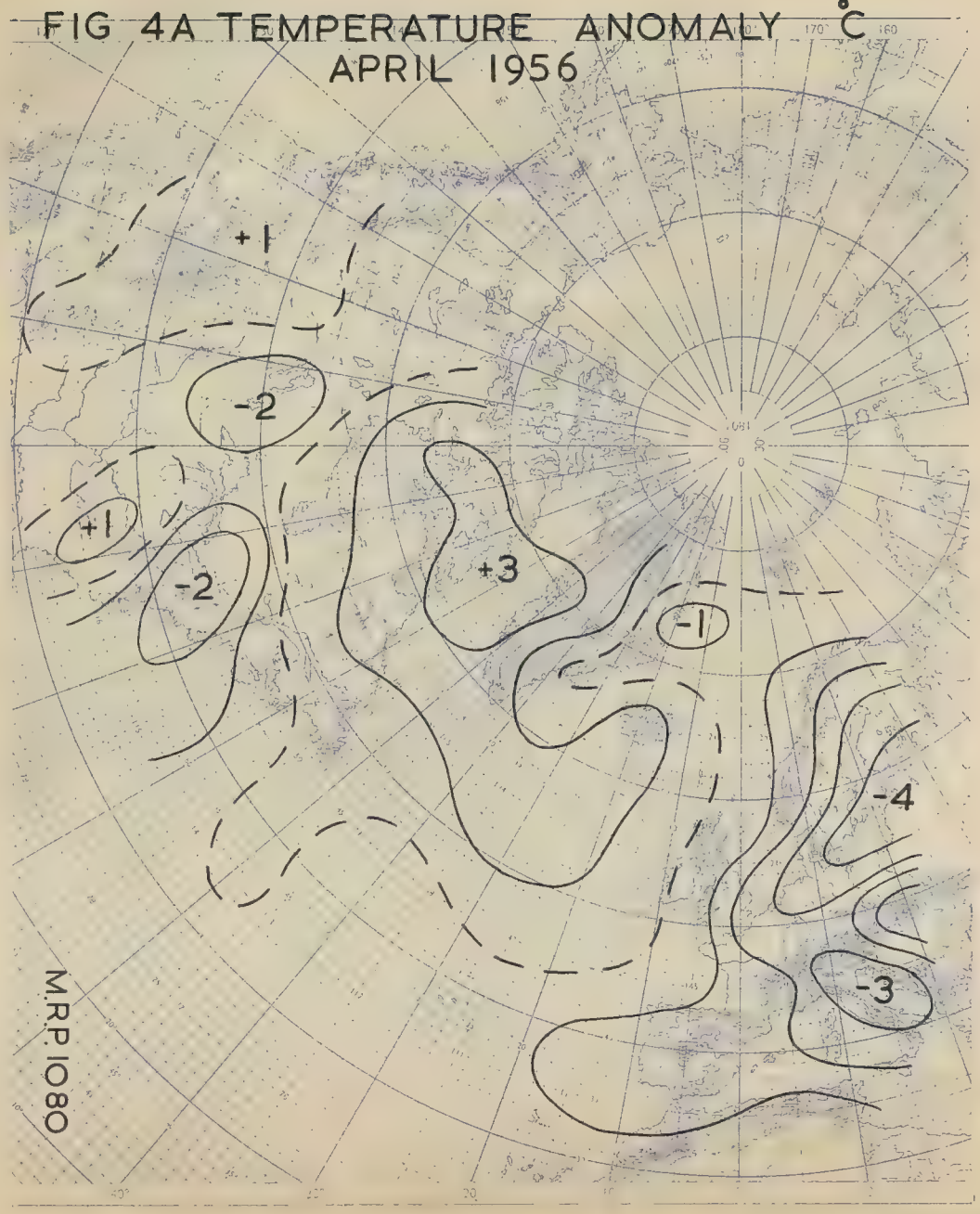

FIG 4B THICKNESS ANOMALY M. °C
APRIL 1956

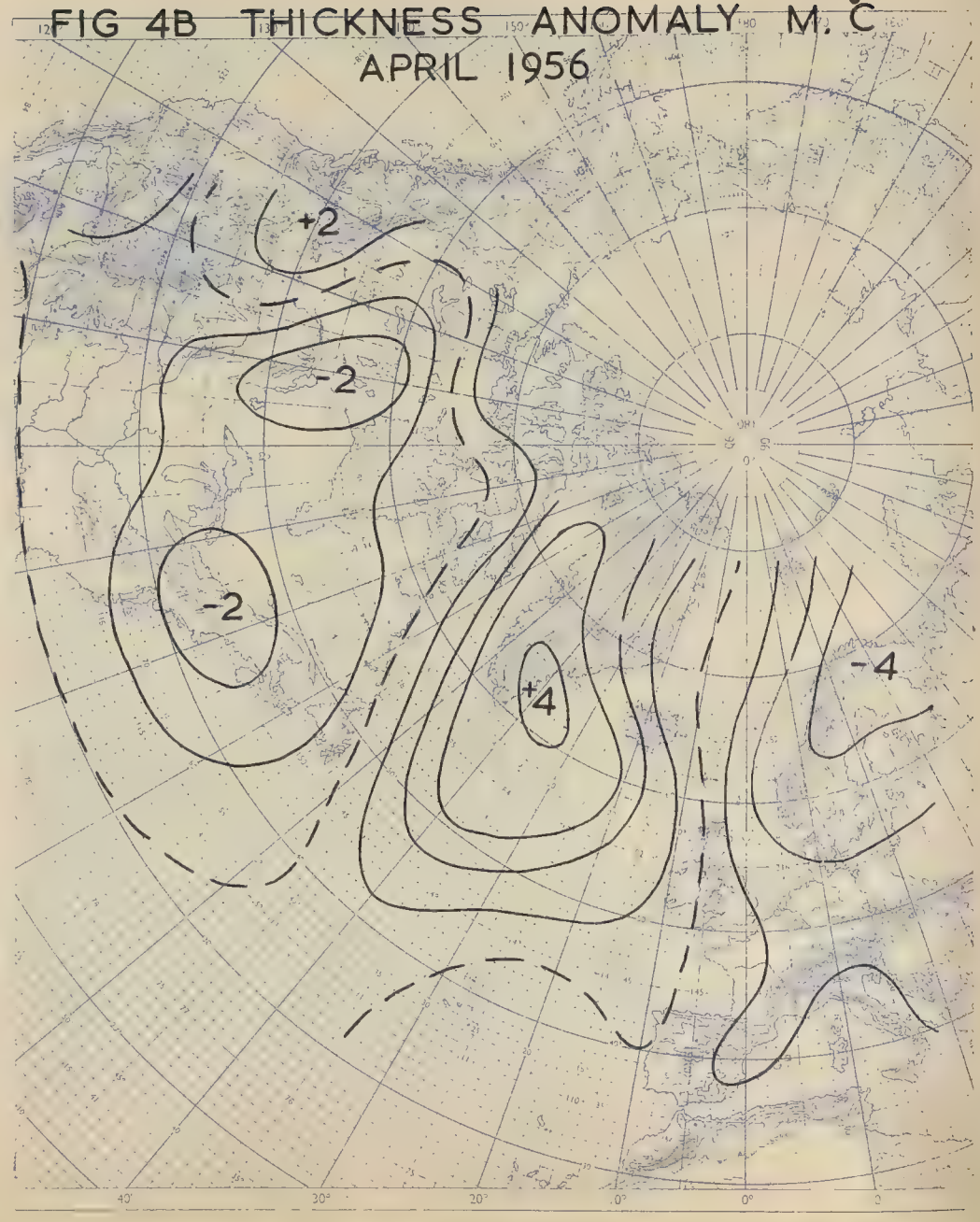

FIG 5A TEMPERATURE ANOMALY °C
MAY 1956

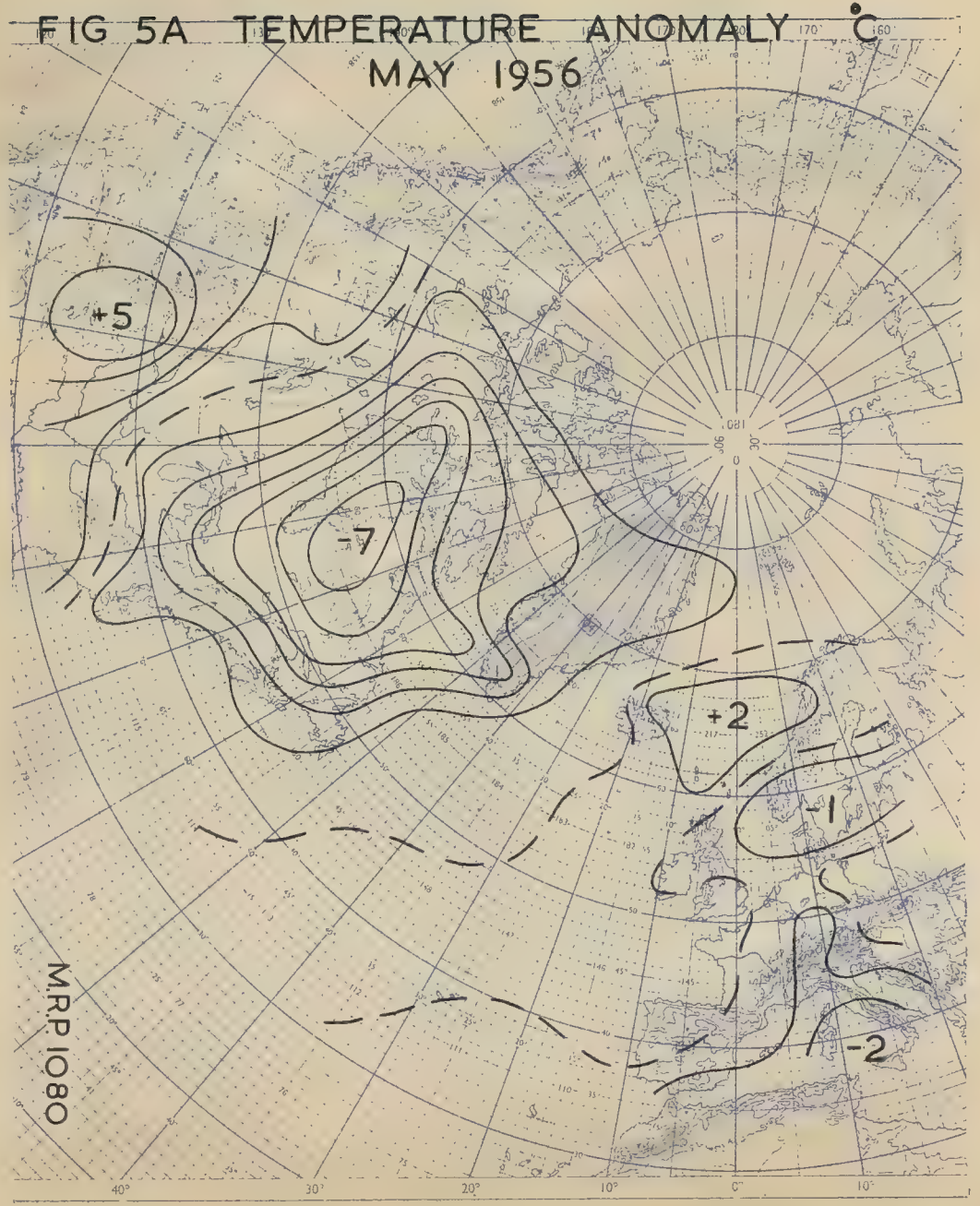

FIG 5B THICKNESS ANOMALY M. °C
MAY 1956

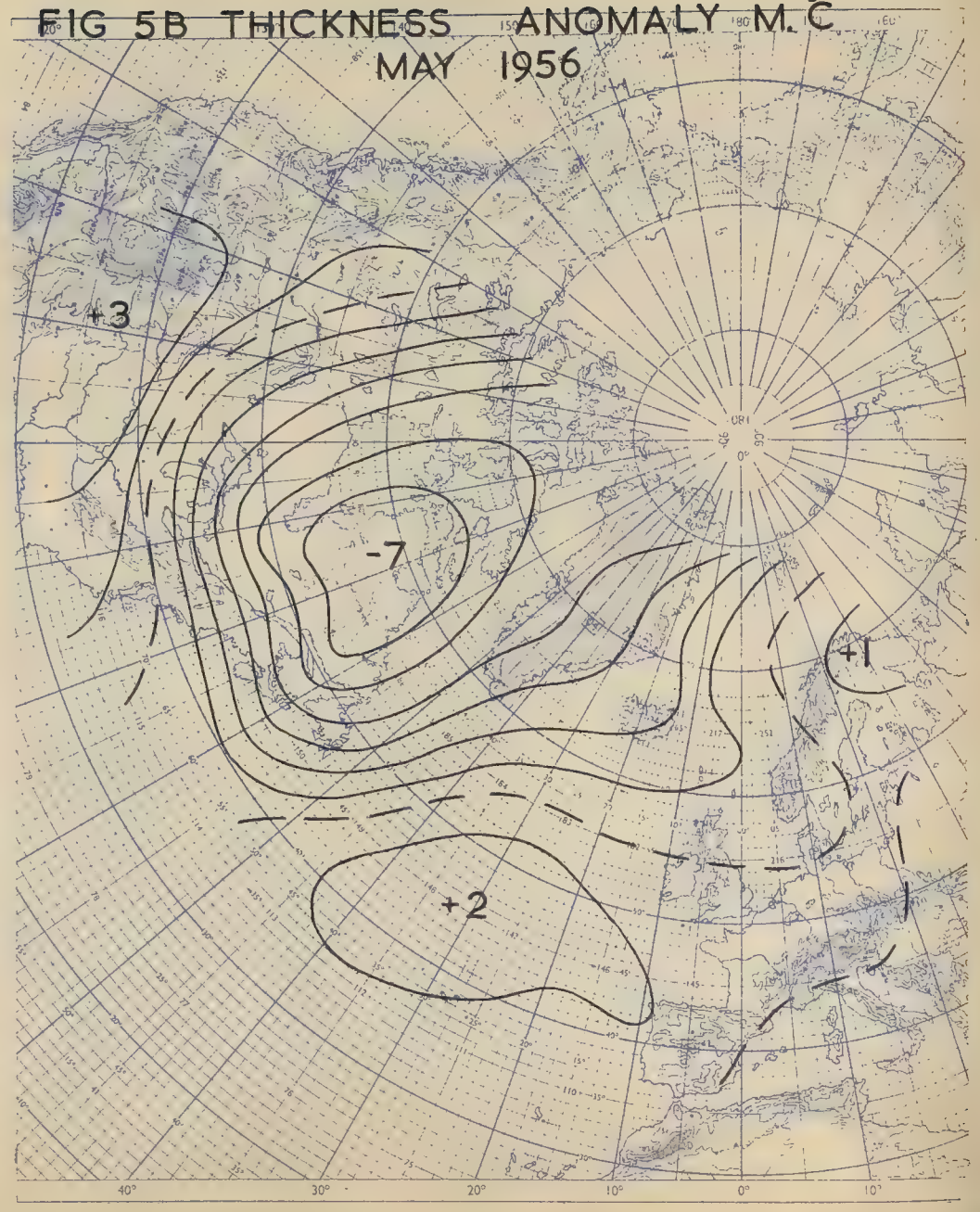

FIG 6A TEMPERATURE ANOMALY °C
JUNE 1956

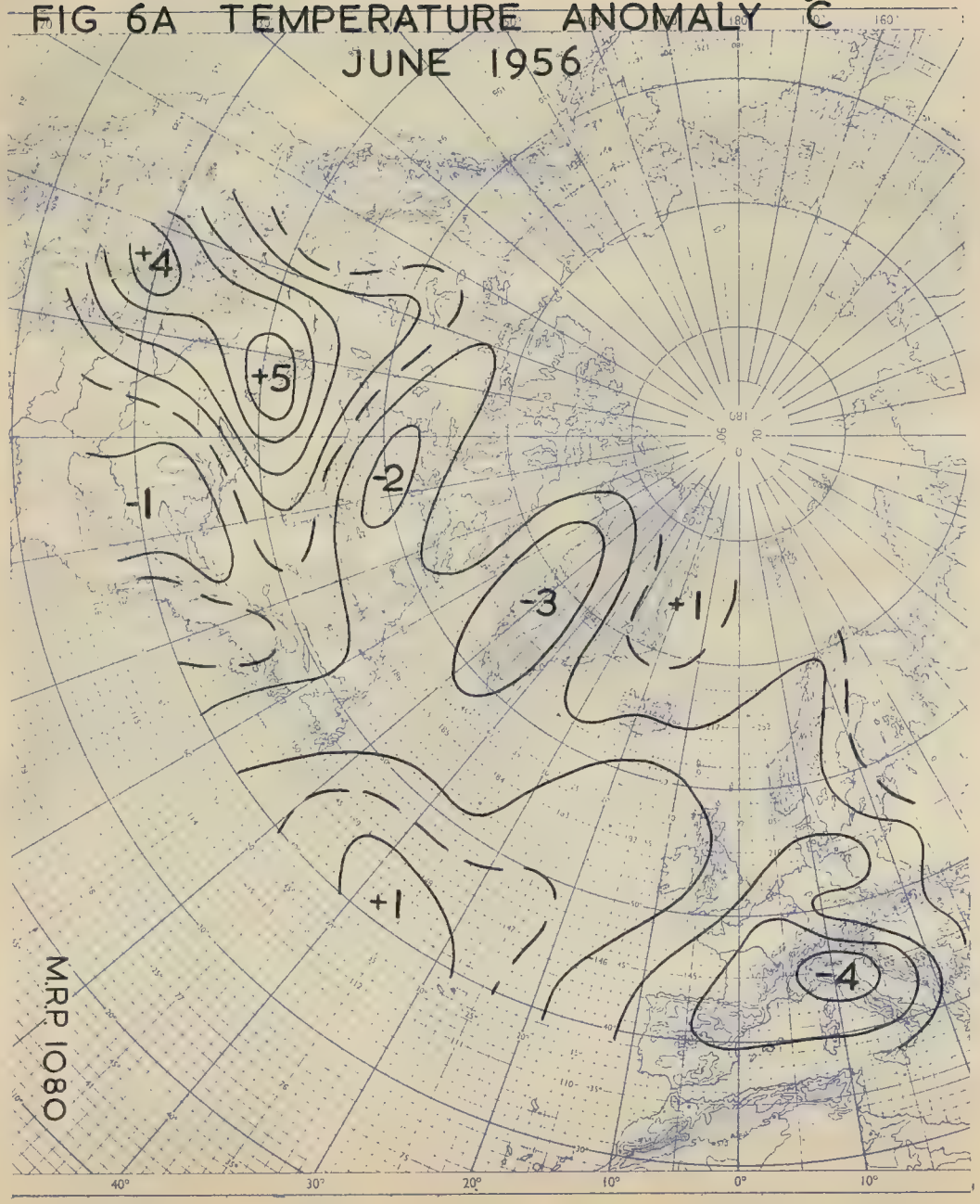

FIG 6B THICKNESS ANOMALY M °C
JUNE 1956

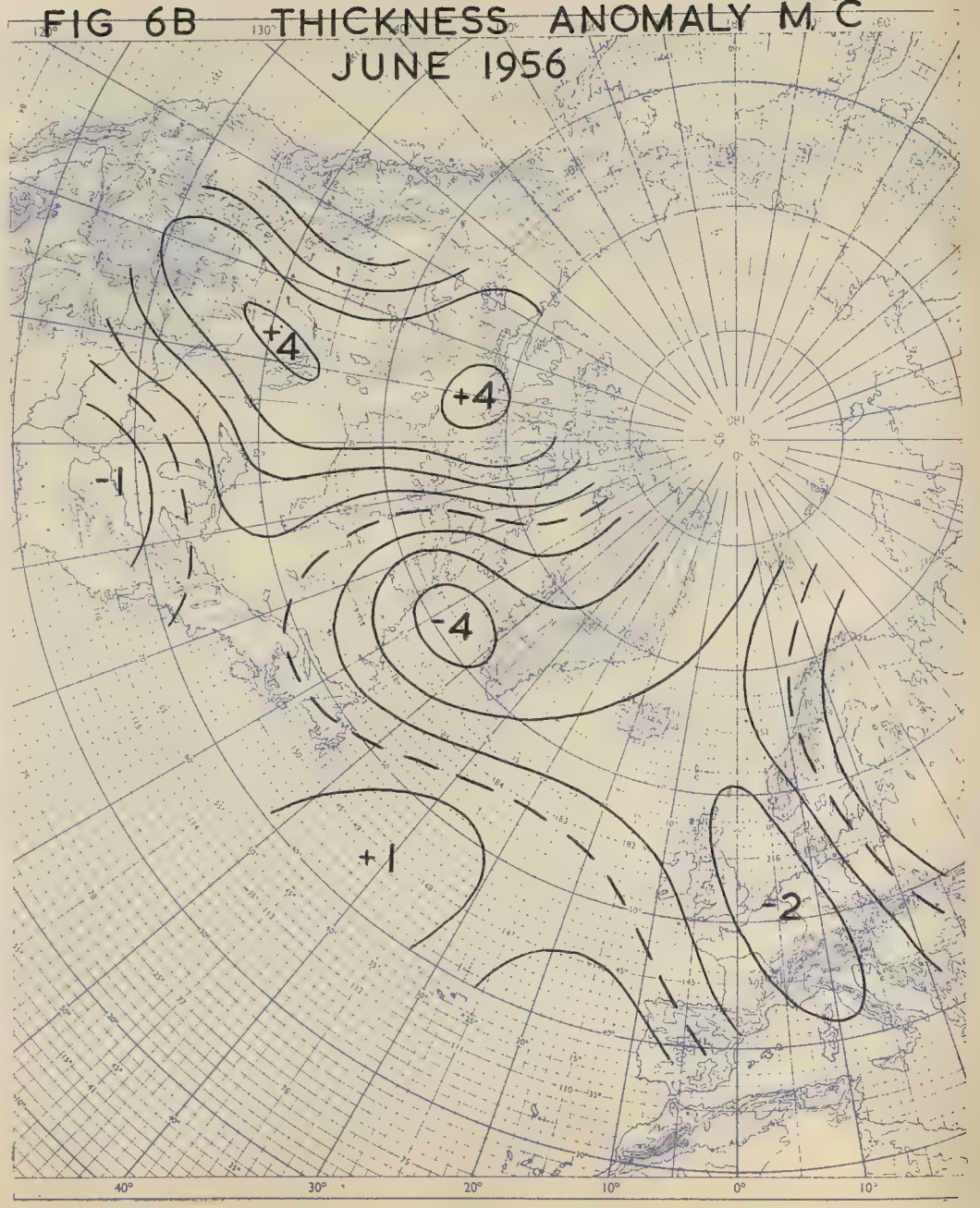

FIG 7A TEMPERATURE ANOMALY °C
JULY 1956

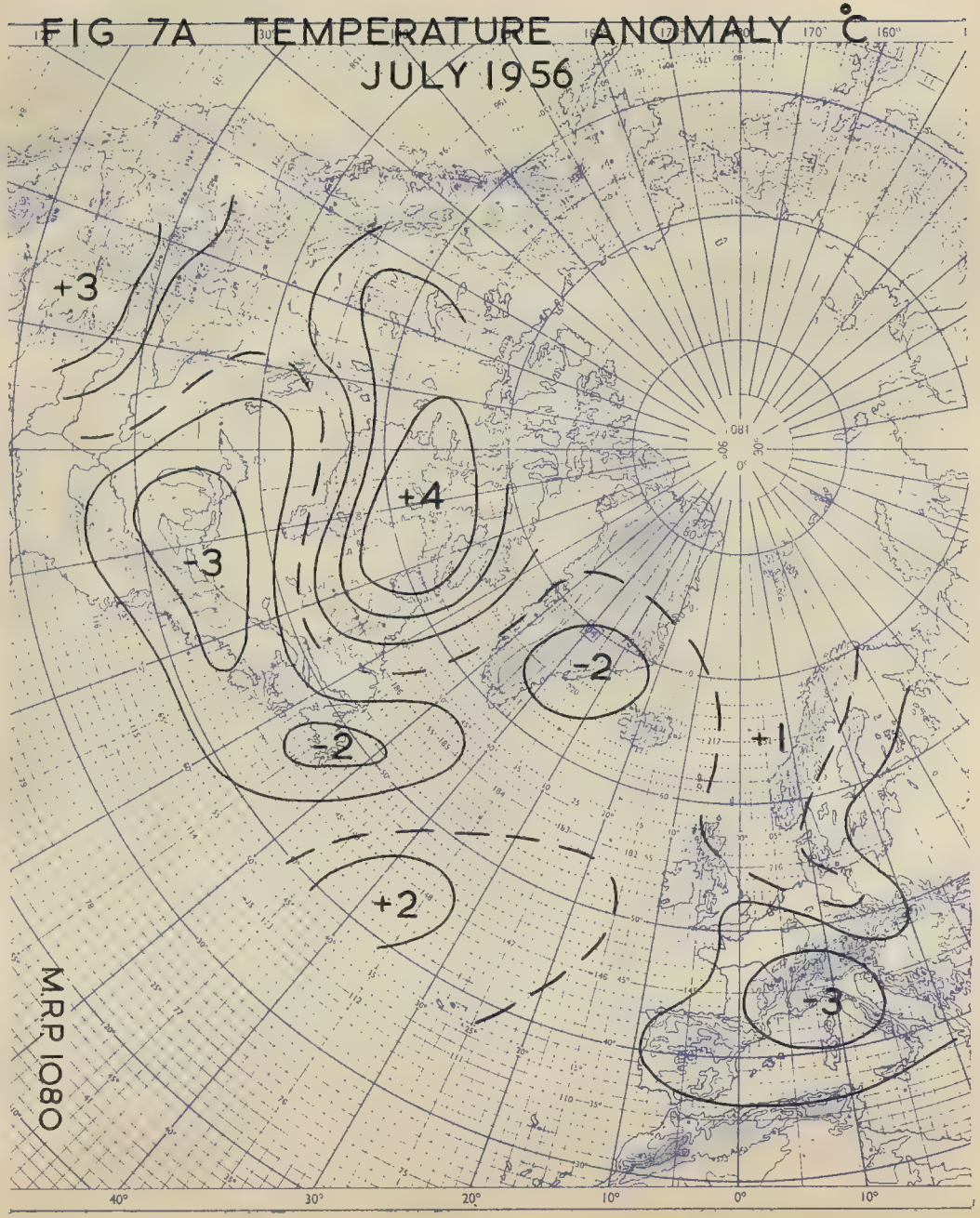

FIG 7B THICKNESS ANOMALY M.°C
JULY 1956

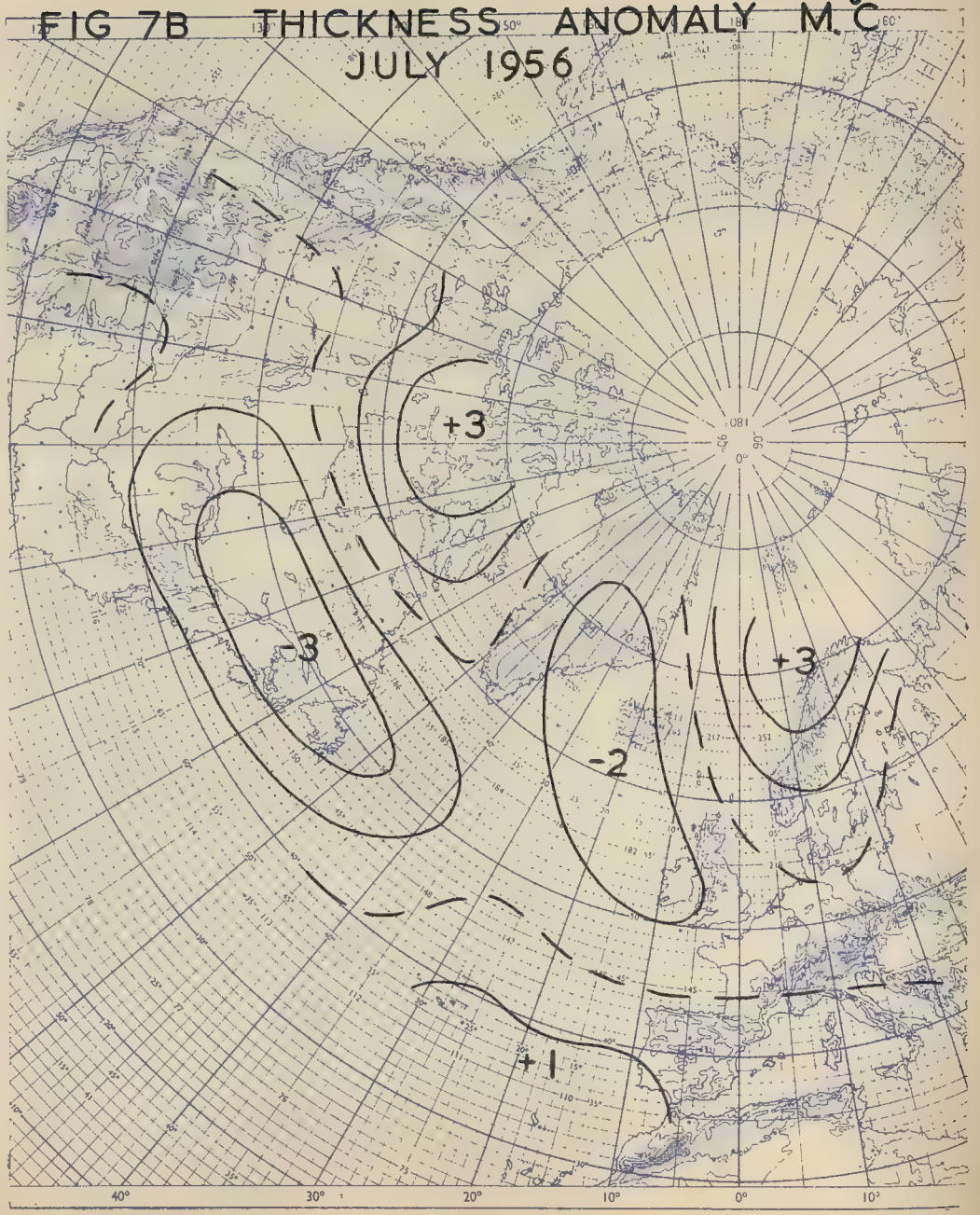

FIG 8A TEMPERATURE ANOMALY °C
AUGUST 1956

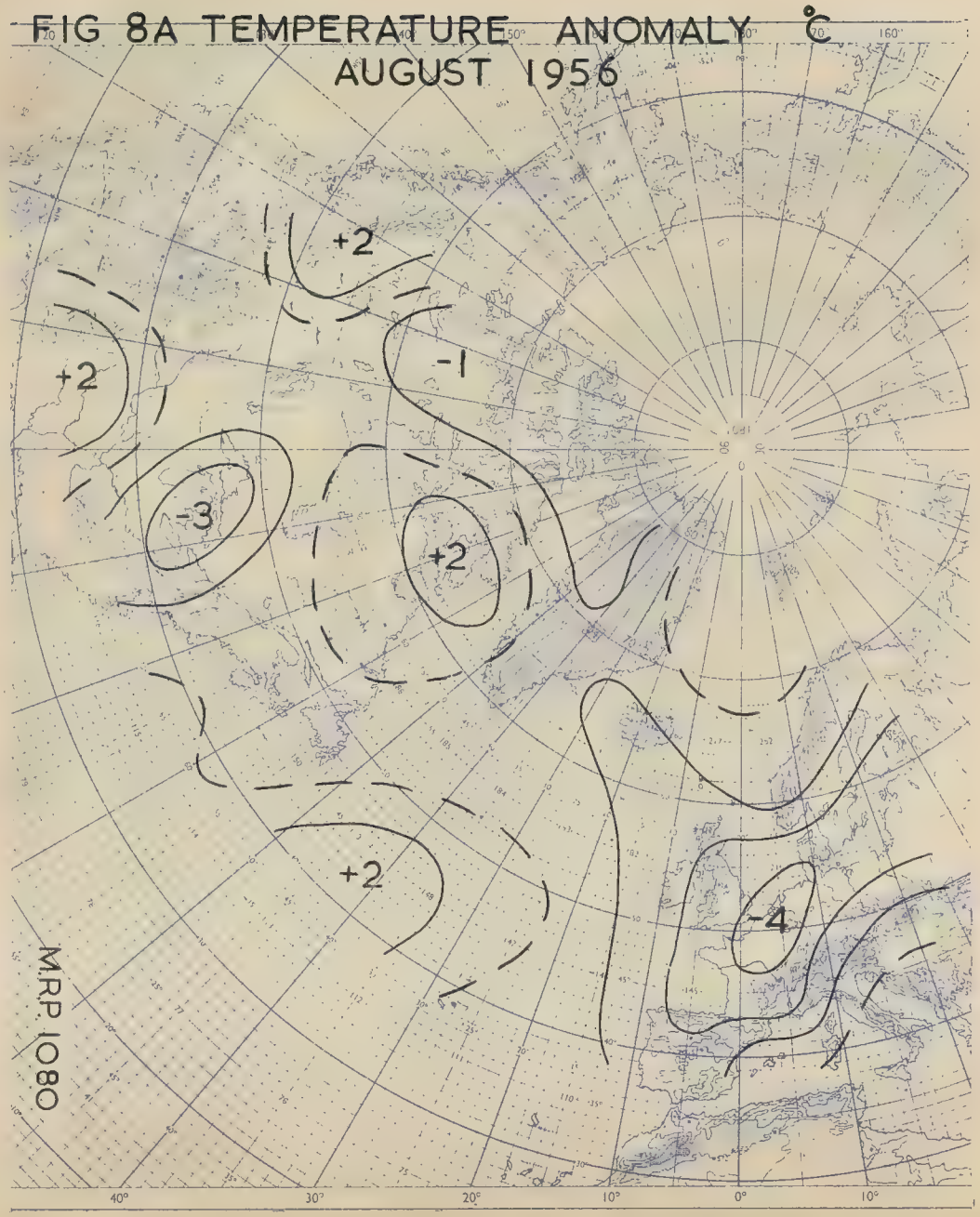

MRP 1080

FIG 8B THICKNESS ANOMALY M. °C
AUGUST 1956

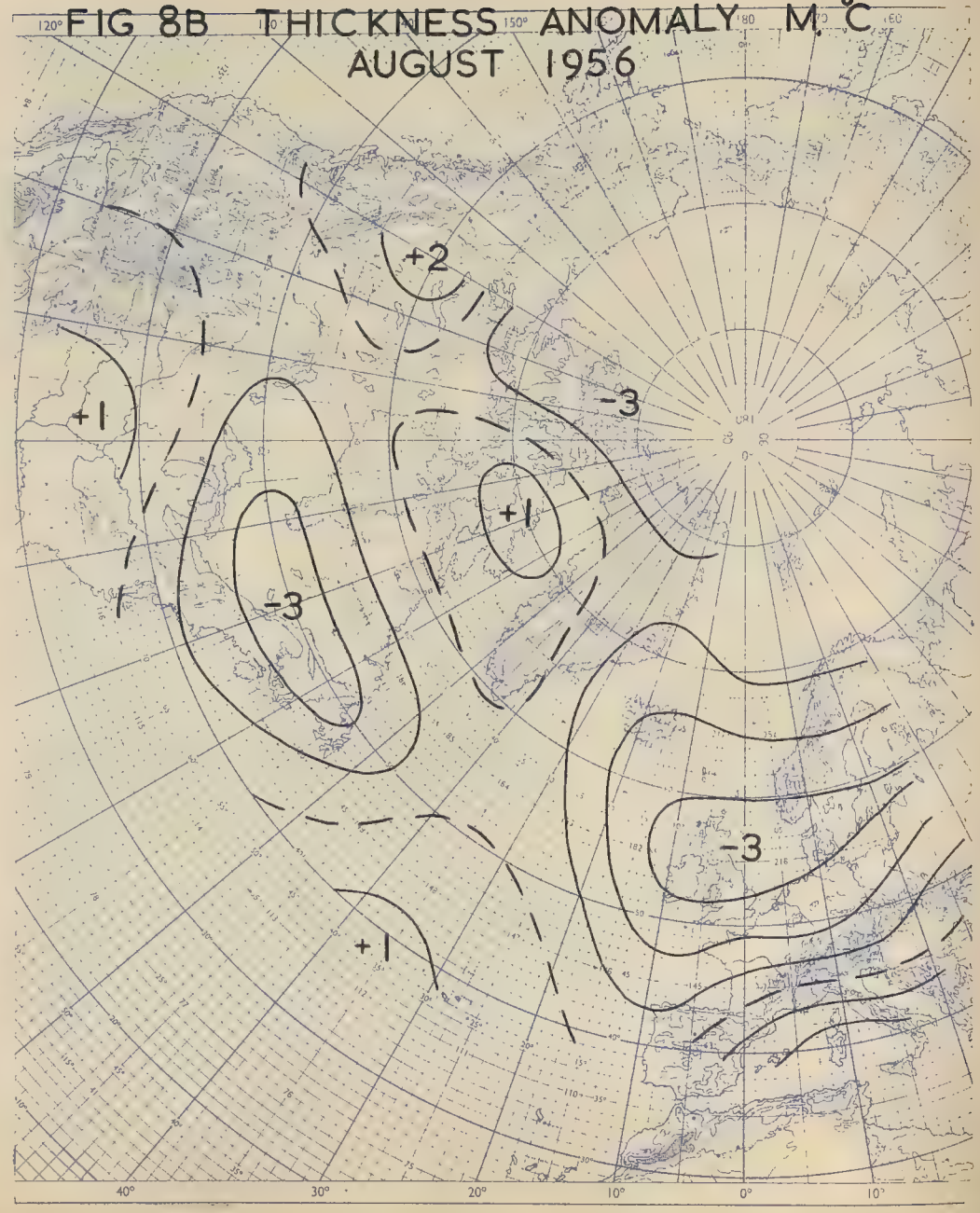

FIG 9A TEMPERATURE ANOMALY °C
SEPTEMBER 1956

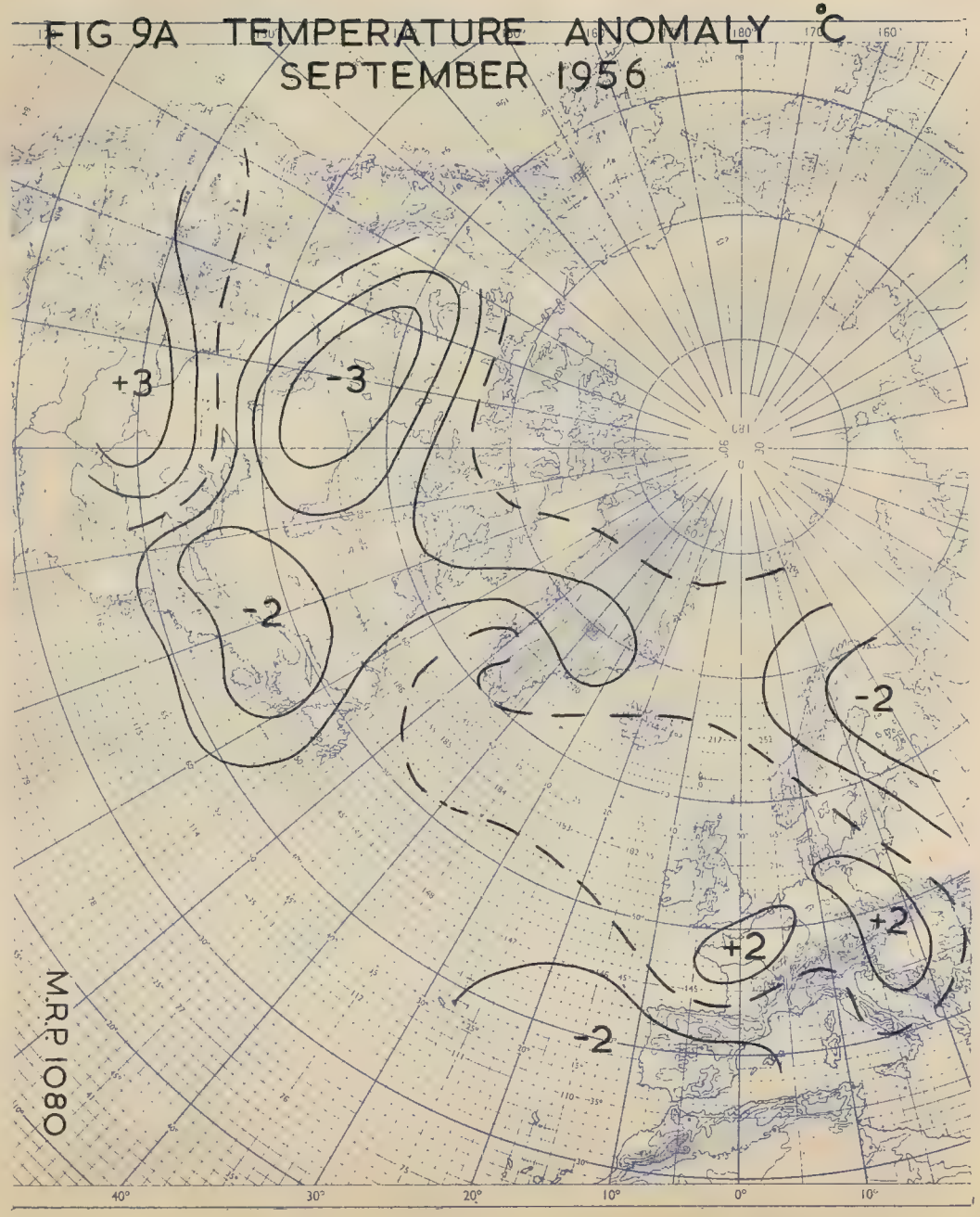

FIG 9B THICKNESS ANOMALY M. °C
SEPTEMBER 1956

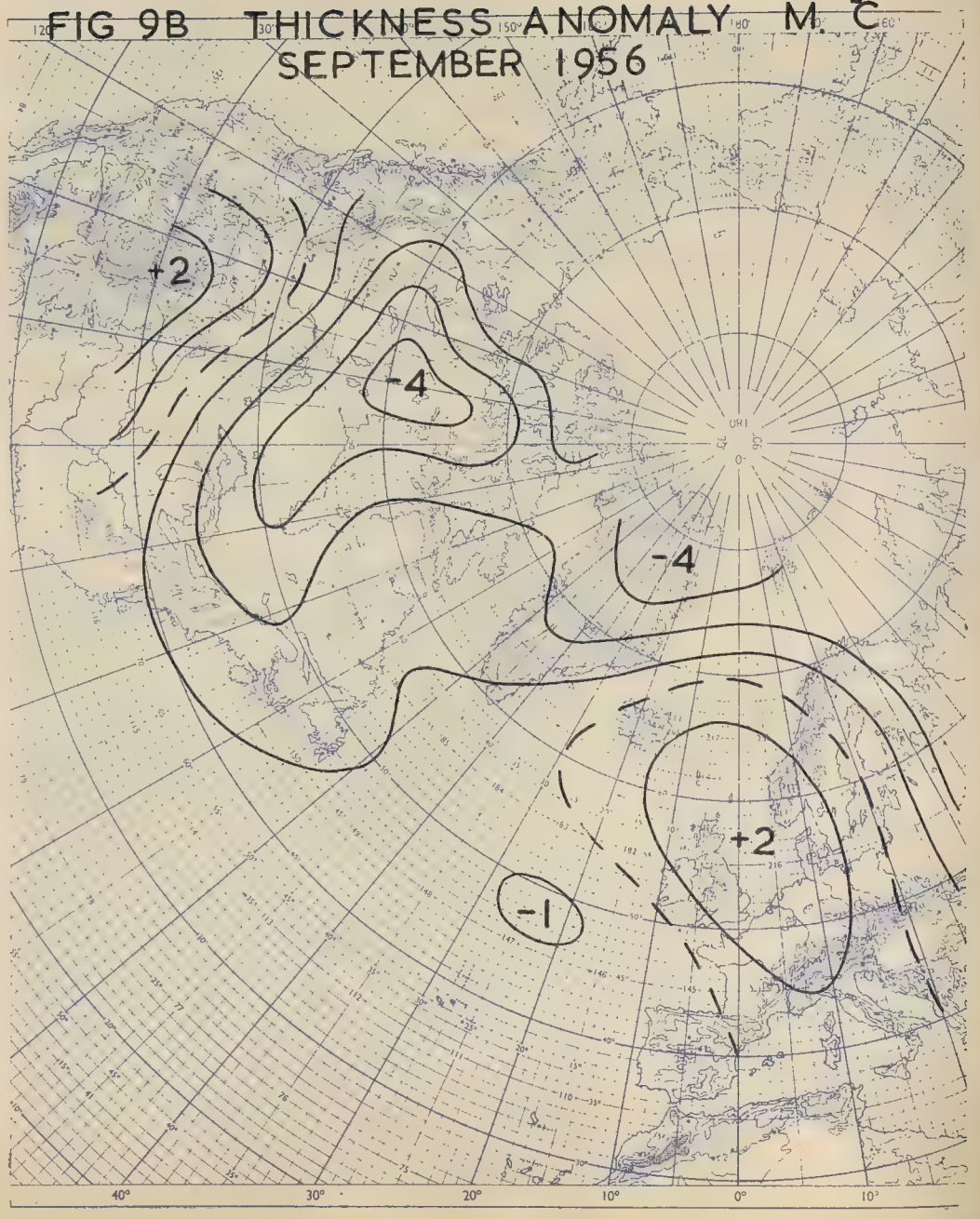

FIG 10A TEMPERATURE ANOMALY °C
OCTOBER 1956

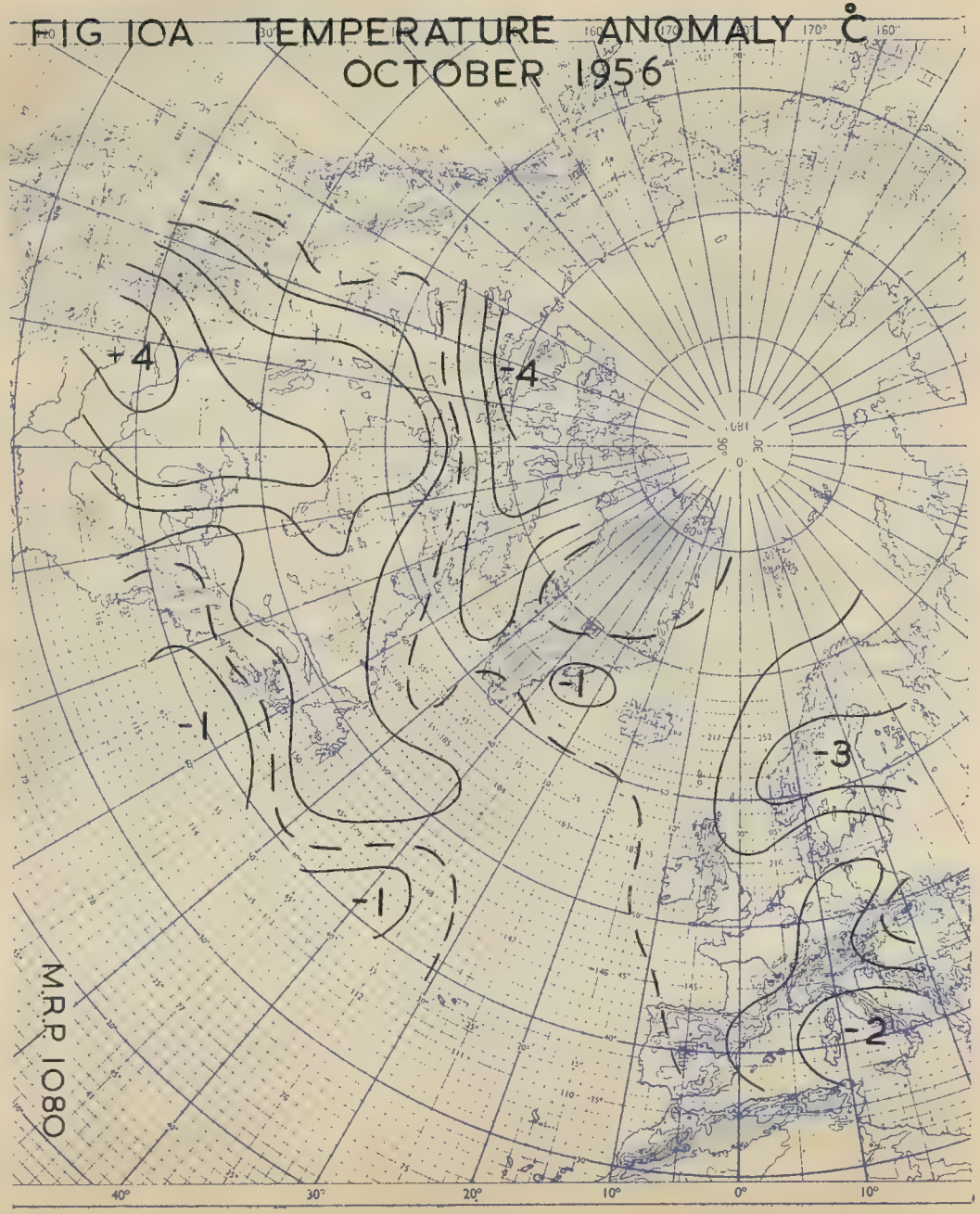

FIG 10B THICKNESS ANOMALY M °C
OCTOBER 1956

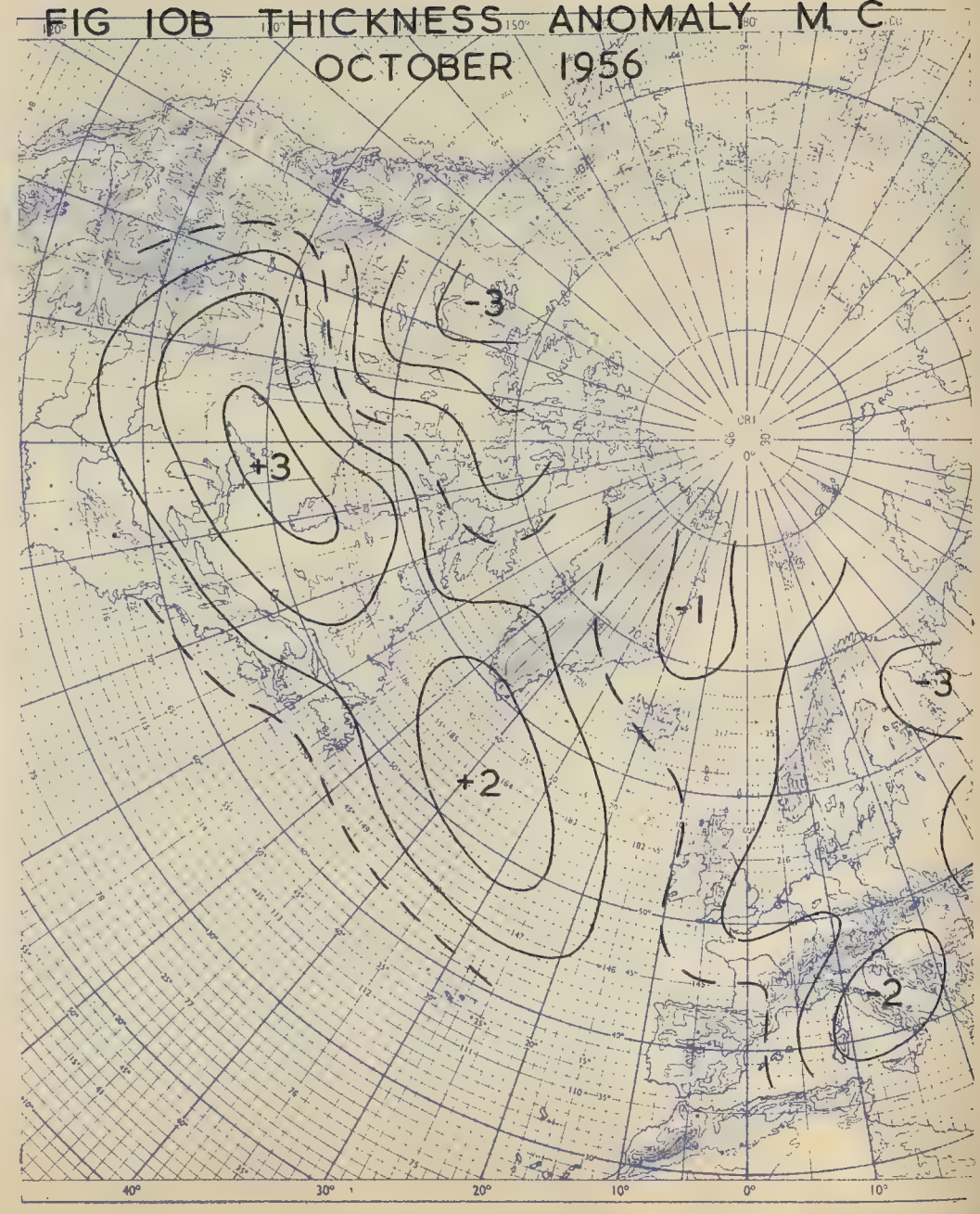

FIG IIA TEMPERATURE ANOMALY °C
NOVEMBER 1956

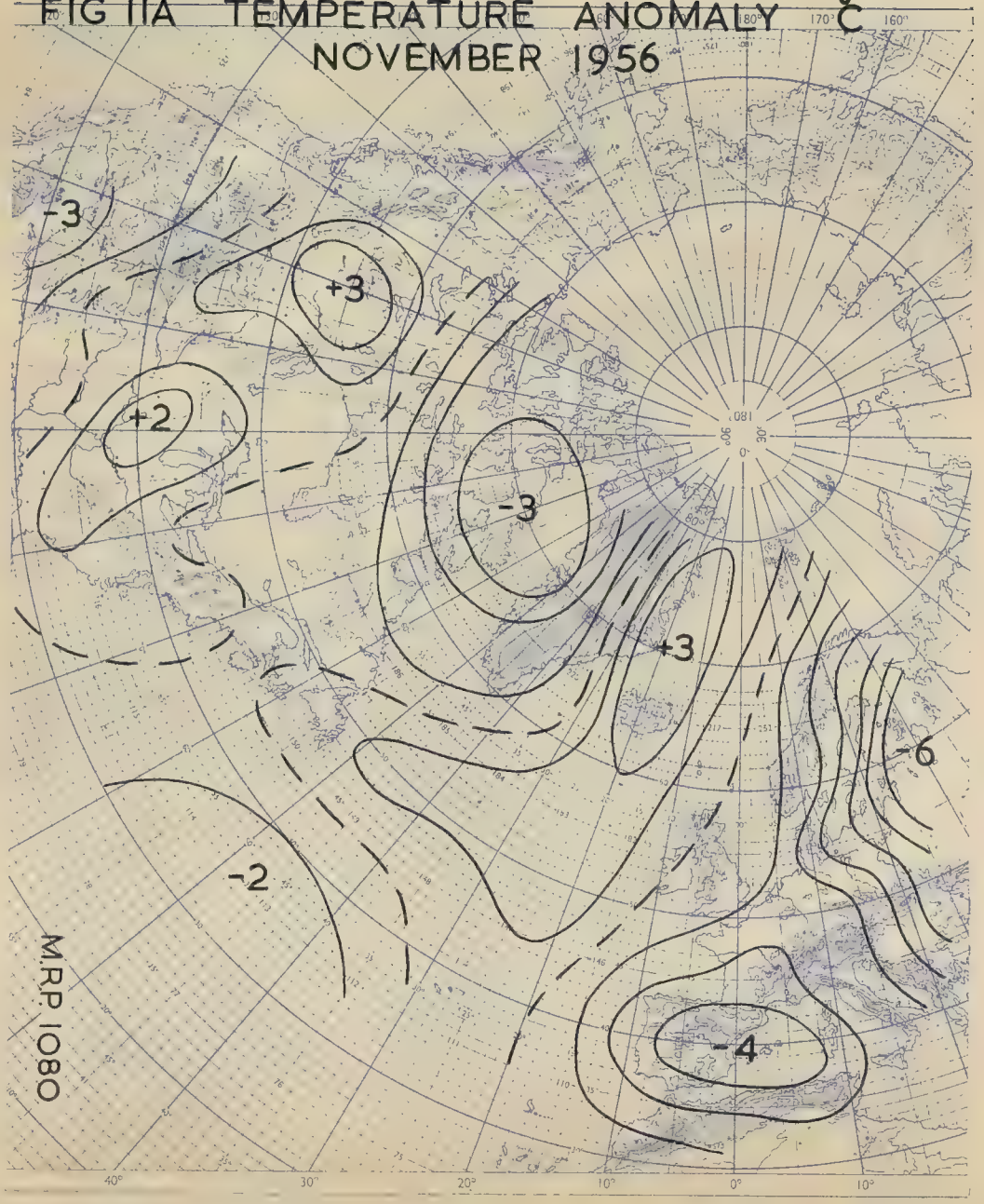

FIG IIB THICKNESS ANOMALY M. °C
NOVEMBER 1956

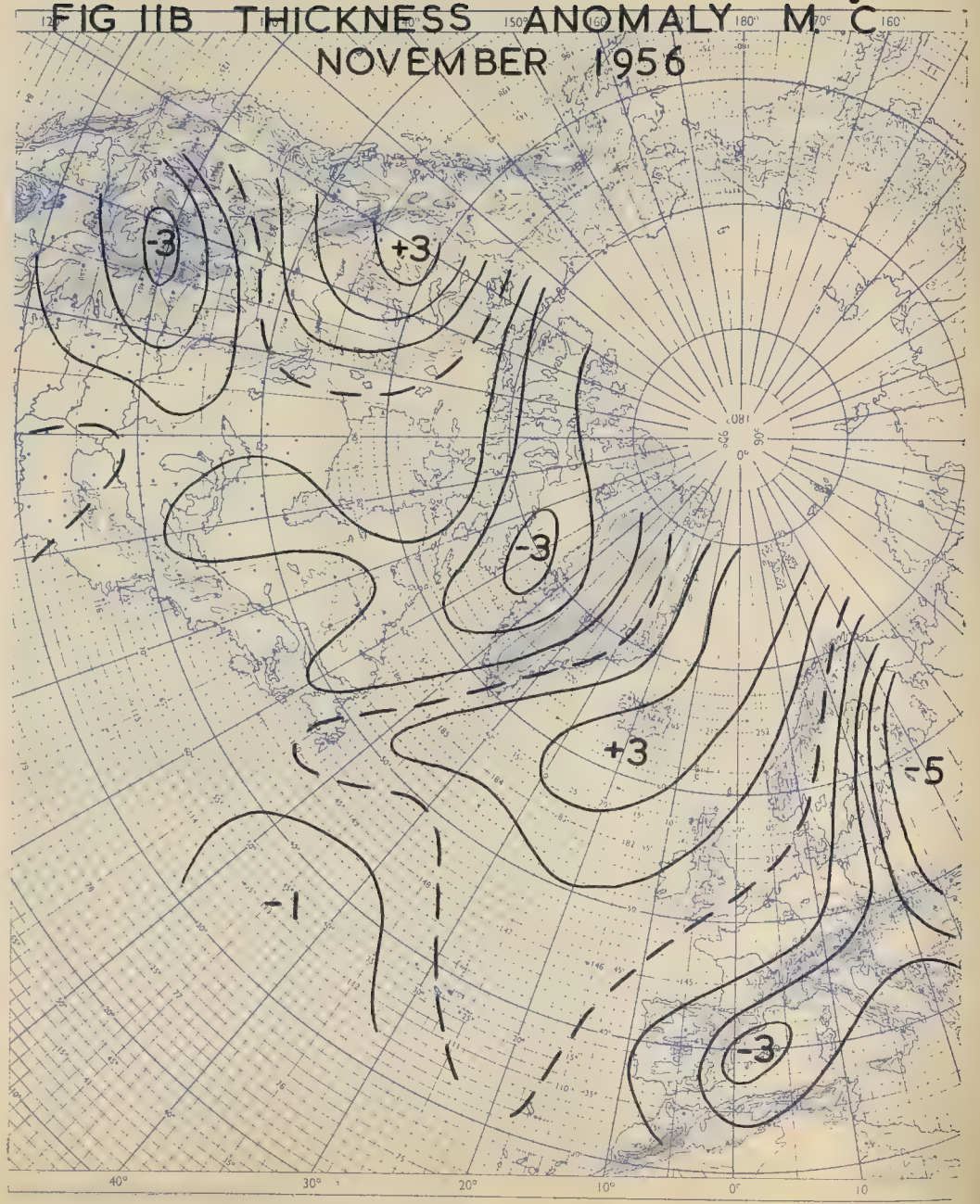

FIG 12A TEMPERATURE ANOMALY °C
DECEMBER 1956

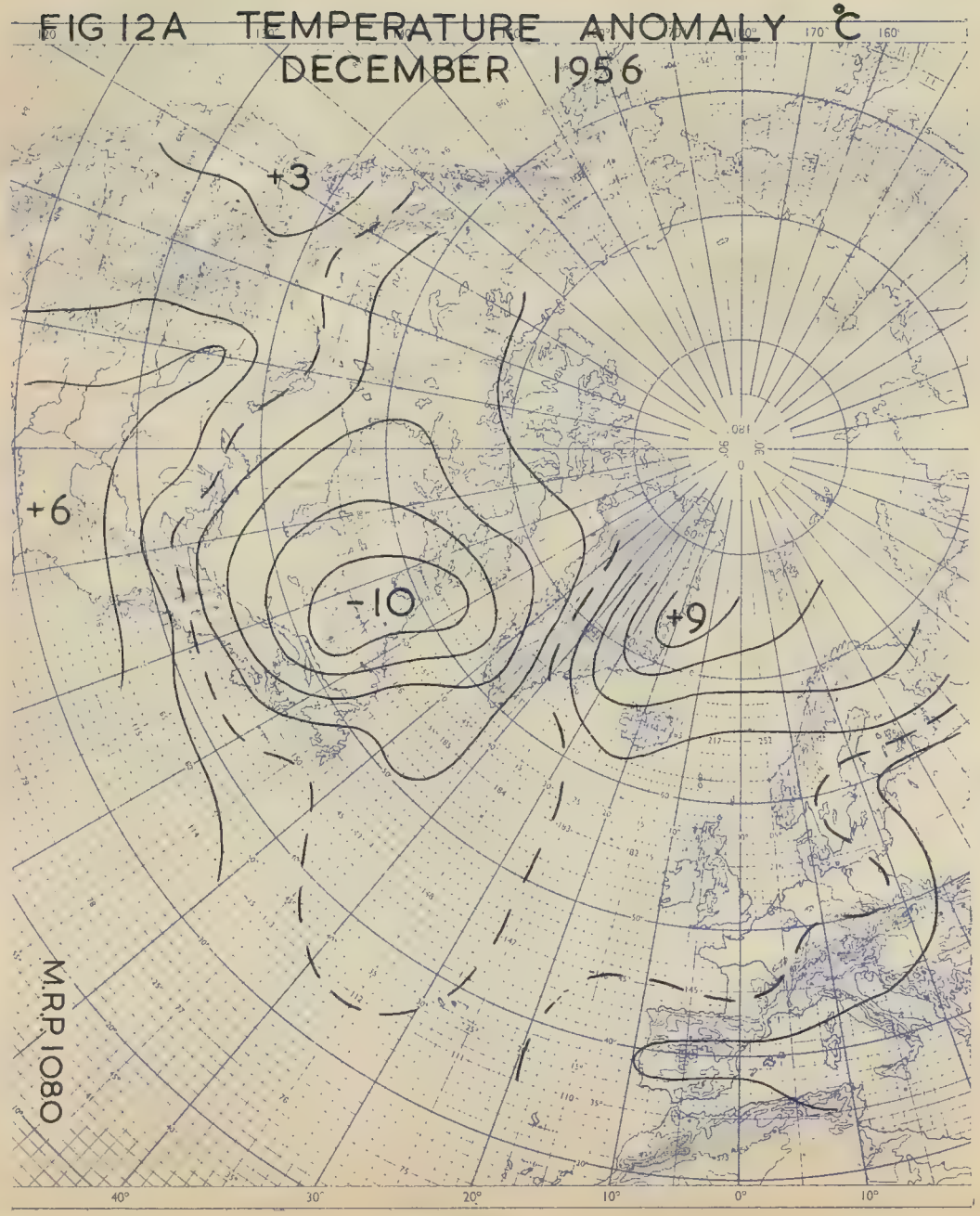

FIG 12B THICKNESS ANOMALY M.°C
DECEMBER 1956

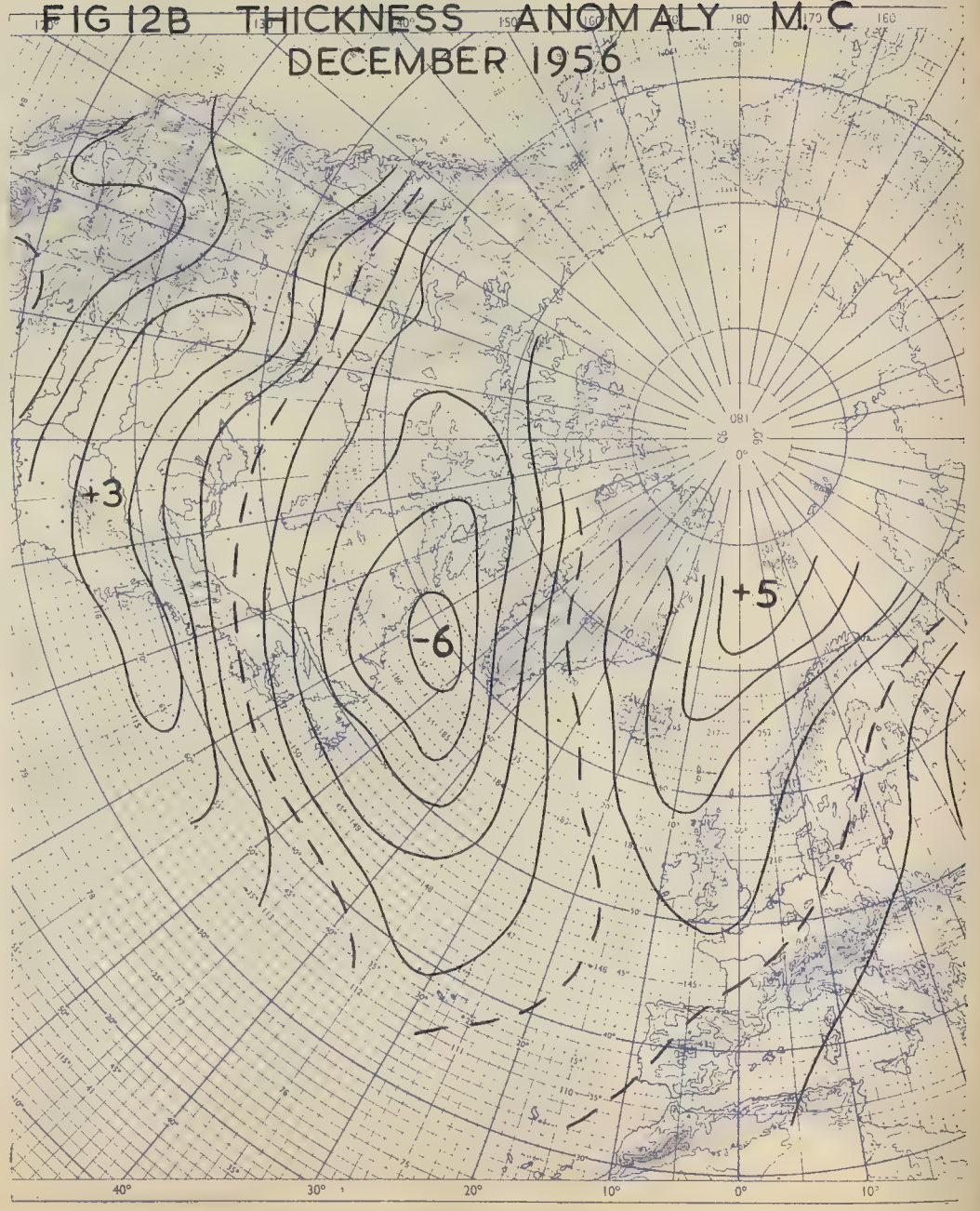

KEY CHART: STATIONS USED FOR COMPARISON OF NORMALS

APPENDIX

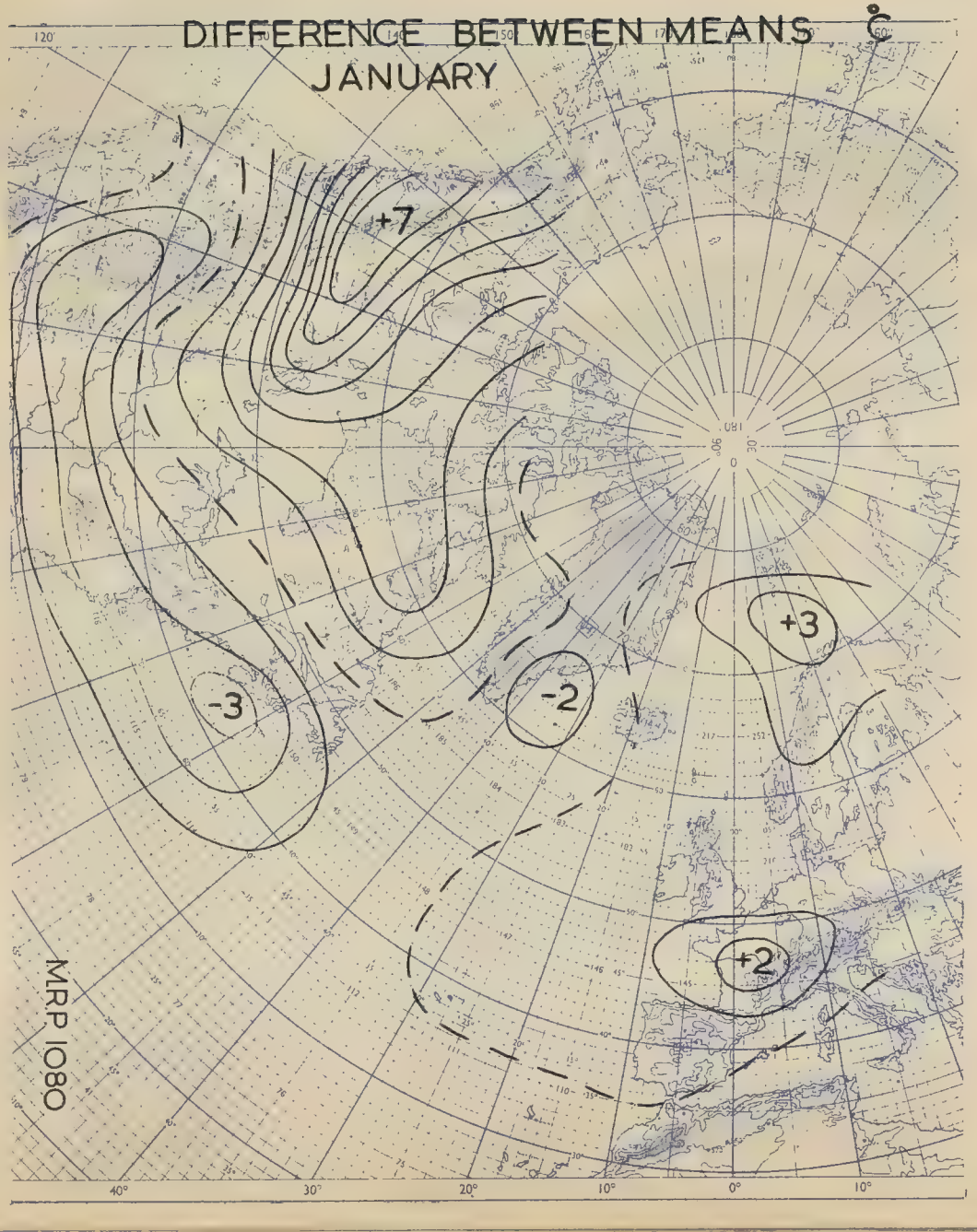
DIFFERENCE BETWEEN MEANS °C
JANUARY
+7
+3
-3
-2
+2
MRP 1080

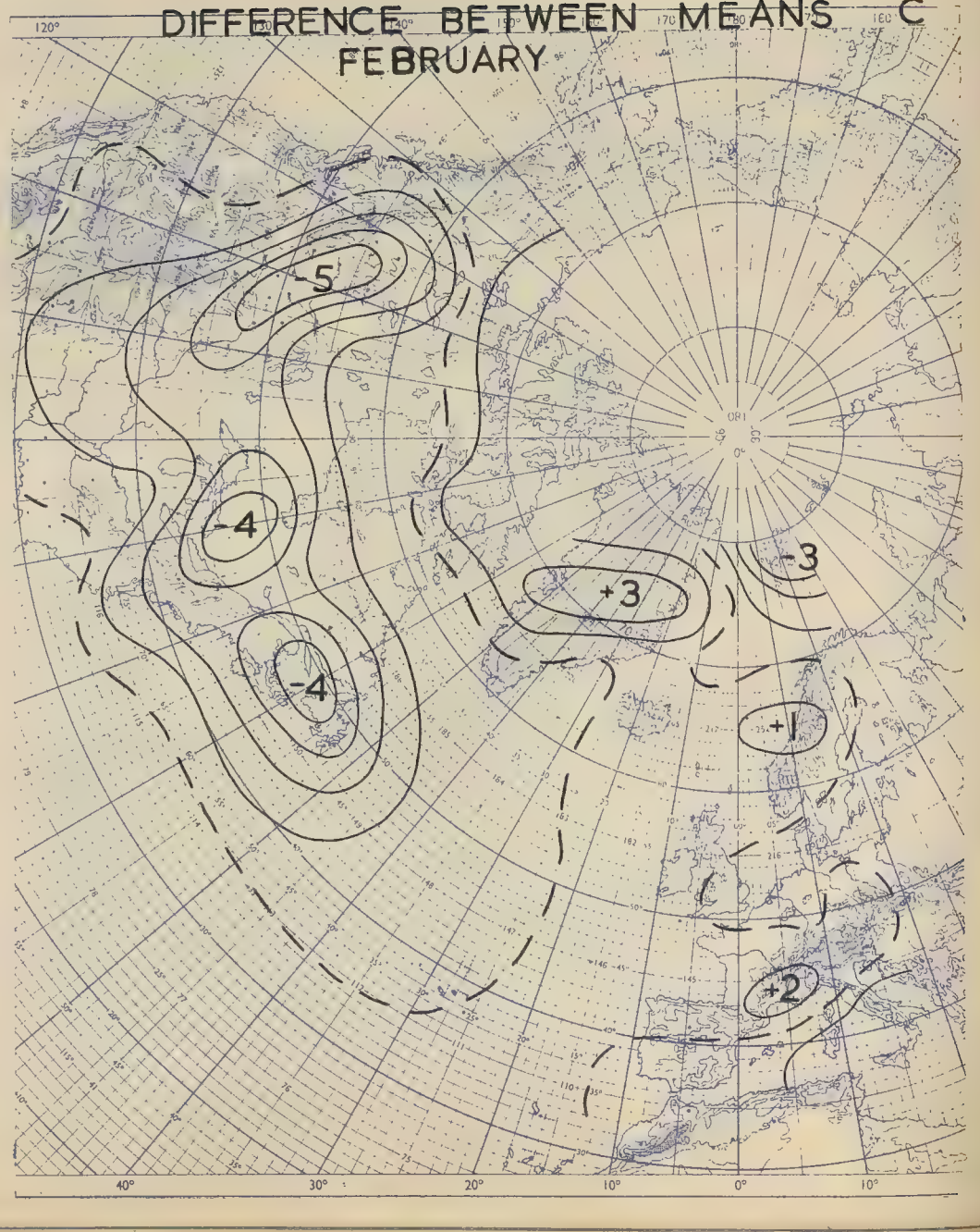
DIFFERENCE BETWEEN MEANS °C
FEBRUARY
-5
-4
-4
+3
-3
+1
+2

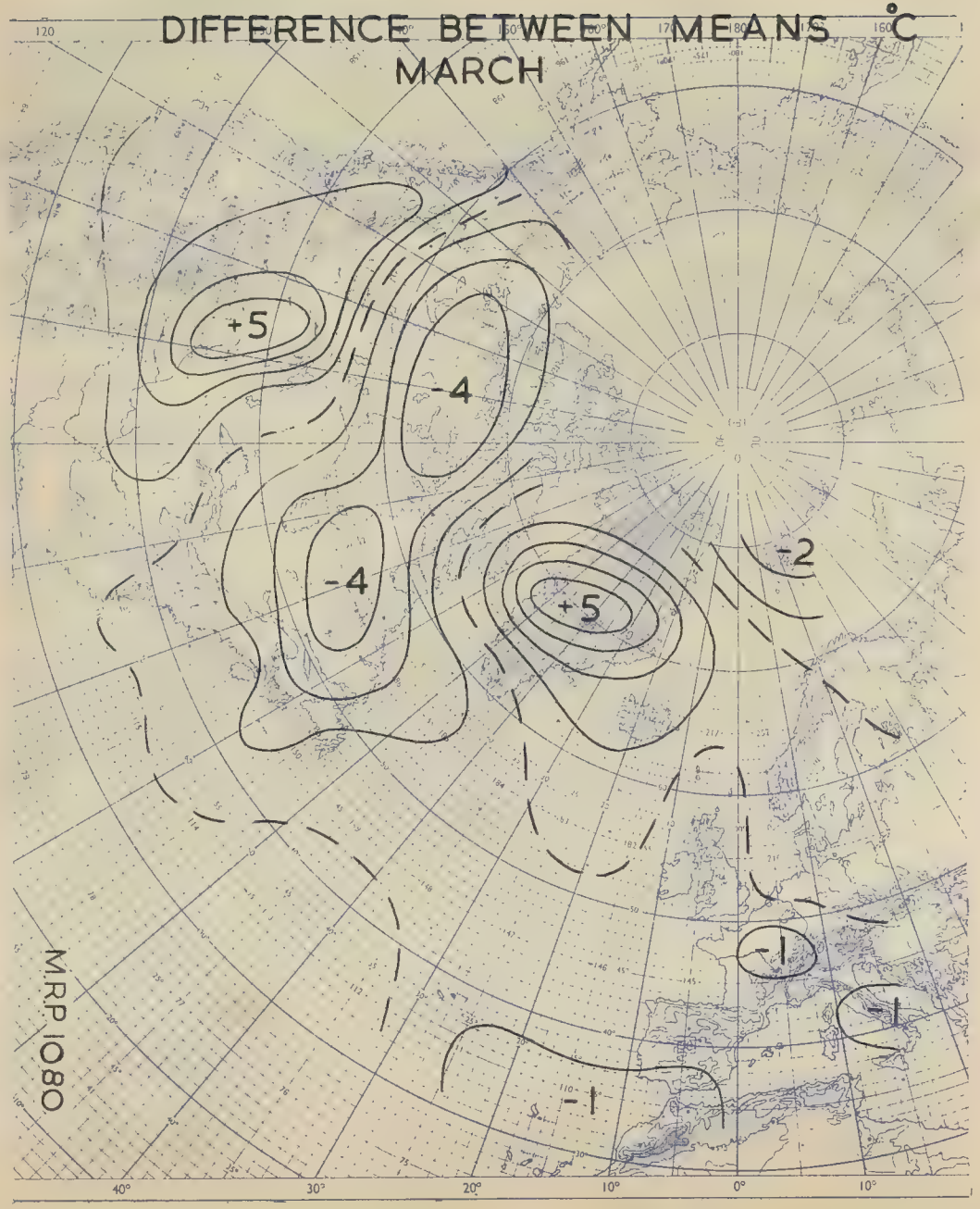
DIFFERENCE BETWEEN MEANS °C
MARCH
+5
-4
-4
+5
-2
-1
-1
-1
M.R.P. 1080

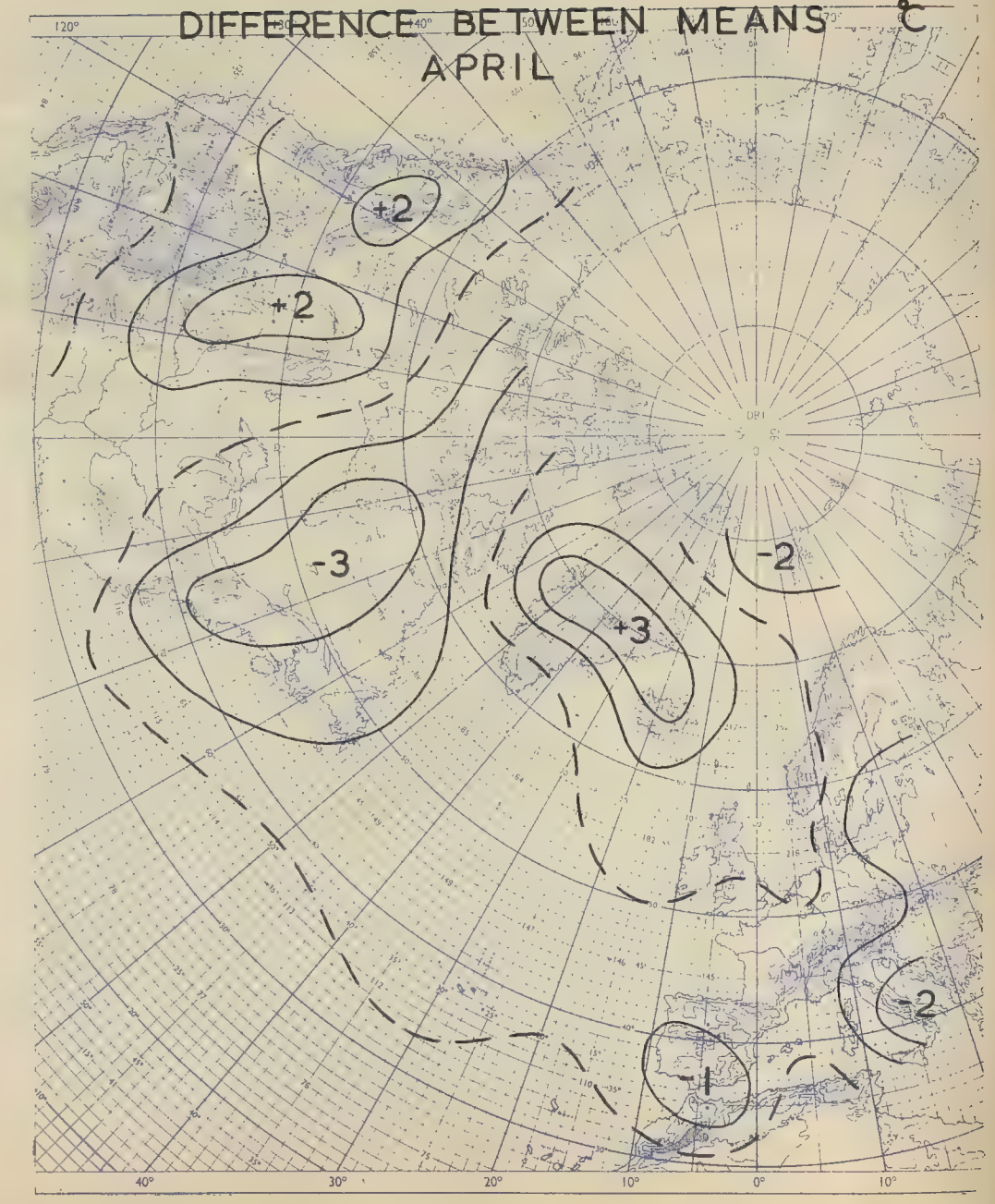
DIFFERENCE BETWEEN MEANS °C
APRIL
+2
+2
-3
+3
-2
-2
-1

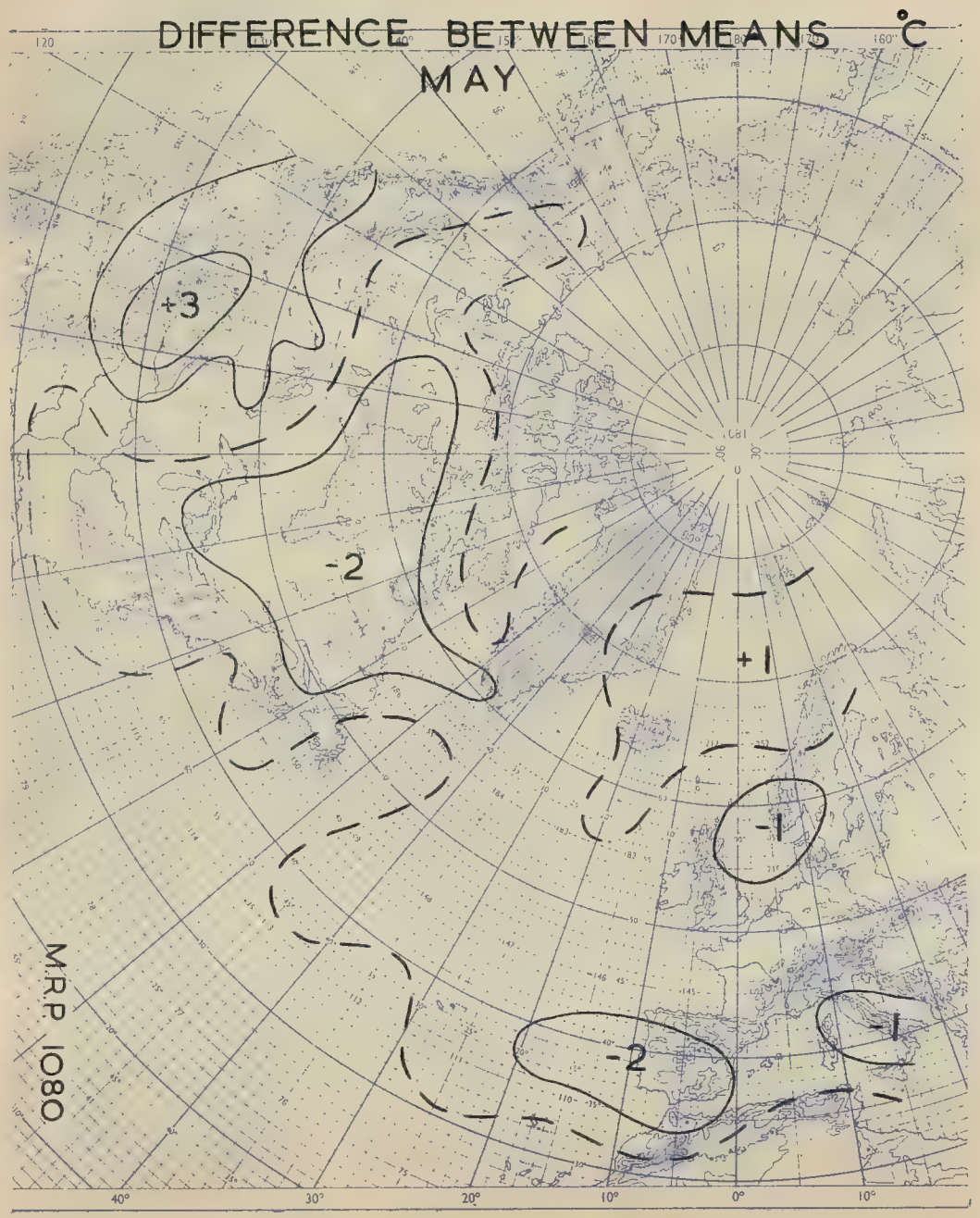
DIFFERENCE BETWEEN MEANS °C
MAY
+3
-2
+1
-1
-2
-1
M.R.P. 1080

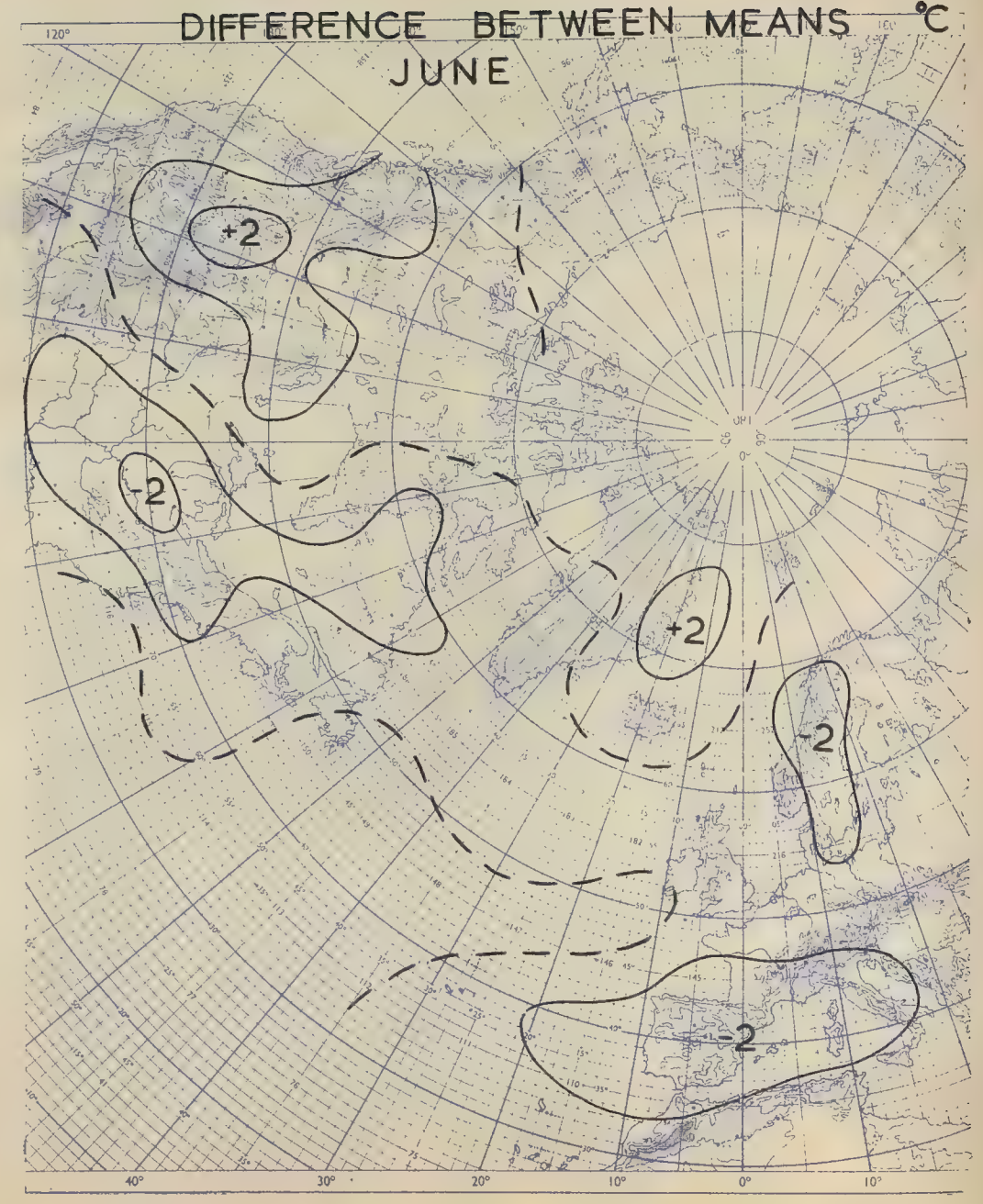
DIFFERENCE BETWEEN MEANS °C
JUNE
+2
-2
+2
-2
-2

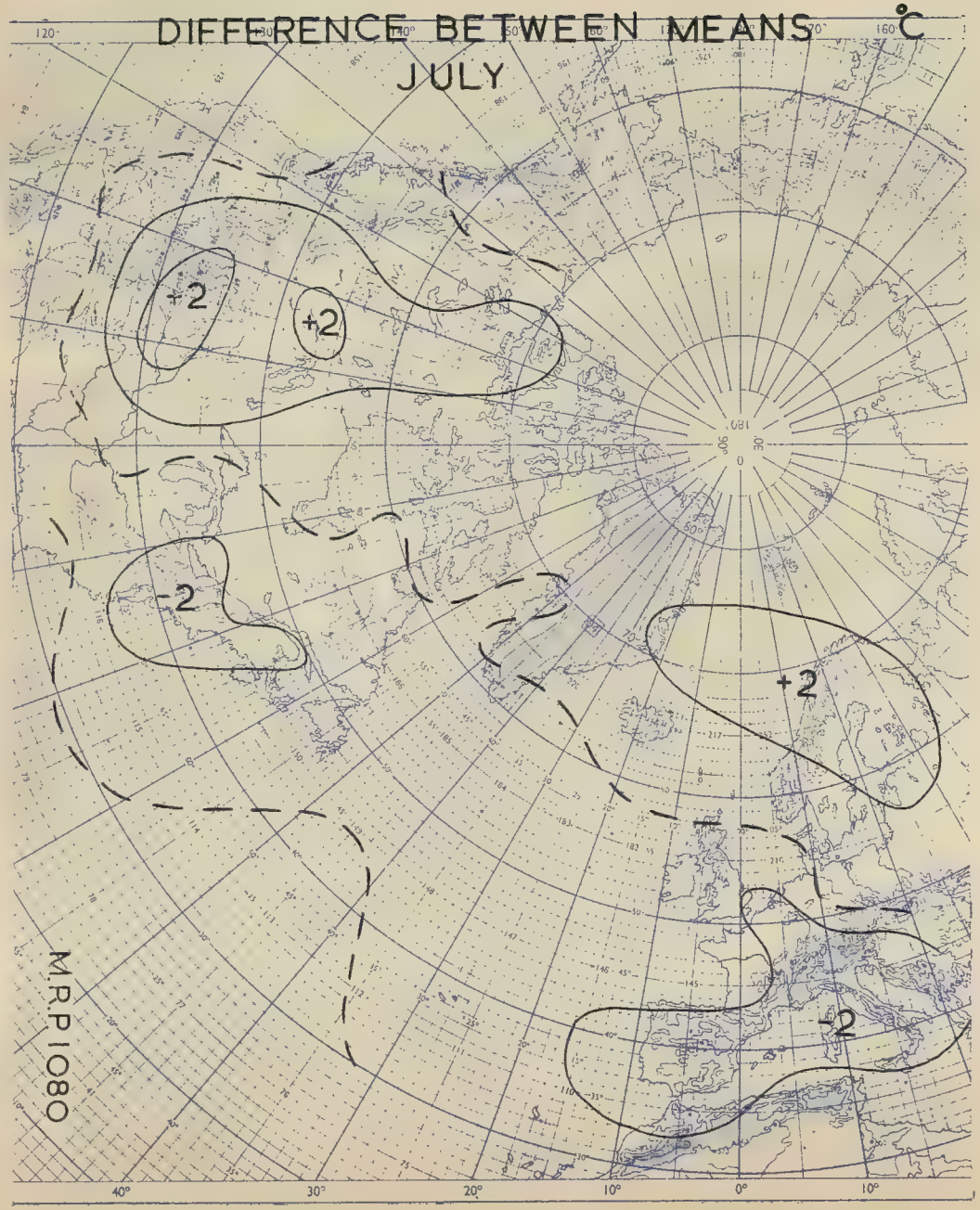
DIFFERENCE BETWEEN MEANS °C
JULY
+2
+2
-2
+2
-2
M.R.P.1080

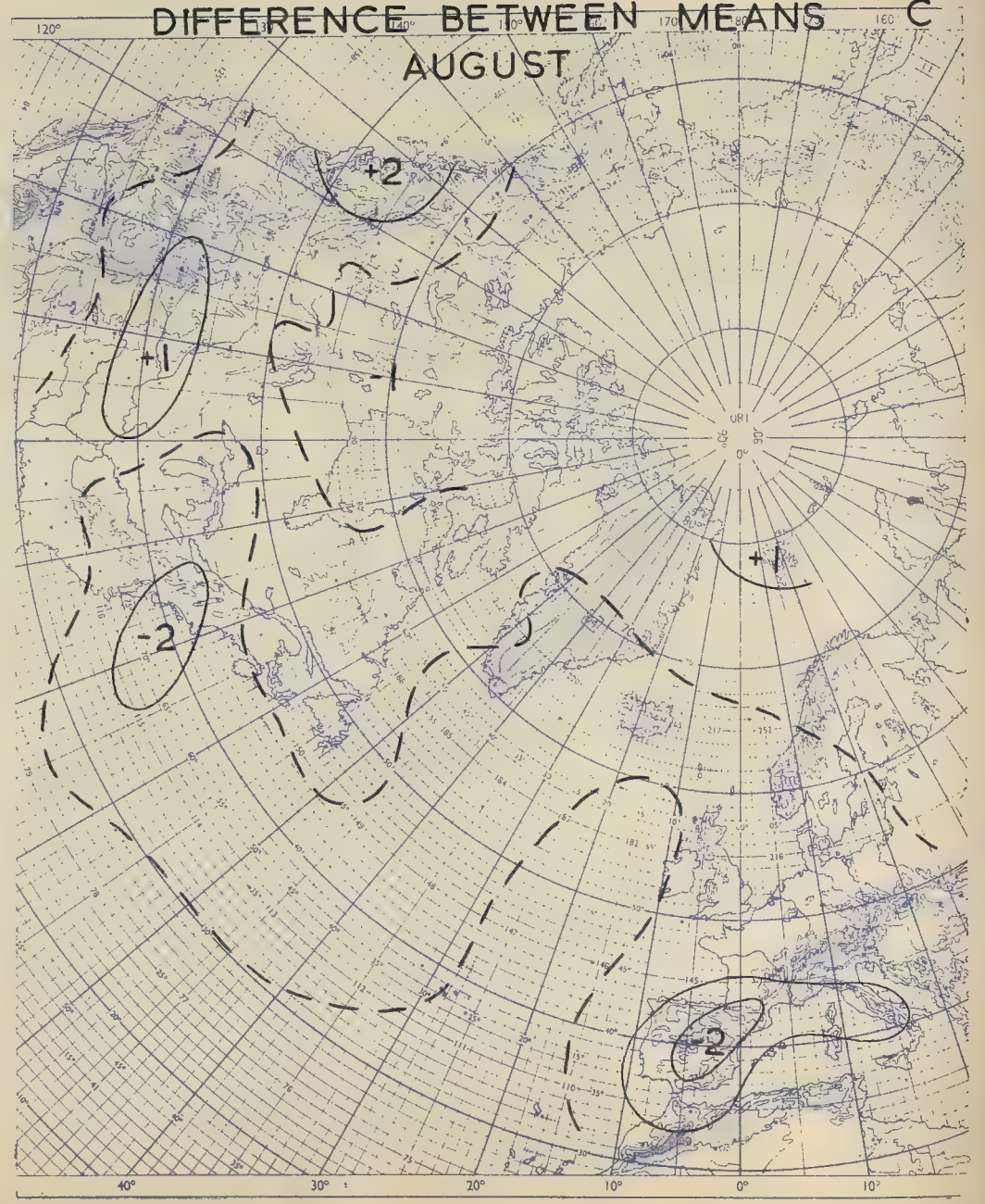
DIFFERENCE BETWEEN MEANS °C
AUGUST
+2
+1
-1
+1
-2
-2

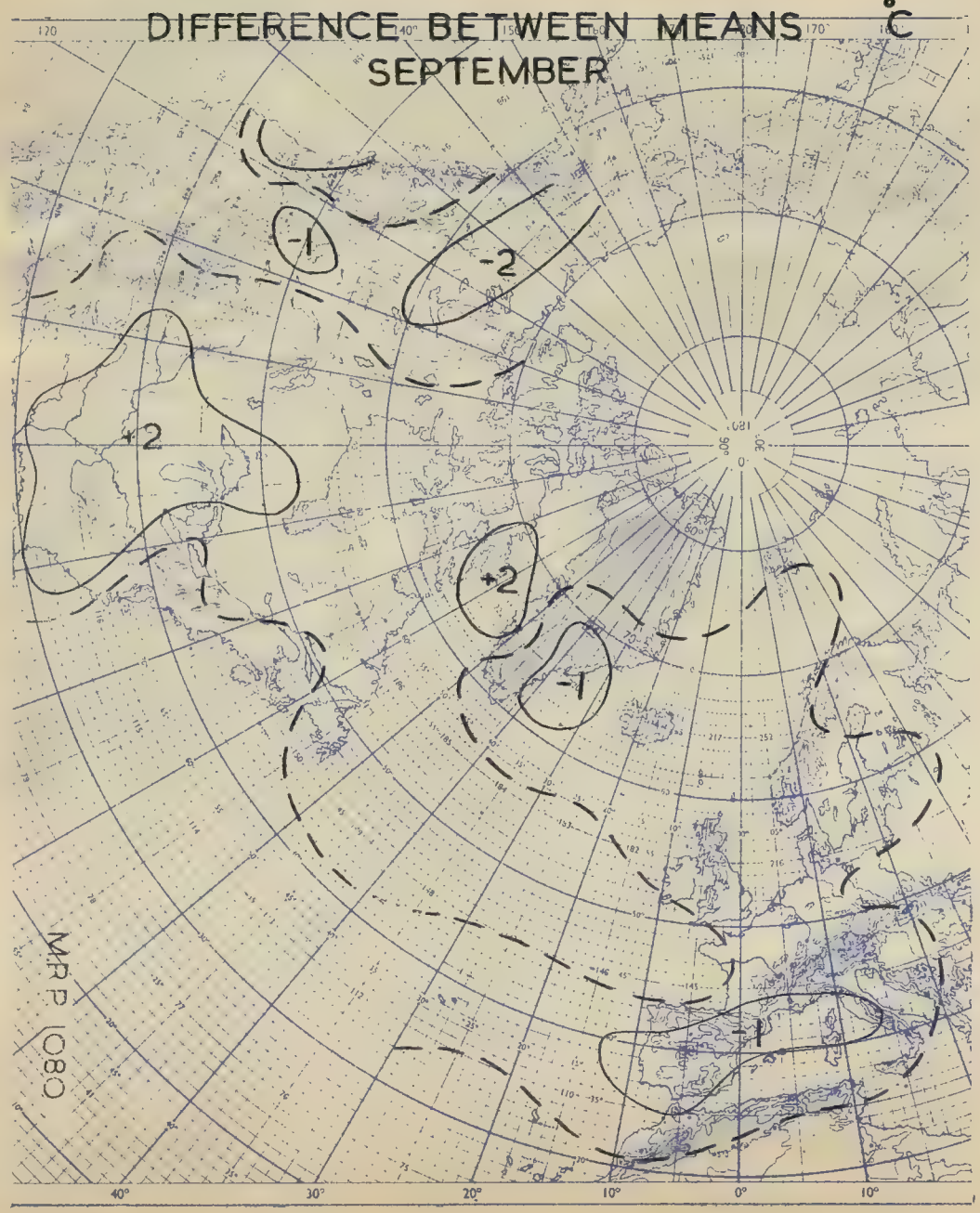
DIFFERENCE BETWEEN MEANS °C
SEPTEMBER
-1
-2
+2
+2
-1
-1
MRP (080)

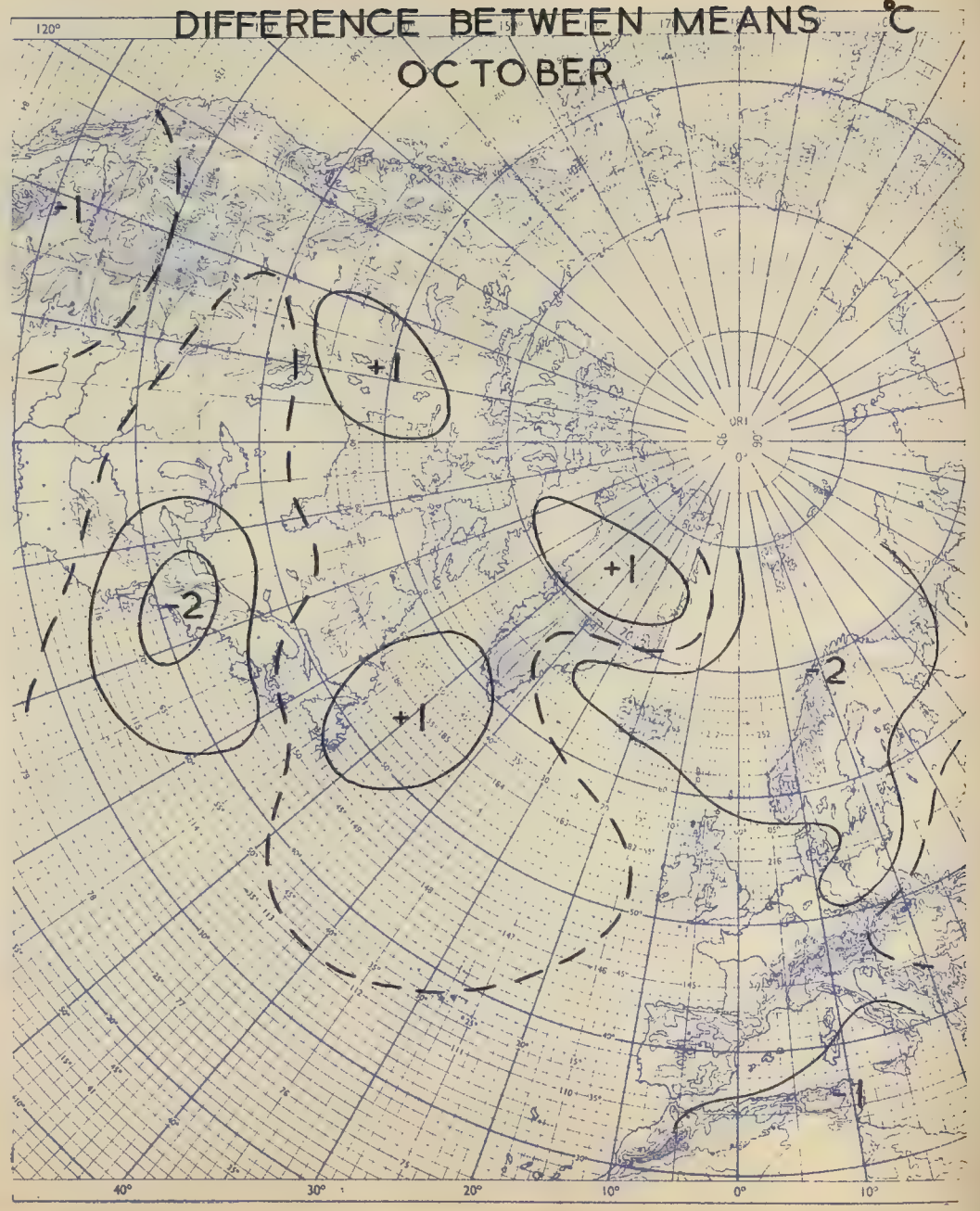
DIFFERENCE BETWEEN MEANS °C
OCTOBER
-1
+1
+1
-2
+1
2
-1

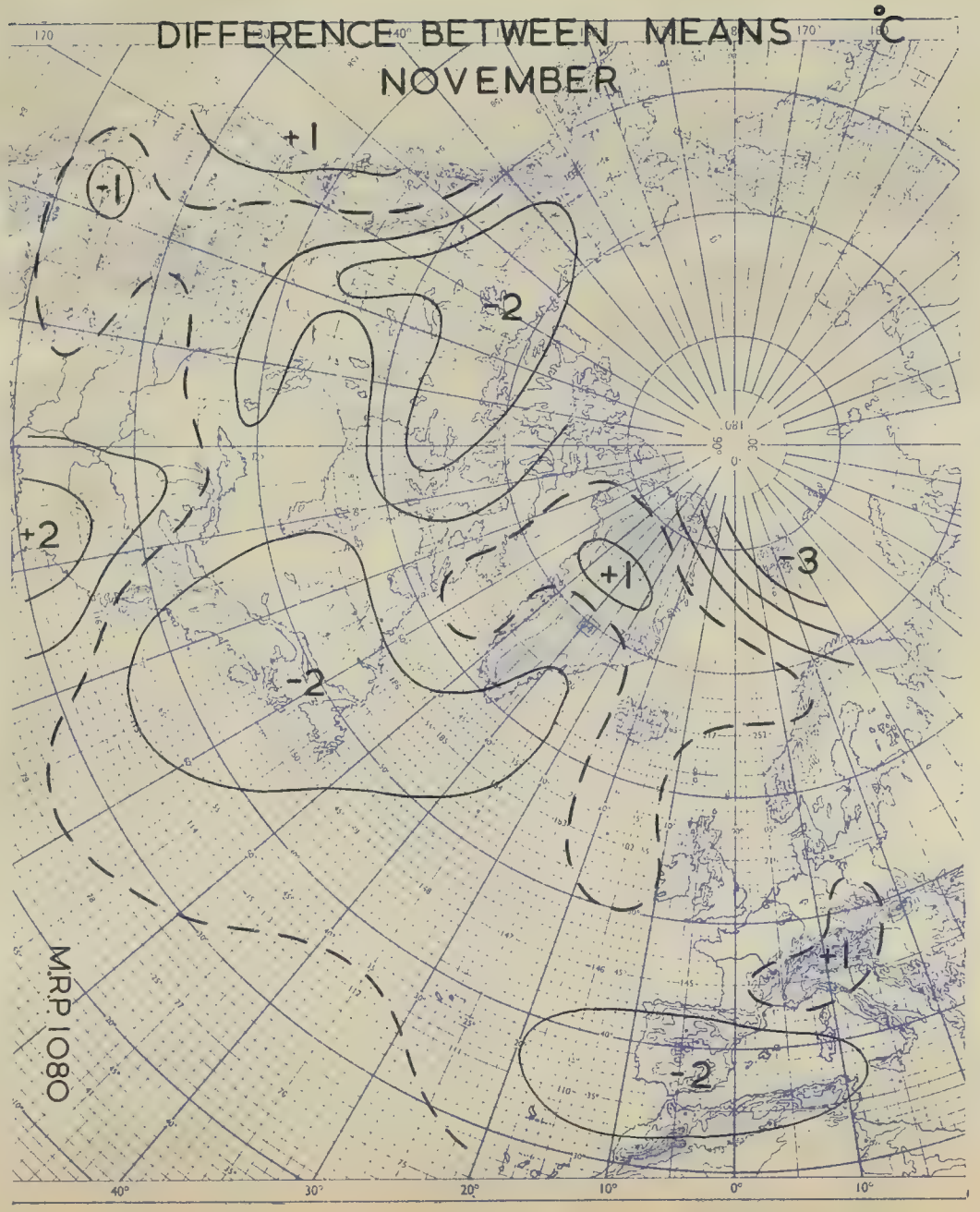
DIFFERENCE BETWEEN MEANS °C
NOVEMBER
+1
+1
-2
+2
-2
+1
-3
-2
+1
-2
MRP 1080

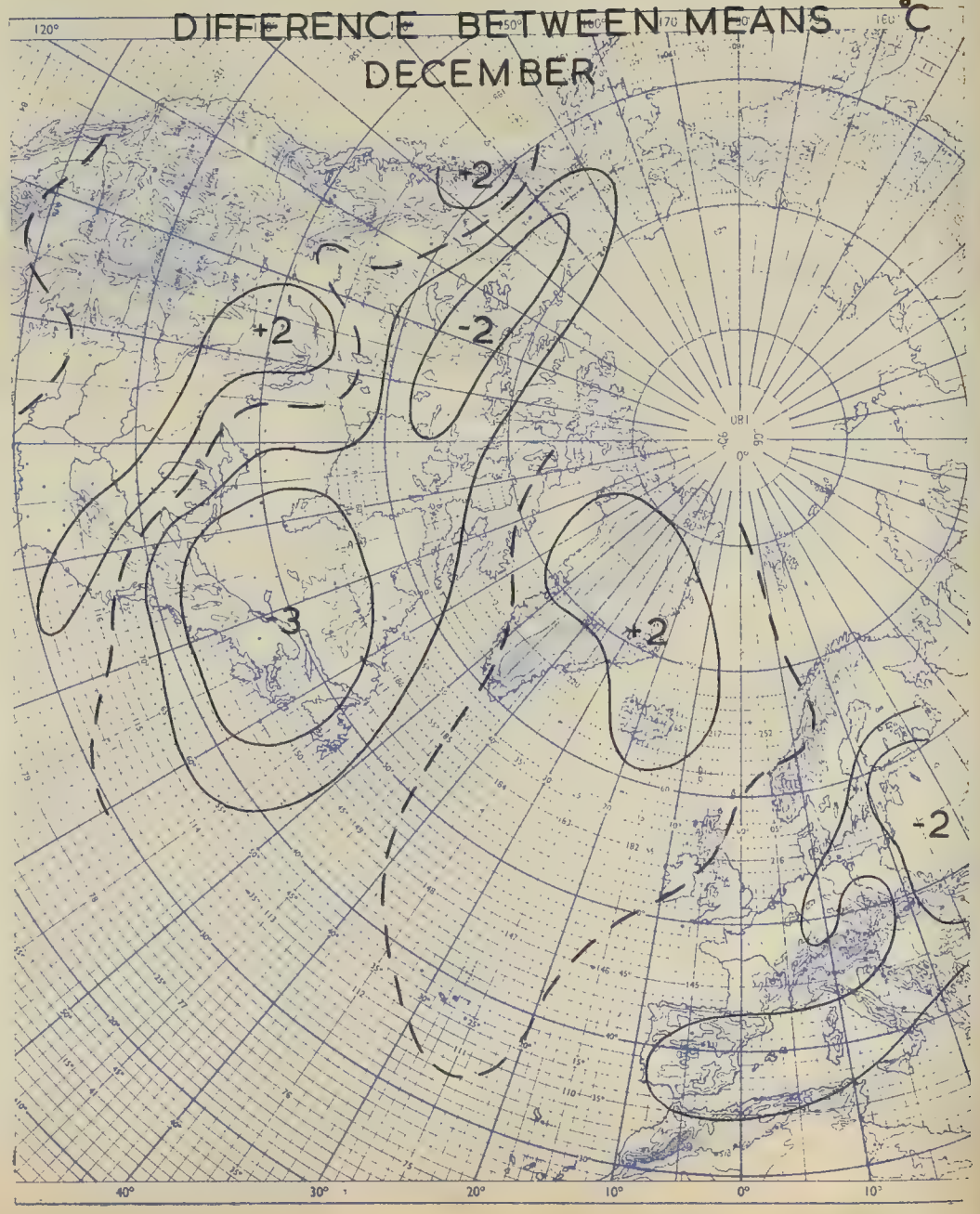
DIFFERENCE BETWEEN MEANS °C
DECEMBER
+2
+2
-2
-3
+2
-2

M.R.P. 1084
S.C.1/133
7th January, 1958

The phosphorous pentoxide electrolytic hygrometer

by

A. W. Brewer

(Clarendon Laboratory Oxford)

AIR MINISTRY

METEOROLOGICAL RESEARCH COMMITTEE

At the time of issue this report has not been published. Any author desiring to quote this paper should refer to it as "A paper of the Meteorological Research Committee (London), M.R.P. No. 1084 by Dr. A.W. BREWER
A copy is available in the Library of the Meteorological Office."

M.R.P. 1084
S.C.I/133
7th January, 1958

AIR MINISTRY

METEOROLOGICAL RESEARCH COMMITTEE

The phosphorous pentoxide electrolytic hygrometer

by

A.W. Brewer (Clarendon Laboratory Oxford)

Since about June, 1956, descriptions of a new hygrometer originating in the Dupont Laboratories, have appeared in the U.S. technical literature (1),(2). and several U.S. instrument firms are now offering hygrometers based on the new principle. All the literature refers to its use at concentrations of a few parts per million (p.p.m.). Since a F.P. (frost point) of -80°C equals 0.4 p.p.m. it is possible that the hygrometer could be used in arctic conditions and in upper atmosphere measurements. This note briefly reviews this possibility.

Principle of operation

The detector consists in principle of a film of phosphoric acid covering a fine grid of platinum electrodes. The electrodes are formed from two fine platinum wires (.004 in. diameter) wound as a two start thread and with a spacing of about .004 in. between adjacent electrodes. A potential difference, which must be greater than 2v and is usually about 50v, is applied between the wires. This electrolyses the water in the phosphoric acid to hydrogen and oxygen, and the phosphoric acid is converted to partially hydrolysed P_2O_5. As this happens the resistance rises and eventually the current is cut off. If now a measured volume of air is passed over the element the P_2O_5 will absorb the water contained in the air and conduct electricity until the water has been electrolysed away. The quantity of electricity passed is determined by the quantity of water absorbed and Faraday's laws of electrolysis, and not by the resistance of the film.

The instrument works as a continuous detector when there is a controlled flow of air, and subject to lag, the current passing depends only on the water content of the air stream.

The absorption of all the water from the air presents difficulties if the air flow exceeds about 200 cc/min, but this is quite convenient as the following approximate calibration shows:

/1 gm H_2O

1 gm H_2O = 10.6×10^3 coulombs

F.P.	Water vapour density gm/cc	Current at 3 cc of air/sec
-80°C	4.5×10^{-10}	14.0 μa
-60°C	8×10^{-9}	250.0 μa
-40°C	1×10^{-7}	3.2 ma
-20°C	8×10^{-7}	25.0 ma
0°C	4.7×10^{-6}	150.0 ma
+20°C	1.7×10^{-5}	540 ma

It will be seen that the currents are quite easily measurable but the range is uncomfortably large. At the large water contents resistive heating is said to be a nuisance. Published accounts claim that the instrument is usable over at least the range of F.P. -80°C to -20°C.

Response time Published data give exponential response times of one minute for increasing water contents and two minutes for decreasing water contents.

Specificity There is no reason to expect any other atmospheric constituent to interfere with its operation.

Construction of the element

The element, as described, is made by winding the platinum wires with copper wires as spacers on a 1 mm to 0.75 mm diameter mandrel for a length of approximately 30 cm; embedding this in Polytetrafluorethylene, removing the mandrel and then dissolving the copper away with acid. In this way the wires are obtained on the outside of a 1 mm (approx) diameter capillary tube 30 cm long. For convenience a coiled coil arrangement is adopted making the final element of reasonable dimensions.

Reliability

Published accounts claim good reliability. One instrument passed to the writer for test failed immediately tests began and this is similar to the experience of the only other person I have met who has actually used one.

Special considerations for meteorological use

Back pressure

The back pressure due to the "Poiseuille" drag in the tube of an element of this construction would be of the order of 20-50 mb depending very much on the actual diameter of the hole and the roughness of the walls, but not on the total pressure. For meteorological purposes this is too large, since, in order to avoid contamination of the air it must be drawn through the element, and this back pressure becomes too large a fraction of the total air pressure.

There is no reason in principle why this should not be overcome by using an annular gap of about 0.5 mm between a cylinder, say 5 mm diameter, and a tube 6mm diameter, but there may be practical difficulties. For this, 2 cm length is sufficient for approximately 99 per cent extraction, with negligible back pressure. The extraction efficiency will improve at high levels due to the increasing diffusion coefficient at low pressures.

/Flow

Flow measurement

At flow rates of about 200 cc/minute our experience is that the most satisfactory method of flow control is to use a small positive displacement piston pump, either driven by a constant speed motor, or with a variable speed motor, and measure the rate of rotation of the motor. For the latter we have used a 40 mm^3 pump running at approximately 5000 r.p.m. and we are making a prototype pump for use with a constant speed motor.

Effect of lag and the wide range of water contents in the atmosphere

A special circumstance arises from the wide range of water contents encountered in the atmosphere. During an ascent when climbing at a rate of say 1500 ft per minute the average rate of fall of water content is greater than through a ratio 1:1/e in two minutes, which is the maximum rate of response claimed for falling water contents. This rate of response is therefore inadequate for use on balloons and would not permit use in aircraft during rapid ascents or descents. For this an expcnential response time of about 30 sec. is desirable.

Conclusion

Though it is by no means free from difficulties it would seem that this is a very hopeful hygrometer which would certainly be suitable for arctic conditions and for some kinds of upper air work.

Mr. Goldsmith at A.E.R.E., is working on a practical development for high altitude work.

Acknowledgment

I am grateful to Mr. A. G. Hamlin, U.K.A.E.A. Capenhurst, for photo copies of American papers on the subject.

References

(1) F. A. Keidel "A novel and inexpensive instrument for accurate analysis for traces of water". Du Pont de Nemours & Co., Inc., Wilmington, Delaware. Presented February 27th, 1956 Pittsburgh conference on Analytical Chemistry and Applied Spectroscopy.

(2) E.S. Taylor "New instrument for the moisture analysis of 'Freon'" Refrigerating Engineering, July, 1956, p.41.

M.R.P. 1098
1st May, 1958.

Index of M.R.Ps.

Approved for General Distribution

Appendix 18 of M.R.P. 200.

AIR MINISTRY

METEOROLOGICAL RESEARCH COMMITTEE

M.R.P. 1098
1st May, 1958

At the time of issue this report has not been published. Any author desiring to quote this paper should refer to it as "A paper of the Meteorological Research Committee (London), M.R.P. No. 1098 A copy is available in the Library of the Meteorological Office."

AIR MINISTRY

METEOROLOGICAL RESEARCH COMMITTEE

Index of M.R.Ps. Approved for General Distribution
Appendix 18 of M.R.P. 200

M.R.P.	TITLE	AUTHOR
1054	Index of M.R.Ps. approved for general distribution (Appendix 17 of M.R.P. 200)	-
1055	Observations from aircraft of temperatures and humidities near stratocumulus cloud	D.G. James
1056	Forecast verification: a critical survey of the literature	D.H. Johnson
1058	Horizontal diffusion in the atmosphere in the light of air trajectories	C.S. Durst A.F. Crossley N.E. Davis
1062	Spectral estimates from subdivided meteorological series	H. Charnock G.D. Robinson
1063	Two-parameter techniques of numerical forecasting applied to a small intense depression	J.S. Sawyer
1064	Temperature, humidity and cloud near fronts in the middle and upper troposphere	J.S. Sawyer
1065	The Southern Circumpolar Westerlies: broad characteristics and apparent associations	H.H. Lamb
1066	Average height of the standard isobaric surfaces over the temperate and tropical regions in July	H. Heastie
1068	The origin of radar 'angels'	W.G. Harper
1069	Some airborne observations of condensation nucleus concentration. I. Variations in the vertical	G.J. Day
1070	The measurement of wind at altitude by airborne instruments	R.J. Murgatroyd N.C. Helliwell
1071	A diagram for obtaining true air temperatures from indicated air temperatures for aircraft resistance thermometers	W.G. Durbin
1073	Convection-diffusion processes below a stable layer - Part II (Porton Technical Paper No. 619)	F.B. Smith
1074	Some observations on the composition of fogs	K.H. Stewart

M.R.P.	TITLE	AUTHOR
1075	Average water-vapour content of the air	J.K. Bannon L.P. Steele
1077	The development of precision aneroids - interim report	R. Frith
1078	Conservation of vorticity at 100 mb	J.R. Probert-Jones
1079	Some measurements of temperature and humidity near the sea surface	H.C. Shellard
1080	The relation between anomalies of surface air temperature and of 1000-500 mb thickness over the Atlantic sector of the Northern Hemisphere	C.A.S. Lowndes
1084	The phosphorus pentoxide electrolytic hygrometer	A.W. Brewer